E1B19K-deleted oncolytic adenoviruses enhance the cytotoxicity of DNA-damaging drugs in pancreatic cancer through deregulation of cell-cycle mechanisms

Constantia Pantelidou

Submitted in partial fulfilment of the requirements of the Degree of Doctor of Philosophy

STATEMENT OF ORIGINALITY

I, Constantia Pantelidou, confirm that the research included within this thesis is my own work or that where it has been carried out in collaboration with, or supported by others, that this is duly acknowledged below and my contribution indicated.

I attest that I have exercised reasonable care to ensure that the work is original, and does not to the best of my knowledge break any UK law, infringe any third party's copyright or other Intellectual Property Right, or contain any confidential material.

I accept that the College has the right to use plagiarism detection software to check the electronic version of the thesis.

I confirm that this thesis has not been previously submitted for the award of a degree by this or any other university.

The copyright of this thesis rests with the author and no quotation from it or information derived from it may be published without the prior written consent of the author.

Signature: *CPantelidou*
Date: 08/09/2014

ACKNOWLEDGEMENTS

First of all I would like to thank my supervisors Dr Gunnel Hallden and Professor Nick Lemoine for giving me the opportunity to undertake this project, and Pancreatic Cancer Research Fund for the project funding. Dr Gunnel Hallden has been a great mentor. I would like to thank her particularly for the encouragement she provided, her understanding, patience and positive attitude. The excellent support she gave to me over the years has been instrumental for completing this PhD course and I am very grateful to her.

I would like to thank current and past members of my team, Dr Stella Man, Dr Katrina Sweeney, Dr Hector Maya, Heike Muller and Dr Gioia Cherubini, for their support, technical assistance, feedback and constructive conversations. I am particularly grateful to Gioia for her teaching, guidance, constructive criticism and stimulating discussions that shaped both the progress of this project and my development as a researcher. I also thank Dr Spiros Linardopoulos (The Institute of Cancer Research), Dr Sarah Martin, Dr Susana Godinho and Dr Sarah McClelland for reagents and valuable comments and suggestions. In addition I would like to express my gratitude to Vipul for his endless help and all the members of the Centre for Molecular Oncology and Tumour Biology who helped me over the years.

I am very thankful to people at work for their advice and for making this experience greatly enjoyable: Gioia, Margot, Delphine, Emma, Eiman, Darling, Muget, Laurent, Guglielmo, Wasfi, Mohiemen, Jay, Ahmet and Tomasz. I would like to thank especially Margot, Delphine, Laurent, Guglielmo, Darling, Ahmet and Tomasz for the good times at the pub on Friday evenings; much needed after long weeks! Also, I would like to say a big thank you to Margot and Delphine for their valuable friendship and huge support. I will always be grateful to them. At last, I would like to thank my family and friends for encouragement, but most of all my partner Richard for being there for me and giving me the strength to carry on.

ABSTRACT

Pancreatic cancer is an aggressive disease with poor prognosis and a high fatality rate. Gemcitabine, the standard first-line chemotherapy for advanced disease, has negligible effects, necessitating the development of new therapies. We previously demonstrated that deletion of the anti-apoptotic gene E1B19K (AdΔ19K) in a replication-selective adenoviral mutant, caused synergistically-enhanced cell-killing when combined with low-dose DNA-damaging drugs in pancreatic cancer xenograft models. To delineate the cellular pathways targeted by the combination treatment we employed AdΔ19K and gemcitabine or irinotecan, with the goal of identifying cellular factors that are essential for the synergistic cell-killing. We hypothesised that AdΔ19K and DNA-damaging drugs act synergistically to deregulate cell-cycle mechanisms.

Pancreatic cancer cell death induced by AdΔ19K and DNA-damaging drugs is apoptotic and time-dependent. AdΔ19K could not block DNA-damage responses (DDR) elicited by the drugs, despite virus-mediated degradation of the DDR factor Mre11. Mre11 siRNA-mediated knockdown augmented the synergistic cell death. Mitotic-index analysis in synchronised cells and immunofluorescence microscopy suggested that AdΔ19K promotes mitotic entry of gemcitabine-treated DNA-damaged cells. Moreover, AdΔ19K inhibited drug-induced accumulation of Claspin, a DDR protein whose degradation is required for checkpoint recovery. Treatment with AdΔ19K and gemcitabine accelerated Claspin degradation, and siRNA-mediated Claspin knockdown enhanced the synergistic cell death. Time-lapse microscopy in histoneH2B mCherry-expressing cells showed that AdΔ19K enhanced gemcitabine-induced mitotic catastrophe, characterised by prolonged mitosis, chromosome missegregation errors, cytokinesis failure and formation of multinucleated cells. Moreover, live-cell imaging revealed that the majority of cells treated with AdΔ19K and gemcitabine die before mitotic entry.

These findings suggest that E1B19K-deleted adenoviruses cannot prevent cell-cycle checkpoint responses elicited by DNA-damaging drugs, but enhance drug-induced cell death by downregulating DDR factors, such as Mre11 and Claspin. Additionally, the virus enhances mitotic catastrophe of DNA-damaged cells escaping cell-cycle checkpoints, eventually leading to increased apoptosis. Through these studies cellular pathways and factors involved in the synergistic cell killing were identified, that could be explored in the future to develop improved targeted therapies for pancreatic cancer.

CONTENTS

ABBREVIATIONS

3-MA: 3-methyladenine

53BP1: p53 binding protein

5-FU: 5-fluorouracil

9-1-1: RAD9–RAD1–HUS1

ABC: ATP-binding cassette

Ad: adenovirus

Ad-DBP: Ad DNA-binding protein

ADP: adenovirus death protein

AIF: apoptosis inducting factor

AP: apurinic/apyrimidinic

Apaf-1: activating factor 1

APC/C: anaphase promoting complex or cyclosome

APE: apurinic/apyrimidinic endonuclease

ATM: ataxia-telangiectasia mutated

ATR: ataxiatelangiectasia and RAD3 related

ATRIP: ATR-interacting protein

Bcl-2: B-cell lymphoma 2

BER: base-excision repair

BLM: bloom syndrome protein

BSA: bovine serum albumin

CAD: caspase activated DNase

CAK: CDK-activating kinase

CAR: coxsackie adenovirus receptor

CD: cytosine deaminase

CDA: cytidine deaminase

Cdc25: cell division cycle 25

CDK: cyclin-dependent kinase

CES: carboxylesterase

CETN2: centrin 2

cFLIP: FLICE-inhibitory protein

Chk1: checkpoint kinase 1

Chk2: checkpoint kinase 2

CK1γ1: Casein kinase 1 γ1

CKI: CDK inhibitor

CPT: camptothecin

CR: conserved region

CRM1: chromosome region of maintenance 1

CT: computed tomography

CtBP: carboxy-terminal binding protein

CtIP: CtBP-interacting protein

CTPsyn: CTP synthase

CUL4A: cullin 4A

CYP3A4: cytochrome P450 3A4

Daxx: death-domain-associated protein

dC: deoxycytidine

dCK: deoxycytidine kinase

dCTD: deoxycytidylate deaminase

DDK: Dbf4 dependent kinase

DDR: DNA-damage response

dFdC: 2'-deoxy-2',2'-difluorocytidine

dFdCDP: dFdC diphosphate

dFdCMP: dFdC monophosphate

dFdCTP: dFdC triphosphate

DISC: death-inducing signaling complex

DMSO: dimethyl sulfoxide

DNA-PK: DNA-dependent protein kinase

DNMTi: DNA methyltransferase inhibitor

dNTPs: deoxyribonucleotide triphosphates

DR: death receptor

DSBs: double-strand breaks

dsDNA: double-stranded DNA

DYRK: dual-specificity tyrosine (Y) phosphorylation-regulated kinase

ECM: extracellular matrix

EGF: epidermal growth factor

ER: endoplasmic reticulum

FADD: Fas-associated death domain

FANCD2: Fanconi-anaemia group D2

FANCM: Fanconi-anaemia group M protein

FBS: fetal bovine serum

FOLFIRI: folinic acid/5-FU and irinotecan

FOLFIRINOX: 5-FU, leucovorin, irinotecan, oxaliplatin

FOXK1/2: Forkhead Box K1 and K2

FSC: Forward Scatter

FVD: fixable viability dye

GADD45: Growth Arrest and DNA Damage 45

GAPs: GTPase-activating proteins

GDP: guanosine diphosphate

GEF: guanine exchange factor

Gem: gemcitabine

GG-NER: global genome nucleotide excision repair

GM-CSF: granulocyte-macrophage colony-stimulating factor

GTP: guanosine triphosphate

HAT: histone acetyltransferase

hCG: human chorionic gonadotropin

HDACs: histone deacetylases

hENT1: equilibrative nucleoside transporter 1

Hh: Hedgehog

HIF-1α: hypoxia-inducible factor 1α

HMGA1: high mobility group A1

HR: homologous recombination

HREs: hypoxia response elements

HSGAGs: heparin sulphate glycosoaminoglycans

Hsp90: heat shock protein 90kDa

HSV1-TK: herpes simplex virus type 1 thymidine kinase

hTERT: human telomerase reverse transcriptase

IAP: inhibitor of apoptosis

IFN: interferon

IL: interleukin

IPMN: mucinous neoplasms

IR: ionizing radiation

Iri: irinotecan

MAD2B: mitotic arrest deficient protein 2B

MAPK: mitogen activated protein kinase

MAPKK: MAPK kinase

MAPKKK: MAPKK kinase

MAST-L: microtubule-associated serine/threonine kinase-like

MCM2-7: minichromosome maintenance 2-7

MCN: mucinous cystic neoplasms

Mdc1: mediator of DNA damage checkpoint 1

Mdm: mouse double minute 2 homolog

MHC: major histocompatibility complex

MK2: MAPK-activated protein kinase 2

MKK: MAPK kinase

MLH: MutL homolog 1

MLP: major late promoter

MMP: matrix metalloproteinase

MMR: mismatch repair

Mps1: monopolar spindle 1

MRI: magnetic resonance imaging

MRN: Mre11-Rad50-Nbs1

MSH: MutS homolog

mTOR: mammalian target of rapamycin

MTS: 3-(4,5- dimethylthiazol-2-yl)-5-(3-carboxymethoxyphenyl)-2-(4-sulfophenyl)- 2H-tetrazolium

NDPK: nucleoside diphosphate kinase

Nek11: NIMA-related kinase 11

NER: nucleotide excision repair

NF: nuclear factor

NF-κB: nuclear factor κB

NHEJ: non-homologous end-joining

NIMA: never in mitosis gene A

NMPK: nucleoside monophosphate kinase

NSCLC: non-small-cell lung cancer

Nup: nucleoporins

OATP1B1: organic anion transporter polypeptide 1B1

P/CAF: p300/CBP-associated factor

P/S: penicillin and streptomycin

PanINs: pancreatic intraepithelial neoplasias

PARP1: poly(ADP-ribose)polymerase 1

PBS: phosphate buffered saline

PCNA: proliferating cell nuclear antigen

PDAC: pancreatic cancer ductal adenocarcinoma

phH3: phospho-histone H3

PI: propidium iodide

PIDD: p53-induced death domain

PIKKs: phosphoinositide 3-kinase related kinases

PKA: protein kinase A

Plk: Polo-like kinase

PML: promyelytic leukaemia

PMS: phenazine methosulfate

PNKP: polynucleotide kinase phosphatase

Pol: polymerase

Pot1: protection of telomeres 1

PP2A: protein phosphatase 2A

ppc: particles per cell

pre-RC: pre-replicative complex

PS: phosphatidylserine

PSA: prostate-specific antigen

PSCs: pancreatic stellate cells

RAD23B: RAD23 homologue B

RanBP1/2: Ran-binding proteins 1/2

Rb: retinoblastoma

RF: replication factor

RFC: RAD17–replication factor C

RGD: arginine-glycine-aspartate

RNR: ribonucleotide reductase

ROC1: cullin 4A regulator of cullins 1

ROS: reactive oxygen species

RPA: replication protein A

SAC: spindle assembly checkpoint

SCF: Skp, Cullin, F-box

SDS: sodium dodecyl sulfate

SDS-PAGE: SDS Polyacrylamide Gel Electrophoresis

shRNA: small hairpin RNA

siRNA: small interference RNA

SN-38G: SN-38 glucuronide

SPOC-1: survival-time associated PHD protein in ovarian cancer 1/PHF13

SSBs: single strand breaks

SSC: Side Scatter

ssDNA: single-stranded DNA

SWI/SNF: SWItch/Sucrose NonFermentable

TBP: TATA binding protein

TC-NER: transcription-coupled nucleotide excision repair

TFIIH: transcription initiation factor IIH

TGF: transforming growth factor

Tim: Timeless

TMS1: target of methylation induced silencing 1

TMZ: temozolomide

TNF: tumour necrosis factor

TopBP1: topoisomerase-binding protein-1

TopI: topoisomerase I

TPX2: Targeting protein for Xklp2

TRF2: Telomere repeat binding factor 2

TRRAP: Transformation/transcription domain-associated protein

TS: thymidylate synthase

UDG: uracil DNA glycosylase

UGT1A1: Uridine-diphosphate glucuronosyltransferase 1A1

USP7: ubiquitin-specific-processing protease 7

UV: ultraviolet

UV-DDB: UV DNA damage-binding protein

UVSSA: UV-stimulated scaffold protein A

VA: virus-associated

VEFF: vascular endothelial growth factor

vp: viral particle

Wip1: wild-type p53 inducible protein 1

XPA: xeroderma pigmentosum group A

XPC: xeroderma pigmentosum complementation group C

XRCC1: X-ray cross complementing protein-1

LIST OF FIGURES

LIST OF TABLES

CHAPTER 1: INTRODUCTION

1.1. Pancreatic cancer

1.1.1. Pancreatic cancer statistics

Pancreatic cancer is the 10th most commonly diagnosed cancer in United Kingdom, with approximately 8,800 new cases diagnosed in 2011 (Cancer Research UK). In United States 46,420 new cases of pancreatic cancer are estimated for 2014 (Siegel et al., 2014). The median age of pancreatic cancer development is 71 years and the risk of developing the disease is significantly increased in individuals older than 55 years of age (Muniraj et al., 2013; Yadav and Lowenfels, 2013). Other risk factors include smoking, alcohol, obesity, family history, non-O blood groups and pancreatitis, with the latter being strongly associated with pancreatic cancer (Muniraj et al., 2013; Yadav and Lowenfels, 2013). Although inherited predisposition to pancreatic cancer exists, 95% of pancreatic cancers are sporadic (Muniraj et al., 2013; Reznik et al., 2014).

In spite of its relatively low occurrence, pancreatic cancer is among the leading causes of cancer deaths worldwide, and one of the few cancers for which there was no substantial improvement in survival rates over the past three decades (Hariharan et al., 2008; Siegel et al., 2014; Siegel et al., 2012). The 5-year survival rate remains less than 6% (Office for National Statistics, 2013; Siegel et al., 2014). Incidence and mortality rates are similar between men and women (Siegel et al., 2014).

1.1.2. Pancreatic cancer histopathology

The exocrine tissue of the pancreas consists of ductal and acinar cells; the latter synthesize and secrete digestive enzymes into the pancreatic ducts which in turn dilute, pH-optimize and transmit the pancreatic secretions into the small intestine (Cleveland et al., 2012). The highly aggressive pancreatic cancer ductal adenocarcinoma (PDAC) accounts for approximately 90% of pancreatic cancer cases (Muniraj et al., 2013). PDAC is a heterogeneous disease and largely arises from pancreatic intraepithelial neoplasias (PanINs), with development into invasive disease driven by acquisition of various genetic alterations (Figure 1) (Muniraj et al., 2013; Reznik et al., 2014). Yet other cystic lesions, namely intraductal papillary mucinous neoplasms (IPMN) and mucinous cystic neoplasms (MCN), can develop into PDAC (Bailey et al., 2014). Although the name and histological features of PDAC imply it arises from the duct cells of the pancreas, there is a strong debate over the cell of origin of pancreatic neoplasms, with evidence for both ductal and acinar cell origin (Bailey et al., 2014).

PDAC is associated with a strong desmoplastic reaction, that is a dense stroma, deposited by activated fibroblasts, called pancreatic stellate cells (PSCs), which are now considered to play a critical role in tumour progression (Apte et al., 2012; Rucki and Zheng, 2014; Wilson et al., 2014). A reciprocal relationship exists between PSCs and cancer cells, which has been shown to promote tumour growth and metastasis (Apte et al., 2012; Apte and Wilson, 2012; Apte et al., 2013). Importantly, stellate cells have been identified both in early-stage PanINs and distant metastatic sites and were also shown to contribute to the immunosuppressive environment that characterizes PDAC (Bayne et al., 2012; Ene-Obong et al., 2013; Wilson et al., 2014; Xu et al., 2010b). As with many other tumours, the microenvironment of ductal adenocarcinoma is infiltrated by various immune cells, the majority of which possess immunosuppressive functions that limit the cytotoxicity of effector T cells, thus contributing to cancer progression (Clark et al., 2007; Hamada et al., 2014). Given the importance of the tumour microenvironment in shaping PDAC development, efforts are currently being made to therapeutically target the pancreatic stroma compartment. Research has demonstrated that dense stroma is associated with

poor prognosis (Erkan et al., 2008) and its targeting was shown to improve the delivery of chemotherapeutic agents (Neesse et al., 2013).

1.1.3. Genetic determinants and molecular biology of pancreatic cancer

Genetic analysis of pancreatic tumours demonstrated that the great majority of genetic alterations that occur in PDAC are somatic mutations and in particular missense mutations, rather than gene amplifications or deletions (Biankin et al., 2012; Jones et al., 2008). Factors involved in numerous signalling pathways, such as DNA-damaging control, apoptosis, invasion, adhesion and even axon guidance have been found to be genetically altered in pancreatic cancers (Biankin et al., 2012; Jones et al., 2008). The most critical factors and pathways are discussed below and the common genetic mutations occurring in PDAC are summarised in Table 1.

Development of pancreatic precursor lesions into PDAC is driven by genetic alterations (Figure 1). One of the earliest mutations observed is constitutive activation of the *KRAS* oncogene, frequently followed by mutational inactivation of the tumour-suppressors *CDKN2A*, *TP53* and *SMAD4* (Figure 1) (Hezel et al., 2006; Reznik et al., 2014; Schneider and Schmid, 2003). Constitutive activation of KRAS occurs in 90% of early-stage PanINs (Kanda et al., 2012) and represents the most frequent (~95%) genetic alteration in PDAC (Biankin et al., 2012; Jones et al., 2008). The mutation is predominantly a glycine (G) to aspartic acid (D) substitution in codon 12, but other activating mutations, for example G13D and G12C, can be found (Bryant et al., 2014; Kanda et al., 2012). The substitution interferes with the binding of Ras GTPase-activating proteins (GAPs), which stimulate the GTPase activity of Ras resulting in hydrolysis of guanosine triphosphate (GTP) to guanosine diphosphate (GDP); oncogenic mutations lead to a constitutive GTP-bound state, which is the active Ras form (Bryant et al., 2014). In pancreatic cancer the effector signalling pathways downstream of oncogenic KRAS are the RAF/MEK/ERK, PI3K/AKT and Ral guanine exchange factor (RalGEF), all promoting cell survival and proliferation (Eser et al., 2014). Oncogenic KRAS has been shown to drive pancreatic cancer initiation and contribute to disease progression and

metastasis (Bryant et al., 2014; Eser et al., 2014). Overexpression of the human epidermal growth factor 2 (EGFR2 or HER2) has also been observed in early stage PanINs and gene amplification has been reported in 10-60% of PDAC patients (Figure 1) (Reznik et al., 2014). EGFR signals through various pathways, including Ras and PI3K, promoting cell growth and proliferation (McCleary-Wheeler et al., 2012).

The progression from early- to intermediate-grade PanINs is characterised by inactivation of the growth suppressor and cell-cycle regulator $p16^{INK4A}$, often occurring through gene deletion (Figure 1) (Hezel et al., 2006; Schneider and Schmid, 2003; Schutte et al., 1997). CDKN2A/$p16^{INK4A}$ inactivation is observed in more than 80% of pancreatic cancers and leads to abrogation of the G1/S checkpoint and loss of growth control (Schneider and Schmid, 2003; Schutte et al., 1997).

TP53 and SMAD4 mutations are not observed until the advanced stages of PanINs (Figure 1) (Reznik et al., 2014). p53 is inactivated in more than 50% of pancreatic cancers, predominantly via missense mutations in its DNA-binding region, resulting in loss of p53 transcriptional functions, which include induction of pro-apoptotic genes and genes that block cell-cycle progression (Hezel et al., 2006; Rozenblum et al., 1997). Inactivation of p53 therefore impacts on regulation of cell growth and proliferation, apoptosis and genomic stability (Hezel et al., 2006). DPC4/SMAD4, a downstream effector of transforming growth factor β (TGFβ), is also inactivated in more than 50% of PDAC cases and its inactivation correlates with poor prognosis (Blackford et al., 2009; Hezel et al., 2006). Loss of SMAD4 function, either through deletion or mutation, impairs the growth-inhibitory effects of TGFβ signalling pathway, but also impacts on tumour angiogenesis independently of TGFβ (Hezel et al., 2006; Reznik et al., 2014). Mutations in the tumour suppressor gene BRCA2 have also been detected in advanced PanINs, albeit to a much lower frequency than TP53 and SMAD4 (Figure 1) (Hruban et al., 2000). BRCA2 is mutated in 7% of PDAC cases, leading to defective DNA repair mechanisms and genomic instability (Koorstra et al., 2008; Reznik et al., 2014).

Besides these high-frequency mutations, other more rare genetic alterations have been detected in PDAC. Such low-frequency (<15%) mutations occur in the DNA mismatch repair genes MutL homolog 1 (MLH1), MutS homolog 2 (MSH2), MSH6, the BRAF oncogene, the cell survival kinase AKT2 and the stress-response MAPK kinase 4 (MKK4), amongst others (Koorstra et al., 2008; Reznik et al., 2014; Schneider and Schmid, 2003).

Table 1: Genetic alterations associated with PDAC

Gene Name	Gene Type	Frequency of alteration	Reference
KRAS	Oncogene	90-95%	(Reznik et al., 2014)
CDKN2A	Tumour suppressor	80-95%	(Reznik et al., 2014)
TP53	Tumour suppressor	50-85%	(Reznik et al., 2014)
SMAD4/DPC4	Tumour suppressor	50-60%	(Reznik et al., 2014)
HER2	Oncogene	10-60%	(Reznik et al., 2014)
AKT2	Oncogene	10-15%	(Koorstra et al., 2008)
BRCA2	Tumour suppressor	7%	(Reznik et al., 2014)
BRAF	Oncogene	5%	(Ottenhof et al., 2011)
MKK4	Candidate tumour suppressor	5%	(Muniraj et al., 2013)
MLH1, MSH2	Genome-maintenance	4%	(Reznik et al., 2014)

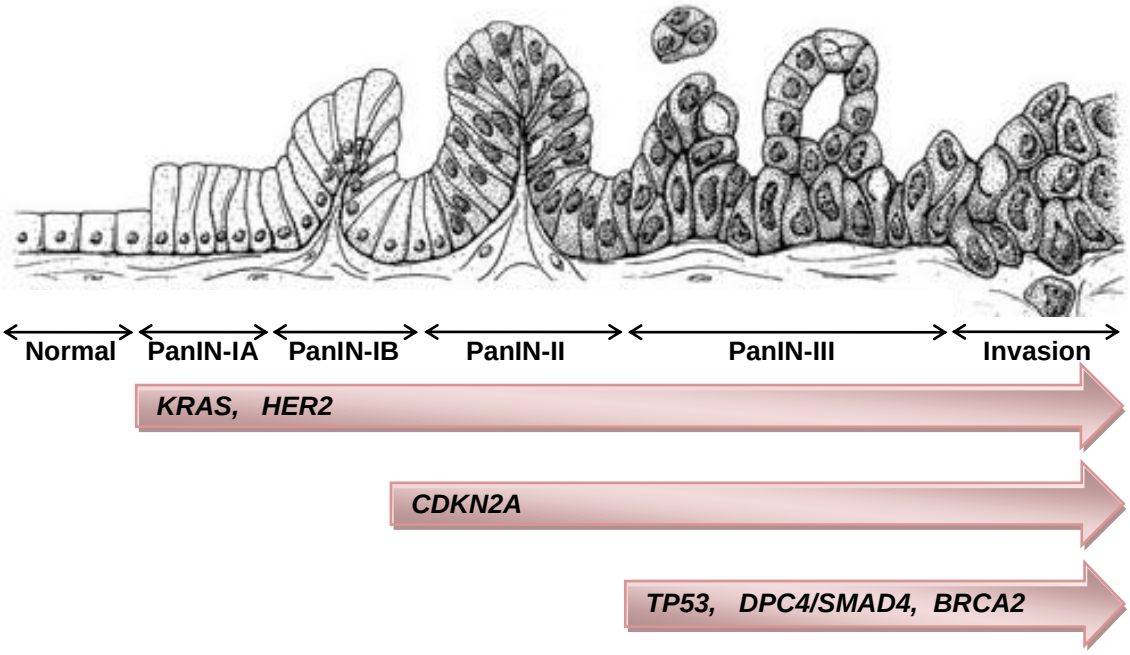

Figure 1: Progression model for pancreatic cancer. Histologically normal pancreatic ductal epithelium develops precursor lesions known as pancreatic

intraepithelial neoplasias (PanINs). The early-stage PanINs are flat (PanIN-IA) or papillary (PanIN-IB) and are characterised by acquisition of activating *KRAS* and *HER2* mutations. Development of nuclear atypia with micropapillary characteristics signifies progression to the intermediate-stage PanIN (PanIN-II), which is concurrent with loss of the tumour suppressor gene *CDKN2A*. Loss of cell polarity, increased cell proliferation and inactivation of the tumour suppressor genes TP53, DPC4/SMAD4 and BRCA2 give rise to the advanced stage PanIN-III (carcinoma in situ). PanIN-III then develops into invasive adenocarcinoma. References (Koorstra et al., 2008; Maitra et al., 2003).

An emerging important player in pancreatic cancer progression is the Hedgehog (Hh) signalling pathway, which controls development patterning, cell proliferation and adult tissue homeostasis and repair (Briscoe and Therond, 2013). In a comprehensive genetic analysis of 24 pancreatic cancers, Jones et al. identified 19 genes of the Hedgehog pathway that were mutated and all tumours examined contained at least one mutation in the Hedgehog pathway (Jones et al., 2008). Experimental evidence suggests that the Hedgehog pathway plays a role in pancreatic carcinogenesis, apoptosis resistance, pancreatic cancer desmoplasia and tumour growth (Bailey et al., 2008; Kelleher, 2011; McCleary-Wheeler et al., 2012), making this pathway an attractive therapeutic target.

Another signalling pathway aberrantly activated in pancreatic cancer is the Notch pathway. The Notch signalling pathway is involved in normal pancreas development, where it regulates cell fate decisions and maintains stem cell populations (Avila and Kissil, 2013). Numerous genes involved in the Notch pathway have been found to be mutated in PDAC cases (Jones et al., 2008). The role of the pathway in pancreatic cancer however remains controversial, as evidence exists for both a role in inhibition of PanIN development and tumour progression (Avila and Kissil, 2013).

A role in PDAC development has also been suggested for the nuclear factor κB (NF-κB) pathway. RelA, one of the subunits of NF-κB, was reported to be aberrantly activated in pancreatic cancers (Wang et al., 1999), while other subunits showed increased expression (Chandler et al., 2004). This signalling pathway has been implicated in pancreatic cancer cell proliferation, apoptotic resistance as well as metastasis (McCleary-Wheeler et al., 2012).

As with many other cancers, a characteristic feature of PDAC is evasion of apoptotic pathways (Fulda, 2009). Apoptotic cells are absent from early- and intermediate-stage PanINs, suggesting anti-apoptotic mechanisms might evolve early in PDAC development (Luttges et al., 2003). Overexpression of inhibitors of apoptosis, such as cIAP2 and Survivin, has been reported in early-stage PanINs increasing through to advanced-stage PanINs and PDAC (Bhanot et al., 2006; Esposito et al., 2007). Moreover, deregulation of death-receptor signalling and overexpression of anti-apoptotic members of the Bcl-2 family are documented contributors to apoptotic resistance in PDAC (Fulda, 2009; Hamacher et al., 2008).

1.1.4. Treatment options

Treatment of pancreatic cancer remains challenging. Although surgery is potentially curative, less than 20% of patients are diagnosed with operable disease, and the rate of relapse following resection is high (Loos et al., 2008; Moss and Lee, 2010). Symptoms often do not occur until the carcinoma has locally advanced or metastasised, which contributes to the low frequency of patients qualifying for surgery (Muniraj et al., 2013). At presentation, imaging techniques, predominantly computed tomography (CT) and magnetic resonance imaging (MRI), are used for diagnosis and staging of pancreatic tumours to define surgical resectability and spread of the tumour (Al-Hawary et al., 2013).

For those patients that surgery is possible, surgical resection is followed by adjuvant chemotherapy or chemoradiotherapy (Liao et al., 2013). For borderline-resectable pancreatic cancers, neoadjuvant chemotherapy or chemoradiotherapy aims to improve surgical resectability of the tumour (He et al., 2014; Polistina et al., 2014). Locally-advanced (unresectable) pancreatic cancers, which represent 25-35% of PDAC cases, are treated with chemotherapy (He et al., 2014; Muniraj et al., 2013), but mainly metastasize within a year (Muniraj et al., 2013). Patients with metastatic disease have a median survival of 6 months and are offered systemic chemotherapy aiming at palliating the symptoms and improving survival (Labianca et al., 2012; Muniraj

et al., 2013). The lack of curative treatment options for advanced stages, necessitates the exploitation of new therapeutic avenues.

Since 1997 the standard chemotherapeutic agent of choice has been the cytidine analogue gemcitabine (Figure 2 and 3) (Mohammed et al., 2014). The mechanisms of action of gemcitabine are discussed in section 1.1.5. Gemcitabine monotherapy remains the only approved treatment option for patients with metastatic pancreatic cancer and poor performance status (Ghosn et al., 2014). Other chemotherapeutic agents, such as the topoisomerase-I inhibitor irinotecan, the uracil analogue 5-fluorouracil (5-FU) and the alkylating agent cisplatin, demonstrated anti-tumour efficacy but have not shown any significant improvement in overall patient survival when evaluated in clinical trials as single agents or in combination with gemcitabine (Ghosn et al., 2014). However, some meta-analyses suggested a survival benefit in patients receiving a combination of gemcitabine with fluoropyrimidines, such as 5-FU, or platinum-derivatives, such as cisplatin (Heinemann et al., 2007; Sultana et al., 2007).

FOLFIRINOX (5-FU, leucovorin, irinotecan, oxaliplatin) has so far been the only gemcitabine-free chemotherapeutic regimen to result in better survival outcomes than gemcitabine in a first-line therapy setting, but its significantly higher toxicity currently limits its use in patients with good performance status (Conroy et al., 2011; Mohammed et al., 2014). Another treatment option for patients with metastatic disease, is the combination of gemcitabine with nab-paclitaxel (a nanoparticle albumin-bound paclitaxel), which has recently demonstrated some positive results over gemcitabine monotherapy (Al-Hajeili et al., 2014; Von Hoff et al., 2013). Despite resulting in less adverse effects than FOLFIRINOX, the gemcitabine-nab-paclitaxel regimen is still less tolerable than gemcitabine monotherapy, thereby it is preferentially used in patients with good performance status (Ghosn et al., 2014). Irinotecan monotherapy and irinotecan-based therapies, such as the folinic acid/5-FU and irinotecan (FOLFIRI) regimen and irinotecan with oxiliplatin, show activity and some clinical benefit as second-line treatments, that is after failure to respond to gemcitabine and gemcitabine-based regimens (Heinemann et al., 2012; Neuzillet et al., 2012; Shi et al., 2012). A nanoliposomal-encapsulated

irinotecan (PEP02 or MM-398) has shown encouraging results as a single-agent or in combination with 5-FU/leucovorin in gemcitabine-refractory pancreatic cancers (Ko et al., 2013) and it is currently in a Phase III trial (https://clinicaltrials.gov/show/NCT01494506).

Clinical trials with targeted therapies have overall demonstrated no positive results for patients with advanced pancreatic cancer (Michl and Gress, 2013). These included antibodies against the vascular endothelial growth factor (VEGF), matrix metalloproteinases (MMPs) inhibitors and tyrosine-kinase inhibitors. The only exception has been the EGF inhibitor erlotinib, which modestly increased patient survival when combined with gemcitabine, leading to its approval as a treatment for metastatic pancreatic cancers (Moore et al., 2007). Given the importance of aberrant signalling in pancreatic cancer, novel targeted therapies are currently being evaluated (Kleger et al., 2014).

1.1.5. DNA-damaging drugs for pancreatic cancer: Mechanisms of action

Gemcitabine (Gemzar®)

Gemcitabine (2'-deoxy-2',2'-difluorocytidine; dFdC) is a deoxycytidine analogue (Figure 2) that can be incorporated into DNA and prevent completion of DNA-strand synthesis (Candelaria et al., 2010). Gemcitabine uptake in the cell is mediated by nucleoside transporters and in particular the human equilibrative nucleoside transporter 1 (hENT1) (Candelaria et al., 2010). High expression of hENT1 in pancreatic cancer tissue has been associated with significantly increased survival in patients treated with gemcitabine (Giovannetti et al., 2006). Inside the cell, gemcitabine (dFdC) is metabolised to its active forms, dFdC diphosphate (dFdCDP) and triphosphate (dFdCTP), by a series of phosphorylation events as depicted in Figure 3. The rate-limiting step in dFdC metabolism is its phosphorylation to dFdC monophosphate (dFdCMP), catalysed by deoxycytidine kinase (dCK), whose expression and activity has also been correlated to clinical outcome (Candelaria et al., 2010). dFdC and dFdCMP can be deaminated to their less-active forms dFdU and dFdUMP, by

cytidine deaminase (CDA) and deoxycytidylate deaminase (dCTD), respectively (Figure 3) (Heinemann et al., 1992).

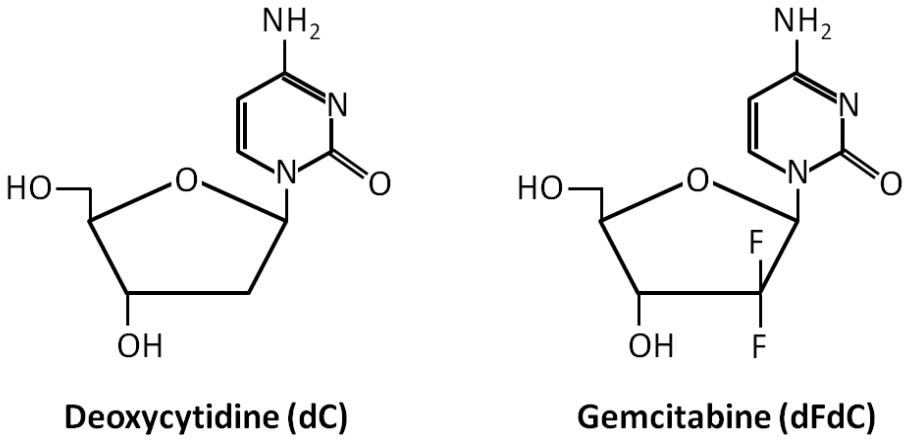

Figure 2: Structure of Deoxycytidine and Gemcitabine. The chemical structure of Gemcitabine (2'-deoxy-2',2'-difluorocytidine; dFdC) differs from deoxycytidine (dC) through replacement of hydrogen atoms with two fluorine atoms at the 2-position of the deoxyribose sugar (Brown et al., 2014; Hertel et al., 1988).

Gemcitabine has several mechanisms of action (Figure 3). First, as a cytidine analogue, dFdCTP is incorporated into DNA, and following the addition of one more nucleotide, DNA polymerization is blocked, leading to a potent inhibition of DNA synthesis (Gandhi et al., 1996; Huang et al., 1991). This process is referred to as "masked chain termination", since the masking of dFdCTP by the terminal deoxynucleotide incorporated, prevents detection and excision of dFdCTP by DNA repair enzymes (Gandhi et al., 1996; Huang et al., 1991). It is worth mentioning that incorporation of gemcitabine into RNA, albeit to a lesser extent than DNA, has also been reported and leads to partial inhibition of RNA synthesis (Ruiz van Haperen et al., 1993; Veltkamp et al., 2008).

A third mechanism of action is self-potentiation, which is achieved through inhibition of several enzymes involved in nucleotide metabolism and results in increased intracellular gemcitabine concentrations and favourable gemcitabine incorporation into DNA (Figure 3). dFdCDP binds and efficiently inhibits ribonucleotide reductase (RNR), thereby blocking production of deoxyribonucleotides required for DNA synthesis and repair (Cerqueira et al.,

2007; Heinemann et al., 1990). This subsequently depletes the cellular pool of deoxyribonucleotide triphosphates (dNTPs), particularly dCTP (Heinemann et al., 1990), leading to decreased feedback inhibition of dCK by dCTP (Sarup et al., 1989) and consequently increased dFdCMP formation (van der Wilt et al., 2000). Depleted dCMP pool also leads to decreased activity of the dCMP deaminase dCTD, thereby reducing deamination and inactivation of dFdCMP by this enzyme (Heinemann et al., 1992). Moreover, it has been reported that high concentrations of dFdCTP inhibit dCTD and CTP synthase (Heinemann et al., 1992; Xu and Plunkett, 1992). The deaminated catabolites of gemcitabine, dFdU and its phosphorylated forms, are often considered inactive. However, dFdUTP was reported to be incorporated into DNA and RNA and dFdU has been shown to be cytotoxic (Veltkamp et al., 2008). In addition, dFdUMP has been shown to inhibit thymidylate synthase (TS), which converts dUMP to dTMP, by yet unknown mechanisms (Bergman et al., 2000; Bergman et al., 2002).

Another mechanism of action of gemcitabine is poisoning of topoisomerase I, an enzyme that cleaves one stand of duplex DNA, relaxes and re-ligates DNA, in order to relieve tension created during replication, transcription, chromosome condensation and segregation (Leppard and Champoux, 2005). Gemcitabine incorporation into DNA was shown to stabilize topoisomerase I cleavage complexes (topoisomerase I-DNA intermediates), due to conformational and electrostatic effects at the gemcitabine-incorporated DNA position (Pourquier et al., 2002). Stabilized topoisomerase I cleavage complexes can interfere with progressing DNA replication and transcription forks leading to the formation of DNA-strand breaks (Pourquier et al., 2002; Pourquier and Pommier, 2001).

As it will be discussed in detail later (section 1.2.10.), the actions of gemcitabine activate a DNA-damage response that results in a cell-cycle arrest and induction of apoptosis. Gemcitabine incorporation into DNA is essential for induction of apoptosis (Huang and Plunkett, 1995). However, the several different inhibitory effects of gemcitabine on DNA synthesis, coupled with self-potentiation mechanisms and topoisomerase I poisoning, are likely to contribute to the potent cytotoxic activity of this unique nucleoside analogue.

Resistance to gemcitabine, which represents a common clinical scenario, can be intrinsic or acquired following prolong treatment. Despite that several factors have been associated with decreased sensitivity to gemcitabine, the mechanisms of gemcitabine resistance remain poorly understood. Altered expression and enzymatic activities of proteins involved in gemcitabine metabolism were the first to be implicated in gemcitabine resistance (Andersson et al., 2009; Bergman et al., 2002). Among these, well-defined mechanisms include the reduced expression of the hENT1 nucleoside transporter (Farrell et al., 2009; Giovannetti et al., 2006) and the activating kinase dCK (Nakano et al., 2007; Ohhashi et al., 2008), as well as increased expression of dFdCDP's target RNR (Bergman et al., 2000; Nakahira et al., 2007; Nakano et al., 2007). Other proteins implicated in gemcitabine resistance include the transcription factors NF-κB and high mobility group A1 (HMGA1), whose overexpression promotes chemoresistance through activation of survival pathways (de Sousa Cavalcante and Monteiro, 2014; Elnaggar et al., 2012).

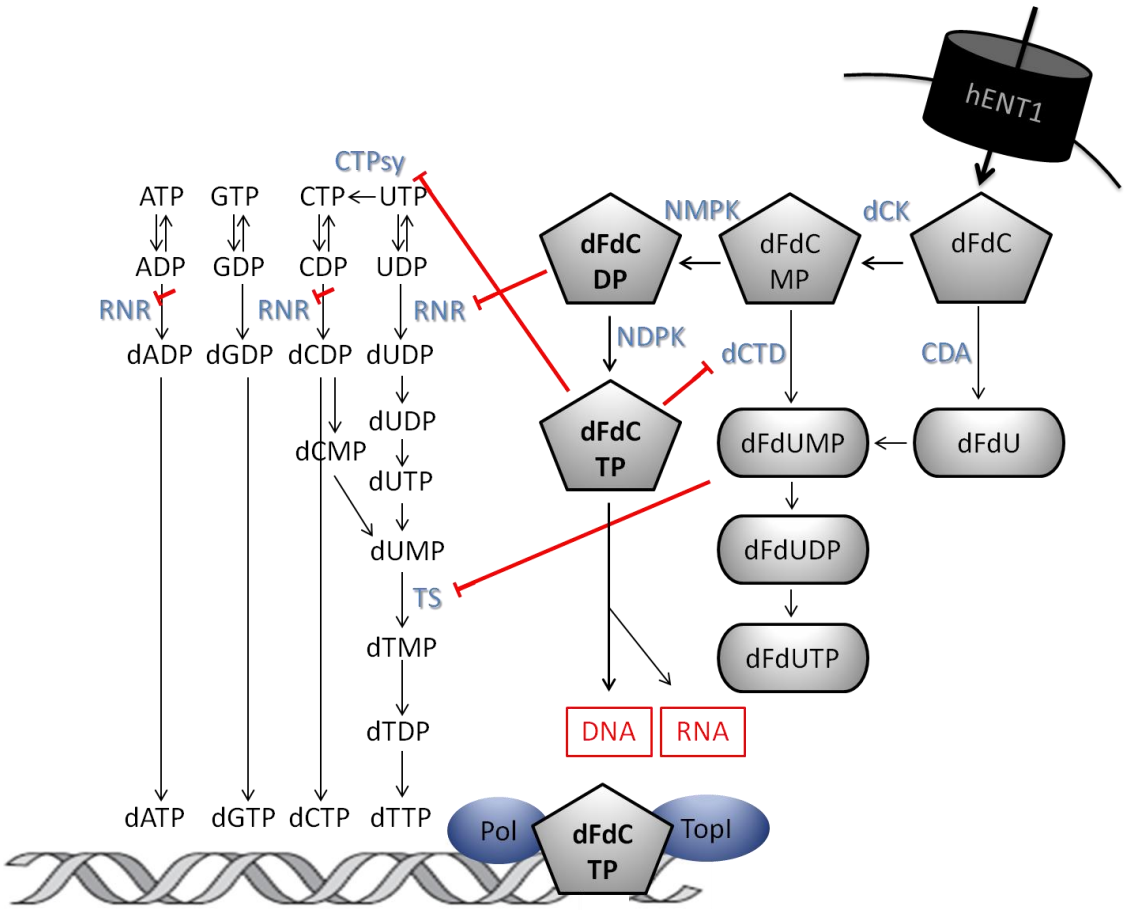

Figure 3: Metabolism and mechanisms of action of gemcitabine. Gemcitabine (dFdC) enters cells via the human equilibrative nucleoside transporter 1 (hENT1). Deoxycytidine kinase (dCK) catalyzes phosphorylation of dFdC to dFdC monophosphate (dFdCMP), which is further phosphorylated to dFdC diphosphate (dFdCDP) by nucleoside monophosphate kinase (NMPK). dFdCDP is in turn phosphorylated to the triphosphate form dFdTMP by nucleoside diphosphate kinase (NDPK). dFdC and dFdCMP can be converted to their less-active metabolites dFdU and dFdUMP through deamination catalysed by cytidine deaminase (CDA) and deoxycytidylate deaminase (dCTD), respectively. dFdUMP can be converted to dFdUDP and subsequently to dFdUTP. Gemcitabine's main mechanism of action is the incorporation of dFdCTP into DNA and to a lesser extend into RNA. After dFdCTP is incorporated into DNA it allows one more nucleotide to be incorporated and then DNA synthesis by DNA polymerase (Pol) is blocked. The terminal nucleotide prevents recognition and removal of dFdCTP by exonucleases (masked chain termination). dFdCTP stabilizes topoisomerase I (TopI) cleavage complexes, which can interfere with progressing DNA replication and transcription forks leading to the formation of DNA-strand breaks. Another mechanism of action is self potentiation (see text for details), achieved through inhibition of ribonucleotide reductase (RNR) by dFdCDP, CTP synthase (CTPsy) by dFdCTP and thymidylate synthase (TS) by dFdUMP, leading to depletion of dNTPs pool and favourable DNA incorporation of dFdCTP. In addition, dFdCTP inhibits dCTD, decreasing inactivation of gemcitabine. References (Candelaria et al., 2010; de Sousa Cavalcante and Monteiro, 2014; Mini et al., 2006; Veltkamp et al., 2008).

Irinotecan (Camptosar™ or Campto®)

Irinotecan (CPT-11) is an analogue of the topoisomerase I inhibitor camptothecin (CPT) and was developed to improve the water solubility of CPT and decrease its side-effects (Mathijssen et al., 2002). Inside the cell, irinotecan (7-ethyl-10-[4-(1-piperidino)-1-piperidino]carbonyloxycamptothecin) is hydrolysed to its active form SN-38 (7-ethyl-10-hydroxycamptothecin) by carboxylesterases (CES), predominantly CES1 and CES2 (Figure 4) (Smith et al., 2006). Irinotecan and SN-38 exist in an anionic carboxylate (open ring) and a non-ionic lactone (closed ring) form and interconversion between these two forms is dependent on pH, with lactone predominating at basic pH (Kobayashi et al., 1999; Mathijssen et al., 2002; Smith et al., 2006). Lactone is the pharmacologically active form of irinotecan and is indispensable for topoisomerase I inhibition and drug cytotoxicity (Ramesh et al., 2010; Smith et al., 2006). Both irinotecan and SN-38 can enter cells through passive diffusion, when in the lactone form, or active transport (de Jong et al., 2006). The organic anion transporter polypeptide 1B1 (OATP1B1 or SLCO1B1) has been implicated in the influx of SN-38 (Nozawa et al., 2005; Yamamoto et al., 2001). Uridine-diphosphate glucuronosyltransferase 1A1 (UGT1A1) further metabolises SN-38 to SN-38 glucuronide (SN-38G) (Figure 4), an inactive product that is excreted through the bile (Gagne et al., 2002; Iyer et al., 1998). Irinotecan, SN-38 and SN-38G and transported out of the cell via members of the ATP-binding cassette (ABC) superfamily of transporters (Figure 4) (Smith et al., 2006). Irinotecan can also be metabolised to its less-active products 7-ethyl-10-[4-(1-piperidino)-1-piperidino] (APC) and 7-ethyl-10-(4-amino-1-piperidino) (NPC) through the action of the cytochrome P450 3A4 (CYP3A4) (Figure 4) (Smith et al., 2006). However, NPC was shown to be converted to SN-38 by CES enzymes (Dodds et al., 1998; Rivory et al., 1996).

SN-38 acts by inhibiting topoisomerase I, which as mentioned above is responsible for relieving tension in DNA created during replication, transcription, chromosome condensation and segregation (Leppard and Champoux, 2005). CPT and its analogues inhibit topoisomerase I by stabilizing topoisomerase I DNA cleavage complexes leading to inhibition of the re-ligation reaction (Hsiang et al., 1985; Hsiang and Liu, 1988; Svejstrup et al., 1991). The stabilized

cleavage complexes prevent DNA replication forks to proceed, generating double-strand DNA breaks, which subsequently activate a DNA-damage response that halts the cell-cycle and induces apoptosis (Hsiang et al., 1989; Mathijssen et al., 2002).

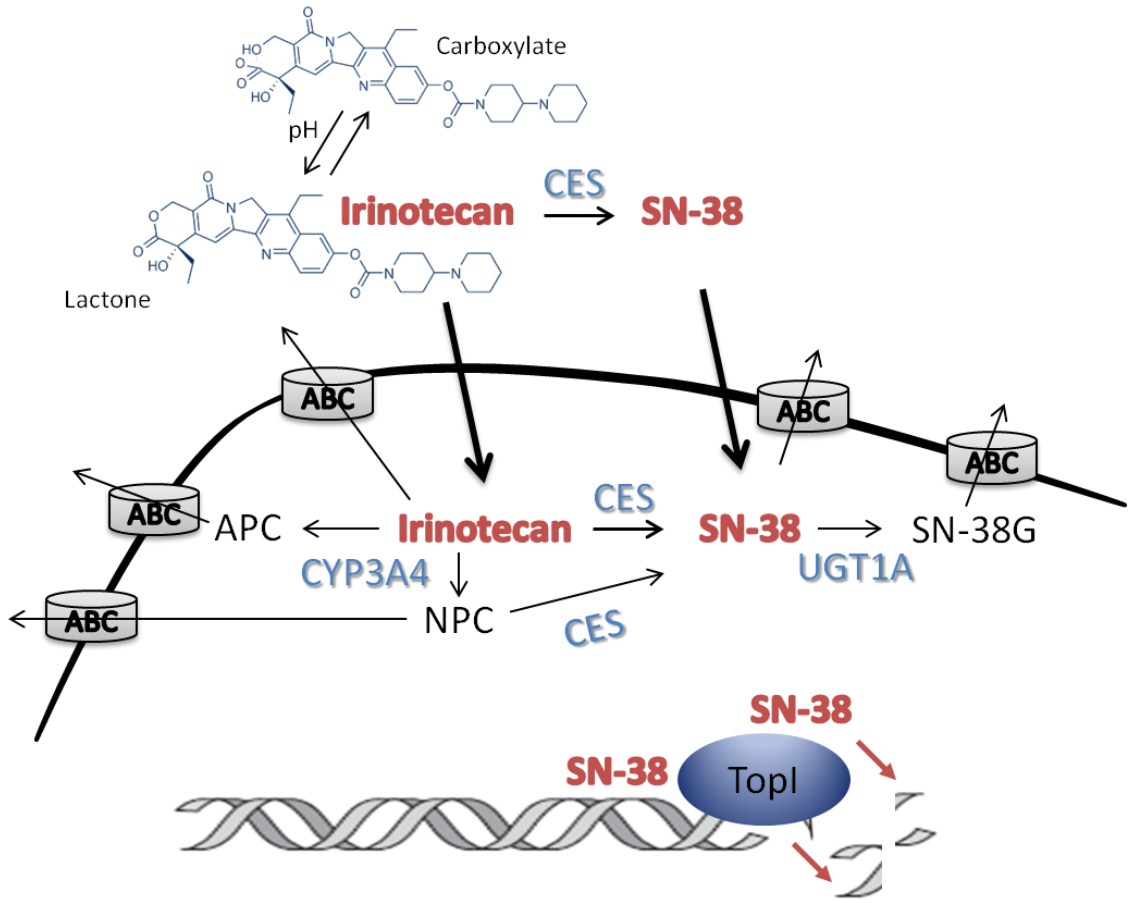

Figure 4: Irinotecan mechanism of action. Irinotecan (CPT-11) is converted to its active metabolite SN-38, by carboxylesterases (CES). The pharmacologically active lactone form of irinotecan and SN-38 can be diffused into the cytoplasm. Once inside the cell, SN-38 acts by stabilizing topoisomerase I cleavage complexes, which prevents DNA replication forks to proceed and leads to their collapse and subsequent formation of double-strand breaks. SN-38 can be metabolised to an inactive form, SN-38G, through the action of Uridine-diphosphate glucuronosyltransferase 1A1 (UGT1A1). In addition, cytochrome P450 3A4 (CYP3A4) inactivates irinotecan by metabolising it to 7-ethyl-10-[4-(1-piperidino)-1-piperidino] (APC) and 7-ethyl-10-(4-amino-1-piperidino) (NPC). NPC however can be converted to SN-38 by CES enzymes. Irinotecan and its metabolites are transported out of the cell via members of the ATP-binding cassette (ABC) superfamily of transporters. References (de Jong et al., 2006; Mathijssen et al., 2002; Smith et al., 2006).

1.2. DNA damage and repair responses

1.2.1. The Cell Cycle

An overview of cell-cycle stages

The cell cycle represents a series of tightly-controlled events that prepare the cell for division into two daughter cells (Morgan, 2007). The mammalian cell cycle, which is completed within approximately 24h, consists of three gap (G) phases (G0, G1, G2), a synthesis (S) phase and mitosis (M) (Figure 5) (Humphrey and Brooks, 2004). The gap and synthesis phases are collectively called interphase. Progression through the cell-cycle phases is irreversible and is therefore strictly regulated by checkpoints, which halt progression if requirements are not met (Humphrey and Brooks, 2004). The key orchestrators of phase transitions are the cyclin-dependent kinase (CDK)-Cyclin complexes, in which Cyclins are the activator subunits and CDKs are the catalytic subunits (Figure 5) (Fisher, 2012; Gallorini et al., 2012). CDKs, which are themselves tightly regulated at several levels, are activated by the CDK-activating kinase (CAK) and inactivated by two families of CDK inhibitors (CKIs); the INK4 and Cip/Kip (Besson et al., 2008; Canepa et al., 2007).

The G0 phase represents a resting or quiescent state, whereby a cell is maintained in the absence of growth signals (Cooper, 2003). Growth signals, such as mitogens, permit cell entry into G1, a phase where the cell is prepared for S-phase through transcription and translation of proteins required for DNA synthesis (Bertoli et al., 2013). Cyclin D bound to either Cdk4 or 6 is the key mediator of G1 events. Progression from G1 to S is controlled by the G1/S checkpoint, which ensures DNA synthesis factors are available and DNA is intact (Cooper, 2003). Once the cell passes this checkpoint, it commits to completion of cell division (Humphrey and Brooks, 2004). During G0 and early G1 the retinoblastoma (Rb) family of pocket proteins inhibit the E2F family of transcription factors, which control expression of S-phase genes (Bertoli et al., 2013). When extracellular signals permit activation of the Cyclin D-Cdk4 and cyclin D-Cdk6 complexes, Rb members are phosphorylated by Cdks and

released from E2F, thereby allowing transcriptional activation of S-phase genes (Bertoli et al., 2013). Amongst the genes transcribed is Cyclin E, which forms a complex with Cdk2 that positively feeds back to the Rb/E2F axis ensuring commitment to cell cycle progression (Bertoli et al., 2013).

S-phase, as the name suggests, is the DNA synthesis stage. A DNA replication licensing system strictly ensures that chromosome replication occurs only once per cycle, while S-phase checkpoints monitor errors occurring during chromosome replication in order to preserve genomic integrity (Labib and De Piccoli, 2011; Wu et al., 2014). Cyclin A-Cdk2 complexes drive S-phase progression and together with Dbf4 dependent kinases (DDKs) activate the pre-replicative complex (pre-RC) assembled on DNA replication origins, leading to initiation of DNA replication (Wu et al., 2014). Successful DNA replication, which lasts approximately 6h, leads to G2 entry whereby the cell synthesises proteins necessary for mitosis (Humphrey and Brooks, 2004). A G2/M checkpoint re-ensures DNA integrity prior to activation of Cyclin B-Cdk1 complexes, which marks the onset of mitosis (Stark and Taylor, 2006).

Mitosis is itself divided into distinct phases, known as prophase, metaphase, anaphase and telophase (Figure 5), that define the onset of mitotic events: nuclear envelope breakdown coupled to chromosome condensation, mitotic spindle formation and DNA alignment, chromosome segregation and nuclear envelope re-assembly (Maiato, 2010). Members of the Aurora and Polo-like (Plk) family of kinases are amongst the key players in coordinating mitotic progression (Maiato, 2010). A spindle assembly checkpoint (SAC) monitors the alignment of chromosomes before segregation and delays the onset of anaphase if chromosomes are not correctly attached to mitotic spindle poles via their kinetochores (Lara-Gonzalez et al., 2012), that is the protein complexes assembled at the centromere of each sister chromatid (Cleveland et al., 2003). Unattached kinetochores stimulate the assembly of SAC components, such as members of the mitotic arrest deficient (Mad) and Bub families and Monopolar spindle 1 (Mps1), which leads to inhibition of the anaphase promoting complex or cyclosome (APC/C), responsible for initiating anaphase (Lara-Gonzalez et al., 2012). When the SAC is satisfied, APC/C, bound to its catalytic subunit Cdc20, targets securin for degradation leading to the release of separase, that

in turn cleaves cohesin responsible for holding the sister chromatids together (Manchado et al., 2010; Peters, 2006). APC/C^{Cdc20} additionally targets Cyclin B for degradation, thus inactivating Cdk1 (Manchado et al., 2010; Peters, 2006). Inactivation of Cdk1 triggers substitution of Cdc20 with Cdh1 in telophase, and APC/C^{Cdh1} targets, amongst others, Aurora-A and Plk1 for degradation to permit mitotic exit (Manchado et al., 2010; Peters, 2006). Following these series of events, cytoplasmic division, known as cytokinesis, occurs (Figure 5) (Fededa and Gerlich, 2012). Cytokinesis involves the formation of an actomyosin ring at the cell cortex, that contracts to form the cleavage furrow, which in turn ingresses giving rise to the midbody (Fededa and Gerlich, 2012). Plasma membrane fission results in midbody abscission, thereby generating two daughter cells (Fededa and Gerlich, 2012).

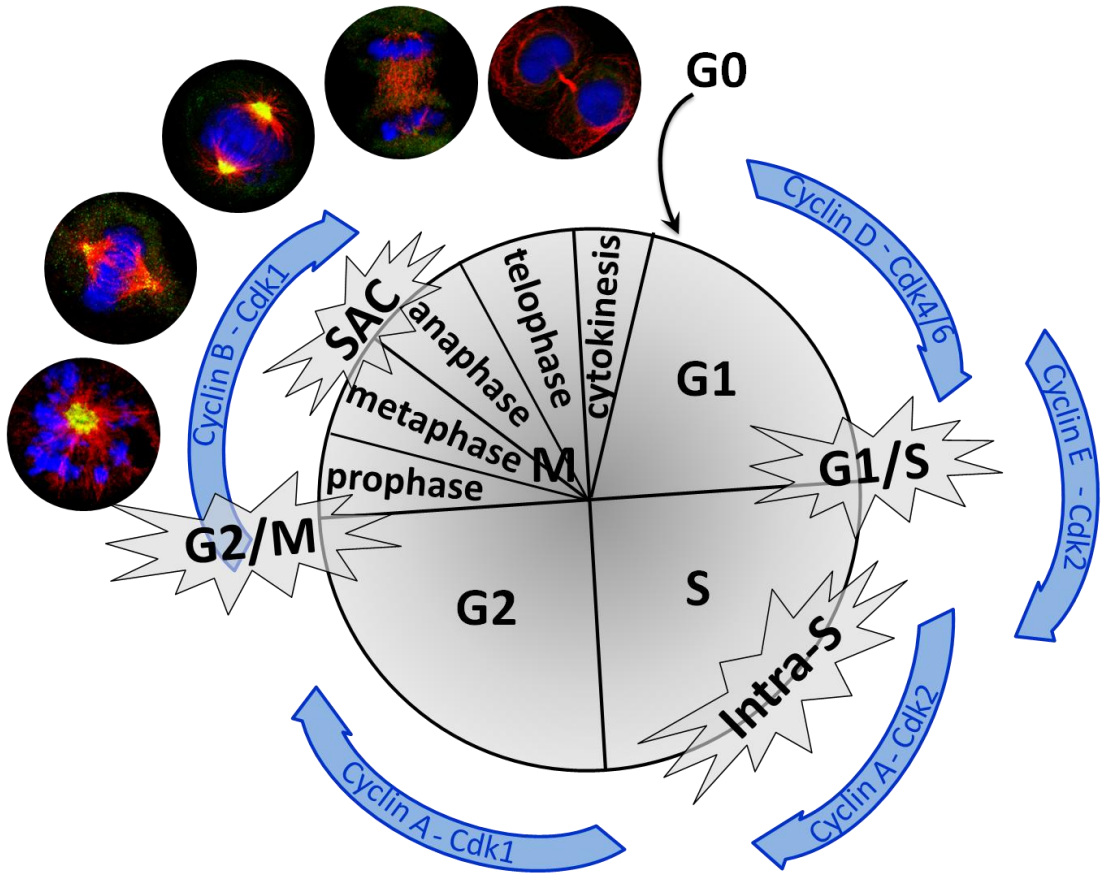

Figure 5: Cell cycle stages. The cell cycle consists of the interphase (G0, G1, S, G2 phases) and mitosis (M phase) and progression through the different stages is driven by Cyclin-Cdk complexes, as depicted. Mitogenic signals permit cell entry from the quiescent G0 phase to G1, where the cell grows and prepares for DNA synthesis. The G1/S checkpoint monitors requirements for entry into S-phase and once the cell passes this transition it commits to cell cycle completion. During S-phase the DNA is replicated and intra-S checkpoints

ensure successful replication before progression to G2. In G2 the cell prepares for division and upon satisfaction of the G2/M checkpoint mitosis initiates. Chromosome condensation, nuclear envelope breakdown and spindle assembly occur during prophase, followed by chromosome alignment at the metaphase plate. When the spindle assembly checkpoint (SAC) has ensured that all chromosomes are properly aligned, the cell progresses to anaphase to segregate the paired chromosomes. In telophase, nuclear re-assembly and chromosome decondensation mark the end of mitosis before cytoplasmic division (cytokinesis) physically separates the two daughter cells. References (Fisher, 2012; Humphrey and Brooks, 2004; Maiato, 2010; Morgan, 2007).

The cell cycle and cancer

Deregulation of the cell cycle is a key hallmark of cancer cells (Williams and Stoeber, 2012). A combination of genetic and epigenetic alterations in the cell-cycle regulatory machinery has been associated with uncontrolled proliferation, genomic instability and aneuploidy that characterizes cancer cells (Diaz-Moralli et al., 2013; Salmela and Kallio, 2013; Williams and Stoeber, 2012). Particularly, growth control at the G1/S transition is lost in the majority of cancer cells, often through inactivation of Rb and CKIs or upregulation of CDKs and Cyclins (Diaz-Moralli et al., 2013; Williams and Stoeber, 2012). Deregulation of the DNA replication licensing system or DNA damage and repair responses represents another common alteration in cancer, which can contribute to chromosome instability (Diaz-Moralli et al., 2013; Williams and Stoeber, 2012). Moreover, overexpression of mitotic kinases, such as Aurora-A/B and Plk1, and mutations in SAC regulators, such as BUBR1 and Mps1, have been observed in tumours (Janssen and Medema, 2011; Salmela and Kallio, 2013). In addition, amplification of centrosomes, which form the microtubule-organising centres or spindle poles in mitosis, is a common feature of tumour cells and it has been linked to carcinogenesis (Chan, 2011).

Given the detrimental consequences of deregulating the cell cycle, it is not surprising that many anti-cancer agents target the cell cycle machinery. For example, DNA replication is a common target of nucleoside analogues and other anti-metabolites (Williams and Stoeber, 2012). In addition, causing lethal DNA damage is one of the major anti-cancer strategies currently employed (Cheung-Ong et al., 2013; Hosoya and Miyagawa, 2014). There have been

considerable efforts in targeting mitosis and its defects in cancer, as cells are particularly vulnerable during this cell-cycle stage (Chan et al., 2012; Janssen and Medema, 2011). Small molecule inhibitors against mitotic kinases, such as Aurora-A and -B, Plk1, Mps1 and Eg5, have been evaluated as anti-cancer therapies and some demonstrated anti-tumour efficacy in clinical trials (Salmela and Kallio, 2013).

1.2.2. Introduction to the DNA damage and repair response

DNA damage checkpoints

Genome integrity is constantly being challenged by endogenous insults arising naturally through metabolic processes, for example reactive oxygen species, or errors in DNA replication, as well as environmental insults, including ultraviolet (UV) radiation and genotoxic agents (Warmerdam and Kanaar, 2010). In order to safeguard genomic stability cells have evolved mechanisms to sense DNA damage and halt cell-cycle progression until the lesions have been repaired. This is referred to as the DNA-damage response (DDR), a complex signal transduction network consisting of sensors, mediators, adaptors and effectors that work together to coordinate cellular processes with the goal of preventing proliferation in the presence of genomic instability (Figure 6) (Bartek and Lukas, 2007). The outcome of the DDR, which depends on the nature of the damage and the context, can vary from a temporary cell cycle arrest with successful DNA repair and resuming of proliferation, to irreversible growth arrest, known as senescence, or even cell death (Bartek and Lukas, 2007). DNA damage checkpoints exist at every cell-cycle phase, besides mitosis. Checkpoint-induced cell-cycle arrest at G1 and G2 phases is overall more durable and robust than S-phase arrest, which is largely transient and results in a subsequent G2 arrest if the damage is not repaired (Bartek et al., 2004). Notably, DNA damage in S-phase can result in three different responses: the DNA replication checkpoint response that deals with stalled replication forks, the Intra-S checkpoint that responds to double-strand breaks (DSBs) and the S-M checkpoint which prevents mitotic entry in response to incomplete DNA replication (Bartek et al., 2004).

The DDR has diverse sensors and signal transducers, depending mainly on the type of DNA lesion, but they all converge on Cyclin-CDK complexes in order to block cell-cycle progression (Figure 6) (Bartek and Lukas, 2007; Warmerdam and Kanaar, 2010). The key mediators of the DDR are the phosphoinositide 3-kinase related kinases (PIKKs) ataxia-telangiectasia mutated (ATM) and ataxiatelangiectasia and RAD3 related (ATR) (Bartek et al., 2004). ATM is primarily activated in response to DSBs, whereas ATR is activated in the presence of single-stranded DNA (ssDNA) generated by stalled replication forks, strand breaks and following recession of DSBs (Figure 6) (Bartek and Lukas, 2007; Lopez-Contreras and Fernandez-Capetillo, 2010). Whereas the activation of ATM and ATR differs at the level of sensors and mediators/adaptors, the signalling cascade initiated following activation of ATM and ATR converges on effector proteins (Cimprich and Cortez, 2008; Lopez-Contreras and Fernandez-Capetillo, 2010). With the exception of checkpoint kinases (Chk) 1 and 2, which appear to be exclusive effectors of ATR and ATM respectively, the vast majority of targets are shared between the two kinases (Chen and Poon, 2008; Cimprich and Cortez, 2008; Lopez-Contreras and Fernandez-Capetillo, 2010). Besides ATM/Chk2 and ATR/Chk1, the p38 mitogen activated protein kinase (MAPK) stress-response pathway is also activated in response to DNA damage (Figure 6).

Overview of DNA repair pathways

Several DNA damage repair pathways exist in higher eukaryotes and the choice of a repair pathway depends on the type of DNA damage as well as the phase of the cell-cycle (Branzei and Foiani, 2008). Single strand breaks (SSBs) and DSBs are mainly repaired through homologous recombination (HR) in S- and G2-phases, and through non-homologous end-joining (NHEJ) in G1 (Branzei and Foiani, 2008). HR operates only in S and G2 phases, as it repairs damaged DNA by using the information from an intact sister chromatid (Branzei and Foiani, 2008). In G1, as chromosomes are not duplicated, the preferred pathway for DSB repair is NHEJ (Branzei and Foiani, 2008). Accumulating evidence suggests that a competition exists between HR and NHEJ proteins

and the balance between them defines the repair choice (Branzei and Foiani, 2008; Lazzaro et al., 2009).

During DNA replication, base-base mismatches are repaired through the mismatch repair (MMR) pathway, while chemical alterations of nucleotide bases are repaired by the base-excision repair (BER) pathway, which also functions in G1 (Branzei and Foiani, 2008). Nucleotide excision repair (NER) is activated in response to bulky lesions that distort the DNA helix, for example those induced by UV, but NER proteins can function together with HR proteins for repair of crosslinks during DNA replication (Branzei and Foiani, 2008).

1.2.3. ATR-mediated DNA-damage response

ATR activation

As mentioned above ATR is activated in the presence of ssDNA, whether this is a result of a stalled replication fork or enzymatic cleavage of DSBs. Stalled replication forks can result for example from direct inhibition of DNA polymerases, depletion of dNTP pools or collision with aberrant DNA structures, including crosslinks and adducts (Bartek et al., 2004; Zegerman and Diffley, 2009). The exact signal that activates ATR is believed to be the extended presence of primed ssDNA, that is normally generated when the minichromosome maintenance 2-7 (MCM2-7) helicase complex unwinds the DNA helix to provide a template for the DNA polymerase (Jossen and Bermejo, 2013).

ssDNA is coated by replication protein A (RPA), which recruits the ATR-interacting protein (ATRIP)-ATR complex (Figure 6) (Cimprich and Cortez, 2008; Lopez-Contreras and Fernandez-Capetillo, 2010). ssDNA-RPA independently recruits the RAD17–replication factor C (RFC) clamp loader (Cimprich and Cortez, 2008; Lopez-Contreras and Fernandez-Capetillo, 2010). Rad17-RFC in turn loads the RAD9–RAD1–HUS1 (9-1-1) complex, which essentially recognises DNA ends near the ssDNA-RPA complex (Cimprich and Cortez, 2008; Lopez-Contreras and Fernandez-Capetillo, 2010). 9-1-1 then

recruits the mediator proteins Claspin and topoisomerase-binding protein-1 (TopBP1), the latter which interacts with and activates ATR (Cimprich and Cortez, 2008; Lindsey-Boltz and Sancar, 2011; Liu et al., 2006; Lopez-Contreras and Fernandez-Capetillo, 2010).

Activated ATR subsequently phosphorylates various targets, but perhaps the most critical effector for transducing the ATR signal is Chk1 (Cimprich and Cortez, 2008; Lopez-Contreras and Fernandez-Capetillo, 2010). ATR-catalysed Chk1 phosphorylation (Ser317 and Ser345) requires the presence of Claspin, which binds and stabilizes Chk1, bringing it in close proximity to ATR (Chini and Chen, 2003; Chini and Chen, 2004; Clarke and Clarke, 2005; Lin et al., 2004; Lindsey-Boltz et al., 2009; Liu et al., 2006; Liu et al., 2012). Chk1 in turn phosphorylates and stabilizes Claspin (Chini and Chen, 2006; Chini et al., 2006; Freire et al., 2006). Accumulating evidence suggests that TopBP1 is required for phosphorylation of most ATR substrates, while Claspin seems to be specific for Chk1 activation (Cimprich and Cortez, 2008; Lindsey-Boltz and Sancar, 2011; Liu et al., 2006; Tanaka, 2010). Claspin is required for normal rates of replication fork progression during an unperturbed DNA replication (Petermann et al., 2008; Tanaka, 2010; Uno and Masai, 2011) and in response to stalled replication forks it becomes phosphorylated and activated (Chini and Chen, 2006; Clarke and Clarke, 2005; Kumagai and Dunphy, 2003; Tanaka, 2010). Claspin phosphorylation occurs in the Chk1-binding domain on Thr916 and Ser945, and it is dependent on ATR but not catalysed by ATR (Chini and Chen, 2006; Clarke and Clarke, 2005; Kumagai and Dunphy, 2003; Lindsey-Boltz et al., 2009; Tanaka, 2010). Multiple kinases have been implicated in the phosphorylation of Claspin, including Chk1 itself (Chini and Chen, 2006), Cdc7 (Kim et al., 2008; Rainey et al., 2013) and Casein kinase 1 γ1 (CK1γ1) (Meng et al., 2011). Another adaptor proposed to be required for efficient Chk1 phosphorylation is the Timeless (Tim)-Tipin complex, suggested to bind ssDNA-RPA and facilitate Claspin recruitment (Leman and Noguchi, 2012).

ATR targets

ATR phosphorylates various substrates at the stalled replication forks, such as RPA and MCM2-7, to promote fork stability and recovery, which is important to

prevent fork collapse and subsequent generation of DSBs (Cimprich and Cortez, 2008; Lopez-Contreras and Fernandez-Capetillo, 2010). ATR also phosphorylates the RecQ helicase bloom syndrome protein (BLM), which was shown to play important roles in replication fork recovery and HR repair (Manthei and Keck, 2013). Other ATR targets present at the stalled replication forks include TopBP1, Rad17, 9-1-1, ATRIP and histone H2A.X (Figure 6); their phosphorylation is believed to amplify the DNA damage signal (Shiotani and Zou, 2009; Warmerdam and Kanaar, 2010). Moreover, ATR phosphorylates proteins involved in DNA repair, such as the HR protein BRCA1, the DNA crosslink repair protein Fanconi-anaemia group D2 (FANCD2), the helicase WRN, the nuclease ExoI and the NER protein xeroderma pigmentosum group A (XPA) (Cimprich and Cortez, 2008; Sirbu and Cortez, 2013; Warmerdam and Kanaar, 2010). ATR also acts to prevent degradation of the R2 subunit of RNR (D'Angiolella et al., 2012). Regulation of RNR in response to replication stress, which serves to adjust dNTP production, has been well documented in yeast, but it remains to be elucidated in human cells (Labib and De Piccoli, 2011; Sirbu and Cortez, 2013; Zegerman and Diffley, 2009).

Chk1 signalling

Once activated, Chk1 dissociates from chromatin and functions to transduce the ATR DNA damage signal by phosphorylating various substrates (Lopez-Contreras and Fernandez-Capetillo, 2010). In response to DNA damage or replication stress Chk1 mediates cell-cycle arrest by controlling the phosphorylation status of CDKs (Figure 6) (Patil et al., 2013). First, Chk1 phosphorylates all three members of the cell division cycle 25 (Cdc25) family of phosphatases (Cdc25A,B,C), which remove inhibitory phosphorylations on CDKs thereby activating them (Aressy and Ducommun, 2008). Chk1-mediated Cdc25A phosphorylation results in its proteasome-mediated degradation, leading to inhibition of CDK1 and CDK2 and subsequent arrest at G1, S or G2 (Patil et al., 2013). Moreover, it was reported that Chk1 phosphorylates the never in mitosis gene A (NIMA)-related kinase 11 (Nek11), which also phosphorylates Cdc25A targeting it for degradation (Melixetian et al., 2009). For Cdc25C, Chk1-mediated phosphorylation creates binding sites for 14-3-3 proteins, which subsequently sequester Cdc25C in the cytoplasm and inhibit

activation of CDK1 (Donzelli and Draetta, 2003; Patil et al., 2013). Chk1-mediated Cdc25B phosphorylation results in the inactivation of CDK1 present at the interphase centrosomes thereby preventing premature mitotic entry (Kramer et al., 2004; Loffler et al., 2006). Another mechanism for Chk1-mediated inhibition of CDK1 activity is the phosphorylation and activation of the Wee1 kinase, which catalyzes an inhibitory phosphorylation on CDK1 (Patil et al., 2013). Therefore, while Chk1-mediated inactivation of CDK2 only occurs through degradation of Cdc25A, multiple mechanisms exist for Chk1-mediated inactivation of CDK1 and inhibition of mitotic entry.

Besides the rapid phosphorylation-driven checkpoint response, a transcriptional response is also induced to sustain the checkpoint signal. Both ATR and Chk1 phosphorylate p53 leading to its stabilization and subsequent transcriptional activation of genes involved in cell-cycle arrest and DNA repair or apoptosis (Stracker et al., 2009). Activating p53 phosphorylations on Ser15 and Ser20 stabilize p53 and recruit transcriptional co-factors, like p300 and CBP, which also act to further stabilize p53 (Meek, 2004). Chk1 also phosphorylates Mouse double minute 2 homolog (Mdm) 4/X, which co-operates with Mdm2 for targeting p53 for degradation, leading to its 14-3-3-mediated sequestration and subsequent stabilisation of p53 (Stracker et al., 2009). The CKI $p21^{CIP1/WAF1}$ is a well-defined gene induced in response to p53 and it is responsible for inhibiting CDK2 thereby preventing Rb dissociation from E2F and leading to G1 arrest (Meek, 2004). Other p53-activated genes involved in cell-cycle arrest are Growth Arrest and DNA Damage (GADD45) and 14-3-3σ (Meek, 2004). Moreover, p53 represses the expression of genes involved in the G2/M transition, such as Cyclin B, Cdk1 and Plk1 (McKenzie et al., 2010; Taylor and Stark, 2001). Interestingly, a study reported that the dissociation of Chk1 from chromatin was concurrent with a reduction in histone H3 (Thr11) phosphorylation and this reduction correlated with the decreased binding of histone acetyltransferase GCN5 to Cyclin B1 and Cdk1 promoters and repression of transcription (Shimada et al., 2008).

Similar to ATR, Chk1 also phosphorylates proteins involved in DNA repair. In the context of DNA crosslink repair, Chk1 phosphorylates the FANCE subunit of the Fanconi-anaemia complementation group resulting in its co-localisation with

FANCD2 (Patil et al., 2013). In addition, Chk1 phosphorylates the HR repair protein Rad51, recruiting it to DNA repair foci (Sorensen et al., 2005).

Homologous recombination (HR) at stalled replication forks

When replication forks stall, ATR signalling promotes fork stabilisation to prevent breakage and ATR phosphorylates and recruits various DNA repair enzymes. HR was shown to play an important role in the repair of damaged replication forks. At stalled replication forks, BRCA2 recruits Rad51 to RPA-coated ssDNA and promotes HR by displacing RPA (Costanzo, 2011; Yeeles et al., 2013). Initially, BRCA2 and Rad51 act to protect fork degradation induced by the exonuclease activity of Mre11, which is thought to enlarge ssDNA gaps (Costanzo, 2011; Costes and Lambert, 2012; Yeeles et al., 2013). Then, HR promotes the re-start of stalled or collapsed replication forks and the Mre11-Rad50-Nbs1 (MRN)-complex, Rad51 and BRCA2 are critical players in this process (Costanzo, 2011; Costes and Lambert, 2012; Yeeles et al., 2013). Damaged forks are also processed by several other enzymes, including helicases, such as WRN and the FA group M protein (FANCM), that unwind DNA, and ATPases, such as SMARCAL1, that re-anneal DNA; all are targets of ATR (Sirbu and Cortez, 2013). The exact sequence of events during processing of stalled replication forks is poorly understood. HR has best been described in the context of DSBs and it is discussed in section 1.2.4.

Base-excision repair (BER)

BER is responsible for the repair of incorrectly incorporated, damaged or modified bases, as opposed to mismatches which are dealt with by MMR (Kim and Wilson, 2012). A frequent incorrectly incorporated base is Uracil, while modified bases can arise through oxidation, alkylation and deamination (Dianov and Hubscher, 2013; Kim and Wilson, 2012). BER also deals with abasic sites (Kim and Wilson, 2012). BER can be activated in response to certain forms of chemotherapy, such as alkylating agents, the autophagy inhibitor 3-methyladenine (3-MA), as well as by ionizing radiation generating reactive oxygen species (ROS), which can oxidize bases (Kim and Wilson, 2012; Parsons and Dianov, 2013).

BER proceeds by excising the damaged base through the action of DNA glycosylases, which results in DNA bending and base flipping (Kim and Wilson, 2012). At least 10 human DNA glycosylases have been identified to date, each with different substrate specificity (Parsons and Dianov, 2013). For example uracil DNA glycosylase (UDG) is responsible for removal of Uracil and 5-FU (Kim and Wilson, 2012). Excision by DNA glycosylase creates an abasic site which is incised by apurinic/apyrimidinic (AP) endonucleases (APE), the most frequently used being APE1, to create an intermediate strand break (Kim and Wilson, 2012). Interestingly, APE1 was implicated in the regulation of DNA binding by various transcription factors, including p53, NF-κB and hypoxia-inducible factor 1α (HIF-1α) (Tell et al., 2009). The next step is cleaning-up of the DNA ends/termini, performed by either DNA polymerase β (Pol β), APE1 or polynucleotide kinase phosphatase (PNKP), depending on the nature of the DNA end (Parsons and Dianov, 2013). If completed successfully, Pol β fills in the gap with a new nucleotide (short-patch BER) followed by DNA stabilization through binding of poly(ADP-ribose)polymerase 1 (PARP1), which recruits the X-ray cross complementing protein-1 (XRCC1) (Kim and Wilson, 2012). XRCC1 together with DNA ligase IIIα perform the sealing step of short-patch BER (Kim and Wilson, 2012; Parsons and Dianov, 2013). However, in some instances the DNA termini are resistant to the "cleaning-up" and replicative DNA polymerases (Pol δ/ε) are required to repair the gap (Parsons and Dianov, 2013). Addition of more than one nucleotide by Pol δ/ε is facilitated by the DNA clamp molecule proliferating cell nuclear antigen (PCNA) and it is followed by DNA ligase I-mediated sealing (Kim and Wilson, 2012; Parsons and Dianov, 2013). This is known as long-patch BER (Kim and Wilson, 2012; Parsons and Dianov, 2013).

Several BER enzymes have been implicated in cancer cell resistance to chemotherapeutic agents and BER inhibition is being evaluated as a sensitizing strategy to chemotherapy (Kim and Wilson, 2012). APE1 is one of these enzymes. Overexpression of APE1 can cause genetic instability, most likely through a collapse of replication forks that can accumulate SSBs and/or DSBs, whereas reduced APE1 expression has been shown to increase sensitivity to ionizing radiation, etoposide and temozolomide (TMZ) (Kim and Wilson, 2012; Parsons and Dianov, 2013). Similarly, suppression of XRCC1 increases sensitivity to ionizing radiation and topoisomerase I inhibitors and it is thought to

be involved in the processing of topoisomerase I-DNA intermediate complexes in response to CPT treatment (Kim and Wilson, 2012). Besides APE1 and XRCC1, the expression and activity of PARP-1, which regulates BER capacity, can increase in response to several chemotherapeutics, such as nucleoside analogues and topoisomerase I inhibitors, and PARP-1 inhibitors are being currently evaluated as anti-cancer agents (Kim and Wilson, 2012; Shah et al., 2013).

Nucleotide-excision repair (NER)

NER removes bulky, helix-distorting lesions that can be generated naturally or by environmental agents, such as UV radiation and cisplatin chemotherapy (Marteijn et al., 2014). NER is considered one of the most versatile types of DNA repair (Marteijn et al., 2014). There are two types of NER: global genome NER (GG-NER), that operates throughout the genome, and transcription-coupled NER (TC-NER), that repairs the template strand of actively-transcribed genes (Kamileri et al., 2012; Scharer, 2013).

In GG-NER, DNA lesions are being recognized by the sensor xeroderma pigmentosum complementation group C (XPC), which forms a complex with the RAD23 homologue B (RAD23B) and centrin 2 (CETN2) (Kamileri et al., 2012; Marteijn et al., 2014). DNA recognition is facilitated by the UV DNA damage-binding protein (UV-DDB) complex and once DNA has been bound, RAD23B dissociates from the complex (Kamileri et al., 2012; Marteijn et al., 2014; Scharer, 2013). UV-DDB forms a complex with cullin 4A (CUL4A)-regulator of cullins 1 (ROC1) E3 ubiquitin ligase and together mediate ubiquitination of XPC and core histones, such as H2A, as well as PARP-1-mediated PARylation of chromatin (Kamileri et al., 2012; Marteijn et al., 2014). Histone acetyltransferases, including p300, are also recruited to enhance chromatin relaxation (Kamileri et al., 2012). These post-translational modifications are thought to stimulate NER and facilitate the repair process (Kamileri et al., 2012; Marteijn et al., 2014).

In TC-NER, as RNA polymerase II (RNA Pol II), that elongates the transcript, stalls at the DNA lesion, a complex containing the ATPases Cockayne

syndrome protein B and A (CSB and CSA) binds RNA Pol II (Kamileri et al., 2012; Marteijn et al., 2014). This follows the binding of the UV-stimulated scaffold protein A (UVSSA) and ubiquitin-specific-processing protease 7 (USP7) (Marteijn et al., 2014).

Following damage recognition, GG-NER and TC-NER proceed in the same pathway which involves recruitment of the transcription initiation factor IIH (TFIIH) complex and lesion verification through the action of its DNA helicases XPB and XPD (Kamileri et al., 2012; Marteijn et al., 2014). XPA binds the altered ssDNA and recruits XPF-ERCC1 and XPG, the endonucleases that catalyze lesion excision leaving a ssDNA gap that is recognized by RPA (Kamileri et al., 2012; Marteijn et al., 2014). Similar to long-patch BER, NER proceeds with the binding of PCNA that recruits replication factors A and C (RFA and RFC) and DNA Pol δ/ε to fill the gap by DNA synthesis, while DNA ligase III-XRCC1 and DNA ligase I perform the final sealing step (Kamileri et al., 2012; Marteijn et al., 2014).

The intermediate ssDNA formed during excision is bound by RPA and has the potential of activating ATR signalling, particularly when the intermediates accumulate due to excision malfunction, excessive damage or various factors that inhibit DNA repair synthesis (Marteijn et al., 2014; Scharer, 2013). In such instances, XPG can be replaced with the exonuclease EXO1, which processes the NER intermediates generating long stretches of ssDNA that activate ATR-mediated DDR (Giannattasio et al., 2010; Sertic et al., 2011).

1.2.4. The ATM-mediated response to double-strand breaks

ATM activation

DSBs, one of the most lethal types of DNA damage, are recognised by the Mre11-Rad50-Nbs1 (MRN) complex**,** which recruits ATM leading to ATM autophosphorylation and activation (Figure 6) (Warmerdam and Kanaar, 2010). ATM directly interacts with MRN through Nbs1 (Warmerdam and Kanaar, 2010). Full activation of ATM was suggested to require acetylation by the Tip60

acetyltransferase (Sun et al., 2005; Sun et al., 2007). Activated ATM then phosphorylates histone H2A.X (γH2AX), which forms a docking site for the mediator of DNA damage checkpoint 1 (Mdc1) adaptor protein (Figure 6). These initial events are important for the subsequent assembly of other DNA damage and repair proteins as well as the amplification of the signal (Bartek and Lukas, 2007; Huen and Chen, 2010). Sustained localization of MRN is achieved through an interaction of Mdc1 with Nbs1 (Huen and Chen, 2010). ATM phosphorylates numerous substrates, including Nbs1, Chk2, BRCA1, p53 and the nuclease Artemis (Warmerdam and Kanaar, 2010).

Recruitment of chromatin remodelling, ubiquitination and DNA repair factors

Chromatin remodelling complexes, such as SWItch/Sucrose NonFermentable (SWI/SNF), are also recruited to γH2AX foci and are thought to relax chromatin for DNA repair protein access (Sirbu and Cortez, 2013). Independently of γH2AX, ATM induces the mono-ubiquitylation of histone H2B and the phosphorylation of the transcriptional co-repressor KAP-1, further relaxing chromatin (Sirbu and Cortez, 2013). Various DNA repair factors are recruited to the sites of DSBs. Among the proteins being recruited are the RING ubiquitin ligases RNF8 and RNF168, which catalyze ubiquitylation at the DSB to further recruit other ubiquitin ligases, like UBC13 (Huen and Chen, 2010; Sirbu and Cortez, 2013). These ubiquitylation events recruit a complex consisting of Abraxas, the ubiquitin-binding protein Rap80, and the DNA repair protein BRCA1 (Huen and Chen, 2010; Sirbu and Cortez, 2013). The p53 binding protein (53BP1) is also recruited and acts as a scaffold for recruitment of other proteins, such as the chromatin modulator EXPAND, as well as an ATM signal amplifier (Panier and Boulton, 2014). Additionally, 53BP1 acts to favour the choice of NHEJ repair in G1, by protecting the ends of DSBs from resection, and it has been suggested that during S-phase, BRCA1 might act to displace 53BP1 in order to favour HR (Bunting et al., 2010; Chapman et al., 2012; Panier and Boulton, 2014).

Chk2 signalling

Chk2 is the best-characterised effector of ATM signalling. ATM phosphorylates Chk2 on Thr-68, which stimulates dimerization and a series of autophosphorylation events on Thr-383 and Thr-387, leading to its full activation (Reinhardt and Yaffe, 2009; Stracker et al., 2009). Despite that Chk2 was reported to phosphorylate Cdc25A leading to proteasomal degradation (Falck et al., 2001), a study has challenged the ability of Chk2 to target Cdc25A for degradation (Jin et al., 2008). Similarly to Chk1 though, Chk2 can phosphorylate Cdc25C leading to 14-3-3-mediated cytoplasmic sequestration and CDK1 inactivation (Figure 6) (Boutros et al., 2006; Donzelli and Draetta, 2003). p53 and Mdm4/X are also phosphorylated by both Chk1 and Chk2 (Stracker et al., 2009). Similarly to ATM, Chk2 phosphorylates BRCA1 promoting BRCA1-mediated repair (Bartek et al., 2001).

DSB repair

Two important pathways for DSB repair are HR and NHEJ (Branzei and Foiani, 2008). The choice of repair pathway depends on the occurrence of DNA end-resection, with DNA end-binding HR and NHEJ proteins competing (Jasin and Rothstein, 2013; Symington and Gautier, 2011). It has been reported that CDK/cyclin B activity is required for the initiation of HR, which is another reason why HR is not utilized in G1 (Lazzaro et al., 2009; Warmerdam and Kanaar, 2010).

As mentioned above, MRN is the first molecule to bind DSBs. For HR, MRN recruits the endonuclease carboxy-terminal binding protein (CtBP)-interacting protein (CtIP), and together they resect DSBs (Lazzaro et al., 2009; Warmerdam and Kanaar, 2010). The E3 ubiquitin ligase BRCA1 is also recruited and interacts with both MRN and CtIP to facilitate HR (Jasin and Rothstein, 2013). Further resection is catalysed by the 5'-3'-exonuclease ExoI, the nuclease/helicase DNA2 and the BLM helicase (Nimonkar et al., 2011; Warmerdam and Kanaar, 2010). DSB resection generates ssDNA overhangs, which are bound by RPA that activates ATR, as described in section 1.2.3. RPA is eventually replaced by the DNA-dependent ATPase Rad51 that results in

invasion of the Rad51-bound strand into the homologous double-stranded DNA (dsDNA) template (Jasin and Rothstein, 2013; Warmerdam and Kanaar, 2010). BRCA2 is an important mediator of the displacement of RPA and its substitution with Rad51 and it is required to promote HR repair (Jasin and Rothstein, 2013).

When the balance tilts towards NHEJ, DNA ends are recognised by the Ku80/70 heterodimer, which recruits the PIKK member DNA-dependent protein kinase (DNA-PK) that provides the catalytic subunit (Warmerdam and Kanaar, 2010). Next, XRCC4, XLF and DNA ligase IV are recruited, which catalyze the ligation of the broken DNA ends (Warmerdam and Kanaar, 2010). The nuclease Artemis is responsible for processing of DSBs that can not directly be ligated, and binds DNA-PK (Warmerdam and Kanaar, 2010).

1.2.5. The p38/MAPK pathway in DNA-damage response

p38MAPK is activated by phosphorylation in its activation loop catalysed by MAPK kinases (MAPKK or MKKs), which are in turn activated by MAPKK kinases (MAPKKKs) depending on the stress signal (Obata et al., 2000). p38MAPK controls many cellular processes, such as transcription and translation, that impinge on cell survival or death decisions (Obata et al., 2000). A number of studies have shown that p38MAPK can be activated in response to various DNA-damaging agents including UV, ionizing radiation and several chemotherapeutic drugs, and that G2/M arrest following DNA damage induced by these agents was p38MAPK-dependent (Reinhardt and Yaffe, 2009; Thornton and Rincon, 2009).

It was later demonstrated that upon activation of p38MAPK, its effector kinase MAPK-activated protein kinase 2 (MK2) is activated which phosphorylates Cdc25B and C, creating 14-3-3 binding sites that lead to nuclear sequestration of Cdc25B/C (Figure 6) (Reinhardt and Yaffe, 2009; Thornton and Rincon, 2009). Additionally, p38MAPK phosphorylates and activates p53 (Thornton and Rincon, 2009). Reinhardt et al. showed that the p38MAPK/MK2 pathway functions downstream of ATM/Chk2 and ATR/Chk1 pathways and Raman et al. further demonstrated that ATM-mediated phosphorylation of the MAPKKK TAO

activates p38MAPK signalling in response to DNA damage (Figure 6) (Raman et al., 2007; Reinhardt et al., 2007). Interestingly, Reinhardt et al. suggested that p53-deficient cells require the p38MAPK/MK2 pathway downstream of ATM/Chk2 and ATR/Chk1 for functional checkpoint responses that lead to survival (Reinhardt et al., 2007).

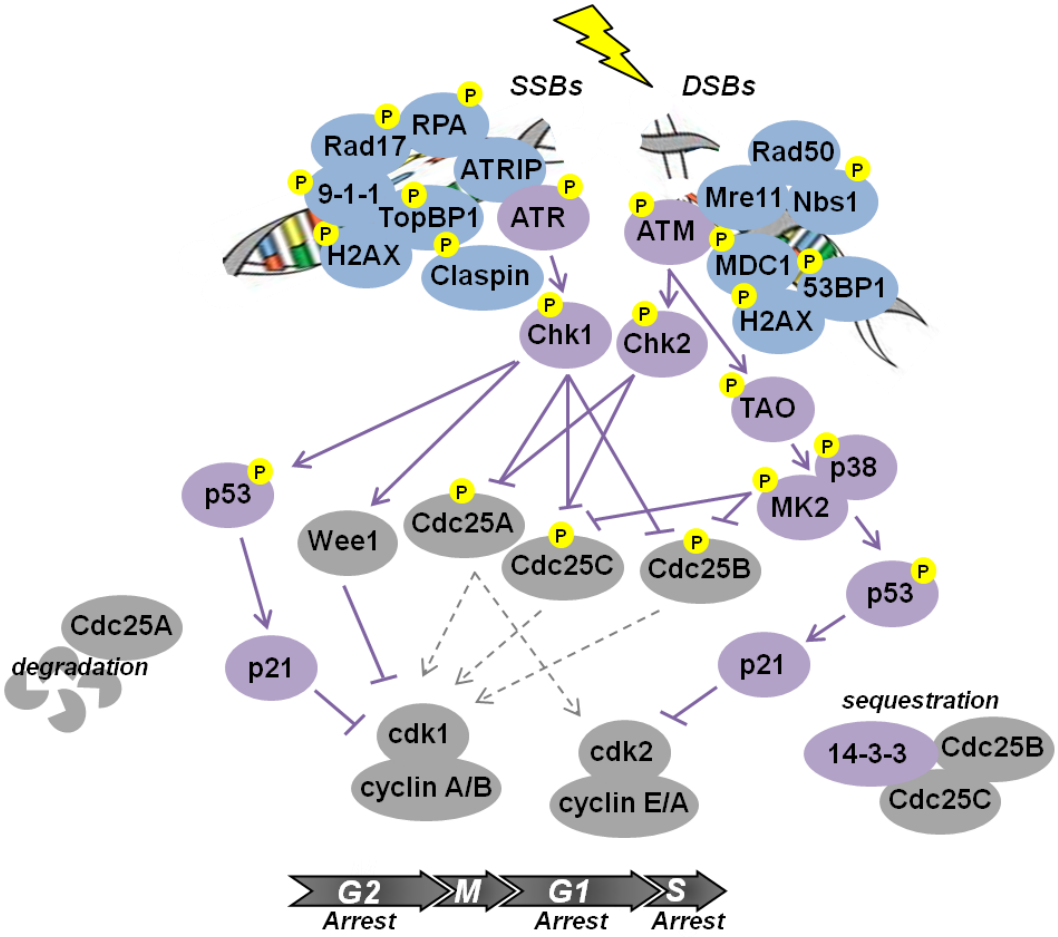

Figure 6: The DNA Damage Response. Single strand breaks (SSBs) get readily coated by RPA, which recruits the ATRIP-ATR complex and Rad17. Rad-17 in turn recruits the 9-1-1 complex which binds the adaptors TopBP1 and Claspin. Activated ATR phosphorylates the sensor and adaptor molecules at SSBs, including H2AX, and its effector Chk1, a phosphorylation event facilitated by Claspin. In response to double strand breaks (DSBs) the Mre11-Rad50-Nbs1 (MRN) complex binds DNA and recruits ATM that gets activated. ATM then phosphorylates H2AX triggering the recruitment of adaptor molecules, such as Mdc1 and 53BP1. ATM phosphorylates and activates its effector Chk2, as well as the MAPKKK TAO, which in turn activates the p38/MK2 kinase complex. Chk1, Chk2 and MK2 phosphorylate members of the Cdc25 family of phosphatases that remove inhibitory phosphorylations on Cdks to activate them. Phosphorylation of Cdc25A by Chk1 and Chk2 leads to its degradation and subsequently Cdk1 and Cdk2 inactivation. Phosphorylation of Cdc25B and Cdc25C by Chk1, Chk2 and MK2 recruits 14-3-3 proteins that sequester Cdc25B/C in the cytoplasm, thus preventing activation of Cdk1. Additionally, ATM, ATR, Chk1, Chk2 and p38/MK2 all phosphorylate and activate p53, stimulating the expression of p21 that acts to inhibit Cdk1-CyclinA/B and Cdk2-

CyclinA/E complexes. The DDR leads to cell cycle arrest at G1, S and/or G2 in order to allow time for DNA damage repair. Chromatin remodelling, ubiquitination and DNA repair factors are also recruited to single- or double-strand breaks (not shown on the diagram for simplicity) to initiate the process of repairing the lesions. References (Bartek and Lukas, 2007; Lopez-Contreras and Fernandez-Capetillo, 2010; Reinhardt and Yaffe, 2009; Sirbu and Cortez, 2013; Warmerdam and Kanaar, 2010).

1.2.6. The DNA-damage response targets mitotic kinases

Besides Cdk1, mitotic kinases that stimulate G2/M transition are inactivated during the DDR, presumably to re-enforce blockade of mitotic entry (Peng, 2013). At the onset of mitosis, Plk1, which is phosphorylated (Th210) and activated by Aurora-A, activates Cdk1 through a number of mechanisms: it directly phosphorylates and activates Cdk1, it phosphorylates and activates Cdc25C and it phosphorylates and inactivates Wee1 (Archambault and Glover, 2009; Petronczki et al., 2008). In response to DNA damage Plk1 was shown to be inactivated in an ATM- and ATR-dependent manner (Hyun et al., 2014; Smits et al., 2000). A study also reported that DNA damage in G2 induces degradation of Plk1 through the E3 ubiquitin ligase APC/C^{Cdh1} (Bassermann et al., 2008). Aurora-A, which was reported to activate Cdc25B, and Aurora-B are also inactivated by the DDR (Cazales et al., 2005; Krystyniak et al., 2006; Monaco et al., 2005).

Protein phosphatase 2A (PP2A) is a well-known antagonist of CDK activities throughout the cell-cycle (Jeong and Yang, 2013; Kurimchak and Grana, 2012). PP2A bound to its regulatory subunit B55 counteracts Cdk1 activities in interphase by de-phosphorylating Cdk1 substrates (Jeong and Yang, 2013). Mitotic entry requires inactivation of PP2A, which was shown to be mediated by the Greatwall kinase, also known as microtubule-associated serine/threonine kinase-like (MAST-L), through its substrates Ensa and ARPP19 (Glover, 2012; Yasutis and Kozminski, 2013). From studies in *Xenopus* extracts it was suggested that Greatwall is inhibited by the DDR (Peng et al., 2011; Peng et al., 2010); it remains to be seen whether this inhibition is conserved in humans. Although the function of Greatwall has been mainly studied in *Xenopus*, subsequent studies indicated the conservation of this function in human cells

and that Greatwall depletion causes a significant G2 delay rescued by inhibiting PP2A (Burgess et al., 2010; Hegarat et al., 2014; Krajewska and van Vugt, 2010; Voets and Wolthuis, 2010).

1.2.7. Recovery from the DNA-damage response: Switching the signal off

As cells complete repair of damaged DNA, the DNA damage checkpoint signal needs to be switched off in order to allow cells to resume cell cycle progression; this process is termed checkpoint recovery (Medema and Macurek, 2011; Peng, 2013). Checkpoint recovery has been mainly studied in the context of G2/M transition and it has emerged that re-activation of the Cyclin B-Cdk1 complex and subsequent mitotic entry is regulated by a balance of activities between DDR and mitotic kinases (Medema, 2010; Medema and Macurek, 2011; Peng, 2013; van Vugt and Yaffe, 2010). It should be noted that Cyclin B-Cdk1 lies in the centre of complex feedback loops occurring during G2/M transition (Medema, 2010; Medema and Macurek, 2011). For example, active Cdk1 inactivates its inhibitor Wee1, while it positively feeds back to its activator Cdc25 and additionally phosphorylates and activates Greatwall, which suppresses the Cdk1-antagonist PP2A (Medema, 2010).

The mitotic kinases Aurora-A and Plk1 have emerged as important regulators of checkpoint recovery. During checkpoint recovery, Aurora-A binds its activating co-factor Bora and phosphorylates Plk1, which subsequently acts to inhibit several components of the DDR as described below (Macurek et al., 2008; Seki et al., 2008). Several groups demonstrated that the mitotic kinase Plk1 phosphorylates Claspin, leading to Skp, Cullin, F-box (SCF)-βTrCP-mediated ubiquitination and subsequent proteasomal degradation (Gewurz and Harper, 2006; Macurek et al., 2008; Mailand et al., 2006; Mamely et al., 2006; Peschiaroli et al., 2006). Claspin degradation prevents further Chk1 activation and promotes recovery from the ATR/Chk1 checkpoint response (Gewurz and Harper, 2006). Plk1 was also shown to inhibit the ATM/Chk2 pathway. First, Plk1 directly phosphorylates Chk2 interfering with its ability to bind substrates and adaptor proteins (Tsvetkov, 2004; van Vugt et al., 2010). Second, Plk1 phosphorylates the adaptor protein 53BP1, which results in its exclusion from

chromatin at the onset and throughout mitosis (van Vugt et al., 2010). It was also shown that following a prime phosphorylation by Cdk1, Plk1 phosphorylates Wee1 leading to SCF-βTrCP-mediated degradation (van Vugt et al., 2004; Watanabe et al., 2005; Watanabe et al., 2004; Yde et al., 2008).

The phosphatase wild-type p53 inducible protein 1 (Wip1 or PPM1D), member of the PP2C family, has also been implicated in checkpoint recovery. Wip1, which is induced in response to various stresses (Lowe et al., 2012), was shown to reverse the ATR-mediated Ser345 phosphorylation on Chk1 resulting in reduced activity, as well as the Ser15 phosphorylation on p53 (Lu et al., 2005). Similar to Wip1, PP2A can reverse ATR-mediated Chk1 phosphorylations on Ser317 and Ser345 (Leung-Pineda et al., 2006). In addition Wip1 de-phosphorylates Mdm2 and Mdm4/X leading to their stabilization and subsequent enhancement of p53 degradation (Lowe et al., 2012; Lu et al., 2008). Another target of Wip1 is the p38MAPK whose Wip1-mediated de-phosphorylation leads to decreased p53 activity (Takekawa et al., 2000). Since Wip1 is transcriptionally induced by p53, Wip1-mediated inhibition of p53 creates a negative feedback loop (Lu et al., 2008). Wip1 also removes the ATM-mediated Thr68 phosphorylation on Chk2, reducing its activity, as well as dephosphorylating ATM itself (Lu et al., 2008). Several groups have shown that Wip1 de-phosphorylates γH2AX, impairing the recruitment of other DDR proteins (Lowe et al., 2012). Moreover, it was proposed that Wip1 attenuates NER and BER through dephosphorylation of the NER proteins XPA and XPC and the Uracil-removing enzyme UNG2 (Lu et al., 2004a; Lu et al., 2004b; Nguyen et al., 2010). Importantly, it was demonstrated that Wip1 overexpression abrogates the intra-S and G2/M checkpoints (Lowe et al., 2012). A direct link between Wip1 activation and checkpoint recovery has been demonstrated (Lindqvist et al., 2009). In this report it was revealed that Wip1 activity is required to maintain the competency of cells to recover and resume cell cycle progression (Lindqvist et al., 2009). However, the requirement of Wip1 for checkpoint recovery was attributed to its ability to antagonise p53-mediated repression of G2 genes, such as Cyclin B and Plk1, rather than the mere dephosphorylation of DDR factors (Lindqvist et al., 2009).

Another transcriptional mechanism for G2/M checkpoint recovery was proposed by Alvarez-Fernandez et al, who showed that checkpoint recovery at G2 requires Cdk1 to phosphorylate and activate the transcription factor FoxM1 thereby inducing FoxM1-mediated expression of Cyclin A, Cyclin B and Plk1 (Alvarez-Fernandez et al., 2010). Interestingly, the authors further suggested that a residual low Cdk1 activity during checkpoint activation is required for cells to be able to recover from the checkpoint response, as inhibition of that activity prevented cells from recovering (Alvarez-Fernandez et al., 2010).

An unresolved question in the field is how mitotic kinases regain activity for checkpoint recovery since they are inhibited by the DDR (Peng, 2013). In a recent review Aimin Peng proposed two models that could explain this paradox (Peng, 2013): The first model, in agreement with Alvarez-Fernandez et al (Alvarez-Fernandez et al., 2010), suggests that a residual low activity of mitotic kinases is maintained despite inhibition by the DDR and that this activity progressively increases as DNA repair is completed and suppressing signals are attenuated. The second model suggests that checkpoint recovery occurs spontaneously regardless of DNA repair completion.

The second model is in agreement with the concept of checkpoint adaptation. Checkpoint adaptation describes the process whereby cells are de-sensitised to the checkpoint signal after prolong periods of checkpoint activation (Bartek and Lukas, 2007; Clemenson and Marsolier-Kergoat, 2009; Syljuasen, 2007). Evidence for checkpoint adaptation in human cells was provided through studies using persistent ionizing radiation (IR) in G2 (Syljuasen, 2007). Following treatment with IR cells can undergo several rounds of division before dying, which could imply an adaptation to the DDR (Syljuasen, 2007). Syljuasen et al. showed that following a sustained IR-induced G2 checkpoint, cells entered mitosis in the presence of DNA lesions, as shown by persistent γH2AX foci (a marker of DNA damage) and checkpoint adaptation required Plk1 activity (Syljuasen et al., 2006). Besides Plk1, it was previously shown that Cyclin B levels gradually accumulate following prolonged IR-induced G2 arrest (Ianzini and Mackey, 1997; Maity et al., 1996). It remains to be seen whether checkpoint adaptation occurs under other forms of genotoxic stress and whether it is a common feature of human cells.

1.2.8. DNA damage-induced apoptosis

Apoptotic pathways

Apoptosis can be activated intrinsically through the mitochondrial pathway and extrinsically through death ligands and receptors (Figure 7). The intrinsic/mitochondrial apoptotic pathway is governed by the B-cell lymphoma 2 (Bcl-2) family of pro- and anti-apoptotic proteins, which include the pro-apoptotic members Bax, Bak, Bad, Bcl-XS, Bid, Bik, Bim and Hrk and the anti-apoptotic members Bcl-2, Bcl-XL, Bcl-W, Bfl-1 and Mcl-1 (Chipuk et al., 2010). When signals shift the balance towards the pro-apoptotic members, BAX and BAK oligomerize to form complexes that create pores in the outer mitochondrial membrane (Chipuk et al., 2010; Elmore, 2007). This leads to loss of the mitochondrial transmembrane potential and mitochondrial release of pro-apoptotic molecules, such as cytochrome-c and Smac/DIABLO (Figure 7) (Chipuk et al., 2010; Elmore, 2007). Cytochrome-c then forms a complex with pro-caspase-9 and apoptotic protease activating factor 1 (Apaf-1), called the apoptosome (Figure 7) (Elmore, 2007). This leads to the cleavage of pro-caspase-9 to caspase-9, which subsequently activates caspase-3 triggering the execution pathway (Elmore, 2007).

Extrinsic apoptosis is activated by the binding of extracellular death ligands (L) of the tumour necrosis factor (TNF) family (TNF-α, FasL, Apo2L/TRAIL, Apo3L) to their respective death receptors (DR) (TNF-R1, Fas, DR4, TRAIL-R1/DR4, TRAIL-R2/DR5, DR3) (Figure 7) (Elmore, 2007). Upon ligand binding, adaptor proteins, mainly Fas-associated death domain (FADD), are recruited and bind to the cytoplasmic tails of the corresponding receptors via their death domains (Elmore, 2007). Pro-caspases 8 and 10 are then recruited and together with the death domains form the death-inducing signaling complex (DISC) (Figure 7) (Elmore, 2007; Fiandalo and Kyprianou, 2012). Pro-caspases are cleaved to their active caspases, a process which can be inhibited by the FLICE-inhibitory protein (cFLIP) (Elmore, 2007; Fiandalo and Kyprianou, 2012). Active caspase-8 cleaves and activates caspase-3 and -7, triggering the execution pathway (Fiandalo and Kyprianou, 2012). The extrinsic apoptotic pathway can also lead to mitochondrial outer membrane permeabilization via activation of BID; cleaved

caspase-8 can activate pro-apoptotic BID which acts to inhibit the anti-apoptotic Bcl-2 family members and promote Bax/Bak oligomerisation (Figure 7) (Li et al., 1998b; Luo et al., 1998).

Extrinsic and intrinsic apoptosis converge to the execution pathway (Figure 7). This is mediated by the execution caspases (-3, -6 and -7), which activate proteases that degrade cellular components (Elmore, 2007). Caspase-3 also cleaves PARP (Elmore, 2007); cleaved PARP is a common marker of apoptosis induction. Independently of caspases, apoptosis-inducing factor (AIF), which is released from the mitochondria, acts to condense chromatin (Elmore, 2007). DNA fragmentation is catalyzed by endonucleases, such as endonuclease G and the Caspase Activated DNase (CAD), which is activated by caspase-3 (Elmore, 2007). Members of the inhibitor of apoptosis (IAP) family, including XIAP, cIAP1/2 and Survivin, antagonize apoptosis by direct binding and inhibition of caspases and Smac/DIABLO (Dubrez et al., 2013).

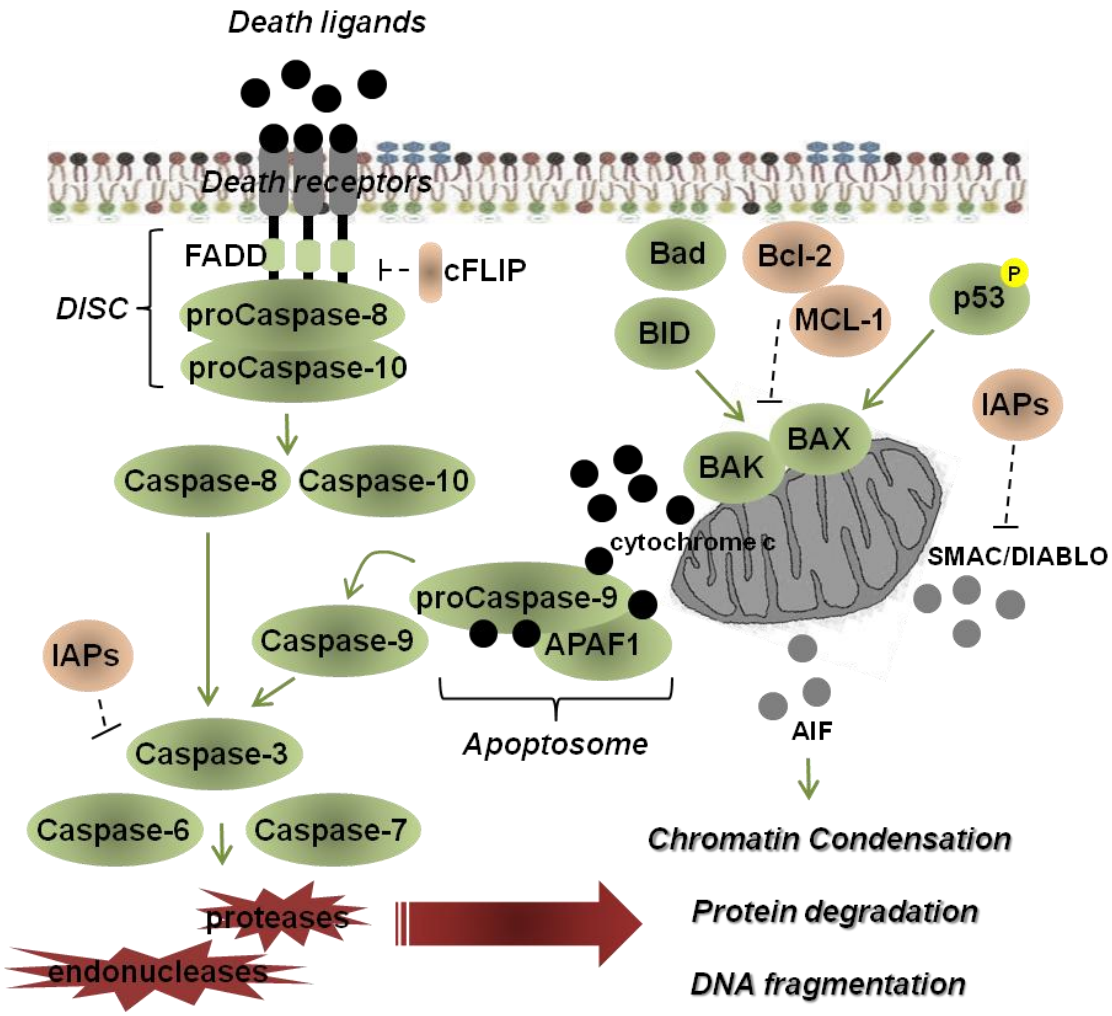

Figure 7: Apoptotic pathways. Apoptosis can be activated intrinsically through the mitochondrial pathway (right side of figure) and extrinsically through death ligands and receptors (left side of figure). The intrinsic pathway is mediated by pro-apoptotic members of the Bcl-2 family (see text for details) and results in the oligomerisation of Bax and Bak that form pores on the outer mitochondrial membrane. This subsequently leads to the release of pro-apoptotic molecules, such as cytochrome C, SMAC/DIABLO and AIF. Cytochrome C together with APAF-1 and pro-caspase-9 form the apoptosome, that results in cleavage and activation of caspase-9. The extrinsic pathway is mediated by death ligands that bind to death receptors to stimulate the assembly of the DISC complex (see text for details), comprised of adaptor death domain molecules, such as FADD, and pro-caspase-10 and -8. Within the DISC pro-caspases are cleaved to form active caspases. The intrinsic and extrinsic pathways converge on execution caspases (-3, -7, -6) that are activated through cleavage by caspase-8 and -9. The execution caspases in turn activate proteases and endonucleases that degrade proteins and DNA. Additionally, released AIF acts to condense chromatin. Apoptosis-inducing factors can be antagonised by anti-apoptotic molecules including IAPs, c-FLIP, Bcl-2 and MCL-1 (see text for details). References (Chipuk et al., 2010; Elmore, 2007; Fiandalo and Kyprianou, 2012).

Activation of apoptosis by the DNA-damage response

ATM, ATR, Chk1 and Chk2 can all phosphorylate and activate p53, as well as stabilize it by downregulating the p53 negative regulators of the Mdm family (Stracker et al., 2009). p53 activation can lead to the transcription of genes involved in cell-cycle arrest and DNA repair or pro-apoptotic genes; the mechanism for the cell fate decision has only recently been fully explored. It was suggested that p53 levels oscillate in distinct pulses and DDR-induced p53 transient pulses can lead to a survival response whereas sustained and constant levels of p53 can support induction of apoptosis (Lahav, 2008; Zhang et al., 2011). It was also demonstrated that these pulses depend on the presence of the Wip1 phosphatase (Batchelor et al., 2008). Moreover, evidence suggests that the Ser15 and Ser20 phosphorylations promote cell-cycle arrest while a delayed Ser46 phosphorylation stimulates full activation and induction of apoptosis (Oda et al., 2000; Zhang et al., 2011). The p53-induced pro-apoptotic genes including BAX, NOXA, BID, PUMA and APAF1 are involved in the intrinsic apoptotic pathway, while DR5, FAS and p53-induced death domain (PIDD) proteins are involved in the extrinsic apoptotic pathway (Meek, 2004; Vousden and Lu, 2002).

In addition to p53, Chk1 and Chk2 have been reported to phosphorylate and stabilize E2F1, promoting E2F1-mediated apoptosis (Stracker et al., 2009). E2F1 stimulates transcription of the p53 homologue p73, which can activate expression of the pro-apoptotic protein PUMA (Roos and Kaina, 2006).

A pro-apoptotic NF-κB pathway has also been implicated in DNA damage-induced apoptosis (Wu and Miyamoto, 2008). ATM binds to and phosphorylates the regulatory subunit NEMO/IKKγ, which leads to monoubiquitination and SUMOylation that activate NEMO (Miyamoto, 2011). The ATM/NEMO complex is then exported to the cytoplasm where NEMO can activate IKKβ (Miyamoto, 2011). IKKβ subsequently targets IκBα for degradation, releasing it from NF-κB, which can now translocate to the nucleus and activate transcription (Miyamoto, 2011). Pro-apoptotic genes induced by NF-κB include the FasL and TNF-α (Nowsheen and Yang, 2012).

As mentioned above, DDR activates BRCA1. BRCA1 has been shown to enhance p53-independent apoptosis when cytoplasmic, and p53 has been shown to be important in DNA-damage induced nuclear export of BRCA1 (Nowsheen and Yang, 2012). In addition, BRCA1 was reported to localize at mitochondria and promote apoptosis (Nowsheen and Yang, 2012).

1.2.9. DNA damage in mitosis

Mitosis prevents DDR activation and DNA repair

Cells escaping DNA damage checkpoints, due to either defective checkpoints or checkpoint adaptation, can initiate mitosis with damaged DNA. As discussed above (section 1.2.6.), DDR proteins are inactivated at the onset of mitosis to allow de-repression of Cdk1 activity that is required to drive mitotic progression, during which the suppressive state of DDR proteins is maintained (Heijink et al., 2013). This is in agreement with observations made decades ago that irradiation of mitotic cells does not lead to mitotic arrest and that cells progress to division (Mazia, 1961; Rieder and Cole, 1998; Zirkle and Bloom, 1953). The point of mitotic commitment is late prophase, as causing DNA damage before this stage can revert the cell to interphase (Rieder, 2011; Rieder and Cole, 1998).

Despite mitotic inactivation of DDR signalling, several studies reported the presence of the MRN complex, Mdc1, RPA and γH2AX, on mitotic chromosomes, suggesting that the initial steps of DNA damage recognition do occur (Heijink et al., 2013). In agreement with MRN and Mdc1 presence on mitotic chromosomes, ATM phosphorylation has also been reported in mitotic cells, however the activation of downstream effectors 53BP1 and Chk2 and subsequent recruitment of ubiquitin ligases RNF8, RNF168 and BRCA1 was blocked (Giunta et al., 2010; van Vugt et al., 2010). Indeed, several studies demonstrated the strict exclusion of 53BP1 from mitotic chromosomes (Belotserkovskaya and Jackson, 2014; Giunta et al., 2010; Giunta and Jackson, 2011; Nelson et al., 2009; van Vugt et al., 2010).

Regarding DNA repair, resection of mitotic DNA ends in *Xenopus* extracts was observed to be dependent on MRN and CtIP but did not lead to ATR/Chk1 activation or Rad51 recruitment (Peterson et al., 2011). The same study as well as another study in human cells reported the presence of the NHEJ complexes Ku on mitotic chromosomes (Gomez-Godinez et al., 2010; Peterson et al., 2011). Despite the presence of some DNA repair proteins and a partial resection of mitotic chromosomes, active and complete DNA repair in mitosis has not been demonstrated. Consistent with the lack of a functional DNA repair machinery in mitosis, it has recently been demonstrated that attempting to repair DNA during mitosis leads to Aurora B-dependent sister telomere fusions, chromosome missegregation and subsequent genetic instability and aneuploidy (Orthwein et al., 2014). Therefore, it seems that cells have evolved mechanisms to suppress DNA repair in mitosis in order to protect telomeres and genome integrity (Belotserkovskaya and Jackson, 2014). The elegant study by Orthwein et al. also revealed that re-activation of RNF8 and 53BP1 was sufficient to initiate DNA repair in mitosis, suggesting a critical role of these molecules in DSB repair (Orthwein et al., 2014; Zlotorynski, 2014). Damaged mitotic chromosomes are instead repaired in the subsequent G1 phase, where DDR activation is permitted (Heijink et al., 2013; Uetake and Sluder, 2010).

In addition to avoiding repair in order to protect telomeres, another rationale for preventing execution of a DDR-mediated arrest in mitosis has emerged from accumulating evidence that mitotic arrest can itself damage DNA (Ganem and Pellman, 2012; Heijink et al., 2013). Early indications for this phenomenon came from observations that cells arrested in mitosis either die or exit mitosis with a subsequent p53-dependent G1 arrest (Ganem and Pellman, 2012). Subsequently it was shown that γH2AX foci could be detected 5-16h after mitotic arrest and further accumulated while cells remained arrested (Dalton et al., 2007; Orth et al., 2012). A study by Orth et al. provided some explanation for the observed DNA damage following prolonged mitosis. It was shown that cells arrested in mitosis for prolonged periods induced partial mitochrondrial membrane permeabilization and cytochrome c release, sufficient to induce CAD-mediated cleavage of DNA but not complete DNA fragmentation (Orth et al., 2012). Accordingly, caspase inhibition inhibited γH2AX foci formation (Orth et al., 2012). Activation of apoptosis during mitosis can be supported by the

observation that the anti-apoptotic proteins Mcl-1 and cFLIP are degraded when cells arrest in mitosis (Harley et al., 2010; Inuzuka et al., 2011; Millman and Pagano, 2011; Sanchez-Perez et al., 2010). Hayashi et al. observed that mitotic arrest triggered deprotection of telomeres (Hayashi et al., 2012), which are normally protected from DDR recognition through coating by the Telomere Repeat binding Factor 2 (TRF2) and Protection Of Telomeres 1 (Pot1) components of the shelterin (de Lange, 2009). Telomere deprotection during prolonged mitosis was associated with Aurora-B mediated TRF2 dissociation and led to ATM activation (Hayashi et al., 2012). Moreover, the study showed that cells with unprotected telomeres arrested in G1 in the presence of a functional p53, whereas p53-deficient cells progressed through the cell cycle eventually becoming aneuploid (Hayashi et al., 2012).

Given that cells do not normally spend more than 60 minutes in mitosis, it can be presumed that mitosis is not a favourable state for a cell. Indeed, mitosis comes with striking reorganization of the cell apparatus (Ganem and Pellman, 2012; Robbins and Gonatas, 1964), including nuclear membrane breakdown (Hetzer, 2010), major cytoskeletal reformations (Heng and Koh, 2010; Kunda and Baum, 2009; Lancaster and Baum, 2014), silencing of transcription (Gottesfeld and Forbes, 1997; Prescott and Bender, 1962) and inhibition of translation (Pyronnet et al., 2001). Remarkably, a study suggested that cells can sense the duration of prometaphase and prevent proliferation of cells that have arrested in mitosis (Uetake and Sluder, 2010). The study showed that when a mother cell spent more than 90 minutes in prometaphase, the daughter cells arrested in the subsequent G1 in a p53- and p38-dependent manner and their proliferation was blocked (Uetake and Sluder, 2010).

Consequences of entering mitosis with DNA damage

Despite the lack of a DNA damage checkpoint in mitosis, it has been reported that mitotic cells exhibiting extensive DNA damage can arrest in metaphase (Mikhailov et al., 2002; Nitta et al., 2004). However, such arrest was demonstrated to be triggered by defects in kinetochore-microtubule attachment that activate the SAC, rather than a DDR, and minor DNA damage does not seem to delay mitotic progression (Heijink et al., 2013; Mikhailov et al., 2002;

Nitta et al., 2004). SAC does not necessarily need be satisfied for cells to exit mitosis, as the prerequisite for mitotic exit is degradation of Cyclin B and/or inactivation of Cdk1 (Rieder and Maiato, 2004). As in the case of any other checkpoint, cells can adapt to or abrogate the SAC and progress to anaphase, or even skip anaphase and cytokinesis (mitotic slippage) (Rieder and Maiato, 2004).

When cells do progress to anaphase, attempting to segregate damaged chromosomes can be detrimental. In recent years, several studies demonstrated that strand breaks, replication stress or any unresolved S-phase DNA structure can lead to chromosome segregation errors, such as chromosome bridges, which form due to the centromeres of a dicentric chromosome being pulled to opposite poles, ultrafine DNA bridges, or lagging chromosomes, which arise when a single kinetochore binds microtubules from two opposite poles pulling with same strength (Bakhoum et al., 2014; Burrell et al., 2013; Chan et al., 2009; Ichijima et al., 2010; Lukas et al., 2011; Mankouri et al., 2013). Lagging chromosomes and other chromatid fragments originating from DSBs or incomplete DNA repair, can be missegregated in daughter cells or excluded from daughter nuclei, leading to the formation of micronuclei (Fenech et al., 2011). Moreover, chromosome bridges and lagging chromosomes can get trapped in the cleavage furrow during cytokinesis and lead to chromosome breakage or cytokinesis delay and/or failure (Ganem and Pellman, 2012; Hayashi and Karlseder, 2013; Janssen et al., 2011).

Cytokinesis failure results in a single daughter cell containing two nuclei (binucleated/tetraploid) and such cells are often arrested in G1 in a p53-dependent manner (Ganem and Pellman, 2007; Normand and King, 2010). However, some tetraploid cells can continue cycling generating chromosomal aberrations and polyploidy and even facilitate tumorigenesis in the absence of p53 (Fujiwara et al., 2005; Ganem and Pellman, 2007; Ganem et al., 2007). Very recently Ganem et al. demonstrated that cytokinesis failure activates the Hippo tumour suppressor pathway which negatively impacts on proliferation by stabilizing p53 and stimulating YAP/TAZ-dependent transcription of genes involved in cell proliferation and death (Ganem et al., 2014; Yu and Guan, 2013). Another consequence of cytokinesis failure is the gaining of one more

centrosome and as centrosomes duplicate in S-phase, tetraploid cell cycle progression could lead to supernumerary centrosomes (Nigg, 2002). Centrosome overduplication (amplification) can also arise in S-phase arrested cells, as a result of uncoupling DNA replication and centrosome duplication and permitting multiple rounds of centrosome duplication (Balczon et al., 1995; Collins et al., 2010; Nigg, 2002; Prosser et al., 2009). Supernumerary centrosomes can generate multiple spindle poles during mitosis and lead to multipolar anaphases and chromosome missegregation, which can in turn result in aneuploidy and genetic instability (Brinkley, 2001; Fukasawa, 2005; Fukasawa, 2007; Marthiens et al., 2012; Nigg, 2002). Interestingly, the majority of cancer cells have evolved mechanisms to cluster supernumerary centrosomes in two spindle poles thus avoiding the poor cell survival associated with multipolar divisions (Brinkley, 2001; Gergely and Basto, 2008; Marthiens et al., 2012).

SAC-mediated arrest of DNA-damaged cells followed by premature mitotic exit (mitotic slippage) also leads to cytokinesis failure (Andreassen et al., 2001; Hayashi and Karlseder, 2013; Huang et al., 2005; Hyun et al., 2012; Nitta et al., 2004; Vakifahmetoglu et al., 2008). Premature mitotic entry of DNA-damaged cells followed by an aberrant mitosis that leads to cell death has often been referred to as mitotic catastrophe. DNA damage-induced mitotic catastrophe was observed decades ago in cancer cells treated with chemotherapy or radiotherapy and it is often coupled to a defective or abrogated G2/M, G1/S or spindle assembly checkpoint (Castedo et al., 2004; Mansilla et al., 2006; Portugal et al., 2010; Roninson et al., 2001; Vakifahmetoglu et al., 2008). Cells with non-functional p53 and/or deficiencies in p21, Chk1 and Chk2 are particularly prone to mitotic catastrophe (Castedo et al., 2004; Portugal et al., 2010; Vakifahmetoglu et al., 2008). DNA damage-induced mitotic catastrophe is associated with premature mitotic entry followed by several mitotic aberrations, including chromosome condensation errors, multipolar spindles and formation of micro- and multi-nucleated cells (Castedo et al., 2004; Roninson et al., 2001; Vakifahmetoglu et al., 2008). Micromultinucleated cells are a prominent feature of mitotic catastrophe and arise through cytokinesis failure and endoreduplication, that is continued cycling in the absence of cell division (Castedo et al., 2004; Roninson et al., 2001; Vakifahmetoglu et al., 2008). A

possible outcome of mitotic catastrophe is death during mitosis that can be caspase-dependent or -independent (Castedo et al., 2004; Portugal et al., 2010; Vakifahmetoglu et al., 2008). Alternatively, cells exit mitosis and progress to G1, where different outcomes are possible: cells can die through apoptotic or necrotic mechanisms, remain arrested (senescent) or re-enter the cell cycle and die following one or more rounds of division (Castedo et al., 2004; Portugal et al., 2010; Vakifahmetoglu et al., 2008). The outcome of mitotic catastrophe is largely cell-context and treatment specific (Portugal et al., 2010).

1.2.10. DDR, apoptosis and the DNA-damaging drugs gemcitabine and irinotecan

Understanding the cellular response to DNA-damaging anti-cancer drugs is critical for identification of cellular factors involved in drug sensitivity or resistance and subsequent development of improved anti-cancer treatments. In the next section I will summarize the current understanding of DNA-damage response and apoptotic pathways activated in response to the DNA-damaging chemotherapeutic drugs gemcitabine and irinotecan.

Gemcitabine

Gemcitabine is a cytidine analogue that inhibits DNA replication and is thus expected to activate the ATR/Chk1 response to stalled replication forks. Indeed, numerous studies demonstrated activation of Chk1 2-24h following 10-500nM gemcitabine treatment of different cancer cell lines, including leukemia, cervical, pancreatic, lung and colon adenocarcinoma (Duong et al., 2013; Ewald et al., 2007; Karnitz et al., 2005; McNeely et al., 2010; Morgan et al., 2005; Parsels et al., 2009). In addition, phosphorylated H2AX was shown to be present at gemcitabine-induced stalled replication forks (Ewald et al., 2007; Karnitz et al., 2005; Parsels et al., 2009) within 2h after treatment and increased with increasing drug concentrations up to 100nM (Ewald et al., 2007). Consistent with the observed activation of the ATR/Chk1 pathway followed by degradation of Cdc25A, gemcitabine induces a potent S-phase arrest within 24h after treatment (Ewald et al., 2007; Parsels et al., 2009; Shi et al., 2001). Shi et al.

reported that 10nM gemcitabine was sufficient to arrest the majority of cells for at least 36h (Shi et al., 2001). Several studies demonstrated that in addition to Chk1, gemcitabine induces phosphorylation of Chk2 that increases as a function of dose or time (Karnitz et al., 2005; Morgan et al., 2005; Parsels et al., 2009). Ewald et al. showed that γH2AX foci co-localise with phosphorylated ATM within 2h after treatment with 100nM gemcitabine and in a separate study the same authors showed that the MRN complex also co-localises with phosphorylated ATM within 2h post-treatment (Ewald et al., 2007; Ewald et al., 2008) Therefore, gemcitabine activates both ATR/Chk1 and ATM/Chk2 pathways.

Pharmacological inhibition or siRNA-mediated knockdown of Chk1, Chk2, ATR, ATM, Rad9, Rad17, Mre11 or Rad50 was shown to sensitize cells to gemcitabine-induced cell death (Duong et al., 2013; Ewald et al., 2007; Ewald et al., 2008; Fredebohm et al., 2013; Karnitz et al., 2005; Morgan et al., 2005; Parsels et al., 2009; Shi et al., 2001). Wee1 inhibition was also found to increase the anti-tumour efficacy of gemcitabine in p53-deficient pancreatic cancer xenografts, by triggering checkpoint abrogation and premature mitotic entry of gemcitabine-treated cells (Rajeshkumar et al., 2011). Azorsa et al. performed a synthetic lethality kinase screen in pancreatic cancer cells and identified Chk1 as the most significant sensitizing target for gemcitabine (Azorsa et al., 2009). The study also identified ATR siRNA as gemcitabine sensitizer, but in disagreement with other studies, ATM and Chk2 knockdown did not significantly alter gemcitabine cytotoxicity (Azorsa et al., 2009). Other kinases identified were CAMK1, STK6, PANK2 and EPHB1 (Azorsa et al., 2009). Extensive literature suggesting that Chk1 inhibition is a potent sensitizer of gemcitabine led to clinical evaluation of various Chk1 inhibitors in combination with gemcitabine in patients with solid tumours, lymphoma and pancreatic cancer (Garrett and Collins, 2011; Hosoya and Miyagawa, 2014). UCN-01, the first inhibitor to be clinically tested, was discontinued because of high toxicities and other inhibitors did not progress to Phase II trials, while SCH900776 in combination with gemcitabine demonstrated some encouraging results (Garrett and Collins, 2011; Hosoya and Miyagawa, 2014). Other Chk1 inhibitors are currently in clinical trials (http://www.clinicaltrials.gov).

Preclinical research showed that inhibition of Chk1 increases gemcitabine-induced DNA damage and triggers premature mitotic entry of gemcitabine-treated cells, leading to catastrophic mitosis and cell death (Garrett and Collins, 2011). In addition, Parsels et al. demonstrated that gemcitabine induces Rad51 foci formation in pancreatic cancer cells, which is prevented upon Chk1 inhibition and moreover, Chk1 inhibition abrogated recovery from gemcitabine-induced replication stress (Parsels et al., 2009). Similarly, another study demonstrated that Chk1 inhibition prevents gemcitabine-induced Rad51 foci formation and HR repair and increases sensitivity to gemcitabine and gemcitabine combined with radiation in pancreatic cancers (Morgan et al., 2010). Gemcitabine-induced upregulation of Rad51 was also observed in non-small-cell lung cancer (NSCLC) cells and downregulation of Rad51 increased sensitivity to gemcitabine and overcame drug resistance (Tsai et al., 2010). In agreement with a survival role of DNA repair, McNeely et al. found that besides premature mitotic entry, Chk1 inhibition promotes the conversion of stalled replication forks into DSBs triggering an ATM and DNA-PK response in HCT116 cells and inhibition of the DNA repair enzymes BRCA2 and XRCC3 increases sensitivity to gemcitabine combined with Chk1 inhibitor (McNeely et al., 2010). Interestingly, in a very recent study Jones et al. showed that following gemcitabine removal, Rad51 and BRCA2 are recruited to stalled replication forks and inhibit fork progression by triggering MUS81- and XPF-mediated fork processing that generates DSBs, suggesting a pro-death role for DNA repair (Jones et al., 2014). Another study found that deficiency in NER, NHEJ, BER or HR repair in Chinese hamster ovary (CHO) cells did not increase sensitivity towards gemcitabine (Crul et al., 2003). Therefore, it seems that there is some controversial evidence regarding the role of DNA repair in gemcitabine cytotoxicity, although abrogation of Rad51-mediated HR repair following Chk1 inhibition does correlate with increased sensitivity to gemcitabine.

Interestingly, two studies examined the ability of gemcitabine to re-activate epigenetically silenced genes. One study demonstrated that gemcitabine can inhibit DNA methyltransferase and activate expression of genes that are epigenetically silenced through DNA CpG methylation, such as VEGFR, RASSF1A and IGFBP3 in different cancer cells lines (Gray et al., 2012). Reactivation of an epigenetically silenced gene, target of methylation induced

silencing 1 (TMS1), by DNA methyltransferase inhibitors (DNMTi) was previously shown to increase sensitivity to gemcitabine (Ramachandran et al., 2010). Another study provided evidence that gemcitabine inhibits *GADD45A*-mediated de-methylation and activation of a reporter gene and can induce hypermethylation and silencing of the *MLH1* gene which is counteracted by Gadd45a (Schafer et al., 2010). The same group previously showed that Gadd45a together with the NER enzyme XPG mediates DNA de-methylation during DNA repair (Barreto et al., 2007). The authors suggested that gemcitabine functions to inhibit NER-mediated DNA de-methylation and activation of epigenetically silenced genes (Schafer et al., 2010). Of note, the synergy between cisplatin and gemcitabine is thought to be mediated by gemcitabine-induced inhibition of NER at sites of cisplatin-induced DNA lesions (Crul et al., 2003; Moufarij et al., 2003; Yang et al., 2000). Despite that the two studies are somewhat contradicting regarding the role of gemcitabine in epigenetic gene regulation which was suggested to be due to differences in drug concentration used, both studies concluded that gemcitabine does not affect the global DNA CpG methylation status (Gray et al., 2012; Schafer et al., 2010).

Achanta et al. previously demonstrated that a complex containing p53 and DNA-PK forms at gemcitabine-incorporated DNA sites preventing further DNA synthesis, and nuclear localisation of the complex coincided with induction of apoptosis (Achanta et al., 2001). Gemcitabine can induce both p53-dependent and independent apoptosis, although a functional p53 increases cell sensitivity to gemcitabine (Elnaggar et al., 2012). Regarding the mitochondrial apoptotic pathway, anti-apoptotic Bcl-XL levels correlate with chemoresistance and targeting of Bcl-XL or expression of the pro-apoptotic Bax increases gemcitabine-induced apoptosis (Elnaggar et al., 2012). The Fas-mediated extrinsic apoptotic pathway was also implicated in gemcitabine-induced apoptosis (Ferreira et al., 2000; Pace et al., 2000). Moreover, several studies demonstrated that the p38MAPK pathway is involved in gemcitabine-induced cytotoxicity in pancreatic cancer cell lines (Bu et al., 2012; Habiro et al., 2004; Koizumi et al., 2005) and a recent study showed that re-expression of p38MAPK overcomes resistance and decreases cell migration in urothelial carcinoma cell lines (Kao et al., 2014). Activation of NF-κB was previously

associated with resistance to gemcitabine through repression of nucleoside transporter gene transcription and stimulation of tumour-associated desmoplasia, and inhibition of the NF-κB pathway was shown by a number of studies to increase sensitivity to gemcitabine (de Sousa Cavalcante and Monteiro, 2014; Elnaggar et al., 2012).

Irinotecan

Irinotecan is a topoisomerase I inhibitor and, as mentioned previously, it acts to stabilize topoisomerase I cleavage complexes, which prevent DNA replication forks to proceed and can lead to the formation of DSBs. In line with its mode of action, several studies demonstrated that treatment with irinotecan causes DNA damage in the form of single- and double-strand breaks (Attia, 2012; Esselen et al., 2013; Petitprez et al., 2013) and induces a time- and dose-dependent increase in H2AX phosphorylation (Davidson et al., 2012; Ma et al., 2012; Petitprez et al., 2013; Rudolf et al., 2012; Rudolf et al., 2013; Takatori et al., 2012). In addition it was demonstrated that irinotecan activates the DDR kinases DNA-PK (Davidson et al., 2012), ATM, p38MAPK, Chk1 and Chk2 (Rudolf et al., 2012; Rudolf et al., 2013; Tse et al., 2007) and induces Rad51 foci formation (Davidson et al., 2012). Rudolf et al. further showed that irinotecan induces p53 phosphorylation leading to increased p53 transcriptional activity and p21 expression (Rudolf et al., 2012). Consistent with DDR activation, irinotecan causes a cell-cycle arrest which initiates as a cell accumulation in S-phase followed by a robust G2 arrest (Attia, 2012; Davidson et al., 2012; Hapke et al., 2002; Ma et al., 2012; Tse et al., 2007). Interestingly, a study showed that irinotecan induces abnormal and polyploid metaphases and formation of micronuclei, suggesting aberrant passage of DNA-damaged cells from mitosis (Attia, 2012).

Similar to gemcitabine, pharmacological inhibition of Chk1 induces premature mitotic entry of irinotecan-treated cells and increases irinotecan cytotoxicity (Ma et al., 2012; Tse et al., 2007). Interestingly, treatment with an inhibitor of the 90kDa heat shock protein (Hsp90), which has been implicated in irinotecan resistance, enhances irinotecan-induced cytotoxicity by abrogating the G2/M checkpoint through depletion of Chk1 and Wee1 (McNamara et al., 2012; Tse et

al., 2009). Chk1 and Hsp90 inhibition was evaluated in Phase I clinical trials in combination with irinotecan, but did not show significant patient responses (Fracasso et al., 2011; Tse et al., 2008).

Whole genome analysis in irinotecan resistant melanoma cell lines revealed a gain in the 14q23.2-31.1 amplicon, encompassing genes involved in DNA repair, such as *RAD51* and *MLH3*, and losses in the loci of DDR genes, such as *TP53, H2AFX* and *CHK1* (Gao et al., 2008). Another study however showed that MLH1 proficiency contributed to stronger irinotecan-induced DDR activation and G2/M arrest and, interestingly, sustained G1 arrest of tetraploid cells (Bhonde et al., 2010). The role of p53 in irinotecan-induced cytotoxicity is somewhat controversial, with some studies reporting involvement of p53 in irinotecan-induced apoptosis (Cao et al., 2010; Rudolf et al., 2012; Takeba et al., 2007) and others implicating p53 in reduced cell sensitivity to irinotecan (Bhonde et al., 2006; Ma et al., 2012).

The p38MAPK pathway has been the focus of several studies of irinotecan cytotoxicity. Rudolf et al. showed in response to high doses of irinotecan a transient and robust p38MAPK activation mediates irinotecan-induced apoptosis, whereas low doses of irinotecan activate a delayed p38MAPK response, whose inhibition increases irinotecan-induced cell death (Rudolf et al., 2013). Other studies found that endogenous p38MAPK activation contributes to irinotecan resistance (Gongora et al., 2008; Paillas et al., 2011) through induction of survival-promoting autophagy (Paillas et al., 2012) and inhibition of p38MAPK increases cell sensitivity to irinotecan (Paillas et al., 2011; Paillas et al., 2012).

Perspective

Collectively, both gemcitabine and irinotecan activate all three branches of the DDR; the ATM/Chk2, ATR/Chk1 and p38MAPK pathways. Chk1 inhibition increases the cytotoxicity of both drugs through checkpoint abrogation that leads to a catastrophic passage of DNA-damaged cells through mitosis. Moreover, p38MAPK activation is implicated in the cytotoxicity of both chemotherapeutic agents, albeit it can also be associated with resistance to

irinotecan. The role of DNA repair in gemcitabine and irinotecan cytotoxicity remains unresolved. Overall, more evidence is warranted to delineate the sequence of events that occur from drug-induced inhibition of DNA synthesis to activation of apoptotic pathways. A better understanding of how different cellular pathways impact on gemcitabine and irinotecan mechanism of action will enable development of improved treatment regimens for solid cancers.

1.3. Adenovirus

1.3.1. Adenovirus biology and life cycle

Human adenoviruses (Ad) belong to the *Adenoviridae* family, which consists of agents that are responsible for many respiratory, ocular and gastrointestinal diseases (Shenk, 2001). Currently there are more than 50 human adenovirus serotypes. These are classified into six subgroups (A to F) based on their ability to agglutinate red-blood cells, with subgroup C viruses, such as Ad2 and Ad5, being the most extensively studied (Leopold and Crystal, 2007; Russell, 2009; Shenk, 2001). The following literature review will be focused on adenovirus type 5 (Ad5).

The adenoviral genome (Figure 8) is approximately 36kb and is composed of linear, double-stranded DNA that does not integrate into host-cell DNA (Shenk, 2001). Adenoviruses have a non-enveloped icosahedral capsid, mainly consisting of the hexon and penton bases and the projecting fiber extensions (Figure 8) (Nemerow et al., 2009; Russell, 2009). The fiber binds the coxsackie adenovirus receptor (CAR) via the knob-domain, while penton binds to cell-surface integrins $\alpha_V\beta3$, $\alpha_V\beta5$, $\alpha_V\beta1$ and $\alpha_3\beta1$ (Goncalves and de Vries, 2006; Russell, 2009). The immunoglobulin CAR is the main receptor for adenovirus in epithelial cells, however, it is the binding to integrins via the arginine-glycine-aspartate (RGD) motif that mediates the internalization of virus into the host-cell (Leopold and Crystal, 2007; Russell, 2009). The heparin sulphate glycosoaminoglycans (HSGAGs) have also been reported to bind to species C adenovirus (Dechecchi et al., 2001). Other minor components of the capsid include the structural polypeptides IIIa, VI, VIII and IX, while several core proteins associate with the viral genome (Table 2 and Figure 8) (Russell, 2009).

Cell entry occurs within a few hours of infection via receptor-mediated endocytosis in clathrin-coated pits and macropinosomes, which pinch off the plasma membrane to generate endocytic vesicles (Leopold and Crystal, 2007; Medina-Kauwe, 2003). It has been suggested that endocytosis requires

reorganisation of the actin cytoskeleton mediated by activation of the Rho family of GTPases (Li et al., 1998a). The acidic environment of the endosomes induces conformational changes in the capsid leading to penton-dependent membrane penetration and rapid escape of the capsid into the cytosol (Leopold and Crystal, 2007; Medina-Kauwe, 2003). Once into the cytosol adenovirus capsid is transported along microtubules and interacts with the motor protein dynein to facilitate translocation to the nucleus (Leopold and Pfister, 2006). Intracellular trafficking towards the nucleus is also mediated by activation of the cAMP-dependent protein kinase A (PKA) and p38/MAPK signalling pathways (Medina-Kauwe, 2003). From the time of cell entry to nuclear docking, adenovirus capsid is progressively dismantled and this is important for cell entry, endosomal lysis and intracellular trafficking (Medina-Kauwe, 2003). When it reaches the nucleus, the capsid forms a stable interaction with the nucleus that involves nucleoporins (Nup) and the export receptor chromosome region of maintenance 1 (CRM1), leading to complete capsid uncoating (Le Sage and Mouland, 2013; Strunze et al., 2011). Dismantled capsid components are sequestered to the perinuclear envelope, while the protein VII-wrapped DNA (Figure 8) is imported into the nucleus with the help of hexon, viral core protein VII, histone H1, import receptor transportin 1, hsp70 and importin-α (Le Sage and Mouland, 2013; Leopold and Crystal, 2007). At this stage of the life cycle, protein VII acts to protect the Ad DNA from being recognised by the DNA damage and repair response, which would otherwise lead to ligation of Ad DNA into concatemers (discussed in section 1.3.2.) (Karen and Hearing, 2011; Schreiner et al., 2013b).

Once the adenovirus genome enters the nucleus it is associated with cellular histones, a process referred to as "chromatinization" of the Ad DNA (Giberson et al., 2012). Protein VI appears to stimulate initiation of viral transcription (Schreiner et al., 2012). Adenovirus gene transcription (Figure 8) occurs in early and late phases, defined by the onset of viral DNA replication, and it is mediated primarily by the cellular RNA Polymerase II complex (Shenk, 2001). Adenovirus 5 expresses at least 36 major proteins (Table 2). Notably, the functions of some of these proteins remain unknown or poorly defined. Upon initiation of early viral gene expression, which occurs through multiple promoters, the E1A gene is immediately and constitutively transcribed (Shenk,

2001). E1A expression is necessary for a productive viral infection (Jones and Shenk, 1979). Each early gene (E1A, E1B, E2A, E2B, E3 and E4) encodes several proteins mainly through differential splicing, that function to promote viral replication and protein synthesis, block host-cell protein synthesis and inhibit apoptosis and immune responses, with the ultimate goal of successful replication and virion production (Table 2) (Berk, 2005; Branton, 1999; Weitzman and Ornelles, 2005). Adenovirus DNA replication, which usually occurs by 6h post-infection, is mediated by the Ad DNA polymerase (Ad-Pol), the Ad DNA-binding protein (Ad-DBP) and the precursor terminal protein (pTP), all produced by the E2 genes (Table 2), but efficient DNA replication and elongation also requires the cellular transcription factors nuclear factor (NF) I, II and III (Goncalves and de Vries, 2006). The synthesis of viral DNA activates transcription of late genes from the major late promoter (MLP) (Figure 8) (Goncalves and de Vries, 2006). Late genes, expressed from the L1-L5 transcription units (Figure 8) (Boyer and Ketner, 1999), are mainly involved in the assembly of infectious virions (Table 2), which occurs in the nucleus by a complex process involving a series of maturation events and eventual loading of viral DNA into empty capsids (D'Halluin, 1995; Goncalves and de Vries, 2006). The adenovirus life cycle is completed within 20-24h and can produce up to 10,000 progeny virions per infected cell, which are subsequently released through cell lysis (Giberson et al., 2012; Shenk, 2001). The process of host cell lysis remains poorly understood, but it was shown to involve the E3-11.6K adenovirus death protein (ADP) and perhaps autophagy (Gros and Guedan, 2010).

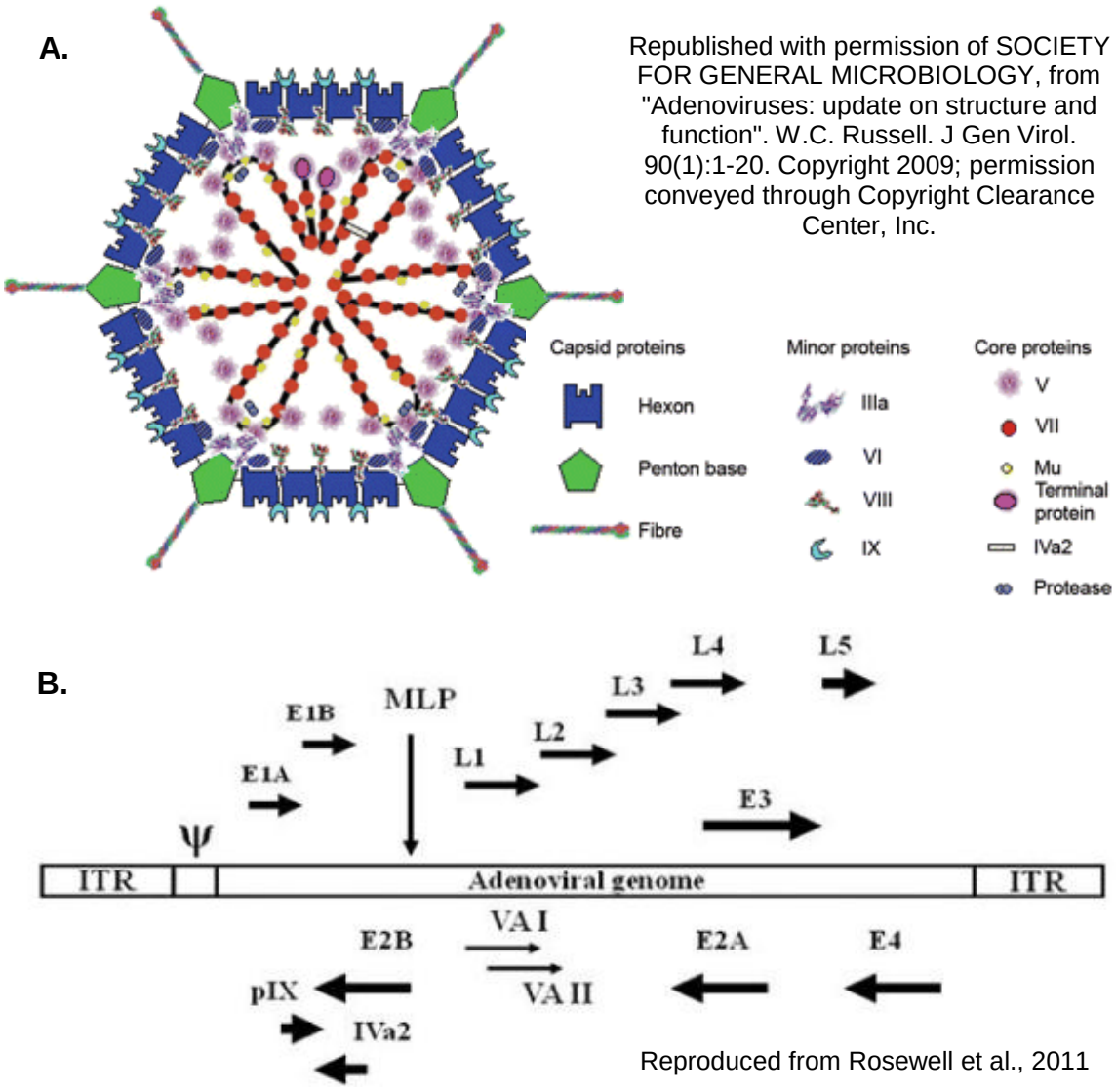

Republished with permission of SOCIETY FOR GENERAL MICROBIOLOGY, from "Adenoviruses: update on structure and function". W.C. Russell. J Gen Virol. 90(1):1-20. Copyright 2009; permission conveyed through Copyright Clearance Center, Inc.

Reproduced from Rosewell et al., 2011

Figure 8: Virion structure and schematic representation of adenovirus type 5 genome. (A) The virion structure of adenovirus 5 is based on cryo-electron microscopy and crystallographic studies. The adenovirus icosahedral capsid is composed of the major capsid proteins, hexon, penton and fibre, the minor capsid proteins and core proteins. The minor capsid protein pIX is located on the outside of the capsid, whereas pIIIa, pVI and pVIII are found in the inner surface. The core proteins pV, pVII and Mu interact with the double-stranded linear genome and the terminal protein coats the termini of adenovirus DNA. References (Nemerow et al., 2009; Russell, 2009). **(B)** The diagram represents the Ad5 genome with arrows illustrating the location and orientation of gene transcription. The genome termini are comprised of inverted terminal repeat (ITR) sequences incorporating the viral origin of replication. Also shown is the packing domain (ψ) involved in virus genome packing into capsids. There are six early RNA Pol II transcription units E1A, E1B, E2A, E2B, E3 and E4, which generate several mRNA transcripts by differential splicing and alternative start codon usage. The major late promoter (MLP) drives expression of a long transcript that produces the late mRNAs L1-L5 through alternative splicing and differential polyadenylation. pIX and IVa2 are intermediate genes. The small virus-associated (VA) I and II RNAs are synthesised by RNA Pol III and act to regulate mRNA translation. References (Goncalves and de Vries, 2006; Rosewell et al., 2011; Shenk, 2001).

Table 2: Adenovirus 5 proteins and their function

Protein	Gene	Function(s) during infection	References
E1A12S	E1A	• Induction of host DNA synthesis • Transcriptional regulation of genes involved in cell-cycle, apoptosis, inflammation, protein translation • Regulation of protein stability through interaction with the 26S proteasome • Induction of apoptosis	(Gallimore and Turnell, 2001; Weitzman and Ornelles, 2005; White, 2006)
E1A13S	E1A	• Transcriptional activation of host and viral genes	(Gallimore and Turnell, 2001)
E1B19K	E1B	• Inhibition of extrinsic and intrinsic apoptosis	(White, 2001; White, 2006)
E1B55K	E1B	• Inhibition of DNA-damage and repair response • Inhibition of p53-dependent apoptosis • Late viral mRNA nuclear export and translation • Blocking of host mRNA nuclear export and protein synthesis	(Weitzman and Ornelles, 2005; White, 2001)
DBP	E2A	• Replication initiation and elongation • Transcriptional regulation • DNA recombination • Virus assembly	(Goncalves and de Vries, 2006; Weitzman and Ornelles, 2005)
Pol	E2B	• DNA polymerisation/replication	(Goncalves and de Vries, 2006)
pTP	E2B	• DNA replication (serves as primer)	(Goncalves and de Vries, 2006)
E3-12.5K	E3	• Uknown	
E3-11.6K (ADP)	E3	• Cell lysis	(Gros and Guedan, 2010)
E3gp19K	E3	• Inhibition of MHC class I cell-surface expression by binding and retaining the heavy chain in endoplasmic reticulum (ER) • Inhibition of the processing of peptides presented by class I MHC • Sequestration of natural killer cell ligands	(Goncalves and de Vries, 2006; Horwitz, 2004; McSharry et al., 2008)
E3-6.7K (CR1α)	E3	• Inhibition of extrinsic apoptosis through TRAIL-R2 internalization and degradation in lysosomes • Directs E3gp19K to ER	(Lichtenstein et al., 2004a; Lichtenstein et al., 2004b; Wilson-Rawls et al., 1994)
E3-10.4K (RIDα)	E3	• Inhibition of extrinsic apoptosis through death receptor internalization and degradation in lysosomes • Inhibition of TNF-induced secretion of arachidonic acid, production of chemokines and NF-κB signal transduction	(Horwitz, 2004; Russell, 2000)
E3-14.9K (RIDβ)	E3	• Inhibition of extrinsic apoptosis through death receptor internalization and degradation in lysosomes • Inhibition of TNF-induced secretion of	(Horwitz, 2004; Russell, 2000)

		arachidonic acid, production of chemokines and NF-κB signal transduction	
E3-14.7K	E3	• Inhibition of TNFα-induced secretion of arachidonic acid	(Horwitz, 2004; Russell, 2000)
E4orf1	E4	• Growth induction through PI3K/mTOR pathway activation	(Weitzman and Ornelles, 2005)
E4orf2	E4	• Unknown	(Russell, 2000)
E4orf3	E4	• Re-organisation of PML bodies • Inhibition of DNA-damage and repair response • Facilitation of S-phase DNA replication	(Weitzman and Ornelles, 2005)
E4orf4	E4	• Growth induction through PI3K/mTOR pathway activation • Disruption of PP2A functions	(Weitzman and Ornelles, 2005)
E4orf6/7	E4	• Inhibition of DNA-damage and repair response • Inhibition of NHEJ DNA repair • Late viral mRNA nuclear export and translation • Blocking of host mRNA nuclear export and protein synthesis • Viral DNA replication	(Weitzman and Ornelles, 2005)
E4-34K	E4	• Uknown	
pIVa2	IVa2	• DNA encapsidation/packing • Activation of late viral gene transcription	(Davison et al., 2003; Goncalves and de Vries, 2006)
pIX	IX	• Cementing of virion structure • Stabilization of capsid	(Goncalves and de Vries, 2006)
Hexon (pII)	L3	• Formation and structure of the virion • Binding of coagulation factors	(Davison et al., 2003; Russell, 2009)
Penton (pIII)	L4	• Cell attachment via integrins • Virus internalization and release from endosome • Formation and structure of the virion • Stabilization of capsid	(Goncalves and de Vries, 2006)
Fiber (pIV)	L5	• Cell attachment via CAR and HSGAG • Blood factor attachment • Formation and structure of the virion	(Goncalves and de Vries, 2006; Russell, 2009)
23K protease	L3	• Cleavage of precursors to produce the mature structural proteins • Virion assembly • Capsid uncoating • Facilitation of cell lysis	(Goncalves and de Vries, 2006; Russell, 2009)
22K	L4	• DNA encapsidation/packaging	(Russell, 2009)
33K	L4	• Formation and structure of the virion	(Davison et al., 2003)
100K	L4	• Formation and structure of the virion • Blockage of protein translation initiation	(Davison et al., 2003; Weitzman and Ornelles, 2005)

Protein IIIa	L1	• Cementing of virion structure	(Davison et al., 2003; Goncalves and de Vries, 2006)
Protein V	L2	• Bridging of viral core and capsid • Possible role in revealing viral DNA for replication and transcription	(Russell, 2009)
Protein VI	L3	• Cementing of virion structure • Disruption of endosomal membrane • Virus maturation	(Davison et al., 2003; Goncalves and de Vries, 2006; Russell, 2009)
Protein VII	L2	• Formation and structure of the virion • DNA encapsidation • Nuclear import of viral DNA • Reduction of early transcription	(Davison et al., 2003; Goncalves and de Vries, 2006; Russell, 2009)
Protein VIII	L4	• Cementing of virion structure	(Davison et al., 2003; Goncalves and de Vries, 2006)
μ or Mu (polypeptide X)	L2	• Cementing of virion structure • Precursor in modulating expression from E2 • DNA packaging	(Davison et al., 2003; Goncalves and de Vries, 2006)
52/55K	L1	• DNA encapsidation	(Goncalves and de Vries, 2006; Russell, 2009)

1.3.2. Regulation of cell-cycle and apoptosis by adenoviral proteins

Adenovirus E1A: Rewiring the host

The adenovirus E1A can be viewed as a viral molecular hub (Pelka et al., 2008) that acts to reprogram host cell gene expression, promote cell-cycle progression and block differentiation, by interacting with a plethora of cellular factors; at least 50 have been identified to date (Berk, 2005; Frisch and Mymryk, 2002; Gallimore and Turnell, 2001; Yousef et al., 2012). The E1A gene encodes five polypeptides (13S, 12S, 11S, 10S and 9S), two of which are the most abundant: the 12S and 13S proteins (Stephens and Harlow, 1987; Ulfendahl et al., 1987). These differ in the conserved region 3 (CR3) which is absent in 12S, while conserved regions 1, 2 and 4 (CR1,2, and 4) are present in both E1A proteins (Gallimore and Turnell, 2001; Pelka et al., 2008). E1ACR3 mediates transcriptional activation of viral and host-cell genes, by binding to

numerous transcription factors and co-factors, including ATF, C-Jun and SP1, as well as the basic transcriptional machinery, including the TATA binding protein (TBP) (Berk, 2005; Jones, 1995; Mymryk and Smith, 1997; Pelka et al., 2008).

The CR1 and CR2 regions have a number of functions, including induction of apoptosis and inhibition of differentiation, but one of the most important functions in the context of infection is deregulation of the cell cycle that promotes S-phase entry (Gallimore and Turnell, 2001). This is largely mediated through interaction with the tumour-suppressor pRb, pRb family members (p107, p130) and the transcriptional co-activator p300/CPB, by binding of the CR2 and CR1 regions (Figure 9) (Felsani et al., 2006; Gallimore and Turnell, 2001). E1A CR2 and CR1 regions interact with the hyperphosphorylated form of pRb displacing E2F, thus enabling E2F-mediated transcription of S-phase genes, such as cyclin A and E (Felsani et al., 2006). The interaction with pRb also displaces histone deacetylases (HDACs) and the BRG1 component of the SWI/SNF chromatin remodelling complex, that are recruited by pRb to repress transcription of target genes (Frisch and Mymryk, 2002).

Another transcriptional co-repressor complex that can be recruited by pRb to suppress E2F-mediated transcription is the CtBP and CtIP (Chinnadurai, 2002). E1A binding to CtBP1/2 displaces CtBP-recruited DNA-binding repressor proteins, such as HDACs, leading to de-repression (Frisch and Mymryk, 2002; Yousef et al., 2012). It has been suggested that E1A might compete with CtIP for binding to CtBP (Schaeper et al., 1998). E1A also directly binds CtIP disrupting the CtIP/Rb and CtIP/p130 complexes (Bruton et al., 2007). Moreover, E1A recruits p300/CBP, which has histone acetyltransferase (HAT) activity, and utilizes it to acetylate CtBP, which reduces its repressor ability (Yousef et al., 2012). CtBP1/2 regulates genes involved in growth, survival and apoptosis and is responsible for repression of the pro-apoptotic genes *BAX* and *NOXA,* the epithelial gene *E-Cadherin*, and the tumour suppressor *PTEN* (Chinnadurai, 2009). It is possible that the interaction of E1A with CtIP might stimulate S-phase entry independently of pRb transcriptional regulation, as Chen et al. previously proposed that CtIP directly counteracts Rb restraint (Chen et al., 2005).

E1A binding to the chromatin remodelling factor and transcriptional co-activator p300/CBP can result in both stimulation of p300/CBP HAT activity and inhibition, depending on the target promoter (Gallimore and Turnell, 2001). For example, it has been reported that the CR3 region in E1A13S protein recruits p300 to activate transcription of viral genes (Pelka et al., 2009). p300/CBP activates p53-mediated transcription of target genes, both by acting as a transcriptional co-activator and by acetylating p53 (Grossman, 2001). In the context of the transcription factor p53, E1ACR1 binding to p300/CBP acts to inhibit its function, thus preventing p53-dependent transcriptional activation and subsequent cell-cycle arrest (Frisch and Mymryk, 2002). Similar to p300/CBP, the CR1 region interacts with the p300/CBP-associated factor (P/CAF) inhibiting its HAT activity, which is required for acetylation of p53 that stimulates p53 binding to promoters of target genes, such as the CKI p21 (Frisch and Mymryk, 2002). It was also reported that E1A-mediated p300 inhibition upregulates the transcription factor c-MYC and subsequently c-MYC-dependent transcription of genes involved in DNA-synthesis (Baluchamy et al., 2007; Kadeppagari et al., 2009; Kolli et al., 2001). Moreover, it was demonstrated that E1A binding to p300/CBP disrupts the interaction of p300/CBP with the APC/C complexes APC5 and APC7, which normally leads to stimulation of p300/CBP HAT activity and subsequent stimulation of p300/CBP-dependent transcription (Turnell and Mymryk, 2006; Turnell et al., 2005). E1A interference with the p300/CBP-APC/C complex inhibited p53-mediated expression of $p21^{CIP1/WAF1}$ and promoted cellular transformation (Turnell and Mymryk, 2006; Turnell et al., 2005).

Another transcriptional regulator complex interacting with E1A is the Transformation/transcription domain-associated protein (TRRAP) and ATPase p400, a member of the SWI/SNF family of chromatin remodelling enzymes (Fuchs et al., 2001). p400, in complex with other chromatin remodelling factors, mediates repression of p21 transcription (Chan et al., 2005) and by inducing p400 E1A might promote p21 repression contributing to inhibition of growth arrest (Samuelson et al., 2005). In addition to suppressing p21 expression, E1A directly binds and inhibits p21 (Chattopadhyay et al., 2001) and the CKI $p27^{kip1}$ (Mal et al., 1996), which would otherwise inactivate Cdk-Cyclin complexes to arrest cells at the G1/S and/or G2/M transitions (Figure 9) (Berk, 2005).

Singhal et al. investigated the effects of E1A on cellular DNA replication and demonstrated that E1A induces the upregulation of genes involved in DNA replication, such as Ctd1, Cdc6, MCM3,4, RFC5, PCNA, PolE2, CyclinE2 and E2F2 (Singhal et al., 2013). The gene upregulation and the capacity to induce replication initiation were significantly higher than in serum-stimulated cells (Singhal et al., 2013). It was further demonstrated that E1A accelerates replication fork progression during early S-phase and induces massive DNA re-replication accompanied by the accumulation of cells with >4N DNA content (Singhal et al., 2013). These effects were partly attributed to the ability of E1A to bind p300/CBP and dissociate the repressor complex present at Myc promoter, leading to Myc induction (Kadeppagari et al., 2009; Sankar et al., 2008; Singhal et al., 2013).

In contrast to the N-terminus, the C-terminus of E1A has been poorly studied and besides the interaction with CtBP, much less is known about the function of C-terminal binding proteins (Yousef et al., 2012). E1ACR4 was reported to bind the pro-survival dual-specificity tyrosine (Y) phosphorylation-regulated kinases (DYRK) 1A and 1B, stimulating their activity, although the functional consequence of the interaction remains unresolved (Pelka et al., 2008; Yousef et al., 2012). DYRKs regulate multiple cellular processes, including survival, proliferation and differentiation (Aranda et al., 2011). DYRK1A/1B exert anti-apoptotic functions, for example by inhibiting caspase-9, and phosphorylate and activate p53 in response to DNA damage (Aranda et al., 2011). Komorek et al. observed that an E1A mutant defective in DYRK1A/1B binding has increased proliferation, transformation and tumour-forming capacities, suggesting that the interaction with DYRKs might suppress E1A-induced proliferation (Komorek et al., 2010). Yousef et al. proposed that E1A interaction with DYRK1A/1B might explain the E1A-mediated inhibition of Rac1 signalling in Ras-transformed cells (Yousef et al., 2012).

Besides DYRKs, the transcription factors Forkhead Box K1 and K2 (FOXK1/2) were also reported to interact with the CR4 region (Komorek et al., 2010). Similar to DYRKs, deleting the FOXK1/2 interacting domain resulted in increased S-phase accumulation and transformation, implying that FOXK1/2 interaction with E1A acts to suppress E1A-induced proliferation (Komorek et al.,

2010). The FOXK1 transcription factor has been associated with transcriptional repression of the p21 and Foxo4 genes in myogenic progenitor cells (Hawke et al., 2003; Shi et al., 2010) and of some serum response factor (SRF)-regulated genes (Freddie et al., 2007). Grant et al. reported that FOXK1 mediates expression of genes involved in G1/S and G2/M transitions (Grant et al., 2012). FOXK2 was proposed to activate IL-2 transcription (Nirula et al., 1997) and promote AP-1-dependent transcription regulation (Ji et al., 2012). Interestingly, FOXK2 was reported to function as a G/T-mismatch DNA-binding protein and become hyperphosphorylated during mitosis in a Cdk-Cyclin dependent manner (Marais et al., 2010). It will be interesting to determine how interaction of E1A with FOXK1/2 impinges on these functions.

Induction of apoptosis by E1A

Besides promoting an S-phase cell state, expression of E1A can induce apoptosis through p53-dependent and -independent mechanisms. The ability of E1A to induce apoptosis is mediated through accumulation of p53, degradation of anti-apoptotic proteins (White, 2006) and hijacking of Myc-dependent transcription via p400 (Chakraborty and Tansey, 2009).

E1A stabilizes p53 in a number of ways (Figure 9) [reviewed in (Gallimore and Turnell, 2001)]. Firstly, inhibition of pRb by E1A leads to stimulation of E2F-mediated transcription of $p19^{ARF}$, an Mdm2 inhibitor, thereby preventing Mdm2-induced p53 degradation (de Stanchina et al., 1998; Sherr, 1998). Secondly, E1A-mediated p300 inhibition also prevents Mdm2-induced p53 degradation, since p300 contributes to Mdm2-induced p53 degradation by either directly binding to p53/Mdm2 or mediating Mdm2 transactivation by p53 (Grossman et al., 1998; Thomas and White, 1998). Thirdly, E1A interacts with and inhibits the ATPase function of the 19S proteasomal regulatory complex leading to increased p53 stability (Turnell et al., 2000; Zhang et al., 2004).

Independently of p53, it was demonstrated that in DNA-damaged cells E1A binds and inhibits the CKI p21, abrogating G1/S arrest and promoting apoptosis (Chattopadhyay et al., 2001). It was recently shown that in response to DNA damage CtIP binds to p21 promoter and activates p21 transcription (Liu et al.,

2014). By interacting with CtIP E1A might displace CtIP from p21 promoters to prevent expression.

The second mechanism of E1A-induced apoptosis involves E1A-mediated degradation of MCL-1. This leads to release of the pro-apoptotic protein BAK from MCL-1, thus allowing it to form complexes with the pro-apoptotic BAX protein at the mitochondrial membrane (Figure 9) (Cuconati et al., 2003). E1A also activates the extrinsic-apoptotic pathway. It can sensitize cells to TNF-α-induced apoptosis, by stimulating the degradation of the anti-apoptotic molecule c-FLIP, thereby allowing TNF-α-mediated caspase-8 activation (Figure 9) (White, 2001).

The third mechanism by which E1A promotes apoptosis depends on its interaction with p400 (Samuelson et al., 2005). It was demonstrated that p400 is required for E1A to induce apoptosis and this is likely the result of p400-E1A interaction promoting p400 association with Myc, stabilizing Myc and stimulating Myc-dependent transcription of apoptotic genes (Chakraborty and Tansey, 2009; Samuelson et al., 2005; Tworkowski et al., 2008).

In addition to E1A, overexpression of one of the products of the E4 transcription unit, E4orf4, induces p53-independent cell-death, with many features of classical apoptosis although requirement for caspase activation was shown to be cell-line dependent (Lavoie et al., 1998; Livne et al., 2001; Marcellus et al., 1998; Robert et al., 2002; Shtrichman and Kleinberger, 1998). Induction of cell death by E4orf4 was shown to depend on its interaction with PP2A (see below) (Li et al., 2009a; Li et al., 2009b; Shtrichman et al., 1999; Shtrichman et al., 2000).

Inhibition of apoptosis by anti-apoptotic viral proteins

In the context of a viral infection, E1A-induced apoptosis is inhibited by the E1B19K and E1B55K proteins, in order to allow productive adenoviral replication (Figure 10) (White, 2001). E1B55K binds and inhibits the function of p53, thus preventing p53-mediated cell-cycle arrest and apoptosis (Berk, 2005). On the other hand, the anti-apoptotic protein E1B19K can inhibit both p53-

dependent (Debbas and White, 1993; Lomonosova et al., 2005) and -independent apoptosis (Chiou and White, 1997; White et al., 1991) and block death-receptor-mediated apoptosis in response to TNF-α, FasL and TRAIL (Gooding et al., 1991; Hashimoto et al., 1991; Tollefson et al., 2001; White et al., 1992). Early studies showed that infection of cells with adenoviruses mutated in the E1B19K gene results in the large plaque phenotype (*lp*) characterised by cellular large clear plaques, the cytocidal (*cyt*) phenotype, characterised by enhanced cytopathic effect, and the degradation (*deg*) phenotype characterised by degradation of cellular and viral DNA (Chinnadurai, 1983; Pilder et al., 1984; Subramanian et al., 1984; Takemori et al., 1984; White et al., 1984). It was later discovered that the enhanced cytopathic effect and the DNA degradation were hallmarks of apoptosis induced by E1A due to lack of E1B19K anti-apoptotic functions (White et al., 1991; White and Stillman, 1987). E1B19K is a Bcl-2 homologue and exerts its anti-apoptotic functions by binding BAK and BAX proteins, preventing oligomerization and pore formation in the mitochondrial membrane which would otherwise lead to the release of pro-apoptotic proteins, such as cytochrome c, from the mitochondria and subsequent activation of caspases (Figure 9) (White, 2006). Inhibition of caspase activation by E1B19K prevents cleavage of apoptotic nucleases, which is necessary during infection to avoid degradation of viral and host-cell DNA (White, 2001). By blocking mitochondrial membrane permeabilization, E1B19K efficiently prevents apoptosis in response to various stimuli that converge on the mitochondria affecting their membrane integrity (White, 2006). In addition to its anti-apoptotic functions, it was demonstrated that E1B19K binds the autophagy protein Beclin-1, disrupts its interaction with Bcl-2 and recruits the C3 catalytic subunit of PI3K (PI3KC3), leading to autophagosome formation (Piya et al., 2011). E1B19K deletion subsequently impaired the ability of adenovirus to induce autophagy (Piya et al., 2011).

The E3 region of adenovirus encodes several proteins that primarily function to evade anti-viral immune responses (Windheim et al., 2004). The E3gp19K protein counteracts immune responses by inhibiting the cell surface expression of the class I major histocompatibility complex (MHC) and by sequestering natural killer cell ligands (Table 2) (Horwitz, 2004; McSharry et al., 2008). Other E3 proteins antagonize pro-apoptotic immune responses by promoting death

receptor internalization and degradation in lysosomes and by inhibiting TNF-induced secretion of arachidonic acid, production of chemokines and NF-κB signal transduction (Table 2) (Horwitz, 2004; Lichtenstein et al., 2004b). In contrast to the other E3 proteins, ADP (E3-11.6kDa) has pro-death functions and is expressed in the late stages of infection to stimulate cell lysis, through non-apoptotic mechanisms (Braithwaite and Russell, 2001; Lichtenstein et al., 2004b). Besides E1B19K and E3 proteins, it was recently shown that E4orf3 and E1B55K act to suppress AIF release from mitochondria and subsequent nuclear entry that leads to nuclear fragmentation, a process that requires activation of PARP-1 (Turner et al., 2014).

Regulation of DNA damage and repair response by adenoviral proteins

Cells infected with adenoviruses stimulate a DNA damage response (DDR) (Figure 9) that needs to be counteracted by the virus in order to enable efficient viral replication (Turnell and Grand, 2012). It has been suggested that the presence of the viral DNA is sufficient to trigger a DDR and it has been shown that viral DNA replication is sufficient to cause phosphorylation of H2AX and activate PARP-1 (Nichols et al., 2009; Turner et al., 2014).

The E4 transcription unit expresses the E4orf 1 to 6/7 polypeptides that have a variety of functions, including enhancing late viral mRNA and protein synthesis, while shutting-off host-cell protein synthesis (Tauber and Dobner, 2001). The most important function for the E4 proteins is evasion of the DDR (Tauber and Dobner, 2001). Infection with E4-deleted adenoviruses stimulates a DDR, since, from a simplistic perspective, the linear double-stranded viral genome is recognised as DSBs by the MRN complex (Weiden and Ginsberg, 1994; Weitzman and Ornelles, 2005). Recognition of viral DNA initiates an ATR- and ATM-mediated signalling cascade, eventually leading to concatemerization of viral DNA through the actions of DNA-PK, DNA ligase IV and Mre11 (Boyer et al., 1999; Carson et al., 2009; Carson et al., 2003; Weiden and Ginsberg, 1994; Weitzman and Ornelles, 2005). During infection, several proteins of the ATR signalling axis, including RPA32, ATR, ATRIP, Rad9, TOPBP1, Rad17 and BLM localize to viral replication centres and it is possible that this results in

inhibition of their functions (Blackford et al., 2008; Carson et al., 2009; Carson et al., 2003; Turnell and Grand, 2012).

E4orf3 and E4orf6 proteins independently inhibit the DDR signalling by targeting the MRN complex (Figure 9) (Carson et al., 2009; Stracker et al., 2002). E4orf3 promotes the reorganization of promyelytic leukaemia (PML) nuclear bodies into track-like structures, whereby it sequesters Mre11 in track-like nuclear structures and cytoplasmic aggresome-like structures (Araujo et al., 2005; Carson et al., 2009; Stracker et al., 2002). By redistributing the MRN complex E4orf3 inhibits ATR signalling (Carson et al., 2009). On the other hand, E4orf6 in a complex with E1B55K recruits ubiquitin ligases that target Mre11, Rad50, Nbs1, p53 as well as the BLM helicase for degradation in aggresomes (Harada et al., 2002; Orazio et al., 2011; Querido et al., 2001; Stracker et al., 2002; Turnell and Grand, 2012). Independently of E1B55K, E4orf3 was found to form nuclear structures whereby histone H3 methylation (Lys9) induced heterochromatin compaction at p53 target promoters, leading to abrogation of p53 DNA binding and silencing of p53-mediated transcription (Soria et al., 2010).

In addition, E4orf6 acts to dissociate the NHEJ repair DNA ligase IV/XRCC4 complex (Jayaram et al., 2008) and the E4orf6/E1B55K complex targets the protein DNA ligase IV for degradation, thereby preventing the ligation step during NHEJ (Baker et al., 2007). E4orf6/E1B55K were found to interact with DNA-PK (Boyer et al., 1999) although no impairment of DNA-PK function has so far been reported in the presence of the viral proteins. Cells stably expressing E4orf6 showed reduced DSB repair capacity in response to IR (Hart et al., 2005). More recently, the E1B55K/E4orf6 complex was found to target the survival-time associated PHD protein in ovarian cancer 1/PHF13 (SPOC-1) and the acetyltransferase TIP60 for degradation (Gupta et al., 2013; Schreiner et al., 2013b). Recent reports suggest that SPOC-1 regulates chromatin compaction and is recruited to DSBs in an ATM-dependent manner where it modulates the choice of NHEJ and HR and kinetics of DNA repair by interacting with other chromatin remodelling factors, such as KAP1 (Kinkley et al., 2009; Mund et al., 2012). Similarly, TIP60 functions in chromatin remodelling, transcriptional regulation and DNA damage and repair response, during which it

acetylates and activates ATM and remodels chromatin to facilitate DNA repair (Sun et al., 2010). Both SPOC-1 and TIP60 were shown to suppress viral gene expression (Gupta et al., 2013; Schreiner et al., 2013b), therefore Ad5-mediated degradation of these factors promotes chromatin relaxation and enhances viral gene transcription. At the same time, degradation of TIP60 should impair ATM activation and degradation of both SPOC-1 and TIP60 would impact on DNA repair (Figure 9). Interestingly, TIP60 associates with the E1A-interacting protein complex p400/TRRAP, which was reported to be recruited to DSBs through Mdc1 and to modulate chromatin structure promoting recruitment of other factors required for DSB repair (Xu et al., 2010a).

Despite targeting of various DDR components, viral infection results in phosphorylation of H2AX and RPA32 (Nichols et al., 2009; Turnell and Grand, 2012). This can be explained partly by the presence of the E1B55K-binding protein E1B-AP5 or hnRNPUL1 at viral replication centres. Blackford et al. showed that E1B-AP5/hnRNPUL1 interacts with ATR, ATRIP and RPA32 in viral replication centres and mediates phosphorylation of RPA32 by ATR (Blackford et al., 2008). hnRNPUL1/2 proteins were reported to be recruited to DSBs by the MRN complex and PARP-1 where they stimulate DNA-end resection, ATR-dependent signaling and DSB repair (Hong et al., 2013; Polo et al., 2012). hnRNPUL1/2 might also regulate PARP-1 transcription (Hong et al., 2013).

The E1A interacting protein CtIP has emerged as an important player in DSB repair. As previously mentioned, the CtIP endonuclease acts together with the MRN complex to resect DNA ends during DSB repair. Expression of AdE1A12S or AdE1A13S was reported to inhibit phosphorylation of CtIP (Bruton et al., 2007), which is mediated by ATM and/or ATR, although it is uncertain whether this is due to the direct interaction of E1A with CtIP or an indirect mechanism. One might speculate that E1A can sequester CtIP from sites of cellular DSBs thus impairing DNA repair.

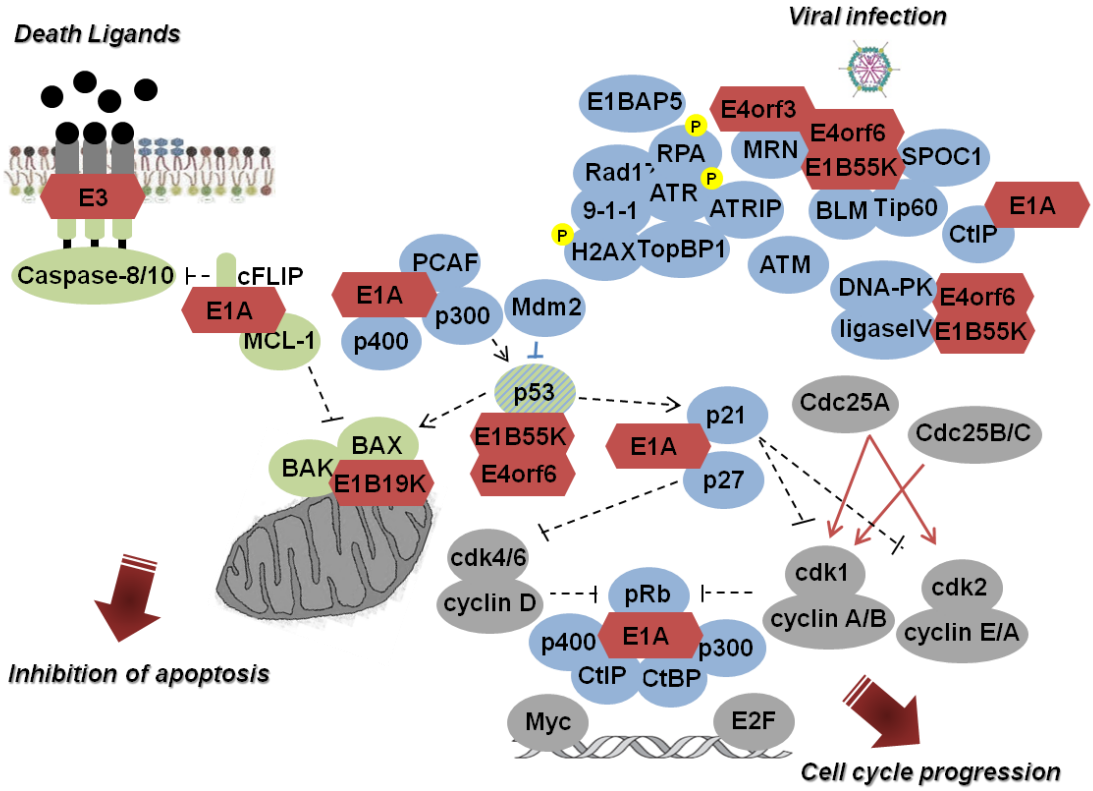

Figure 9: Regulation of cell cycle and apoptosis by adenoviral proteins. Adenovirus infection ultimately leads to S-phase entry, inactivation of DNA damage and repair responses and inhibition of apoptosis. E1A acts to stimulate S-phase entry through inhibition of pRb and the CKIs p21 and p27, as well as dissociation of chromatin remodelling and HAT factors, including p300/CBP, CtBP, CtIP and p400 (see text for details). This leads to activation of E2F- and Myc-dependent transcription of cell-cycle genes. In addition, E1A stabilizes p53 and inhibits the anti-apoptotic proteins c-FLIP and MCL-1. However, induction of apoptosis is efficiently counteracted by E1B19K, E4orf6/E1B55K and E3 viral proteins. E1B19K and E3 proteins inhibit intrinsic and extrinsic apoptotic pathways as depicted on the diagram, while E4orf6/E1B55K blocks p53-dependent apoptosis. E4orf3 and the E4orf6/E1B55K complex are predominantly responsible for inactivation of a DNA damage and repair response that is initiated following viral infection. E4orf3 sequesters the Mre11 subunit of MRN complex in PML nuclear tracks and E4orf6/E1B55K target Mre11, Nbs1, p53, BLM, Tip60, SPOC-1 and ligase IV for proteasomal degradation (see text for details). E4orf6/E1B55K also interact with DNA-PKs and inhibit NHEJ repair.

Other cellular factors targeted by adenoviral proteins

E4orf3 reorganizes the TIF1α/TRIM24 into the PML-containing nuclear tracks (Yondola and Hearing, 2007) and targets TIF1γ/TRIM33 for proteasomal degradation (Forrester et al., 2012). TIF1α/TRIM24 is overall associated with chromatin silencing (Ikeda and Inoue, 2012; Napolitano and Meroni, 2012) and interestingly, it is a E3 ubiquitin ligase targeting p53 for degradation but in response to DNA damage undergoes ATM-dependent degradation (Jain et al., 2014). TIF1γ/TRIM33 is also associated with transcriptional repression (Agricola et al., 2011) and has been implicated in the regulation of TGF-β signalling (Fattet et al., 2013) and PARP-dependent DNA damage response (Kulkarni et al., 2013). E1B55K interacts with another member of the TIF family, TIF1β/KAP1/TRIM28, which is required for DSB repair during which it gets phosphorylated by ATM (Forrester et al., 2012). The functional consequences of the E1B55K-TIF1β interaction are unknown, but it could be possible that the interaction further disrupts DSB repair signalling. It is likely that the TIF family members possess anti-viral activities; TIF1γ was shown to attenuate viral gene expression (Forrester et al., 2012) and other TRIM family members function in antiviral immune response (Jefferies et al., 2011).

Another protein targeted for degradation is the death-domain-associated protein (Daxx). Daxx is a PML-interacting protein that binds to other chromatin remodelling proteins, such as ATRX and HDACs, to repress transcription of various genes, including NF-κB, E2F1 and p53, but it also regulates apoptosis (Salomoni, 2013; Salomoni and Khelifi, 2006). In addition it interacts with Mdm2 and promotes p53 degradation, although during DNA damage the interaction is disrupted by an ATM-mediated phosphorylation event (Tang et al., 2013). Daxx was shown to repress Ad5 replication and together with its binding partner ATRX acts to inhibit viral gene expression (Schreiner et al., 2013a; Schreiner et al., 2010). Schreiner et al. showed that Daxx acts to suppress the immediate early E1A promoter and that core protein VI inhibits Daxx to enable initiation of viral transcription (Schreiner et al., 2012). As early viral proteins are synthesised Daxx is targeted by E1B55K that recruits E3 ubiquitin ligases, independently of E4orf6, to target Daxx for degradation. The E1B55K/E4orf6 complex also

targets ATRX for proteasomal degradation (Schreiner et al., 2013a; Schreiner et al., 2010).

Effects of adenovirus on mitosis

Regulation of mitosis by adenovirus is poorly studied and the current literature on how adenovirus might affect mitotic progression is scarce. Interestingly, in a microarray gene expression analysis in Ad5-infected cells it was revealed that mitosis-associated genes were significantly upregulated throughout the viral life cycle (Miller et al., 2007). Such genes encoded for subunits of the anaphase promoting complex, mitotic checkpoint proteins and proteins that regulate spindle formation, chromosome condensation and chromosome segregation (Miller et al., 2007).

Several studies reported that adenovirus infection can cause mitotic abnormalities (Braithwaite et al., 1983; Cherubini et al., 2006; Connell et al., 2008; Ingemarsdotter et al., 2010; Lavia et al., 2003; Murray et al., 1982). Adenovirus alters the microtubule cytoskeleton and stabilizes microtubules in the early hours post-infection in order to promote its transport towards the nucleus (Warren et al., 2006). Despite that adenovirus utilizes microtubules for trafficking, adenoviral particles were not found to be associated with spindle and astral microtubules during mitosis (Strunze et al., 2005). Ingemarsdotter et al. observed that altered organisation of microtubules and stabilization was still evident at 48h post-infection with a replication-selective adenovirus and interestingly, reported that the microtubule network is important for adenoviral non-lytic cell exit (Ingemarsdotter et al., 2010).

Cherubini et al. demonstrated that an E1B55K-deleted adenovirus and to a lesser extend wild-type Ad5 induce polyploid cells and hypercondensed mitotic chromosomes and upregulate the SAC protein Mad2 (Cherubini et al., 2006). Moreover, the oncolytic virus *dl*922-947 was reported to cause chromosome alignment issues, spindle multipolarity and cytokinesis failure (Connell et al., 2008). In another study, expression of E1A induced polyploidy, prolonged mitosis and chromosome segregation defects (Hernando et al., 2004). The authors observed that Mad2 expression was upregulated and suggested that

this could be due to E1A-mediated deregulation of the Rb/E2F pathway, since Mad2 transcription was found to be regulated by E2F (Hernando et al., 2004). Another study reported that E1A utilizes the CBF/NF-Y transcription factors to stimulate the expression of Cdk1 (Kao et al., 1999).

E1A can induce centrosome amplification and subsequent multipolar spindles and this was shown to require a functional RanGTPase network (De Luca et al., 2003; Lavia et al., 2003). The RanGEF RCC1 promotes the active and predominantly nuclear GTP-bound form of Ran, whereas RanGAPs and RanBP1/2 (Ran-binding proteins 1/2) stimulate the GTPase activity of Ran, promoting the inactive GDP-bound form which primarily localises in the cytoplasm (Clarke and Zhang, 2008). Besides the role of RanGTPase in interphase nucleocytoplasmic transport, RanGTP promotes the nucleation of microtubules at centrosomes, stabilizes microtubules and regulates spindle assembly and nuclear envelope assembly during mitosis (Clarke and Zhang, 2008). It interacts with importin-β, dissociating spindle assembly factors, including TPX2, NuMa and Lamin B, from the importin-α/β dimer and enabling their localisation to spindle poles and microtubules (Clarke and Zhang, 2008). De Luca et al. demonstrated that the N-terminus of E1A interacts with Ran and that E1A downregulates RCC1-mediated nucleotide exchange on Ran *in vitro,* leading to centrosome overduplication (De Luca et al., 2003). It was previously suggested that Ran might regulate centrosome duplication through RCC1-mediated association of Ran with Crm1 (exportin 1) and subsequent Crm1-mediated binding of nucleophosmin (NPM) to centrosomes; disruption of this process results in centrosome amplification (Budhu and Wang, 2005).

As previously mentioned, E1A binding to p300/CBP disrupts p300/CBP-APC/C complexes. Besides the role of p300/CBP-APC/C in G1/S transcriptional regulation, CBP was also found to interact with APC/C and stimulate the ubiquitin ligase activity during mitosis (Turnell et al., 2005). Knockdown of CBP disrupted APC/C-mediated ubiquitination and subsequent degradation of Cyclin B and Plk1, and prolonged mitotic exit (Turnell et al., 2005). Therefore E1A interference with p300/CBP-APC/C can potentially lead to APC/C deregulation, prolonged mitosis and inhibition of mitotic exit, although this has not been experimentally verified. Prolonged mitosis was indeed previously reported

following E1A expression (Hernando et al., 2004). It was recently shown that the ubiquitin ligase activity of APC/C^{Cdc20} can be regulated by TIF1γ, and knockdown of TIF1γ disrupted APC/C^{Cdc20} function resulting in SAC activation, prolonged mitosis and chromosome alignment errors (Sedgwick et al., 2013). Since TIF1γ is targeted for degradation by adenovirus E4orf3 it is likely that APC/C^{Cdc20} function towards mitotic substrates is impaired during adenovirus infection, leading to deregulated mitosis.

Several independent studies established that E4orf4 binds to the B55 regulatory subunit of the PP2A holoenzyme (Horowitz et al., 2013; Li et al., 2009a; Mui et al., 2013; Shtrichman et al., 1999; Shtrichman et al., 2000). PP2A-B55 functions in mitotic entry and exit by counteracting Cdk1-mediated phosphorylations and inactivates Cdk1 by de-phosphorylating Wee1, Cdc25 and Greatwall (Hegarat et al., 2014; Jeong and Yang, 2013; Wurzenberger and Gerlich, 2011). E4orf4 interaction with B55 was shown to disrupt PP2A phosphatase activity *in vitro* and at least two PP2A targets, 4E-BP1 and p70S6K, were found to be hyperphosphorylated *in vivo* and another substrate, p107 was prevented from accessing PP2A (Li et al., 2009a; Mui et al., 2013). In *Saccharomyces cerevisiae*, E4orf4-mediated interaction with PP2A resulted in mislocalisation of PP2A, activation of Cdk1 in S-phase and premature activation of APC^{Cdc20} as a consequence of uncoupling Cdk1 and APC activity (Mui et al., 2010). Another study in *Saccharomyces cerevisiae* reported that E4orf4 interacts with PP2A and APC/C and inhibits APC^{Cdh1} and perhaps APC^{Cdc20} activity (Kornitzer et al., 2001).

The ability of E4orf4 to interfere with PP2A activity results in upregulation of Cdk1 and E4orf4-induced G2/M arrest and cell death (Li et al., 2009a; Li et al., 2009b; Mui et al., 2013; Shtrichman et al., 1999; Shtrichman et al., 2000). Cell death in lung carcinoma cells was accompanied by mitotic catastrophe, characterised by formation of micro- and multi-nucleated cells (Li et al., 2009b). Interestingly, a study reported that E4orf4 activates the myosin II motor and recruits endosomes to stimulate actin polymerisation, through regulation of the Rho GTPases RhoA, Rac1 and Cdc42 and this is required for E4orf4-induced cell death (Robert et al., 2006).

Despite the characterisation of E4orf4 functions when overexpressed, its role during the viral life cycle remains poorly defined. Mui et al. proposed that during viral infection the interaction of E4orf4 with PP2A might serve the delivery of specific substrates to PP2A, like in the instance of the mRNA splicing factor ASF/SF2/SRSF1 (Mui et al., 2013). Nevertheless, given the important roles of PP2A-B55 during mitosis E4orf4 interference with PP2A activity is likely to impact on mitotic progression.

Besides its role in DNA damage and repair response, the E1B55K/E4orf6 target SPOC-1 has been implicated in mitosis. The expression of SPOC-1 significantly increases in late G2 and mitosis and it localizes to mitotic chromosomes (Kinkley et al., 2009). Depletion of SPOC-1 resulted in chromosome condensation defects and chromosome alignment and segregation errors, suggesting it regulates mitotic chromosome architecture and condensation (Kinkley et al., 2009). Therefore, degradation of SPOC-1 by adenovirus can result in mitotic chromosome condensation errors.

A study reported that the E3-11.6K ADP protein interacts with the mitotic arrest deficient protein 2B (MAD2B) and found that MAD2B overexpression reduced the rate of cell lysis, suggesting that MAD2B attenuates ADP-mediated cell lysis (Ying and Wold, 2003). MAD2B (Rev7 or MAD2L2) is known to inhibit the activity of both APC^{Cdh1} and APC^{Cdc20} (Chen and Fang, 2001; Pfleger et al., 2001) functioning at the metaphase-to-anaphase transition (Listovsky and Sale, 2013) and co-localizes with clathrin light chain A (CLTA) and the RanGTPase at mitotic spindles where it was suggested to function in chromosome alignment and spindle assembly (Medendorp et al., 2009; Medendorp et al., 2010). The functional consequences of ADP-MAD2B interaction are not known, but it could potentially impinge on the function of MAD2B as a mitotic regulator.

Taken together, several studies reported adenovirus-mediated aberrant effects on mitosis but the mechanisms underlying these effects remain largely unidentified. A number of adenoviral proteins interact with mitosis-associated factors and appreciation of the functional consequences of these interactions would improve our understanding of the relationship between adenovirus and host, with subsequent impact on advancing of adenovirus-based therapeutics.

1.3.3. Replication-selective oncolytic adenoviruses as a promising anti-cancer strategy

Due to their many appealing features as therapeutic tools, adenoviruses are amongst the most widely used viruses in cancer gene therapy, both as engineered oncolytic mutants or as non-lytic vectors delivering therapeutic genes (Dyer and Herrling, 2000; Good et al., 2011; Vorburger and Hunt, 2002). Replication-selective oncolytic adenoviruses represent a novel anticancer strategy, with demonstrated efficacy, tumour-selectivity and overall safety for several mutants, in preclinical and clinical studies (Kirn, 2000; Liu et al., 2007; Parato et al., 2005; Yamamoto and Curiel, 2010). Oncolytic virotherapy using adenovirus has many advantages: tumour-specific cytotoxicity with limited infection of normal tissue, mild side-effects, potential of 10^4-fold amplification of the initial dose, ability of co-delivering therapeutic genes, activation of different cell-death pathways including anti-tumour immune responses and no development of treatment resistance (Hallden and Portella, 2012).

Replication-selective oncolytic adenoviruses are engineered to replicate specifically in cancer cells, by taking advantage of cancer-specific alterations (Alemany, 2007). One approach to achieve tumour-selective replication is to drive viral gene expression by tissue- or tumour-specific promoters, such as the prostate-specific antigen (PSA) promoter or enhancer used in prostate cancer (Dilley et al., 2005; Small et al., 2006; Yu et al., 1999). Another example is the use of hypoxia response elements (HREs) to drive viral gene expression in the hypoxic tumour environment (Choi et al., 2012) and the human telomerase reverse transcriptase (hTERT) promoter, which takes advantage of the high expression of hTERT observed in tumour, but not normal cells (Shay and Wright, 2011; Stewart and Bertuch, 2010). The most frequently used approach is to engineer tumour-selectivity by deleting viral genes that function to inactivate tumour-suppressor proteins in normal cells, since such functions are often already inactivated in cancer cells (Bischoff et al., 1996; McCormick, 2003). This concept formed the basis for the development of the first clinically-tested replication-selective oncolytic adenovirus *dl*1520 (Onyx-015) (McCormick, 2003). *dl*1520 is deleted in the E3B immune-regulatory region and the E1B55K gene, responsible for inactivating p53. It was hypothesised that the

mutant virus would replicate efficiently in cancer cells with non-functional p53, but not in normal cells (Bischoff et al., 1996) and indeed that was demonstrated as discussed next.

1.3.4. The evolution of replication-selective oncolytic adenoviruses: a clinical perspective

Clinical trials with ONYX-015

A total of 18 phase I and II clinical trials have been conducted using *dl*1520, 8 of which combined *dl*1520 with chemotherapy (Aghi and Martuza, 2005; Liu et al., 2007; Parato et al., 2005). Patients with a variety of cancers have been evaluated, with both primary and metastatic tumours, including head and neck squamous cell carcinoma, colorectal carcinoma, liver and lung metastases, using several routes of administration, including intra-tumoural, intra-vesicular, intra-venous and via the hepatic artery (Aghi and Martuza, 2005; Kirn, 2000). Tumour-selectivity and overall safety were demonstrated; *dl*1520 was well-tolerated, causing only flu-like symptoms, without significant toxicity in liver or other normal tissue (Kirn, 2000; McCormick, 2003; Toth and Wold, 2010). However, the efficacy of *dl*1520 as a single agent was poor, while more encouraging results were obtained in combination with chemotherapy, such as 5-FU and cisplatin (Aghi and Martuza, 2005; Heise and Kirn, 2000; Kirn, 2000). In a Phase I trial in patients with unresectable pancreatic cancer *dl*1520 was well-tolerated but no objective responses were demonstrated (Mulvihill et al., 2001).

Subsequent studies revealed that the attenuated potency of *dl*1520 could be attributed to the loss of critical functions of the E1B55K/E4orf6 complex, such as viral late mRNA nuclear export and translation, and subsequent blocking of host mRNA nuclear export and protein synthesis (Babiss and Ginsberg, 1984; Babiss et al., 1985; Beltz and Flint, 1979; O'Shea et al., 2004). Deletion of the E3B genes was later shown to also decrease viral efficacy by more rapid macrophage-mediated clearance of the virus (Suzuki et al., 2002; Wang et al., 2003). Moreover, in contrast to initial findings, several studies reported that

*dl*1520 could replicate in certain primary cells and that its replication in tumour cells was not dependent on p53 status, but rather complementation of late viral nuclear mRNA export functions (Goodrum and Ornelles, 1998; Hall et al., 1998; O'Shea et al., 2004; Rothmann et al., 1998; Turnell et al., 1999). Despite this, the almost identical H101 (Shanghai Sunway Biotech) was reported to have a 79% response rate in combination with cisplatin and 5-FU in a phase III trial in China (Xia et al., 2004), which subsequently led to its approval as a treatment for head and neck cancer in China (Garber, 2006).

Clinical trials with *dl*1520 combined with chemotherapy illustrated that the greatest anti-tumour efficacy was observed in patients with head and neck cancer. *dl*1520 combined with 5-FU and cisplatin in patients with recurrent head and neck cancer demonstrated significant objective responses over monotherapy and importantly, chemotherapy-induced toxicity was not increased in the presence of virus (Khuri et al., 2000). Similarly, the H101 phase III trial in China demonstrated that the response rate following treatment with cisplatin and 5-FU was doubled in the presence of H101 and toxicity was low (Xia et al., 2004). In other types of cancer less-encouraging patient responses were observed from combinations of chemotherapy with *dl*1520, however in some cases chemosensitization was demonstrated. Intra-vascular administration of *dl*1520 with intravenous injection of 5-FU and leucovorin in patients with colorectal cancer metastasised to the liver, resulted in anti-tumoral activity and chemosensitization in 2/11 patients (Reid et al., 2001). Ultrasound-guided tumour injection of *dl*1520 in combination with gemcitabine in a Phase I/II trial in patients with locally advanced adenocarcinoma of the pancreas or with metastatic disease, resulted in partial regressions in 2/21 patients, minor responses in 2/21 patients and stable disease in 6/21 patients (Hecht et al., 2003). These results demonstrate that, at least some patients, did benefit from a combination of *dl*1520 with chemotherapy compared to chemotherapy alone. It needs to be kept in mind though that most of these trials mainly assessed safety without considerable optimisation of treatment schedule and it can be appreciated that dosing and administration schedule significantly affect the efficacy of combination treatments.

Several lessons have been learnt from the *dl*1520 trials and clearly, the data point towards a need for more efficacious oncolytic adenoviruses. In an attempt to improve the potency and selectivity of *dl*1520, the mutant was armed with the suicide fusion-gene Escherichia coli cytosine deaminase (CD)-herpes simplex virus type 1 thymidine kinase (HSV1-TK) (Ad5-CD/TK*rep*) (Freytag et al., 1998). In one trial, patients with recurrent prostate cancer following radiotherapy were recruited, while in a second trial Ad5-CD/TK*rep* was combined with radiation therapy in patients with newly-diagnosed prostate cancer (Freytag et al., 2002; Freytag et al., 2003). The results showed low toxicity and patient responses, albeit transient. A 5-year follow-up reported that the oncolytic virotherapy delayed salvage therapy by at least 2 years, suggesting possible long-term beneficial effects in patients (Freytag et al., 2007b). The potency of Ad5-CD/TK*rep* has since been further improved, by increasing the catalytic activity of the fusion gene, and ADP expression to improve viral efficacy and spread. The newly-modified virus, Ad5-yCD/*mut*TK_{SR39}*rep*-ADP, is currently in a phase II/III clinical trial in combination with radiotherapy in patients with newly-diagnosed prostate cancer (Barton et al., 2006; Freytag et al., 2007a).

Improving anti-tumour efficacy by more selective viral engineering

Studies aiming at improving viral potency while retaining tumour selectivity, demonstrated that deletion of the pRb-binding region in the E1ACR2 domain increases tumour-selectivity, since pRb inactivation is complemented in the majority of cancer cells due to deregulated G1/S growth control (Sherr, 1996). *dl*922-947 and the very similar Ad5-Δ24, demonstrated high tumour-selectivity and increased potency *in vivo* in a number of studies (Fueyo et al., 2000; Heise et al., 2000; Kirn et al., 1998; Lamfers et al., 2002), while anti-tumour efficacy was further enhanced in combination with chemotherapy (Bhattacharyya et al., 2011; Conrad et al., 2005; Gomez-Manzano et al., 2006; Radhakrishnan et al., 2010). In addition to E1ACR2, E1B19K deletion was shown to prevent viral spread in normal tissue through tumour necrosis factor (TNF)-induced apoptosis, and enhance anti-tumour efficacy (Harrison et al., 2001; Kim et al., 2002; Leitner et al., 2009; Liu et al., 2004; Sauthoff et al., 2000; White et al., 1992).

Arming oncolytic adenoviral mutants with therapeutic genes

Arming of oncolytic viruses with therapeutic genes in order to improve potency has been widely adopted. Pre-clinical examples include adenoviral-mediated delivery of pro-apoptotic genes, such as TRAIL (Chen et al., 2009; Mao et al., 2014; Zhu et al., 2013), to enhance cell death, and delivery of small hairpin or interference RNAs (shRNAs or siRNAs) against survival factors, such as the IAP survivin (Shen et al., 2010; Shen et al., 2009; Wang et al., 2012; Yin et al., 2008). Currently, a considerable focus of the field has been the arming of oncolytic adenoviruses with immunomodulatory genes aiming at enhancing anti-tumour immune responses. Anti-tumour efficacy has been demonstrated in pre-clinical models using adenoviruses armed with various cytokines, such as the granulocyte-macrophage colony-stimulating factor (GM-CSF) (Thorne, 2013), interleukin 24 (IL-24) (He et al., 2013; Zhang et al., 2012; Zhu et al., 2012; Zhuo et al., 2013), IL-15 (Zhao et al., 2014), IL-18 and IL-12 (Choi et al., 2011).

Preliminary clinical testing of oncolytic viruses armed with GM-CSF as an immunostimulatory therapeutic gene has been showing some positive responses in cancer patients, but further clinical trials are required to fully evaluate the potential of such viruses (Bramante et al., 2014; Burke et al., 2012; Cerullo et al., 2010; Koski et al., 2010). The CG0070 virus expresses GM-CSF under the control of the human E2F-1 promoter to take advantage of upregulated E2F-1 due to defective retinoblastoma pathway in bladder cancers (Ramesh et al., 2006). CG0070 is currently in a phase II safety and efficacy study (http://clinicaltrials.gov/show/NCT01438112) and an integrated phase II/III, open label, randomized and controlled study (http://clinicaltrials.gov/show/NCT02143804) in patients with invasive bladder cancer. Another example is the E1B-deleted adenovirus Ad/L523S armed with the immunogenic lung cancer antigen L523S, which has proven to be safe in a phase I trial with non-small-cell lung cancer patients, however no further clinical testing has been reported (Nemunaitis et al., 2006). The use of oncolytic viruses as immunotherapy for cancer is at the present time an intense and exciting area of research (Chiocca and Rabkin, 2014; Hemminki, 2014; Prestwich et al., 2009; Stanford et al., 2008; Tong et al., 2012).

Improving infectability

Numerous studies have also focused on the improvement of infectivity. Adenovirus infection depends on the availability of CAR and integrins, and CAR deficiency in many tumour cells represents a major obstacle in adenovirus-based gene therapy (Yamamoto and Curiel, 2010). Thus, a major focus has been to achieve CAR-independent adenovirus transduction. Strategies being used include modifications of the fiber-knob and incorporation of fiber-knob domains from adenovirus serotypes that do not depend on CAR for cell-entry (Pesonen et al., 2011; Yamamoto and Curiel, 2010).

An example is the oncolytic adenovirus Ad5-Δ24-RGD, an Ad5-Δ24-based virus containing an RGD insertion in the fiber to allow infection through $\alpha_v\beta$ integrins (Fueyo et al., 2003), which are often constitutively-expressed in tumours (Weis and Cheresh, 2011). Ad5-Δ24-RGD showed encouraging results in pre-clinical models (Fueyo et al., 2003; Guse et al., 2007; Kangasniemi et al., 2006) and a phase I clinical trial with Ad5-Δ24-RGD in patients with recurrent ovarian cancer demonstrated overall safety and potential anti-tumour efficacy, with stable disease in 71% of patients after 1 month (Kimball et al., 2010). A phase I trial with Ad5-Δ24-RGD in patients with recurrent glioblastomas is currently on-going, with the aim to determine maximum tolerable doses of virus as well as safety and preliminary efficacy (http://www.clinicaltrials.gov/show/NCT01582516). Another phase I trial for recurrent glioblastoma is currently evaluating the efficacy of Ad5-Δ24-RGD with the drug temozolomide (http://www.clinicaltrials.gov/show/NCT01956734). A phase 1b clinical trial is expected to open soon and it will evaluate safety and efficacy of Ad5-Δ24-RGD with or without interferon gamma (IFNγ) treatment in patients with glioblastoma or gliosarcoma (http://www.clinicaltrials.gov/show/NCT02197169). Further modifications of Ad5-Δ24-RGD were introduced to improve selectivity and replication, giving rise to the ICOVIR virus (Oncos Therapeutics, Inc), which contains an E2F-1 promoter with additional palindromes of E2F-responsive sites controlling E1A-Δ24 expression (Rojas et al., 2009). ICOVIR could be safely administrated in patients with advanced solid tumours and resulted in stabilization or reduction in tumour size in 5 out of 12 patients, encouraging further clinical testing

(Nokisalmi et al., 2010; Rojas et al., 2009). ICOVIR is currently in a phase I trial for patients with locally advanced or metastatic melanoma (http://www.clinicaltrials.gov/show/NCT01864759).

Another virus utilising RGD for improved infectivity is Ad5.SSTR/TK.RGD, which also expresses a therapeutic TK suicide gene and a somatostatin receptor (SSTR) that allows for gene transfer imaging (Kim et al., 2012). This virus was evaluated in a phase I clinical trial in patients with recurrent gynecologic cancer, showing safety but moderate efficacy with 5 out of 13 patients maintaining stable disease (Kim et al., 2012).

Improving viral spread and limiting clearance

Research is also aiming at improving viral spread within the tumour bed, as the extracellular matrix (ECM) in the tumour stroma could limit efficient viral distribution (Choi et al., 2012). Adenoviruses expressing ECM modulators, such as relaxin and decorin, have demonstrated improved spread and efficacy in tumour spheroids and *in vivo* xenograft models (Choi et al., 2010; Kim et al., 2006).

Perhaps the biggest limitation in developing oncolytic adenoviruses as anti-cancer therapies is the host anti-viral immune response and the sequestration of adenovirus from the blood by liver macrophages (Kupffer cells) and coagulation factors (Ferguson et al., 2012; Thaci et al., 2011). These host factors are partly responsible for the transient efficacy of most clinically evaluated oncolytic viruses (Ferguson et al., 2012; Thaci et al., 2011). Anti-viral immune responses, which include the complement system (part of innate immunity) and neutralising antibodies (adaptive/acquired immunity), occurring during systemic delivery, represent a major hurdle in oncolytic virotherapy (Nayak and Herzog, 2010; Randall and Goodbourn, 2008). One approach to limit antibody neutralization is to coat adenoviruses with chemical conjugates, such as co-polymers of poly N-(2-hyrdoxypropyl) methacrylamide which was shown to evade neutralization and also decrease liver uptake of the virus *in vivo* (Fisher and Seymour, 2010). Another approach that has been employed is the encapsulation of adenoviruses into liposomes that was shown to limit virus

neutralisation by the immune system (Liu et al., 2011; Wan et al., 2013; Yang et al., 2010). In order to limit viral liver and spleen uptake, Shashkova et al depleted Kupffer cells and pre-treated xenografts with the anticoagulant drug warfarin before intravenous adenoviral injection, demonstrating circumvention of macrophage and hepatocyte binding of adenovirus and enhanced anti-tumour efficacy (Shashkova et al., 2008). It remains to be seen whether these results will translate into patients.

1.3.5. Replication-selective oncolytic adenoviruses: Mechanisms of cytotoxicity

Although much is known about how individual adenoviral proteins regulate cell-death pathways, the precise mechanisms that govern adenovirus-mediated cell-lysis during infection are poorly understood, let alone the different oncolytic mutants. As reviewed below accumulating evidence suggests that replication-selective oncolytic adenoviruses utilize multiple mechanisms to induce cytotoxicity.

Ad5-Δ24 (E3-deleted) and Ad5-Δ24-RGD with intact E3 region were shown to induce a necrosis-like programmed cell-death, independent of caspases and the presence or absence of ADP, in non-small-cell lung carcinoma cells (Abou El Hassan et al., 2004). Abnormal chromatin condensation and nuclear-swelling, characteristic of necrosis, was observed following adenovirus infection, and although apoptotic phosphatidylserine (PS) externalization could be detected after Annexin V staining, cell-death was caspase-independent (Abou El Hassan et al., 2004). Baird et al. exploited the mode of cell-death induced by *dl*922-947 in ovarian cancer cells, and despite some observed nuclear-swelling and apoptotic morphological characteristics, programmed cell-death could not be attributed to apoptosis or pure necrosis (Baird et al., 2008). Autophagy was also examined as a potential mode of cell-death but was rather found to act as a cell-survival response (Baird et al., 2008). Autophagy is generally considered as a pro-survival mechanism in response to cellular stresses, and involves the engulfment of proteins and organelles by autophagosomes and their degradation upon fusion with lysosomes (Yang and

Klionsky, 2010). However, autophagy is also a type of programmed cell-death and is intricately involved in crosstalk with apoptotic pathways (Fimia and Piacentini, 2010).

Another group used glioma, cervical and prostate cancer cell lines to assess the anti-tumour mechanisms of an oncolytic adenovirus with hTERT promoter driving E1A expression (Ito et al., 2006). In contrast to Baird et al., this group demonstrated that hTERT-Ad-induced tumour-specific cell-death was autophagic, mediated though inhibition of the mammalian target of rapamycin (mTOR) signalling. Blockade of autophagy was shown to reduce hTERT-Ad-induced cytotoxicity in glioma cells (Ito et al., 2006). Following this study, several publications further implicated autophagy in adenovirus-induced glioma cell-death, and growing evidence suggests that, at least in glioma cells, adenovirus-induced cell lysis is linked to autophagy (Jiang et al., 2008). A study evaluating the therapeutic potential of Ad5-Δ24-RGD in glioblastoma stem-cells, revealed that Ad5-Δ24-RGD induces autophagic cell-death, as judged by the formation of autophagic vacuoles and upregulation of autophagic markers, which co-localized with the viral fiber protein near the area of tumour necrosis in xenografts (Jiang et al., 2007). Another publication confirmed induction of complete autophagic flux by Ad5-Δ24-RGD in glioma cells and further associated autophagy to cell-lysis (Jiang et al., 2011b). Interestingly, in leukemia but not glioma cells, autophagy triggered caspase activation, which contributed to adenoviral-induced lysis (Jiang et al., 2011b). Consistent with findings in glioma cells, a study in lung adenocarcinoma cells demonstrated that autophagy was associated with enhanced viral replication and oncolysis (Rodriguez-Rocha et al., 2011).

Botta et al. reported that *dl*922-947 activated autophagy in glioma cell lines, as evidenced by formation of acidic vesicles, LC3II expression and p62 downregulation (Botta et al., 2012). However, in contrast to other studies but in agreement with Baird et al., it was proposed that *dl*922-947-induced autophagy acted as a cell survival mechanism. The proposal was a result of various findings. First, the AKT/mTOR pathway that negatively regulates autophagy was activated following infection, while the ERK1/2 pathway that positively regulates autophagy was inhibited. Second, MEK inhibition enhanced *dl*922-947

cytotoxicity, whereas rapamycin-induced autophagy attenuated *dl*922-947 cytotoxicity. Moreover, inhibiting autophagy with chloroquine enhanced *dl*922-947 anti-tumour efficacy both *in vitro* and *in vivo* (Botta et al., 2012).

Another study in glioma cells, showed that oncolytic Ad-Survivin-RGD (RGD-modified adenovirus with the tumour-specific promoter survivin driving E1A expression) increased apoptosis and upregulated caspase-3 and BAX mRNA levels (Ulasov et al., 2007). However, at the protein level, despite cytochrome c release, no BAX or p53 upregulation was detected, and caspase-3 was not activated. Electron microscopy experiments revealed the presence of autophagic vacuoles. The authors concluded that conditionally replicating Ad-Survivin-RGD-induced cell-death was autophagic (Ulasov et al., 2007).

Using *dl*922-947 in ovarian cancer cells, Flak et al. demonstrated that knocking-down or over-expressing p21 reduced or enhanced, respectively, both E1A expression and *dl*922-947-induced cytotoxicity both *in vitro* and *in vivo* (Flak et al., 2010). This group previously demonstrated that *dl*922-947 induces the formation of cells with >4N DNA content and mitotic defects, such as multipolar spindles, and that *dl*922-947-induced cytotoxicity correlated with its ability to induce extensive DNA-damage and host-cell DNA over-replication (Connell et al., 2011). *dl*922-947-induced DNA-damage and over-replication were mediated by the ATR/Chk1-target Cdc25A, which was transcriptionally upregulated by the virus, and over-expression of Cdc25A increased *dl*922-947-induced DNA-damage and cytotoxicity (Connell et al., 2011).

Taken together, the evidence so far shows that cytotoxicity mechanisms differ between different cell- and tumour-types, and also for different replication-selective oncolytic adenoviruses. This is not surprising given the various distinct modifications being made to different oncolytic adenoviruses, as well as the expected genetic variations among different tumour cell lines. Numerous studies have clearly demonstrated that autophagy mediates oncolytic adenovirus-induced cytotoxicity in glioma cells, but besides A549 lung cancer cells, the evidence for such mechanism in other tumour cells remains poor. Therefore further studies are required before assigning a primary role of autophagy in adenovirus-induced oncolysis. Furthermore, when oncolytic

adenoviruses are administered to a host with intact immune system, immune-factors may alter the major mode of virus-induced cell death. Several recent reports have described new concepts of cell killing in connection with virus-induced oncolysis *in vivo*, such as immunogenic cell death (Guo et al., 2014; Inoue and Tani, 2014). It has been suggested that the immune-response to virus infection constitutes the major mechanism whereby oncolytic viruses eliminate tumours clinically, and consequently the terminology oncolytic immunotherapy rather than oncolytic virotherapy was proposed (Guo and Bartlett, 2014; Hemminki, 2014; Pesonen et al., 2012).

1.3.6. Replication-selective oncolytic adenoviruses combined with chemotherapy: Mechanisms of cytotoxicity

Numerous pre-clinical studies demonstrated that combining oncolytic adenoviruses with other cytotoxic agents greatly enhances anti-tumour efficacy. Increased therapeutic responses have been demonstrated upon adenovirus combination with anthracyclins, such as doxorubicin and mitomycine C, anti-metabolites, such as gemcitabine and 5-FU, platinum-based chemotherapeutics, such as cisplatin, alkylating agents, such as temozolomide, topoisomerase inhibitors, such as irinotecan and mitoxantrone, and mitotic inhibitors, including paclitaxel and docetaxel (Bressy and Benihoud, 2014; Hallden and Portella, 2012; Jiang et al., 2011a). While a plethora of studies demonstrated enhanced anti-tumour efficacy when oncolytic adenoviruses are combined with chemotherapy, a handful of studies have thoroughly examined the mechanisms underlying the synergistic anti-tumour effects. The interactions of adenoviral proteins and drugs are likely to occur by convergence on pathways and host-cell factors that induce tumour cell killing. Understanding of such interactions is necessary for further clinical developments.

Combination with alkylating agents

Ulasov et al. demonstrated that combining the chemotherapeutic autophagy-inducing agent temozolomide with the oncolytic Ad-Survivin-pk7 virus, enhances cytotoxicity in glioma cells through autophagic cell-death. However, *in*

vivo anti-tumour efficacy was attributed to induction of both autophagy and apoptosis (Ulasov et al., 2009). It was similarly reported that temozolomide-induced autophagy was the mechanism underlying therapeutic synergy when this drug was combined with OBP-405 (hTERT-Ad-RGD) in glioblastoma cells (Yokoyama et al., 2008). Fueyo's group showed that temozolomide synergizes with Ad-Δ24-RGD to induce cytotoxicity in glioma cells and the combination treatment improves survival in a mouse model (Alonso et al., 2007). Ad-Δ24-RGD abrogated temozolomide-induced G2/M arrest and blocked p300 recruitment to promoters of the DNA repair enzyme 6-methylguanine-DNA methyltransferase (MGMT), which has been previously associated with resistance of glioma cells to temozolomide. Ad-Δ24-RGD-mediated interaction with p300, a well-known target of E1A, inhibited MGMT expression (Alonso et al., 2007).

Combination with anthracyclins or platinum-based agents

Interestingly, a study showed that Ad5-Δ24RGD synergised with doxorubicin to induce cytotoxicity in osteosarcoma cell lines, but not in primary osteosarcoma cells (Graat et al., 2006). Synergistic effects correlated with the ability of doxorubicin to induce G2 cell-cycle arrest, which was not evident in primary cells perhaps due to their slow growth rate. Adenovirus cell attachment, internalization and replication was previously reported to be enhanced in G2/M phase (Bernt et al., 2002; Steinwaerder et al., 2000) and in this study doxorubicin inhibited viral replication only in the non-arresting primary cells (Graat et al., 2006).

You et al. showed that SG511 (chimeric fiber and E1B55K-deleted Ad) enhanced efficacy of the DNA-damaging drug cisplatin, by downregulating anti-apoptotic MCL-1 and increasing apoptosis through the intrinsic/mitochondrial pathway, in colon and cervical cancer cells (You et al., 2012). Increased apoptosis was also observed when cisplatin was combined with adenovirus lacking E1B55K and E1B19K (AdΔE1B19/55) in a human cervical cancer xenograft model (Yoon et al., 2006). In addition, synergistic induction of apoptosis was greatly enhanced when both E1B55K and E1B19K were deleted, as opposed to deletion of only E1B55K (Yoon et al., 2006).

Combination with topoisomerase inhibitors

A study in glioma cells showed that AdΔ24 enhanced irinotecan-induced cytotoxicity and AdΔ24 injection of glioma xenografts followed by irinotecan treatment significantly prolonged survival (Gomez-Manzano et al., 2006). Viral replication was unaffected and chemosensitization was attributed to AdΔ24-induced upregulation of topoisomerase I expression and activity as well as S-phase cell accumulation (Gomez-Manzano et al., 2006). The suggestion was based on previous publications reporting enhanced effect of irinotecan and camptothecin in S-phase cells (Darzynkiewicz et al., 1992; Li et al., 1972).

Our group previously demonstrated significantly improved anti-tumor efficacy upon combination of mitoxantrone with the *dl*922–947 oncolytic adenovirus in both *in vitro* and *in vivo* prostate cancer models (Radhakrishnan et al., 2010). Treatment with mitoxantrone, before or at the same time as virus infection, increased viral uptake in a dose-dependent manner and E1A expression, while it attenuated virus replication (Radhakrishnan et al., 2010). E1A expression was sufficient for chemosensitisation, as shown by E1A overexpression in the absence of replication, consistent with previous reports (Cheong et al., 2008; Ueno et al., 2000). The ability of virus to accumulate cells in S-phase was not affected in the presence of drugs, which could have also enhanced the effects of the drug. Moreover while both virus and mitoxantrone increased topoisomerase II expression, their combination did not further increase expression, excluding it as the mechanism of chemosensitisation (Radhakrishnan et al., 2010).

Combination with anti-metabolites

In esophageal squamous cell carcinoma cells a replication-selective adenovirus lacking E1B55K (Ad-delE1B55) enhanced cytotoxicity in combination with 5-FU, etoposide and mitomycin C, but not cisplatin (Ma et al., 2010). The lack of enhanced cytotoxicity upon Ad-delE1B55 and cisplatin combination was attributed to a cisplatin-induced G1 arrest, as all other agents induced S-phase cell accumulation followed by progression to G2/M (Ma et al., 2010). The study also evaluated different treatment schedules; simultaneous administration of

Ad-delE1B55 and 5-FU and Ad infection before or after 5-FU treatment. Simultaneous treatment with Ad-delE1B55 and 5-FU was more efficacious in inducing apoptosis compared to the sequential treatments. Regarding drug-mediated effects on virus, 5-FU initially decreased viral replication, although long-term viral progeny production was not significantly inhibited; E1A expression was unaffected (Ma et al., 2010).

Combination of Ad5/3-Δ24 with gemcitabine in an orthotopic murine model of peritoneally spread ovarian cancer, significantly increased survival as compared to either monotherapy and ~60% of mice remained alive at the end of the experiment (Raki et al., 2005). Of note, gemcitabine decelerated Ad5/3-24 replication, but total virus yield was not reduced. The authors suggested that slower replication could benefit anti-tumour efficacy by enhancing tumour penetration and viral spread before oncolysis. Another proposed mechanism for the observed synergistic effect, was virus-mediated enhancement of chemotherapy-induced cytotoxicity, although this was not further examined (Raki et al., 2005). Lee et al studied the synergistic cytotoxic effect of an E1B- and E3-deleted adenovirus (AdE1A) and gemcitabine in hepatocellular carcinoma cell lines. By stably transfecting cells with E1A, they demonstrated that E1A sensitised cells to gemcitabine through enhancement of apoptosis (Lee et al., 2003). Gemcitabine treatment increased expression of NF-κB and PARP and enhanced caspase-mediated PARP cleavage. However, in the presence of E1A gemcitabine-induced upregulation of NF-κB expression and PARP expression and cleavage were suppressed. Overexpression of NF-κB or PARP decreased apoptosis, suggesting a protective role for these two factors in gemcitabine-induced apoptosis (Lee et al., 2003).

Combination of an hTERT-promoter dependent oncolytic adenovirus (Ad5/3hTERTE1) with gemcitabine enhanced cytotoxicity in pancreatic cancer cells and *in vivo* xenografts (Onimaru et al., 2010b). It was shown that gemcitabine increased hTERT promoter activity and subsequently E1 expression and infectivity, which led to increased E1-induced chemosensitization (Onimaru et al., 2010b). The same group also demonstrated that gemcitabine can increase CMV promoter activity in an adenoviral vector, thus increasing gene expression (Onimaru et al., 2010a). Interestingly, this

group later reported that adenovirus infectability and cytotoxicity were higher in gemcitabine-resistant cells compared to sensitive cell clones (Yasui et al., 2011).

Another group proposed that the increased anti-tumour efficacy of gemcitabine combined with an E1ACR2-mutated and E1B55K-deleted adenovirus (AxdAdB-3) in renal cell carcinoma and bladder cancer cells could be attributed to the ability of the virus to increase S-phase entry, although this was not examined in the presence of gemcitabine (Wang et al., 2013; Wang et al., 2011). The hTERT promoter-driven virus OB-301 exhibited a therapeutic synergism in combination with gemcitabine in xenograft models of lung cancer (Liu et al., 2009). In contrast to other studies, gemcitabine did not affect viral replication or expression of E1A. OB-301 accumulated cells in S-phase, which was attributed to the increased phosphorylation of Akt and increased expression of E2F1, leading to downregulation of Rb levels. The authors proposed that the cell-cycle effects of OB-301 could account for the increased gemcitabine cytotoxicity, however S-phase accumulation was not studied in combination-treated cells (Liu et al., 2009).

Combination with radiotherapy

Insights into the mechanisms underlying synergy of oncolytic adenoviruses with DNA-damaging therapeutics can be also gained from studies combining viruses with radiation. Similar to DNA-damaging chemotherapeutic drugs, irradiation induces DNA-damage in the form of DSBs (Jakob et al., 2009; Sokolov et al., 2005). One study in prostate cancer cells using radiotherapy in combination with Ad5/3-Δ24-hCG (Ad3 receptor-retargeted Ad5Δ24 virus expressing the secretable marker human chorionic gonadotropin (hCG)) reported that the virus reduced Mre11 levels and Chk2 activation and downregulated DNA-repair proteins in combination-treated cells, which also exhibited enhanced autophagy (Rajecki et al., 2009). Cell-cycle and mTOR pathways were also deregulated. The authors suggested that Ad5/3-Δ24-hCG prevented repair of irradiation-induced DSBs and accumulated DNA-damage which eventually led to induction of autophagy, but not apoptosis (Rajecki et al., 2009). In agreement, Kuroda et al. showed that OBP-301 (hTERT promoter-driven E1 expression) synergizes

with irradiation via inhibition of DNA-repair pathways, exerted by E1B55K-mediated degradation of the MRN complex in oesophageal and lung cancer cell lines (Kuroda et al., 2010).

Combination with mitotic inhibitors

A group examined the mechanism underlying synergy of *dl*922-947 with the microtubule-stabilizing chemotherapeutic drug paclitaxel in ovarian cancer cells (Ingemarsdotter et al., 2010). They demonstrated that the combination treatment induced mitotic aberrations coupled with increased cdk1-cyclin B activity, which led the authors to suggest that synergy was mediated through induction of mitotic slippage and caspase-dependent apoptosis, as shown by Annexin V staining and caspase-3 activation (Ingemarsdotter et al., 2010).

Adenovirus-mediated sensitization to the microtubule-stabilizing agent docetaxel, has been mainly attributed to E1A-mediated cell-cycle effects (Radhakrishnan et al., 2010; Yu et al., 2001). Accordingly, our team has demonstrated that E1A12S expression is sufficient for prostate cancer cell sensitization to docetaxel (Miranda et al., 2012).

Libertini et al. demonstrated that combining the Aurora-B inhibitor AZD1152 with *dl*922-947 in anaplastic thyroid carcinoma (ATC) cells and *in vivo* models results in enhanced anti-tumour efficacy (Libertini et al., 2011). Cell death induced by the combination treatment did not show the classical features of apoptosis, despite caspase-3 activation and appearance of cells with less than 2N DNA content (sub-G1). AZD1152 with or without *dl*922-947 arrested cells in G2/M and the increased sub-G1 fraction observed with the combination treatment correlated with a decrease in polyploid (>4N DNA content) cells, suggesting mitotic catastrophe. AZD1152 decreased phosphorylation of histone H3, a mitotic marker and Aurora-B substrate, consistent with Aurora-B inhibition leading to premature mitotic exit. Interestingly, *dl*922-947 also decreased phosphorylation of histone H3 24h post-infection and together with AZD1152 phosphorylation was diminished. The authors suggested that adenovirus prematurely ends mitosis in order to switch the cell machinery to viral replication (Libertini et al., 2011).

Conclusions

Studies combining oncolytic adenoviruses and chemotherapy have clearly demonstrated enhanced cytotoxicity compared to either single agents and have highlighted the importance of optimising the treatment schedules. Collectively, the mechanisms responsible for enhanced anti-tumour efficacy when replication-selective oncolytic adenoviruses are combined with cytotoxic drugs, are predominantly cell-cycle dependent, but vary with different chemotherapeutic agents. Several studies reported that drug-induced S-phase or G2 arrest can favour viral replication and, vice versa, adenovirus-induced S-phase accumulation can enhance the efficacy of drugs. In some instances abrogation of cell-cycle checkpoints was implicated in virus-mediated chemosensitization. A number of reports also demonstrated drug-mediated beneficiary effects on adenovirus, such as increased E1A expression, viral uptake or promoter activity, whereas other studies reported that drugs can attenuate viral replication. Importantly, E1A is the main viral protein that has been implicated in chemosensitization and some groups reported E1A expression alone to be sufficient. Specific cellular targets of the combination treatments were not always investigated and/or identified. Regarding the type of cell death, both autophagy and apoptosis have been reported, although apoptosis seems to be the predominant mode of cell death when oncolytic adenoviruses are combined with chemotherapy.

Clearly, more thorough investigations are warranted in order to gain insights into adenovirus-mediated chemosensitization. In light of the recent interest in evaluating several oncolytic adenoviral mutants in clinical trials in combination with already approved chemotherapeutic drugs, it is essential to determine how these agents synergise with virus. The dismal prognosis for pancreatic cancer patients highlights the importance of improving on current therapies by investigating whether selected adenoviral mutants could enhance cell killing by drugs such as gemcitabine. By establishing the cellular mechanisms for the improved inhibition of cancer growth it might also be possible to further improve on treatment strategies by developing alternative targeted therapies.

1.4. Research rationale

1.4.1. Background to the project

Replication-selective oncolytic adenoviruses represent a promising anticancer strategy, with demonstrated efficacy, tumour-selectivity and overall safety for several mutants, in preclinical and clinical studies (Kirn, 2000; Liu et al., 2007; Parato et al., 2005; Yamamoto and Curiel, 2010). Clinical trials with the prototype oncolytic mutant *dl*1520 indicated the need for more efficacious oncolytic adenoviruses. Deletion of the E1ACR2 region that takes advantage of the frequent inactivation of pRb/p16 pathways in tumours, was extensively demonstrated to increase both tumour selectivity and viral potency (Fueyo et al., 2000; Heise et al., 2000; Kirn et al., 1998; Lamfers et al., 2002; Lockley et al., 2006; Stolarek et al., 2004). However, E1ACR2-deleted mutants were also reported to replicate in normal proliferating cells (Heise et al., 2000). To enhance the efficacy and specificity of E1ACR2-deleted mutants our team has introduced the E1B19K deletion, which was demonstrated to enhance viral spread and anti-tumour efficacy and lower toxicity to normal tissue (Harrison et al., 2001; Leitner et al., 2009; Liu et al., 2004; Liu et al., 2005; Sauthoff et al., 2000). The E1ACR2- and E1B19K-deleted adenovirus (AdΔΔ; (Oberg et al., 2010)) takes advantage of the high anti-tumour potency of E1ACR2-deleted mutants and the improved efficacy and tumour-selectivity of the E1B19K-deleted mutants.

Since pancreatic cancers show prevalent genetic alterations in pRb/p16, cell cycle and cell death pathways, it was hypothesised that the E1B19K-deleted (AdΔ19K) and E1ACR2- and E1B19K-deleted (AdΔΔ) mutants would efficiently target and render pancreatic cancer cells susceptible to cytotoxic drugs. Indeed, our group demonstrated that both mutants have high anti-tumour efficacy in pancreatic cancer cell lines and *in vivo* xenografts (Cherubini et al., 2011; Leitner et al., 2009; Oberg et al., 2010). In addition, AdΔ19K potently sensitized pancreatic cancer cells to gemcitabine-induced apoptosis, both *in vitro* and *in vivo* (Leitner et al., 2009), and this ability was retained in the AdΔΔ mutant, which additionally was shown to potentiate irinotecan-induced cell death

(Cherubini et al., 2011). The enhanced anti-tumour efficacy that was demonstrated when DNA-damaging drugs are combined with E1B19K-deleted mutants, suggests that this combination treatment holds promise as an improved therapeutic strategy for pancreatic cancer.

1.4.2. Aims and objectives of the project

The current project is a continuation of the previously published results (Cherubini et al., 2011; Leitner et al., 2009; Oberg et al., 2010). The project aims to elucidate the mechanisms underlying the enhanced cell killing observed when E1B19K-deleted adenoviruses are combined with DNA-damaging chemotherapeutic drugs in pancreatic cancer cells and identify potential biomarkers of the treatment response. The overall goal is to identify cellular factors that can be targeted in future drug development of improved oncolytic viruses or small molecule anticancer therapeutics targeting pancreatic cancer. We hope that the findings from these studies will aid in the development of anticancer agents that can improve on the current dismal prognosis for patients afflicted with pancreatic cancer.

The major purpose with the work in this thesis is to determine the mechanisms of action for the AdΔ19K mutant in combination with the DNA-damaging drugs gemcitabine and/or irinotecan in pancreatic cancer cells. Employing the Ad∆19K rather than the Ad∆∆ mutant, will allow the identification of potential factors specifically targeted during virus-mediated sensitization to the DNA-damaging chemodrugs. The study intends to delineate the sequence of events leading to cell death when AdΔ19K and DNA-damaging drugs are combined in the pancreatic cancer cell lines PT45 and MIAPaCa-2.

The hypothesis is that cellular processes activated in response to the DNA-damaging drugs and Ad∆19K converge on signalling pathways to synergistically induce cell killing. Particularly, we hypothesise that Ad∆19K and DNA-damaging drugs act synergistically to deregulate cell-cycle mechanisms. Therefore a major objective is to determine how Ad∆19K in combination with DNA-damaging drugs affect cell cycle progression, with a particular focus on DNA

damage responses. First, using cell viability, death and apoptotic assays I will verify previous findings by our team, that the E1B19K deletion in wild-type adenovirus type 5 enhances drug-induced cell death. Then I will determine changes in cell-cycle progression in response to the combination of AdΔ19K with gemcitabine and/or irinotecan compared to single-agent treatments through the use of flow-cytometry. I intend to investigate DNA damage checkpoint responses to the combination treatment and particularly how the presence of adenovirus in drug-treated cells affects the expression of DNA-damage response factors. In addition, I will characterise the effects of the combination treatment on mitotic progression by employing a combination of immunofluorescence microscopy and live-cell imaging techniques. The identification of factors differentially regulated in combination-treated versus single-agent-treated cells will be verified using a battery of molecular tools, including siRNA-mediated knockdown and small molecule inhibitors.

CHAPTER 2: METHODS

2.1. Chemical Reagents

Gemcitabine (Gemzar®) was purchased from Eli Lilly (IN, USA) and reconstituted in 0.9% Sodium Chloride Injection solution (127mM; stored at 4ºC). Irinotecan (Campto®) hydrochloride injection (20mg/ml; stored at 4ºC) was from Hospira UK Ltd and the pan-caspase inhibitor Calbiochem® Z-VAD(OMe)-FMK (Caspase Inhibitor I; 5mM in dimethyl sulfoxide (DMSO)) was from Millipore (MA, USA). Staurosporine (1mM in DMSO), RNAse A solution (33mg/ml in Tris-HCl/glycerol), Tween-20, Triton-X100 and bovine serum albumin (BSA) were from SIGMA-ALDRICH (MO, USA). Propidium Iodide (PI; 1mg/ml in water) and ProLong Gold antifade reagent with DAPI were purchased from Thermo Fisher Scientific (CA, USA). MG-132 (25mg/ml in DMSO) was from Enzo Life Sciences Ltd (UK), cycloheximide (25mM in water) was from Abcam Plc (UK) and thymidine (100mM in water) was from Alfa Aesar (MA, USA). The fixable viability dye (FVD) eFluor® 506 was purchased from eBioscience (CA, USA) and kept in aliquots at -80ºC. The small molecule inhibitor monastrol (20mM in DMSO) was from SIGMA-ALDRICH. The Plk1 inhibitor BI-2536 (10mM in DMSO) and the Aurora-B inhibitor AZD1152-HQPA (Barasertib; 201mM in DMSO) were purchased from Selleckchem (TX, USA). The Mps1 inhibitor (10mM in DMSO) was a generous gift from Dr Spiros Linardopoulos (The Institute of Cancer Research, London UK).

2.2. Cell lines, culture conditions and cell infection/treatment

2.2.1. Origin of cell lines

The human pancreatic adenocarcinoma cell lines PT45 (Prof H. Kalthoff, Kiel, Germany) and MIAPaCa-2 (ATCC, VA, USA) are derived from primary PDAC

tumours. The cell lines were STR-profiled (LGC Standards, UK and Cancer Research UK) and verified to be identical to the profiles reported by the suppliers and to the original vial.

2.2.2. Cell culture conditions

Cells were grown at 37°C and 5% CO_2 in DMEM supplemented with 10% Fetal Bovine Serum (FBS) and 1% penicillin and streptomycin (Penicillin 10000 units/ml, Streptomycin 10mg/ml; P/S). DMEM, FBS and P/S were purchased from PAA and after August 2013 from SIGMA-ALDRICH. DMEM contained 4.5g/L glucose, L-glutamine, sodium pyruvate and sodium bicarbonate. Cells were sub-cultured twice a week, by removing medium, washing with phosphate buffered saline (PBS) and trypsinizing (1x Trypsin from PAA or later SIGMA-ALDRICH). PT45 and MIAPaCa-2 cells were used at passage 18-30 and 3-15, respectively. Cells were frozen at $1x10^6$ cells/ml in 10% DMSO/30% FBS in DMEM and stored in liquid N_2.

2.2.3. Cell seeding, infection/treatment and harvesting from 6-well plates

In all experiments cells were seeded in 10% FBS/1% P/S DMEM at the specified densities for 16-24 hours (h). For cell infection with adenoviruses in 6-well plates, the medium was changed to 1ml serum-free DMEM -/+ the indicated dose of virus. 2h later the medium was replaced with 10% FBS/1% P/S DMEM -/+ the indicated dose of drug(s). At the specified times post-infection cell harvesting from 6-well plates was done as follows: supernatant was collected, unless otherwise stated, cells were washed in PBS and trypsinised, followed by addition of 10% FBS/1% P/S DMEM to inactivate the trypsin. The supernatant was mixed with the cell suspension, followed by centrifugation at 1200rpm for 5 minutes (min) using an Allegra X-22 centrifuge (Beckman Coulter, Inc, CA, USA) and removal of supernatant, leaving the cell pellet. The cell pellet was washed in PBS and processed as specified.

2.3. Viruses

The species C wild type adenovirus type 5 Ad5tg, was derived from pTG3602 (a kind gift from Dr Majid Mehtali Transgéne, Strasbourg, France). Ad5tg and the corresponding mutant deleted in the anti-apoptotic E1B19K gene (AdΔ19K) were previously constructed and characterized by members of our team (Leitner et al., 2009; Oberg et al., 2010). Viruses were amplified in human embryonic kidney 293 (HEK293) cells and/or A549 human lung adenocarcinoma epithelial cells, purified and validated by Ms Heike Muller according to previously described methods (Oberg et al., 2010; Wang et al., 2003). PCR verification of Ad5tg and AdΔ19K viruses is shown in figure 10. Ad5tg and AdΔ19K had viral particle (vp) counts of $5.5x10^{11}$vp/ml and $2.3x10^{12}$vp/ml, respectively, and infectious units (plaque-forming units; pfu) of $1.97x10^{10}$pfu/ml and $1.98x10^{11}$pfu/ml, respectively. The resulting ratios of particle to infectious units were 28 and 12 vp/pfu for Ad5tg and AdΔ19K, respectively.

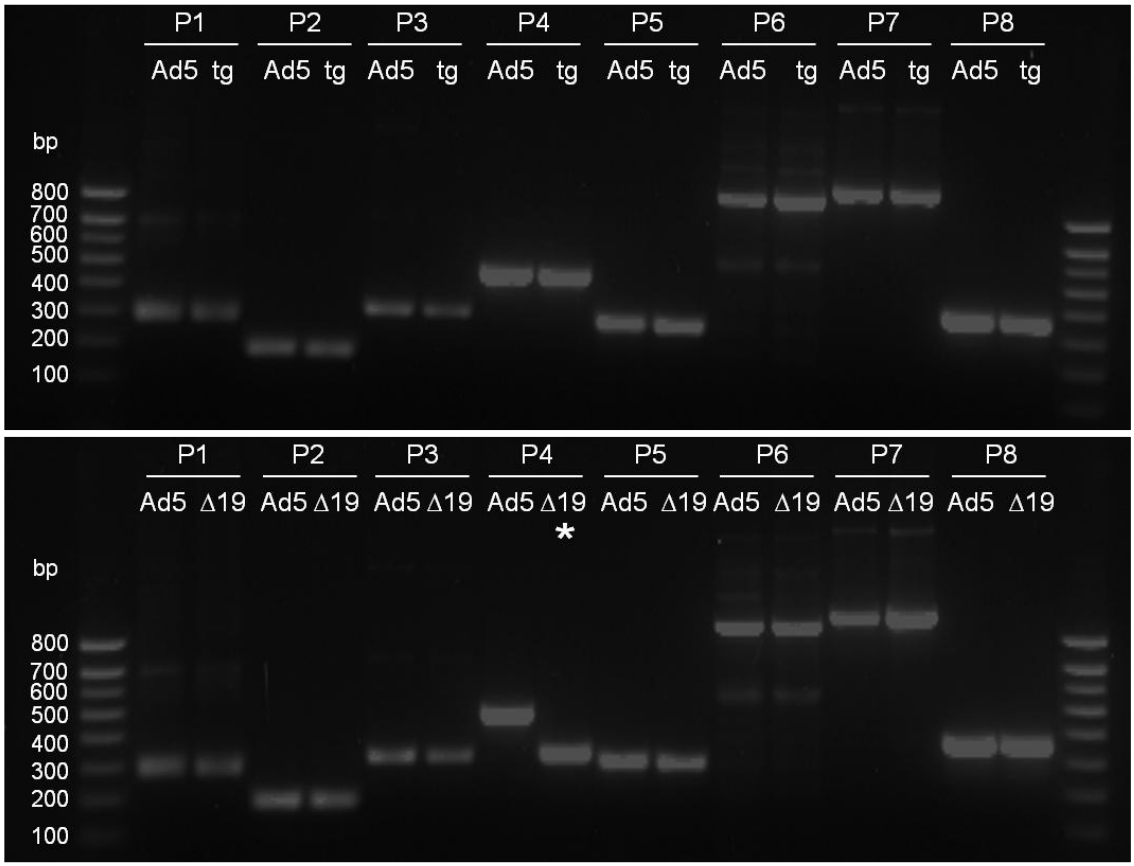

Figure 10: PCR verification of Ad5tg and AdΔ19K. Primers 1-8 (P1-8) identifying the adenoviral E1A, E1B55K, E1B19K, E3B and E3gp19K regions (Table 3) were used for PCR amplification of DNA extracted from wild-type Ad5tg and the AdΔ19K mutant. PCR products from these reactions were

compared with PCR fragments generated from the amplification of the control wild-type Ad5 DNA. Upper panel shows the comparison of Ad5tg (tg) with Ad5 and bottom panel shows the comparison of AdΔ19K (Δ19) with Ad5, with an asterisk denoting the mutated region. Courtesy of Ms Heike Muller.

Table 3: Primer sets for Ad5 PCR verification

Primer	5' binding site	3' binding site	Target region	Expected band size
1	476	853	E1A	377 bp
2	767	1029	E1A	262 bp
3	1069	1453	E1A	384 bp
4	1554	2086	E1B19K	532 bp
5	2073	2440	E1B55K	367 bp
6	2383	3434	E1B55K	1051 bp
7	29915	31038	E3B	1123 bp
8	28715	29135	E3-gp19K	420 bp

2.4. KRAS, TP53 and CDKN2A PCR mutational analysis

2.4.1. DNA extraction

DNA was extracted from PT45 and MIAPaCa-2 cells using the QIAamp DNA Blood Mini Kit, according to the manufacturer's instructions (QIAGEN, Netherlands). In brief, cell pellets were re-suspended in 200µl PBS, and 20µl QIAGEN protease was added per sample followed by addition of 200µl Buffer AL and 10min incubation at 56ºC. 200µl of 100% ethanol were added and DNA was purified using the spin protocol according to the manufacturer's instructions. DNA was eluted in 200µl Buffer AE and assessed for purity (ratio A_{260}/A_{280}=1.8-2.0 and ratio A_{260}/A_{230}=2.0-2.2) and concentration using the NanoDrop^{TM}1000 Spectrophotometer (Thermo Fisher Scientific).

2.4.2. Polymerase chain reaction (PCR) protocol

PT45 and MIAPaCa-2 DNA was analysed for mutations in exon 1 of the KRAS gene, exons 1-3 of CDKN2A gene and exons 5-8 of TP53 gene. Primers for the cellular gene amplifications are given in table 4. Gene amplification was performed in a 50µl PCR reaction mix containing 1µM forward or reverse primer, 200µM NTP mix (Life Technologies, Thermo Fisher Scientific), 1 unit AmpliTaq Gold DNA Polymerase, 1x GeneAmp PCR Gold buffer, 1.5mM $MgCl_2$ (all from Applied Biosytems, Thermo Fisher Scientific) and 1µg DNA, in a PTC-225 Peltier Thermal cycler (MJ Research, Inc, Canada), using the following program: 7min denaturation at 95ºC, 30 seconds(s) incubation at 95ºC, 45s annealing at the specified temperatures, 45s elongation at 72ºC and 30s incubation at 95ºC for 34 cycles and extension at 72ºC. A gradient (55-62ºC) of annealing temperatures was initially set-up to determine the optimal annealing temperature for each primer set (Figure 11), which was: 55.2ºC for KRAS, 57ºC for CDKN2A(p16) exons 1-3 and TP53 exon 8, and 56.2ºC for TP53 exon 5, 6 and 7.

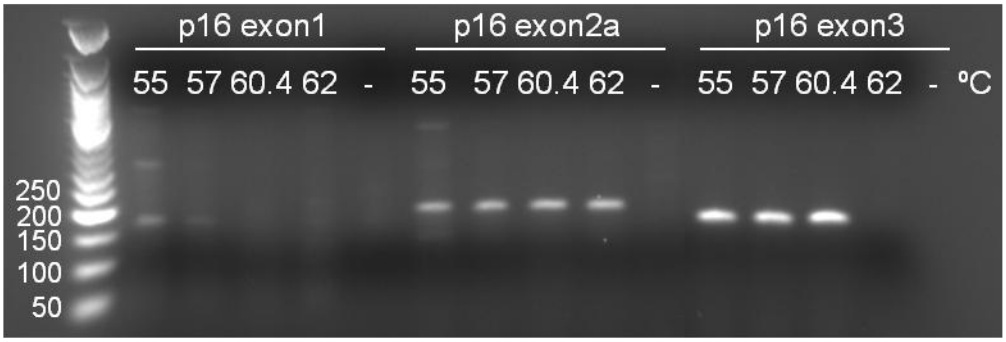

Figure 11: Example of annealing temperature optimisation. PCR reactions were performed at the annealing temperatures indicated on the figure and a sample from each reaction was mixed with 6x blue/orange loading dye (Promega, WI, USA) and loaded on a 1% agarose gel (in 1x Tris-Borate EDTA). The example shown is for CDKN2A (p16) exon 1, 2a and 3 primers. The optimisation was performed using DNA from human umbilical vein endothelial cells (HUVEC). Hyphen indicates the negative control, which was a PCR reaction in the absence of DNA. DNA ladder numbers are in base pairs (bp).

2.4.3. DNA sequencing

The purity and specificity/size of the amplified DNA was assessed by agarose gel electrophoresis (1% agarose gel in 1x Tris-Borate EDTA) before submission for Sanger sequencing at the Barts and the London Genome Centre. TP53 exon 6 amplification resulted in more than one DNA fragment as visualised by agarose gel electrophoresis. Therefore, the specific DNA fragment was excised from the agarose gel, extracted and purified using the QIAquick gel extraction kit (QIAGEN), according to manufacturer's instructions, and then submitted for sequencing. DNA sequencing data were analysed using Chromas software (Technelysium Pty Ltd, Australia) and nucleotide sequences were aligned with National Center for Biotechnology Information (NCBI) reference sequences for each gene (NG_007524 for KRAS and NM_000546.5 for TP53) using nucleotide BLAST (NCBI). Identified nucleotide changes were translated to amino acid changes using translated and protein BLAST (NCBI). The PCR mutational analysis was performed in conjunction with Dr Yang Kee Stella Man.

2.5. Cell viability assays

PT45 and MIAPaCa-2 cells were seeded at $8x10^3$ and $1x10^4$ cells/well, respectively, in 200µl/well of 96-well plates for 16-24h. The medium was decanted and replaced with 90µl of 2% FBS/1% P/S DMEM -/+ drugs. Drug concentration was fixed at doses previously determined to kill 20-40% of cells. Ad5tg or AdΔ19K was added in 10µl medium containing the respective 10x concentration, to make up a total volume of 100µl/well. To generate virus dose-response curves, 5-fold dilutions starting at $1x10^5$ particles per cell (ppc) were prepared. Otherwise, fixed concentrations of both drugs and viruses were prepared. Each condition was in triplicate wells.

72h post-infection cell-viability was assessed using the CellTiter 96® AQeous Non-Radioactive Cell Proliferation Assay (Promega) according to the manufacturer's instructions. The assay comprises of the tetrazolium compound [3-(4,5- dimethylthiazol-2-yl)-5-(3-carboxymethoxyphenyl)-2-(4-sulfophenyl)- 2H-tetrazolium] (MTS) and the electron coupling reagent phenazine methosulfate (PMS). Medium was decanted and replaced with 100µl serum-free DMEM containing 20% MTS and 1% PMS at 100µl/well, followed by cell incubation at

37°C and 5% CO_2. In metabolically active cells, dehydrogenases convert MTS into a soluble formazan dye, which absorbs at 490nm and the absorbance of the dye is directly proportional to the number of live cells in the well (Dunigan et al., 1995). Cells were incubated with DMEM/MTS/PMS until the absorbance of the untreated cells reached 1.6-1.9 (typically 1-2h for MIAPaCa-2 cells and 3-6h for PT45 cells). Absorbance was read at 490nm using a microplate reader (Opsys MR from Dynex Technologies, VA, USA).

Cell viability calculated from the absorbance values was expressed as percentages and used to indirectly calculate the percentages of cell death. The absorbance of the DMEM/MTS/PMS solution in the absence of cells (background absorbance; $A_{background}$) was subtracted from the absorbance values of untreated and treated cells. In cell viability assays generating dose-response curves, the percentage cell death of virus or drug was calculated by normalising the absorbance of virus- or drug-treated (A_{virus} or A_{drug}) cells to that of untreated cells ($A_{untreated}$), using the following formula:

$$\% \text{ Cell death virus or drug} = 100 - \left[100 \times \left(\frac{(A_{virus} \text{ or } A_{drug}) - (A_{background})}{(A_{untreated}) - (A_{background})} \right) \right]$$

When virus was combined with drugs, the absorbance of the double treatment ($A_{virus+drug}$) was normalised to the absorbance of drug-treated cells (A_{drug}) as shown by the following formula:

$$\% \text{ Cell death virus + drug} = 100 - \left[100 \times \left(\frac{(A_{virus+drug}) - (A_{background})}{(A_{drug}) - (A_{background})} \right) \right]$$

When two drugs were combined with virus, the absorbance was normalised to that of the cells treated with the two drugs. When cell viability assays were performed using fixed doses of both viruses and drugs, the absorbance of all treated cells was normalised to the absorbance of untreated cells only. Effective concentrations (EC) killing 50% of cells (EC_{50} values) were derived from

sigmoidal dose-response curves, generated using non-linear regression analysis (Graphpad Prism Software, CA, USA) with the following formula:

$$Y = \text{Bottom} + \frac{(\text{Top} - \text{Bottom})}{1 + 10^{(\text{LogEC50} - X) \cdot \text{HillSlope}}}$$

(LogEC50 is the X value when the response is halfway between the Bottom and the Top of the curve)

2.6. Trypan blue inclusion cell death assay

PT45 cells were seeded at $1.5x10^5$ cells/well in 6-well plates, infected, treated and harvested as described in section 2.2.3. Cell suspension was mixed with 0.4% Trypan blue dye (Bio-Rad Laboratories, Inc, CA, USA) at 1:1 ratio and 10µl in duplicates were loaded onto a dual-chambered counting slide (Bio-Rad). Cell count and viability were assessed using a TC20^{TM} automated cell counter (Bio-Rad). Percentage cell viability was recorded and used to calculate cell death.

2.7. Apoptotic assays

PT45 or MIAPaCa-2 cells were seeded at $2x10^5$ cells/well in 6-well plates, infected and treated as described in section 2.2.3. Where indicated, 25µM of zVAD was added simultaneously with gemcitabine. Staurosporine was used at 1µM for 16h in PT45 cells and at 0.5µM for 24h in MIAPaCa-2 cells.

2.7.1. TUNEL/PI assay

72h post-infection cells were harvested, fixed and stained using the APO-BrdU kit (BD Biosciences Pharmingen, CA, USA) according to the manufacturer's guidelines. Briefly, $1\text{-}2x10^6$ cells were suspended in 1% w/v parafolmaldehyde/PBS, kept on ice for 1h, then washed in PBS and fixed in 70% ethanol (30min on ice). Cells were washed in wash buffer and incubated (1h, 37°C) in DNA-labelling solution, containing Br-dUTP. Cells were washed in rinse buffer and incubated (30min, 22°C) in antibody-staining solution, containing FITC-labelled anti-BrdU antibody. 350µl of PI/RNAse staining buffer

was added (30min, 22°C) and cells were analysed by flow-cytometry as detailed below. All reagents were supplied by the kit (BD Biosciences).

2.7.2. Cleaved Caspase-3/PI assay

At the indicated times post-infection cells were harvested, fixed and stained using the FITC Active Caspase-3 Apoptosis Kit (BD Biosciences Pharmingen) according to the manufacturer's guidelines. Briefly, cell pellet was washed with PBS twice and resuspended in BD Cytofix/Cytoperm™ solution at a concentration of $1x10^6$ cells/ml. Following a 20min incubation on ice, cells were pelleted and washed twice with 1x BD Perm/Wash™ buffer. Cells were incubated in FITC Rabbit Anti-Active Caspase-3 antibody (supplied by the kit) diluted in BD Perm/Wash™ buffer solution (30min, 22°C). Following washing with BD Perm/Wash™ buffer, cell pellet was re-suspended in 250µl of PI (50µg/ml)/RNAse A (100µg/ml) solution and incubated for 30min at 22°C.

2.7.3. Flow-cytometric analysis

Flow-cytometric data acquisition was performed using BD CellQuest^{TM} software operated on a BD FACSCalibur instrument (both from Becton Dickinson, NJ, USA). PI and FITC signals were detected in the FL-3 and FL-1 channel, respectively, of the 488nm argon laser. Dot plots of Side Scatter (SSC-H) vs Forward Scatter (FSC-H) were used to exclude debris, followed by doublet exclusion using the area and width of the FL2 channel. Acquisition stopped when 20000 events were acquired in the doublet-exclusion gate. Cell-cycle specific apoptosis was measured by plotting the FL1-H channel, where FITC was detected, against the FL3-H channel, where propidium iodide was detected, and gates for apoptotic G1, S, G2/M and >4N cells where applied. Post-acquisition data analysis was performed using the FlowJo v7.6.5 software (Tree star, Inc, OR, USA) and bar charts were plotted using GraphPad Prism v5 software.

2.8. Viral genome amplification assay

PT45 cells were seeded at $7.5x10^4$ cells/well in 6-well plates, infected, treated and harvested (excluding supernatant) at 4, 24, 36, 48 and 72h post-infection, as described in section 2.2.3. Cell suspension was transferred to microcentrifuge tubes and spun at 1200rpm for 5min using a benchtop microcentrifuge (5415C from Eppendorf, Germany). Cell pellets were snap-frozen and stored at -80ºC until all time-points were collected. DNA was extracted as described in section 2.4.1. Total DNA was diluted to 15ng/µl and used for quantitative PCR (qPCR) analysis of the viral E2A gene using the standard curve method. The cellular GAPDH gene was used as an internal control.

2.8.1. Quantitative PCR protocol

Two qPCR reactions were set-up per sample with each containing 1x SYBR® Green PCR master mix (Applied Biosystems), 200nM of forward and reverse primers and 60ng DNA (with the exception of standards) in 20µl volume. The primer sequences are given in table 4. qPCR was performed in MicroAmp® optical 96-well reaction plates covered with MicroAmp® optical adhesive film (Applied Biosystems), using an Applied Biosystems 7500 Instrument. Melting (dissociation) curves for each primer set were generated for primer quality control. A standard curve was generated for each gene tested, using 10-fold serial dilutions, and used for determination of E2A and GAPDH quantity in unknown samples. E2A quantity was normalised to GAPDH and the E2A/GAPDH quantity ratios in 24, 36, 48 and 72h samples were normalised to the average E2A/GAPDH quantity ratio of the duplicates at 4h post-infection (input DNA).

2.9. Quantification of E1A protein expression by flow-cytometry

PT45 and MIAPaCa-2 cells were seeded at $2.5x10^5$ and $3x10^5$ cells/well, respectively, in 6-well plates, infected, treated and harvested (excluding supernatant) as described in section 2.2.3. $0.5\text{-}1x10^6$ cells/ml were

resuspended in ice-cold 3% BSA/1% sodium azide/PBS, pelleted and fixed in 0.5ml 100% methanol. Samples were stored at -20°C (10min minimum incubation in methanol) until all time-points were collected. Cells were washed twice in 1% BSA/PBS and permeabilised in 0.5ml of 0.5% Triton-X100/PBS for 15min at 22°C, followed by wash in 0.1% Triton/PBS and incubation with anti-E1A antibody diluted in 3% BSA/PBS (30min at 22°C). Cells were washed once with PBS and incubated with anti-mouse FITC-conjugated antibody diluted in 3% BSA/PBS (30min at 22°C). Details for the antibodies are given in table 6. Cells were washed twice in PBS, resuspended in 3% BSA/ 1% sodium azide/PBS and analysed by flow cytometry using a BD FACSCalibur instrument. Cell debris was excluded and 20000 events were acquired per sample. FITC was detected using the FL1 channel of the 488nm argon laser. Data were analyzed using the FlowJo v7.6.5 software (Tree star, Inc).

2.10. mRNA analysis by reverse transcriptase qPCR

PT45 cells were seeded at $2x10^5$ cells/well in 6-well plates, infected, treated and harvested (excluding supernatant) as described in section 2.2.3. RNA was extracted using the RNeasy Mini Kit (QIAGEN) according to the manufacturer's instructions. Briefly, cell pellet was resuspended in 350µl of buffer RLT and the lysate was transferred to QIAshredder spin columns, centrifuged and mixed with 350µl of 70% ethanol. Lysate was transferred to an RNeasy spin column, washed once with buffer RW1 and twice with buffer RPE, followed by elution in 50µl of RNase-free water. RNA was assessed for purity (ratio A_{260}/A_{280}=1.8-2.0 and ratio A_{260}/A_{230}=2.0-2.2) and concentration using the NanoDrop™1000 Spectrophotometer (Thermo Fisher Scientific).

RNA was diluted to the concentration of the least concentrated sample and purified from contaminating DNA using the DNA-*free*™ kit (Ambion) according to the manufacturer's instructions. Briefly, RNA was treated with recombinant DNase I (rDNase I) in DNase I buffer and incubated at 37°C for 20min, followed by a 2min incubation with the DNase inactivation reagent, centrifugation and transferring of the pure RNA in fresh microcentrifuge tubes. 1µg of RNA was reversed transcribed using the TaqMan® Reverse Transcription Reagents Kit

(Applied Biosystems), according to the manufacturer's instructions. A 50µl reaction mix was set-up, containing 1x TaqMan® Reverse Transcription Buffer, 5.5mM $MgCl_2$, 500µM deoxyNTPs mixture, 2.5µM random hexamers, 0.4units/µl RNase inhibitor, 1.25units/µl MultiScribe® Reverse Transcriptase and 1µg RNA. Reverse transcription was performed using a DNA Engine Dyad® Peltier thermal cycler (MJ Research) by incubating at 25°C for 10min, followed by 30min incubation at 48°C and a 5min incubation at 95°C. 20ng of complementary DNA (cDNA) were used in qPCR analysis of viral E1A and Penton genes and the cellular Claspin and GAPDH genes. qPCR analysis using the standard curve method was performed as described in section 2.8.1. Primer sequences are shown in table 4. Claspin, E1A and penton quantities were normalised to GAPDH internal control. For E1A mRNA analysis, E1A/GAPDH ratio was normalised to penton/GAPDH ratio in order to remove the effect of viral replication and measure E1A expression as a function of viral late gene expression (indicative of replication).

Table 4: Primer sequences used for PCR

Gene	Primer	Primer sequence
GAPDH	Forward	TGGGCTACACTGAGCACCAG
	Reverse	GGGTGTCGCTGTTGAAGTCA
E2A	Forward	GGATACAGCGCCTGCATAAAAG
	Reverse	CCAATCAGTTTTCCGGCAAGT
E1A	Forward	TGCCAAACCTTGTACCGGA
	Reverse	CGTCGTCACTGGGTGGAAA
Penton	Forward	GATCGGAAAACCTCTCGAGAAA
	Reverse	CGTAGGAGGGAGGAGGACCTT
CLSPN	Forward	ACAGTGATTCCGAAACAGA
	Reverse	TGCTCCTCGGCACTGTCATA
KRAS exon 1	Forward	GGCCTGCTGAAAATGACTGA
	Reverse	GTCCTGCACCAGTAATATGC
CDKN2A exon 1	Forward	TCTGCGGAGAGGGGGAGAGCAGGCA
	Reverse	GCGCTACCTGATTCCAATTC
CDKN2A exon 2A	Forward	ACAAGCTTCCTTTCCGTCATGCCG
	Reverse	CCAGGCATCGCGCACGTCCA

CDKN2A exon 2B	Forward	TTCCTGGACACGCTGGTGGT
	Reverse	CCAGGTCCACGGGCAGA
CDKN2A exon 3	Forward	CCGGTAGGGACGGCAAGAG
	Reverse	CTGTAGGACCCTCGGTGACTGATGA
TP53 exon 5	Forward	TTCCTCTTCCTGCAGTACTCC
	Reverse	GCCCCAGCTGCTCACCATCG
TP53 exon 6	Forward	CGATGGTGAGCAGCTGGGGC
	Reverse	AGTTGCAAACCAGACCTCA
TP53 exon 7	Forward	TCCTAGGTTGGCTCTGAC
	Reverse	CAAGTGGCTCCTGACCTGGA
TP53 exon 8	Forward	CCTATCCTGAGTAGTGGTAA
	Reverse	CCTGCTTGCTTACCTCGCT

2.11. Cell cycle and mitotic-index analysis in unsynchronised cells

PT45 or MIAPaCa-2 cells were seeded at $2x10^5$ cells/well in 6-well plates, infected, treated and harvested as described in section 2.2.3. Cells were fixed with 70% ethanol (30min, 4°C) and stored at 4°C. All centrifugations henceforth were performed at 2000rpm for 3min using the Allegra X-22 centrifuge. When all time-points had been collected, fixed cells were centrifuged, ethanol was removed and cells were washed with 1ml of PBS.

For mitotic index analysis cells were washed with 1ml of 1% FBS/PBS and incubated in 100µl of anti-phospho-histone H3 antibody diluted in 1% FBS/PBS (30min at 22°C). Following wash in 3ml of 1% FBS/PBS, cells were incubated in 100µl of Alexa Fluor® 488 antibody diluted in 1% FBS/PBS (30min at 22°C). Details for the antibodies are given in table 6. Cells were washed with 3ml of 1% FBS/PBS. For PI staining, cells were incubated in 300µl of PI (50µg/ml) / RNAse A (100µg/ml) solution (30min, 22°C). Immediately after staining data were acquired as described in section 2.7.3. The exact gating strategy is shown in figure 12.

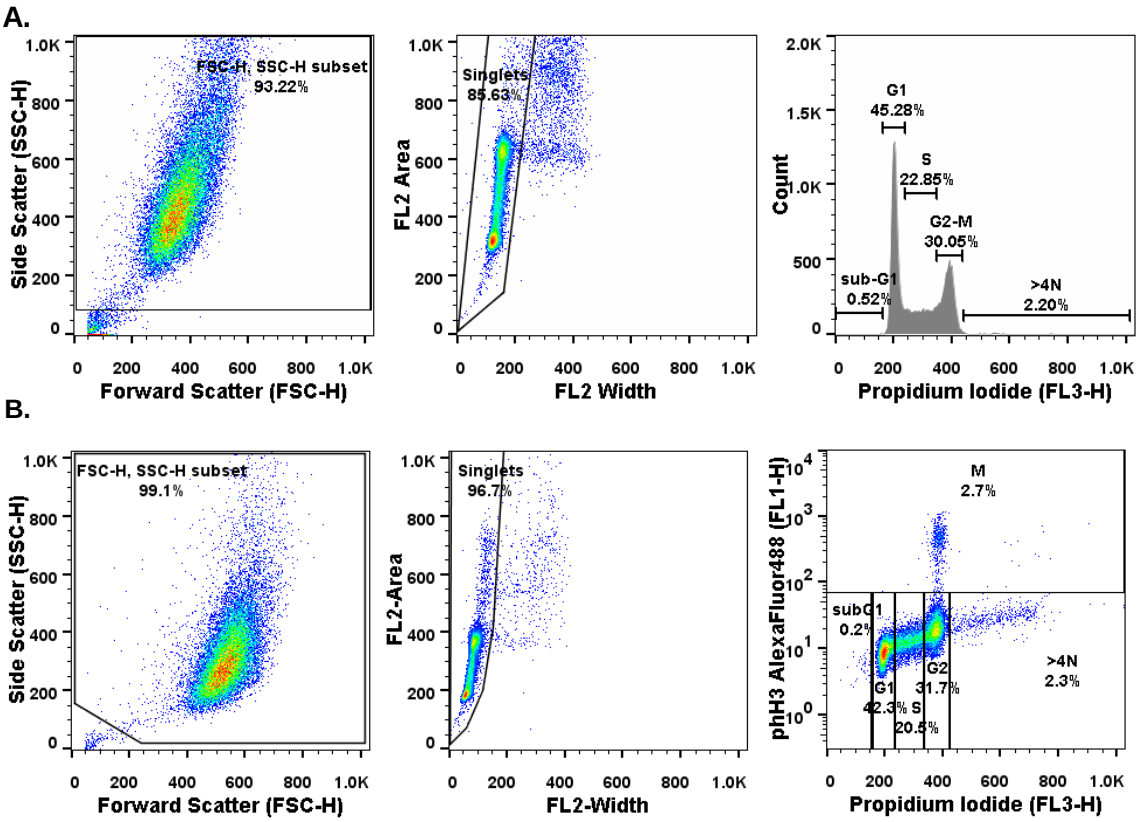

<u>Figure 12:</u> Gating strategy for cell cycle and mitotic index analysis. Dot plots of Side Scatter (SSC-H) vs Forward Scatter (FSC-H) were used to exclude debris, followed by doublet exclusion using the area and width of the FL2 channel. Acquisition stopped when 20000 events were acquired in the singlets gate. **(A)** Cell cycle distribution was assessed by plotting a histogram of propidium iodide fluorescence (FL3-H channel of the 488nm argon laser). **(B)** For mitotic index analysis phospho-histone H3 (phH3) fluorescence (FL1-H channel of the 488nm argon laser) was plotted against propidium iodide (FL3-H channel). Gates for subG1, G1, S, G2, M and >4N cells where applied as indicated on the graph. The examples shown are from mock-infected PT45 cells.

2.12. Cell cycle and mitotic-index multicolour flow-cytometric analysis in synchronised cells

2.12.1. Cell synchronisation and treatment

PT45 cells were seeded at 2.5x10^5 cells/well in 6-well plates and 13-15h later treated with 2.5mM thymidine for synchronisation in early S-phase. 24h after treatment, cells were released from the thymidine block by washing twice with PBS (pre-warmed to 37ºC) and incubating in 1ml serum-free DMEM -/+ 300pcc

of Ad5tg or AdΔ19K. 2h later the medium was replaced with 10% FBS/ 1% P/S DMEM -/+ 5nM gemcitabine.

2.12.2. Cell harvesting, fixing and staining

At the indicated times post-infection, supernatant and cells were harvested as described in section 2.2.3, washed with PBS and incubated with 250µl of the fixable viability dye (FVD) eFluor® 506 (equilibrated to 22 ºC) diluted 1:1000 in PBS. Following a 30min incubation at 4ºC, cells were washed in PBS and fixed with cold 70% ethanol (30min, 4ºC). Cells were stored at 4ºC until all time-points had been collected. All centrifugations henceforth were performed at 2000rpm for 3min.

Cells were washed with 1ml of 1% FBS/PBS and permeabilised using cold 0.25% Triton X-100 diluted in 1% FBS/PBS. Following a 10min incubation at 4ºC, cells were centrifuged and incubated in 100µl of primary antibody solution for 30min at 22°C. The primary antibody solution consisted of rabbit polyclonal anti-phospho-histone H3 and mouse monoclonal anti-E1A antibodies diluted in 1% FBS/PBS. Following two washes in 2ml of 1% FBS/PBS, cells were incubated in 100µl of secondary antibody solution for 30min at 22°C. The secondary antibodies used were anti-rabbit Alexa Fluor® 488 and anti-mouse Alexa Fluor® 647 diluted in 1% FBS/PBS. Cells were then washed with 3ml of 1% FBS/PBS and incubated in 200µl of PI (50µg/ml) / RNAse A (100µg/ml) solution (30min, 22°C). Details for the antibodies are given in table 6.

2.12.3. Multicolour flow-cytometric analysis

Cells were immediately acquired using the BD FACSDiva™ software operated on the BD LSRFortessa™ cell analyzer (both from Becton Dickinson). PI and Alexa Fluor® 488 signals were detected in the B695/40 and B5300/30 filters, respectively, of the 488nm blue laser. FVD eFluor® 506 and Alexa Fluor® 647 signals were detected in the V525/50 filter of the 405nm violet laser and R670/14 filter of the 640nm red laser, respectively. Cell debris and doublets were excluded, followed by gating of live cells and acquisition of 20000 events,

as demonstrated in figure 13. Data were analyzed using the FlowJo v7.6.5 software and plotted using GraphPad Prism v5 software.

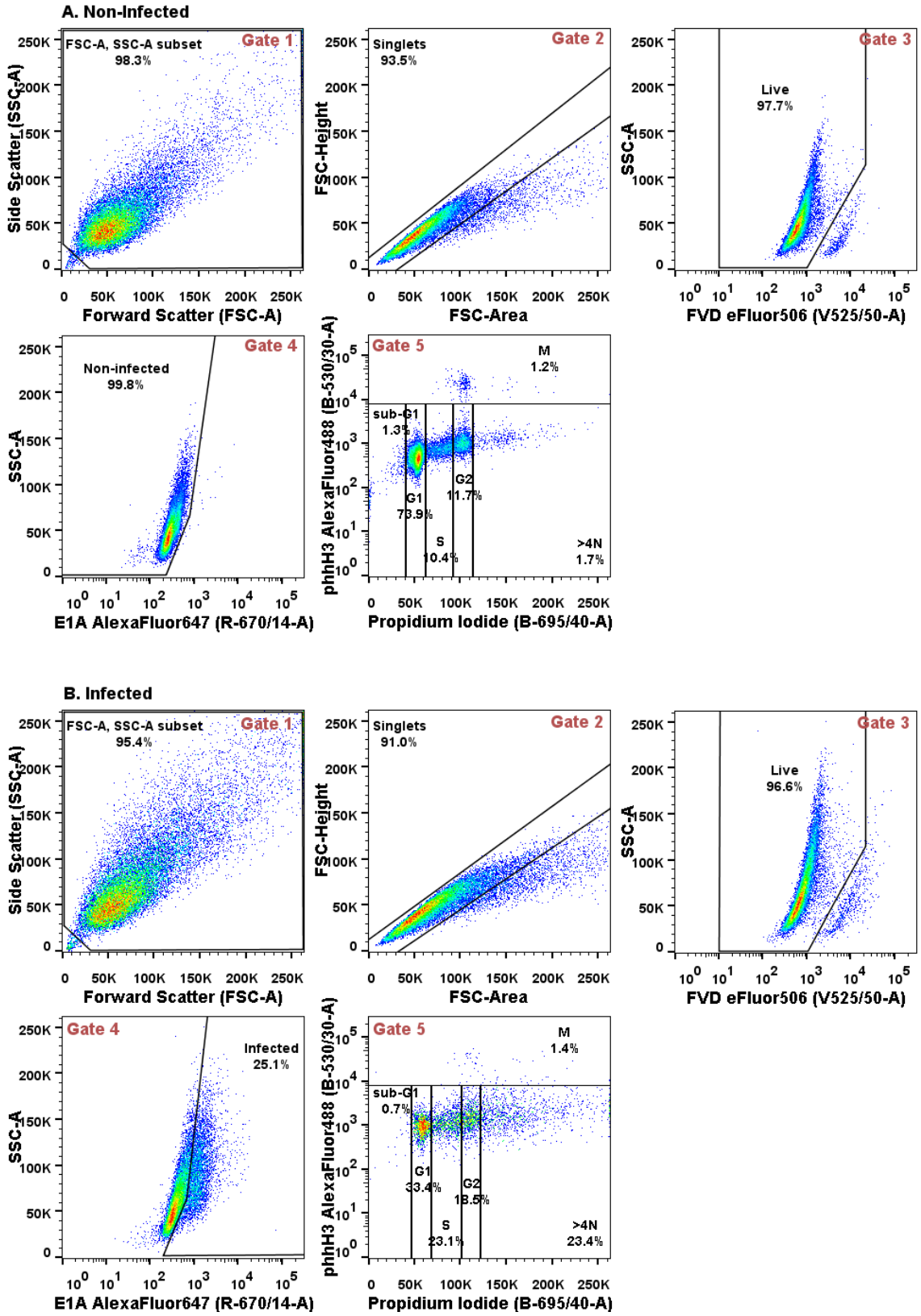

Figure 13: Gating strategy for multicolour flow-cytometry. Dot plots of Side Scatter (SSC-A) vs Forward Scatter (FSC-A) were used to exclude debris (gate

1), followed by doublet exclusion using the height and width of the FSC channel (gate 2). Singlets were then gated on a dot plot of SSC-A vs V525/50-A, to exclude FDV eFluor®506 positive, that is dead, cells (gate 3). Acquisition stopped when 20000 events were acquired in the live-cells gate (gate 3). Live cells were next assessed for E1A expression by plotting SSC-A against R-670/14-A. E1A-negative non-infected (untreated or gemcitabine-treated) cells **(A)** or E1A-positive infected cells **(B)** were then gated (A and B gate 4). Gated non-infected or infected cells were assessed for phospho-histone H3 and propidium iodide expression by plotting B-530/30-A against B-695/40-A. Gates for subG1, G1, S, G2, M and >4N cells where applied as indicated on the graph (gate 5). The example shown is from mock-infected **(A)** and Ad5tg-infected **(B)** PT45 cells 72h post-infection.

2.13. Immunoblot analysis

2.13.1. Protein extraction and quantitation

PT45 and MIAPaCa-2 cells were seeded at $1.5x10^5$ and $2x10^5$ cells/well, respectively, in 6-well plates, infected, treated and harvested as described in section 2.2.3. Cells were lysed in RIPA buffer (50mM Tris pH 8.0, 150mM NaCl, 1% Triton X-100, 0.5% sodium deoxycholate, 0.1% SDS) supplemented with protease inhibitor cocktail and PhosSTOP phosphatase inhibitor (Roche Diagnostics, Switzerland). Cell lysates were incubated on ice (15min), centrifuged (15min, 16100xg, 4°C) to remove pelleted debris and stored at -80ºC.

Cell lysates were quantitated for protein using the Bradford assay as follows: Samples from cell lysates were diluted (1:10-20) in water and 5µl of the diluted lysate were mixed with 195µl of 1x Bradford dye reagent (Bio-Rad) diluted in water, in duplicate wells of a 96-well plate. A standard curve was generated by serial dilutions of BSA (New England Biolabs, UK) starting from 1mg/ml. Absorbance was detected using the 560/8nm filter of the Victor3^{TM}-1420 multilabel plate reader (PerkinElmer, MA, USA). Background absorbance detected in the blank well (5µl water and 195µl Bradford dye reagent) was subtracted from all the absorbance values. The average of the duplicate absorbance from the BSA standards was used to construct a standard curve of Absorbance vs Protein concentration, from which the equation of the straight line was derived and used to calculate the protein concentration of the unknown

samples (multiplied by the dilution factor). Cell lysates were mixed with 2X sample Laemmli buffer (0.125M Tris-HCl pH6.8, 20% glycerol, 4% SDS, 0.01% bromophenol blue and freshly-added 10% β-mercaptoethanol) and incubated for 5min at 95ºC.

2.13.2. SDS-PAGE and immunobloting

Equal amounts (typically 30µg) of protein were resolved by SDS Polyacrylamide Gel Electrophoresis (SDS-PAGE). For immunoblot analysis of claspin 60µg of protein were loaded on gels. The percentage of SDS-PAGE resolving gels ranged from 6% to 15% according to the protein of interest, while the stacking gel was always 4%. SDS-PAGE gels were custom-made using ProtoGel 30% (w/v) acrylamide/methylene bisacrylamide solution (37.5:1 ratio), 4x ProtoGel Resolving buffer, 4x ProtoGel Stacking Buffer, TEMED (all from National Diagnostics, GA, USA) and 10% w/v ammonium persulfate (APS). A PageRuler™ prestained or PageRuler™ Plus prestained protein ladder (Fermentas, Thermo Fisher Scientific) was used as protein size standards. SDS-PAGE was performed at 120V using the Mini-PROTEAN® Tetra cell system (Bio-Rad) and in the presence of Tris-Glycine SDS-PAGE Buffer (National Diagnostics) diluted to 1x in water. Proteins were then transferred to nitrocellulose membranes (Hybond-ECL, GE Healthcare, UK) using the Trans-Blot® SD semi-dry electrophoretic transfer cell (Bio-Rad) at 20V, typically for 40min. For immunoblot analysis of claspin, wet protein transfer was performed using the Mini Trans-Blot® electrophoretic transfer cell system (Bio-Rad) at 400mA for 2h.

Membranes were blocked in 0.1% Tween-20/ 5% BSA or milk (Marvel Morrison's) diluted in Tris-buffered saline (TBS) for 1h at 22°C, and incubated (overnight, 4°C) in primary antibodies diluted in blocking buffer. Membranes were washed three times (5min each) in 0.1% Tween-20/TBS, and incubated (1h at 22°C or 2h at 4°C) in secondary antibodies diluted in blocking buffer. Membranes were washed three to five times (5min each) in 0.1% Tween-20/TBS and immunodetection was performed using enhanced chemiluminescence substrate ECL and ECL-Plus (PerkinElmer). Protein bands were visualised on X-ray films (FujiFilm) or using the G:Box iChemi-XT imaging

system (Syngene, UK). Densitometric analysis was done using the NIH ImageJ software. Details of the antibodies used are given in table 6.

2.14. siRNA-mediated knockdown followed by immunoblotting and cell viability, viral genome amplification and cell cycle assays

2.14.1. siRNA transfection

PT45 cells were seeded at $2x10^5$ cells/well in 6-well plates. 16-20h later cells were left untransfected or transfected with 25nM of siGENOME non-targeting (NT) siRNA #1 control, siGENOME SMARTpool Claspin (CLSPN) siRNA or siGENOME SMARTpool MRE11A siRNA, using 10µl DharmaFECT1 transfection reagent (all purchased from Dharmacon, GE Healthcare) and according to the manufacturer's instructions. siRNA sequences are shown in table 5. Briefly, siRNAs and DharmaFECT were diluted separately in serum-free DMEM and incubated for 5min, followed by addition of siRNA to DharmaFECT solution and 20min incubation at 22ºC. Cell medium was replaced with 1.6ml of serum-free DMEM and 0.4ml of siRNA/DharmaFECT solution was added to each well. After 6h medium was replaced with 10% FBS/1% P/S DMEM.

24-32h later non-transfected, siNT-, siCLSPN- and siMRE11-transfected cells were harvested as described in section 2.2.3, counted and re-seeded in 96-well plates for use in cell viability assays or 6-well plates for use in immunoblotting, cell-cycle analysis and viral genome amplification assays. Cell seeding was at $8x10^3$ cells/well in 96-well plates and $2x10^5$ cells/well in 6-well plates for 16-24h.

2.14.2. Cell viability, viral genome amplification and cell cycle assays

For cell viability assays, cells were treated with AdΔ19K -/+ drugs to generate dose-response curves as detailed in section 2.5. and cell viability was assessed at 72h post-infection by MTS assay (see section 2.5.). For viral genome amplification assessment, siNT-, siCLSPN- and siMRE11-transfected cells were infected, treated, harvested (at 48h) and DNA was extracted for use in viral genome amplification assays, as detailed in section 2.8. For cell cycle analysis, non-transfected, siNT-, siCLSPN- and siMRE11-transfected cells were infected

and treated as described in section 2.2.3. At 24h, 48h and 72h post-infection cells were harvested and processed as detailed in section 2.12.2. for use in cell-cycle and mitotic index analysis by multicolour flow-cytometry (see section 2.12.3.).

2.14.3. Immunoblot analysis to monitor siRNA-mediated knockdown

At 48, 72, 96 and 120h post-transfection, non-transfected, siNT-, siCLSPN- and siMRE11-transfected cells were harvested, lysed and processed for immunoblot analysis as detailed in section 2.13., with the exception of the electrophoresis procedure for Claspin detection. During these studies Claspin and Vinculin were resolved in NuPAGE® Novex 3-8% Tris-Acetate pre-cast gels in the presence of NuPAGE® Tris-Acetate SDS Running Buffer using the XCell SureLock® Mini-Cell (all from Life Technologies Thermo Fisher Scientific). Protein transfer and immunodetection were carried out as before (see section 2.13.2.).

Table 5: siRNA sequences

siRNA	Catalogue No	Target sequence
siGENOME non-targeting #1	D-001210-01-05	
siGENOME SMARTpool CLSPN	D-005288-01	GGAAAUACCUGGAGGAUGA
	D-005288-03	GCAGAUGGGUUCUUAAAUG
	D-005288-02	GGACGUAAUUGAUGAAGUA
	D-005288-04	GAAUUUAUAUGCUGGGAAA
siGENOME SMARTpool MRE11A	D-009271-01	GAUGAGAACUCUUGGUUUA
	D-009271-02	GAAAGGCUCUAUCGAAUGU
	D-009271-03	GCUAAUGACUCUGAUGAUA
	D-009271-04	GAGUAUAGAUUUAGCAGAA

2.15. Immunofluorescence microscopy analysis

2.15.1. Cell seeding and treatment

For immunofluorescence microscopy analysis of mitotic cells, PT45 and MIAPaCa-2 cells were seeded at $5x10^4$ cells/well on coverslips (Menzel-Gläser, Germany) in 6-well plates. For immunofluorescence microscopy analysis of interphase cells, PT45 cells were seeded on coverslips at $2.5x10^4$ cells/well, or $5x10^4$ cells/well when cells would be treated with gemcitabine. 16-24h later cells were infected and treated as described in section 2.2.3. At the indicated times post-infection cells were processed as follows:

2.15.2. Methanol Fixation Method

Cells were fixed in 100% ice-cold methanol (20min, 4°C), followed by 20min blocking in 5% FBS/PBS and incubation (overnight, 4°C) in primary antibodies (Aurora-A, α-tubulin or Ad-E1A as specified) diluted in 5% FBS/PBS. Cells were washed three times in PBS and incubated (1h, 22°C) in secondary antibodies (anti-mouse AlexaFluor® 488 and anti-rabbit AlexaFluor® 594) diluted in 5% FBS/PBS. Coverslips were washed twice in PBS and once in distilled water. Details for the antibodies are given in table 6.

2.15.3. Parafolmaldehyde Fixation Method

Cells were washed twice in PBS and fixed (10min, 22°C) in 4% parafolmaldehyde/PBS (made from 16%(w/v) folmaldehyde (TAAB, UK)), followed by two washes in PBS and permeabilization (10min, 22°C) in Triton buffer (0.5% Triton X-100, 20mM Hepes KOH pH7.9, 50mM NaCl, 3mM $MgCl_2$, 300mM Sucrose). Cells were washed twice in PBS, blocked in 0.05% Tween-20/3% BSA/PBS (15min, 22°C) and incubated (overnight, 4°C) in rabbit polyclonal anti-phospho-histoneH2A.X and mouse anti-Ad-DBP antibodies diluted in blocking buffer. Coverslips were washed twice in blocking buffer and incubated (1h, 22°C) in AlexaFluor® 488 goat anti-mouse and AlexaFluor® 594 goat anti-rabbit IgG (H+L) antibodies diluted in blocking buffer. Details for the

antibodies are given in table 6. Coverslips were washed twice in blocking buffer, once in PBS and once in distilled water.

2.15.4. Mounting and analysis

Following staining, all coverslips were allowed to dry (30min, 22°C) and mounted on slides (ESCO optics, NJ, USA) using the ProLong Gold antifade reagent with DAPI. Slides were analysed using a Zeiss Axioplan epifluorescent microscope, where cell counting was performed. Images were acquired using the confocal laser scanning microscope Zeiss LSM510 META.

2.15.5. γH2AX analysis in interphase cells

Images from 10-20 fields were acquired using the 40x objective of the confocal laser scanning microscope Zeiss LSM510 and used for cell counting. Cell counting in separate channels was performed using the NIH ImageJ software. Quantification of total γH2AX fluorescence intensity was performed as follows:

Channels were separated and converted to greyscale. The red (γH2AX) channel was used for measurements of area, mean grey value and integrated density. The mean grey value is defined as "the sum of the gray values of all the pixels in the selection, divided by the number of pixels" (Ferreira and Rasband, 2012). The integrated density is defined as "the sum of the values of the pixels in the image or selection. This is equivalent to the product of Area and Mean Gray Value" (Ferreira and Rasband, 2012). To measure **background fluorescence**, a region of the image containing no cells was selected and the mean grey value was measured. This was repeated twice and the mean grey values from the three selected regions were averaged to produce the average background fluorescence of the image. Then the area and integrated density of the entire image were measured. The **corrected total γH2AX fluorescence intensity** was calculated by multiplying the area of the image by the average background fluorescence and subtracting the product from the integrated density of the entire image. This was then divided by the number of cells in the image to give the **total γH2AX fluorescence intensity per non-infected cell.** In the presence of virus, area and integrated density were measured only in the

infected region of the image (as indicated by Ad-DBP expression) and corrected total γH2AX fluorescence intensity was calculated using the above equation. This was then divided by the number of infected cells to give the **total γH2AX fluorescence intensity per infected cell.**

2.16. PT45 histone H2B-mCherry stable cell line generation

PT45 cells were seeded in a T75 flask until 90% confluency was reached. Cells were transfected with 5µg of histoneH2B-mCherry construct (a gift from Dr Spiros Linardopoulos, The Institute of Cancer Research, London UK) using 16µl Lipofectamine™ 2000 (Life Technologies Thermo Fisher Scientific), according to the manufacturer's instructions. The following day transfected cells were harvested, washed in PBS and fluorescently sorted using the BD FACSAria™ cell sorter (Becton Dickinson) based on mCherry expression (detected in the YG610/20-A filter of the yellow-green 561nm laser). During the first cell sort 20% of cells were positive for mCherry (Figure 14). Sorted cells were cultured in 20% FBS/1% P/S DMEM and a week later the culture was up-scaled in 10% FBS/1% P/S DMEM. The PT45 histoneH2B-mCherry cells were fluorescently sorted by flow-cytometry another three times until more than 90% of cells expressed mCherry (Figure 14).

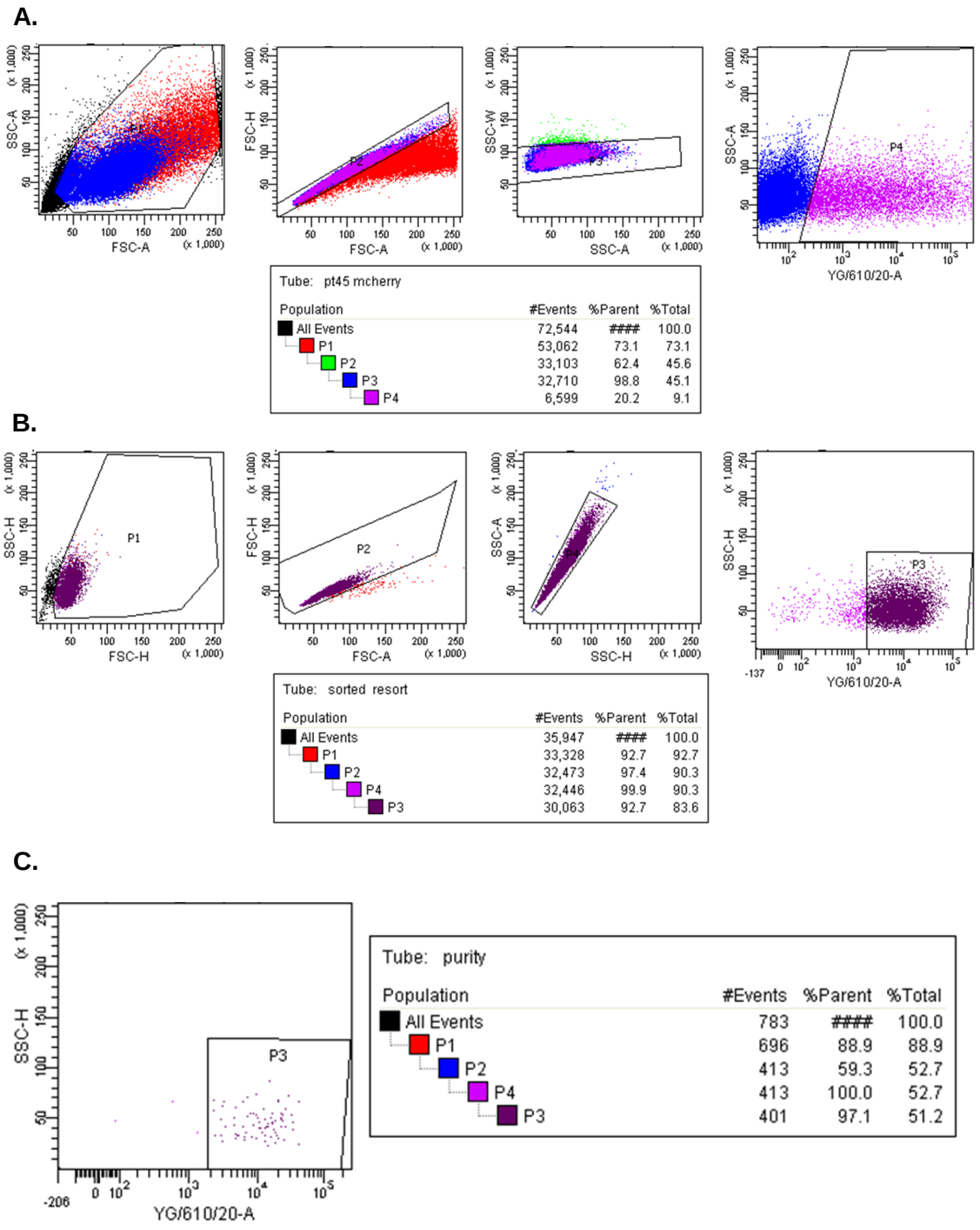

Figure 14: Fluorescently-assisted cell sorting of PT45 histone H2B-mCherry cells. Dot plots of Side Scatter (SSC-A) vs Forward Scatter (FSC-A) were used to exclude debris (gate P1). Next, doublets were excluded using the height and area of the FSC channel (gate P2) and doublet exclusion was confirmed using the width and area of the SSC channel. Singlets were then assessed for mCherry expression by plotting SSC-A vs YG/610/20-A (where mCherry signal was detected). **(A)** First sort after cell transfection. The P4 gate shows the % cells positive for mCherry. **(B)** Fourth sort. The P3 gate shows the % cells positive for mCherry **(C)** Assessment of the FACS sorting purity for the fourth sort. P3 gate shows the % cells sorted as positive for mCherry.

2.17. Time-lapse microscopy

PT45 cells stably expressing histone H2B-mCherry were seeded at $2x10^4$ cells/well in 6-well plates and 20-24h later treated with 2.5mM thymidine for synchronization. Cells were released from the thymidine block 24h later, washed twice with PBS (pre-warmed to 37ºC) and incubated in 1ml serum-free DMEM -/+ 300pcc of AdΔ19K. 2h later the medium was replaced with 10% FBS Leibovitz's L15 medium (Life Technologies) -/+ 5nM gemcitabine. L15 medium instead of DMEM was chosen due to the lack of CO_2 supply in the time-lapse system. Leibovitz's L15 medium is designed to support the growth of cells in CO_2-free systems and it is buffered by phosphates, instead of sodium bicarbonate and higher levels of free-base amino-acids, sodium pyruvate and galactose (instead of glucose).

24h post-infection cells were subjected to a 72h time-lapse imaging by phase-contrast and fluorescence microscopy. The time-lapse system comprised of a Zeiss Axiovert 200M fluorescence microscope with a camera and a motorised stage. Images from 3 different fields per condition were acquired every 15min from 24 to 96h post-infection using the 40x objective. Data from 3 independent experiments were analysed using AxioVision Rel. 4.9.1 (Carl Zeiss, Germany) and NIH ImageJ software.

Table 6: Antibodies used in immunoblotting (IM), immunofluorescence microscopy (IF) and flow-cytometry (FC); shown in alphabetical order

Antigen	Species	Clone	Origin	Method	Dilution
Primary Antibodies					
Actin	goat	C-11 polyclonal	SantaCruz Biotechnology, Inc (TX, USA)	IM	1:1000
Ad-DBP	mouse	monoclonal	Gift*	IF	1:1000
Aurora-A (IAK-1)	mouse	monoclonal	BD Biosciences	IF	1:500
E1A	mouse	M58 monoclonal	Labvision, Thermo Fisher Scientific	IF	1:400
				FC	1:200
Claspin	rabbit	polyclonal	Cell Signalling Technology (MA, USA)	IM	1:1000
Phospho-Chk1 (Ser296)	rabbit	133D3 polyclonal	Cell Signalling Technology	IM	1:1000
Phospho-Chk2 (Thr68)	rabbit	C13C1 polyclonal	Cell Signalling Technology	IM	1:1000
Phospho-histoneH2A.X (Ser139)	rabbit	polyclonal	Cell Signalling Technology	IM	1:1000
				IF	1:150
Phospho-histoneH3 (S10)	rabbit	polyclonal	Abcam plc	IM	1:1000
				FC	1:250
Mre11	rabbit	polyclonal	Genetex Inc. (CA, USA)	IM	1:5000
Nbs1 p95	rabbit	polyclonal	Abcam plc	IM	1:1000
Phospho-Plk1 (T210)	rabbit	polyclonal	Enzo Life Sciences	IM	1:1000
Plk1	mouse	monoclonal	Abcam plc	IM	1:1000
α-tubulin	rabbit	polyclonal	Abcam plc	IM	1:2000
				IF	1:400
Vinculin (SPM227)	mouse	monoclonal	Abcam plc	IM	1:2000

Secondary Antibodies					
Alexa Fluor 488 IgG (H+L)	rabbit	polyclonal	Life Technologies, Thermo Fischer Scientific	FC	1:125
Alexa Fluor 488 IgG (H+L)	mouse	monoclonal		IF	1:1000
Alexa Fluor 594 IgG (H+L)	rabbit	polyclonal		IF	1:1000
Alexa Fluor 647 IgG (H+L)	mouse	monoclonal		FC	1:125
Immunoglobulins/FITC	mouse	monoclonal	Dako (Denmark)	FC	1:20
immunoglobulins/HRP	goat, rabbit, or mouse	polyclonal	Dako	IM	1:2000

*anti-Ad-DBP (37.3) antibody was a gift from Dr Gioia Cherubini and originally from K. Benihoud, Institut Gustave Roussy, Villejuif, France.

CHAPTER 3: RESULTS

3.1. E1B19K deletion in Ad5 enhances chemodrug-induced pancreatic cancer cell killing

3.1.1. Confirmation of *KRAS*, *TP53* and *CDKN2A* mutations in PT45 and MIAPaCa-2 cell lines

PT45 and MIAPaCa-2 cell lines are derived from primary PDAC tumours and were previously reported to exhibit activating KRAS mutations, inactivating TP53 mutations and homozygous CDKN2A (p16) deletion, while retaining a wild-type SMAD4/DPC4 gene (Berrozpe et al., 1994; Caldas et al., 1994; Moore et al., 2001; Sun et al., 2001). In addition to the STR-profiling (section 2.2.1), in order to confirm the presence of mutations, we performed PCR mutational analysis and the results are summarised in table 7.

Assessment of the PCR-amplified p16 exons 1, 2 and 3 by agarose gel electrophoresis demonstrated the absence of this gene from PT45 and MIAPaCa-2 DNA. As shown in figure 15A, the p16 exon 3 PCR product is not detectable in PT45 and MIAPaCa-2 cells, in contrast to other pancreatic cancer cell lines, such as Suit-2 and Panc04.03, as well as HUVEC cells (Figure 15A). Sequencing of PCR-amplified KRAS exon 1 revealed the presence of missense mutations in both cell lines. In PT45 cells, a heterozygous G to A substitution was detected at position 10574 (nucleotide reference sequence NG_007524), corresponding to a glycine (G) to aspartic acid (D) amino acid change at codon 13 (protein reference sequence P01116) (Figure 15B, upper left panel). In MIAPaCa-2 cells, a homozygous G to T substitution was detected at position 10570, which leads to a glycine (G) to cystine (C) amino acid change at codon 12 (Figure 15B upper right panel). For TP53 mutational analysis we examined

exons 5, 6, 7 and 8. No mutations were detected in TP53 exons 5 and 6, while exon 7 and 8 exhibited missense mutations in MIAPaCa-2 and PT45 cells, respectively. PT45 cells exhibited a G to A substitution at position 1041 (nucleotide reference sequence NM_000546.5) of the TP53 exon 8, creating an arginine (R) to lysine (K) amino acid change at codon 280 (Figure 15B, bottom left panel). In MIAPaCa-2 cells, a C to T substitution was evident at position 944, corresponding to an arginine (R) to tryptophan (W) amino acid substitution at codon 248, which lies in exon 7 (Figure 15B bottom right panel).

Taken together, the PCR mutational analysis revealed the absence of CDKN2A (p16) in PT45 and MIAPaCa-2 cells, in agreement with previous literature reports of a homozygous CDKN2A deletion (Moore et al., 2001). In addition, the activating G13D and G12C KRAS mutations in PT45 and MIAPaCa-2 cells respectively, and the inactivating R280K and R248W TP53 missense mutations in PT45 and MIAPaCa-2 cells respectively, were confirmed (Moore et al., 2001).

Table 7: Summary of mutation analysis in PT45 and MIAPaCa-2 cells.

	PT45	MIAPaCa-2
CDKN2A exons1-3	Homozygous deletion	Homozygous deletion
➢ ***Effect on protein***	Absence	Absence
KRAS exon 1	G 13 D	G 12 C
➢ ***Effect on protein***	Constitutive activation	Constitutive activation
TP53 exon 5	-	-
➢ ***Effect on protein***	-	-
TP53 exon 6	-	-
➢ ***Effect on protein***	-	-
TP53 exon 7	-	R 248 W
➢ ***Effect on protein***	-	Impaired DNA-binding
TP53 exon 8	R 280 K	-
➢ ***Effect on protein***	Impaired DNA-binding	-

Hyphen (-) indicates absence of mutation

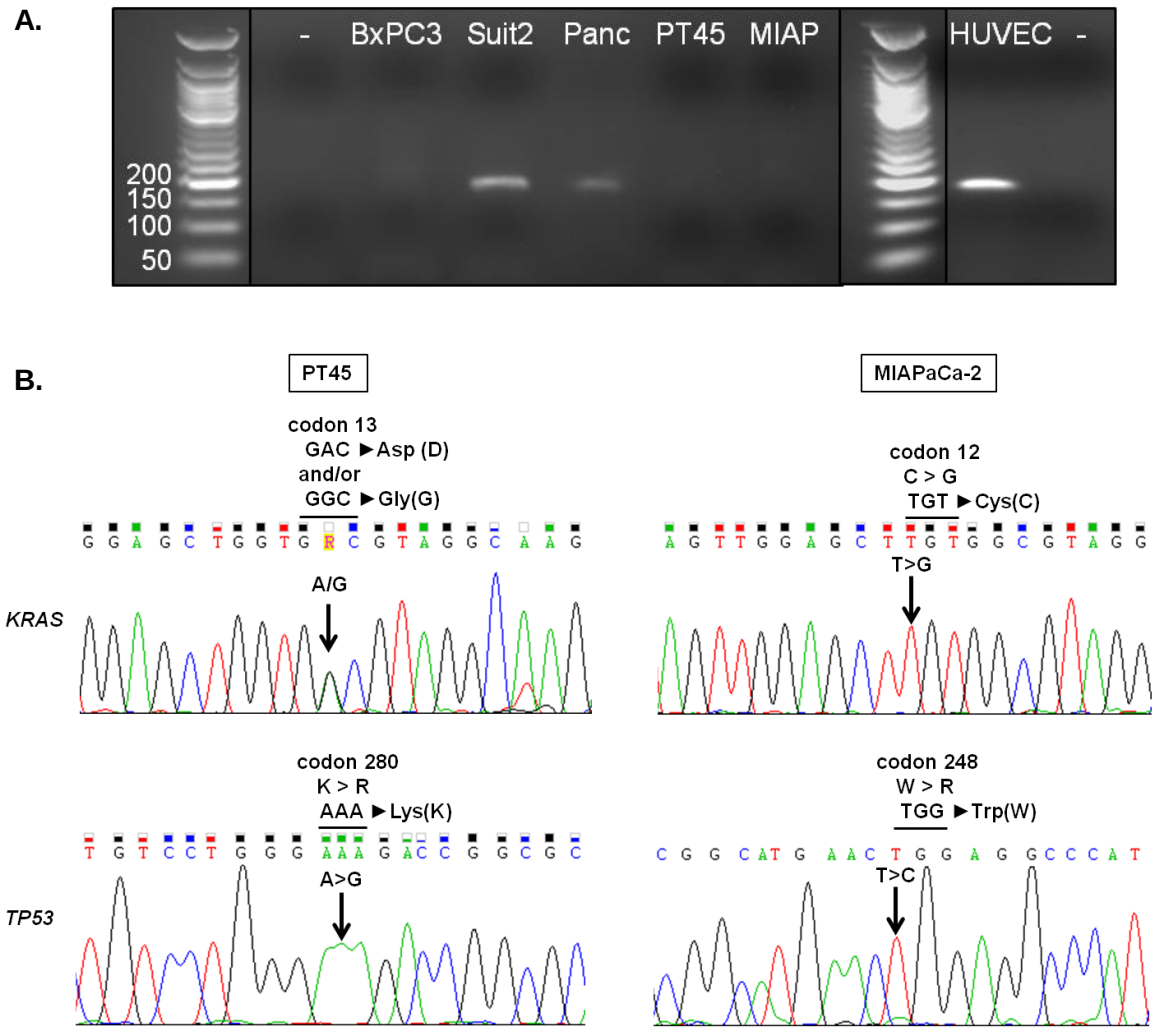

Figure 15: Confirmation of *KRAS*, *TP53* and *CDKN2A* mutations in PT45 and MIAPaCa-2 cell lines. DNA extracted from cells was PCR-amplified for exons 1,2 and 3 of CDKN2A gene, exon 1 of KRAS gene and exons 5-8 of TP53 gene, as detailed in the methods. **(A)** Agarose gel electrophoresis of PCR-amplified exon 3 of CDKN2A (p16) gene from pancreatic cancer cell lines BxPC3, Suit-2, Panc0403, PT45 and MIAPaCa-2 and HUVEC cells. Hyphen indicates a blank negative control and vertical black lines designate points of gel cropping. DNA ladder numbers are in base pairs (bp). **(B)** Amplified DNA was sequenced and aligned with NCBI reference sequences for each gene. The portion of the DNA sequencing chromatogram containing the specified mutations is shown. Arrows indicate base alterations and the subsequent amino acid substitutions at the specified codons are shown. The studies were performed in conjunction with Dr Yang Kee Stella Man.

3.1.2. E1B19K-deletion in Ad5 enhances pancreatic cancer cell killing induced by DNA-damaging drugs

Our team previously demonstrated that the E1B19K deletion in wild-type Ad5 promotes gemcitabine- and irinotecan-induced apoptosis in pancreatic cancer cells and that the enhanced cell death observed when Ad∆19K is combined with cytotoxic drugs is inhibited by the pan-caspase inhibitor zVAD (Cherubini et al., 2011; Leitner et al., 2009; Oberg et al., 2010). Ad∆19K-induced cell death was not inhibited by zVAD in the absence of drugs, while gemcitabine-induced cell killing could be attenuated (Cherubini et al., 2011; Leitner et al., 2009). In order to verify these findings and the conditions previously used, cell viability assays were carried out in PT45 and MIAPaCa-2 cells. Dose-response curves to Ad5tg and Ad∆19K with or without addition of fixed doses of gemcitabine, irinotecan and the pan-caspase inhibitor zVAD were generated 72h post-infection and EC_{50} values were derived. The doses of drugs used were selected from previous data in the team (by Dr Gioia Cherubini) and verified to kill approximately 30% of cells.

In PT45 cells Ad5tg had an average EC_{50} value of 121.2±31.7 ppc (Figure 16B). Addition of gemcitabine or irinotecan sensitized PT45 cells to Ad5tg, as shown by the shift of the curve to the left (Figure 16A left panel). However, the decreased EC_{50} values in the presence of gemcitabine or irinotecan (67.6±16.9 and 72.5±26.8 ppc, respectively) were not significantly different from that of Ad5tg alone (Figure 16B). Gemcitabine and irinotecan sensitized PT45 cells to Ad5tg-induced cell death to the same extend, as indicated by the sensitization ratio (Figure 16C). In contrast to Ad5tg, the EC_{50} value of Ad∆19K (207.3±19.0 ppc) was significantly reduced to 52.8±12.2 and 34.5±16.2 ppc upon addition of gemcitabine and irinotecan, respectively (Figure 16B). Gemcitabine enhanced Ad∆19K-induced cell death to a greater extent than irinotecan, as indicated by the sensitization ratio (Figure 16C). In the presence of the pan-caspase inhibitor zVAD the dose-response curves to Ad∆19K combined with gemcitabine or irinotecan, shifted to the right suggesting de-sensitization (Figure 16A right panel). However, there was not a statistically significant increase of the average EC_{50} values or decrease of the sensitization ratios in the presence of zVAD (Figure 16B and C).

The cytotoxicity of Ad5tg and AdΔ19K was 3-fold and 5-fold higher in MIAPaCa-2 cells compared to PT45 cells (EC_{50} values of 44.6±17.2 and 41.6±7.5 ppc in MIAPaCa-2 cells compared to 121.2±31.7 and 207.3±19.0 ppc in PT45 cells), with no significant differences between viruses. In contrast to PT45 cells, addition of gemcitabine did not enhance Ad5tg-induced MIAPaCa-2 cell death (Figure 16D, left panel). In fact, there was a trend towards increased EC_{50} value (134.9±47.3 ppc) when Ad5tg and gemcitabine were combined (Figure 16E) and the sensitization ratio was below 1 (Figure 16F), suggesting gemcitabine de-sensitizes MIAPaCa-2 cells to Ad5tg. On the contrary, addition of irinotecan showed a trend towards a decreased Ad5tg EC_{50} value (20.5±10.9 ppc) (Figure 16E). Addition of gemcitabine or irinotecan increased AdΔ19K cytotoxicity (Figure 16D). The E_{C50} value of AdΔ19K combined with gemcitabine was significantly lower in comparison to Ad5tg combined with gemcitabine, but not significantly lower from that of AdΔ19K (Figure 16E). Irinotecan-mediated sensitization to AdΔ19K appeared higher compared to gemcitabine and was abolished in the presence of the pan-caspase inhibitor zVAD (Figure 16F). Gemcitabine-induced enhancement of AdΔ19K cytotoxicity showed a trend towards inhibition by zVAD (Figure 16E and F).

These data confirm that E1B19K deletion in Ad5 increases sensitization of pancreatic cancer cells to gemcitabine- and irinotecan-induced cell death. However, zVAD-mediated inhibition of sensitization was not significant under the current conditions and was only clearly demonstrated in response to AdΔ19K combined with irinotecan in MIAPaCa-2 cells. Overall, drug-combinations with AdΔ19K resulted in more potent cell killing than combinations with the wild type virus. In addition, the two cell lines show different levels of sensitivity to both viruses and drugs. Firstly, MIAPaCa-2 cells were more sensitive to adenovirus compared to PT45. Secondly, gemcitabine-mediated enhancement of AdΔ19K cytotoxicity was stronger than irinotecan in PT45 cells but weaker in MIAPaCa-2 cells.

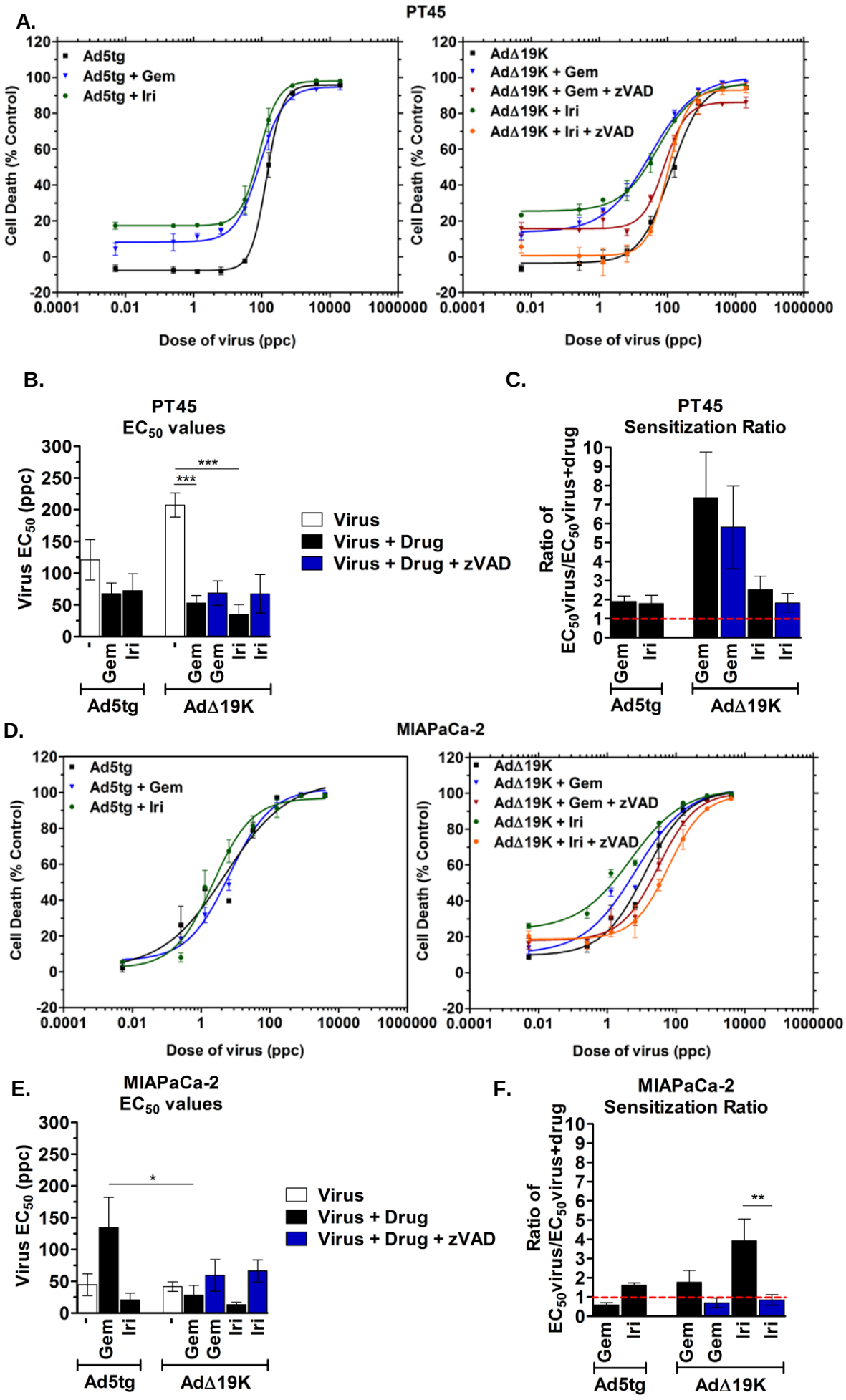
A.
PT45
Ad5tg
Ad5tg + Gem
Ad5tg + Iri
AdΔ19K
AdΔ19K + Gem
AdΔ19K + Gem + zVAD
AdΔ19K + Iri
AdΔ19K + Iri + zVAD
Cell Death (% Control)
Dose of virus (ppc)
B.
PT45
EC50 values
Virus EC50 (ppc)
Virus
Virus + Drug
Virus + Drug + zVAD
Gem
Iri
Ad5tg
AdΔ19K
C.
PT45
Sensitization Ratio
Ratio of EC50virus/EC50virus+drug
D.
MIAPaCa-2
E.
MIAPaCa-2
EC50 values
F.
MIAPaCa-2
Sensitization Ratio

Figure 16: E1B19K deletion in Ad5tg increases sensitization of pancreatic cancer cells to death by DNA-damaging drugs. Cell viability assays of PT45 and MIAPaCa-2 cells treated with Ad5tg or AdΔ19K -/+ addition of gemcitabine (Gem) or irinotecan (Iri). Where indicated, 25µM of the pan-caspase inhibitor zVAD was added. Survival was assessed by MTS assay 72h.p.i. **(A and D)** Representative Ad5tg and AdΔ19K dose-response curves (left and right panels, respectively) -/+ fixed doses of DNA-damaging drug(s) (PT45: 2nM Gem, 3µM Iri. MIAPaCa-2: 10nM Gem, 5µM Iri) with or without addition of 25µM of the pan-caspase inhibitor zVAD. Cell death was normalized to control (untreated cells or drug(s)-treated cells). Error bars indicate standard deviation (S.D.) of technical triplicates. **(B and E)** EC_{50} values (in ppc) derived from virus dose-response curves -/+ fixed doses of drug(s). Error bars represent standard error of the mean (S.E.M.) of at least three independent experiments. *.p<0.05, ***.p<0.001 (one-way ANOVA with Bonferroni's multiple comparison test). Drug cytotoxicity (%) ± S.E.M. was: 27±3.4% and 29.3±6.5% with 2nM and 10nM gemcitabine, respectively, 26.5±2.9% and 30.9±1.7% with zVAD plus 2nM and 10nM gemcitabine, respectively, 23.3±5.4% and 28.6±1.2% with 3µM and 5µM irinotecan, respectively and 19.1±6.5% and 29.9±4.4% with zVAD plus 3µM and 5µM irinotecan, respectively. **(C and F)** Sensitization ratio (ratio of virus EC_{50}/combination EC_{50}). Red dotted lines indicate a ratio of 1 (= no sensitization). **.p<0.01 (one-way ANOVA with Bonferroni's multiple comparison test).

3.1.3. AdΔ19K and gemcitabine induce pancreatic cancer cell killing in a more-than-additive manner

Throughout the present studies different doses of AdΔ19K and gemcitabine causing less than 30% cell killing were used, dependent on differences in drug batches and changes with increasing passaging of cells. To demonstrate that the cell death induced by AdΔ19K and gemcitabine was at least additive at these different doses, I performed cell viability assays with the different fixed doses of AdΔ19K and gemcitabine and in the absence or presence of zVAD. All the conditions used in this thesis are summarised in figure 17.

In both PT45 and MIAPaCa-2 cells, cell death induced by AdΔ19K, gemcitabine and their combination is dose-dependent (Figure 17A and B). In PT45 cells combinations of AdΔ19K and gemcitabine induced more-than-additive cell killing at all doses tested (theoretical additive value is shown in red dotted lines) (Figure 17A). Cell death induced by the combination was significantly higher compared to both single treatments when the high dose (300ppc) of AdΔ19K was combined with gemcitabine (Figure 17A). In response to 300ppc AdΔ19K and 5nM gemcitabine cell killing was significantly higher than the theoretical additive value (shown by a red asterisk). Besides a trend towards decreased cell death at 100ppc AdΔ19K and 2nM gemcitabine, zVAD did not appear to inhibit cell death induced by the combination treatment (Figure 17A). In MIAPaCa-2 cells, gemcitabine and AdΔ19K induced cell death in a more-than-additive manner at most doses tested (theoretical additive value is shown in red dotted lines) (Figure 17B). Similar to PT45 cells, significantly higher cell death compared to both single treatments was evident when 300ppc AdΔ19K were combined with gemcitabine (Figure 17B). In the presence of zVAD, there was a trend towards decreased cell death induced by AdΔ19K and gemcitabine at all doses tested (Figure 17B).

Collectively, in both cell lines most combinations of AdΔ19K and gemcitabine promoted cell death in a more-than-additive manner. Despite this, cell killing induced by the combination treatment was significantly higher compared to both single treatments only when the high dose (300ppc) of AdΔ19K was used.

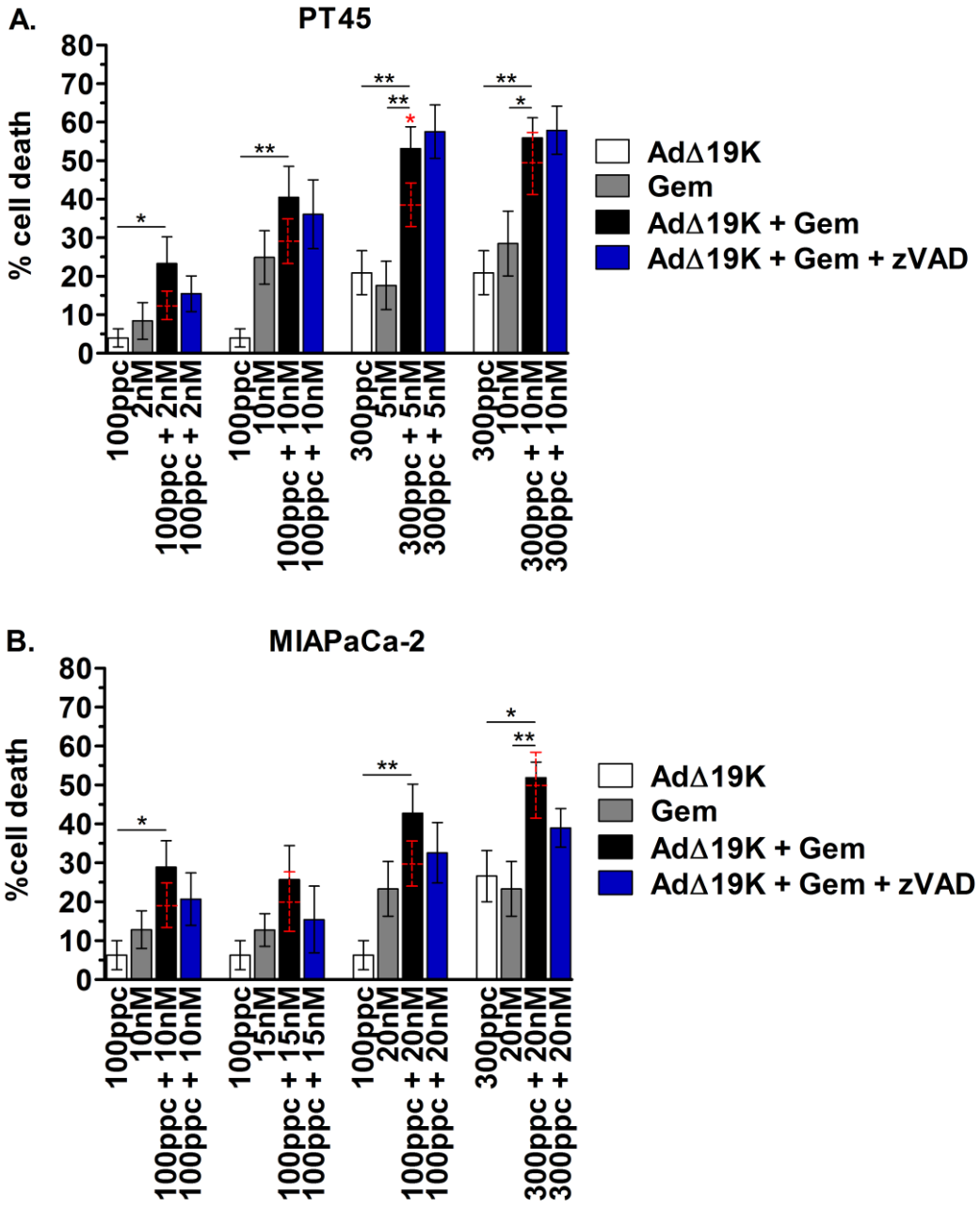

Figure 17: AdΔ19K and gemcitabine induce pancreatic cancer cell killing in a more-than-additive manner. Cell viability assays in **(A)** PT45 and **(B)** MIAPaCa-2 cells treated with AdΔ19K, gemcitabine (Gem) or their combination at the indicated doses. Where indicated, 25μM of the pan-caspase inhibitor zVAD was added. Cell viability was assessed by MTS assay at 72h.p.i. Error bars represent S.E.M. of 6 independent experiments. *.p<0.05, **.p<0.01 (one-way ANOVA with Bonferroni's multiple comparison test). Red dotted lines indicate the theoretical additive mean ± S.E.M of the two treatments combined and red asterisks indicate significant difference of the actual mean from the theoretical additive mean (one-sample t-test).

3.1.4. The combination of AdΔ19K with DNA-damaging drugs induces more-than-additive and time-dependent cell killing

In order to directly assess cell death over time, rather than cell viabilty (MTS assay) and confirm that E1B19K deletion enhances cell death induced by gemcitabine and irinotecan, the trypan blue inclusion test of cell death was employed. The trypan blue dye is not cell-membrane permeable and therefore only cells with non-intact membranes will incorporate the dye (Strober, 2001). Trypan-blue positive, that is dead cells, were quantified at 24, 48, 72, 96 and 120h post-infection in PT45 cells.

Cell death induced by AdΔ19K combined with gemcitabine or irinotecan was first detected at 48h, with 10% of cells dying (9.4±1.9% and 11.2±1.2% for AdΔ19K combined with gemcitabine or irinotecan respectively) (Figure 18A and B). At 72h cell death increased by 3-fold to reach 41.5±5.3% and 39.7±4.2% for AdΔ19K combined with gemcitabine and irinotecan, respectively (Figure 18A and B). A further increase in cell death in response to AdΔ19K and drugs was observed from 72h to 96h, with values reaching 66.9±3.6% and 75±1.4% for AdΔ19K combined with gemcitabine or irinotecan respectively (Figure 18A and B). The maximum cell death observed in response to gemcitabine and AdΔ19K was 69.3±2.9% (Figure 18A) while for irinotecan and AdΔ19K was 84.3±2.5% (Figure 18B), both at 120h. The combination of AdΔ19K with either drug, induced cell death in a more-than-additive manner at 48, 72 and 96h post-infection and that was significantly higher than the theoretical additive value, indicated by a yellow dotted line (Figure 18A and B; yellow asterisks denote statistical significance). At 72h, 96h and 120h Ad5tg enhanced gemcitabine-induced cell death, but was significantly lower compared to AdΔ19K combined with gemcitabine for the 72h and 92h time-points (Figure 18A). Cell death in response to AdΔ19K and irinotecan was also significantly higher compared to Ad5tg and irinotecan at 72, 96 and 120h (Figure 18B). AdΔ19K significantly enhanced gemcitabine and irinotecan-induced cell death from 48 to 120h (Figure 18A and B). 96h post-infection virus-mediated cell death became evident and increased by around 2-fold by 120h (Figure 18A and B). Overall, there was no significant induction of cell death by gemcitabine at this low dose,

while irinotecan induced cell death 96h and 120h post-treatment (Figure 18A and B).

Collectively, cell death induced by AdΔ19K and DNA-damaging drugs started at 48h and increased with time, reaching a plateau at 96h-120h, with the biggest increases observed between 48 and 72h post-treatment. AdΔ19K significantly enhanced drug-induced cell death from 48 to 120h and the combination of gemcitabine or irinotecan with AdΔ19K, but not Ad5tg, induced cell death in a more-than-additive manner at most time-points. The highest synergistic response was seen at 72h post-treatment.

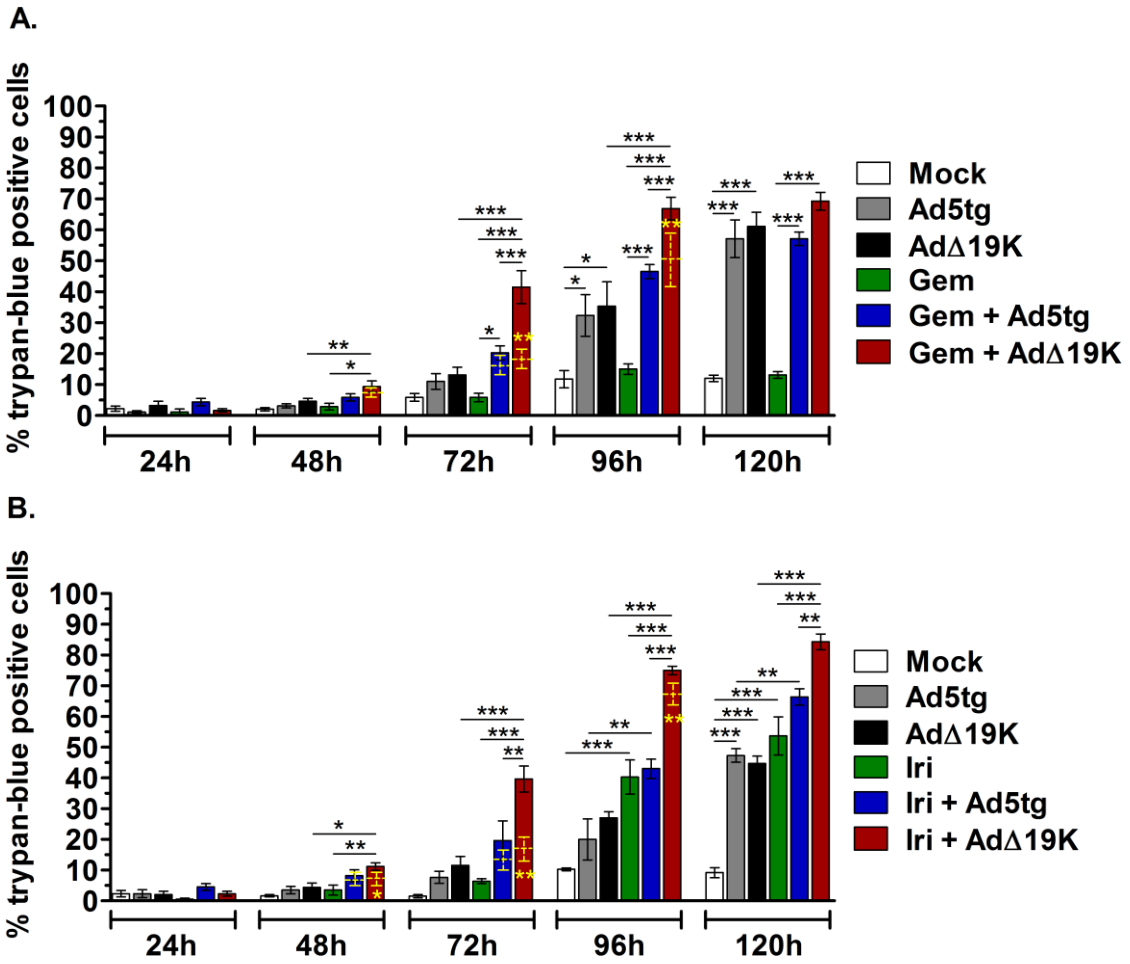

Figure 18: The combination of AdΔ19K with DNA-damaging drugs induces more-than-additive and time-dependent cell killing. PT45 cells were treated with 300ppc of Ad5tg or AdΔ19K -/+ addition of **(A)** 5nM Gem or **(B)** 5μM Iri. Cell death was assessed by trypan-blue dye incorporation at the indicated times. Error bars represent S.E.M. of 3-4 independent experiments. *.p<0.05, **.p<0.01, ***.p<0.001 (one-way ANOVA with Bonferroni's multiple comparison test). Yellow dotted lines indicate the theoretical additive mean ± S.E.M. of the two treatments combined and yellow asterisks indicate significant difference of the actual mean from the theoretical additive mean (one-sample t-test).

3.1.5. AdΔ19K and gemcitabine synergize to induce apoptosis of PT45 cells

Assessment of apoptosis in PT45 cells using the TUNEL assay

Previous studies in our team suggested that cell death in response to AdΔ19K and gemcitabine occurs through enhancement of gemcitabine-induced apoptosis (Leitner et al., 2009). However, I did not observe significant inhibition of the enhanced cell death by the pan-caspase inhibitor zVAD in cell viability assays (Figure 16B and 17A). In order to examine whether cell death induced by AdΔ19K and gemcitabine is apoptotic, the TUNEL assay was employed. The TUNEL assay utilizes the TdT-dependent addition of Br-dUTP to the termini of single- and double-stranded DNA, thus labelling fragmented DNA, one of the last apoptotic events (Darzynkiewicz et al., 2008; Li and Darzynkiewicz, 1995). DNA fragmentation in PT45 cells was assessed by flow-cytometry 72h post-infection, since the greatest more-than-additive induction of cell death was observed at this time-point (Figure 18A). Propidium iodide was used in conjunction with TUNEL to identify DNA fragmentation at specific DNA contents, thereby allowing association of apoptosis induction with specific cell-cycle phases. Representative flow cytometry profiles for each condition can be found in Appendix 1 (section 5.1.; Figure 65A).

Treatment with staurosporine, employed as a positive control for apoptosis induction, demonstrated that DNA fragmentation was successfully detected, despite some variability, while apoptosis was almost undetectable in mock-infected cells (Figure 19A). When AdΔ19K was combined with gemcitabine, a synergistic increase in DNA fragmentation was observed which reached 18.2±6% (Figure 19A). In contrast, no enhanced DNA fragmentation was observed upon combination of Ad5tg and gemcitabine. DNA fragmentation was less than 1% following infection with Ad5tg or AdΔ19K and just over 1% in cells treated with gemcitabine (Figure 19A).

Detection of cell-cycle specific apoptosis using a combination of TUNEL and propidium iodide staining, revealed that in response to AdΔ19K and gemcitabine 56.5±1.8% of apoptotic cells display DNA fragmentation at the G1

phase (Figure 19B). This was significantly higher than the apoptotic G1 fraction of gemcitabine-treated cells (17.7±3.7%) as well as cells treated with a combination of Ad5tg and gemcitabine (19.7±10.8%) (Figure 19B). A smaller fraction of cells treated with AdΔ19K and gemcitabine showed DNA fragmentation in S and G2/M phases (23.4±3.3% and 17.5±3.9%, respectively). The majority of gemcitabine-treated cells underwent DNA fragmentation in G2/M (44.8±8.4%) and S-phase (34.5±0.9%) and gemcitabine combined with Ad5tg showed a similar apoptotic profile to gemcitabine (Figure 19B). The modest DNA fragmentation seen with Ad5tg and AdΔ19K alone occurred mostly in G1 phase (Figure 19B). The sub-G1 cell-fraction was excluded from the analysis.

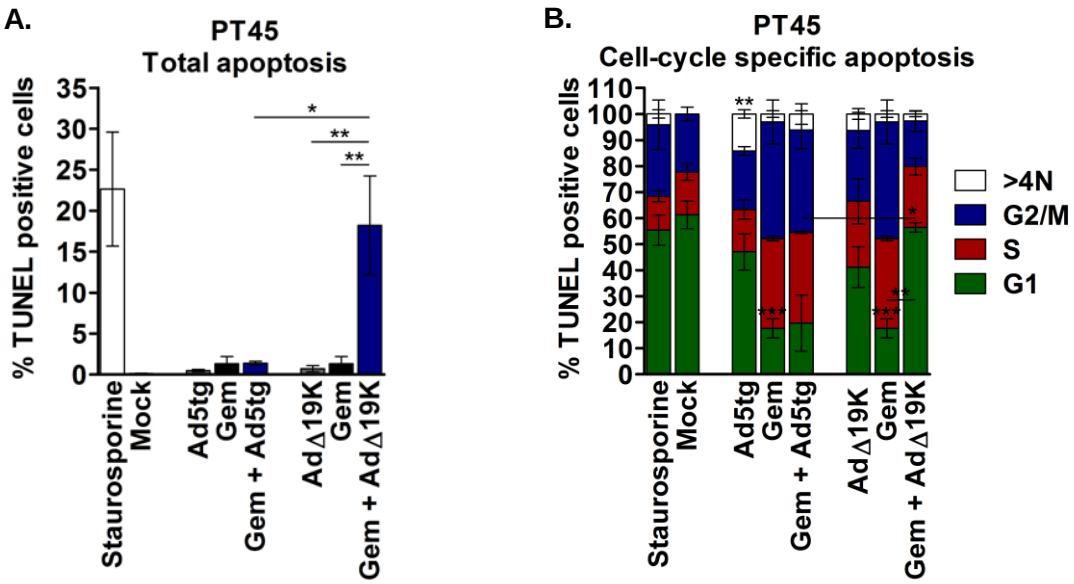

Figure 19: AdΔ19K and gemcitabine induce DNA-fragmentation in PT45 cells in a more-than-additive manner. PT45 cells were treated with 300ppc of Ad5tg or AdΔ19K, +/- addition of 10nM gemcitabine (Gem). Staurosporine-treated and mock-infected cells were used as positive and negative controls, respectively. Apoptosis was assessed at 72h by flow-cytometric analysis of TUNEL and propidium iodide (PI) for DNA-content analysis as detailed in the methods. **(A)** Total apoptosis expressed as % of cells positive for TUNEL **(B)** Cell-cycle specific apoptosis. TUNEL expression was quantified in cells with DNA-content of 2N (G1-phase), 2-4N (S-phase), 4N (G2/M-phase) and >4N (polyploid cells), as determined by PI staining. Apoptosis in each cell-cycle phase was expressed as % of total apoptosis in the condition. Error bars represent S.E.M. of 3-4 independent experiments. *.p<0.05, **.p<0.01, ***.p<0.001 (one-way ANOVA with Bonferroni's multiple comparison test).

Table 8: Figure 19B statistical comparisons

DNA content	Treatment comparison	Statistical significance
>4N	Mock vs Ad5tg	** .p<0.01
2N (G1-phase)	Mock vs Gem	***.p<0.001
2N (G1-phase)	Gem vs Gem + AdΔ19K	**.p<0.01
2N (G1-phase)	Gem + Ad5tg vs Gem + AdΔ19K	* .p<0.05

Assessment of apoptosis in PT45 cells using the cleaved Caspase-3 assay

In order to verify the observations of the TUNEL assay using a different apoptotic marker, a cleaved caspase-3 assay was utilised. Expression of cleaved and thus activated caspase-3 was assessed by flow-cytometry at 72h after treatment of PT45 cells with Ad5tg or AdΔ19K with or without 5nM or 10nM gemcitabine. Cells were co-stained with propidium iodide to allow assessment of apoptosis at specific cell-cycle phases. Representative flow cytometry profiles for each condition can be found in Appendix 1 (section 5.1.; Figure 65B).

38±4.8% of cells treated with AdΔ19K and 5nM gemcitabine activated caspase-3 and this significantly increased when the dose of gemcitabine was increased to 10nM, reaching 52±3.2% (Figure 20A). Caspase-3 activation was clearly more-than-additive, since AdΔ19K only induced 6.2±1.2% apoptosis and gemcitabine less than 5% at either dose (Figure 20A). Ad5tg and gemcitabine also activated caspase-3 in a more-than-additive manner, but was significantly lower compared to the combination of AdΔ19K and gemcitabine (Figure 20A). Addition of the pan-caspase inhibitor zVAD significantly reduced apoptosis to 11.7±3% in response to AdΔ19K and gemcitabine (Figure 20A).

49.7±3.2% of AdΔ19K-infected cells with activated caspase-3 had a DNA content of >4N and 25.4±1.9% were in G2 or mitosis (Figure 20B). Similarly, the majority of Ad5tg-infected cells activating caspase-3 had a DNA content of >4N (36±1.7%) and 4N (29.9±4%) (Figure 20B). Induction of apoptosis by gemcitabine was equally distributed in G1, S and G2/M phases when used at 5nM, whereas at 10nM of the drug, most caspase-3 cleavage occurred in S-phase cells (50.4±4.4%) (Figure 20B). 45.3±4.1% of apoptotic cells following

treatment with AdΔ19K and gemcitabine had a DNA content of 4N, suggesting they were in G2 or mitosis (Figure 20B). This was significantly higher than the G2/M-apoptotic fraction of cells infected only with AdΔ19K. On the other hand, the >4N apoptotic fraction in AdΔ19K-infected cells was significantly reduced in the presence of gemcitabine at either drug dose (Figure 20B). The decrease of apoptosis by zVAD did not significantly change the apoptotic profile of cells treated with AdΔ19K and gemcitabine (Figure 20B). When the dose of gemcitabine was increased to 10nM and combined with AdΔ19K, cleaved caspase-3 expression was equally distributed between cells in S-phase and G2/M, as opposed to mostly G2/M seen with the lower dose of the drug (Figure 20B). The combination of gemcitabine with Ad5tg activated caspase-3 mostly in cells with a DNA-content of 4N (G2/M) (47.6±3.3%) and, as with Ad5tg alone, 34.6±2.2% of apoptotic cells had a DNA-content of >4N (Figure 20B).

Taken together, assessment of apoptosis in PT45 cells suggested that cell death induced by AdΔ19K and gemcitabine after 72h is apoptotic. The TUNEL assay demonstrated that approximately 20% of PT45 cells treated with a combination of AdΔ19K and gemcitabine displayed DNA fragmentation with the majority of them apoptosing in the G1 phase. The cleaved-caspase-3 method showed that approximately 40% of PT45 cells treated with AdΔ19K and gemcitabine activate apoptosis after 72h. In contrast to cell-viability assays, apoptosis induced by AdΔ19K and gemcitabine was significantly inhibited by the pan-caspase inhibitor zVAD in PT45. The majority of caspase-3 cleavage in response to AdΔ19K and gemcitabine occurred in PT45 cells with a DNA content of 4N, as opposed to >4N or equally distributed between all phases with AdΔ19K or gemcitabine alone, respectively. In addition, increasing the dose of gemcitabine increased the number of cells activating caspase-3 in S-phase both with gemcitabine alone and in combination with AdΔ19K.

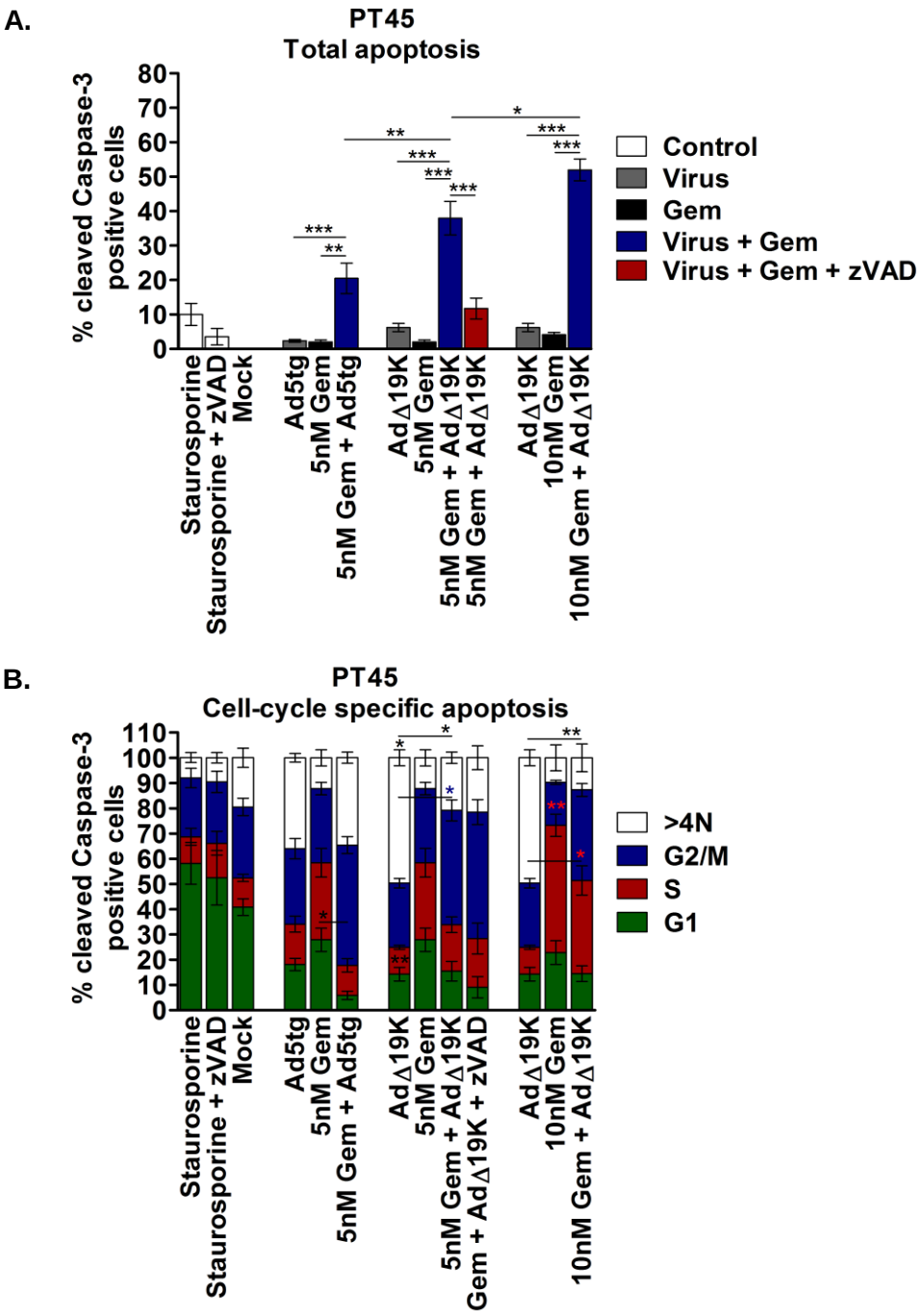

<u>Figure 20</u>: AdΔ19K and gemcitabine induce caspase-3 cleavage in PT45 cells in a more-than-additive manner. PT45 cells were treated with 300ppc of Ad5tg or AdΔ19K -/+ addition of gemcitabine (Gem) at the indicated doses. Where indicated 25μM of the pan-caspase inhibitor zVAD was added. Staurosporine and mock-infection (no treatment) were used as positive and negative controls, respectively. Apoptosis was assessed at 72h by flow-cytometric analysis of cleaved caspase-3 expression and PI for DNA-content analysis, as detailed in the methods. **(A)** Total apoptosis expressed as % of cells positive for cleaved caspase-3. **(B)** Cell-cycle specific apoptosis. Cleaved caspase-3 expression was quantified in cells with DNA-content of 2N (G1-phase), 2-4N (S-phase), 4N (G2/M-phase) and >4N (polyploid cells), as determined by PI staining. Apoptosis in each cell-cycle phase was expressed as % of total apoptosis in the condition. Error bars represent S.E.M. of 3-4 independent experiments. *.p<0.05, **.p<0.01, ***.p<0.001 (one-way ANOVA with Bonferroni's multiple comparison test).

Assessment of apoptosis in MIAPaCa-2 cells using the cleaved Caspase-3 assay

Assessment of apoptosis using the cleaved caspase-3 method was also utilised in MIAPaCa-2 cells. In this cell line, apoptosis was assessed at 48, 72 and 96h following treatment with Ad5tg or AdΔ19K -/+ gemcitabine. Representative flow cytometry profiles for each condition at 72h can be found in Appendix 1 (section 5.1.; Figure 65C).

At 48h, AdΔ19K and gemcitabine induced caspase-3 cleavage in 3.8±0.2% of cells (Figure 21A 48h). This number increased modestly with time reaching 13.7±1.8% by 96h. Activation of caspase-3 in response to AdΔ19K and gemcitabine was more-than-additive only at 48h and there was no significant decrease in apoptosis in the presence of zVAD (Figure 21A). At all time-points tested cleaved caspase-3 expression was significantly higher when gemcitabine was combined with AdΔ19K, compared to gemcitabine alone, but was the same as AdΔ19K alone at 72h and 120h (Figure 21A). In addition, combining gemcitabine with AdΔ19K resulted in significantly higher caspase-3 cleavage than the combination of gemcitabine with Ad5tg, which induced caspase-3 cleavage in a less-than-additive manner at all time-points tested (Figure 21A). Similarly, AdΔ19K-induced caspase-3 activation was significantly higher at 96h compared to Ad5tg alone (Figure 21A 96h).

Assessment of cell-cycle specific apoptosis at 48h did not show any significant differences between the various treatments (Figure 21B 48h). In cells treated with AdΔ19K or gemcitabine, the highest percentage of caspase-3 cleavage was seen in G1-phase (44.9±16.7% and 34.3±3.4%, respectively) and the second highest in G2/M (27.2±8.4% and 28.5±6.5%, respectively) (Figure 21B 48h). In response to their combination, 32.4±3.4% of cells with cleaved caspase-3 were in G2 or mitosis and 28.4±0.4% in G1-phase (Figure 21B 48h).

At 72h and 96h the apoptotic DNA-content profile of the combination treatment resembled more that of AdΔ19K rather than gemcitabine; caspase-3 was activated in cells with >4N, 2N and 4N DNA content as opposed to mainly 2N seen with gemcitabine (Figure 21B 72h and 96h). 29.4±8% of apoptotic cells

had a DNA-content of >4N, 26.5±4% were in G1 and 25.5±1.7% were in G2/M 72h following treatment with AdΔ19K and gemcitabine (Figure 21B 72h). Similarly, at 96h caspase-3 cleavage induced by AdΔ19K and gemcitabine was 29.3±1.4% in G1-phase cells, 27.3±4.2% in G2/M-phase cells and 25.6±6.9% in cells with >4N DNA content (Figure 21B 96h). At this time-point the apoptotic G1 fraction was significantly higher in response to gemcitabine compared to its combination with AdΔ19K (Figure 21B 96h).

In contrast, the apoptotic DNA-content profile of the combination of Ad5tg with gemcitabine resembled that of gemcitabine at 96h and a significant increase in the apoptotic G1 fraction was evident when gemcitabine was present in Ad5tg-infected cells (Figure 21B 96h). In the absence of gemcitabine, AdΔ19K-induced caspase-3 cleavage was equally distributed in 2N and >4N DNA-content cells at 72h and 96h (Figure 21B). Ad5tg-induced apoptosis occurred mostly in G1 at 72h but, similar to AdΔ19K, was equally displayed in 2N and >4N DNA-content cells at 96h (Figure 21B).

In summary, induction of apoptosis by AdΔ19K and gemcitabine in MIAPaCa-2 cells increased with time but was overall modest and the effect was more-than-additive only at 48h. Despite the weak induction of apoptosis by AdΔ19K and gemcitabine, this was still higher than apoptosis observed in response to Ad5tg and gemcitabine. AdΔ19K and gemcitabine induced apoptosis throughout the cell cycle phases. The presence of AdΔ19K in gemcitabine-treated cells did not appear to change the S-phase and 4N apoptotic profile, but promoted caspase-3 activation in cells with >4N DNA content. The small reduction in apoptosis in the presence of zVAD appeared to occur in these polyploid cells (Figure 21B). Since such cells are most likely to occupy G2/M, the cumulative apoptosis in 4N and >4N cells (50%<) suggests that, similar to PT45 cells, caspase-3 activation following gemcitabine and AdΔ19K treatment occurs preferentially in G2/M phase.

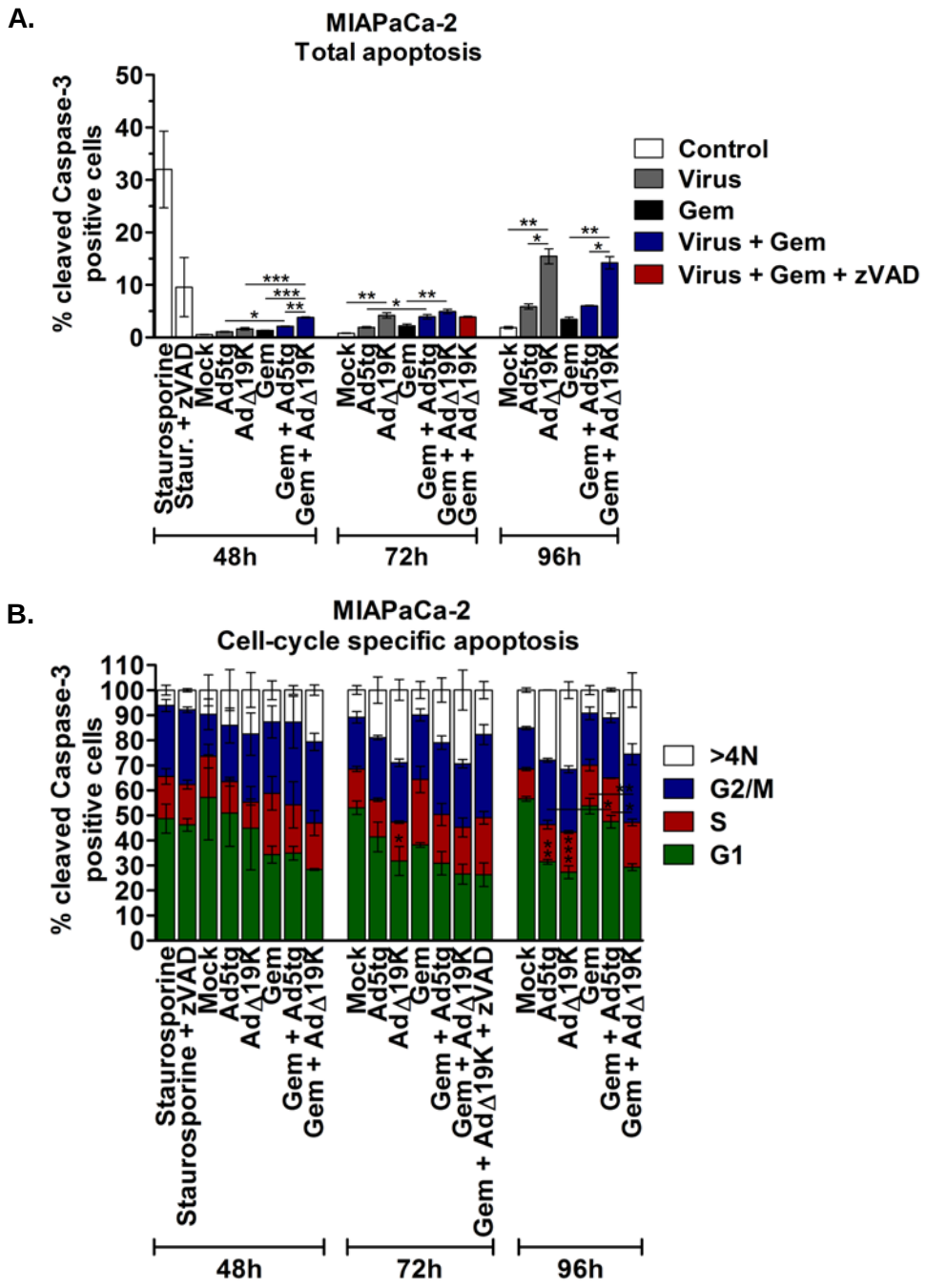

<u>Figure 21</u>: AdΔ19K and gemcitabine induce modest caspase-3 cleavage in MIAPaCa-2 cells. MIAPaCa-2 cells were treated with 100ppc of Ad5tg or AdΔ19K -/+ 15nM gemcitabine (Gem). Where indicated 25μM of the pan-caspase inhibitor zVAD was added. Staurosporine (0.5μM 24h) and mock-infection (no treatment) were used as positive and negative controls, respectively. Apoptosis was assessed at 72h by flow-cytometric analysis of cleaved caspase-3 expression and PI for DNA-content analysis, as detailed in the methods. **(A)** Total apoptosis expressed as % of cells positive for cleaved caspase-3. **(B)** Cell-cycle specific apoptosis. Cleaved caspase-3 expression was quantified in cells with DNA-content of 2N (G1-phase), 2-4N (S-phase), 4N (G2/M-phase) and >4N (polyploid cells), as determined by PI staining. Apoptosis in each cell-cycle phase was expressed as % of total apoptosis in the treatment. Error bars represent S.E.M. of 2-3 independent experiments. *.p<0.05, **.p<0.01, ***.p<0.001 (one-way ANOVA with Bonferroni's multiple comparison test).

Conclusions from studies assessing cell death in PT45 and MIAPaCa-2 cells

Cell viability, death and apoptotic assays demonstrated that suboptimal doses of AdΔ19K and DNA-damaging drugs induce cell killing in a more-than-additive manner. Despite that in PT45 cell viability assays the pan-caspase inhibitor zVAD did not significantly inhibit cell death, apoptotic assays demonstrated that cell death induced by AdΔ19K and gemcitabine after 72h is apoptotic and can be prevented in the presence of zVAD. In MIAPaCa-2 cells, cell death induced by irinotecan and AdΔ19K is caspase-dependent, since it was inhibited in the presence of zVAD. The observations that induction of caspase-3 cleavage by gemcitabine and AdΔ19K in MIAPaCa-2 cells was modest and that cell killing by the combination treatment showed a trend towards inhibition in the presence of zVAD, suggests that MIAPaCa-2 cell killing in response to gemcitabine and AdΔ19K is partly apoptotic.

Assessment of cell-cycle specific apoptosis in PT45 and MIAPaCa-2 cells showed that addition of AdΔ19K to gemcitabine-treated cells overall increases caspase-3 activation in cells with 4N and >4N DNA content compared to gemcitabine alone. This suggests that combination-treated cells are more likely to undergo apoptosis in G2 and/or mitosis. In addition, the increased DNA fragmentation in PT45 cells with 2N DNA content suggests that the final stages of apoptosis after AdΔ19K and gemcitabine treatment might occur in cells that have gone through mitosis and entered G1. Furthermore, it was demonstrated that the enhanced cell killing is time-dependent and occurs predominantly between 48h and 96h after combination treatment. These findings are suggestive of a delayed onset of apoptosis that might require cell-cycle progression and/or accumulation of damaging factors that are eventually fatal.

3.1.6. The enhanced cell killing is not dependent on viral replication, as gemcitabine inhibits viral genome amplification

Our group previously showed that the enhanced cell death observed when AdΔ19K is combined with gemcitabine is independent of viral replication, since gemcitabine strongly inhibited AdΔ19K genome amplification (Leitner et al., 2009). In order to verify this finding with the conditions used in the present study, Ad5tg and AdΔ19K genome amplification was assessed in PT45 cells with or without gemcitabine treatment, 24, 36, 48 and 72h post-infection. Viral DNA at each time-point was normalized to the DNA present at 4h post-infection.

As shown in figure 22, from 24h to 36h post-infection Ad5tg and AdΔ19K DNA increased by 5- and 9-fold, respectively, and after 12h there was another 2-fold increase for both viruses. By 72h post-infection both viruses had amplified their DNA by 20-fold (Figure 22). Interestingly, at 24h the DNA of AdΔ19K was significantly less compared to Ad5tg, but AdΔ19K showed a trend towards a higher rate of DNA amplification than Ad5tg at all other time-points tested (Figure 22). Treatment with gemcitabine significantly inhibited viral genome amplification at 24h and 72h and a trend towards inhibition was observed at all other time-points (Figure 22). Despite the observed inhibition in the presence of gemcitabine, some genome amplification did occur and by 72h post-infection Ad5tg and AdΔ19K had amplified their DNA by 3.4- and 6-fold, respectively (Figure 22). The greatly decreased viral genome amplification in the presence of gemcitabine confirmed that the enhanced cell killing in response to AdΔ19K and gemcitabine was largely replication-independent under the current experimental conditions.

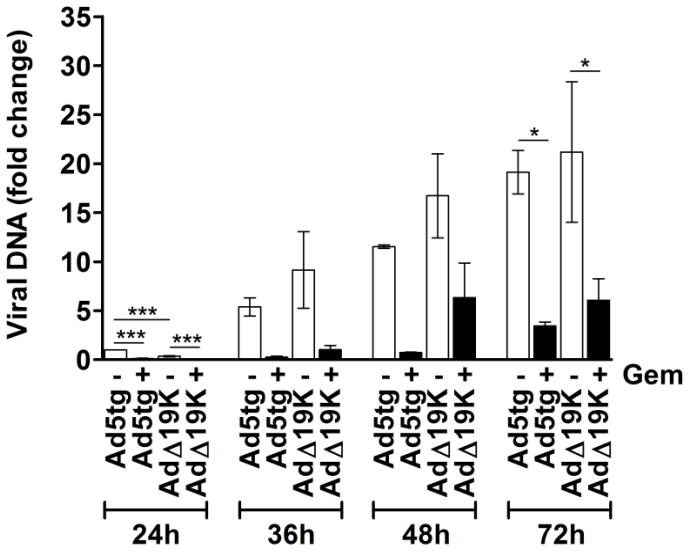

<u>Figure 22</u>: Gemcitabine inhibits viral DNA replication. PT45 were treated with 300ppc of Ad5tg or AdΔ19K -/+ 5nM gemcitabine (Gem). DNA was extracted at 4, 24, 36, 48 and 72hpi and analysed by qPCR for viral genome amplification (Ad-E2A). Viral DNA was normalized to input DNA (4h) and cellular GAPDH and expressed as fold-change relative to Ad5tg 24h. Error bars represent S.E.M. of 2 independent experiments. *.p<0.05, ***.p<0.001 (one-way ANOVA with Bonferroni's multiple comparison test).

3.1.7. Gemcitabine increases E1A mRNA and protein expression

In addition to viral genome amplification, the expression of Ad-E1A was assessed both at mRNA and protein levels. Quantification of E1A expression at the protein level was performed by flow-cytometry in PT45 and MIAPaCa-2 cells 16, 24 and 48h post-infection with Ad5tg or AdΔ19K in the absence or presence of gemcitabine.

16h post-infection with Ad5tg or AdΔ19K, 14.7±2.4% and 15.5±2.5% of PT45 cells, respectively, were positive for E1A (Figure 23A). The presence of gemcitabine had no effect on the number of E1A-positive cells at this time. At 24h E1A-positive cells increased by 6% for Ad5tg and 14% for AdΔ19K (Figure 23A). In the presence of gemcitabine there was a 2.7-fold increase in the number of E1A-positive AdΔ19K-infected cells from 16h to 24h. The frequency of E1A-positive cells in response to AdΔ19K and gemcitabine was significantly higher compared to Ad5tg and gemcitabine and showed a trend towards increase compared to AdΔ19K alone (Figure 23A). At 48h gemcitabine significantly increased E1A expression for both viruses (Figure 23A).

In the MIAPaCa-2 cell line, 14.8±3.2% and 21±2.2% of cells showed E1A expression 16h after infection with Ad5tg and AdΔ19K respectively (Figure 23B). Addition of gemcitabine to AdΔ19K-infected cells increased the number of E1A-positive cells to 30.9±0.2%, which was significantly higher than Ad5tg-infected E1A-positve cells following addition of gemcitabine (16.5±3.1%) (Figure 23B). From 16h to 24h, E1A expression had not significantly changed under any condition. At these time-points there was a trend towards increased E1A expression in AdΔ19K-infected cells compared to Ad5tg, regardless of gemcitabine treatment (Figure 23B). However, by 48h E1A expression was equal for Ad5tg and AdΔ19K infected cells (26.9±5.4% and 26.8±7.7%, respectively) (Figure 23B). At 48h, gemcitabine treatment showed a strong trend towards increased numbers of E1A positive cells, which reached 39.8±4.6% and 45.9±3.6% following Ad5tg and AdΔ19K infection respectively (Figure 23B).

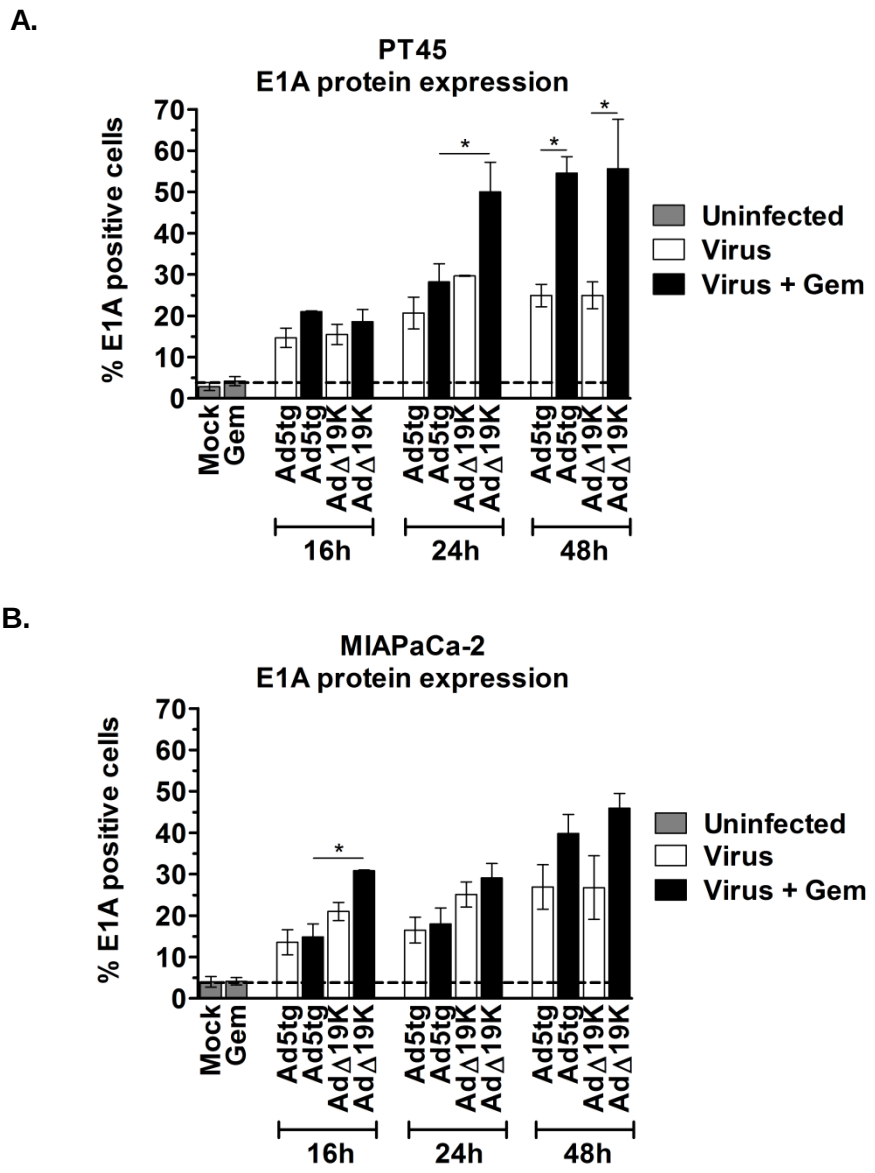

Figure 23: Gemcitabine increases E1A protein expression at specific times post-infection. (A) PT45 and **(B)** MIAPaCa-2 cells were treated with (A) 300ppc or (B) 100ppc of Ad5tg or AdΔ19K -/+ (A) 5nM or (B) 10nM gemcitabine (Gem), harvested, permeabilised and fixed at the indicated times. E1A expression was assessed by flow-cytometry using an E1A primary antibody and a FITC-labelled secondary antibody. The dotted line indicates baseline (background) fluorescence. Error bars represent S.E.M. of 3-4 independent experiments. *.$p<0.05$ (one-way ANOVA with Bonferroni's multiple comparison test).

Assessment of E1A mRNA expression was performed by qPCR in PT45 cells 16 and 24h post-infection. Normalisation of E1A mRNA levels to penton mRNA at each time-point allowed for accurate measurement of E1A transcript levels. As seen in figure 24, treatment of Ad5tg or AdΔ19K-infected cells with gemcitabine resulted in a trend towards increased E1A mRNA expression at 16h. The difference became more evident at 24h, where gemcitabine significantly increased E1A mRNA levels in AdΔ19K-infected cells (Figure 24). E1A mRNA expression was significantly higher in response to gemcitabine and AdΔ19K compared to gemcitabine and Ad5tg (Figure 24). In the absence of gemcitabine, AdΔ19K exhibited a tendency for increased E1A mRNA levels compared to Ad5tg at both time-points (Figure 24).

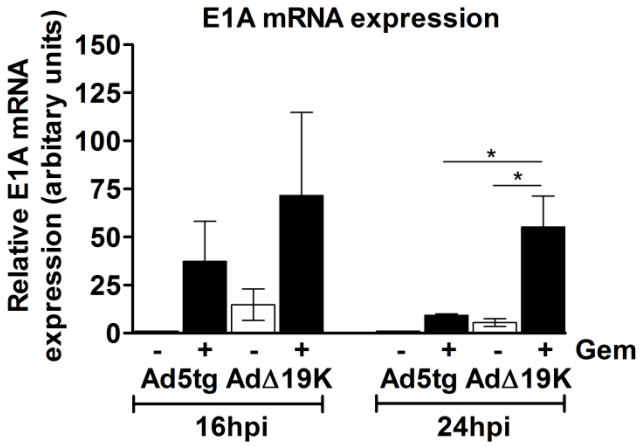

Figure 24: Gemcitabine increases AdΔ19K E1A mRNA expression in PT45 cells. PT45 cells were treated with 300ppc of Ad5tg or AdΔ19K -/+ 5nM Gem. RNA was extracted at 16 and 24h post-infection for qPCR analysis. Ad5 E1A mRNA expression was normalised to Ad5 penton and GAPDH internal control and expressed as fold difference versus Ad5tg. Error bars represent S.E.M. of 3 independent experiments. *.p<0.05 (one-way ANOVA with Bonferroni's multiple comparison test).

To summarize, gemcitabine increased E1A protein expression in Ad5tg- and AdΔ19K-infected PT45 cells 48h after treatment. At 24h more E1A-positive PT45 cells were observed in response to the combination of gemcitabine with AdΔ19K compared to the combination with Ad5tg. The same effect was seen in MIAPaCa-2 cells at 16h. Assessment of E1A mRNA in PT45 cells suggested that gemcitabine promotes higher levels of E1A mRNA expression in AdΔ19K-infected cells, which is also reflected in the higher E1A protein levels. Gemcitabine likely stimulates viral uptake in PT45 cells as previously shown in MIAPaCa-2 and other pancreatic cancer cell lines (Bhattacharyya et al.).

3.2 Adenovirus cannot prevent the DNA-damage response elicited by DNA-damaging drugs

3.2.1. Cell-cycle distribution effects in PT45 and MIAPaCa-2 cells

Previous work by our group had suggested that gemcitabine causes cell-cycle arrest at the G1/S transition and that addition of adenovirus increases the sub-G1 fraction (Leitner et al., 2009). To confirm these findings in PT45 and MIAPaCa-2 cells, cell-cycle distribution was assessed over time by flow-cytometric analysis of DNA content. Representative cell-cycle histograms can be found in Appendix 2 (section 5.1.; Figure 66).

Time-course of cell-cycle distribution in PT45 cells

In PT45 cells, gemcitabine caused an early S-phase arrest, with 54.5±5.4% of cells arrested in S-phase after 24h of treatment (Figure 25A). No significant changes in the number of S-phase arrested cells were observed in the presence of adenovirus (53.3±4.3% with Ad∆19K and 54.5±6.5% with Ad5tg) (Figure 25B S-phase). As a result of the cell accumulation in S-phase, G1 and G2/M fractions were significantly reduced whenever gemcitabine was present (Figure 25B G1-phase and G2/M-phase).

At 48h half of gemcitabine-treated cells were still arrested in S-phase (52.8±8%, Figure 25B S-phase) and again, addition of Ad5tg or Ad∆19K did not alter the cell-cycle profile of gemcitabine-treated cells (Figure 25A). It should be noted that from 24h to 48h gemcitabine-treated cells move from early S-phase to mid-S-phase, as it can be seen by the cell-cycle histograms (See Appendix 2 Figure 66A; section 5.1.). Both at 24 and 48h, the G1 fraction of gemcitabine-treated cells was significantly reduced compared to cells receiving no gemcitabine treatment, irrespectively of the presence adenovirus (Figure 25B G1-phase). At 48h an increased sub-G1 fraction became apparent in the presence of gemcitabine with or without infection with adenovirus (Figure 25B sub-G1).

At 72h 37.3±5.4% of gemcitabine-treated cells remained in S-phase, an accumulation that was significantly higher compared to mock-infected cells without gemcitabine, while the G2 fraction increased to 15.3±2.3% (Figure 25B S- and G2/M-phase). 72h following treatment with gemcitabine and Ad5tg or AdΔ19K, 31.4±6.1% and 36±4.8% of cells, respectively, were in S-phase and 19.8±2% and 16.4±1.2% of cells, respectively, were in G2/M (Figure 25B S- and G2/M-phase). At the 72h time-point the G1 cell fraction modestly increased in the presence of gemcitabine compared to 48h suggesting passage of cells from G2/M to G1, although it was still significantly lower compared to cells without gemcitabine treatment (Figure 25B G1-phase). The sub-G1 cell fraction at 72h in the presence of gemcitabine, with or without adenovirus infection, was again significantly higher compared to cells without gemcitabine (Figure 25B sub-G1). From 72h onwards, the number of gemcitabine-treated cells with or without adenovirus infection present in the G1-phase remained the same up to 120h and was still significantly lower in comparison to cells receiving no gemcitabine treatment (Figure 25B G1-phase).

At 96h and 120h the S-phase fraction in gemcitabine-treated cells (22.8±4.3% and 20.7±2.4%, respectively) remained significantly higher compared to mock-infected cells (Figure 25B S-phase). In contrast, S-phase cells were not significantly more 96h and 120h after gemcitabine treatment combined with either virus, compared to virus alone (Figure 25B S-phase). In addition, there were more cells in G2/M at 96h following treatment with Ad5tg and gemcitabine, compared to Ad5tg without gemcitabine (Figure 25B G2/M). At 96h sub-G1 was significantly higher in response to gemcitabine or gemcitabine with AdΔ19K, compared to mock- or AdΔ19K-infected cells, respectively (Figure 25B sub-G1). Similarly, at 120h addition of gemcitabine to mock-, Ad5tg- or AdΔ19K-infected cells increased the sub-G1 cell fraction, but cells treated with a combination of gemcitabine and AdΔ19K had significantly more sub-G1 than cells treated only with gemcitabine (Figure 25B sub-G1).

Infection with AdΔ19K significantly increased S- and G2/M-phase cells at 120h compared to mock-infection and subsequently less cells were present in G1 (Figure 25B S-, G1- and G2/M-phase). Similar tendency was observed with Ad5tg. Moreover, following AdΔ19K infection there was a significant

accumulation of cells with a DNA content of >4N from 72h onwards, which was reduced 120h after addition of gemcitabine (Figure 25B >4N). Ad5tg also induced accumulation of cells with a DNA content of >4N by 120h, but this was significantly lower in comparison to AdΔ19K and remained unaffected by the presence of gemcitabine (Figure 25B >4N).

A.

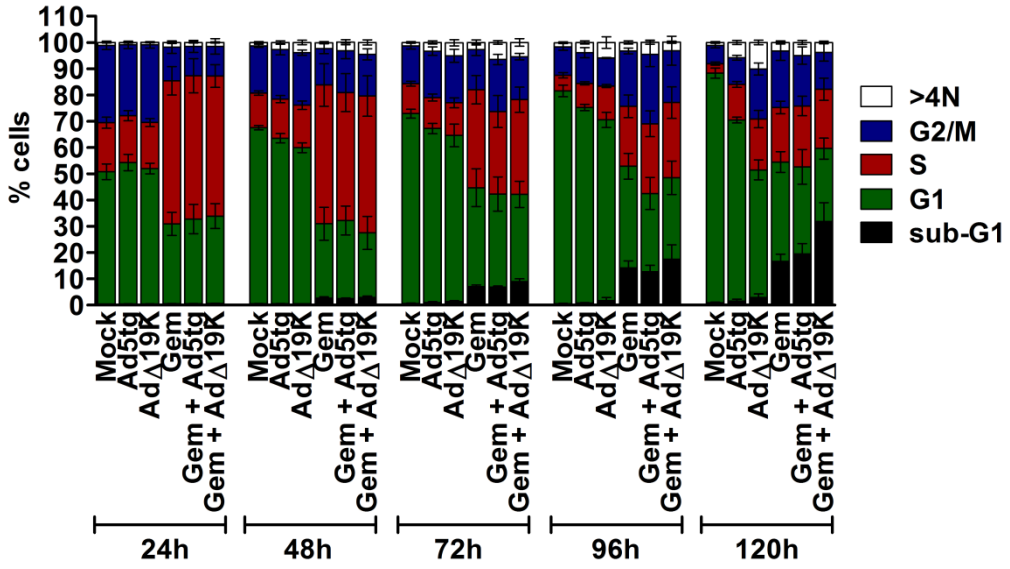

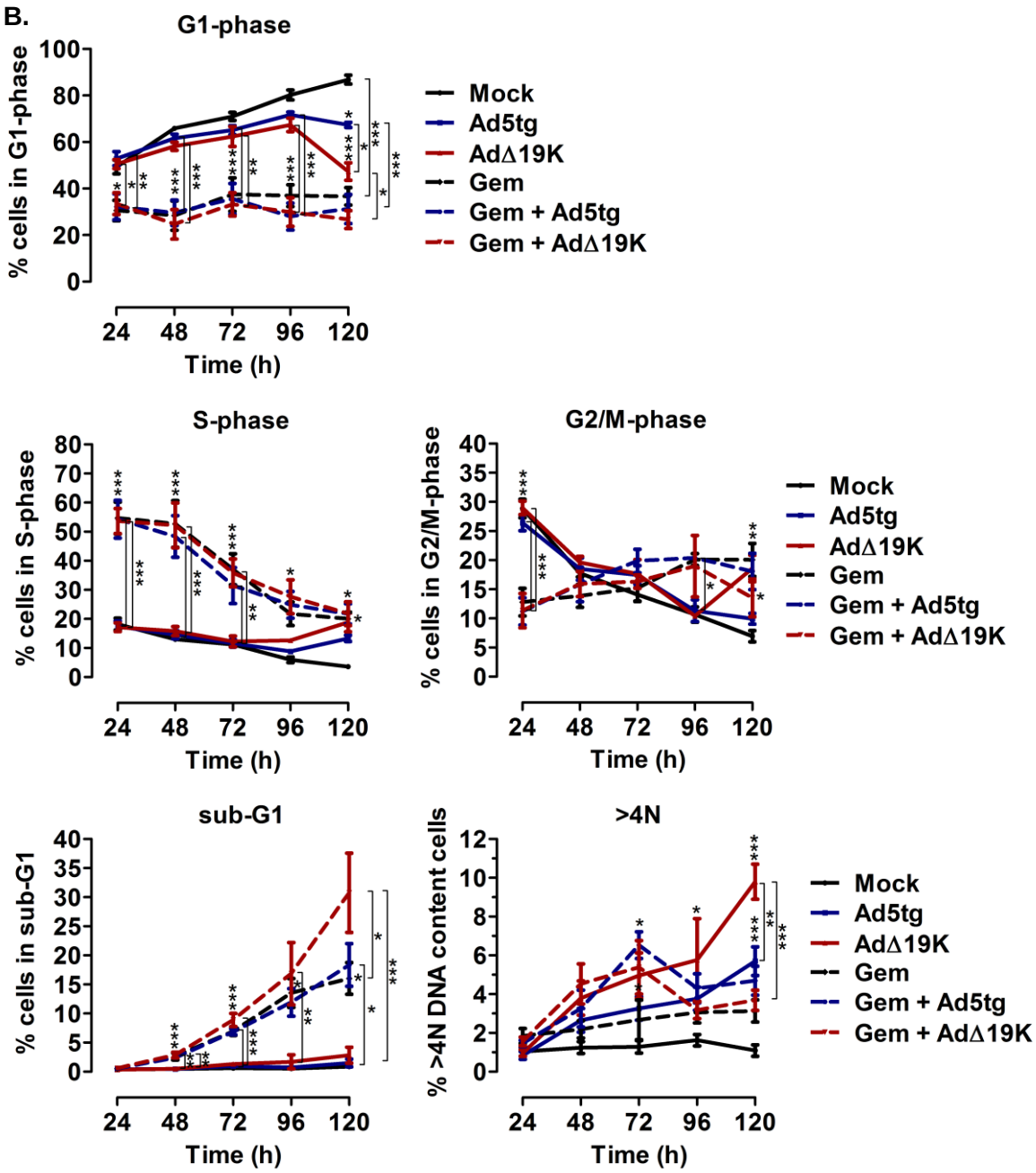

Figure 25: Time-course of cell-cycle distribution in PT45 cells. PT45 cells were treated with 100ppc of Ad5tg or AdΔ19K -/+ 10nM gemcitabine (Gem) and harvested at the indicated times post-infection for cell-cycle analysis. Mock-infection represents untreated cells. **(A)** Cell-cycle distribution. **(B)** Separate plots of % cells in G1-phase, S-phase, G2/M-phase and with DNA content of <2N (sub-G1) and >4N. Error bars represent S.E.M. of at least 3 independent experiments. *.p<0.05, **.p<0.01, ***.p<0.001 (one-way ANOVA with Bonferroni's multiple comparison test). Experiments were performed in conjunction with Dr Gioia Cherubini.

Time-course of cell-cycle distribution in MIAPaCa-2 cells

Similar to PT45 cells, MIAPaCa-2 cells accumulated in S-phase up to 72h following treatment with gemcitabine (Figure 26A), with subsequent reduction of the G1-phase (Figure 26B G1-phase). At 48h, 42.2±6.2% and 25.1±3% of cells were in S and G2/M respectively, following treatment with gemcitabine. Addition of Ad5tg or AdΔ19K did not significantly alter these frequencies. However, there was a tendency towards reduced S-phase fractions; 39.2±6.2% and 27.6±2.6% of cells were in S and G2/M following treatment with gemcitabine and Ad5tg, and 33.9±5.1% and 28.1±3.2% of cells were in S and G2/M following treatment with gemcitabine and AdΔ19K (Figure 26B S- and G1-phase). From 48h to 72h cells treated with gemcitabine or gemcitabine and Ad5tg showed an approximately 10% reduction in S-phase and about 10% increase in G1-phase, whereas cells treated with gemcitabine and AdΔ19K showed no reduction of S-phase (Figure 26B S- and G1-phase). At 72h and 120h after treatment with gemcitabine or gemcitabine and AdΔ19K, significantly more cells were seen in sub-G1 compared to mock- or AdΔ19K-infection, respectively (Figure 26B sub-G1). After 120h of treatment with gemcitabine or gemcitabine and AdΔ19K, more S-phase cells were observed, in comparison to mock or AdΔ19K, respectively (Figure 26B S-phase). At 120h there were more cells accumulating in G1 following treatment with gemcitabine compared to treatment with gemcitabine and viruses (Figure 26B G1).

Ad5tg significantly increased S- and G2/M-phase cells 120h post-infection and a similar trend was observed with AdΔ19K (Figure 26B S- and G2/M-phase). By 120h adenovirus severely perturbed the cell cycle, as it can be appreciated by the cell-cycle histograms found in Appendix 2 (section 5.1.; Figure 66B). Both viruses accumulated cells with a DNA content of >4N, although with AdΔ19K the accumulation was earlier and stronger than Ad5tg and reached 62.2±3.3% by 120h (Figure 26B >4N). As seen in figure 26B, the presence of gemcitabine in AdΔ19K-infected cells inhibited the accumulation of >4N cells from 72h onwards. Reduced >4N cell-fraction was also observed 120h following addition of gemcitabine to Ad5tg-infected cells (Figure 26B >4N).

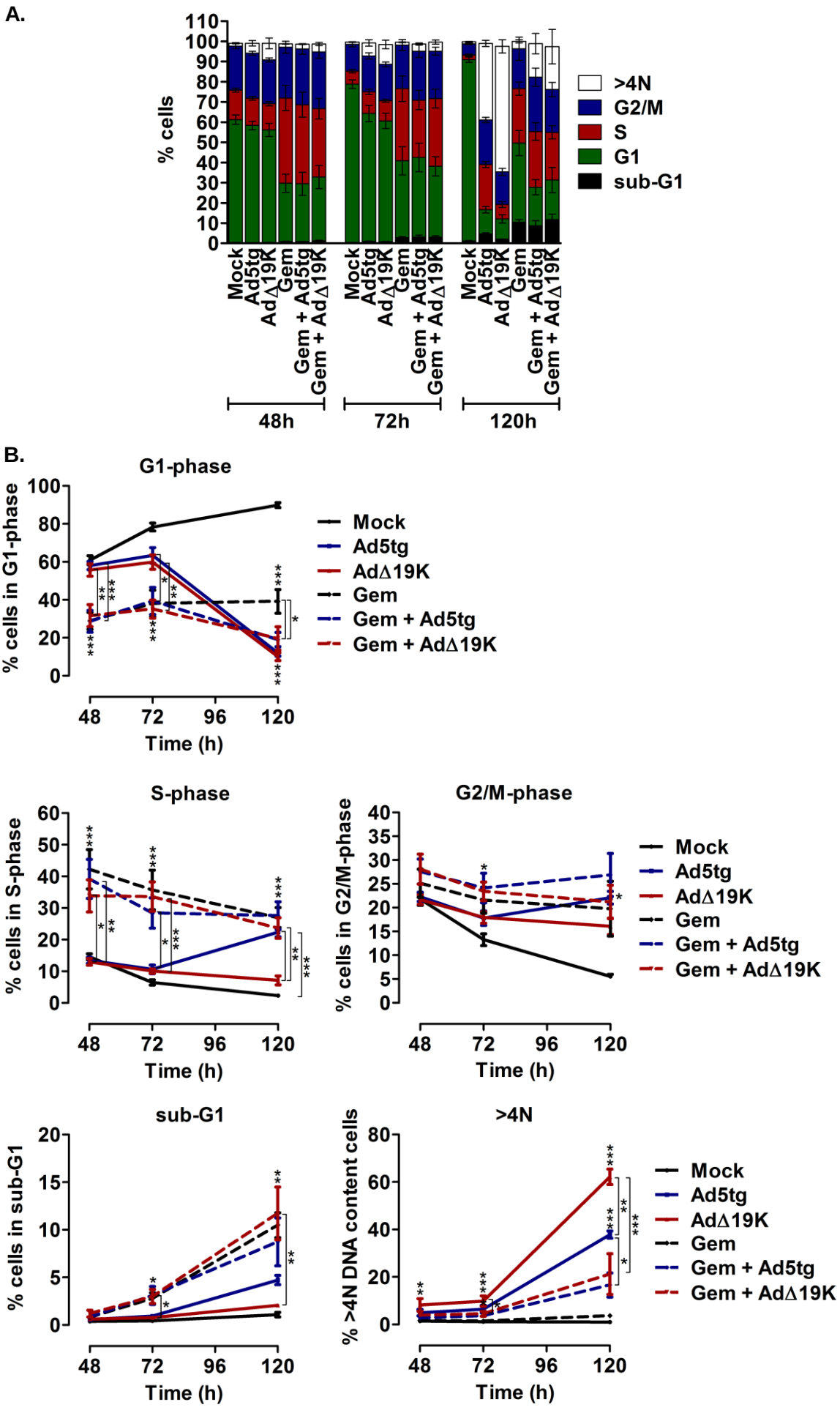
A.
% cells
>4N
G2/M
S
G1
sub-G1
Mock
Ad5tg
AdΔ19K
Gem
Gem + Ad5tg
Gem + AdΔ19K
48h
72h
120h
B.
G1-phase
% cells in G1-phase
S-phase
% cells in S-phase
G2/M-phase
% cells in G2/M-phase
sub-G1
% cells in sub-G1
>4N
% >4N DNA content cells
Time (h)

Figure 26: Time-course of cell-cycle distribution in MIAPaCa-2 cells. MIAPaCa-2 cells were treated with 300ppc of Ad5tg or AdΔ19K -/+ 10nM gemcitabine (Gem) and harvested at the indicated times post-infection for cell-cycle analysis. Mock-infection represents untreated cells. **(A)** Cell-cycle distribution. **(B)** Separate plots of % cells in G1-phase, S-phase, G2/M-phase and with DNA content of <2N (sub-G1) and >4N. Error bars represent S.E.M. of at least 3 independent experiments. *.p<0.05, **.p<0.01, ***.p<0.001 (one-way ANOVA with Bonferroni's multiple comparison test).

Summary

In conclusion, in PT45 cells gemcitabine caused an S-phase arrest which was gradually relieved, with cells passing to G2/M and G1-phases and some dying, as suggested by the gradual increase of sub-G1 cell fraction. Addition of either Ad5tg or AdΔ19K did not significantly affect the cell-cycle distribution of gemcitabine-treated cells, with the exception of a sub-G1 increase in the presence of AdΔ19K. Furthermore, infection with AdΔ19K increased the frequency of S- and G2/M-phase cells and accumulated a cell fraction with >4N DNA content, that was reduced in the presence of gemcitabine. Similarly, following treatment with gemcitabine, MIAPaCa-2 cells arrested in S-phase and gradually moved to G2/M and G1. Up to 72h no significant differences were seen between cells treated with gemcitabine and cells treated with gemcitabine and viruses, while at 120h there were more cells in G1-phase in response to gemcitabine compared to gemcitabine with viruses. Both viruses perturbed the cell-cycle resulting in an accumulation of a >4N cell-fraction, but with AdΔ19K the accumulation was more potent.

3.2.2. Combining AdΔ19K with gemcitabine or irinotecan does not prevent the activation of the DDR elicited by the drugs, but increases DNA damage

PT45 cells

Arrest of cells in S-phase following treatment with gemcitabine led us to assess activation of the DNA-damage response. Firstly, we examined whether any DNA damage was present, using the DNA-damage marker phospho-histone H2A.X (Ser139). Immunoblot analysis of phospho-histone H2A.X (pH2AX) in PT45 cells showed that 24h after gemcitabine treatment there was a 2-fold increase in pH2AX protein levels, that modestly increased up to 72h (Figure 27A). The presence of AdΔ19K in gemcitabine-treated cells significantly increased phosphorylation of histone H2AX at 48h, with a trend towards increases also at 24h and 72h (Figure 27A). The presence of Ad5tg in gemcitabine-treated cells showed a tendency towards elevated phosphorylation of histone H2AX at 48h (Figure 27A). Infection with Ad5tg or AdΔ19K alone appeared to increase pH2AX protein levels at 48h and 72h, but did not reach statistical significance (Figure 27A).

In order to assess activation of the DNA-damage response we examined phosphorylation of the checkpoint kinases Chk1 and Chk2. As shown in Figure 27B, gemcitabine induced Chk1 phosphorylation at 24h, with a gradual decrease from 24h to 72h. In response to gemcitabine combined with either Ad5tg or AdΔ19K pChk1 was induced to a similar extend as with gemcitabine alone (Figure 27B). No Chk1 phosphorylation was apparent following infection with Ad5tg or AdΔ19K (Figure 27B). Chk2 phosphorylation increased 48h and 72h after treatment with gemcitabine and this pattern was also seen when gemcitabine was combined with Ad5tg or AdΔ19K (Figure 27C). A trend towards increased phospho-Chk2 protein levels was observed when AdΔ19K was present in gemcitabine-treated cells, compared to gemcitabine without AdΔ19K (Figure 27C). No obvious Chk2 phosphorylation could be detected in Ad5tg- or AdΔ19K-infected cells (Figure 27C).

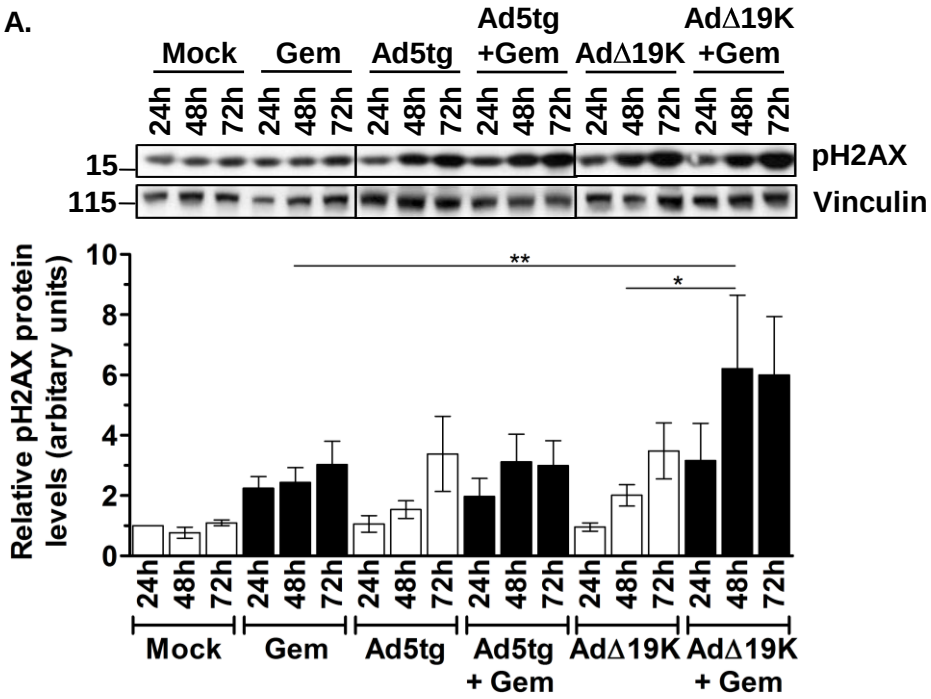
A.
Mock
Gem
Ad5tg
Ad5tg +Gem
AdΔ19K
AdΔ19K +Gem
24h 48h 72h
15
115
pH2AX
Vinculin
Relative pH2AX protein levels (arbitary units)
**
*
Mock
Gem
Ad5tg
Ad5tg + Gem
AdΔ19K
AdΔ19K + Gem

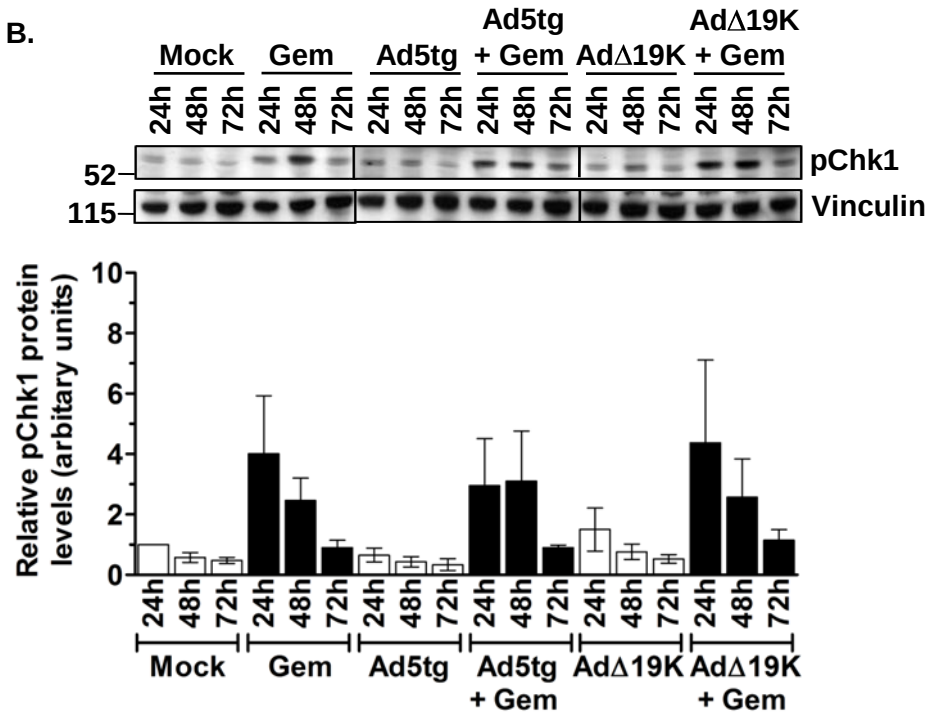
B.
Mock
Gem
Ad5tg
Ad5tg + Gem
AdΔ19K
AdΔ19K + Gem
24h 48h 72h
52
115
pChk1
Vinculin
Relative pChk1 protein levels (arbitary units)
Mock
Gem
Ad5tg
Ad5tg + Gem
AdΔ19K
AdΔ19K + Gem

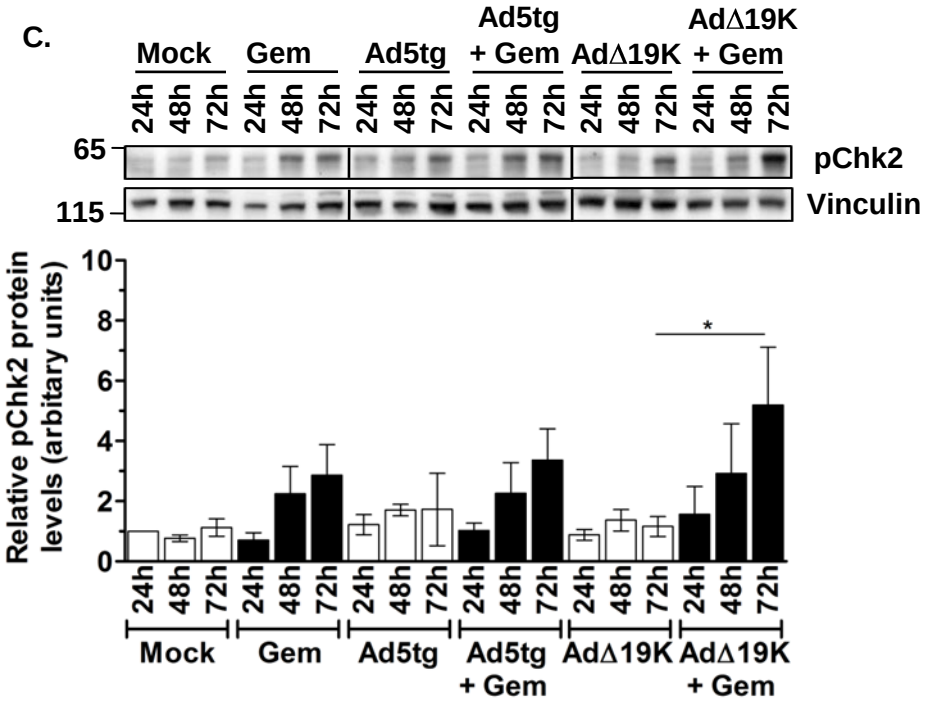

Figure 27: Combining AdΔ19K with gemcitabine does not prevent the activation of the DNA-damage response elicited by the drug, but increases DNA damage in PT45 cells. PT45 cells were treated with 100ppc Ad5tg or AdΔ19K -/+ 10nM gemcitabine (Gem) and harvested at the indicated times for immunblot analysis of pH2AX, pChk1 and pChk2. **(A)** Average phospho-histoneH2A.X (pH2AX, Ser139) protein levels expressed relative to the loading control, as quantified by densitometric analysis. A representative immunoblot of pH2AX (15kDa) with vinculin (130kDa) as a loading control is also shown. Numbers indicate MW size marker (kDa) **(B)** Average phospho-Chk1 (pChk1, Ser345) protein levels expressed relative to the loading control, as quantified by densitometric analysis. A representative immunoblot of pChk1 (56kDa) with vinculin (130kDa) as a loading control is also shown. **(C)** Average phospho-Chk2 (pChk1, Thr68) protein levels expressed relative to the loading control, as quantified by densitometric analysis. A representative immunoblot of pChk2 (56kDa) with vinculin (130kDa) as a loading control is also shown. Vertical lines on immunoblots indicate points of cropping. Error bars represent S.E.M. of 2-3 independent experiments. *.p<0.05, **.p<0.01 (one-way ANOVA with Bonferroni's multiple comparison test). The sample preparation and immunobotting was performed in collaboration with Dr Gioia Cherubini.

We next sought to examine whether the inability of adenovirus to prevent the activation of the DNA-damage response elicited by gemcitabine was also evident in response to the DNA-damaging drug irinotecan. Preliminary immunoblot analysis in PT45 cells showed that irinotecan induces phosphorylation of histoneH2AX that increases from 24h to 72h post-treatment, phosphorylation of Chk1 that peaks at 48h and phosphorylation of Chk2 that remains constant from 24 to 72h (Figure 28). In contrast to gemcitabine, the presence of Ad5tg or AdΔ19K in irinotecan-treated cells did not seem to further increase phosphorylation of histoneH2AX (Figure 28). The preliminary data suggested that irinotecan-induced phosphorylation of Chk1 might be increased in the presence of viruses at 24h and reduced at 48h (Figure 28). Irinotecan-induced Chk2 phosphorylation seemed to increase in the presence of viruses after 72h (Figure 28). Therefore, these preliminary studies suggested that similar to the findings with gemcitabine, adenovirus cannot prevent activation of the DNA-damage response elicited by irinotecan.

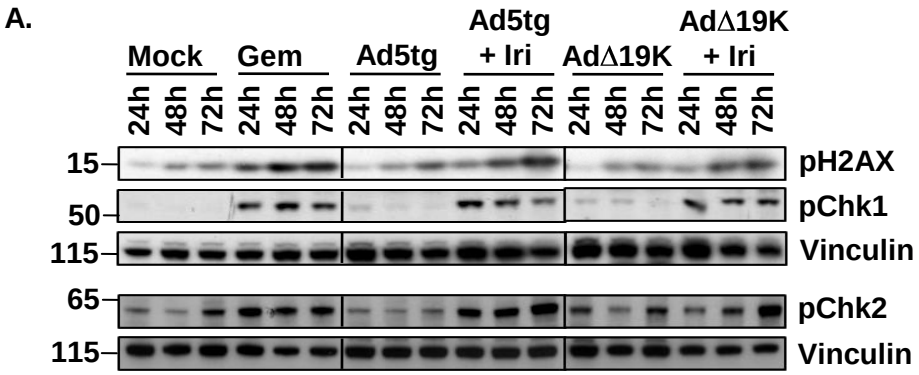

B.

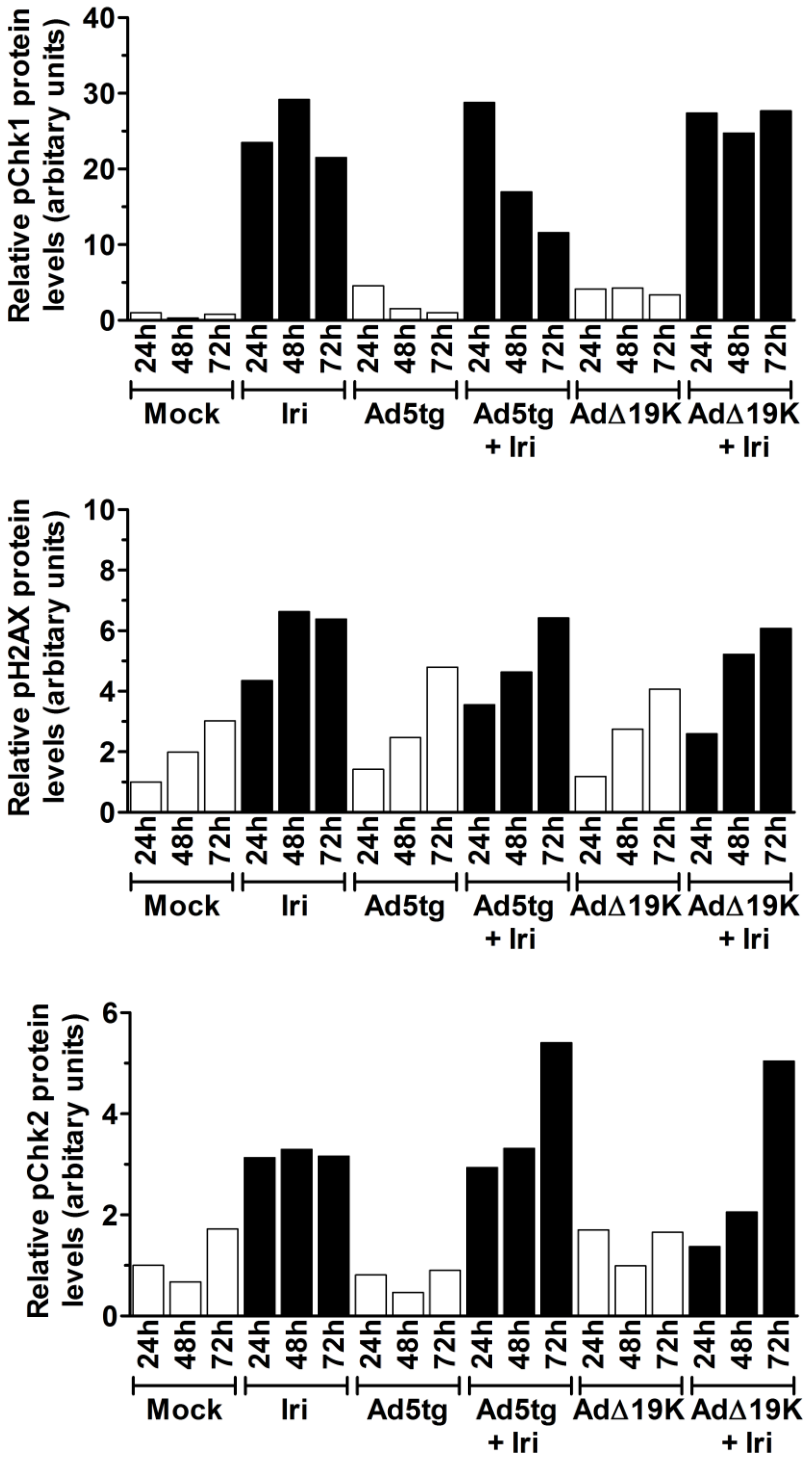

<u>Figure 28</u>: Preliminary data in PT45 cells suggest that combining AdΔ19K with Irinotecan does not prevent the activation of the DNA-damage response elicited by the drug. PT45 cells were treated with 100ppc Ad5tg or AdΔ19K -/+ 12.5μM irinotecan (Iri) and harvested at the indicated times for immunblot analysis of pH2AX, pChk1 and pChk2. **(A)** Immunoblot of pH2AX (Ser139, 15kDa), pChk1 (Ser345, 56kDa) and pChk2 (Thr68, 62kDa) with vinculin (130kDa) as a loading control. **(B)** Quantification of pH2AX, pChk1 and pChk2 protein levels by densitometric analysis (expressed relative to the loading control). n =1. The sample preparation and immunoblotting were performed by Dr Gioia Cherubini and Ms Ana Mozetic.

MIAPaCa-2 cells

In order to examine whether adenovirus affects the activation of the DNA-damage response following gemcitabine or irinotecan treatment in MIAPaCa-2 cells, immunoblot analysis for phosphorylation of Chk1 and histoneH2AX was performed at 24h and 48h.

Gemcitabine induced phosphorylation of histoneH2AX at 24h, which increased by 3-fold at 48h post-treatment (Figure 29A and B). In the presence of AdΔ19K gemcitabine-induced histoneH2AX phosphorylation significantly increased; 2-fold compared to gemcitabine at 48h (Figure 29A and B). In contrast, the presence of Ad5tg did not affect gemcitabine-induced histoneH2AX phosphorylation and similar phospho-histoneH2AX protein levels were observed between gemcitabine and gemcitabine combined with Ad5tg (Figure 29A and B). Phospho-histoneH2AX levels were significantly higher in cells treated with gemcitabine and AdΔ19K, compared to gemcitabine and Ad5tg (Figure 29B). Similar to gemcitabine, irinotecan induced histoneH2AX phosphorylation at 48h but to a greater extent, with a 9-fold increase compared to 24h (Figure 29A and C). In the presence of either Ad5tg or AdΔ19K irinotecan-induced histoneH2AX phosphorylation at 48h was significantly increased (2-fold; Figure 29A and C). In addition, there was a trend towards increased phospho-histoneH2AX levels at 24h following treatment with irinotecan and either Ad5tg or AdΔ19K (Figure 29C). In the absence of drugs, infection with Ad5tg or AdΔ19K appeared to increase histoneH2AX phosphorylation by 2-3-fold compared to mock-infected cells but was not statistically significant (Figure 29B and C).

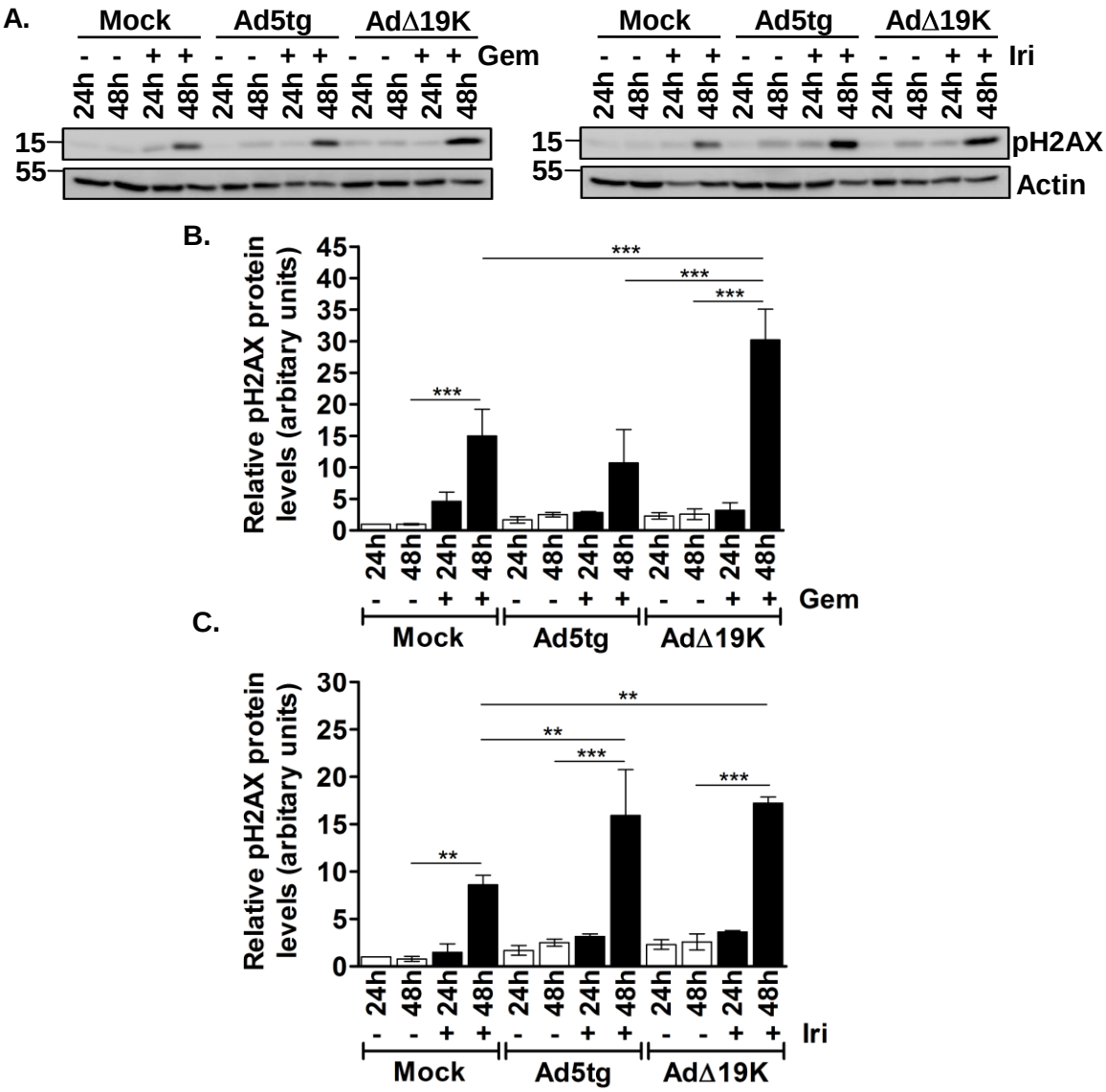

Figure 29: Combining AdΔ19K with gemcitabine or irinotecan increases DNA-damage in MIAPaCa-2 cells. MIAPaCa-2 cells were treated with 300ppc Ad5tg or AdΔ19K -/+ 20nM gemcitabine (Gem) or 15µM Irinotecan (Iri) and harvested at the indicated times for immunoblot analysis of phosphorylated histoneH2A.X (Ser139). **(A)** Representative immunoblots of pH2AX (Ser139, 15kDa) with actin (42kDa) as a loading control. **(B)** Average pH2AX protein levels in mock-, Ad5tg- or AdΔ19K-infected cells -/+ gemcitabine. **(C)** Average pH2AX protein levels in mock-, Ad5tg- or AdΔ19K-infected cells -/+ irinotecan. The pH2AX protein levels were quantified by densitometric analysis and expressed relative to the loading control. Error bars represent S.E.M. of 2 independent experiments. **.p<0.01, ***.p<0.001 (one-way ANOVA with Bonferroni's multiple comparison test).

Chk1 was phosphorylated 24h post-treatment with gemcitabine and the phosphorylation appeared to increase at 48h (Figure 30A and B). Similar upregulation of phospho-Chk1 levels was observed in response to the combination of gemcitabine with either Ad5tg or AdΔ19K (Figure 30A and B). Analogous to gemcitabine, irinotecan induced phosphorylation of Chk1, which peaked at 48h (Figure 30A and C). In the presence of viruses irinotecan-induced Chk1 phosphorylation showed a tendency towards decreased levels at 24h, especially in the presence of AdΔ19K (Figure 30A and C). At 48h similar phospho-Chk1 levels were observed in cells treated with irinotecan and irinotecan combined with either virus (Figure 30A and C). No Chk1 phosphorylation was detectable following infection with adenoviruses in the absence of drugs (Figure 30A-C).

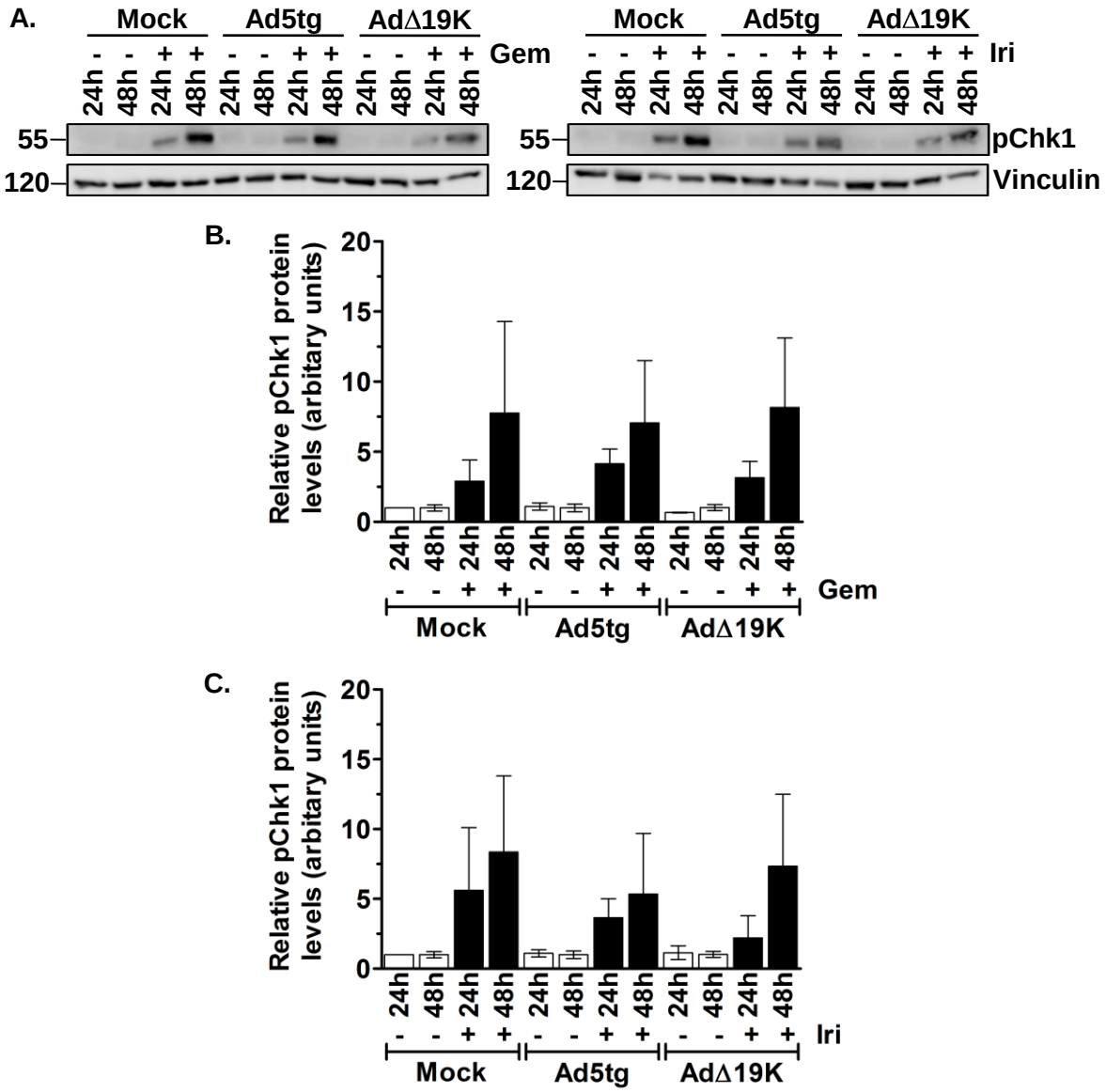

Figure 30: Combining AdΔ19K with gemcitabine or irinotecan does not prevent the activation of the DNA-damage response elicited by the drugs in MIAPaCa-2 cells. MIAPaCa-2 cells were treated with 300ppc Ad5tg or AdΔ19K -/+ 20nM gemcitabine (Gem) or 15µM Irinotecan (Iri) and harvested at the indicated times for immunoblot analysis of phospho-Chk1 (Ser345). **(A)** Representative immunoblots of pChk1 (Ser345, 56kDa) with vinculin (130kDa) as a loading control. **(B)** Average phospho-Chk1 protein levels in mock-, Ad5tg- or AdΔ19K-infected cells -/+ gemcitabine. **(C)** Average phospho-Chk1 protein levels in mock-, Ad5tg- or AdΔ19K-infected cells -/+ irinotecan. Phospho-Chk1 protein levels were quantified by densitometric analysis and are expressed relative to the loading control. Error bars represent S.E.M. of 2 independent experiments.

Summary

In PT45 cells gemcitabine induces phosphorylation of Chk1 at 24 and 48h post-treatment and Chk2 phosphorylation at 48 and 72h, indicating activation of the DNA-damage response. In contrast, adenovirus infection efficiently prevented activation of the DNA-damage response. However, in the presence of gemcitabine, Ad5tg or AdΔ19K could not prevent phosphorylation of Chk1 and Chk2 and overall, gemcitabine-induced activation of the DNA-damage response was not significantly affected by the presence of viruses. Despite this, AdΔ19K significantly increased gemcitabine-induced histoneH2AX phosphorylation at 48h, suggesting increased DNA damage. Preliminary data suggested that similar to gemcitabine, adenovirus cannot prevent activation of the DNA-damage response elicited by irinotecan in PT45 cells. In MIAPaCa-2 cells, both gemcitabine and irinotecan activated Chk1 24-48h post-treatment. The presence of adenovirus in gemcitabine- or irinotecan-treated cells did not significantly alter drug-induced induction of phospho-Chk1, suggesting that, like in PT45 cells, adenovirus is unable to prevent activation of the DNA-damage response elicited by the drugs. However, AdΔ19K did increase gemcitabine and irinotecan-induced phosphorylation of histoneH2A.X. Therefore, it can be concluded that in response to AdΔ19K and DNA-damaging drugs the ATR/Chk1 and ATM/Chk2 pathways are activated to similar extent as with drugs alone, but the combination treatment leads to augmented phospho-histoneH2A.X expression, implying increased DNA damage and/or replication stress.

3.2.3. AdΔ19K-mediated Mre11 and Nbs1 downregulation persists in the presence of gemcitabine and irinotecan

Upon infection adenovirus efficiently blocks the activation of the DNA-damage response, by degrading the Mre11 and Nbs1 components of the MRN complex (Turnell and Grand, 2012). Following the finding that adenovirus is unable to block the DNA-damage response elicited by gemcitabine or irinotecan, we wondered whether it was still able to degrade the MRN complex. Immunoblot analysis for Mre11 and Nbs1 was therefore carried out in PT45 cells.

In the absence of drugs, adenovirus efficiently downregulated Mre11 expression, with significant decreases seen at 48h and 72h post-AdΔ19K infection and 72h post-Ad5tg infection (Figure 31A and B). Similarly, Nbs1 protein levels were significantly reduced from 24h to 72h post-infection with either virus (Figure 31A and C). Gemcitabine did not seem to affect Mre11 or Nbs1 protein levels compared to mock-treated cells (Figure 31A-C). However, 72h after treatment with gemcitabine and AdΔ19K, Mre11 expression was significantly decreased compared to gemcitabine (Figure 31A and C). In the presence of gemcitabine, AdΔ19K and Ad5tg showed a trend towards Mre11 and Nbs1 downregulation at all time-points tested.

Similar results were obtained in response to irinotecan (Figure 32A-C). Mre11 and Nbs1 protein levels were significantly decreased 24h and 72h post-Ad5tg infection, with a trend towards a decrease at 48h (Figure 32A-C). AdΔ19K significantly reduced Mre11 expression after 48h and 72h, and Nbs1 expression at 48h, with a trend towards decreases at all other time-points (Figure 32A-C). Analogous to gemcitabine, irinotecan did not alter the protein levels of Mre11 or Nbs1 (Figure 32A-C). In the presence of irinotecan, AdΔ19K downregulated Mre11 expression and a significant decrease in Mre11 protein levels compared to irinotecan was seen at 72h (Figure 32A and B). A tendency towards Mre11 downregulation was also seen 24 and 48h following irinotecan and Ad5tg treatment (Figure 32A and B). No significant decreases in Nbs1 protein levels were detected in cells treated with AdΔ19K and irinotecan, despite a trend towards reduced levels compared to irinotecan, particularly at 72h (Figure 32A

and C). In the presence of irinotecan Ad5tg did not seem to be as potent as AdΔ19K in downregulating Nbs1 expression (Figure 32C).

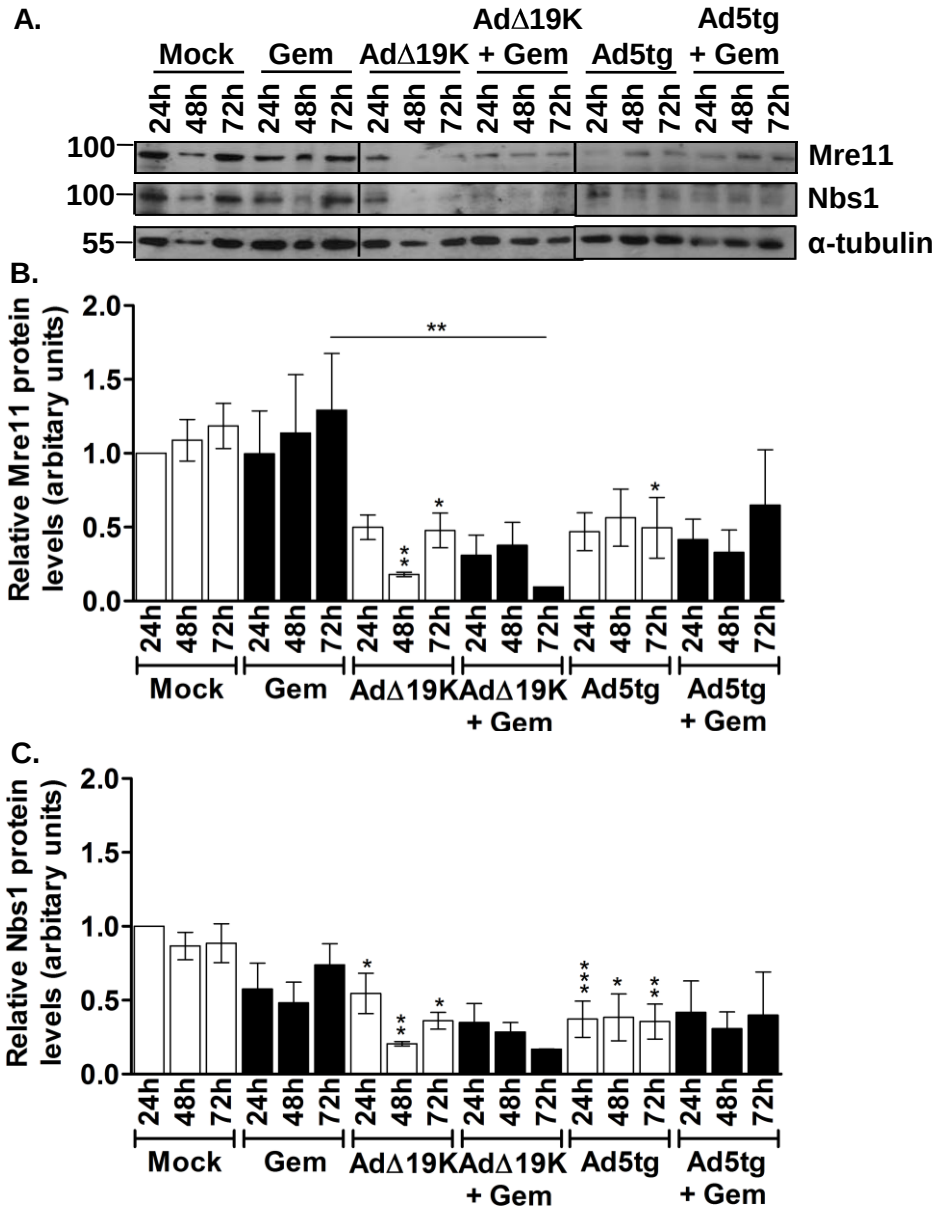

<u>Figure 31</u>: AdΔ19K-mediated Mre11 and Nbs1 downregulation persists in the presence of gemcitabine. PT45 cells were treated with 300ppc Ad5tg or AdΔ19K -/+ 5nM gemcitabine (Gem) and harvested at the indicated times for immunblot analysis of Mre11 and Nbs1. **(A)** Representative immunoblot of Mre11 (81kDa) and Nbs1 (95kDa). α-tubulin (55kDa) was used as a loading control. Numbers indicate MW size marker (kDa). Vertical lines on the immunoblot indicate points of cropping. **(B and C)** Quantification of protein levels by densitometric analysis. Mre11 and Nbs1 protein levels were expressed relative to the loading control. Error bars represent S.E.M. of 3 independent experiments. *.p<0.05, **.p<0.01, ***.p<0.001 (one-way ANOVA with Bonferroni's multiple comparison test).

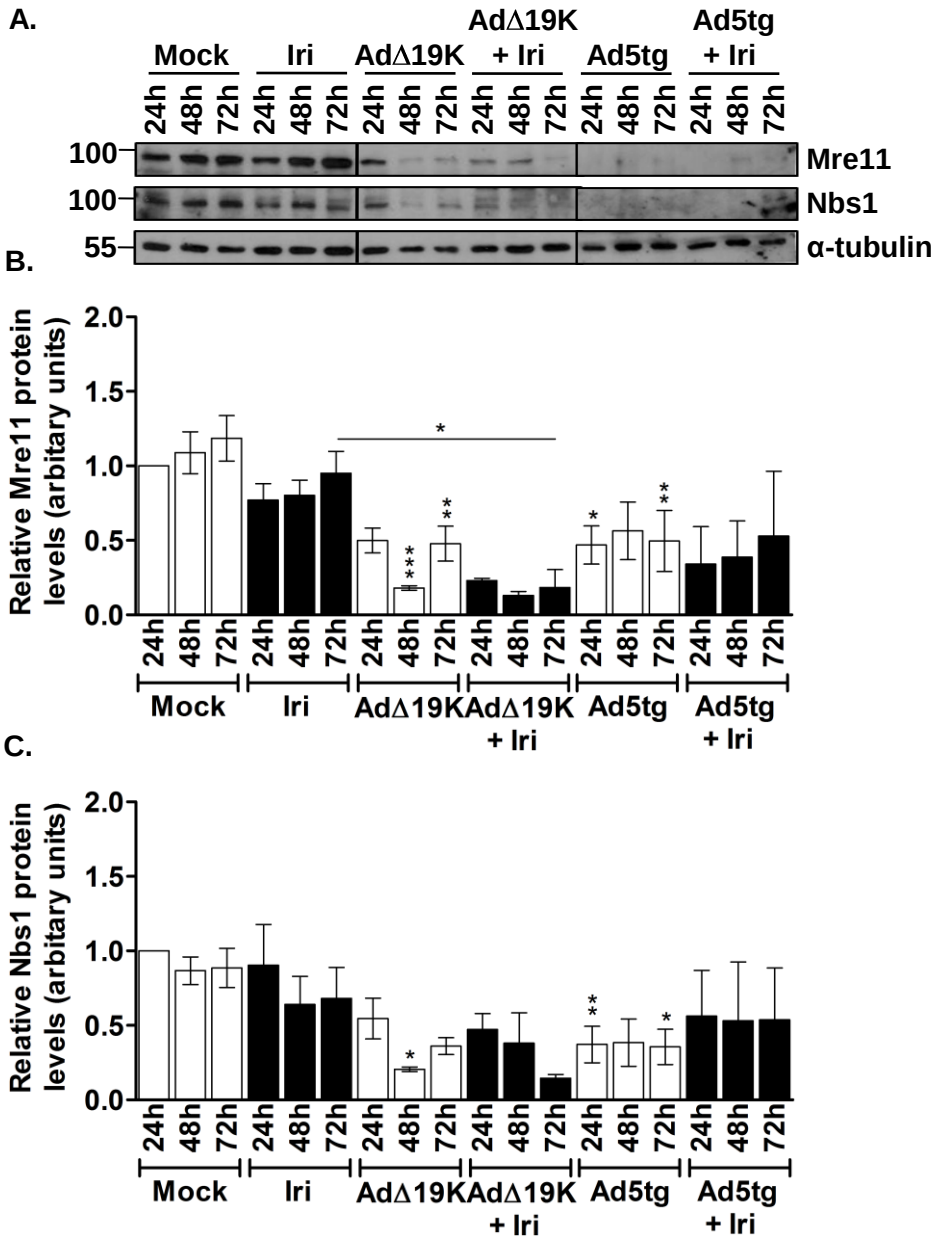

Figure 32: AdΔ19K-mediated Mre11 and Nbs1 downregulation persists in the presence of irinotecan. PT45 cells were treated with 300ppc Ad5tg or AdΔ19K -/+ 5μM irinotecan (Iri) and harvested at the indicated times for immunblot analysis of Mre11 and Nbs1. **(A)** Representative immunoblot of Mre11 (81kDa) and Nbs1 (95kDa). α-tubulin (55kDa) was used as a loading control. Vertical lines on the immunoblot indicate points of cropping. **(B and C)** Quantification of protein levels by densitometric analysis. Mre11 and Nbs1 protein levels were expressed relative to the loading control. Error bars represent S.E.M. of 3 independent experiments. *.p<0.05, **.p<0.01, ***.p<0.001 (one-way ANOVA with Bonferroni's multiple comparison test).

Mre11 and Nbs1 expression was also assessed in MIAPaCa-2 cells following mock, Ad5tg or AdΔ19K infection in the absence or presence of gemcitabine. As shown in figure 33, AdΔ19K downregulated Mre11 and Nbs1 protein levels only at 48h post-infection, whereas Ad5tg decreased Mre11 and Nbs1 expression 24h though to 72h post-infection. In response to gemcitabine, a modest upregulation of Mre11 and Nbs1 was observed at 24h, while no obvious change was seen after 48h and 72h compared to mock-infected cells (Figure 33A-C). In cells treated with a combination of gemcitabine and AdΔ19K, Mre11 and Nbs1 protein levels were reduced at 48h (Figure 33A-C). In contrast, no downregulation of Mre11 and Nbs1 was observed upon treatment with gemcitabine and Ad5tg (Figure 33A-C).

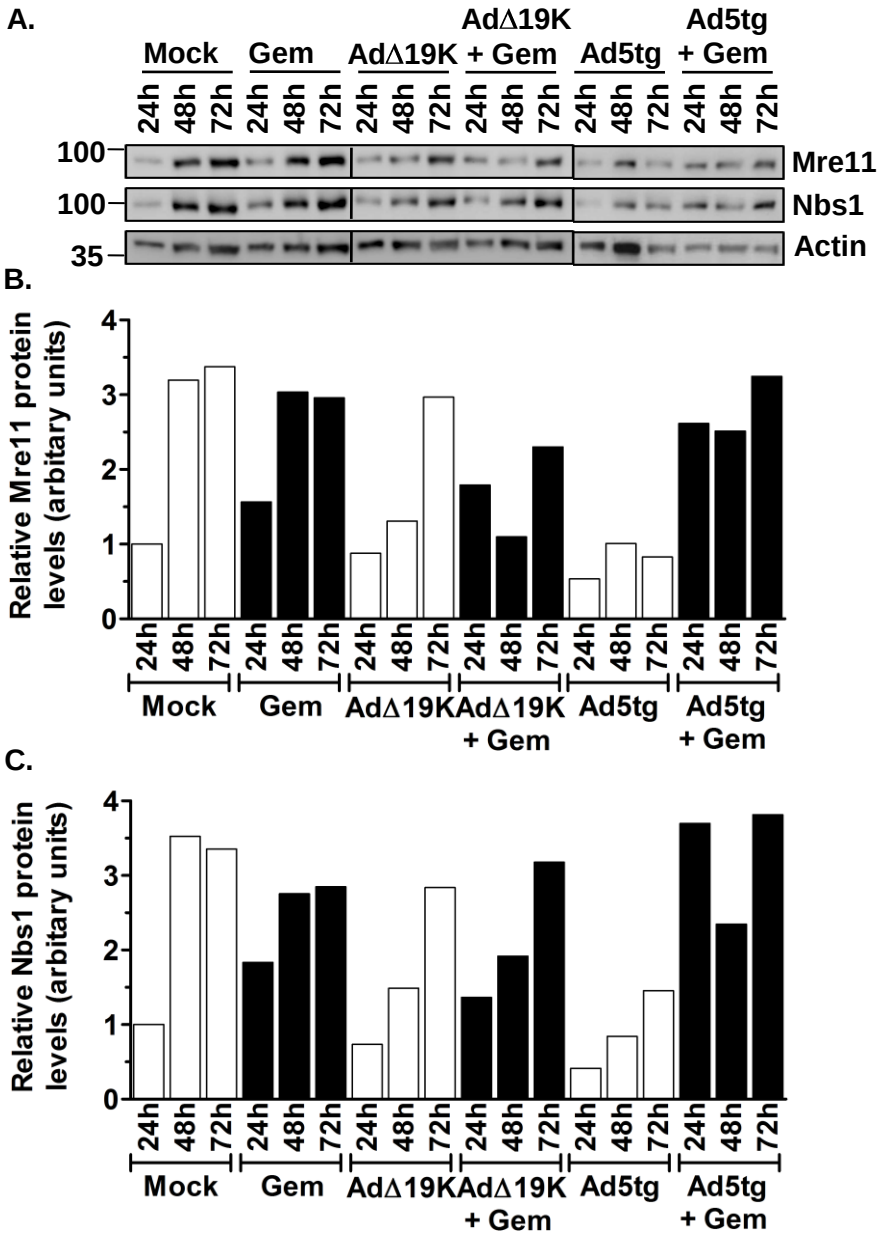

<u>Figure 33</u>: Preliminary data in MIAPaCa-2 cells suggest that AdΔ19K induces Mre11 and Nbs1 downregulation at 48h, that persists in the presence of gemcitabine. MIAPaCa-2 cells were treated with 300ppc Ad5tg or AdΔ19K -/+ 20nM gemcitabine (Gem) and harvested at the indicated times for immunoblot analysis of Mre11 and Nbs1. **(A)** Immunoblot of Mre11 (81kDa) and Nbs1 (95kDa). Actin (42kDa) was used as a loading control. **(B and C)** Mre11 and Nbs1 protein levels were quantified by densitometric analysis and expressed relative to the loading control. One experiment.

It can be concluded that both viruses downregulate Mre11 and Nbs1 protein levels in PT45 cells and in the presence of gemcitabine or irinotecan AdΔ19K is still able to downregulate Mre11 expression up to 72h after treatment. Preliminary data suggest that Ad5tg-mediated downregulation of Mre11 and Nbs1 expression in MIAPaCa-2 cells is more efficient compared to AdΔ19K in the absence of gemcitabine. However, in the presence of gemcitabine AdΔ19K, but not Ad5tg, decreased Mre11 and Nbs1 protein levels 48h post-treatment. Taken together, the immunoblot analysis for DDR proteins suggested that in both cell lines drug-induced activation of the DDR is not impaired by adenovirus but persistent virus-induced degradation of the MRN complex in the presence of drugs might inhibit DNA repair leading to increased DNA damage and/or replication stress.

3.2.4. Mre11 knockdown increases cell death induced by AdΔ19K and DNA-damaging drugs

Observing that in the presence of gemcitabine or irinotecan AdΔ19K can still downregulate Mre11 and Nbs1 expression, prompted me to investigate whether this downregulation was important for AdΔ19K-mediated sensitization of PT45 cells to DNA-damaging drugs. A 6-day experiment was setup, during which cells were transfected with a non-targeting siRNA or siRNA against Mre11, harvested and seeded for use in cell viability assays and immunoblot analysis for monitoring Mre11 knockdown. Cell viability was assessed 72h post-infection with AdΔ19K in the absence or presence of fixed doses of gemcitabine or irinotecan. The time of cell viability assessment corresponded to 120h post-transfection. As shown in figure 34, Mre11 was efficiently knocked-down throughout the course of the experiment, with 80-90% knockdown being achieved 48h to 120h post-transfection, compared to the non-targeting siRNA control.

Assessment of cell viability demonstrated that Mre11 knockdown decreased the EC_{50} value of AdΔ19K by 2-fold compared to the non-targeting siRNA control (Figure 35A). The EC_{50} value of AdΔ19K in combination with 2nM or 5nM

gemcitabine significantly dropped by 3- and 5-fold, respectively, following Mre11 knockdown (Figure 35A). Similarly, a significant 4-fold decrease in the EC_{50} value of AdΔ19K and irinotecan was observed when Mre11 was knocked-down (Figure 35A).

The sensitization ratio in response to AdΔ19K and 2nM gemcitabine showed a trend towards increase in cells where Mre11 was knocked-down compared to the control siRNA (Figure 35B). When AdΔ19K was combined with the higher dose of gemcitabine or irinotecan the sensitization ratio significantly increased following Mre11 knockdown (Figure 35B). Interestingly, knocking-down Mre11 enhanced gemcitabine-induced cytotoxicity and showed a tendency to enhance irinotecan-induced cell death (Figure 35C).

In conclusion, knockdown of Mre11 enhanced AdΔ19K-mediated cytotoxicity both in the absence and presence of drugs, although greater reductions in the EC_{50} values following Mre11 knockdown were observed when AdΔ19K was combined with drugs. Moreover, gemcitabine- and irinotecan-mediated sensitization to AdΔ19K was significantly enhanced when Mre11 was knocked-down compared to the same treatment in cells with the non-targeting siRNA. Besides AdΔ19K, gemcitabine-induced cytotoxicity was also enhanced following Mre11 knockdown. Therefore, AdΔ19K-mediated downregulation of Mre11 is important for cell death induced by AdΔ19K and DNA-damaging drugs.

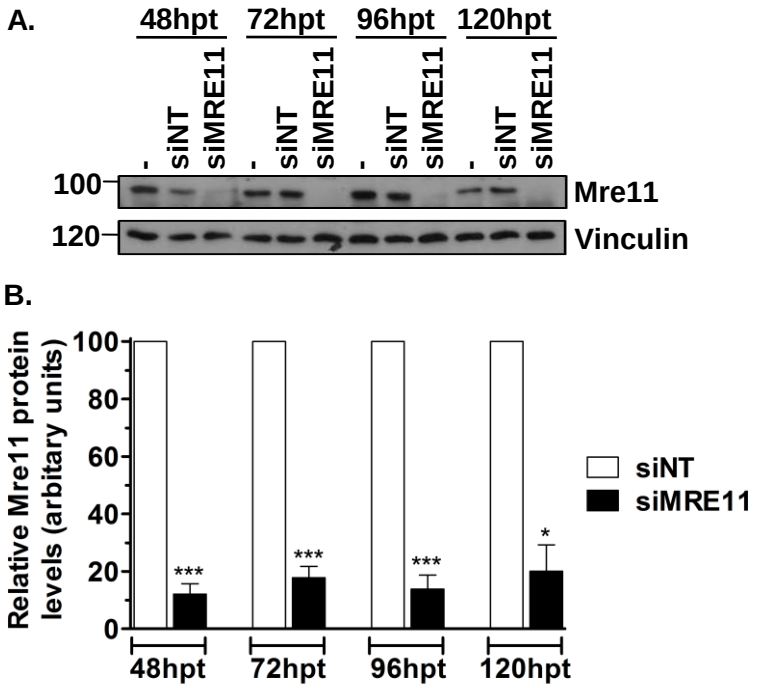

Figure 34: Mre11 is efficiently knocked-down for up to 120h post-transfection. PT45 cells were transfected with siRNA against MRE11 (siMRE11) or non-targeting siRNA (siNT). 24h post-transfection cells were pooled, re-seeded in 6-well plates and harvested for immunoblot analysis at the indicated hours post-transfection (hpt). **(A)** Representative immunoblot of Mre11 (81kDa). Vinculin (130kDa) was used as a loading control. Numbers indicate MW size marker (kDa). **(B)** Quantification of protein levels by densitometric analysis. Mre11 protein levels were normalised to the loading control and expressed as % of siNT at each time-point Error bars represent S.E.M. of 4 independent experiments. *.p<0.05, ***.p<0.001 (one-sample t-test comparing to 100%).

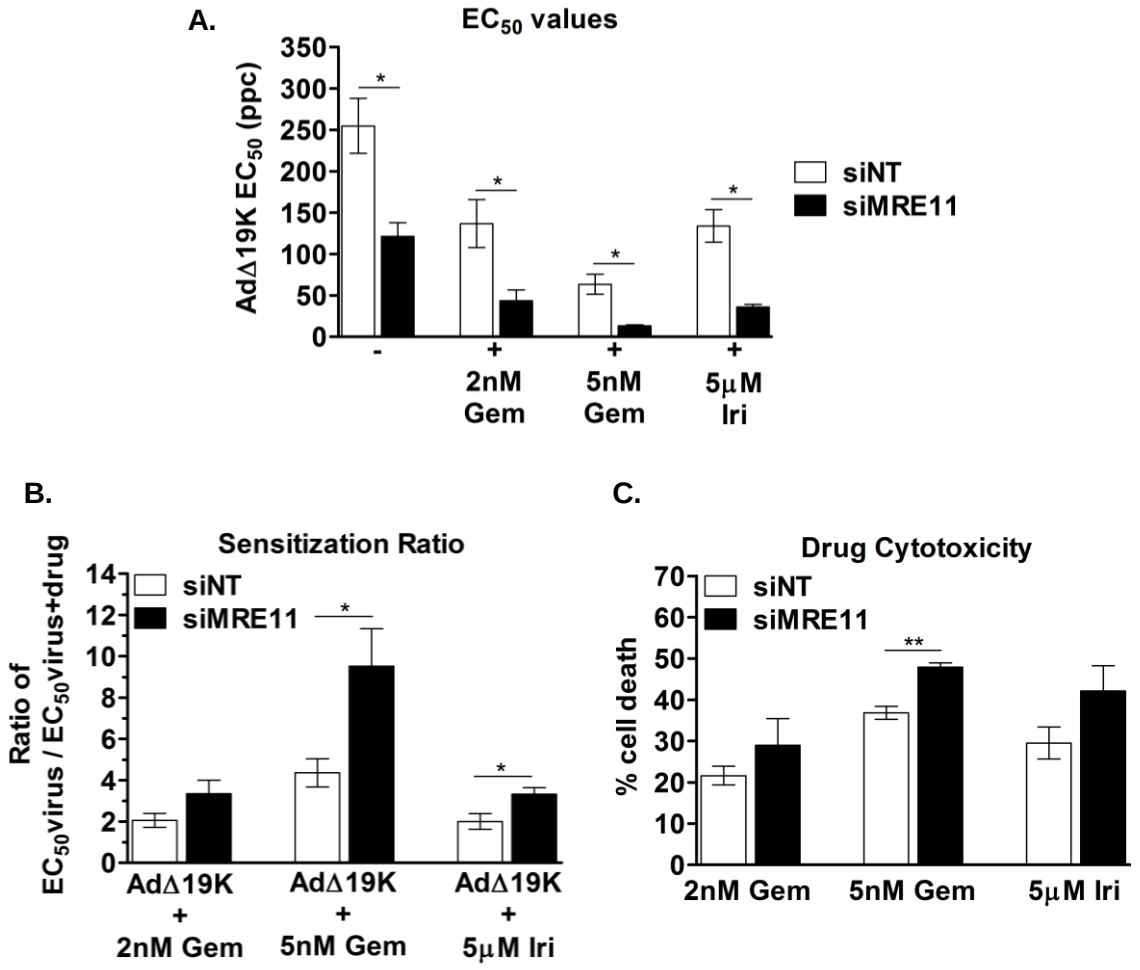

<u>Figure 35</u>: Mre11 knockdown increases cell death induced by AdΔ19K and DNA-damaging drugs. PT45 cells were transfected with siRNA against MRE11 (siMRE11) or non-targeting siRNA (siNT) 24h post-transfection cells were pooled and re-seeded in 96-well plates. 24h later (i.e. 48h post-transfection) cells were treated with 5-fold dilutions of AdΔ19K -/+ fixed doses of gemcitabine (Gem) or irinotecan (Iri) to generate dose-response curves. Cell viability was assessed by MTS assay at 72h post-infection, which corresponded to 120h post-transfection. **(A)** EC_{50} values for AdΔ19K -/+ gemcitabine (Gem) or irinotecan (Iri) at the indicated doses in cells transfected with MRE11 or NT siRNA. **(B)** Sensitization ratio (AdΔ19K EC_{50} / AdΔ19K+Gem or Iri EC_{50}). **(C)** Drug cytotoxicity. % cell death induced by gemcitabine or irinotecan in cells transfected with siMRE11 or siNT. Error bars represent S.E.M. of 4 independent experiments. *.p<0.05, **.p<0.01 (Unpaired t-test).

3.2.5. Mre11 knockdown does not significantly affect viral DNA amplification

Following the observation that Mre11 knockdown enhances AdΔ19K-mediated cytotoxicity, we wondered whether this was a result of increased viral replication. qPCR analysis for Ad-E2A was performed in PT45 cells transfected with an siRNA against MRE11 or a non-targeting siRNA and treated with AdΔ19K with or without gemcitabine for 48h. The time for the qPCR-analysis of viral genome amplification corresponds to 96h post-transfection.

Knocking-down Mre11 did not significantly affect AdΔ19K DNA amplification, although there was a trend towards increased DNA in the absence of gemcitabine (Figure 36). Surprisingly, treatment with gemcitabine in cells transfected with the non-targeting siRNA control did not decrease viral genome amplification (Figure 36). In response to the combination of AdΔ19K with gemcitabine, genome amplification showed a tendency towards decrease when Mre11 was silenced compared to the control siRNA (Figure 36). Therefore, under these experimental conditions knocking-down Mre11 does not seem to significantly affect AdΔ19K DNA amplification regardless of the presence of gemcitabine.

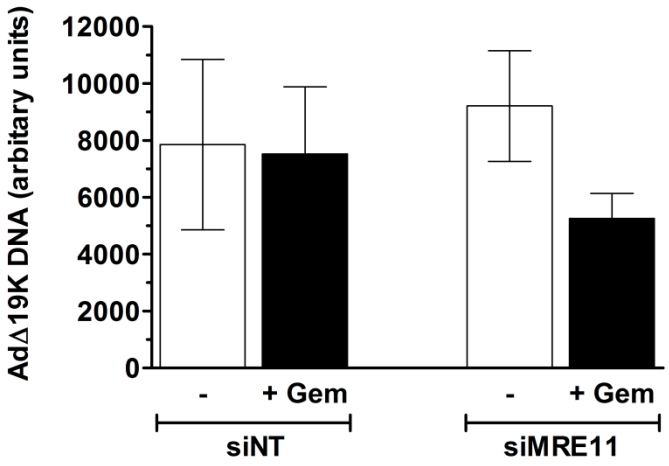

Figure 36: Mre11 knockdown does not significantly affect viral DNA amplification. PT45 cells were transfected with siRNA against MRE11 or a non-targeting (NT) siRNA. 48 hours post-transfection cells were treated with 300ppc AdΔ19K -/+ 5nM gemcitabine (Gem). DNA was extracted at 4 and 48hpi and analysed by qPCR for viral genome amplification (Ad-E2A). Viral DNA was normalized to input DNA (4h) and cellular GAPDH. Error bars represent S.E.M. of 2 independent experiments.

3.2.6. Mre11 knockdown has no significant effect on cell-cycle distribution

Concluding that enhanced viral replication was likely not responsible for the enhanced cell death induced by AdΔ19K and gemcitabine when Mre11 is knocked-down, led me to investigate any changes in the cell-cycle distribution of AdΔ19K and gemcitabine treated cells. Following transfection of cells with siRNA against Mre11 or control siRNA and treatment with AdΔ19K and gemcitabine, cell-cycle and mitotic index analysis were performed 24, 48 and 72h post-treatment (corresponding to 72, 96 and 120 h post-transfection).

Knocking-down Mre11 did not significantly alter the cell-cycle distribution of cells treated with AdΔ19K, gemcitabine or their combination (Figure 37A-D). After 24h of knocking-down Mre11 resulted in a very modest tendency towards enhanced and attenuated S-phase fraction in cells treated with gemcitabine or gemcitabine and AdΔ19K, respectively (Figure 37B). The same trend was observed at 72h (Figure 37B). In addition, Mre11 knockdown resulted in a moderate trend towards higher mitotic index 24h to 72h post-AdΔ19K infection (Figure 37D). It can thus be concluded that knockdown of Mre11 does not significantly affect the cell-cycle distribution in response to AdΔ19K and gemcitabine.

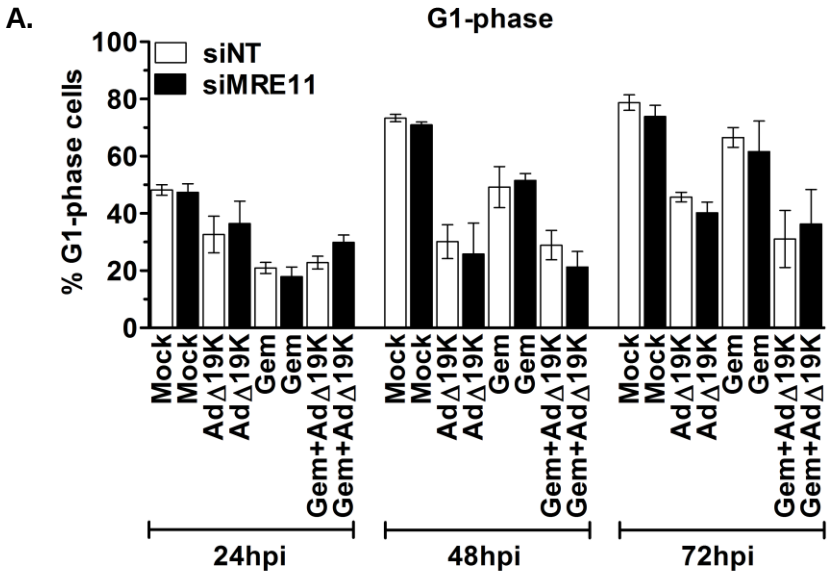

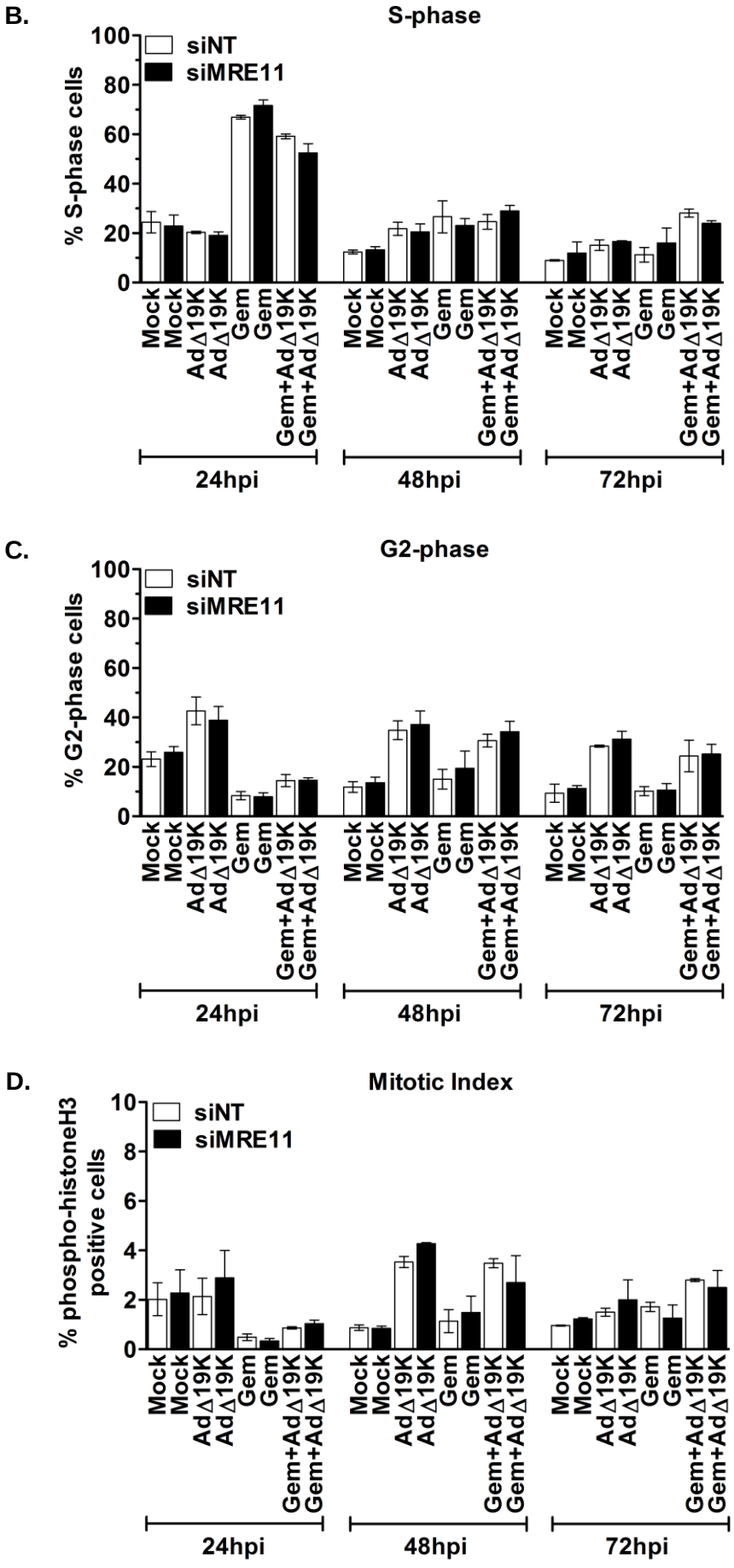

Figure 37: Mre11 knockdown has no significant effect on cell-cycle distribution. (A-D) PT45 cells were transfected with siRNA against MRE11

(siMRE11) or non-targeting (NT) siRNA (siNT) and treated with 300ppc AdΔ19K -/+ 5nM gemcitabine (Gem) 48h post-transfection. At 24, 48 and 72hpi cells were stained with a fixable-viability dye (FVD) and fixed for cell-cycle analysis. Cells were stained with propidium iodide (for DNA-content analysis), an anti-phospho-histone H3 antibody (for mitotic index analysis) and an anti-E1A antibody (for identification of infected cells) and analysed by flow-cytometry. Dead cells, as identified from their incorporation of FVD, were excluded from the analysis. In the presence of AdΔ19K only E1A-positive cells were analysed for propidium iodide and phospho-histone H3 expression. **(A)** % cells in G1 phase **(B)** % cells in S phase **(C)** % cells in G2 phase **(D)** % cells in mitosis. Error bars represent S.E.M. of 2 independent experiments. *.p<0.05 (one-way ANOVA with Bonferroni's multiple comparison test).

3.2.7. γH2AX foci mark the sites of AdΔ19K- and gemcitabine-induced DNA damage

Immunoblot analysis for the DNA-damage marker phospho-histoneH2A.X had suggested that the presence of AdΔ19K in gemcitabine-treated cells increases DNA damage. To confirm this observation we performed immunofluorescence microscopy studies of phospho-histoneH2A.X, which would allow visualization of the foci that phospho-histoneH2A.X forms at sites of DNA-damage (γH2A.X foci). In these studies an Ad-DBP antibody was used to allow identification of infected cells. The analysis was performed 24h and 36h post-treatment with AdΔ19K with or without gemcitabine. Representative immunofluorescence microscopy images for each condition at 24h and 36h are shown in figure 38A.

Firstly, quantification of the number of cells displaying more than 5 (5<) γH2A.X foci was performed (Figure 38B). Gemcitabine induced the formation of γH2A.X foci in 44.2±3.6% of non-infected cells 24h post-treatment, a significant increase compared to mock-infected cells (Figure 38B left panel). The proportion of cells displaying γH2A.X foci in response to gemcitabine increased to 58.9±5.4% by 36h, again significantly higher than untreated cells (Figure 38B left panel). In response to AdΔ19K, 24.3±0.8% of infected cells showed γH2A.X foci 24h post-infection and this was significantly increased to 47.8±5.1% when gemcitabine was added (Figure 38B right panel). However, the number of γH2A.X-positive cells was similar between gemcitabine and gemcitabine combined with AdΔ19K (Figure 38B). At 36h the number of AdΔ19K-infected cells displaying γH2A.X

foci increased by 3-fold to reach 72.8±3.8% and addition of gemcitabine did not further increase this percentage (Figure 38B right panel). Once more, the proportion of cells having γH2A.X foci following treatment with gemcitabine with or without AdΔ19K was similar (61.9±2.7% and 58.9±5.4%, respectively) (Figure 38B).

Having seen that there was no increase in the number of cells positive for γH2A.X when AdΔ19K was present in gemcitabine-treated cells, I speculated whether an increase in total γH2A.X fluorescence intensity could be detected. It is possible that more and/or brighter γH2A.X foci occur per cell and such effect would have not been detected when counting the number of cells positive for γH2A.X. A second analysis was thus performed, in which total γH2AX fluorescence intensity was measured in non-infected or AdΔ19K-infected cells and expressed as fluorescence intensity per cell (Figure 38C).

The total γH2AX fluorescence intensity 24h after treatment with gemcitabine was 2.4-fold higher compared to untreated cells, but the difference was not statistically significant (Figure 38C left panel). At 36h total γH2AX fluorescence intensity in response to gemcitabine significantly increased compared to 24h and was 3.7-fold higher than untreated cells (Figure 38C left panel). The presence of gemcitabine in AdΔ19K-infected cells resulted in a trend towards increased γH2AX fluorescence intensity (2-fold) at 24h and it significantly increased the γH2AX fluorescence intensity at 36h (Figure 38C right panel). γH2AX fluorescence intensity at 24h was 18,361±4,925 in gemcitabine-treated cells compared to 29,162±12,008 in cells treated with gemcitabine and AdΔ19K, suggesting there could be an increase (Figure 38C). At 36h similar γH2AX fluorescence intensity was observed in gemcitabine-treated cells with or without AdΔ19K (Figure 38C). Regarding the infectability of cells, 9.1±2.7% and 14.1±1.8% of cells were positive for Ad-DBP 24h and 36 post-infection, respectively, whereas in the presence of gemcitabine the number of Ad-DBP-positive cells increased to 21±4.7% and 42.9±11.1% for 24h and 36h, respectively (Figure 38D).

In conclusion, gemcitabine and AdΔ19K individually induced the formation of γH2AX foci. Their combination increased the number of γH2AX-positive cells and the fluorescence intensity compared to AdΔ19K but not compared to gemcitabine. Therefore, these studies showed that AdΔ19K does not increase gemcitabine-induced DNA damage up to 36h.

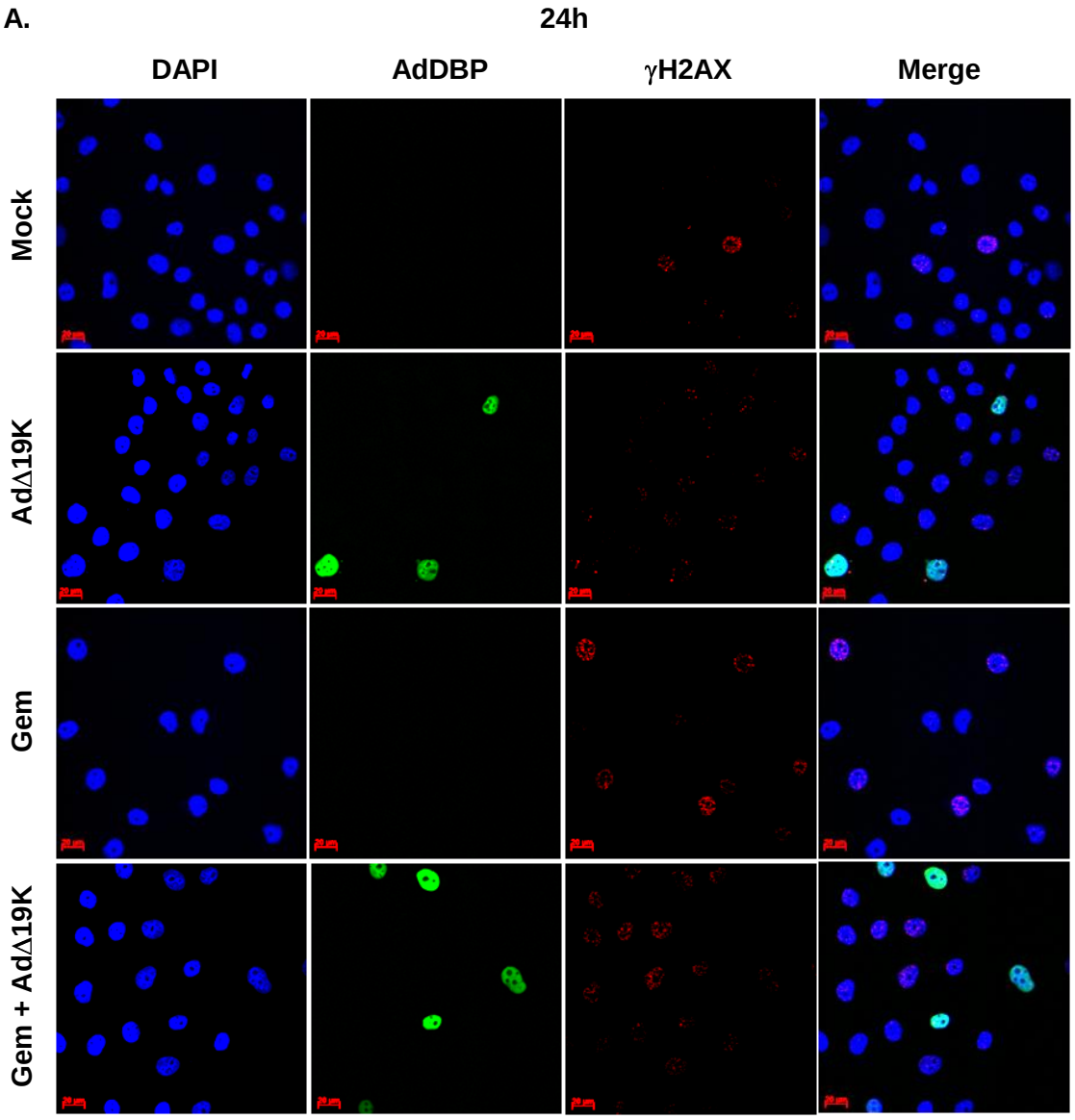

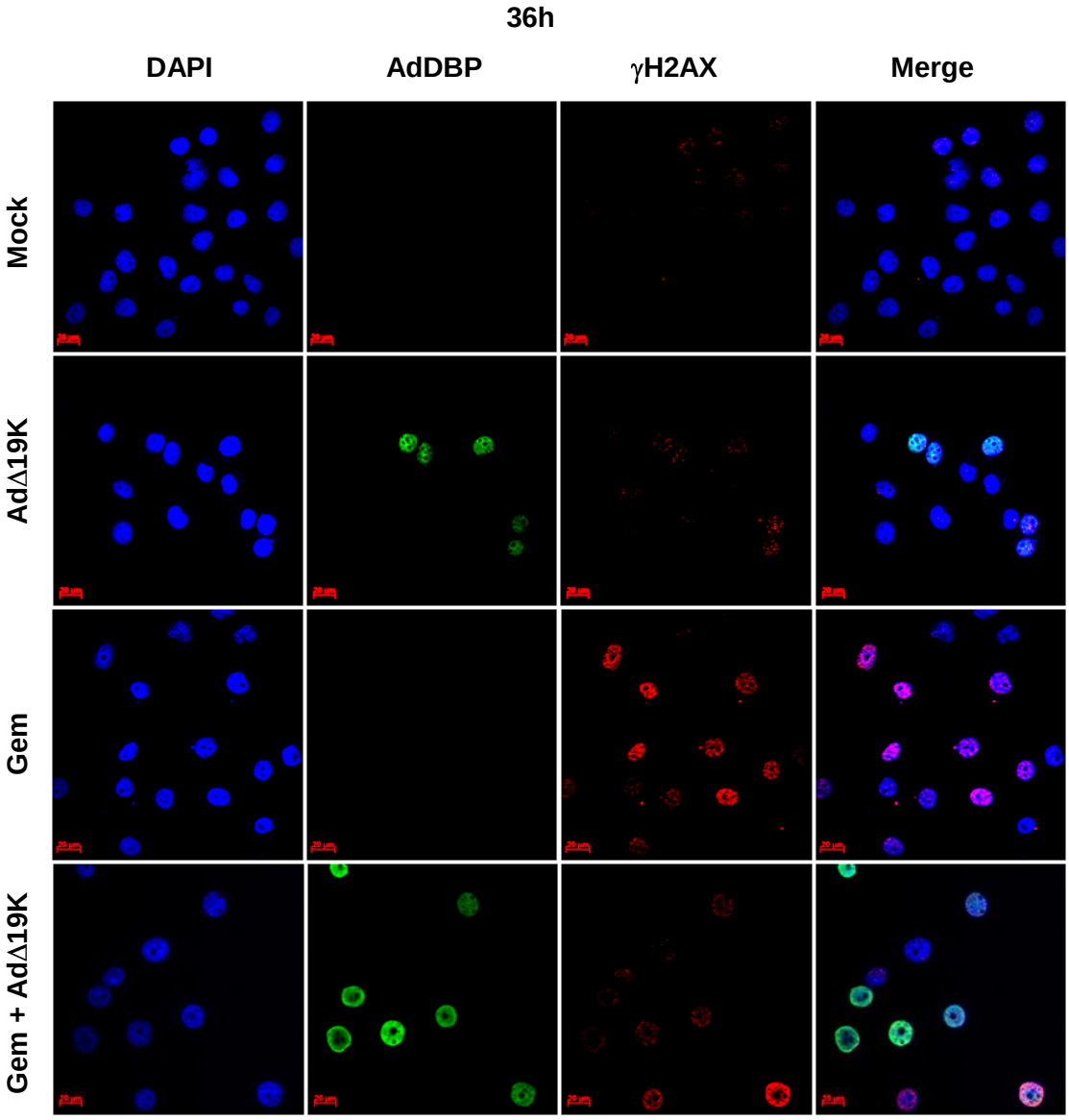
36h
DAPI
AdDBP
γH2AX
Merge
Mock
AdΔ19K
Gem
Gem + AdΔ19K

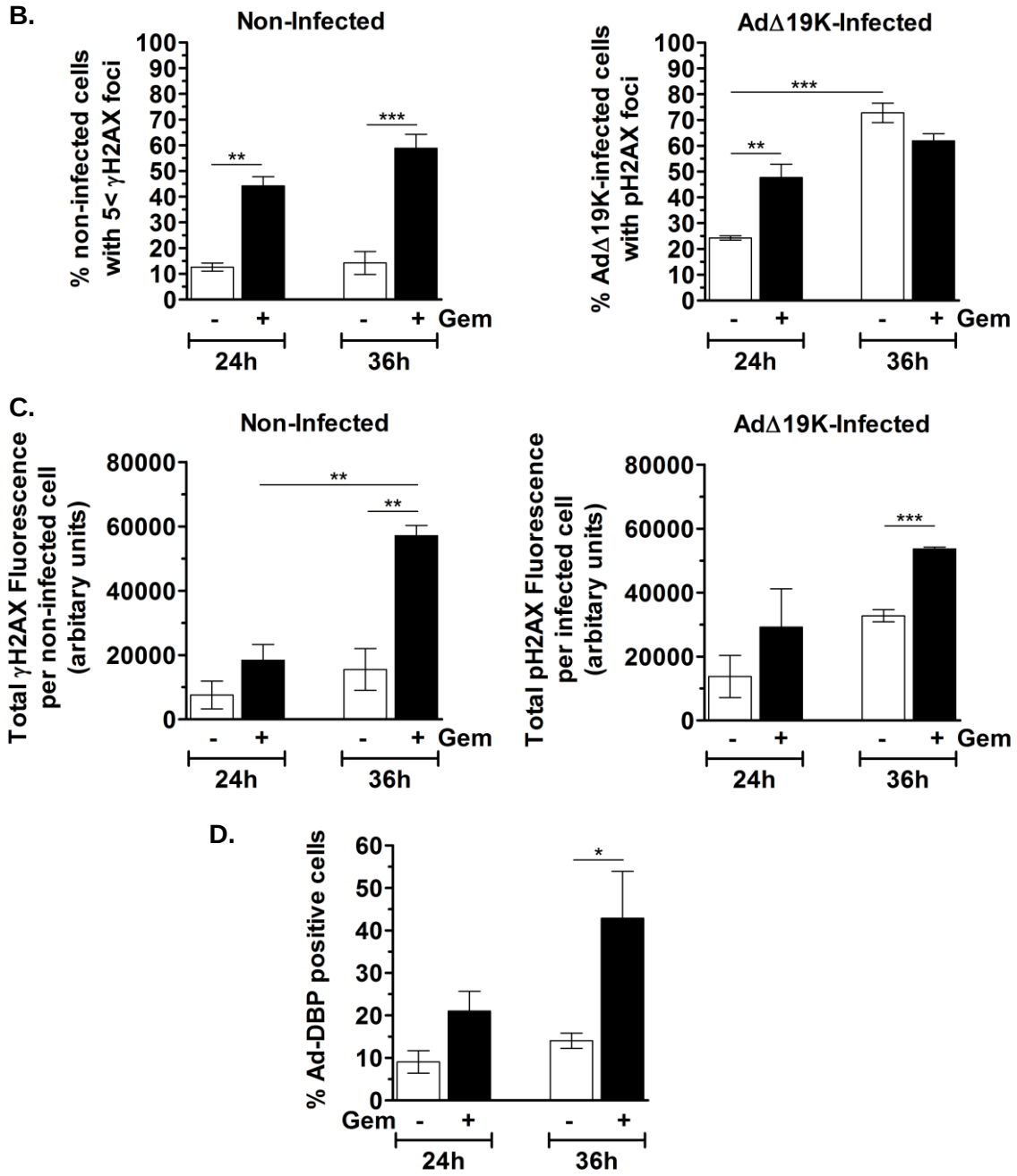

Figure 38: Ad∆19K and gemcitabine induce DNA-damage. PT45 cells were treated with 300ppc of Ad∆19K -/+ 5nM gemcitabine (Gem) and fixed at the indicated times for immunofluorescence microscopy analysis of γH2AX and Ad-DBP. Images from 10-20 fields were acquired using the 40x objective of the confocal laser scanning microscope Zeiss LSM510 and used for counting at least 200 cells per treatment. **(A)** Representative DAPI, Ad-DBP, γH2AX and merged images from each treatment at 24h and 36h. **(B)** Quantification of non-infected or Ad∆19K-infected cells displaying more than 5 (5<) γH2AX foci, expressed as % of total non-infected or infected cells respectively. **(C)** Quantification of total γH2AX fluorescence intensity per non-infected or Ad∆19K-infected cell (expressed as γH2AX fluorescence in non-infected or infected area normalised to the area background fluorescence divided by the number of cells in the area). **(D)** Quantification of Ad∆19K positive cells, as measured by Ad-DBP expression, expressed as frequency (%). Quantification was done using NIH ImageJ software as described in the methods. Error bars

represent S.E.M. of 3 independent experiments. *.p<0.05, **.p<0.01, ***.p<0.001 (one-way ANOVA with Bonferroni's multiple comparison test).

3.2.8. Cells treated with adenovirus and gemcitabine display DNA damage in mitosis

In order to understand whether DNA damage induced by AdΔ19K and gemcitabine is repaired, immunofluorescence microscopy analysis of phosphorylated histoneH2A.X was carried out in mitotic cells, as persistence of γH2AX foci in mitosis would suggest failure to repair DNA damage. PT45 cells treated with Ad5tg or AdΔ19K with or without gemcitabine were subjected to immunofluorescence microscopy analysis of phospho-histoneH2A.X and Ad-DBP, as a marker for infected cells, 48h and 72h post-treatment. The γH2AX analysis was categorised into cells displaying more than 5 (5<) foci and cells displaying a pan-chromosomal γH2AX signal, in which γH2AX staining occupied the majority of mitotic DNA. Representative images of non-infected and infected mitotic cells displaying γH2AX foci or a pan-chromosomal γH2AX staining are shown in figure 39A.

Ad-DBP expression demonstrated that less than 5% of mitotic cells were infected with either Ad5tg or AdΔ19K at 48h or 72h (Figure 39D). In the presence of gemcitabine 12.9±3.8% and 12.9±3.6% of mitotic cells were infected with Ad5tg and AdΔ19K, respectively, at 48h, and 4.5±2.3% and 5.2±0.4% of mitotic cells were infected with Ad5tg and AdΔ19K, respectively, at 72h (Figure 39D).

At 48h following treatment with gemcitabine 68±3.2% and 25.6±2.8% of mitotic cells showed γH2AX foci and pan-chromosomal γH2AX staining, respectively, suggesting that gemcitabine-induced DNA damage is passed on to mitosis (Figure 39B). Very similar frequencies were observed 72h post-treatment with gemcitabine (Figure 39B). At both time-points the γH2AX signal was significantly stronger compared to cells without gemcitabine (Figure 39B). 48h post-infection with AdΔ19K 100% of mitotic cells were positive for γH2AX, with 38.2±6.1% of them having a pan-chromosomal γH2AX staining (Figure 39C).

This was significantly higher compared to mock-infected cells, as denoted by the red asterisks (Figure 39C). The presence of gemcitabine increased the number of AdΔ19K-infected cells displaying a pan-chromosomal γH2AX staining to 53.2±2.1%, which was significantly higher compared to gemcitabine and gemcitabine combined with Ad5tg at 48h (Figure 39C). In contrast to AdΔ19K, Ad5tg infection did not result in 100% of mitotic cells being positive for γH2AX and the number of Ad5tg-infected cells displaying a pan-chromosomal γH2AX staining did not increase when gemcitabine was added, nor was it higher than gemcitabine alone at 48h (Figure 39C). In contrast to 48h, the presence of gemcitabine 72h post-Ad5tg infection significantly increased the pan-chromosomal γH2AX staining, which was also significantly higher than gemcitabine without virus (Figure 39C). At 72h AdΔ19K induced more pan-chromosomal γH2AX signal than Ad5tg (Figure 39C). Addition of gemcitabine to AdΔ19K significantly increased the proportion of cells having pan-chromosomal signal to 65.2±1.6% and this was significantly more than gemcitabine or gemcitabine with Ad5tg (Figure 39C).

In conclusion, gemcitabine- and AdΔ19K-induced DNA damage was not repaired before mitotic entry and all mitotic cells were positive for γH2AX at 48h and 72h post-treatment. However, treatment with a combination of gemcitabine and AdΔ19K did result in an increased pan-chromosomal γH2AX staining compared to either single treatment or a combination of gemcitabine with Ad5tg.

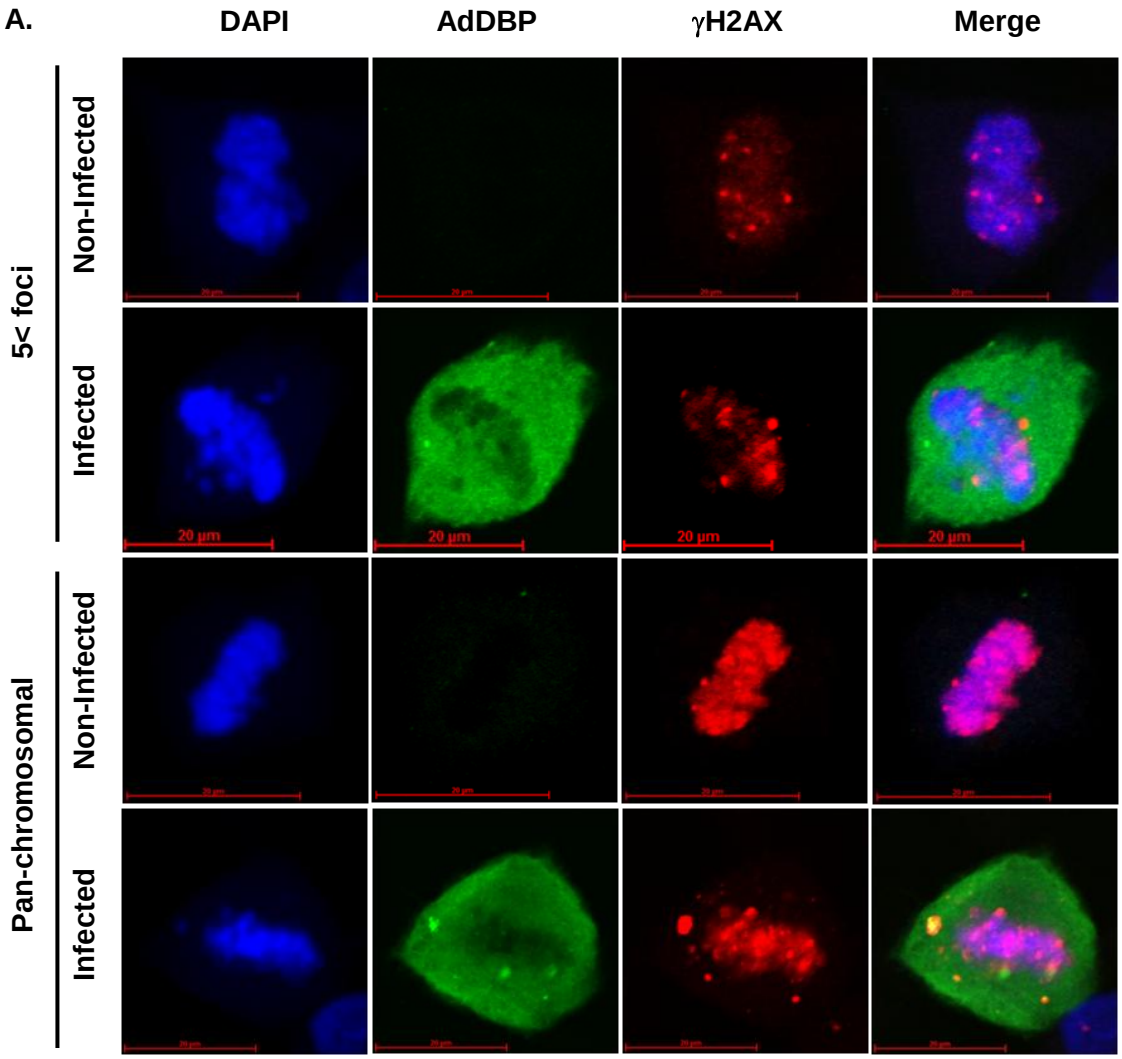
A.
DAPI
AdDBP
γH2AX
Merge
5< foci
Non-Infected
Infected
Pan-chromosomal
Non-Infected
Infected
20 μm

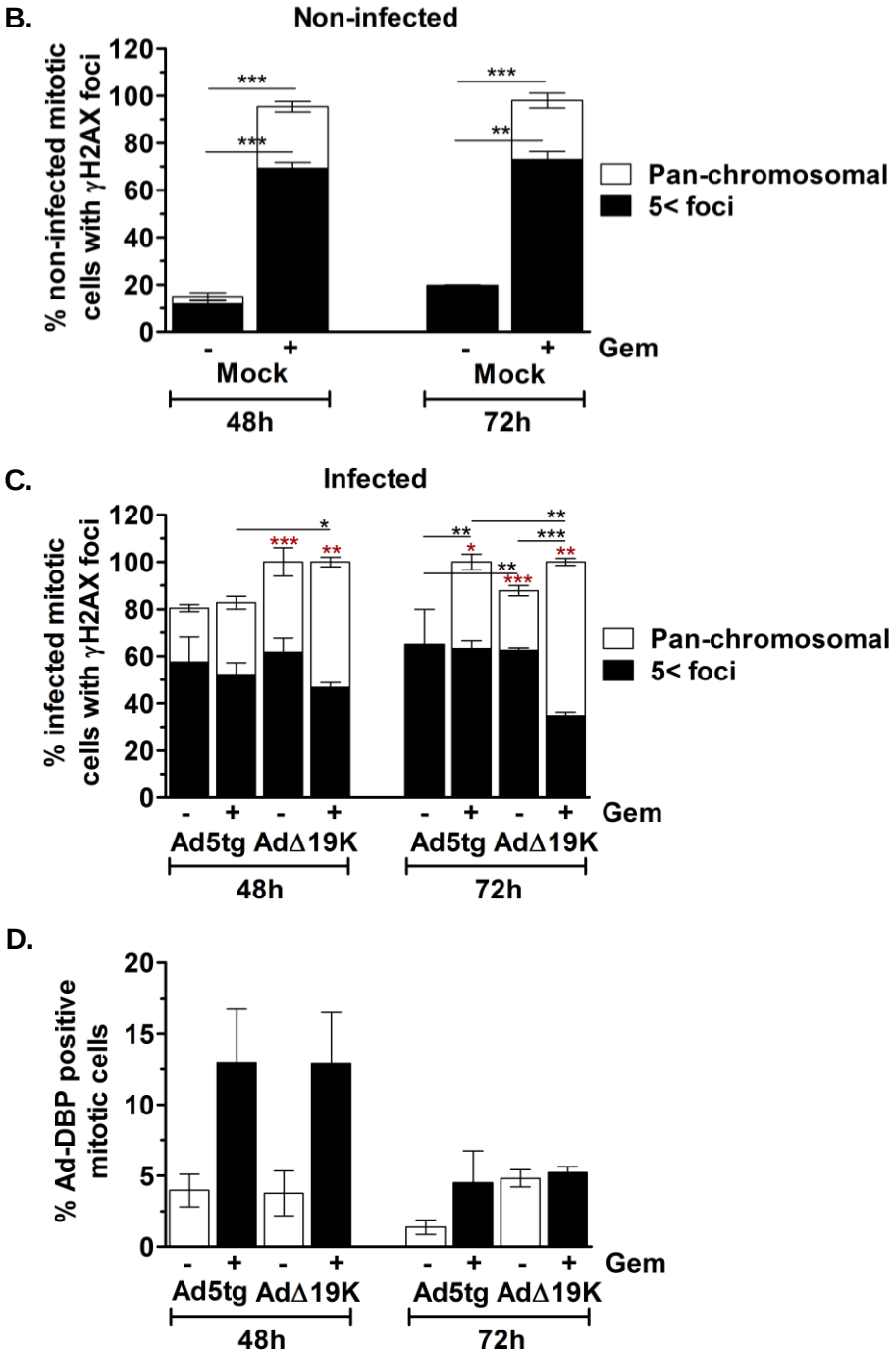

Figure 39: Cells treated with adenovirus and gemcitabine display DNA damage in mitosis. PT45 cells were seeded on coverslips, treated with 300ppc of Ad5tg or AdΔ19K -/+ 10nM gemcitabine (Gem) and fixed at the indicated times for immunofluorescence microscopy analysis of γH2AX and Ad-DBP. At least 150 mitotic cells were counted per treatment using a Zeiss Axioplan epifluorescent microscope and categorised into γH2AX-negative mitoses, mitoses with more than 5 (5<) γH2AX foci and pan-chromosomal γH2AX staining **(A)** Examples of non-infected or infected mitotic cells with 5< γH2AX foci and pan-chromosomal γH2AX staining. DAPI, Ad-DBP, γH2AX and merged images are shown. Images were acquired using the 60x objective of the confocal laser scanning microscope Zeiss LSM510. **(B)** Quantification of γH2AX-positive non-infected mitoses, expressed as % of total non-infected

mitoses. **.p<0.01, ***.p<0.001. (Unpaired t-test). **(C)** Quantification of γH2AX-positive infected mitoses, expressed as % of total infected mitoses. *.p<0.05, **.p<0.01, ***.p<0.001. (one-way ANOVA with Bonferroni's multiple comparison test). Red asterisks indicate statistical significance in comparison to non-infected cells. **(D)** Quantification of infected mitoses as measured by Ad-DBP expression, expressed as frequency. Error bars represent S.E.M. of 2 independent experiments, each with 2 technical replicates.

3.2.9. AdΔ19K does not accelerate the slippage of gemcitabine-arrested S-phase cells, but promotes mitotic entry and prevents their gradual G1-arrest after escape

We next questioned whether AdΔ19K could accelerate the progression of gemcitabine-treated cells through the cell-cycle, since it was previously reported that adenovirus can override cell-cycle checkpoints (Cherubini et al., 2006; Connell et al., 2008). In order to answer this question, cell-cycle synchronisation was necessary. Cells were synchronised in early S-phase using a thymidine block and released into medium containing Ad5tg or AdΔ19K with or without gemcitabine. In these studies a viability dye was employed to allow exclusion of dead cells and an E1A antibody was used to identify infected cells. Cell-cycle and mitotic index analysis was performed by multicolour flow-cytometry at 6, 12, 24, 30, 36, 48, 54, 60 and 72h post-treatment. For assessment of cell synchronisation, the cell-cycle distribution of total cells (both infected and non-infected in conditions where virus was present) 6h and 12h post-thymidine release is shown in figure 40A. Figure 40B shows the cell-cycle distribution of only E1A-positive cells (in conditions where virus was present). Representative flow-cytometry profiles can be found in Appendix 3 (section 5.1.; Figure 67).

At 6h post-thymidine release the majority of cells had progressed from S- to G2-phase in all conditions (Figure 40A; 6h). At 12h post-thymidine release 49.6±1.1% of mock-infected cells progressed to G1-phase, while a 34.4±2.5% remained in G2 (Figure 40A; 12h). In response to Ad5tg and AdΔ19K cell passage from G2 to mitosis and then G1 appeared to be slower than in mock-infection (Figure 40A; 12h). At 12h post-thymidine release Ad5tg- or AdΔ19K-infected E1A-positive cells were accumulated in G2-phase (Figure 40B; 12h). By 24h cell-cycle distribution was similar between mock-, Ad5tg- and AdΔ19K-

infected cells (Figure 40B; 24h). However, from 36h and 48h onwards the S- and G2-phase cell-fraction, respectively, in Ad5tg- and AdΔ19K-infected cells was significantly higher than mock-infected cells (Figure 40B).

Gemcitabine-induced S-phase arrest initiated at 12h and peaked at 36h reaching 57.3±5.9% (Figure 40B). From 36 to 48h approximately 35% of gemcitabine-treated cells progressed from S to G2 and mitosis and another fraction entered G1 (Figure 40B). From 48h onwards gemcitabine-treated cells kept entering G1 and by 72h 61±1.9% of cells had accumulated in G1 (Figure 40B).

At 12h post-thymidine release gemcitabine addition significantly increased the S-phase fraction of Ad5tg- and AdΔ19K-infected E1A-positive cells, which also appeared to be higher compared to gemcitabine (Figure 40B; 12h). This suggested that gemcitabine-induced S-phase arrest might be initially stronger in the presence of viruses. In addition, the presence of Ad5tg or AdΔ19K in gemcitabine-treated cells increased the G2 cell-fraction, since, as also observed in the absence of gemcitabine, E1A-positive cells appeared to have moved slower from G2 to G1 (Figure 40B 12h). Surprisingly, despite a trend towards higher S-phase at 12h, the presence of viruses significantly decreased gemcitabine-induced S-phase arrest at 24h and 30h (Figure 40B). Moreover, up to 36h AdΔ19K infection in the presence of gemcitabine resulted in increased G2-phase compared to gemcitabine (Figure 40B). At 36h cells treated with a combination of gemcitabine and AdΔ19K had reached maximum S-phase arrest (48.3±4.9%). From 36 to 48h a fraction of gemcitabine and AdΔ19K-treated cells progressed from S to G2 and another fraction had entered S-phase, as suggested by the decrease in G1 (Figure 40B; 36h versus 48h). From 48h to 72h small fractions of gemcitabine and AdΔ19K-treated cells kept progressing through the different phases, but overall no significant changes in their cell-cycle distribution were observed during this 24h period (Figure 40B). Significantly less and more cells were present in G1 and S-phase, respectively, 48 to 72h after gemcitabine was combined with viruses, compared to gemcitabine (Figure 40B). In addition, significantly more cells were present in G2-phase 60 to 72h after gemcitabine was combined with viruses, compared to gemcitabine (Figure 40B).

Both viruses showed a trend towards increased mitotic index from 30h onwards, with significant increases at 48h and 54h post-Ad5tg infection and at 60h post-AdΔ19K infection (Figure 40C). Gemcitabine significantly decreased the mitotic index at 12h and remained low until 36h since cells were arrested in S-phase (Figure 40C 36h). 48h following gemcitabine treatment the mitotic index reached 3.5±0.4%, as cells escaped from the S-phase block (Figure 40C; 48h). The presence of either virus in gemcitabine-treated cells showed a tendency to increase the mitotic index throughout the time-course and significant increases were seen from 48h to 72h (Figure 40C). The mitotic index in response to gemcitabine and AdΔ19K was 2 to 4-fold higher than gemcitabine throughout the time-course, with the biggest difference observed at 60h (Figure 40C).

To summarize, in response to either virus, the E1A-positive cells accumulated in S and G2 phases throughout the time-course. Gemcitabine-induced S-phase arrest peaked at 36h and was followed by cell progression to G2 and mitosis and gradual cell arrest in G1. In contrast, following the S-phase arrest, cells treated with gemcitabine and AdΔ19K did not accumulate in G1, but rather occupied S and G2 with some progression through the different phases being observed. Notably, AdΔ19K significantly increased the mitotic index of gemcitabine-treated cells from 48h to 72h. In conclusion, AdΔ19K did not accelerate the slippage of gemcitabine-arrested S-phase cells to G2. However, it prevented the gradual G1 arrest of gemcitabine-treated cells by keeping them accumulated in S and G2 phases and at the same time it promoted their mitotic entry.

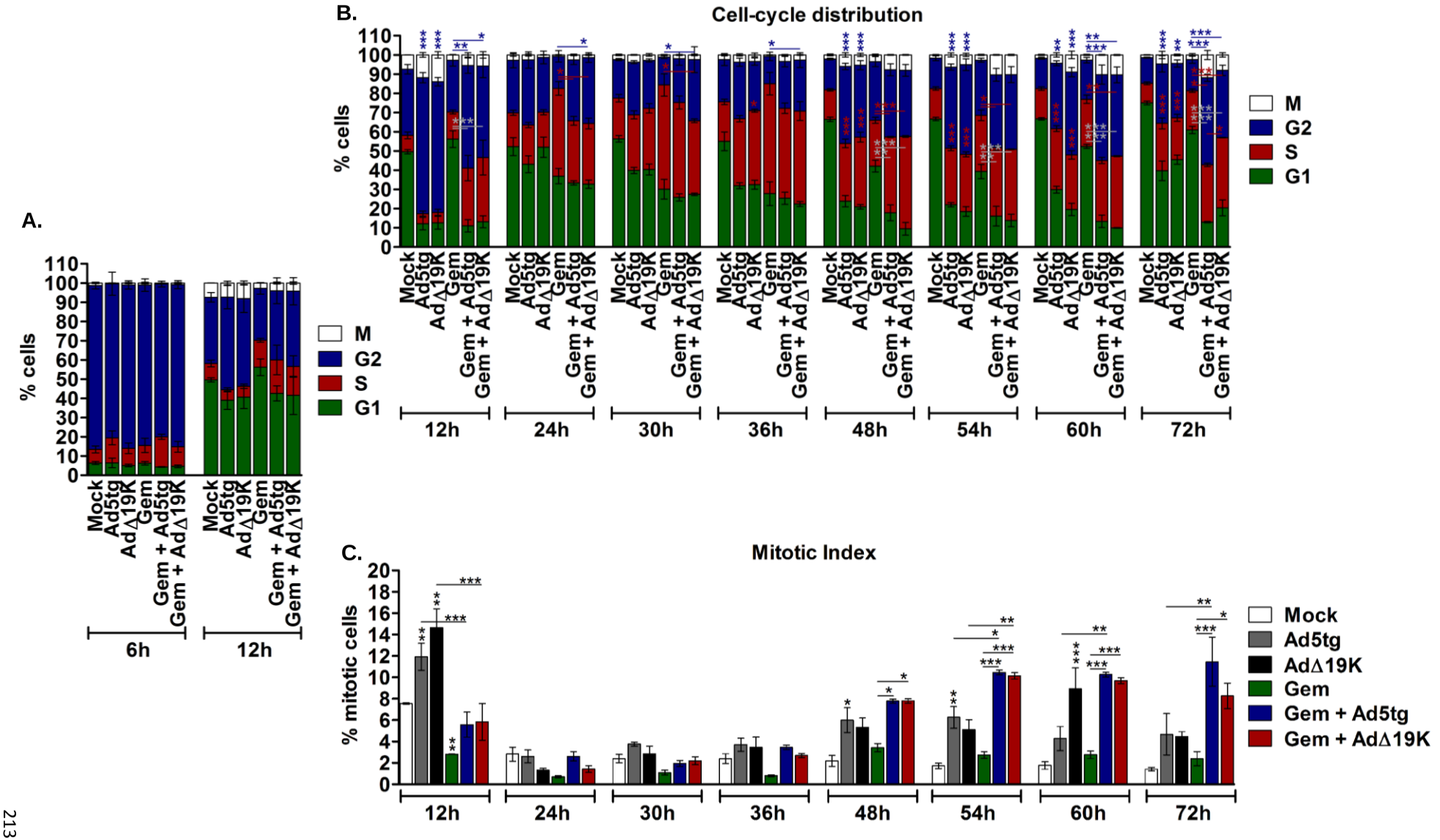
A.
% cells
M
G2
S
G1
Mock
Ad5tg
AdΔ19K
Gem
Gem + Ad5tg
Gem + AdΔ19K
6h
12h
B.
Cell-cycle distribution
% cells
12h
24h
30h
36h
48h
54h
60h
72h
C.
Mitotic Index
% mitotic cells
Mock
Ad5tg
AdΔ19K
Gem
Gem + Ad5tg
Gem + AdΔ19K

Figure 40: **AdΔ19K does not accelerate the slippage of gemcitabine-arrested S-phase cells, but promotes mitotic entry and prevents their gradual G1-arrest after escape.** PT45 cells were treated with 2.5mM thymidine for 24h and released from the thymidine block in 0% FBS DMEM -/+ 300ppc Ad5tg or AdΔ19K. 2h later medium was replaced with 10% FBS DMEM -/+ 5nM gemcitabine (Gem). At the indicated times post-infection cells were stained with FVD eFluor506 and fixed for cell-cycle analysis. Cells were stained with propidium iodide (for DNA-content analysis), a phospho-histone H3 antibody (for mitotic index analysis) and an E1A antibody (for identification of infected cells) and analysed by flow-cytometry. Dead cells, as identified from their incorporation of FVD, were excluded from the analysis. **(A)** Cell-cycle distribution of total cells (non-infected and infected) at 6h and 12h post-treatment, shown as % cells in G1-phase, S-phase, G2-phase and mitosis (M). **(B)** Cell-cycle distribution of non-infected or infected cells, shown as % cells in G1-phase, S-phase, G2-phase and mitosis (M). **(C)** Mitotic Index (% cells in mitosis). Error bars represent S.E.M. of 4 independent experiments. *.$p<0.05$ **.$p<0.01$, ***.$p<0.001$ (one-way ANOVA with Bonferroni's multiple comparison test).

3.3. AdΔ19K inhibits Gemcitabine-induced accumulation of Claspin, which contributes to the enhanced cell death

3.3.1. AdΔ19K inhibits drug-induced upregulation of Claspin at the protein level

Based on the observation that AdΔ19K and Ad5tg enhance the mitotic entry of gemcitabine-treated cells that enter mitosis in the presence of DNA damage, we questioned whether adenovirus abrogates the G2/M checkpoint. We explored whether adenovirus could regulate Claspin, a checkpoint protein that was previously demonstrated to play a role in G2/M checkpoint abrogation in cells infected with HPV (Spardy et al., 2009). In response to replication stress or DNA-damage, Claspin accumulates and mediates ATR-dependent phosphorylation and activation of Chk1 (Chini and Chen, 2004; Kumagai and Dunphy, 2000). For cells to recover from the DNA-damage checkpoint response and enter mitosis Claspin needs to be degraded, by a mechanism involving the ubiquitin ligase complex β-TrCP-SCF, Aurora-A and Plk-1 (Freire et al., 2006; Macurek et al., 2008; Mamely et al., 2006). The E7 oncoprotein of HPV was shown to increase the proteasomal degradation of claspin, thereby attenuating DNA damage responses and promoting mitotic entry (Spardy et al., 2009). To gain insight into the mechanism underlying the enhanced mitotic entry of gemcitabine-treated DNA-damaged cells, we examined Claspin expression by immunoblot analysis in PT45 cells.

Gemcitabine significantly increased claspin expression 24h and 48h post-treatment (Figure 41A and B, left panels). AdΔ19K infection in gemcitabine-treated cells significantly decreased gemcitabine-induced upregulation of claspin to almost basal levels at both 24h and 48h (Figure 41A and B, left panels). A trend towards attenuation of gemcitabine-induced claspin upregulation was also observed when Ad5tg was present in gemcitabine-treated cells (Figure 41A and B, left panels). No significant changes in Claspin

expression were detected following Ad5tg or AdΔ19K infection in the absence of gemcitabine, although AdΔ19K showed a tendency towards decreased Claspin protein levels (Figure 41A and B, left panels).

Preliminary immunoblot analysis of Claspin expression following treatment with irinotecan, suggested that similar to gemcitabine, irinotecan upregulated claspin protein levels at 24h and 48h post-treatment (Figure 41A and B, right panels). The presence of AdΔ19K in irinotecan-treated cells inhibited irinotecan-induced Claspin accumulation at 24h and 48h post-treatment, with a stronger inhibition observed at 48h (Figure 41A and B, right panels). Ad5tg did not affect irinotecan-induced upregulation of Claspin expression at 24h, but it appeared to attenuate it at 48h (Figure 41A and B, right panels).

Therefore, gemcitabine-induced upregulation of claspin expression is strongly inhibited in the presence of AdΔ19K in PT45 cells. Preliminary data suggest that AdΔ19K also inhibits irinotecan-induced upregulation of claspin protein levels in PT45 cells.

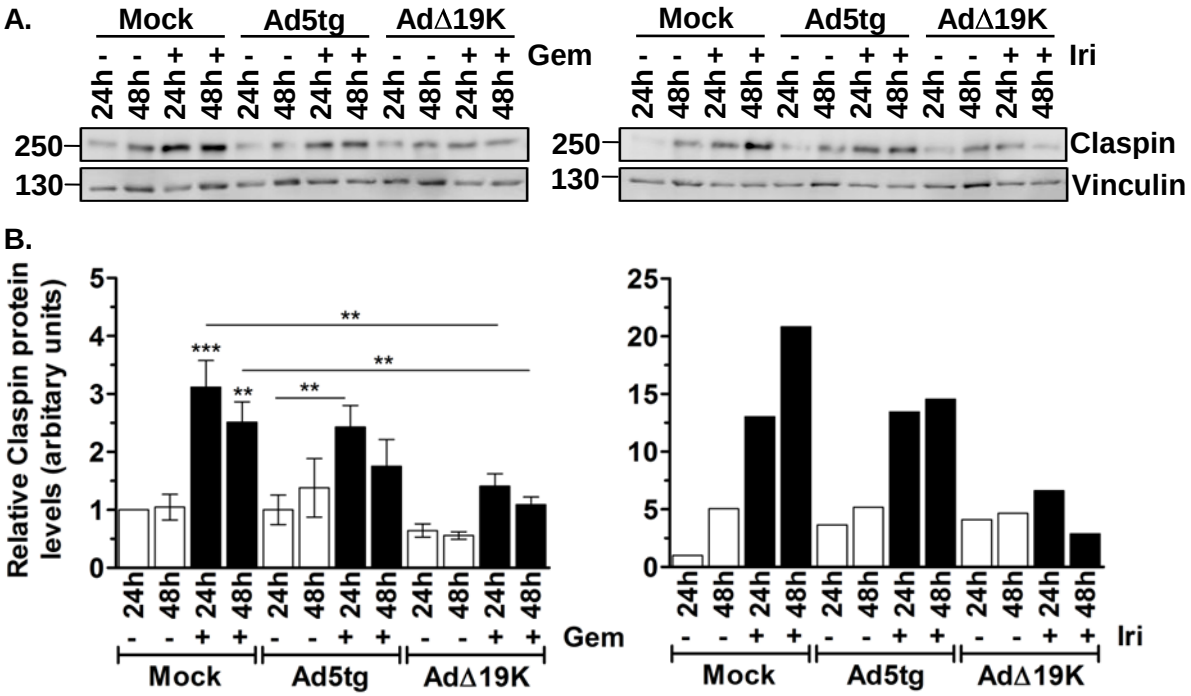

Figure 41: AdΔ19K inhibits drug-induced upregulation of Claspin at the protein level in PT45 cells. PT45 cells were treated with 300ppc Ad5tg or AdΔ19K -/+ 10nM gemcitabine (Gem) or 5μM irinotecan (Iri) and harvested at the indicated times for immunblot analysis of Claspin. **(A)** Representative immunoblots of Claspin (250kDa) with vinculin (130kDa) as a loading control. Numbers indicate MW size marker (kDa). **(B)** Quantification of protein levels by densitometric analysis. Claspin protein levels were expressed relative to the loading control. Error bars represent S.E.M. of 3 independent experiments. **.p<0.01, ***.p<0.001 (one-way ANOVA with Bonferroni's multiple comparison test). Immunoblotting for Claspin in response to irinotecan was done once.

We next asked whether AdΔ19K-mediated inhibition of drug-induced Claspin accumulation also occurs in MIAPaCa-2 cells. Immunoblot analysis of claspin expression demonstrated that, analogous to PT45 cells, treatment of MIAPaCa-2 cells with gemcitabine results in a significant upregulation of Claspin protein levels at 24h and 48h post-treatment (Figure 42A and B, left panels). The presence of AdΔ19K or Ad5tg in gemcitabine-treated cells showed a trend towards attenuation of gemcitabine-induced claspin upregulation, but unlike PT45 cells no significant inhibition was detected (Figure 42A and B, left panels). Claspin protein levels were significantly higher 24h after treatment with gemcitabine and either virus, compared to AdΔ19K or Ad5tg (Figure 42A and B,

left panels). Similar to PT45 cells, irinotecan significantly increased the expression of claspin in MIAPaCa-2 cells 24 to 48h after treatment (Figure 42A and B, right panels). Once more, AdΔ19K or Ad5tg infection of irinotecan-treated cells showed a tendency towards attenuation of irinotecan-induced claspin upregulation (Figure 42A and B, right panels). No significant changes in Claspin expression were observed in response to AdΔ19K or Ad5tg infection (Figure 42A and B). Thus, in contrast to PT45 cells drug-induced upregulation of Claspin expression in MIAPaCa-2 cells is not significantly inhibited by AdΔ19K, although a trend towards attenuation was observed.

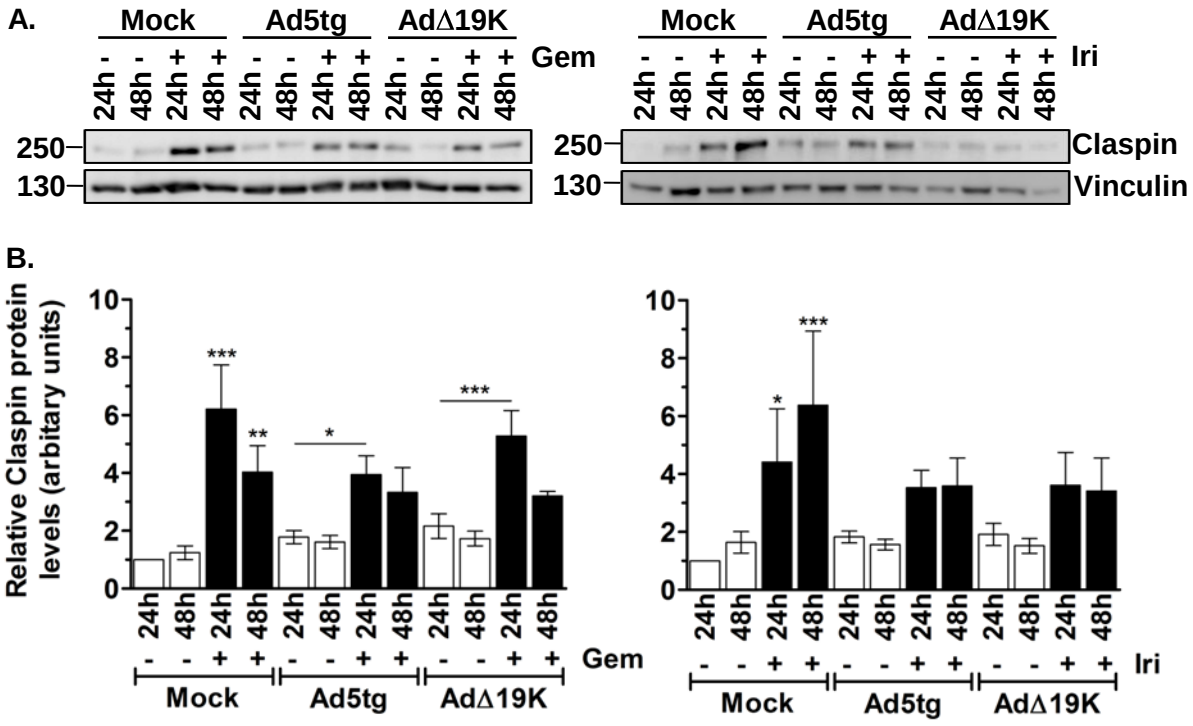

Figure 42: Infection of MIAPaCa-2 cells with AdΔ19K shows a trend towards attenuation of drug-induced upregulation of Claspin expression. MIAPaCa-2 cells were treated with 300ppc Ad5tg or AdΔ19K -/+ 20nM gemcitabine (Gem) or 15μM irinotecan (Iri) and harvested at the indicated times for immunblot analysis of Claspin. **(A)** Representative immunoblots of Claspin (250kDa) with vinculin (130kDa) as a loading control. Numbers indicate MW size marker (kDa). **(B)** Quantification of protein levels by densitometric analysis. Claspin protein levels were expressed relative to the loading control. Error bars represent S.E.M. of 3 independent experiments. *.p<0.05, **.p<0.01, ***.p<0.001 (one-way ANOVA with Bonferroni's multiple comparison test).

3.3.2. AdΔ19K induces the phosphorylation of Plk1 that persists in the presence of DNA-damaging drugs

The interesting observation that AdΔ19K inhibited drug-induced upregulation of Claspin expression in PT45 cells, prompted us to further investigate the mechanism underlying this inhibition. We hypothesised that AdΔ19K might inhibit drug-induced upregulation of claspin expression by increasing the proteolytic turnover of Claspin. To test this hypothesis, we first examined the expression of Plk1, since during checkpoint recovery phosphorylated Plk1 (Thr210) targets Claspin for degradation (Freire et al., 2006; Macurek et al., 2008; Mamely et al., 2006).

Immunoblot analysis of phospho-Plk1 (Thr210) in PT45 cells revealed that AdΔ19K and Ad5tg induce the phosphorylation of Plk1 at 48h post-infection (Figure 43A and B). AdΔ19K-induced upregulation of phospho-Plk1 levels was significantly stronger than Ad5tg (Figure 43A and B). No Plk1 phosphorylation was observed in response to gemcitabine (Figure 28A and B, left panels). In response to the combination of gemcitabine with AdΔ19K phospho-Plk1 expression was significantly higher than gemcitabine without AdΔ19K, suggesting that AdΔ19K-induced phosphorylation of Plk1 persists in the presence of gemcitabine (Figure 43A and B, left panels). Significantly higher phospho-Plk1 levels were observed when gemcitabine was combined with AdΔ19K in comparison to its combination with Ad5tg (Figure 43A and B, left panels). As observed with gemcitabine, treatment with irinotecan did not induce Plk1 phosphorylation (Figure 43A and B, right panels). When irinotecan was combined with Ad5tg or AdΔ19K phospho-Plk1 expression showed a trend towards upregulation, but no significant differences were detected compared to irinotecan alone (Figure 43A and B, right panels).

Therefore, at 48h post-treatment, AdΔ19K, but not DNA-damaging drugs, induce the phosphorylation of Plk1 that persists in the presence of drugs. Upregulation of phospho-Plk1 expression after checkpoint activation suggests that Claspin is targeted for degradation in the presence of AdΔ19K and DNA-damaging drugs.

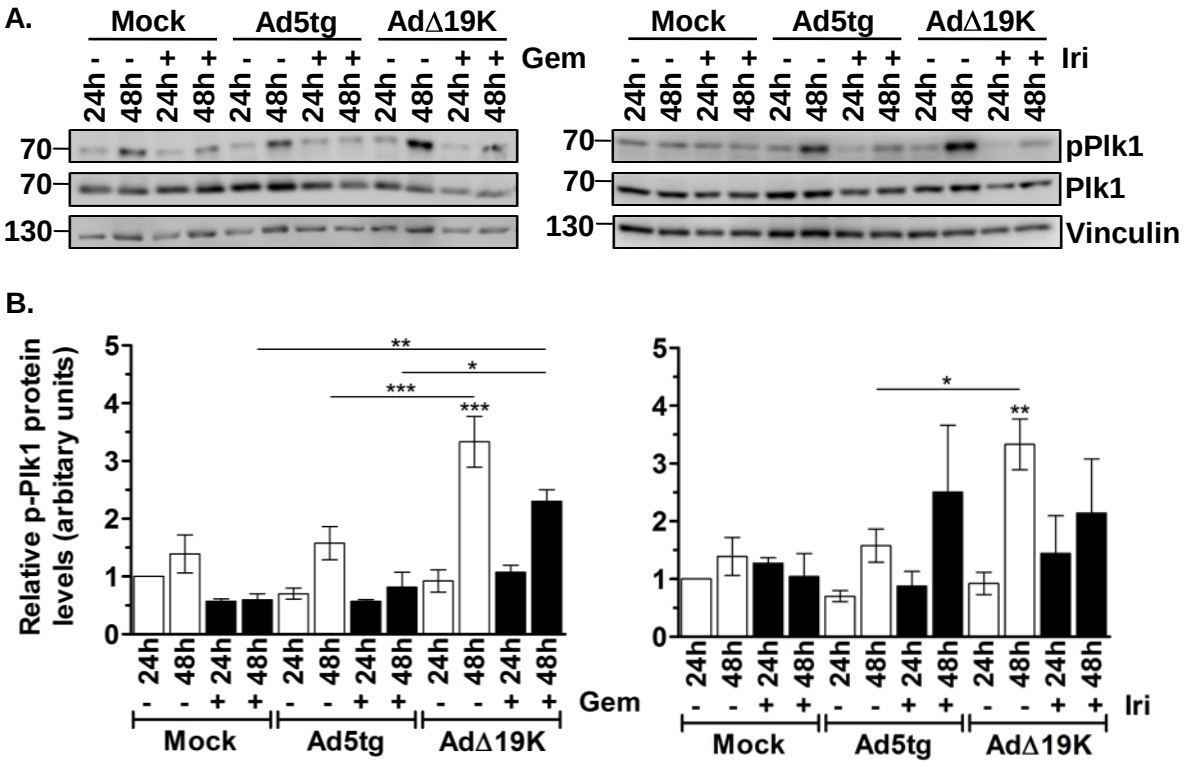

Figure 43: AdΔ19K induces the phosphorylation of Plk1 that persists in the presence of DNA-damaging drugs. PT45 cells were treated with 300ppc Ad5tg or AdΔ19K -/+ 10nM gemcitabine (Gem) or 5µM irinotecan (Iri) and harvested at the indicated times for immunblot analysis of phosphorylated (Thr210) and total Plk1. **(A)** Representative immunoblots of phopsho-Plk1 (pPlk1) and total Plk1 (68kDa) with vinculin (130kDa) as a loading control. Numbers indicate MW size marker (kDa). **(B)** Quantification of protein levels by densitometric analysis. phospho-Plk1 protein levels were expressed relative to total Plk1 and the loading control. Error bars represent S.E.M. of 2 independent experiments. *.p<0.05, **.p<0.01, ***.p<0.001 (one-way ANOVA with Bonferroni's multiple comparison test).

3.3.3. The presence of AdΔ19K in gemcitabine-treated cells promotes Claspin degradation

The observation that AdΔ19K induces the phosphorylation of Plk1 both in the absence and presence of DNA-damaging drugs, suggested that AdΔ19K might regulate the degradation of Claspin. We therefore sought to investigate the stability of Claspin using a cycloheximide chase assay. Cycloheximide blocks protein synthesis and thereby allows the study of protein degradation. At 24h and 48h following mock, Ad5tg or AdΔ19K infection in the absence or presence of gemcitabine, PT45 cells were treated with cycloheximide for 0, 2, 4 and 6h and subjected to immunoblot analysis of Claspin expression (Figure 44A and 45A; 24h and 48h, respectively). Claspin half-life was determined by plotting the quantified protein levels against the time after cycloheximide treatment (Figure 44B and 45B; 24h and 48h, respectively).

Assessment of claspin degradation demonstrated that the half-life of claspin under basal conditions is 207±37min 24h post-mock infection (Figure 44C). Infection with Ad5tg did not affect the half-life of claspin (200±20min) at 24h, whereas AdΔ19K infection showed a tendency to decrease Claspin half-life (178±36min) at 24h. Treatment with gemcitabine, regardless of the presence of viruses, resulted in a trend towards increased claspin half-life at 24h (Figure 44C). Nevertheless, no significant changes were observed in the stability of claspin at 24h post-treatment. At 48h post-mock infection claspin half-life was 289±24min (Figure 45C). Analogous to 24h, Ad5tg did not significantly change the half-life of Claspin 48h post-infection, while infection with AdΔ19K showed a tendency towards reduced Claspin half-life (184±41min) (Figure 45C). In contrast to 24h, at 48h there was no trend towards stabilisation of Claspin following treatment with gemcitabine (Figure 45C). The combination of gemcitabine with Ad5tg did not affect the degradation of claspin, which had a similar half-life to mock-infected cells (245±5min) (Figure 45C). On the contrary, treatment with a combination of gemcitabine and AdΔ19K resulted in a claspin half-life of 152±23min, which was significantly decreased compared to mock-infected cells (Figure 45C). In conclusion, claspin stability was significantly decreased 48h following treatment with AdΔ19K and gemcitabine, suggesting

that Claspin degradation is accelerated in response to AdΔ19K and gemcitabine.

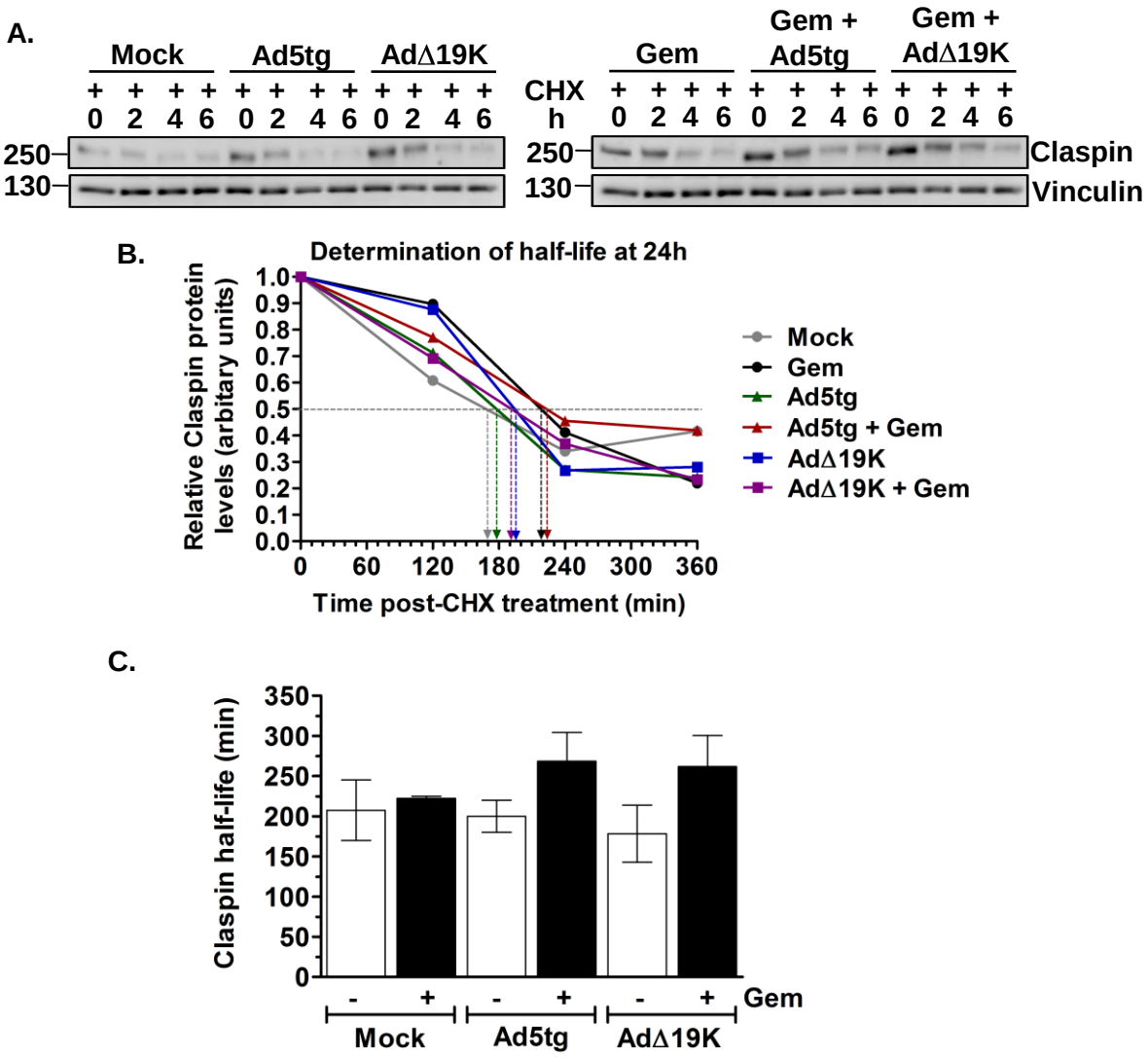

Figure 44: Gemcitabine and adenovirus have no effect on the half-life of claspin at 24h. PT45 cells were treated with 300ppc of Ad5tg or AdΔ19K -/+ addition of 10nM gemcitabine (Gem). At 24h post-infection, 3μM of the protein synthesis inhibitor cycloheximide (CHX) was added to study protein degradation. Cells were harvested at 0, 2, 4 and 6 hours post-cycloheximide treatment and prepared for immunoblot analysis of claspin expression. **(A)** Representative immunoblots of Claspin (250kDa) with vinculin (130kDa) as a loading control. Numbers indicate MW size marker (kDa). **(B)** Example of determination of claspin half-life. Claspin protein levels were quantified by densitometric analysis, normalised to the loading control and expressed relative to the 0h time-point of each treatment (set to 1). Half-life was derived from plotting claspin protein levels against time post-CHX treatment (minutes) and determining the time at which protein level was at 0.5 (indicated by dotted lines). **(C)** Average claspin half-lives (minutes) from 2 independent experiments. Error bars represent S.E.M.

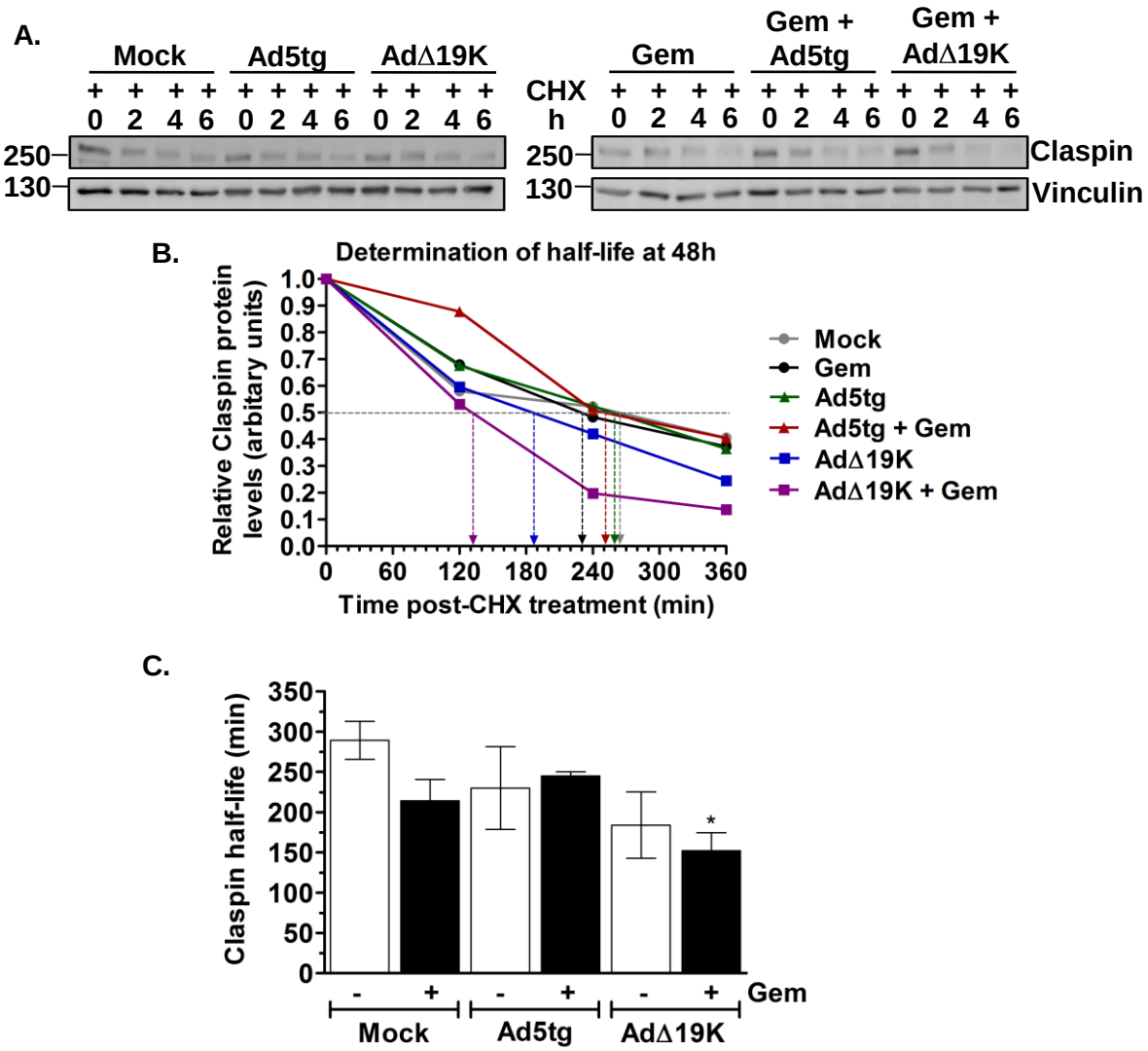

Figure 45: The combination of gemcitabine and AdΔ19K decreases the half-life of claspin at 48h. PT45 cells were treated with 300ppc of Ad5tg or AdΔ19K -/+ addition of 10nM gemcitabine (Gem). At 48h post-infection, 3μM of the protein synthesis inhibitor cycloheximide (CHX) was added to study protein degradation. Cells were harvested at 0, 2, 4 and 6 hours post-cycloheximide treatment and prepared for immunoblot analysis of claspin expression. **(A)** Representative immunoblots of Claspin (250kDa) with vinculin (130kDa) as a loading control. Numbers indicate MW size markers (kDa). **(B)** Example of determination of claspin half-life. Claspin protein levels were quantified by densitometric analysis, normalised to the loading control and expressed relative to the 0h time-point of each treatment (set to 1). Half-life was derived from plotting claspin protein levels against time post-CHX treatment (minutes) and determining the time at which protein level was at 0.5 (indicated by dotted lines). **(C)** Average claspin half-lives (minutes) from 3-4 independent experiments. Error bars represent S.E.M. *.p<0.05 (one-way ANOVA with Bonferroni's multiple comparison test).

3.3.4. AdΔ19K inhibits gemcitabine-induced Claspin synthesis

The accelerated degradation of claspin 48h after treatment with AdΔ19K and gemcitabine did not seem sufficient *per se* to explain the strong inhibition of gemcitabine-induced Claspin accumulation by AdΔ19K. We therefore asked whether AdΔ19K and gemcitabine could also affect Claspin protein synthesis. To gain insight into this question, we utilized the proteasomal inhibitor MG-132 to study protein synthesis. MG-132 was added 48h following treatment of PT45 cells with AdΔ19K and gemcitabine and the accumulation of newly synthesized Claspin was assessed by immunoblot analysis at 0, 2 and 6h post-MG-132 treatment as shown in figure 46A and B.

When proteasomal degradation was blocked following treatment with MG-132 newly synthesised claspin accumulated in mock- and AdΔ19K-infected cells (Figure 46B). Gemcitabine treatment showed a tendency towards increased accumulation of claspin (Figure 46B). In contrast, in response to a combination of gemcitabine with AdΔ19K Claspin protein levels did not increase following MG-132 treatment and were rather reduced (Figure 46B). After 6h of MG-132 treatment significantly decreased Claspin levels were observed in cells treated with a combination of gemcitabine with AdΔ19K compared to gemcitabine without AdΔ19K (Figure 46B). This suggested that the presence of AdΔ19K in gemcitabine-treated cells prevents gemcitabine-induced accumulation of newly synthesized Claspin.

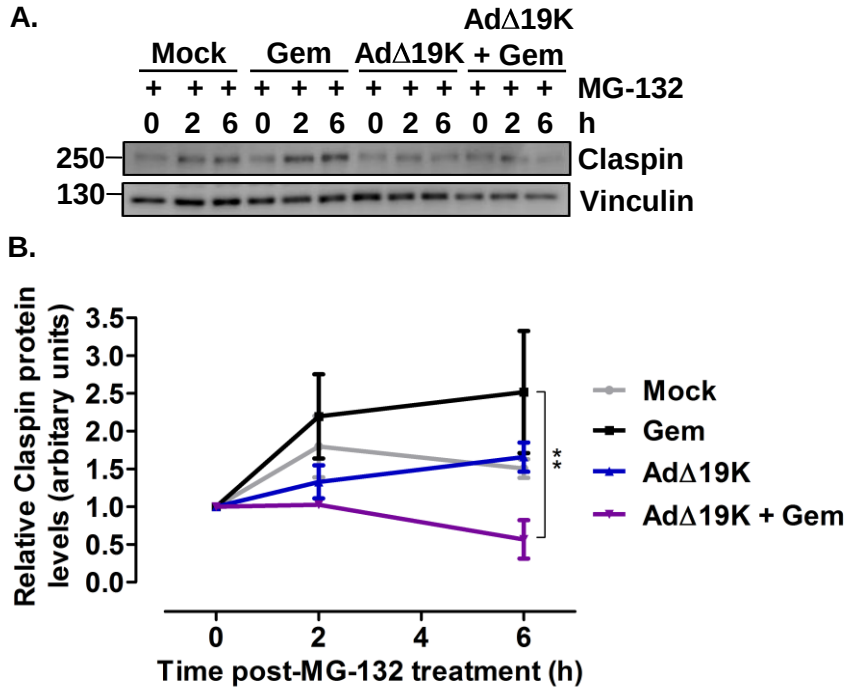

Figure 46: AdΔ19K prevents gemcitabine-induced accumulation of newly synthesized Claspin following proteasomal inhibition. PT45 cells were treated with 300ppc of AdΔ19K -/+ addition of 10nM gemcitabine (Gem). At 48h post-infection, 10μM of the proteasome inhibitor MG-132 was added to study protein synthesis. Cells were harvested at 0, 2 and 6 hours post-MG-132 treatment and prepared for immunoblot analysis of claspin expression. **(A)** Representative immunoblots of Claspin (250kDa) with vinculin (130kDa) as a loading control. Numbers indicate MW size marker (kDa). **(B)** Averages of newly synthesised Claspin protein levels at 0, 2 and 6h post-MG-132 treatment. Claspin protein levels were quantified by densitometric analysis, normalised to the loading control and expressed relative to the 0h time-point of each treatment (set to 1). Error bars represent S.E.M. of 3 independent experiments. **.p<0.01 (two-way ANOVA with Bonferroni's multiple comparison test).

Based on the observation that AdΔ19K prevented gemcitabine-induced accumulation of newly synthesized Claspin following proteasomal inhibition, I sought to further investigate changes in Claspin synthesis. Claspin mRNA levels were therefore assessed by qPCR analysis.

At 24h post-treatment with gemcitabine, Claspin mRNA levels appeared to be upregulated (Figure 47). The presence of either Ad5tg or AdΔ19K in gemcitabine-treated cells did not affect gemcitabine-induced upregulation of Claspin mRNA expression at 24h (Figure 47). At 48h post-treatment with gemcitabine Claspin mRNA expression was significantly increased (Figure 47). Addition of Ad5tg to gemcitabine-treated cells did not affect gemcitabine-induced upregulation of Claspin mRNA levels (Figure 47). On the contrary, the combination of AdΔ19K with gemcitabine significantly decreased Claspin mRNA levels compared to gemcitabine (Figure 47). Infection alone with Ad5tg or AdΔ19K did not appear to affect the mRNA expression of Claspin at any time (Figure 47). These results therefore suggest that at 48h post-infection AdΔ19K inhibits gemcitabine-induced upregulation of Claspin mRNA expression but does not affect basal claspin mRNA expression.

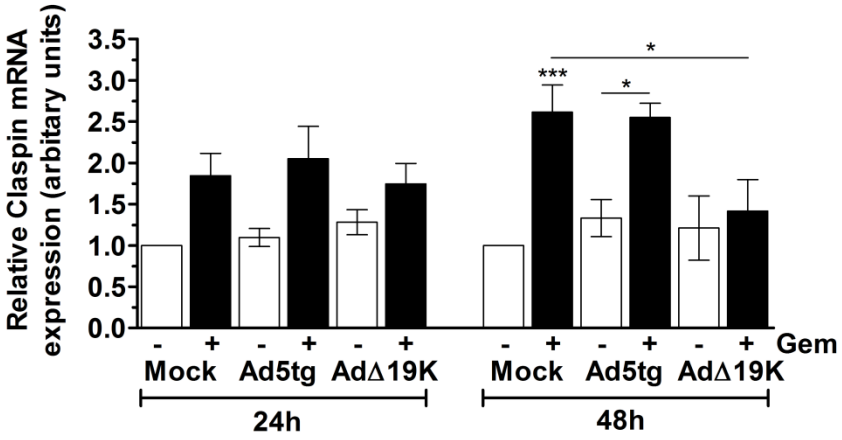

Figure 47: AdΔ19K inhibits gemcitabine-induced upregulation of Claspin mRNA expression. PT45 cells were treated with 300ppc of Ad5tg or AdΔ19K -/+ addition of 5nM gemcitabine (Gem). RNA was extracted at 24 and 48hpi for qPCR analysis of claspin mRNA expression. GAPDH mRNA expression was used as an internal/loading control. Claspin mRNA expression was normalised to that of GAPDH and expressed relative to mock-infection (set to 1). Error bars represent S.E.M. of 3 independent experiments. *.p<0.05, ***.p<0.001 (one-way ANOVA with Bonferroni's multiple comparison test).

3.3.5. Claspin knockdown increases cell death induced by AdΔ19K and DNA-damaging drugs

The above studies demonstrated that infection with AdΔ19K inhibits gemcitabine-induced Claspin accumulation, through downregulation of Claspin synthesis and acceleration of Claspin degradation. In order to understand whether AdΔ19K-mediated downregulation of Claspin accumulation in response to gemcitabine is important for AdΔ19K- and gemcitabine-induced cell death, we decided to knock-down Claspin using siRNA. PT45 cells were transfected with non-targeting (NT) or an anti-Claspin (CLSPN) siRNA and analysed in cell viability assays. The transfected cells were also analysed by immunoblotting for monitoring of Claspin knockdown. Cell viability was assessed 72h post-infection with AdΔ19K in the absence or presence of fixed doses of gemcitabine or irinotecan. The time of cell viability assessment corresponded to 120h post-transfection.

Unexpectedly the expression of Claspin at 48h post-transfection was very low, possibly due to cells having been re-seeded only 24h before (Figure 48; siNT). Nevertheless, the knockdown of Claspin was 30% at 48h post-transfection, which corresponded to the time of virus infection in cell-viability assays. At 72h post-transfection the maximum knockdown was reached, which was approximately 70% compared to the non-targeting siRNA control (Figure 48). After this time Claspin knockdown appeared to be less effective, with 40% and 30% knockdown observed at 96h and 120h post-transfection, respectively (Figure 48).

Assessment of cell viability in cells with Claspin knockdown showed a trend towards decreased AdΔ19K EC_{50} values, both in the absence and presence of gemcitabine or irinotecan (Figure 49A). The sensitization ratio in response to AdΔ19K and 2nM or 5nM gemcitabine significantly increased when Claspin was silenced, compared to the siRNA control (Figure 49B). Moreover, in response to AdΔ19K combined with irinotecan, Claspin knockdown showed a tendency towards increased sensitization ratio (Figure 49B). Knocking-down claspin did not affect drug-induced cytotoxicity (Figure 49C). It can be concluded that Claspin knockdown enhances cell death induced by gemcitabine and AdΔ19K,

suggesting that downregulation of claspin in response to AdΔ19K is important for induction of increased cell death by the combination treatment.

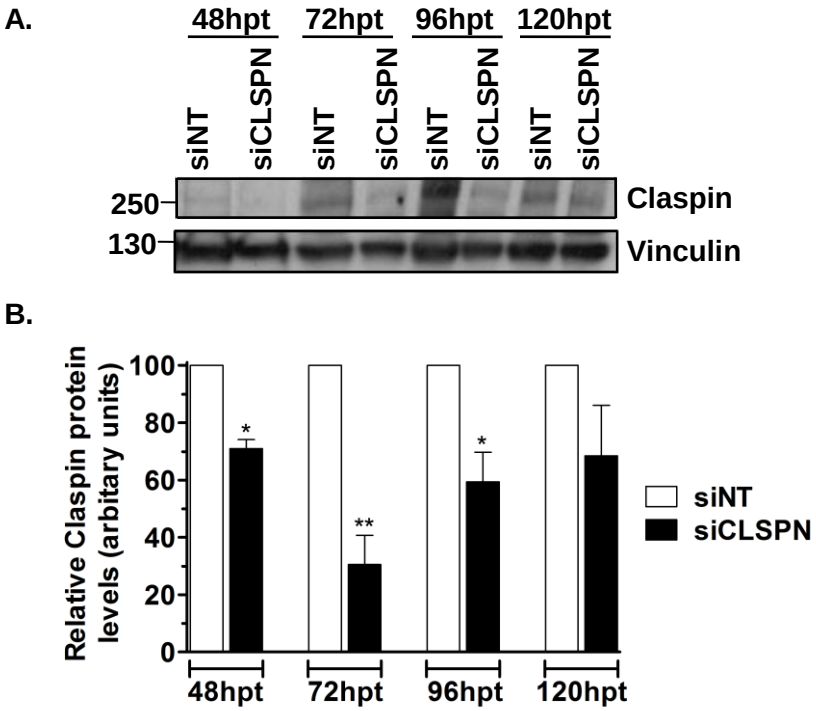

Figure 48: Claspin knockdown peaks at 72h post-transfection and protein levels remain low up to 120h post-transfection. PT45 cells were transfected with siRNA against claspin (siCLSPN) or non-targeting siRNA (siNT). 24h post-transfection cells were pooled, re-seeded in 6-well plates and harvested for immunoblot analysis at the indicated hours post-transfection (hpt). **(A)** Representative immunoblot of claspin (250kDa). Vinculin (130kDa) was used as a loading control. Numbers indicate MW size marker (kDa). **(B)** Quantification of protein levels by densitometric analysis. Claspin protein levels were normalised to the loading control and expressed as % of siNT at each time-point. Error bars represent S.E.M. of 5 independent experiments. *.p<0.05, **.p<0.01 (one-sample t-test comparing to 100%).

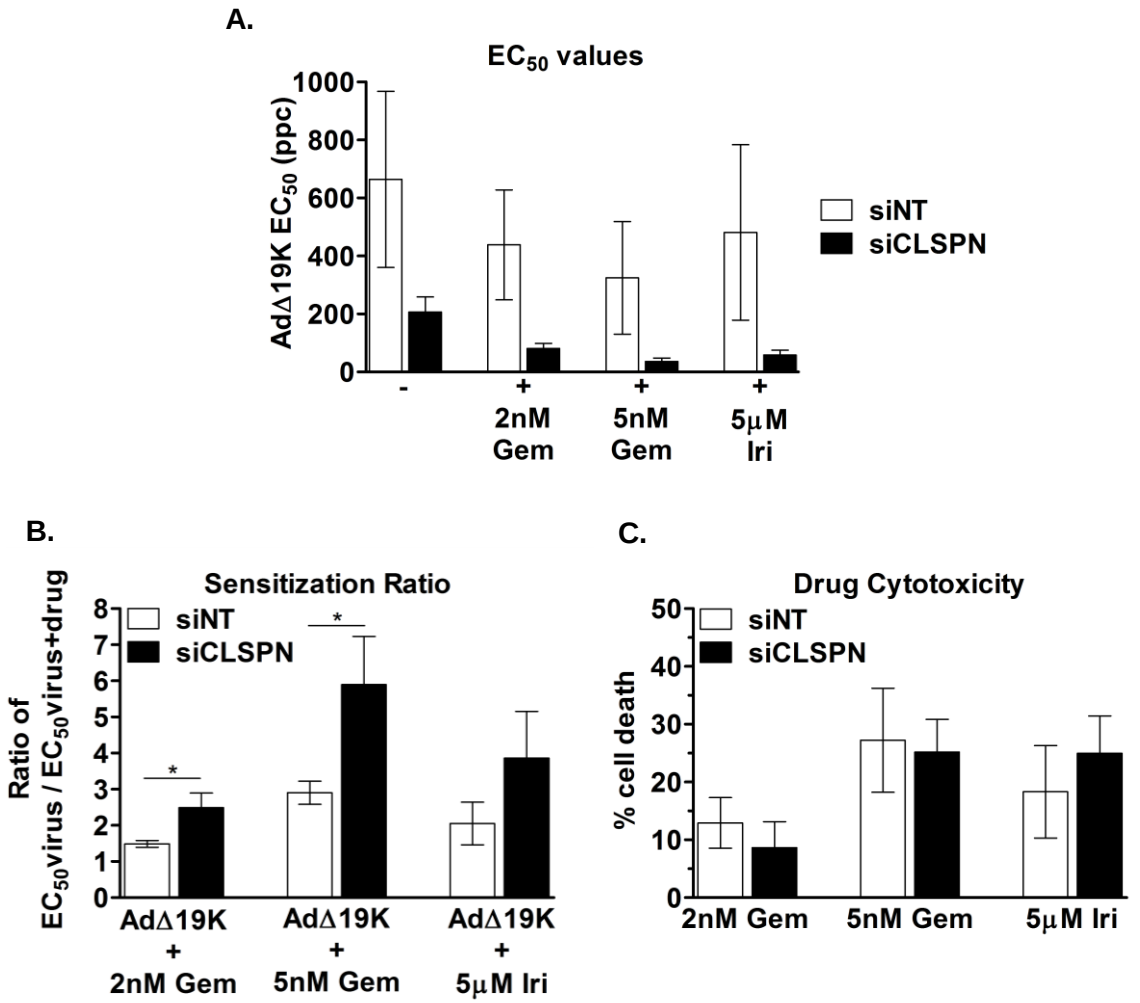

<u>Figure 49</u>: Claspin knockdown increases cell death induced by AdΔ19K and DNA-damaging drugs. PT45 cells were transfected with siRNA against claspin (siCLSPN) or non-targeting (NT) siRNA. 24h post-transfection (6-wells), cells were pooled, re-seeded in 96-well plates and treated with 5-fold dilutions of AdΔ19K -/+ fixed doses of gemcitabine (Gem) or irinotecan (Iri) to generate dose-response curves. Cell viability was assessed by MTS assay at 72hpi (corresponding to 120h post-transfection). **(A)** EC_{50} values for AdΔ19K -/+ gemcitabine (Gem) or irinotecan (Iri) at the indicated doses in cells transfected with CLSPN or NT siRNA. **(B)** Sensitization ratio (AdΔ19K EC_{50} / AdΔ19K+Gem or Iri EC_{50}). **(C)** Drug cytotoxicity. % cell death induced by gemcitabine or irinotecan in cells transfected with CLSPN or NT siRNA. Error bars represent S.E.M. of 5 independent experiments. *.p<0.05 (Unpaired t-test).

3.3.6. Claspin knockdown in combination-treated cells does not affect viral replication, but attenuates the S-phase arrest and increases the mitotic index

In order to examine whether the enhanced cell death with AdΔ19K and gemcitabine in Claspin knockdown cells, was a result of enhanced viral replication, AdΔ19K genome amplification was assessed. qPCR analysis of Ad-E2A demonstrated that Claspin knockdown does not significantly affect AdΔ19K genome amplification in the absence of gemcitabine (Figure 50). In the presence of gemcitabine, AdΔ19K genome amplification showed a trend towards decrease when Claspin was knocked-down compared to the control siRNA (siNT) (Figure 50). Therefore, the enhanced cell death induced by AdΔ19K and gemcitabine when claspin was knocked-down, was not a result of enhanced viral replication.

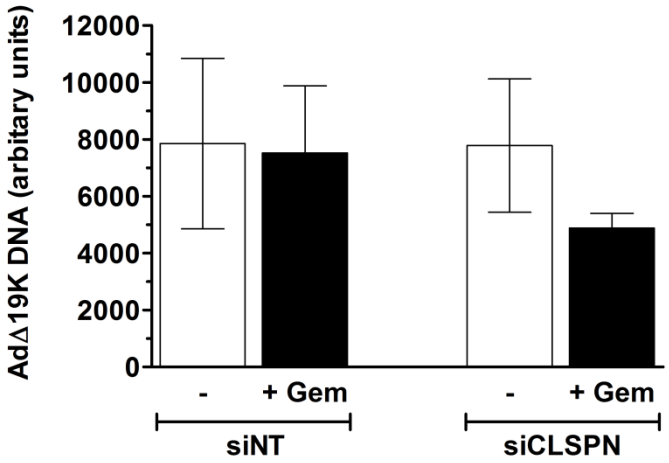

Figure 50: Claspin does not significantly affect AdΔ19K DNA amplification. PT45 cells were transfected with siRNA against Claspin (CLSPN) or non-targeting (NT) siRNA. At 48h post-transfection cells were treated with 300ppc AdΔ19K -/+ 5nM gemcitabine (Gem). DNA was extracted at 4 and 48hpi and analysed by qPCR for viral genome amplification (Ad-E2A). Viral DNA was normalized to input DNA (4h) and cellular. Error bars represent S.E.M. of 2 independent experiments.

To investigate whether Claspin knockdown results in changes in the cell-cycle distribution of cells treated with AdΔ19K and gemcitabine, cell-cycle and mitotic index analysis was performed in PT45 cells transfected with control or anti-claspin siRNA. Knocking-down Claspin significantly increased the G1 cell-fraction and decreased the S-phase fraction 24h post-treatment with AdΔ19K and gemcitabine (Figure 51A and B). This suggests that gemcitabine-induced S-phase arrest of AdΔ19K-infected cells is either delayed or weakened when Claspin is knocked-down. Moreover, the mitotic index of cells treated with AdΔ19K and gemcitabine was significantly higher (2-fold) following Claspin knockdown compare to the non-targeting knockdown (Figure 51D). No other changes in the cell-cycle distribution were observed when claspin was knocked-down (Figure 51A-D). Therefore, the enhanced cell death induced by AdΔ19K and gemcitabine following the knockdown of Claspin might be a result of cell-cycle changes, that is an attenuated S-phase arrest followed by an increased mitotic index.

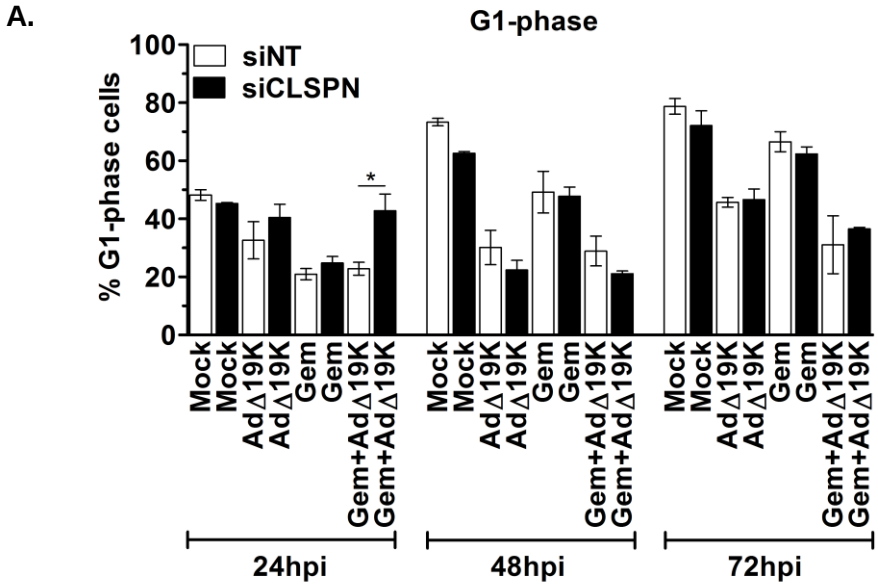

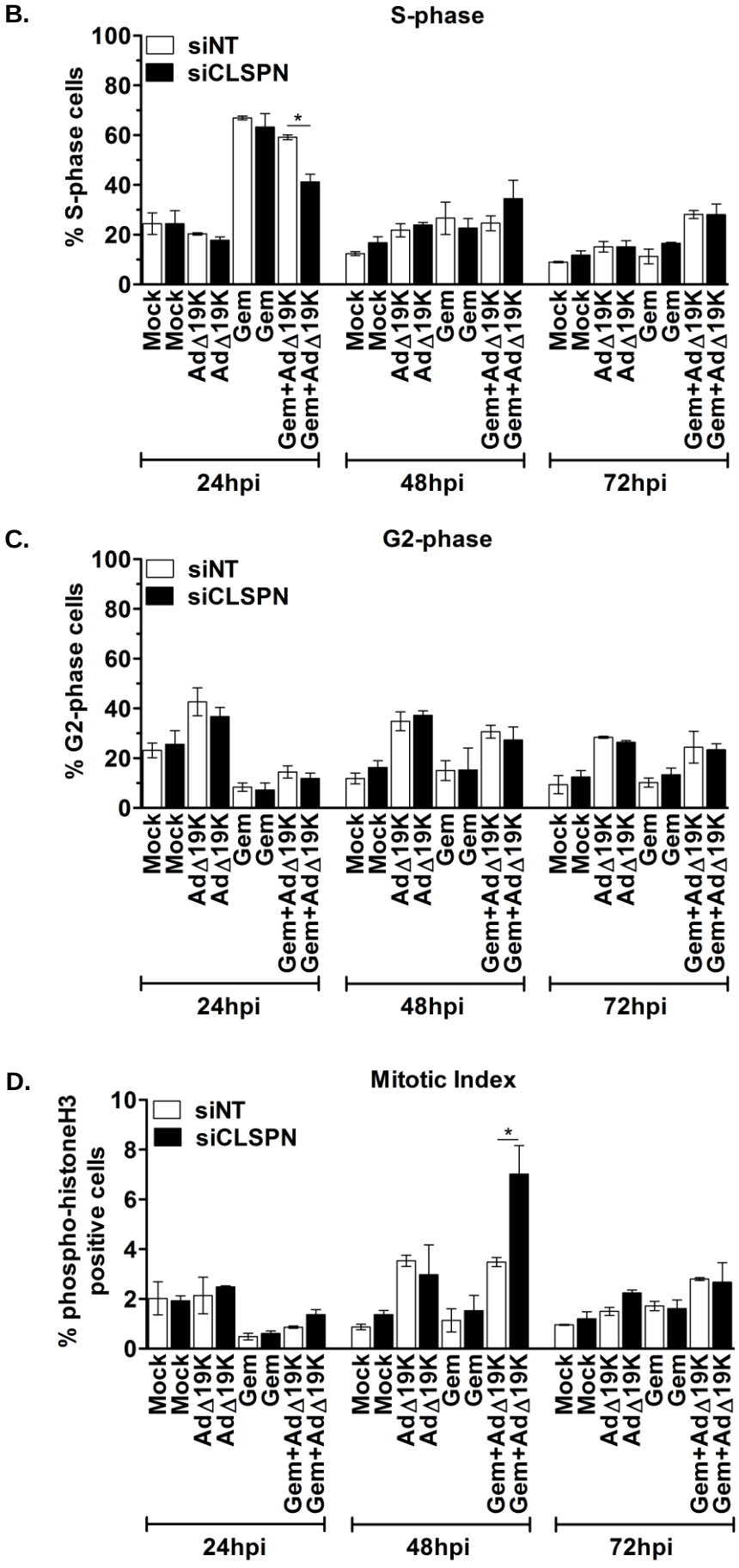

Figure 51: Claspin knockdown decreases S-phase arrest at 24h and increases the mitotic index at 48h post-treatment with AdΔ19K and

gemcitabine. PT45 cells were transfected with siRNA against Claspin (CLSPN) or non-targeting (NT) siRNA and treated with 300ppc AdΔ19K -/+ 5nM gemcitabine (Gem) 48h post-transfection. At 24, 48 and 72hpi cells were stained with FVD and fixed for cell-cycle analysis. Cells were stained with propidium iodide (for DNA-content analysis), an anti-phospho-histone H3 antibody (for mitotic index analysis) and an anti-E1A antibody (for identification of infected cells) and analysed by flow-cytometry. Dead cells, as identified from their incorporation of FVD, were excluded from the analysis. In the presence of AdΔ19K only E1A-positive cells were analysed for propidium iodide and phospho-histone H3 expression. **(A)** % cells in G1 phase **(B)** % cells in S phase **(C)** % cells in G2 phase **(D)** % cells in mitosis. Error bars represent S.E.M. of 2 independent experiments. *.$p<0.05$ (one-way ANOVA with Bonferroni's multiple comparison test).

3.4. Cells treated with gemcitabine and AdΔ19K go through aberrant mitosis

3.4.1. Adenovirus and gemcitabine induce spindle multipolarity

Based on the observation that AdΔ19K promotes the mitotic entry of gemcitabine-treated cells that have unrepaired DNA damage, we sought to investigate whether these mitotic cells exhibit any aberrations. In order to assess mitotic cells, immunofluorescence microscopy analysis of α-tubulin, to mark the mitotic spindle and Aurora-A, to mark spindle poles was performed 48h post-treatment. In the presence of gemcitabine I observed the appearance of cells with multipolar, instead of bipolar, spindles. Example images of bipolar and multipolar spindles are shown in figure 52A.

Quantification of spindle multipolarity in PT45 cells demonstrated that 20±4% of mitotic cells exhibit multipolar spindles in response to gemcitabine (Figure 52B). Less than 2% of mitotic cells displayed spindle multipolarity following infection with Ad5tg or AdΔ19K (Figure 52B). When gemcitabine was combined with Ad5tg or AdΔ19K 35±7% and 33±3% of mitotic cells, respectively, exhibited multipolar spindles and this was significantly higher compared to either virus without gemcitabine (Figure 52B). Preliminary immunofluorescence microscopy analysis in MIAPaCa-2 cells demonstrated similar results (Figure 52C). Gemcitabine induced spindle multipolarity in 18% of mitotic MIAPaCa-2 cells and infection with Ad5tg or AdΔ19K increased gemcitabine-induced spindle multipolarity to 43% and 51%, respectively (Figure 52C). Hence, treatment with gemcitabine induces the formation of multipolar spindles in mitotic cells, which is increased in the presence of adenoviruses in PT45 cells. Preliminary data demonstrate a similar trend in MIAPaCa-2 cells.

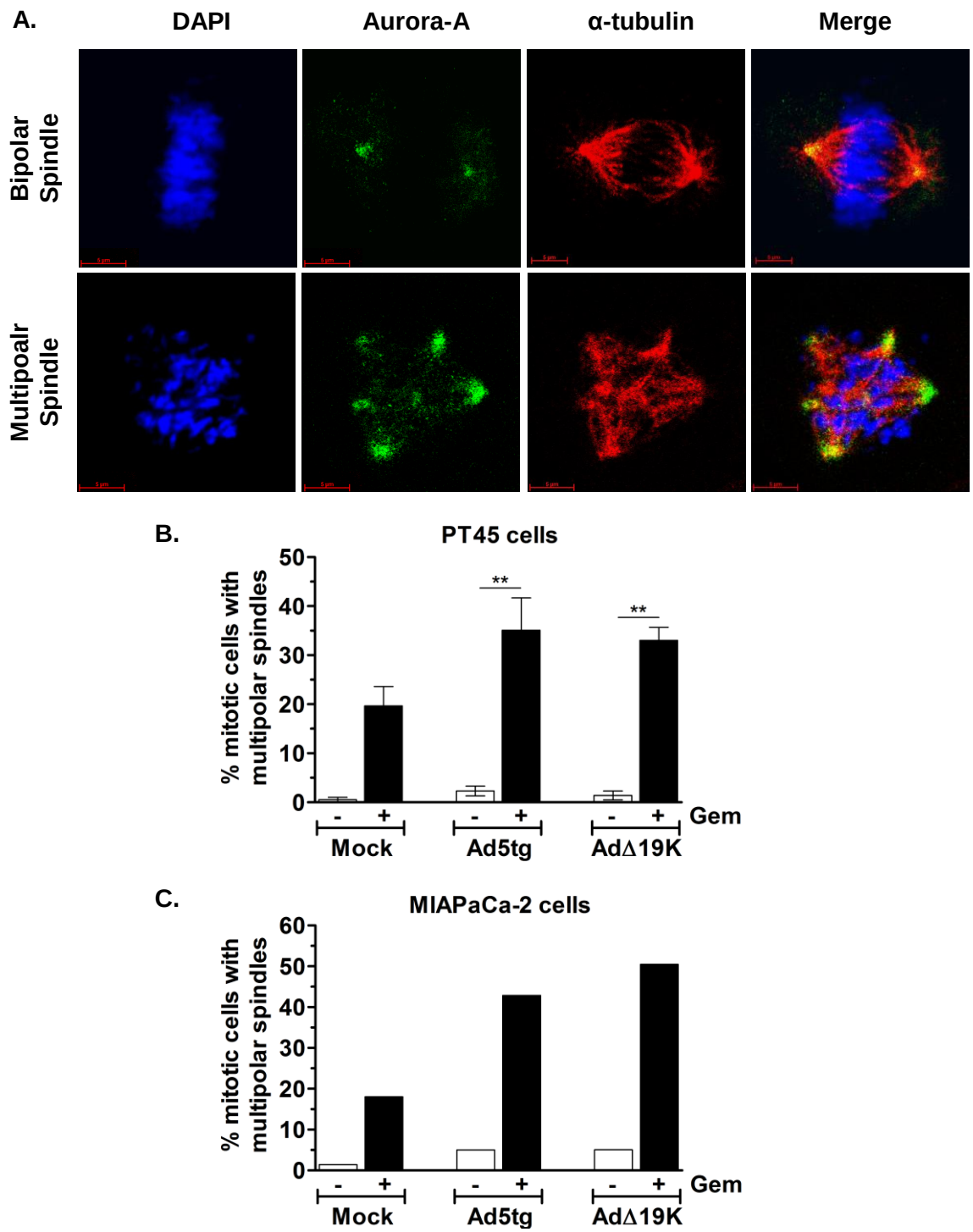

Figure 52: Adenovirus and gemcitabine induce spindle multipolarity. Cells were seeded on coverslips and treated with 300ppc of Ad5tg or AdΔ19K -/+ addition of **(B)** PT45 cells, 10nM or **(C)** MIAPaCa-2 cells, 20nM gemcitabine (Gem). At 48h.p.i cells were prepared for immunofluorescence microscopy analysis of nuclear DAPI, Aurora-A and α-tubulin. At least 150 mitotic cells were counted per treatment and spindle multipolarity was quantified. **(A)** Example of nuclear DAPI (blue), Aurora-A (green), α-tubulin (red) and merged images in PT45 cells with bipolar or multipolar spindles. Images were acquired using the 60x objective of the confocal laser scanning microscope Zeiss LSM510. **(B)** Quantification of spindle multipolarity in PT45 cells, expressed as frequency (%). Error bars represent S.E.M of two independent experiments. **.p<0.01 (one-way ANOVA with Bonferroni's multiple comparison test). **(C)** Quantification

of spindle multipolarity in MIAPaCa-2 cells, expressed as frequency (%). One experiment.

3.4.2. Adenovirus inhibits time-dependent accumulation of multinucleated cells induced by gemcitabine

During the immunofluorescence microscopy studies I observed the appearance of cells with micronuclei and multiple fragmented nuclei, an indication of aberrant mitosis. In order to assess cell multinucleation in response to treatments I performed another immunofluorescence microscopy analysis for α-tubulin and Ad-E1A, to mark infected PT45 cells. A pilot time-course experiment suggested that the frequency of cell multinucleation was low before 60h post-treatment, thus I performed the analysis at 60, 72h and 96h post-treatment. Example images of multinucleated non-infected or infected cells are shown in figure 53A.

Very few multinucleated cells were detected following mock-, Ad5tg or AdΔ19K infection (Figure 53B and C). In response to gemcitabine 7±1.5%, 9.4±0.4% and 13.4±2.1% of cells were multinucleated at 60, 72h and 96h post-treatment, respectively (Figure 53B). Gemcitabine-induced multinucleation was significantly higher in comparison to mock-infected cells without gemcitabine (Figure 53B). Moreover, gemcitabine-induced formation of multinucleated cells increased from 60h to 96h post-treatment, suggesting a time-dependent accumulation of these aberrant cells (Figure 53B). Infection of gemcitabine-treated cells with Ad5tg resulted in 5.8±0.4%, 9±1.6% and 7.8±1.9% of multinucleated cells at 60, 72h and 96h post-treatment, respectively, demonstrating that multinucleated cells did not accumulate over time (Figure 53C). Similarly, no time-dependent accumulation of infected multinucleated cells was observed in response to the combination of gemcitabine and AdΔ19K; 10.3±1.5%, 7.7±1% and 8.3±2.2% of cells exhibited multinucleation at 60, 72h and 96h post-treatment, respectively (Figure 53C). The presence of Ad5tg or AdΔ19K in gemcitabine treated cells significantly decreased the number of multinucleated cells at 96h post-treatment (Figure 53B vs C, red asterisks). Therefore, after 60h post-treatment gemcitabine induces an accumulation of multinucleated cells, which is inhibited in the presence of Ad5tg or AdΔ19K.

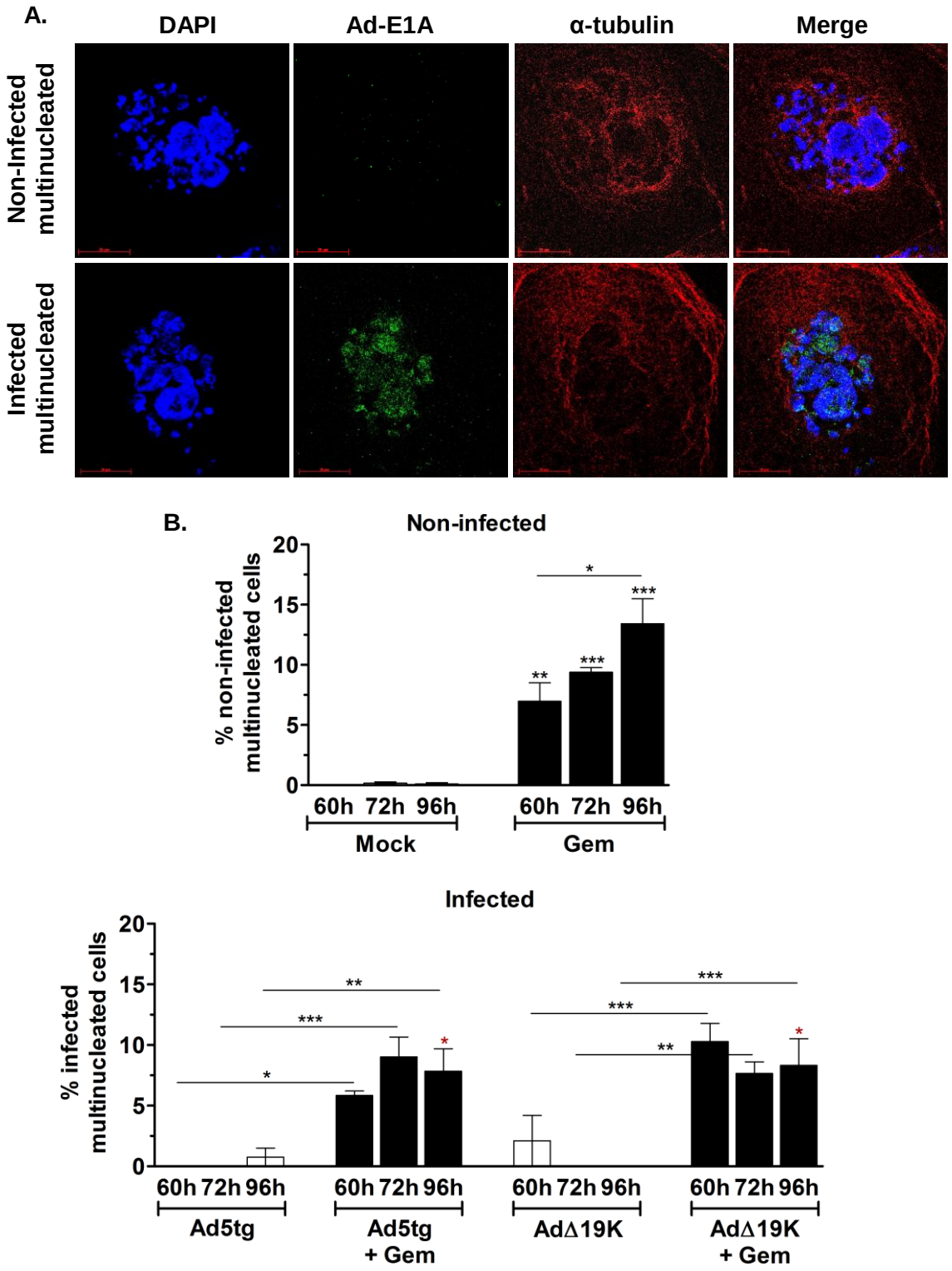

Figure 53: Adenovirus inhibits time-dependent accumulation of multinucleated cells induced by gemcitabine. Cells were seeded on coverslips and treated with 300ppc of Ad5tg or AdΔ19K -/+ addition of 5nM gemcitabine (Gem). At the indicated times post-infection cells were prepared for immunofluorescence microscopy analysis of nuclear DAPI, Ad-E1A and α-tubulin. At least 300 cells were counted per treatment and multinucleation was quantified. **(A)** Example of nuclear DAPI (blue), Ad-E1A (green), α-tubulin (red) and merged images in non-infected and infected multinucleated cells. Images were acquired using the 60x objective of the confocal laser scanning

microscope Zeiss LSM510. **(B)** Quantification of multinucleation in non-infected and infected cells, expressed as % of total non-infected and infected, respectively. *.p<0.05, **.p<0.01, ***.p<0.001 (two-way ANOVA with Bonferroni's multiple comparison test). Red asterisks indicate statistical significance in comparison to non-infected cells. Error bars represent S.E.M of at least three independent experiments.

3.4.3. Mitotic accumulation enhances cell death in response to AdΔ19K and gemcitabine

Following the observation that cells treated with AdΔ19K and gemcitabine develop various mitotic aberrations, we sought to understand whether passage through mitosis was important for the enhanced cell death observed in response to AdΔ19K and gemcitabine. To explore this, we utilised various mitotic inhibitors to perturb different mitotic stages and events and assessed cell viability in response to AdΔ19K and gemcitabine.

The Eg5 inhibitor monastrol increases mitotic index and enhances gemcitabine-induced sensitization to AdΔ19K

Monastrol is a selective inhibitor of the mitotic kinesin Eg5. By inhibiting Eg5 monastrol prevents separation of spindle poles resulting in monoastral spindles, activation of the spindle assembly checkpoint (SAC) and subsequent mitotic arrest (Kapoor et al., 2000; Mayer et al., 1999). We utilised monastrol in cell-viability assays to understand whether activation of the SAC and mitotic arrest affects cell death in response to AdΔ19K and gemcitabine. Monastrol was added simultaneously to AdΔ19K and gemcitabine, at a dose that killed no more than 30% of cells. To examine whether the selected dose was sufficient to induce a mitotic arrest, immunoblot analysis of phopsho-histone H3 in cells treated with monastrol was carried out. Phopsho-histone H3 levels were increased 24h and 48h post-treatment with monastrol, suggesting mitotic enrichment (Figure 54D).

Cell viability assays 72h post-treatment with AdΔ19K and monastrol demonstrated that addition of monastrol significantly sensitizes cells to AdΔ19K-induced cytotoxicity (Figure 54A). Notably, a 90% reduction in the EC_{50} value of

AdΔ19K was observed when monastrol was present (Figure 54A). Similarly, addition of monastrol to cells treated with AdΔ19K and gemcitabine, significantly decreased the EC_{50} value (by 3.5-fold) (Figure 54A). Consequently, the sensitization ratio in response to AdΔ19K and gemcitabine significantly increased upon addition of monastrol, suggesting that monastrol enhanced cell death induced by AdΔ19K and gemcitabine (Figure 54B). Gemcitabine-induced cytotoxicity was unaffected by the addition of monastrol (Figure 54C).

In order to understand how monastrol affects the cell-cycle distribution in response to AdΔ19K and gemcitabine, cell-cycle and mitotic index analysis was performed 24h, 48h and 72h post-treatment. Monastrol-induced mitotic arrest was 15.6±5.1% after 24h and it decreased to 7.7±1.3% and 3.6±1% by 48h and 72h respectively (Figure 54E). Moreover, monastrol significantly increased the G2 cell-fraction after 48h and 72h, compared to mock-infected cells without monastrol (Figure 54E). In cells treated with a combination of AdΔ19K, gemcitabine and monastrol, the mitotic index was 9.8±2% after 24h, as opposed to 0.6±0.2% observed in the absence of monastrol (Figure 54E). Interestingly, the presence of monastrol significantly decreased the S-phase arrest from 54±2% to 29.3±4.7%, 24h post-treatment with AdΔ19K and gemcitabine (Figure 54E). Besides a trend towards increased mitotic index no significant changes in the cell-cycle distribution were observed at 48h and 72h when monastrol was present in AdΔ19K and gemcitabine treated cells (Figure 54E). It is possible that this increase in the number of cells in mitosis is contributing to the sensitisation in response to monastrol.

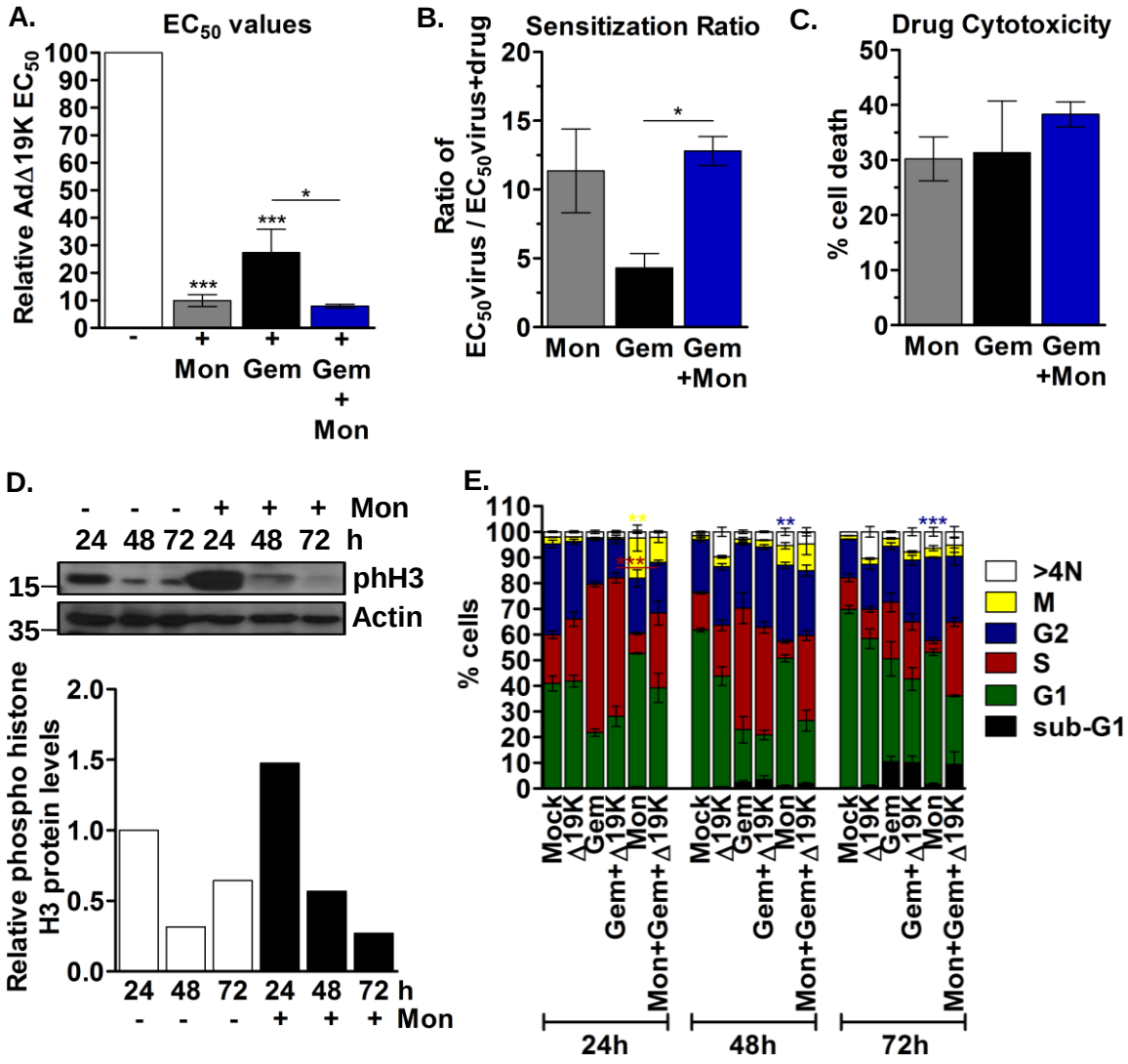

Figure 54: The Eg5 inhibitor monastrol increases mitotic index and enhances gemcitabine-induced sensitization to AdΔ19K. (A-C) Cell viability assays in PT45 cells treated AdΔ19K -/+ 5nM gemcitabine (Gem) and/or 200μM monastrol (Mon). Cell viablity was assessed by MTS assay 72h.p.i. Error bars represent S.E.M. of three independent experiments. *.p<0.05, ***.p<0.001 (one-way ANOVA with Bonferroni's multiple comparison test). **(A)** EC_{50} values (ppc) derived from AdΔ19K dose-response curves -/+ fixed doses of drug(s). Cell death was normalized to control (untreated cells or drug(s)-treated cells). EC_{50} values are expressed as % of AdΔ19K EC_{50}. **(B)** Sensitization ratio (ratio of virus EC_{50}/combination EC_{50}). **(C)** Drug cytotoxicity (% cell death). **(D)** PT45 cells were treated with 200μM monastrol (Mon) or left untreated and harvested at 24, 48 and 72h post-treatment for immunoblot analysis of phospho-histone H3 (phH3; Ser10, 17kDa) with actin (42kDa) as loading control. Numbers indicate MW size marker (kDa). Phospho-histone H3 protein levels were quantified by densitometric analysis, normalised to the loading control and expressed relative to untreated cells at 24h. One experiment. **(E)** Cell-cycle distribution; PT45 cells were treated with 300ppc AdΔ19K (Δ19K) -/+ 5nM gemcitabine (Gem) and/or 200μM monastrol (Mon) and fixed at 24, 48 and 72h post-infection for cell-cycle and mitotic index analysis. Error bars represent S.E.M. of three independent experiments. **.p<0.01, ***.p<0.001 (one-way ANOVA with Bonferroni's multiple comparison test).

An Mps1 inhibitor accelerates mitosis and inhibits gemcitabine-induced sensitization to AdΔ19K

We next utilised a selective inhibitor of Mps1 (Naud et al., 2013), a mitotic kinase required for the activation and maintenance of the SAC (Lan and Cleveland, 2010; Liu and Winey, 2012). Inhibition of Mps1 has been reported to result in abrogation of the SAC and premature mitotic exit (Jemaa et al., 2013; Kwiatkowski et al., 2010; Liu and Winey, 2012; Tardif et al., 2011). As with monastrol, the Mps1 inhibitor was added simultaneously to AdΔ19K and gemcitabine in cell-viability assays, at a dose that killed approximately 30% of cells.

Immunoblot analysis demonstrated that the selected dose of the Mps1 inhibitor indeed suppressed phosphorylation of histone H3, suggesting acceleration of mitosis (Figure 55D). In cell viability assays 72h post-treatment with AdΔ19K with or without gemcitabine, addition of the Mps1 inhibitor showed a trend towards increased AdΔ19K EC_{50} value, suggesting de-sensitization to AdΔ19K-induced cell death (Figure 55A). The presence of the Mps1 inhibitor in cells treated with a combination of AdΔ19K with gemcitabine significantly increased the EC_{50} value to the levels of AdΔ19K without gemcitabine (Figure 55A). This suggested that the Mps1 inhibitor blocks gemcitabine-induced sensitization to AdΔ19K (Figure 55A). Subsequently, the sensitization ratio of gemcitabine and AdΔ19K dropped to 1.1±0.1, a ratio that suggests no enhancement of AdΔ19K-induced cytotoxicity (Figure 55B). Mps1 inhibition had no effect on gemcitabine-induced cell death (Figure 55C).

We then examined any effects of Mps1 inhibition on the cell-cycle distribution of cells treated AdΔ19K and gemcitabine. Cell-cycle and mitotic index analysis indicated that the Mps1 inhibitor significantly diminishes the mitotic index 24h post-treatment and shows tendency towards decreased mitotic index at later time-points (Figure 55D). After 72h the Mps1 inhibitor had increased the proportion of cells in G2-phase and the fraction of cells with >4N DNA content, as compared to mock-infected cells (Figure 55D). The presence of the Mps1 inhibitor did not significantly change the cell-cycle distribution of cells treated with gemcitabine and AdΔ19K (Figure 55D). However, a trend towards

decreased mitotic index was observed when the Mps1 inhibitor was combined with gemcitabine and AdΔ19K, compared to gemcitabine and AdΔ19K without Mps1 inhibitor at 48h and 72h (Figure 55D). It is possible that acceleration of mitosis contributes to the inhibition of cell death when the Mps1 inhibitor is present in cells treated with gemcitabine and AdΔ19K .

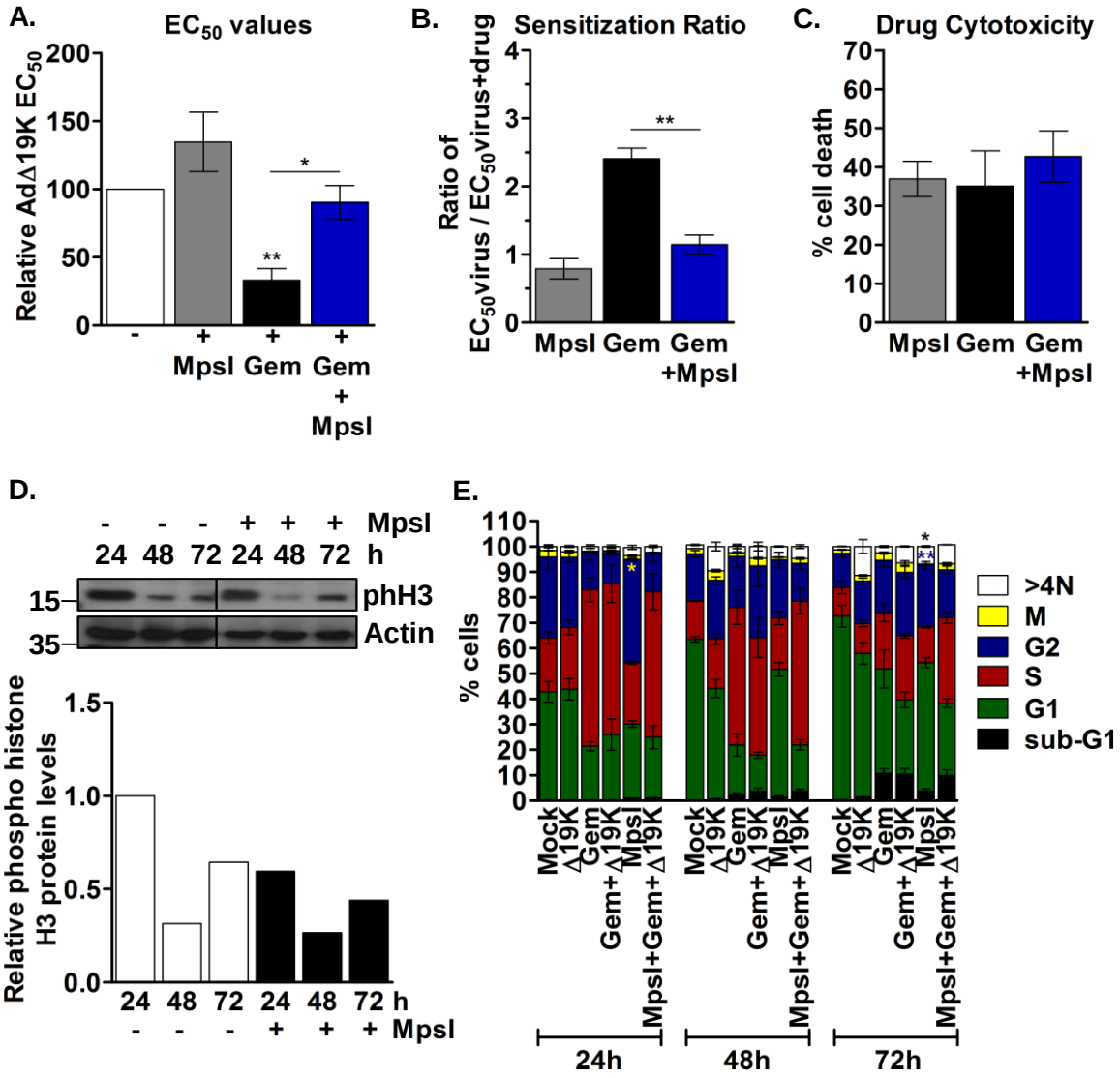

Figure 55: An Mps1 inhibitor accelerates mitosis and inhibits gemcitabine-induced sensitization to AdΔ19K. (A-C) Cell viability assays in PT45 cells treated with 5-fold dilutions of AdΔ19K -/+ 5nM gemcitabine (Gem) and/or 2.5μM Mps1 inhibitor (MpsI). Cell viability was assessed by MTS assay 72h.p.i. Error bars represent S.E.M. of three independent experiments. *.p<0.05, **.p<0.01 (one-way ANOVA with Bonferroni's multiple comparison test). **(A)** EC_{50} values (ppc) derived from AdΔ19K dose-response curves -/+ fixed doses of drug(s). Cell death was normalized to control (untreated cells or drug(s)-treated cells). EC_{50} values are expressed as % of AdΔ19K EC_{50}. **(B)** Sensitization ratio (ratio of virus EC_{50}/ combination EC_{50}). **(C)** Drug cytotoxicity (% cell death). **(D)** PT45 cells were treated with 2.5μM Mps1 inhibitor (MpsI) or left untreated and harvested at 24, 48 and 72h post-treatment for immunoblot

analysis of phospho-histone H3 (phH3; Ser10, 17kDa) with actin (42kDa) as loading control. Numbers indicate MW size marker (kDa) and lines indicate blot cropping. Phospho-histone H3 protein levels were quantified by densitometric analysis, normalised to the loading control and expressed relative to untreated cells at 24h. One experiment. **(E)** Cell-cycle distribution. PT45 cells were treated with 300ppc AdΔ19K (Δ19K) -/+ 5nM gemcitabine (Gem) and/or 2.5μM Mps1 inhibitor (MpsI) and fixed at 24, 48 and 72h post-infection for cell-cycle and mitotic index analysis. Error bars represent S.E.M. of three independent experiments. *.p<0.05, **.p<0.01 (one-way ANOVA with Bonferroni's multiple comparison test).

An Aurora-B inhibitor accelerates mitosis but its effect on gemcitabine-induced sensitization to AdΔ19K is inconclusive

AZD1152-HQPA is the active metabolite of AZD1152, a selective inhibitor of Aurora-B (Azzariti et al., 2011; Keen et al., 2005). Consistent with a function of Aurora-B in mitotic exit, treatment with AZD1152 accelerates mitosis and induces polyploidy (Azzariti et al., 2011; Mortlock et al., 2007). Following the observation that Mps1 inhibition, which accelerates mitosis, strongly inhibited cell death induced by AdΔ19K and gemcitabine we utilized AZD1152-HQPA as an alternative inhibitor that accelerates mitotic progression. AZD1152-HQPA was used at a dose that killed no more than 30% of cells in cell-viability assays. Immunoblot analysis confirmed that at 1μM the Aurora-B inhibitor efficiently diminishes phosphorylation of histone H3, suggesting acceleration of mitosis (Figure 56A).

Cell viability assays revealed that, in contrast to the Mps1 inhibitor, the Aurora-B inhibitor significantly decreased the EC_{50} value of AdΔ19K, indicating enhancement of AdΔ19K-induced cytotoxicity (Figure 56B). Aurora-B inhibition did not significantly change gemcitabine-induced cytotoxicity (Figure 56D). When AdΔ19K was combined with gemcitabine, addition of the Aurora-B inhibitor showed a tendency towards a modest increase of the EC_{50} value, suggesting it might attenuate cell death induced by AdΔ19K and gemcitabine (Figure 56B). The sensitization ratio in cells treated with AdΔ19K, gemcitabine and AZD1152-HQPA was variable, as in two experiments AZD1152-HQPA decreased the sensitization ratio of AdΔ19K and gemcitabine whereas in another two experiments it increased it (Figure 56C). Therefore, the effect of

the Aurora-B inhibitor on gemcitabine-mediated sensitization to AdΔ19K cell death is inconclusive and would require further investigation.

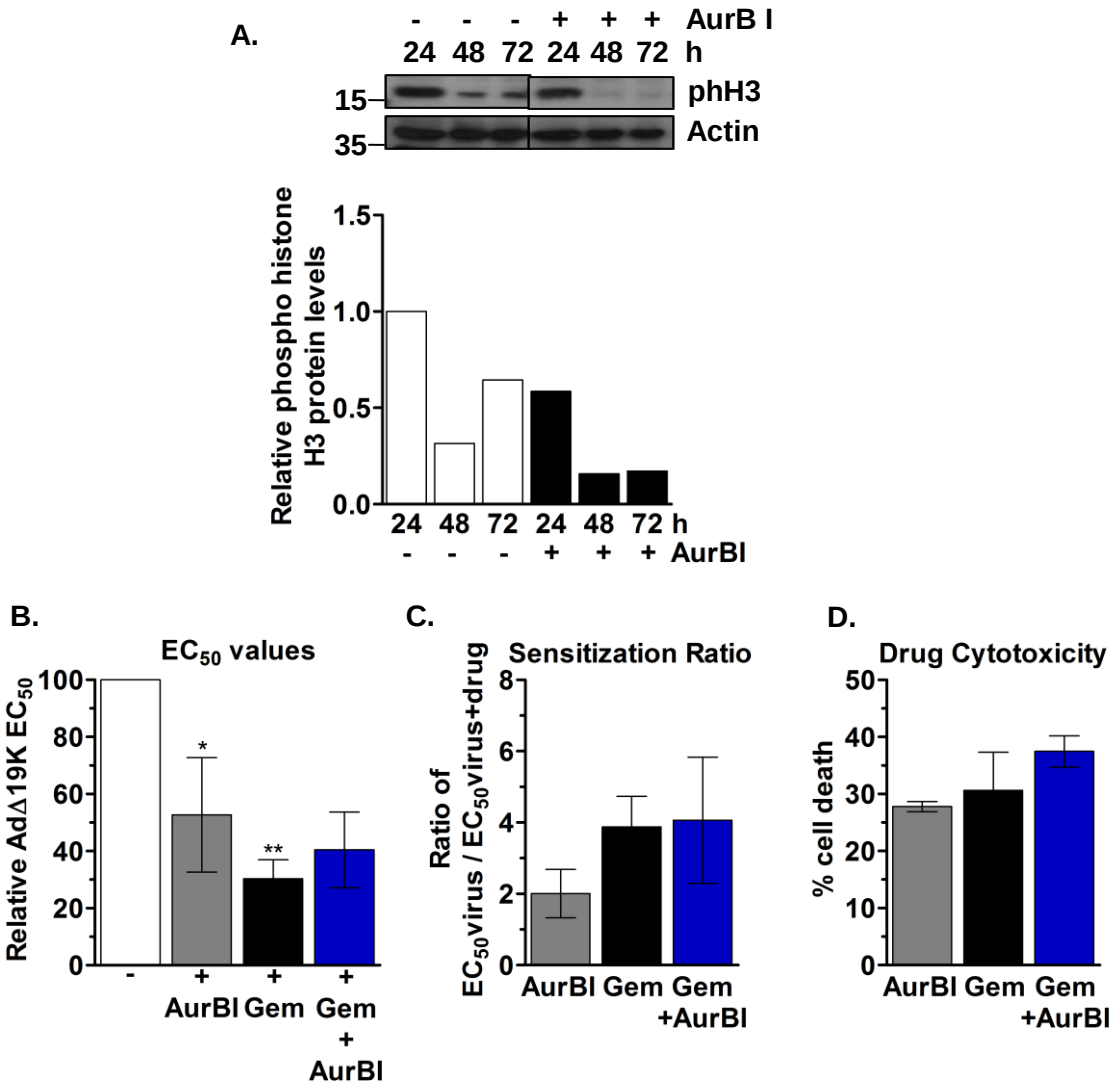

Figure 56: An Aurora-B inhibitor accelerates mitosis but its effect on gemcitabine-induced sensitization to AdΔ19K is inconclusive. (A) PT45 cells were treated with 1µM Aurora-B inhibitor (AurBI) or left untreated and harvested at 24, 48 and 72h post-treatment for immunoblot analysis of phospho-histone H3 (phH3 Ser10 17kDa) with actin (42kDa) as loading control. Numbers indicate MW size marker (kDa) and lines indicate blot cropping. Phospho-histone H3 protein levels were quantified by densitometric analysis, normalised to the loading control and expressed relative to untreated cells at 24h. One experiment. **(B-D)** Cell viability assays in PT45 cells treated with 5-fold dilutions of AdΔ19K -/+ 5nM gemcitabine (Gem) and/or 1µM Aurora-B inhibitor (AurBI). Cell viability was assessed by MTS assay 72h.p.i. Error bars represent S.E.M. of four independent experiments. *.p<0.05, **.p<0.01 (one-way ANOVA with Bonferroni's multiple comparison test). **(B)** EC_{50} values (ppc) were derived from AdΔ19K dose-response curves -/+ fixed doses of drug(s). Cell death was normalized to control (untreated cells or drug(s)-treated cells). EC_{50} values are expressed as % of AdΔ19K EC_{50}. **(C)** Sensitization ratio (ratio of virus EC_{50}/combination EC_{50}). **(D)** Drug cytotoxicity (% cell death).

Plk1 inhibition arrests cells in mitosis and shows a trend towards enhanced gemcitabine-induced sensitization to AdΔ19K

BI-2536 is a selective inhibitor of Plk-1 and it has been reported to result in the formation of monopolar spindles, followed by activation of the SAC and mitotic arrest (Lenart et al., 2007; Steegmaier et al., 2007). The Plk1 inhibitor was of particular interest for two reasons. Firstly, Plk1 inhibition could prevent Claspin degradation at the G2/M transition and provide insight into whether the accelerated degradation of claspin observed in response to gemcitabine and AdΔ19K contributes to enhanced cell death. Secondly, SAC activation and mitotic arrest in monastrol-treated cells demonstrated enhancement of gemcitabine- and AdΔ19K-induced cell death. Thus BI-2536 could be utilized as an alternative activator of the SAC that causes mitotic arrest to confirm the results obtained with monastrol.

Incorporation of BI-2536 in cell viability assays revealed that Plk1 inhibition significantly decreases the EC_{50} value of AdΔ19K by 40%, suggesting enhancement of AdΔ19K-mediated cytotoxicity (Figure 57A). Addition of the Plk1 inhibitor in cells treated with gemcitabine and AdΔ19K showed a trend towards a reduced EC_{50} value of gemcitabine and AdΔ19K (Figure 57A). Similarly, the sensitization ratio of gemcitabine and AdΔ19K showed a tendency towards an increase in the presence of the Plk1 inhibitor, but did not reach statistical significance (Figure 57B). The Plk1 inhibitor caused less than 30% cell death and did not affect gemcitabine-induced cytotoxicity (Figure 57C).

In order to assess the cell-cycle effects of the Plk1 inhibitor, cell-cycle and mitotic index analysis was carried out. BI-2536 caused 32% of cells to arrest in mitosis 24h after treatment (Figure 57D). The arrest was gradually alleviated with 12% and 6% of cells remaining in mitosis after 48h and 72h, respectively, and was accompanied by an increase in the fraction of cells having >4N DNA content (Figure 57D). This preliminary study suggested that addition of the Plk1 inhibitor in cells treated with gemcitabine and AdΔ19K decreases the S-phase arrest and increases mitotic-index at 24h post-treatment (Figure 57D). At 48h and 72h increased mitotic index and >4N cell fraction were observed in cells

treated with gemcitabine, AdΔ19K and BI-2536, compared to gemcitabine and AdΔ19K (Figure 57D).

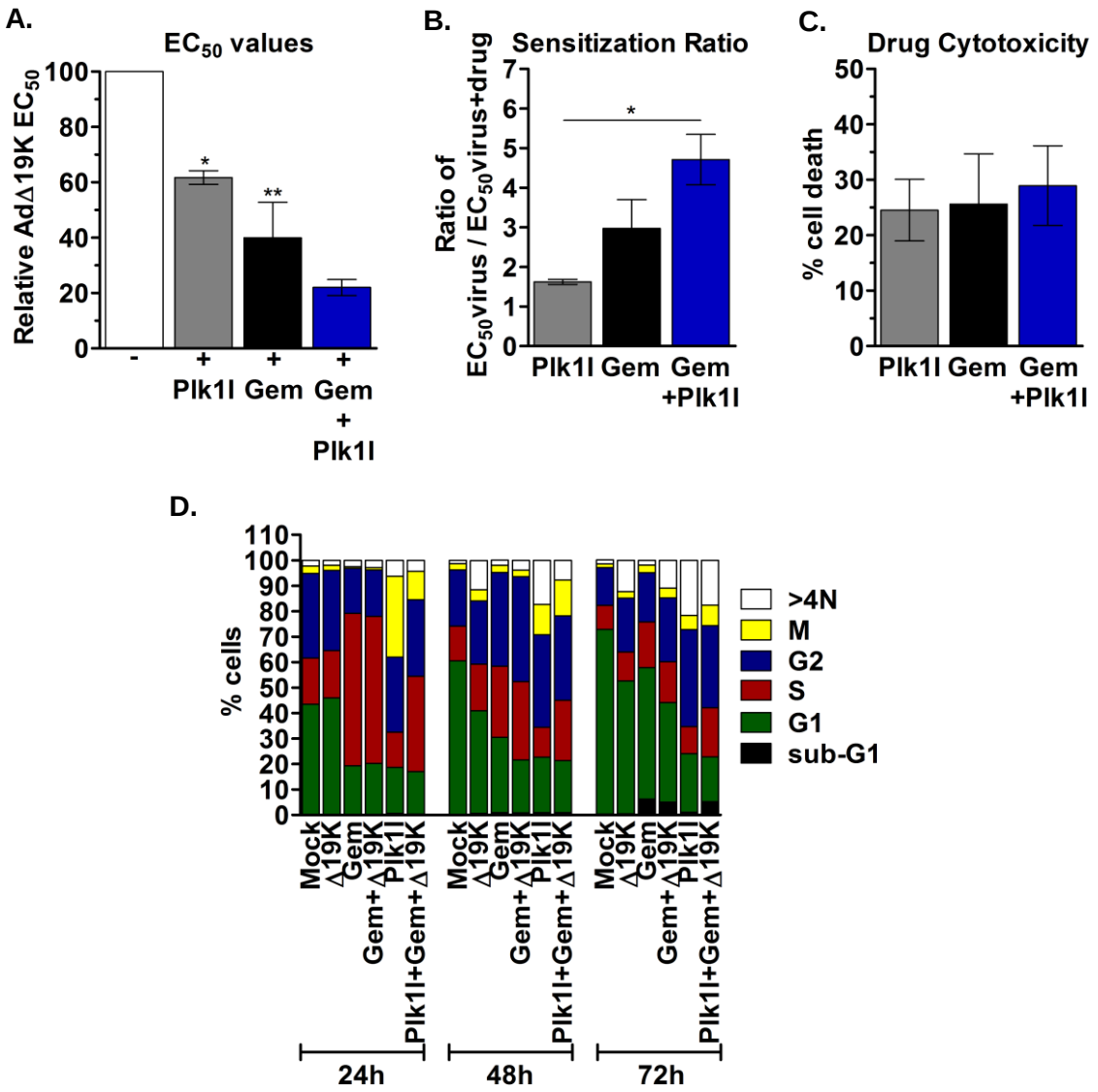

Figure 57: A Plk1 inhibitor arrests cells in mitosis and enhances gemcitabine-induced sensitization to AdΔ19K. (A-C) Cell viability assays in PT45 cells treated with 5-fold dilutions of AdΔ19K -/+ 5nM gemcitabine (Gem) and/or 4nM Plk1 inhibitor (Plk1I). Cell viability was assessed by MTS assay 72h.p.i. **(A)** EC_{50} values (ppc) were derived from AdΔ19K dose-response curves -/+ fixed doses of drug(s). Cell death was normalized to control (untreated cells or drug(s)-treated cells). EC_{50} values are expressed as % of AdΔ19K EC_{50}. **(B)** Sensitization ratios (ratio of virus EC_{50}/ combination EC_{50}). **(C)** Drug cytotoxicity (% cell death). Error bars represent S.E.M. of three independent experiments. *.p<0.05, **.p<0.01 (one-way ANOVA with Bonferroni's multiple comparison test). **(D)** PT45 cells were treated with 300ppc AdΔ19K (Δ19K) -/+ 5nM gemcitabine (Gem) and/or 4nM Plk1 inhibitor (Plk1I) and fixed at 24, 48 and 72h post-infection for cell-cycle analysis. Cells were stained with propidium iodide (for DNA-content analysis), and anti-phospho-histone H3 antibody (for mitotic index analysis) and analysed by flow-cytometry. One experiment.

Summary of the effects of mitotic inhibitors

To summarize, Eg5 inhibition by monastrol and subsequent SAC activation strongly enhanced AdΔ19K-induced cytotoxicity both in the absence and presence of gemcitabine. The monastrol-induced enhancement of cell killing in response to AdΔ19K and gemcitabine might be mediated through a decrease of S-phase arrest and an increase of mitotic index. Similar to the findings with monastrol, Plk1 inhibition enhanced AdΔ19K-mediated cytotoxicity and showed a tendency towards enhancement of gemcitabine- and AdΔ19K-induced cell death. The presence of the Plk1 inhibitor in cells treated with gemcitabine and AdΔ19K appeared to decrease the S-phase arrest and increase the mitotic index and >4N cell-fraction. The cell-viability and cell-cycle effects of the Plk1 inhibitor resembled those observed with monastrol, suggesting that the two inhibitors share similar mechanisms of action on cells treated with gemcitabine and AdΔ19K. Interestingly, the same cell-cycle effects were observed in response to Claspin knockdown that also promotes AdΔ19K- and gemcitabine-mediated cell death.

On the other hand, inhibition of the SAC protein Mps1 prevented the enhanced cell death observed in response to gemcitabine and AdΔ19K, through attenuation of AdΔ19K-mediated cytotoxicity and acceleration of mitosis. However, acceleration of mitosis in response to Aurora-B inhibition only showed a modest trend towards decreased cytotoxicity of the AdΔ19K and gemcitabine combination and rather yielded inconclusive effects on the sensitization ratio. Moreover, in contrast to the impaired AdΔ19K cytotoxicity observed when Mps1 was inhibited, AdΔ19K-mediated cell killing was enhanced by Aurora-B inhibition. Since both inhibitors decreased the mitotic index, this suggests that accelerated mitosis *per se* is likely not responsible for the effects on AdΔ19K-mediated cytotoxicity.

3.4.4. Gemcitabine prolongs mitosis and induces segregation errors, multipolar divisions and cytokinesis failure that are enhanced by AdΔ19K

AdΔ19K does not affect the time of mitotic entry or mitotic duration, while treatment with gemcitabine delays and prolongs mitosis

Based on the observations that the combination of AdΔ19K with gemcitabine induces mitotic aberrations and that cell death in response to AdΔ19K and gemcitabine is sensitive to SAC and mitotic perturbations, I wished to further characterize mitotic progression and its importance for AdΔ19K- and gemcitabine-induced cell death. I stably transfected PT45 cells with a histone H2B-mCherry construct, to fluorescently mark chromatin, synchronised the cells using thymidine block and performed time-lapse video microscopy experiments from 24h to 96h post-treatment with AdΔ19K and gemcitabine. The objectives of the study were first, to characterize mitotic progression, that is time of mitotic entry, mitotic duration, chromosome segregation and mitotic exit, and secondly, to assess whether cell death induced by AdΔ19K with gemcitabine occurs before or after mitotic progression.

Assessment of the mitotic index showed that mock- or AdΔ19K-infected cells divided mostly between 24h and 40h post-infection, with a reduced mitotic index being observed from 40h through to 96h post-infection (Figure 58A). In contrast to previous phospho-histoneH3 analysis by flow cytometry, infection with AdΔ19K did not increase the mitotic index (Figure 58A). As expected, treatment with gemcitabine significantly decreased the mitotic index until 40h post-treatment (Figure 58A). The mitotic index in response to gemcitabine was less than 5% until 56h post-treatment, after which it increased for 16h (56-72h post-treatment) and dropped again until the end of the time-course (Figure 58A). In contrast to previous observations, the presence of AdΔ19K in gemcitabine-treated cells did not significantly increase the mitotic index and the number of mitotic cells was overall similar to gemcitabine without AdΔ19K (Figure 58A).

Regarding the time of mitotic entry, mock-infected cells entered mitosis throughout the time-course, with the median time of mitotic entry being 35h post-infection (Figure 58B). Addition of gemcitabine increased the median time

of mitotic entry to 54h, with the majority of cells entering mitosis between 38 and 64h post-treatment (Figure 58B). The median time that AdΔ19K-infected cells entered mitosis was 36h, while addition of gemcitabine to AdΔ19K-infected cells increased the median time of mitotic entry to 61h (Figure 58B). Most cells treated with a combination of AdΔ19K and gemcitabine entered mitosis between 51 and 70h post-infection, which appeared delayed compared to gemcitabine (Figure 58B).

Mock- and AdΔ19K-infected cells divided with a median mitotic duration of 45min, despite that several cells were observed to deviate from that median time and remain in mitosis for up to 11h or even 22h (figure 58C). Treatment with gemcitabine prolonged mitotic duration, which ranged from 30min to 32h (figure 58C). The majority of gemcitabine-treated cells spent 1.25h to 7.5h in mitosis, with a median mitotic duration of 2.75h (figure 58C). Infection of gemcitabine-treated cells with AdΔ19K increased the median mitotic duration to 4.5h, but the range of mitotic duration appeared smaller compared to gemcitabine and was 30min to 14.5h (figure 58C).

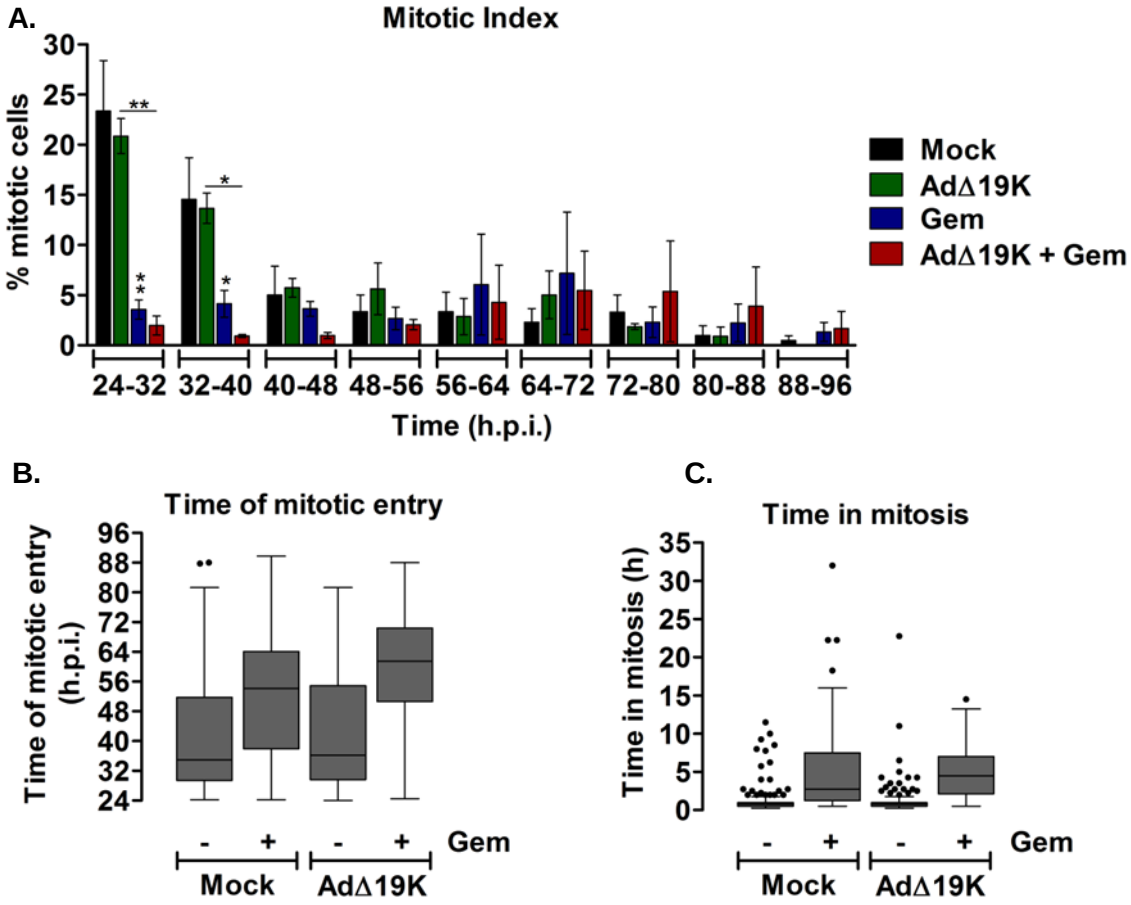

<u>Figure 58</u>: AdΔ19K does not affect the time of mitotic entry or mitotic duration, while treatment with gemcitabine delays and prolongs mitosis. PT45 cells stably expressing histone H2B-mCherry were subjected to thymidine block and released in 0% FBS DMEM -/+ 300ppc AdΔ19K. 2h later, medium was replaced with 10% FBS L15 -/+ 5nM gemcitabine (Gem). 24h post-infection cells were subjected to a 72h time-lapse imaging by phase-contrast and fluorescence microscopy as detailed in the methods. Images from 3 different fields per condition were acquired every 15min from 24 to 96h post-infection. **(A)** Mitotic index. Mitotic cells were quantified within each 8h time period indicated and expressed as % of total cells counted in the beginning of the 8h time period. Error bars represent S.E.M of three independent experiments. *.p<0.05, **.p<0.01 (one-way ANOVA with Bonferroni's multiple comparison test). **(B)** Time of mitotic entry. Tukey's box-and-whisker plots (with whiskers spanning 1.5xIQR and outliers shown) showing the time of mitotic onset, defined as the time of nuclear envelope breakdown. Mitotic cells from each independent experiment were pooled together. At least 100 mitotic cells were analysed. **(C)** Time in mitosis. Tukey's box-and-whisker plots (with whiskers spanning 1.5xIQR and outliers shown) showing the duration of mitosis, defined from the time of nuclear envelope breakdown until the time of sister chromatid separation. Mitotic cells from each independent experiment were pooled together. At least 100 mitotic cells were analysed.

Gemcitabine induces segregation errors, multipolar divisions and cytokinesis failure with a trend towards further increases in the presence of AdΔ19K

As mentioned above, gemcitabine-treated cells frequently exhibited spindle multipolarity and severe chromosome alignment issues. Such aberrant cells often divided with multipolar, instead of bipolar, anaphases. Examples of bipolar and mulitpolar divisions are shown in figure 59A. Quantification of bipolar and multipolar divisions showed that the frequency of multipolar divisions in mock- and AdΔ19K-infected cells was low (5.3±3% and 8.2±2%, respectively) and these were mostly tripolar divisions (Figure 59B). In response to gemcitabine, 42.9±10.6% of divisions were multipolar; significantly higher than mock-infected cells (Figure 59B). The presence of AdΔ19K in gemcitabine-treated cells showed a tendency towards increased frequency of multipolar anaphases (63.4±6.8%). Multipolar anaphases were significantly more frequent in cells treated with gemcitabine and AdΔ19K, compared to AdΔ19K (Figure 59B).

Assessment of chromosome segregation revealed errors, that is, anaphase bridges and lagging chromosomes (Figure 59A). The frequency of segregation errors in mock-infected cells was relatively high (37.8±1.7%) and significantly increased to 88.5±2.7% when gemcitabine was added (Figure 59C). Chromosomse segregation errors exhibited a trend towards an increase in the presence of AdΔ19K (44.1±7.6%) and when gemcitabine was present the frequency significantly increased to 98.8±1.2% (Figure 59C). Virtually all combination-treated cells divided with segregation errors. The frequency of chromosome segregation errors was 10% higher in cells treated with a combination of gemcitabine and AdΔ19K, compared to gemcitabine (Figure 59C).

A small percentage of cytokinesis failure (Figure 59A) was observed in mock- and AdΔ19K-infected cells (Figure 59D). In response to gemcitabine, the extent of cytokinesis failure was highly variable between the 3 independent experiments. The mean frequency of cytokinesis failure in gemcitabine-treated cells was 15.3±8.8% in the absence of AdΔ19K, and almost doubled to 31.1±11.4% when AdΔ19K was present (Figure 59D).

A.

Bipolar Anaphase

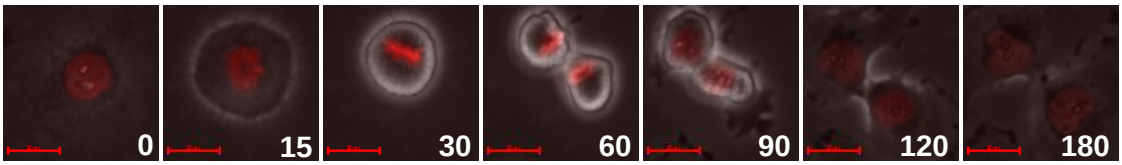

Multipolar Anaphase

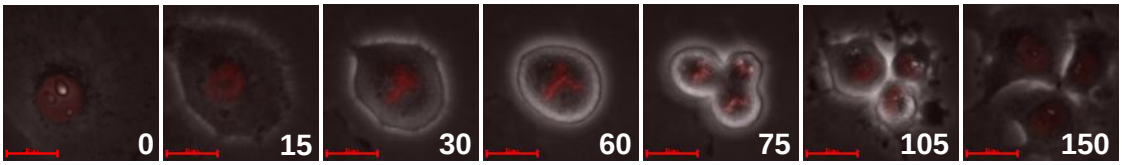

Segregation Errors: Anaphase bridge

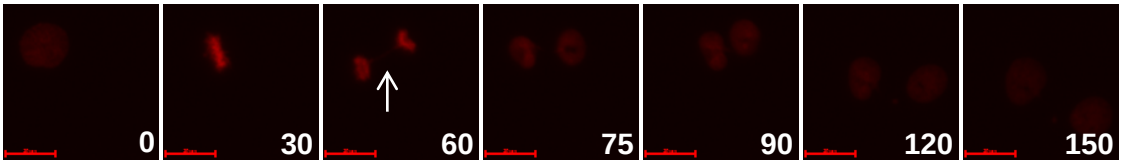

Segregation Errors: Lagging chromosome

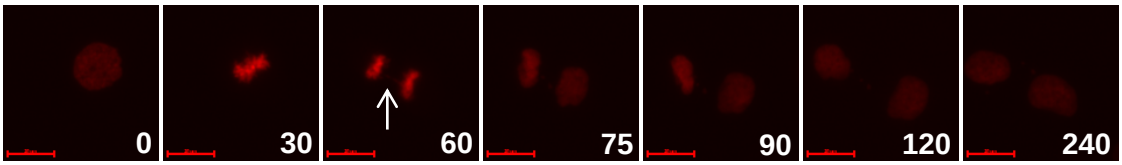

Cytokinesis Failure

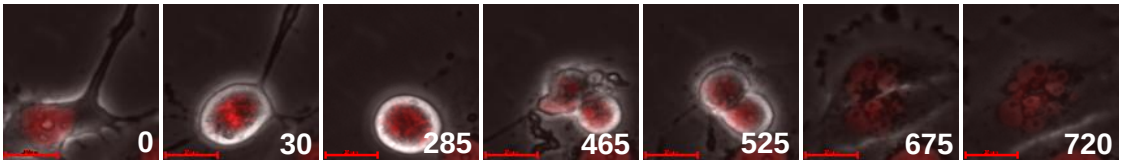

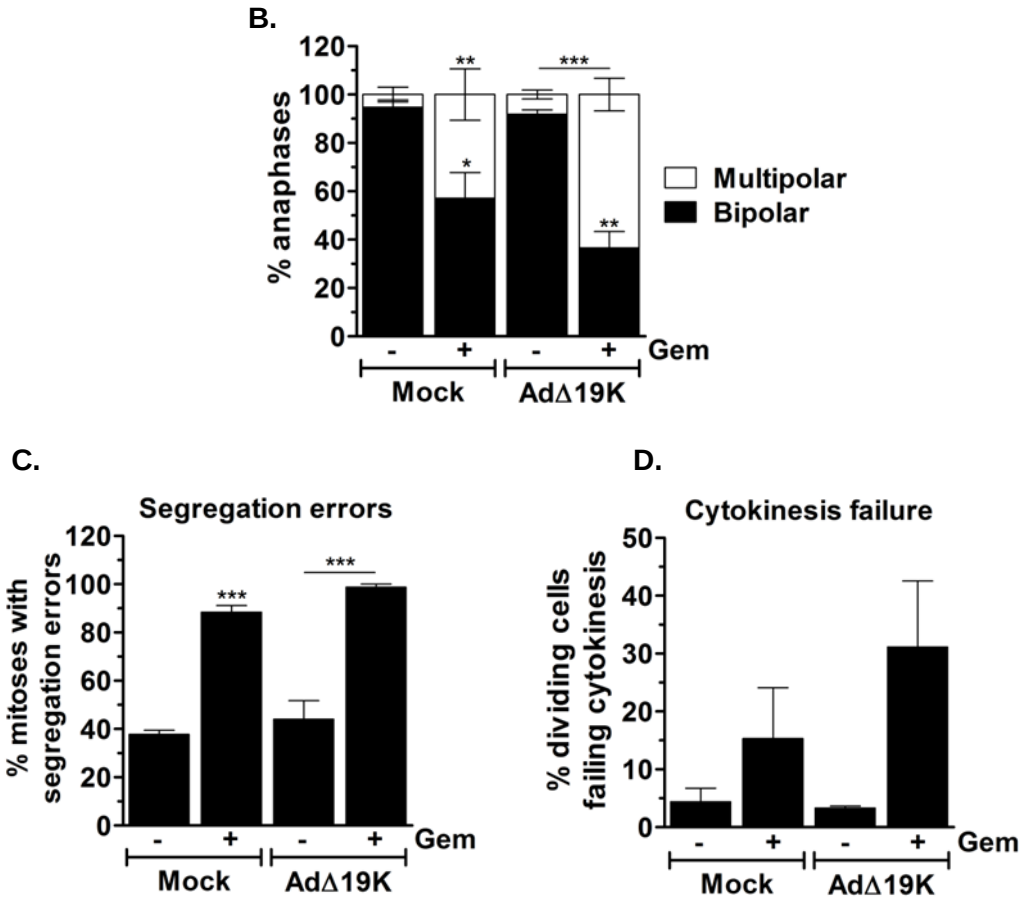

<u>Figure 59</u>: Gemcitabine induces segregation errors, multipolar divisions and cytokinesis failure with a trend towards increases in the presence of AdΔ19K. PT45 cells stably expressing histone H2B-mCherry were subjected to thymidine block and released in 0% FBS DMEM -/+ 300ppc AdΔ19K. 2h later medium was replaced with 10% FBS L15 -/+ 5nM gemcitabine (Gem). 24h post-infection cells were subjected to a 72h time-lapse imaging by phase-contrast and fluorescence microscopy as detailed in the methods. Images from 3 different fields per condition were acquired every 15min from 24 to 96h post-infection. At least 100 mitotic cells were analysed for aberrations during chromosome segregation and cytokinesis. **(A)** Example images of bipolar and multipolar anaphases, segregation errors (anaphase bridges or lagging chromosomes) and cytokinesis failure. Numbers indicate time (in min). **(B)** Frequency (%) of bipolar and multipolar anaphases. **(C)** Frequency (%) of chromosome segregation errors. **(D)** Frequency (%) of cytokinesis failure. Error bars represent S.E.M of three independent experiments. *.p<0.05, **.p<0.01 ***.p<0.001 (one-way ANOVA with Bonferroni's multiple comparison test).

Gemcitabine-induced mitotic aberrations result in formation of micro- and multi-nucleated cells that are increased in the presence of AdΔ19K

To assess the consequences of mitotic abnormalities, daughter cells were analysed for the presence of micronuclei and multinucleation. Daughter cells were categorised into mononucleated when one intact nucleus was observed, micronucleated when one or more small nuclei were associated with the daughter cell nucleus and multinucleated when two or more nuclei were present (Figure 60A). As expected, in mock-infected cells the majority (71±2.1%) of daughter cells were mononucleated and 26.4±1.6% had micronuclei, explaining the high frequency of the observed segregation errors (Figure 60B). Similarly, 67±1.8% of dividing AdΔ19K-infected cells generated mononucleated daughter cells and 29.5±1.5% resulted in the formation of micronuclei (Figure 60B). The frequency of multinucleated cells was low in both mock- and AdΔ19K-infected cells.

Treatment with gemcitabine significantly increased the frequency of multinucleation in mock-infected cells (Figure 60B), as previously observed (Figure 53B). Significantly less mononucleated daughter cells were also observed and overall the most frequent phenotype of gemcitabine-treated daughter cells was micronucleation (45.9±10.1) (Figure 60B). In cells treated with a combination of gemcitabine and AdΔ19K, equal frequencies of micronucleated and multinucelated daughter cells were observed (45.6±.6.8% ad 43.9±8.7%, respectively). Mononucleated daughter cells were significantly decreased when AdΔ19K was added to gemcitabine-treated cells, as the frequency of multinucleated daughter cells increased (Figure 60B). The occurrence of micronucleation was the same between gemcitabine and gemcitabine combined with AdΔ19K (Figure 60B). Therefore, the high rate of segregation errors following gemcitabine treatment results in micronucleated and multinucleated daughter cells and only a minority of daughter cells has a single intact nucleus. Addition of AdΔ19K, appeared to increase the frequency of gemcitabine-induced multinucleation and nearly all daughter cells were either micro- or multi-nucleated.

A.

Mononucleated daughter cells

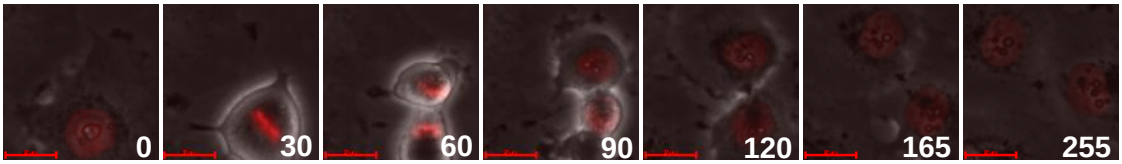

Micronucleated daughter cells

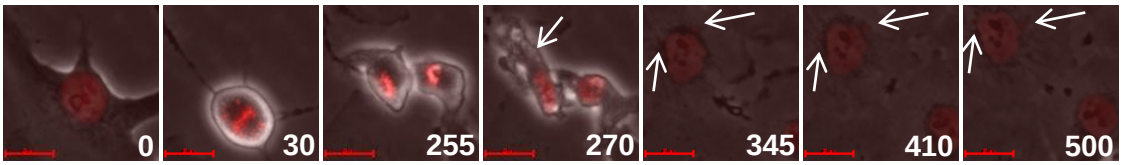

Multinucleated daughter cells

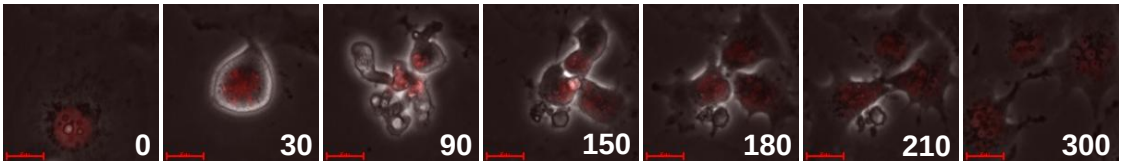

B.

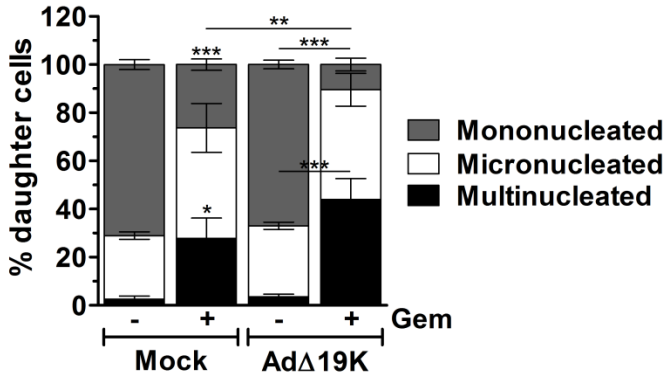

<u>Figure 60</u>: Gemcitabine-induced mitotic aberrations result in formation of micro- and multi-nucleated cells that are increased in the presence of AdΔ19K. PT45 cells stably expressing histone H2B-mCherry were subjected to thymidine block and released in 0% FBS DMEM -/+ 300ppc AdΔ19K. 2h later, medium was replaced with 10% FBS L15 -/+ 5nM gemcitabine (Gem). 24h post-infection cells were subjected to 72h time-lapse imaging by phase-contrast and fluorescence microscopy as detailed in the methods. Images from 3 different fields per condition were acquired every 15min from 24 to 96h post-infection. At least 150 daughter cells were analysed for the presence of micronuclei or multiple nuclei. **(A)** Example images of mononucleated, micronucleated and multinucleated daughter cells. Numbers indicate time (in min). **(B)** Frequency (%) of mononucleated, micronucleated and multinucleated daughter cells. Error bars represent S.E.M of three independent experiments. *.p<0.05, **.p<0.01 ***.p<0.001 (one-way ANOVA with Bonferroni's multiple comparison test).

The majority of cell death induced in response to AdΔ19K and gemcitabine occurs before mitotic entry

I next quantified cell death in response to the various treatments and assessed the proportion of cells dying before mitotic entry (pre-mitotic cell death), during mitosis (mitotic cell death) or after passage through mitosis (post-mitotic cell death) as well as the time of cell death (Figure 61). A total of 32% of mock-infected cells died throughout the time-course, suggesting some toxicity of the experimental conditions (Figure 61A). AdΔ19K-induced cell death was significantly higher than in mock-infected cells from 88h to 96h post-infection, whereas gemcitabine-induced cell death was not significantly different from cell death occurring in mock-infected cells without gemcitabine (Figure 61A). In response to the combination of gemcitabine with AdΔ19K cell death initiated at 48h and gradually increased, peaking at 88-96h during which 34.8±5.3% of cells died (Figure 61A). As expected, AdΔ19K significantly increased cell death in response to gemcitabine from 72h onwards (Figure 61A).

In mock- and AdΔ19K-infected cells the majority of cells died after cell division with 0% and 1% of cells dying during mitosis in mock-infected and AdΔ19K-infected, respectively (Figure 61B). Following treatment with gemcitabine 55.6±16.2% of cells died before mitotic entry and 39.9±11.7% of cells died after division (Figure 61B). Approximately 5% of gemcitabine-treated cells were also observed to die during mitosis (Figure 48B). When gemcitabine was combined with AdΔ19K the great majority of cell death (81.9±6.5%) occurred before cells entered mitosis and 17.2±5.6% of cells died after completing mitosis (Figure 61B). Post-mitotic cell death was significantly reduced in AdΔ19K-infected cells treated with gemcitabine, compared to Ad∆19K infection alone (Figure 61B).

The median time of cell death was 75h and 86h post-infection for mock-infected cells dying before or after mitosis, respectively (Figure 61C). In response to AdΔ19K, the majority of pre-mitotic cell death occurred from 54h to 80h post-infection with a median time of 68h that was lower than in mock-infected cell (Figure 61C). Post-mitotic cell death also occurred earlier in AdΔ19K- compared to mock-infected cells, with a median time of 79h and a range of 45 to 96h post-infection (Figure 61C). In response to gemcitabine the majority of pre-mitotic

cell death occurred from 66h to 90h post-treatment with a median time of 81h (Figure 61C). When AdΔ19K was present gemcitabine-treated cells died earlier, with a median pre-mitotic cell death time of 71h (Figure 61C). The timing of post-mitotic cell death in response to gemcitabine was similar between gemcitabine and gemcitabine with AdΔ19K and had a median value of 86h and 83h in the absence or presence of AdΔ19K, respectively (Figure 61C). Gemcitabine-treated cells died in mitosis from 71 to 90h post-treatment (median time 80h). When AdΔ19K was present, mitotic death of gemcitabine-treated cells started as early as 44h and showed a median time of 76h (Figure 61C).

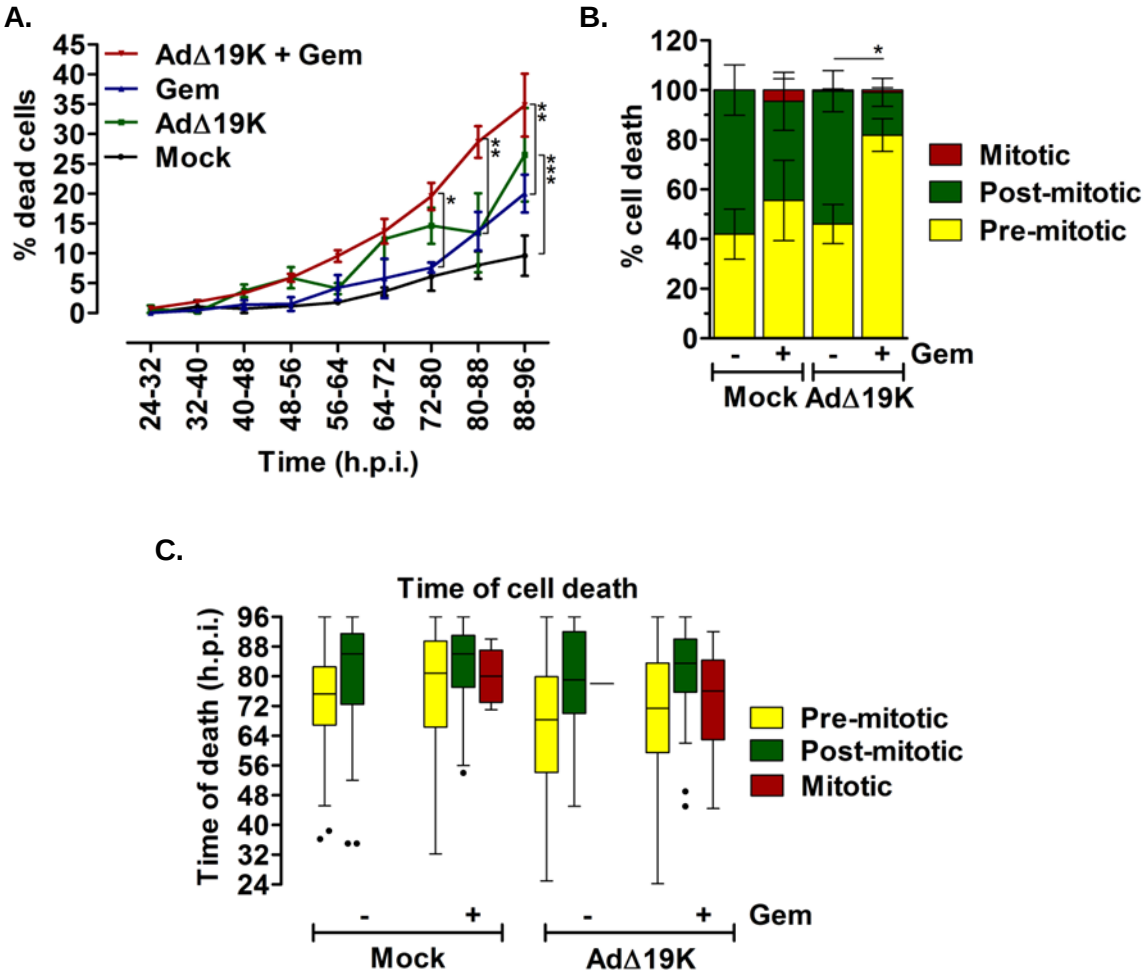

Figure 61: The majority of cell death induced in response to AdΔ19K and gemcitabine occurs before mitotic entry. PT45 cells stably expressing histone H2B-mCherry were subjected to thymidine block and released in 0% FBS DMEM -/+ 300ppc AdΔ19K. 2h later medium was replaced with 10% FBS L15 -/+ 5nM gemcitabine (Gem). 24h post-infection cells were subjected to a 72h time-lapse imaging by phase-contrast and fluorescence microscopy as detailed in the methods. Images from 3 different fields per condition were

acquired every 15min from 24h to 96h post-infection. **(A)** Frequency of cell death. Dying cells were quantified within each 8h time period indicated and expressed as % of total cells counted in the beginning of the 8h time period. 100-400 total cells were counted per experiment. Error bars represent S.E.M of three independent experiments. *.p<0.05, **.p<0.01, ***.p<0.001 (one-way ANOVA with Bonferroni's multiple comparison test). **(B)** Dying cells from 24h to 96h were categorized into cells dying before mitotic onset (pre-mitotic death), cells dying during mitosis (mitotic death) and cells dying after completion of mitosis (post-mitotic death) and expressed as % of total cells dying. *.p<0.05 (one-way ANOVA with Bonferroni's multiple comparison test). **(C)** Tukey's box-and-whisker plots (with whiskers spanning 1.5xIQR and outliers shown) showing the time (in hours post-infection) of pre-mitotic, mitotic and post-mitotic cell death for each condition. 100-600 dead cells per condition were recorded.

In addition to cell death, the overall fate of cells in response to each treatment was analysed. Fate was categorised into cells that divided and died (no division - death), cells that divided and survived (no division - survival), cells that divided and survived (division - survival) and cells that divided and died in interphase or mitosis (division - death in interphase and division - death in mitosis, respectively). Examples of each cell fate are shown in figure 62A. The fate profiles of 100 cells from each condition are shown in figure 62C.

As expected, in mock-infected cells the most frequent fate was division followed by survival (51.6±10.3%) (Figure 62B). 23.5±6.1% of mock-infected cells survived without division and around 26% died either before or after division (Figure 62B). In response to AdΔ19K 12.4±8.3% and 34.6±16.2% of cells survived with no division or following division, respectively (Figure 62B). A total of 53% of AdΔ19K-infected cells died, mostly in interphase following division (Figure 49B). The most frequent fate of gemcitabine-treated cells was survival without division, which was observed in 44.3±6% of cells (Figure 62B). Compared to mock-infection, the frequency of cells surviving after division was significantly reduced when gemcitabine was present (Figure 62B). A total of 41% of cells died following treatment with gemcitabine and death occurred more frequently before division (Figure 62B). In response to gemcitabine and AdΔ19K the majority of cells that were tracked died without division (58±4.2%), a frequency that was significantly higher than each single treatment (Figure 62B). A total of 29% of cells survived treatment with gemcitabine and AdΔ19K and 12.3±4.2% died following division (Figure 62B).

A.

No division - Death

No division - Survival

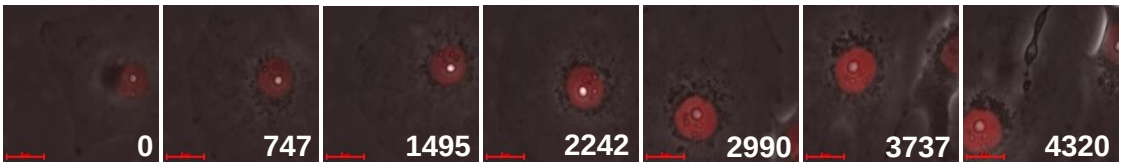

Division - Death in Interphase

Division - Survival

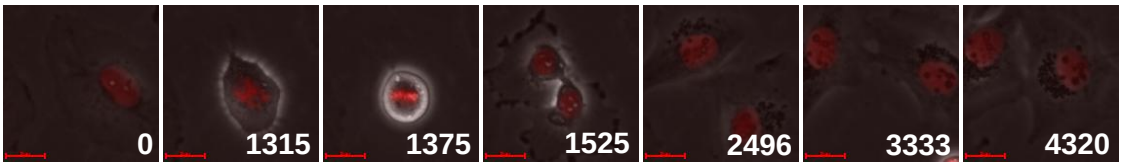

Division - Death in mitosis

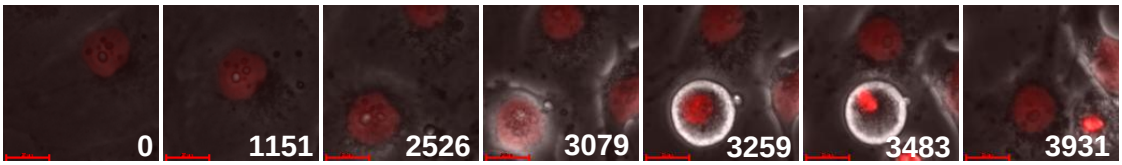

B.

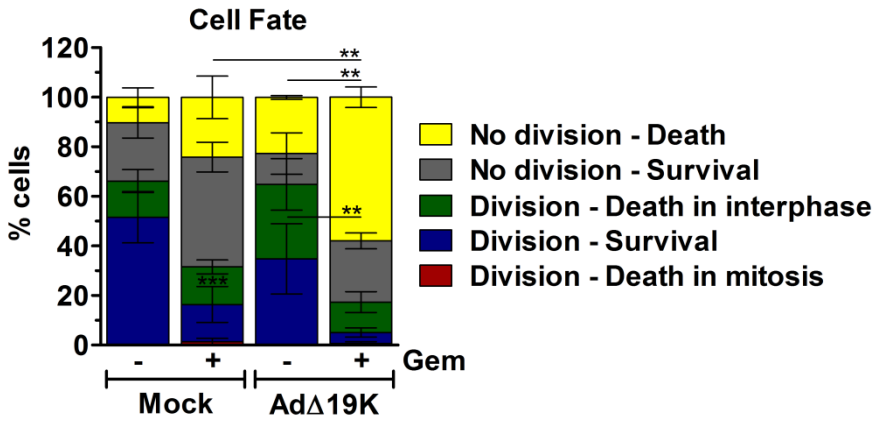

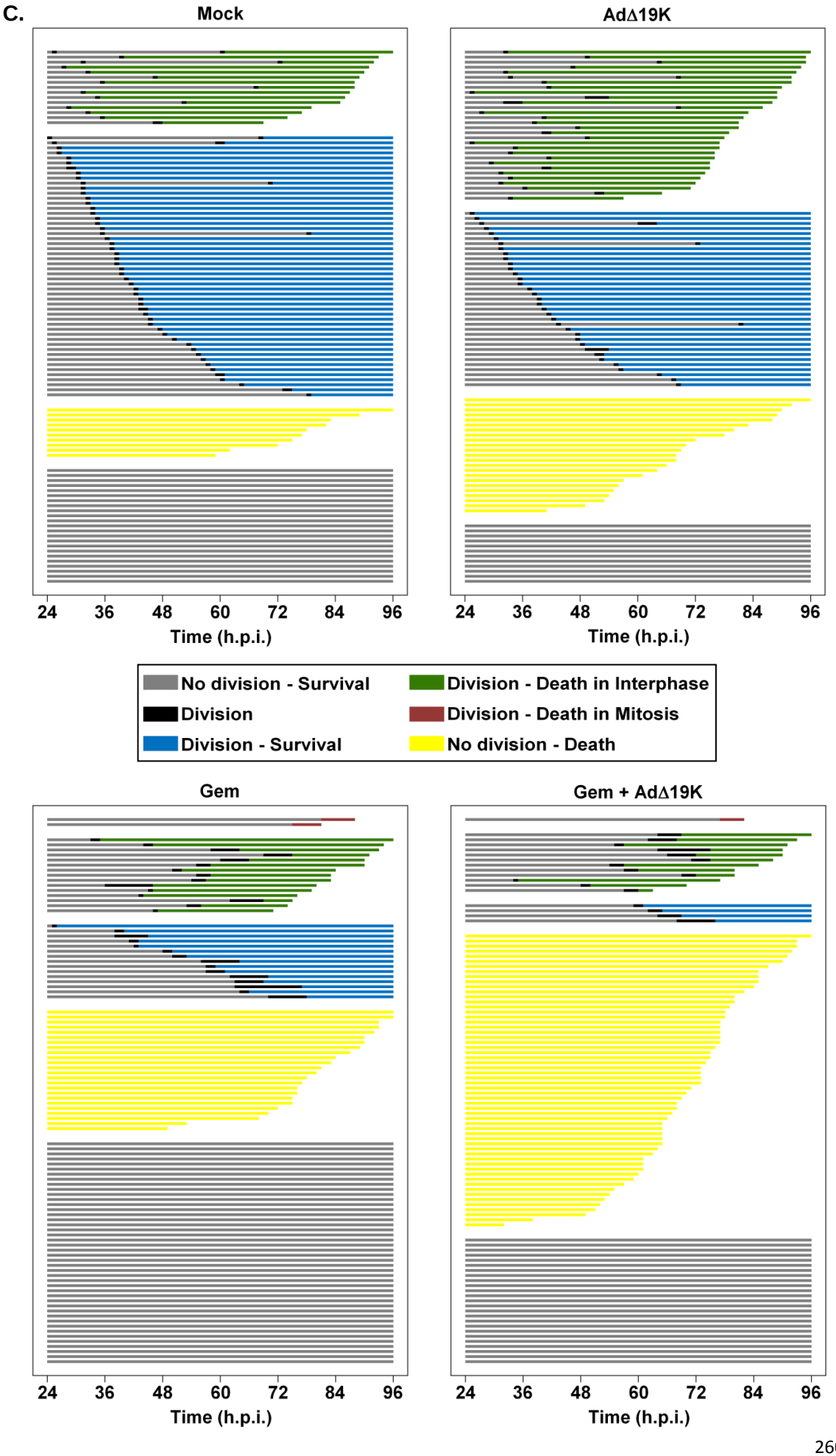
C.
Mock
AdΔ19K
24
36
48
60
72
84
96
Time (h.p.i.)
No division - Survival
Division
Division - Survival
Division - Death in Interphase
Division - Death in Mitosis
No division - Death
Gem
Gem + AdΔ19K

Figure 62: Fate profiles. PT45 cells stably expressing histone H2B-mCherry were subjected to thymidine block and released in 0% FBS DMEM -/+ 300ppc AdΔ19K. 2h later medium was replaced with 10% FBS L15 -/+ 5nM gemcitabine (Gem). 24h post-infection cells were subjected to a 72h time-lapse imaging by phase-contrast and fluorescence microscopy as detailed in the methods. Images from 3 different fields per condition were acquired every 15min from 24 to 96h post-infection. At least 400 cells per condition were analyzed for their fate. **(A)** Example images of each cell fate. Numbers indicate time (in min) **(B)** Frequency of each cell fate per condition. Error bars represent S.E.M of three independent experiments. **.p<0.01, ***.p<0.001 (one-way ANOVA with Bonferroni's multiple comparison test). **(C)** Representative cell fate profiles (showing 100 cells) in each condition. Each line represents a cell.

Conclusions from time-lapse microscopy studies

AdΔ19K infection had no effect on the time of mitotic entry or time in mitosis (duration). In contrast, gemcitabine treatment, regardless of the presence of virus, delayed mitotic entry and prolonged mitotic duration, suggesting activation of the SAC. It was observed that the majority of cells with prolonged mitosis exhibited chromosome alignment issues partly due to spindle multipolarity. The presence of AdΔ19K in gemcitabine-treated cells enhanced the effects of gemcitabine, by delaying mitotic entry and increasing the time in mitosis. This suggested that combination-treated cells exhibited more severe chromosome alignment issues thus taking longer to satisfy the SAC.

In response to gemcitabine, a high frequency of segregation errors, multipolar divisions and cytokinesis failure occurred. Addition of AdΔ19K to gemcitabine-treated cells resulted in a tendency towards increased segregation errors, multipolar divisions and cytokinesis failure, with virtually all combination-treated cells exhibiting chromosome segregation abnormalities and the majority of cells undergoing multipolar divisions. The high rate of segregation errors following gemcitabine treatment resulted in micronucleated and multinucleated daughter cells and only a minority of daughter cells had a single intact nucleus. Addition of AdΔ19K appeared to increase the frequency of gemcitabine-induced multinucleation and nearly all daughter cells were either micro- or multi-nucleated.

Regarding cell death, AdΔ19K-induced cell killing occurred almost equally before or after mitosis and earlier compared to mock-infected cells. More than half of gemcitabine-treated cells died before mitotic entry and addition of AdΔ19K both increased and accelerated pre-mitotic cell death. In response to gemcitabine, post-mitotic cell death occurred at later times post-treatment, consistent with the delayed mitotic entry, and addition of AdΔ19K did not significantly change the timing of post-mitotic cell death. Furthermore, gemcitabine treatment caused some mitotic cell death, which appeared accelerated in the presence of AdΔ19K. Importantly, the majority of enhanced cell death observed when AdΔ19K was combined with gemcitabine occurred before passage through mitosis. No major cell fate was observed in response to AdΔ19K alone but the two most frequent cell fates were division with or without death. Gemcitabine treatment resulted in most cells surviving without division, whereas when gemcitabine was combined with AdΔ19K the majority of cells died before division.

CHAPTER 4: DISCUSSION

Pancreatic cancer is an aggressive disease with poor prognosis and a high fatality rate. Gemcitabine, the standard first-line chemotherapy for advanced disease, has negligible effects, necessitating the development of new therapies. We previously demonstrated that deletion of the anti-apoptotic protein E1B19K in a replication-selective adenoviral mutant (AdΔΔ; E1ACR2- and E1B19K-deleted) caused synergistically-enhanced cell killing when combined with low-dose DNA-damaging drugs in pancreatic cancer cell models and greatly improved efficacy *in vivo* in tumour xenograft models (Cherubini et al., 2011). These findings were reproduced by a virus deleted only in the E1B19K gene (AdΔ19K) establishing that this deletion is responsible for the synergistic cell killing in combination with DNA-damaging drugs (Leitner et al., 2009). To delineate the cellular pathways targeted by the combination treatment we employed AdΔ19K combined with either gemcitabine or irinotecan with the goal of identifying cellular factors that are essential for the synergistic cell killing. We hypothesised that AdΔ19K and DNA-damaging drugs act synergistically to deregulate cell-cycle mechanisms.

The present study has confirmed previous findings by our team that pancreatic cancer cell death induced by AdΔ19K and gemcitabine is apoptotic (Leitner et al., 2009). This study has further showed that induction of cell killing by the combination treatments is more-than-additive and time-dependent. The data suggested that neither AdΔ19K nor Ad5tg could block DNA-damage responses elicited by the drugs, despite virus-mediated degradation of the DNA-damage response and repair factor Mre11. Mre11 siRNA-mediated knockdown augmented the synergistic cell death induced by AdΔ19K and DNA-damaging drugs, suggesting that virus-mediated Mre11 downregulation contributes to the enhanced cell killing. Mitotic index analysis in synchronised cells and immunofluorescence microscopy suggested that AdΔ19K promotes mitotic entry of gemcitabine-treated DNA-damaged cells. Moreover, AdΔ19K inhibited drug-

induced mRNA and protein accumulation of Claspin, a DNA-damage response protein whose degradation is required for G2/M checkpoint recovery. Treatment with AdΔ19K and gemcitabine accelerated Claspin degradation in cycloheximide-chase assays and siRNA-mediated Claspin knockdown enhanced the synergistic cell death. Time-lapse microscopy in histone H2B mCherry-expressing cells, as well as immunofluorescence microscopy studies, revealed that AdΔ19K enhanced gemcitabine-induced aberrant mitosis, characterised by spindle multipolarity, chromosome alignment issues and subsequent SAC activation, chromosome missegregation errors, cytokinesis failure and formation of micro- and multi-nucleated cells. Importantly though, AdΔ19K prevented the gemcitabine-induced accumulation of multinucleated cells. Despite that the majority of cell killing in response to gemcitabine and AdΔ19K appeared to occur in S/G2-arrested cells before mitotic entry, passage through a prolonged aberrant mitosis enhanced induction of cell death.

4.1. Differential sensitivity of PT45 and MIAPaCa-2 cells to virus and drug

PT45 and MIAPaCa-2 cells exhibited different sensitivity to chemodrugs and adenovirus infection in cell-viability assays. Dose-response curves to viruses demonstrated that MIAPaCa-2 cells are 3-5-fold more sensitive to adenovirus compared to PT45 cells (Figure 16), but more resistant to gemcitabine and irinotecan, since higher drug doses were required to cause 30% cell death (Figure 16). The sensitivity of MIAPaCa-2 to gemcitabine was almost 5-fold lower compared to PT45 cells, in agreement with previous published results from our group (Cherubini et al., 2011). Moreover, gemcitabine-mediated cell sensitization to AdΔ19K was weaker than in PT45 cells (Figure 16C and F).

Both cell lines lack p16 and have constitutively active K-Ras and transcriptionally non-functional p53, as confirmed by PCR mutational analysis (Figure 15). Thus the differential sensitivity to virus and drug in the two cell lines cannot be attributed to differences in the most frequent genetic alterations occurring in PDAC However other unidentified genetic variations are likely to contribute to the dissimilar sensitivities. In addition to genetic variation, differential virus sensitivity might be a result of discrepancies in the rate of viral

uptake, spread and genome amplification between the two cell lines. Hamdan et al. reported that CAR and αvβ5 expression levels are comparable between PT45 and MIAPaCa-2 cells and despite increased αvβ3 expression in PT45 cells, adenovirus uptake was almost 4-fold higher in MIAPaCa-2 cells (Hamdan et al., 2011). Augmented viral transduction might therefore be responsible for the increased adenovirus sensitivity of these cells compared to PT45 cells. Moreover, previous published data from our team indicated that the rate of adenovirus production, including intracellular and released viral particles, was higher at 24-48h in MIAPaCa-2 cells compared to PT45, suggesting that viral spread is accelerated in MIAPaCa-2 cells at these times post-infection (Cherubini et al., 2011). Hence, increased viral uptake and spread can explain the increased sensitivity of MIAPaCa-2 cells to adenovirus. Despite that MIAPaCa-2 cells were more sensitive to virus, the degree of sensitisation in combination with gemcitabine was higher in the PT45 cells. It is possible that the less efficient gemcitabine-mediated cell killing in MIAPaCa-2 cells could not further improve on virus-induced cell death.

4.2. E1B19K deletion in Ad5 permits apoptosis induction

Cell viability, cell death and apoptotic assays confirmed previous findings by our group that deleting E1B19K in wild-type Ad5 potently sensitizes pancreatic cancer cells to chemodrug-induced apoptosis (Cherubini et al., 2011; Leitner et al., 2009). Dose-response curves to virus demonstrated lower EC_{50} values when AdΔ19K was combined with suboptimal doses of DNA-damaging drugs compared to Ad5tg (Figure 16). In MIAPaCa-2 cells particularly, the combination of gemcitabine with Ad5tg appeared antagonistic and this was efficiently overcome by combining gemcitabine with AdΔ19K, in agreement with previous reports by our group (Cherubini et al., 2011). Moreover, in PT45 cell death assays, the cytotoxicity of the combination of AdΔ19K with either gemcitabine or irinotecan was significantly higher than the combination of Ad5tg with either drug (Figure 18). Similarly, apoptotic assays demonstrated that DNA fragmentation and caspase-3 activation are induced to significantly higher extent in response to AdΔ19K and gemcitabine, compared to Ad5tg and gemcitabine (Figures 19-21).

The enhanced apoptotic responses observed when chemotherapeutic agents are combined with E1B19K-deleted mutants as opposed to wild-type Ad5 can be rationally attributed to the anti-apoptotic functions of E1B19K. Firstly, deleting E1B19K attenuates the ability of the virus to antagonise extrinsic, intrinsic, p53-dependent or -independent apoptosis that can be induced in response to viral infection and cytotoxic drugs. Secondly, the ability of E1A to induce p53-dependent and -independent apoptosis can be counteracted by E1B19K, as previously reported (Rao et al., 1992; White, 2001; White et al., 1991). Therefore, deleting E1B19K should stimulate E1A-induced apoptosis. Indeed, it has been reported that deletion of E1B19K produces a large plaque phenotype indicative of accelerated viral spread and this effect was due to early cell lysis and subsequent earlier release of progeny virions (Chinnadurai, 1983; Gros and Guedan, 2010; Sauthoff et al., 2000; Subramanian et al., 2006; Takemori et al., 1984). Although E1A-induced p53-mediated apoptosis can also be counteracted by E1B55K, in the context of tumour cells with non-functional p53 E1A-induced apoptosis is expected to occur independently of p53.

In line with the ability of E1B19K to counteract E1A functions, White et al. reported that deletion of E1B19K increased E1A expression and subsequently E1A-dependent transcription of viral genes, leading to increased viral replication (White et al., 1988; White et al., 1986). Other studies also reported increased viral replication in pancreatic tumour cells infected with other E1B19K-deleted mutants that had additional gene deletions (Liu et al., 2004; Liu et al., 2005). Previous studies by our group using the AdΔ19K and AdΔΔ mutants in PT45 and MIAPaCa-2 cells did not detect significant differences in viral replication or production compared to wild-type Ad5 (Cherubini et al., 2011; Leitner et al., 2009).

In my studies, I observed a trend towards higher levels of viral DNA amplification for AdΔ19K compared to Ad5tg up to 72h after infection in PT45 cells. I also observed a slight trend towards increased E1A mRNA expression in AdΔ19K- versus Ad5tg-infected cells at 16h-24h (Figure 24). This increase was paralleled by a trend towards more cells expressing the E1A protein when infected with AdΔ19K compared to Ad5tg at 16h-24h post-infection in MIAPaCa-

2 cells and at 24h in PT45 cells (Figure 23). However, Leitner et al, reported that E1A expression was not increased in Ad∆19K-infected PT45 cells compared to Ad5 up to 72h post-infection, although quantification of the immunoblot data was not performed (Leitner et al., 2009). Furthermore, I observed that the differences in E1A mRNA and protein expression between Ad5tg and Ad∆19K became significant in the presence of gemcitabine (Figure 22-23). A possible explanation for the discrepancies between my study and that of Leitner et al. regarding the E1A expression might be the timing, the methods of analysis and the use of a wild type Ad5 from a different source. Ad5tg is the backbone for Ad∆19K (not the commercial Ad5), which was obtained from Dr M. Mehtali in the form of a plasmid (pTG3602) (Chartier et al., 1996). We found that Ad5tg is slightly less adapted to growth in cultured cells than the serially passaged wild type Ad5 (unpublished findings). Furthermore, in my E1A mRNA experiments I normalised E1A mRNA expression to penton mRNA to accurately measure the relative increase in E1A per virus particle, independently of replication. In the study by Leitner et al, E1A was normalised to cellular 18S RNA (Leitner et al., 2009) also at later time-points than in my study. In addition, I analysed E1A protein expression in live cells only, using flow-cytometry, which is a more accurate quantitative method than immunoblotting. The immunoblot data presented by Leitner et al might have included protein from dead cells (which would be more frequent with the Ad∆19K infection) and possibly underestimated the E1A levels when normalising to actin. Interestingly, I found that E1A levels were higher with Ad∆19K-infection than with Ad5tg at the early time-points (before 24h), while at 48h the levels were similar. These results indicate that E1A is expressed more potently at earlier stages from the Ad∆19K virus than from Ad5tg and might more efficiently initiate the higher levels of cell killing in combination with DNA-damaging drugs. It has been established that E1A induction of viral transcription/replication is not dose-dependent once a sufficiently high threshold level has been reached, however, it is likely that the initial higher levels of E1A expressed from Ad∆19K play an important role in modulating the cellular responses to other factors involved in the enhanced cell killing with drugs.

An increased viral spread and E1A expression upon E1B19K deletion would explain the significantly higher accumulation of cells with >4N DNA content

observed following infection with AdΔ19K as compared to Ad5tg (Figures 25-26). E1A was previously shown to induce DNA re-replication leading to accumulation of cells with >4N DNA content (Singhal et al., 2013). In addition, this virus-induced host DNA over-replication has been associated with oncolytic adenovirus cytotoxicity in ovarian cancer cells (Connell et al., 2011). Indeed, the more virus-sensitive MIAPaCa-2 cell line supported higher levels of >4N cell accumulation compared to the PT45 cell line (compare Figures 25 and 26). This also implies that AdΔ19K should be more cytotoxic than Ad5tg. Cell viability and death assays did not support such notion (Figures 16 and 18), however in apoptotic assays AdΔ19K appeared to induce more caspase-3 cleavage than Ad5tg (Figures 20A and 21A). Moreover, virus-induced apoptosis occurred preferentially in cells with >4N DNA content (Figures 20B and 21B). Therefore it can be perceived that E1B19K deletion permits apoptosis induction in the infected cells but this does not translate to overall increased virus cytotoxicity in the absence of chemotherapeutic drugs.

4.3. Effects of gemcitabine on adenovirus

Data presented in this thesis demonstrated that gemcitabine inhibits viral DNA replication but increases E1A mRNA and protein expression levels (Figures 22-24). The inhibitory effect of gemcitabine on adenoviral DNA replication, late gene expression and virion production was previously demonstrated by our and other groups and was observed to be relieved at later times post-infection (72h-96h) (Bhattacharyya et al.; Cherubini et al., 2011; Leitner et al., 2009; Raki et al., 2005). The inhibitory effect is believed to be the result of blocked host DNA replication, as other DNA replication inhibitors, such as aphidocholin and the gemcitabine analogue arabinofuranosylcytosine (Ara-C), can also suppress viral replication (Feldman and Rapp, 1966; Habara et al., 1980; Leitner et al., 2009; Michaelis et al., 2002; Musk et al., 1990). In addition, blockage of DNA replication by gemcitabine inhibited the ability of the virus to induce DNA re-replication, as significant decreases in AdΔ19K-mediated accumulation of cells with >4N DNA content were evident in the presence of gemcitabine (Figure 25B and 26B).

Increased E1A expression as well as increased frequency of Ad-DBP positive cells observed in immunofluorescence studies (Figure 38) following Ad∆19K infection are likely the result of enhanced viral uptake in the presence of gemcitabine. Our group previously reported that gemcitabine increases adenoviral uptake in MIAPaCa-2, Suit-2 and other pancreatic cancer cell lines, most likely through increased integrin expression (Bhattacharyya et al.). Onimarou et al. also reported increased infectivity of Suit-2 cells by the oncolytic virus Ad5/3hTERTE1 in the presence of gemcitabine (Onimaru et al., 2010b). Gemcitabine inhibited Ad5tg and Ad∆19K DNA replication to similar extent, suggesting that the enhanced cell death induced by gemcitabine and Ad∆19K is largely independent of viral replication. However, gemcitabine-induced increases in viral uptake and increased E1A expression is expected to contribute to Ad∆19K-mediated potentiation of gemcitabine-induced cell death.

4.4. Ad∆19K and DNA-damaging drugs induce more-than-additive and time-dependent apoptotic cell killing

Cell viability, death and apoptotic assays demonstrated that suboptimal doses of Ad∆19K and DNA-damaging drugs induce cell killing in a more-than-additive manner (Figures 17-21). Cell death induced by Ad∆19K and DNA-damaging drugs is time-dependent (Figures 18, 21 and 61A). In PT45 cells, the highest synergistic response was observed at 72h and the biggest increase in the more-than-additive cell death occurred between 48h and 72h and to a lesser extent between 72h and 96h post-treatment. 72h following treatment of PT45 cells with 300ppc Ad∆19K and 5nM gemcitabine cell killing reached 53.2±5.7% as measured by cell-viability assays (Figure 17A) and 41.5±5.3% as measured by cell-death assays (Figure 18A). The higher cytotoxicity detected in cell-viability assays compared to cell-death assays was also observed in response to single treatments. For example, gemcitabine-induced cell death was 17.6±6.3% as assessed by cell-viability assays (Figure 17A), whereas in cell death assays gemcitabine did not result in significant cell killing (Figure 18A). Live-cell imaging studies confirmed that these doses of gemcitabine are mainly cytostatic, with some cell death occurring after 80h of treatment (Figure 61A).

The differences among cell viability and death assays can be explained by the fact that the MTS cell viability assay measures dehydrogenase activity as an indirect measurement of cell viability, whereas the trypan-blue dye incorporation assay provides a direct assessment of cell death. Decreased mitochondrial activity likely does not always translate to cell killing.

In cell viability assays, addition of the pan-caspase inhibitor zVAD in dose-response curves to the virus with fixed dose of drug, showed a trend towards inhibition of the cell death induced by AdΔ19K and gemcitabine or irinotecan in PT45 cells, while more potent inhibition was observed in MIAPaCa-2 cells (Figure 16). Previous published results from our group, using the same technical conditions, demonstrated almost complete abrogation of the enhanced cell death when AdΔ19K or AdΔΔ were combined with gemcitabine or irinotecan in PT45 cells; addition of zVAD reversed the shift of the virus dose-response curve induced by addition of drug (Cherubini et al., 2011; Leitner et al., 2009). In the present study, zVAD-induced attenuation of the sensitization was evident from the dose-response curves (Figures 16A and 16D, left panels), however significant increase in the average EC_{50} values derived from multiple experiments was not achieved following addition of zVAD (Figures 16B and 16E). The underlying cause for this discrepancy is not known but could be influenced by cell passage number or source and batch of reagents. Nevertheless, subsequent apoptotic assays clearly demonstrated that the enhanced cell killing in PT45 cells is apoptotic (Figures 19 and 20) and is inhibited in the presence of zVAD (Figure 20). This is evidenced, for example, by the observation that gemcitabine and AdΔ19K induced caspase-3 cleavage to the same extent (38±4.8%; Figure 20) as membrane permeabilization detected by the trypan-blue dye incorporation assay (41.5±5.3%; Figure 18A). The observation that the frequency of DNA fragmentation at 72h (Figure 19) was half the frequency of caspase-3 activation (Figure 20) can be attributed to the fact that DNA fragmentation is downstream of caspase-3 cleavage. Delayed occurrence of nuclear fragmentation following caspase-3 activation was previously reported (Davoli et al., 2002; Sasaki et al., 2000). The findings in MIAPaCa-2 cells, suggest that cell killing in response to irinotecan and AdΔ19K is caspase-dependent, and in response to gemcitabine and AdΔ19K cell death shows at least partial dependency on caspases (Figures 16-17 and 21A).

Overall, the presence of AdΔ19K in gemcitabine-treated promoted caspase-3 activation in cells with 4N and >4N DNA content, suggesting preference for induction of apoptosis in G2/M phases (Figures 20B and 21B).

4.5. AdΔ19K cannot prevent the DNA damage response elicited by the cytotoxic drugs

Treatment of PT45 cells with AdΔ19K and gemcitabine results in S-phase arrest that, as with gemcitabine alone, peaks at 36h (Figure 40B), which is in agreement with published data on the kinetics of gemcitabine-induced arrest (Shi et al., 2001). However, in contrast to gemcitabine-treated cells that escape the block and gradually arrest in G1 by 72h, AdΔ19K-infected gemcitabine-treated cells preferentially occupied S and G2/M phases preventing the G1 accumulation (Figure 40B). From 36h to 72h, fractions of AdΔ19K-infected gemcitabine-treated cells progressed through the cell-cycle, either from G1 to S or from S to G2/M phases (Figure 40B). Therefore in the presence of gemcitabine AdΔ19K promotes progression through some cell-cycle phases but avoids a G1 arrest. While the presence of Ad5tg in gemcitabine-treated cells resulted in similar cell-cycle distribution, AdΔ19K was overall more potent in promoting S-phase occupancy, suggesting that this might be a key event in triggering cell death. In this regard, a higher E1A activity, responsible for the more potent S-phase induction in AdΔ19K-infected cells, would be central to AdΔ19K-mediated sensitization to gemcitabine. Despite that the cell-cycle distribution analysis in MIAPaCa-2 cells was not performed as comprehensively as in PT45 cells, the data suggest that a similar sequence of events might occur. At the latest times post-treatment the presence of AdΔ19K significantly reduced G1 occupancy of gemcitabine-treated cells and promoted >4N cell accumulation (Figure 26), suggesting G2/M preference and again pointing towards a role of E1A.

In both PT45 and MIAPaCa-2 cells drug-induced cell-cycle arrest was accompanied by activation of the ATR/Chk1 pathway and histone H2AX phosphorylation (Figures 27-30). The kinetics of Chk1 phosphorylation

however, differed between cell lines and drugs. For example, in PT45 cells gemcitabine-induced Chk1 phosphorylation peaked at 24h and subsided through to 72h with concomitant increase in Chk2 phosphorylation (Figure 27), while irinotecan-induced Chk1 and Chk2 phosphorylation persisted from 24h to 72h (Figure 28). In MIAPaCa-2 cells Chk1 phosphorylation induced by either drug peaked at 48h (Figure 30). This suggests that the kinetics of DNA-damage response (DDR) activation do not define the ability of virus to chemosensitize cells. Activation of the ATR/Chk1 and ATM/Chk2 pathways by gemcitabine and irinotecan is in agreement with published reports (Ewald et al., 2007; Ewald et al., 2008; Karnitz et al., 2005; Morgan et al., 2005; Parsels et al., 2009; Rudolf et al., 2012; Tse et al., 2007).

Drug-induced Chk1 phosphorylation was largely unaffected by the presence of Ad∆19K (Figures 27-30), however interestingly, there was a trend towards more potent activation of Chk2 at 72h (Figure 27-28). The increase in Chk2 phosphorylation in drug- and Ad∆19K-treated PT45 cells occurred at a time where Ad∆19K efficiently downregulated Mre11 and Nbs1, diminishing their expression (Figures 31-32). Adenovirus-induced Mre11-Rad50-Nbs1 (MRN) degradation in the context of viral infection prevents activation of the DNA damage and repair that would otherwise lead to concatemerization of viral DNA (Turnell and Grand, 2012; Weitzman and Ornelles, 2005). However, in the presence of gemcitabine and irinotecan adenovirus-mediated degradation of the MRN complex was not sufficient to prevent activation of the DDR, as evidenced by the Chk1/2 phosphorylation. In parallel experiments, using an adenovirus deleted in the E4 region, we observed activation of Chk1/2 , and no degradation of the MRN complex (Dr Gioia Cherubini, unpublished data).

The observation that Chk2 activation might increase 72h following treatment with Ad∆19K and drugs at a time when the MRN complex is degraded seems conflicting. Chk2 is primarily activated by ATM and MRN is required for ATM activation (Warmerdam and Kanaar, 2010). It is possible that residual MRN expression is sufficient to activate ATM/Chk2. Alternatively, Chk2 phosphorylation could be mediated by ATR. Although the evidence for ATR-mediated Chk2 phosphorylation *in vivo* is limited, it has been suggested that in the absence of active ATM Chk2 might be activated by ATR (Matsuoka et al.,

2000; Pabla et al., 2008; Wang et al., 2006). DNA-PK-mediated phosphorylation of Chk2 and H2AX cannot be ruled out either, since both are substrates of this kinase (An et al., 2010; Li and Stern, 2005). Interestingly, DNA-PK and p53 recruitment to gemcitabine-stalled replication forks was previously associated with induction of apoptosis (Achanta et al., 2001) and irinotecan also activates DNA-PK (Davidson et al., 2012). Regardless of the upstream kinase, a strengthened Chk2 signal at a time when cell death is significantly induced would suggest accumulation of DNA damage. In immunoblot analysis, phosphorylation of histone H2AX, as a marker for DNA damage, appeared stronger in the combination treatment compared to gemcitabine or AdΔ19K alone at 72h but a significant increase was only evident at 48h (Figure 27A). On the other hand, preliminary data with irinotecan in PT45 cells suggested that the increased Chk2 activation was not accompanied by an increase in histone H2AX phosphorylation (Figure 28). In MIAPaCa-2 cells, Chk2 phosphorylation was not evaluated, however, the combination of AdΔ19K with either gemcitabine or irinotecan significantly increased histone H2AX phosphorylation at 48h compared to single treatments (Figure 29), suggesting that DNA damage might accumulate. In this cell line, preliminary data suggested that AdΔ19K downregulates Mre11 and Nbs1 at 48h post-infection both in the absence and presence of drugs (Figure 33). Nevertheless, whether an increase in Chk2 phosphorylation is associated with increased DNA damage and is implicated in the enhanced cell death, awaits further investigation.

Interestingly, in both cell lines increased phospho-histone H2AX was not readily observed in cells treated with Ad5tg and gemcitabine (Figure 27A and 29B), nor was Ad5tg-mediated downregulation of Mre11 significant in the presence of either gemcitabine or irinotecan, although slight decreases were observed (Figures 31-33). Hence, at least in the presence of gemcitabine it appears that AdΔ19K-induced Mre11 downregulation accompanied by an increase in histone H2AX signal correlates with the enhanced cell death. This notion is further supported by the finding that siRNA-mediated knockdown of Mre11 significantly enhanced cell death induced by gemcitabine and AdΔ19K in PT45 cells (Figure 35). Mre11 knockdown also potentiated cell death in response to irinotecan and AdΔ19K (Figure 35). Since knocking-down Mre11 also increased AdΔ19K

cytotoxicity and it was previously reported that Mre11 negatively affects viral DNA replication (Mathew and Bridge, 2007), we examined viral DNA amplification following Mre11 knockdown. The data suggested that in the absence of drugs silencing Mre11 shows a trend towards increased Ad∆19K replication, whereas in the presence of gemcitabine viral DNA replication showed a trend towards attenuation (Figure 36). Surprisingly however, when cells were transfected with non-targeting siRNA, gemcitabine-induced decrease in viral DNA amplification was not evident and this might imply some interference of the siRNA transfection. Therefore, the possibility that Mre11 has no significant effect on viral DNA replication regardless of the presence of drugs, needs to be further investigated, in order to determine whether the experimental conditions cause the effect or whether it is a true effect.

Silencing Mre11 did not affect cell-cycle distribution of combination-treated cells (Figure 37), implying that gemcitabine-induced cell-cycle arrest does not involve Mre11. These findings point towards a more central role of the ATR/Chk1 rather than the ATM/Chk2 pathway in mediating gemcitabine-induced DDR, regardless of the presence of virus. This is further supported by the observation that gemcitabine-induced Chk1 activation preceded that of Chk2 and Chk2 phosphorylation increased as the Chk1 signal subsided (Figure 27). In agreement with another study (Ewald et al., 2008), silencing Mre11 increased gemcitabine cytotoxicity, albeit by only 10% (Figure 35C) suggesting some role of Mre11 in survival after gemcitabine treatment. Ewald et al. did not find that MRN recruitment to gemcitabine-induced stalled replication forks was associated with the presence of strand breaks (Ewald et al., 2008). It has now been shown that MRN recruitment to stalled replication forks is involved in the re-start of stalled or collapsed forks (Costanzo, 2011). Therefore, Mre11 recruitment to gemcitabine-induced stalled forks mediates repair and recovery from the replication stress and this explains the survival role of Mre11 in response to gemcitabine. With this in mind, Ad∆19K-induced Mre11 degradation should impair the recovery from gemcitabine-induced stalled forks potentially leading to replication fork collapse and formation of strand breaks, which would explain the increase in Chk2 signal at 72h. This hypothesis was not examined in the present study but since silencing of Mre11 potentiates the cytotoxicity of the Ad∆19K and gemcitabine combination it is plausible that this

is due to accumulation of unrepaired DNA damage. A similar mechanism is expected to account for the increased cytotoxicity when Mre11 is silenced in cells treated with irinotecan and AdΔ19K, although it is unknown whether Mre11 is involved in DNA repair of irinotecan-induced damage; the DNA repair events occurring in response to irinotecan remain largely undefined.

It should be noted that the potential effect of AdΔ19K on DNA repair of drug-induced DNA damage is currently a speculation, as there is no evidence so far to suggest that DNA repair occurs following gemcitabine or irinotecan treatments. Chk1/2 signals persist up to 72h post-drug treatment, suggesting lack of DNA damage checkpoint recovery. In addition, immunofluorescence microscopy assessment of γH2AX in mitosis demonstrated that nearly all gemcitabine-treated mitotic cells exhibit γH2AX foci 48-72h post-treatment (Figure 39B) suggesting failure to repair DNA damage before mitotic entry. Addition of AdΔ19K significantly increased the pan-chromosomal γH2AX signal in gemcitabine-treated cells (Figure 39C), which could suggest a global accumulation of DNA damage prior to apoptosis. This is further supported by the observation that the pan-chromosomal γH2AX staining in cells treated with AdΔ19K and gemcitabine was increased from 48h to 72h and was significantly stronger compared to Ad5tg combined with gemcitabine. Co-localisation studies with other DDR proteins and utilisation of pan-caspase inhibitors should provide some insights into the significance of the pan-chromosomal γH2AX staining in mitotic cells in response to AdΔ19K and gemcitabine in future studies. Pan-chromosomal γH2AX staining patterns in mitotic cells are largely unexplored and the only literature reports describing a global H2AX phosphorylation pattern refer to interphase cells. The pan-nuclear H2AX phosphorylation in interphase cells has been associated with DNA repair following UV radiation, pre-apoptotic responses, replication stress or checkpoint abrogation (Ewald et al., 2007; Marti et al., 2006; Murga et al., 2009; Solier and Pommier, 2014).

In immunofluorescence microscopy analysis of phospho-histone H2AX in interphase cells, γH2AX foci marked sites of gemcitabine-induced stalled replication forks (Figure 38), as the number of cells displaying γH2AX foci was equal to the number of cells arrested in S-phase at the time, in agreement with

literature reports (Ewald et al., 2007; Karnitz et al., 2005; Parsels et al., 2009). γH2AX foci were also detected in AdΔ19K-infected cells (Figure 38). The presence of foci is in contrast to the widespread nuclear-wide accumulation of phospho-histone H2AX in adenovirus-infected cells reported by Nichols et al. (Nichols et al., 2009). However other studies did observe foci formation instead of the diffused nuclear signal (Connell et al., 2011; Karen and Hearing, 2011). The reason behind the discrepancies in γH2AX signal distribution after adenovirus infection is not well understood; the H2AX phosphorylation patterns might be cell-context specific. Nevertheless, the γH2AX discrete nuclear foci detected in AdΔ19K-infected cells are consistent with DDR foci, and might suggest the presence of strand breaks or replication stress. Indeed it was previously shown that adenovirus can induce host DNA strand breaks, attributed to E1A activity (Caporossi and Bacchetti, 1990; Connell et al., 2011). The presence of AdΔ19K in gemcitabine-treated cells did not increase the number of cells displaying γH2AX foci nor the total H2AX signal intensity up to 36h post-treatment (Figure 38). Yet, since γH2AX foci likely marked sites of gemcitabine-induced stalled replication forks, addition of AdΔ19K should not be expected to increase replication stalling. If DNA replication was affected by AdΔ19K the effect would rather be increased replication fork progression (Singhal et al., 2013). γH2AX foci assessment by immunofluorescence microscopy was not performed at 48h, which was the time histone H2AX phosphorylation increased in immunoblotting in AdΔ19K and gemcitabine treated cells. However pilot immunofluorescence microscopy evaluation of γH2AX foci at this time suggested signal saturation with difficulties in observing additive effects between AdΔ19K and gemcitabine. In retrospect, with the presence of stalled replication forks it is difficult to assess occurrence of DNA damage in the form of strand breaks using γH2AX foci assays. Moreover, the presence of viral DNA, stalled replication forks and the initiation of cell death at 48h post-treatment generating DNA fragments would likely interfere with assessment of DNA strand breaks when other methods, besides γH2AX assays, are used; for example TUNEL and comet assays.

Overall, it appears that a fraction of gemcitabine-arrested cells escape the cell-cycle block without apparent DNA repair as they enter mitosis with γH2AX foci.

This suggests adaptation to the checkpoint response. The possibility that DNA repair is attempted but not successfully completed or that NHEJ or NER repair occurs at later times in G1 phase is not excluded. Cells treated with gemcitabine and AdΔ19K might accumulate more DNA damage, although further research is required to confirm this. Any attempted DNA repair, either Mre11- or NHEJ-dependent, is expected to be inhibited by the presence of AdΔ19K further accumulating DNA damage.

4.6. Claspin as a target of AdΔ19K and gemcitabine treatment

The present study has identified the DDR protein Claspin as cellular factor targeted during treatment with AdΔ19K and gemcitabine (Figure 63). In PT45 cells, gemcitabine induced a 2-3-fold increase in Claspin mRNA transcript levels paralleled by increased protein levels (Figures 41 and 47). Similarly, irinotecan treatment in PT45 cells, and gemcitabine and irinotecan treatments in MIAPaCa-2 cells upregulated claspin expression (Figures 41-42). In drug-treated PT45 cells the presence of AdΔ19K, but not Ad5tg, prevented Claspin accumulation at both 24h and 48h post-treatment (Figure 41). The inhibition was demonstrated to be the result of both decreased Claspin synthesis and stability. Addition of AdΔ19K in gemcitabine-treated PT45 cells prevented accumulation of newly synthesised claspin following MG132-mediated proteasomal inhibition (Figure 46). Analysis of Claspin mRNA expression confirmed that AdΔ19K, but not Ad5tg, impairs gemcitabine-induced upregulation of claspin mRNA at 48h (Figure 47). Claspin expression is cell-cycle regulated, with levels peaking in S/G2-phases followed by a rapid proteasomal degradation before the onset of mitosis (Bennett and Clarke, 2006; Chini and Chen, 2003). Therefore the drug-induced upregulation of claspin expression can be attributed to the S-phase arrest and activation of the ATR/Chk1 pathway (Figure 63). However, the decrease in claspin expression observed when AdΔ19K is present in gemcitabine-treated cells cannot be the result of cell-cycle changes since combination-treated cells show the same cell-cycle distribution as gemcitabine. Claspin transcription is regulated by the NF-κB and E2F1 transcription factors (Iwanaga et al., 2006; Kenneth et al., 2010). Whereas E2F1-mediated transcription is induced by adenovirus, NF-κB-

dependent transcription is repressed through suppression of IKK activity by E1A (Cook et al., 2002; Shao et al., 1999; Shao et al., 1997). Consequently, it is likely that AdΔ19K-mediated suppression of Claspin synthesis in the presence of gemcitabine is mediated through E1A-dependent inhibition of NF-κB (Figure 63). The higher E1A expression from AdΔ19K compared to Ad5tg could then explain the failure of Ad5tg to inhibit Claspin expression. The possibility that decreased Claspin expression could be the mere consequence of combination-treated cells entering mitosis, since Claspin expression is lost in mitotic cells (Mamely et al., 2006), is not excluded, but seems unlikely. The higher mitotic index observed in combination-treated synchronised cells compared to gemcitabine alone (Figure 40D) was seen with both Ad5tg and AdΔ19K combinations with gemcitabine, however, claspin expression was only decreased in response to AdΔ19K and gemcitabine.

In addition to claspin expression, cycloheximide-chase assays demonstrated that claspin stability is significantly reduced in PT45 cells treated with AdΔ19K and gemcitabine (Figure 45). Following DNA damage and/or replication stress Aurora-A-dependent activation of Plk1 targets Claspin for degradation through the ubiquitin ligase complex β-TrCP-SCF and this event is required for checkpoint recovery and mitotic entry (Bennett and Clarke, 2006; Freire et al., 2006; Macurek et al., 2008; Mailand et al., 2006; Mamely et al., 2006). AdΔ19K induced phosphorylation of Plk1 at 48h that persisted to a lesser extent in the presence of drugs (Figure 43). Therefore the reduced stability of claspin in response to AdΔ19K and gemcitabine is likely the consequence of accelerated Plk1-mediated claspin degradation. This suggests that following DDR activation AdΔ19K promotes mitotic entry of gemcitabine-treated cells by accelerating the degradation of claspin (Figure 63).

Ad5tg was also able to induce Plk1 phosphorylation, albeit to significantly smaller degree than AdΔ19K, and in the presence of gemcitabine significant Plk1 phosphorylation was not observed. To the best of my knowledge, Plk1 phosphorylation during adenovirus infection has not been previously reported. The phosphorylation was specifically induced at 48h post-infection and is probably associated with increased mitotic entry as compared to mock-infected synchronised cells (Figure 40D). Preliminary data also suggested that Plk1

phosphorylation was paralleled by Aurora-A stabilization (data not shown). One possibility is that the induced Plk1 phosphorylation is merely the consequence of mitotic entry. However the same mitotic index was observed in combination-treated cells that did not display as strong Plk1 phosphorylation as adenovirus alone. In addition, there were no differences in the mitotic index of Ad5tg compared to AdΔ19K at a time when Plk1 phosphorylation was stronger in AdΔ19K-infected cells (Figure 40D). Alternatively, adenovirus-mediated potential disruption of PP2A phosphatase activity through E4orf4 could stabilize phospho-Plk1, as PP2A was shown to de-phosphorylate Plk1, at least in response to DNA damage (Jang et al., 2007).

Despite that AdΔ19K blocked gemcitabine-induced claspin protein accumulation both at 24h and 48h, reduction in claspin mRNA levels or stability was not observed at 24h post-treatment. The mechanism leading to decreased protein levels at 24h remains to be elucidated. Nonetheless, the observation that in the presence of drugs AdΔ19K, but not Ad5tg, exerted the effects on claspin expression and stability suggests that this mechanism might be associated with the enhanced cell death. Indeed siRNA-mediated silencing of Claspin potentiated cell death induced by AdΔ19K and DNA-damaging drugs (Figure 49). The knockdown did not significantly affect drug cytotoxicity but appeared to enhance AdΔ19K-induced cell death. Assessment of viral DNA amplification suggested that the enhanced cytotoxicity of the combination treatment when Claspin is silenced, is independent of viral DNA replication (Figure 50). Cell cycle analysis in claspin knocked-down cells revealed an increase in the G1 cell fraction accompanied by a decrease in S-phase arrest at 24h and an increase in the mitotic index at 48h post-treatment with AdΔ19K and gemcitabine (Figure 51). Remarkably, the effect of claspin knockdown on cell-cycle distribution was specific for AdΔ19K and gemcitabine. The inhibition of S-phase entry suggests that Claspin is important for the S-phase induction in cells treated with AdΔ19K and gemcitabine. Moreover, Claspin appears to regulate mitotic entry of combination-treated cells, since Claspin knockdown increased the mitotic index. These findings further support the notion that AdΔ19K-induced inhibition of Claspin accumulation in the presence of gemcitabine mediates the increased mitotic entry of combination-treated cells.

In contrast to the findings with Claspin knockdown, pharmacological inhibition of Plk1 did not inhibit cell death induced by AdΔ19K and gemcitabine and rather appeared to enhance their cytotoxicity (Figure 57). However, similar to claspin knockdown the inhibitor decreased the S-phase arrest and increased the mitotic index of combination-treated cells and additionally enhanced the formation of polyploid (>4N) cells (Figure 57D). This could suggest that the activity of Plk1 and by extension the degradation of claspin is not important for the combination treatment to induce cell death. On the other hand, the cell-cycle effects of Plk1 inhibition might have been sufficient to increase cytotoxicity and perhaps masked the effects of merely inhibiting Plk1-induced claspin degradation on cell death. Expression of a degradation-resistant Claspin mutant would aid to understand whether Claspin degradation is an important event in the enhanced cell death.

A perplexing issue in these studies is the Claspin-Chk1 relationship. Since Claspin is required for efficient ATR-dependent Chk1 activation, Claspin downregulation is expected to impact Chk1 activation; yet Chk1 phosphorylation was largely unaffected in response to AdΔ19K and gemcitabine. However, viral infection is limited to 30-50% of cells and it is likely that the remaining cells express high levels of Chk1. Activation of Chk1 was not determined when Claspin was knocked-down. Of note, a study reported that Claspin depletion does not perturb initial Chk1 phosphorylation but it rather affects the sustainability of Chk1 signal at later times in the DDR (Chini et al., 2006). Certainly phospho-Chk1 levels were not normalised to total Chk1 expression, which has not been assessed in these studies, thereby increases or decreases in Chk1 phosphorylation might have been missed. In addition, the immunoblot analysis was performed in the presence of 100ppc of adenovirus, while during the Claspin studies a higher dose of virus (300ppc) was used. It is therefore possible that at higher virus doses the effects on Chk1 phosphorylation might become apparent.

In MIAPaCa-2 cells AdΔ19K-induced downregulation of claspin in the presence of drugs was far less potent than in PT45 cells and was similar to the effect of Ad5tg (Figure 42). It is possible that adenovirus is less efficient in suppressing NF-κB-dependent transcription in these cells. It is interesting that MRN

downregulation was also less efficient in these cells compared to PT45. Therefore it seems that adenovirus-mediated cell-cycle effects in the presence of drugs are attenuated in MIAPaCa-2 compared to PT45 cells. Certainly, the possibility that Mre11 and Caspin downregulation might not be crucially involved in the potent cell death induced by AdΔ19K and DNA damaging-drugs in MIAPaCa-2 cells cannot be ruled out. Mre11 and Claspin knockdown studies in these cells should provide some answers.

An obvious question arising though these studies is whether adenovirus regulates claspin in the absence of drugs. I did not observe significant changes in the expression or stability of Claspin in virus-infected cells without drug treatment. There was a trend towards decreased claspin half-life in AdΔ19K-infected cells, but it is probably the consequence of increased Plk1 phosphorylation. It is possible that significant upregulation of Claspin is necessary for virus-induced effects to become apparent, since basal Claspin levels are relatively low. Alternatively, the increased viral uptake and subsequent higher E1A expression in the presence of gemcitabine potentiates the virus-induced effects on Claspin. The E7 oncoprotein of human papillomavirus (HPV) was recently shown to increase the proteasomal degradation of claspin, thereby attenuating DNA damage responses and promoting mitotic entry (Spardy et al., 2009). Whether claspin is a target of adenovirus during infection requires further investigation.

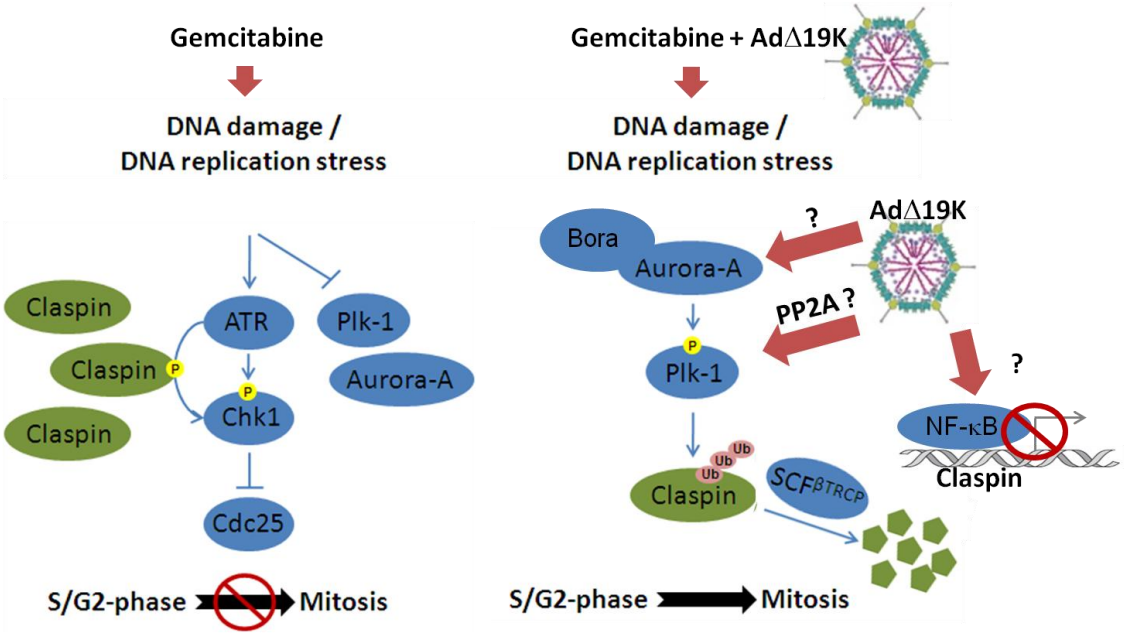

Figure 63: Proposed model of Claspin regulation in response to gemcitabine and AdΔ19K. In response to gemcitabine-induced DNA damage/replication stress Claspin accumulates and sustains the ATR-mediated phosphorylation of Chk1 limiting mitotic entry. In the presence of AdΔ19K gemcitabine-induced accumulation of Claspin is prevented, as a result of both decreased expression and increased proteolytic turnover through the Bora-Aurora-A/Plk1 pathway. AdΔ19K might act to suppress NF-κB-mediated transcriptional activation of Claspin, thereby keeping Claspin expression at basal levels. In addition, AdΔ19K induces the phosphorylation of Plk1. This might occur through AdΔ19K-mediated disruption of PP2A phosphatase activity towards Plk1, leading to constitutive phosphorylation and activation of Plk1. Alternatively, AdΔ19K might act to stabilize Aurora-A and its binding partner Bora, leading to overactivation of the Aurora-A/Plk1 pathway. The protein stabilization could potentially occur through interference with the activity of APC/C.

4.7. Effects of the combination treatment on mitosis

Phospho-histone H3 analysis by flow-cytometry in synchronised PT45 cells demonstrated that the presence of AdΔ19K in gemcitabine-treated cells increased the mitotic index following escape from the cell-cycle block (Figure 40D). The effect was also observed in mitotic index analysis in unsynchronised cells (Figures 37D and 51D). This is in line with accelerated Claspin degradation which promotes mitotic entry. Claspin knockdown further increased the mitotic index of combination-treated cells. Despite these consistent observations during phospho-histone H3 analysis, live-cell imaging did not confirm accelerated mitotic entry of combination-treated cells compared to gemcitabine alone (Figure 58). In fact, gemcitabine-treated cells appeared to initiate mitosis earlier whereas the bulk of mitotic entry in combination-treated cells occurred at later times (Figure 58A and B). It is true that there was high variability between the three independent time-lapse studies in terms of mitotic index and cell death capacity, primarily arising from variations in cell behaviour. In addition, the experimental conditions were toxic to a certain extent as judged by the increased cell killing of mock-infected cells (Figure 61A). The toxicity might had an impact on the mitotic index, particularly in the instance of multiple growth-limiting conditions; thymidine pre-treatment for cell synchronisation, virus infection and gemcitabine treatment. Another possibility is that the lack of a marker for infection in the time-lapse microscopy studies prevented differences between gemcitabine and infected gemcitabine-treated cells from becoming apparent. In the phospho-histone H3 mitotic index analysis staining for E1A expression permitted the selective assessment of E1A-positive cells as opposed to total infected and uninfected cells in the population.

Perhaps the scenario of false positive phospho-histone H3 cells detected by flow cytometry should not be ruled out either. Histone H3 becomes phosphorylated on Ser10 by Aurora-A/B during mitotic chromosome condensation (Crosio et al., 2002; Prigent and Dimitrov, 2003), and phospho-histone H3 is a widely used marker of mitosis. However, histone H3 phosphorylation has been also detected in apoptotic cells and was associated with chromatin condensation (Park and Kim, 2012). The increases in the phospho-histone H3 phosphorylation in combination-treated cells versus

gemcitabine occurred at a time (48-72h) where cell death is induced and apoptotic assays showed caspase-3 activation in G2/M cells. On the other hand, histone H3 phosphorylation was specifically detected in cells with 4N and >4N DNA content (see Appendix 3; section 5.1.) when cells with non-intact plasma membranes, that is dying cells, had been excluded from the analysis; this supports the notion that phosphorylation represents mitotic entry rather than apoptosis.

The consequences of mitotic entry following escape from the gemcitabine-induced cell-cycle block were detrimental. Time-lapse microscopy experiments revealed that the majority of gemcitabine-treated cells arrested in mitosis for hours (Figure 58C) with difficulties in chromosome alignment, suggesting activation of the SAC. Chromosome alignment issues are likely the result of damaged DNA compromising the correct stable attachment of kinetochores to microtubules (Hayashi and Karlseder, 2013; Rieder and Maiato, 2004). Another abnormality that might have contributed to mitotic delay is the presence of multipolar spindles. Immunofluorescence microscopy studies had suggested that a fraction of cells treated with gemcitabine exhibit multipolar spindles (Figure 52). Multipolar spindles can arise though over-duplication or splitting of centrioles, the paired structure that makes up each centrosome (Gergely and Basto, 2008; Maiato and Logarinho, 2014). Several studies reported that S/G2 arrest following DNA damage can result in uncoupling of DNA replication and centrosome duplication, resulting in centrosome over-duplication (Balczon et al., 1995; Collins et al., 2010; Kuriyama et al., 2007; Nigg, 2002; Prosser et al., 2009). A role for Plk1 in coordinating the centriole duplication cycle with the cell cycle has been suggested (Loncarek et al., 2010). Centriole splitting ('disengagement'), which can also result from DNA damage, can permit the duplication of centrioles leading to centrosome amplification (Saladino et al., 2009). Damaged DNA and mitotic arrest can also lead to centrosome splitting during mitosis (Hut et al., 2003; Maiato and Logarinho, 2014). The literature therefore suggests that gemcitabine-induced spindle multipolarity could either be the result of centriole splitting during mitosis or centriole splitting and/or overduplication during the S-phase arrest. Multipolar spindles *per se* do not trigger SAC activation, but can delay mitosis through the perturbation of the

microtubule-kinetochore attachment (Gergely and Basto, 2008; Kwon et al., 2008; Rieder and Maiato, 2004).

Adenoviral infection in the presence of gemcitabine appeared to increase the frequency of spindle multipolarity by nearly 2-fold both in PT45 and MIAPaCa-2 cells (Figure 52) and the induction of spindle multipolarity by the combination treatment could be regarded as a more-than-additive effect. Adenovirus E1A is able to induce centrosome amplification through deregulation of the RanGTPase network (De Luca et al., 2003), thus accounting for the increased spindle multipolarity in the combination treatments. In time-lapse microscopy experiments the presence of AdΔ19K in gemcitabine-treated cells enhanced the mitotic arrest (median mitotic duration 4.5h versus 2.75h in gemcitabine-treated cells; Figure 58C), suggesting that combination-treated cells took longer to satisfy the SAC. This could be a consequence of increased frequency of cells exhibiting multipolar spindles observed in immunofluorescence microscopy studies and/or increased DNA damage. On the other hand, adenovirus infection might be sufficient to increase mitotic delay. A study reported prolonged mitosis following E1A expression (Hernando et al., 2004) and E1A-mediated perturbation of p300/CBP-APC/C complexes could result in prolonged mitosis due to failure of APC/C to target Cyclin B and other mitotic proteins for degradation required for mitotic exit (Turnell and Mymryk, 2006). Moreover, given that TIF1γ knockdown was reported to disrupt APC/C^{Cdc20} function leading to SAC activation, prolonged mitosis and chromosome alignment errors (Sedgwick et al., 2013), E4orf3-mediated degradation of TIF1γ is likely to result in a similar phenotype.

Consistent with the presence of spindle multipolarity, nearly half of gemcitabine-treated mitotic cells underwent multipolar instead of bipolar divisions (Figure 59B). Despite that it has been reported that supernumerary centrosomes can often cluster to favour bipolar divisions, the cell capacity of this mechanism varies between cell lines (Marthiens et al., 2012) and it appears that PT45 cells are not efficient in clustering their extra centrosomes. The presence of AdΔ19K in gemcitabine-treated cells enhanced the frequency of multipolar anaphases (Figure 59B), consistent with the observation that combination-treated cells show increased frequency of spindle multipolarity. In addition to multipolar

divisions, gemcitabine treatment resulted in a very high frequency of segregation errors, such as anaphase bridges and lagging chromosomes, and in the presence of AdΔ19K all mitotic cells exhibited such errors (Figure 59B). This was somewhat expected, given that accumulating experimental evidence suggests that such errors can arise from unresolved S-phase DNA structures and replication stress (Chan et al., 2009; Ichijima et al., 2010; Mankouri et al., 2013). Regarding adenovirus, Hernando et al. previously reported that E1A expression resulted in chromosome segregation defects (Hernando et al., 2004). Other studies reported that adenovirus can cause DNA strand breaks (Caporossi and Bacchetti, 1990; Connell et al., 2011) and together with the stress E1A imposes on DNA replication (Singhal et al., 2013), it is highly likely that adenovirus-infected mitotic cells would exhibit chromosome segregation errors further contributing to gemcitabine-induced aberrant mitosis.

Cytokinesis failure was another feature of gemcitabine-induced aberrant mitosis that showed a trend towards increase in the presence of AdΔ19K (Figure 59C). The observed failed cytokinesis was predominantly a defect in midbody abscission and could have resulted from lagging or bridging chromosomes trapped in the cleavage furrow (Ganem and Pellman, 2012; Hayashi and Karlseder, 2013; Janssen et al., 2011). Cytokinesis failure was mainly associated with multipolar divisions, which explains the increased frequency of cytokinesis failure in combination-treated cells. Infection with the *dl*922-947 oncolytic mutant was previously reported to result in spindle multipolarity and cytokinesis failure (Connell et al., 2008). As a consequence of gemcitabine-induced chromosome segregation defects, micronucleated and multinucleated daughter cells were generated (Figure 60). Multinucleation was frequently associated with cytokinesis failure, but not restricted to it; multiple fragmented nuclei, arising from chromosome breakage during segregation, were also being generated, suggestive of compromised DNA integrity. In combination-treated cells only a minority of daughter cells were mononucleated and a higher frequency of multinucleation was observed compared to gemcitabine. The literature suggests that multinucleated cells can be eliminated through death but can also survive and either arrest in G1 or continue cycling, particularly in a p53-deficient cell-context (Decordier et al., 2008). In the current studies I did occasionally observe both micronucleated and multinucleated cells entering

mitosis. In immunofluorescence microscopy experiments these multinucleated cells were observed to accumulate over time in response to gemcitabine alone (Figure 53B), suggesting that they fail to die at least up to 96h post-treatment. It is highly likely that multinucleated cells generated following gemcitabine treatment arrest in G1, given the gradual increase of G1 cell fraction in response to gemcitabine (Figure 40). Up to 96h the post-division survival of gemcitabine-treated cells was approximately 20% (Figure 62B). Considering the high frequency of mitotic errors, the generation of micro- and multi-nucleated daughter cells and the evidence of post-mitotic survival, gemcitabine treatment could lead to generation of aneuploid and polyploid cells. The presence of AdΔ19K in gemcitabine-treated cells prevented accumulation of multinucleated cells (Figure 53B) and the post-mitotic survival of combination-treated cells was diminished (Figure 62B). This evidence together with the fact that infected cells are eventually lysed, suggests that combination of gemcitabine with AdΔ19K would be essential for preventing the survival of polyploid and aneuploid cells.

It should be noted that throughout the time-lapse microscopy studies AdΔ19K alone did not significantly affect mitotic progression. However, modest trends towards increased frequency of segregation errors and multipolar divisions were observed. An obvious drawback of the study was the lack of a marker for infection, which would have permitted selective assessment of infected cells and accurate evaluation of the effects of adenovirus on mitosis. Nevertheless, the effects of adding AdΔ19K in gemcitabine-treated cells were apparent in most instances, perhaps due to increased viral uptake and gene expression. Some of the mitotic aberrations observed in the presence of AdΔ19K, such as cytokinesis failure and multinucleation, might be a consequence of E4orf4-mediated disruption of PP2A activity. Overexpression of AdE4orf4 was shown to induce G2/M arrest followed by formation of micro- and multi-nucleated cells, cytokinesis failure, mitotic catastrophe and cell death (Cabon et al., 2013; Li et al., 2009b), and E4orf4 cytotoxicity was previously shown to depend on its interaction with PP2A (Li et al., 2009a; Li et al., 2009b; Shtrichman et al., 1999; Shtrichman et al., 2000). The current study has not addressed whether wild type Ad5 induces similar mitotic aberrations, but it is possible that, due to higher E1A expression, AdΔ19K expresses higher levels of E4orf4 and therefore induces more mitotic aberrations than wild type Ad5.

Cell viability assays suggested that pharmacological induction of mitotic arrest by small molecule inhibitors of Eg5 and Plk1 enhanced cell death induced by the combination of AdΔ19K and gemcitabine (Figure 54 and 57). Both inhibitors increased the mitotic index and decreased S-phase arrest of combination-treated cells (Figure 54E and 57D). Importantly, the inhibitors did not affect the cytotoxicity of gemcitabine in the absence of virus (Figure 54C and 57C). These findings suggest that mitotic accumulation of combination-treated cells is important for cell death induction. It is possible that prolonged mitosis enhances the cell death by further causing DNA damage, as suggested by accumulating evidence in the literature (Ganem and Pellman, 2012; Heijink et al., 2013). Despite that pharmacological induction of mitotic arrest consistently augmented cell killing in response to AdΔ19K and gemcitabine, the reverse, that is acceleration of mitosis, did not yield as consistent effects on the cytotoxicity of the combination treatment. SAC impairment and acceleration of mitosis by an Mps1 inhibitor almost completely prevented the enhanced cell death (Figure 55A/B), whereas acceleration of mitosis through inhibition of Aurora-B only showed a modest trend towards attenuation of cell death induced by AdΔ19K and gemcitabine (Figure 56B). While the inhibitors did not significantly affect gemcitabine cytotoxicity, AdΔ19K cytotoxicity was affected in opposite manners by the inhibitors; Mps1 inhibition impaired AdΔ19K cytotoxicity and Aurora-B inhibition enhanced it (Figure 55-56). These opposing effects on virus-induced cell death might explain the differential impact of the inhibitors on the killing of combination-treated cells. Nonetheless, since both inhibitors accelerated mitosis, it is possible that abrogation of prolonged mitosis *per se* does not impair cell death in response to AdΔ19K and gemcitabine. In this regard, abrogation of the enhanced cell death through Mps1 inhibition might indicate that Mps1 is involved in the induction of cell death by AdΔ19K and gemcitabine independently of its functions in mitosis. Interestingly, some literature reports implicated Mps1 in the DDR (Liu and Winey, 2012). Mps1 was shown to be important for efficient checkpoint-mediated arrest by phosphorylating and activating Chk2 (Wei et al., 2005) Additionally, in response to IR Chk2 phosphorylates and stabilizes Mps1, which forms nuclear foci that colocalize partially with γ-H2AX (Yeh et al., 2009). In my studies, Mps1 inhibition showed a modest trend towards increased S-phase arrest of combination-treated cells at 48-72h, but this weak cell-cycle effect is unlikely to account for the 2-3-fold

effect on cell death (Figure 55). It is currently not well understood how Aurora-B or Mps1 inhibition might impact on cell death in response to the combination treatment and clearly further investigation is required.

Finally, an interesting finding of the present study is that the combination of AdΔ19K with the Eg5 inhibitor monastrol greatly enhances cell killing of pancreatic cancer cells. Remarkably, monastrol reduced the EC_{50} value of AdΔ19K by 90% and displayed greater synergy with AdΔ19K than gemcitabine (Figure 54A/B). Plk1 and Aurora-B inhibitors also potentiated cell death when combined with AdΔ19K, albeit to a lesser extent than monastrol. The same Aurora-B inhibitor was previously shown to significantly inhibit the growth of anaplastic thyroid carcinoma xenografts in combination with the oncolytic adenovirus *dl*922-947 (Libertini et al., 2011). Therefore, the combination of oncolytic adenoviruses with mitotic inhibitors could be a promising therapeutic avenue for pancreatic cancers.

4.8. Concluding remarks

Data presented in the current study suggest that the more-than-additive and time-dependent cell death in response to AdΔ19K and DNA-damaging drugs occurs both in cells blocked in S and G2 phases and following an aberrant, prolonged passage through mitosis (Figure 64). The findings indicate that AdΔ19K cannot prevent the activation of the DNA damage checkpoint responses elicited by the drugs, but it downregulates the DNA damage response factors Mre11 and Claspin, contributing to the induction of cell death. Mre11 downregulation is likely to prevent any attempted DNA repair and this might accumulate DNA damage, whereas AdΔ19K-mediated downregulation of Claspin in the presence of drugs contributes to cell death by promoting mitotic entry (Figure 64). Moreover, AdΔ19K enhances gemcitabine-induced aberrant mitosis, characterised by spindle multipolarity, chromosome alignment issues and subsequent SAC activation, chromosome missegregation errors, cytokinesis failure and formation of micro- and multi-nucleated cells (Figure 64). Importantly though, Ad∆19K prevents the gemcitabine-induced accumulation of multinucleated cells and diminishes post-mitotic survival of daughter cells.

Through these studies cellular pathways and factors involved in the synergistic cell killing were identified that could be explored in the future to develop improved targeted therapies for pancreatic cancer. Moreover, these studies revealed potential novel cellular factors that are affected by adenovirus and demonstrated the potential synergistic cytotoxicity of Ad∆19K combined with mitotic inhibitors, such as the Eg5 inhibitor monastrol or the Plk1 inhibitor BI-2536, in pancreatic cancer cells.

I conclude that the ability of Ad∆19K to deregulate DNA damage and repair responses and promote aberrant mitosis is crucial for triggering cell killing in response to low doses of DNA-damaging drugs (Figure 64). This conclusion is in agreement with other studies reporting that adenovirus-induced chemosensitization is mediated through abrogation of DNA repair mechanisms (Kuroda et al., 2010; Rajecki et al., 2009) or induction of mitotic aberrations (Ingemarsdotter et al., 2010). A number of studies reported that adenovirus-induced S-phase accumulation enhances the efficacy of DNA-damaging drugs, although most studies did not assess S-phase in cells treated with the combination of drug and virus (Liu et al., 2009; Ma et al., 2010; Wang et al., 2013; Wang et al., 2011). The presence of Ad∆19K in gemcitabine-treated cells increased S-phase cell occupancy at 12h and after 48h post-treatment (Figure 40B). The initial increase in S-phase could have enhanced the efficacy of gemcitabine. In addition, drug-induced increased viral uptake and subsequent increased expression of E1A and other early viral proteins, likely enhances the cell-cycle effects of Ad∆19K contributing to the more-than-additive cell death in response to the combination treatment. Increased E1A activity in particular, is possibly essential for enhancing the apoptotic cell death, since several studies demonstrated that E1A is sufficient for chemosensitization (Cheong et al., 2008; Lee et al., 2003; Miranda et al., 2012; Radhakrishnan et al., 2010; Ueno et al., 2000).

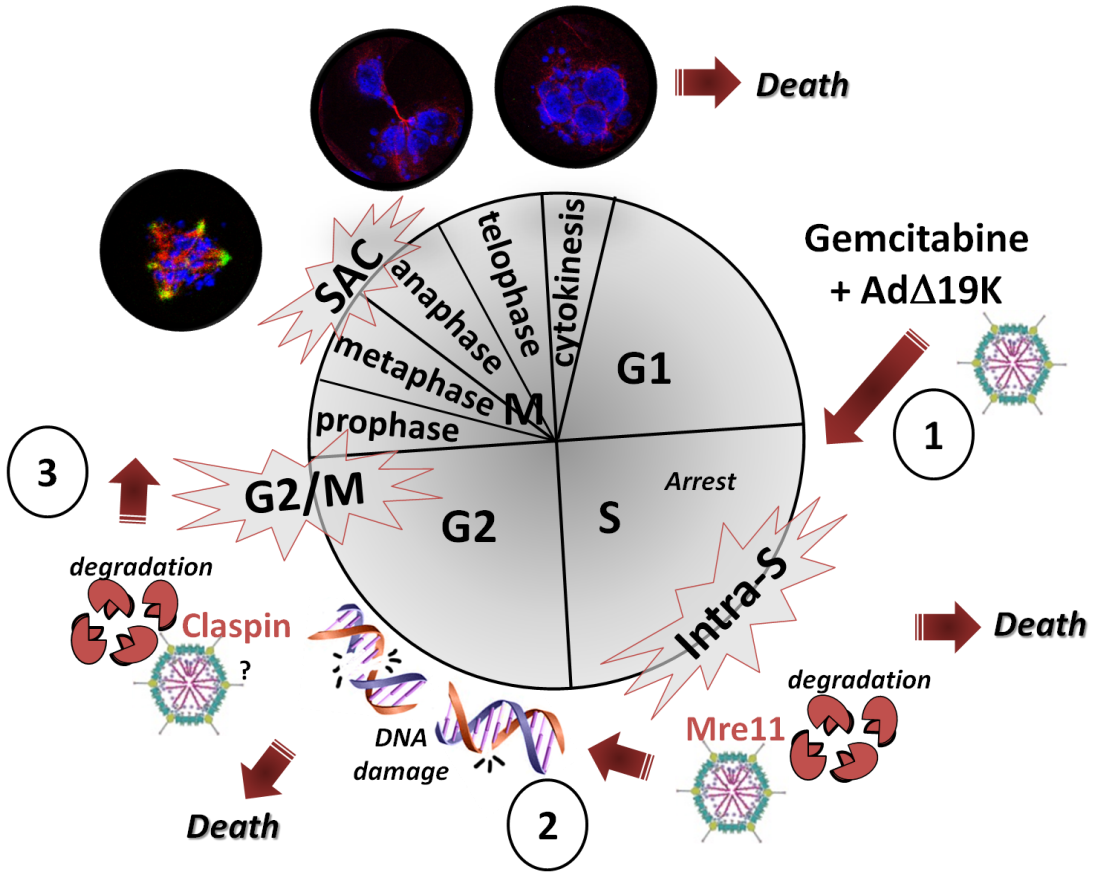

Figure 64: Proposed sequence of events leading to cell death in response to gemcitabine and AdΔ19K. Treatment with AdΔ19K and gemcitabine induces activation of the DNA damage response and causes S-phase arrest (step 1). AdΔ19K induces the degradation of Mre11, possibly leading to abrogation of DNA repair and accumulation of DNA damage (step 2). This contributes to cell death. The presence of AdΔ19K in gemcitabine-treated cells prevents accumulation of Claspin through decreased synthesis and increased degradation, thereby promoting mitotic entry of combination-treated cells (step 3). During mitosis, AdΔ19K enhances gemcitabine-induced mitotic aberrations, leading to increased spindle multipolarity, chromosome alignment issues and subsequent SAC activation, chromosome missegregation errors, cytokinesis failure and formation of micro- and multi-nucleated cells. Passage through mitosis further enhances cell death in response to AdΔ19K and gemcitabine. Not depicted on the figure is the increased expression of adenovirus E1A, which is expected to contribute to the cell-cycle deregulation and increased apoptosis.

4.9. Future directions

To support the proposed mechanisms for the enhanced cell killing in response to AdΔ19K and DNA-damaging drugs, it will be essential to establish that the combination treatment results in increased DNA damage. Methods other than γH2AX assays should be employed, for example pulsed-field gel electrophoresis. In addition, it will be important to demonstrate DNA repair responses following drug treatment, in order to reinforce the notion that AdΔ19K-induced abrogation of DNA repair processes contributes to chemosensitization. Moreover, the effects of AdΔ19K-induced downregulation of Claspin on activation and sustainability of the ATR/Chk1 signalling should be further investigated, for example through a comprehensive time-course analysis of Claspin and Chk1 phosphorylation status. It will be interesting to further investigate the significance of the increased Chk2 signal in response to the combination treatment, for example by using small molecule inhibitors. Finally, the proposed AdΔ19K-induced increased mitotic entry of drug-treated cells should be confirmed using other mitotic markers and immunofluorescence microscopy methods and examined in the presence of irinotecan.

In future studies, it will be interesting to determine DNA replication dynamics in the presence of AdΔ19K and gemcitabine in order to better understand the mechanisms of action of the combination treatment. Identifying other DDR factors affected by the adenovirus in the presence of drugs, is intriguing too. For instance, the RecQ helicase BLM has been implicated in the processing and recovery of stalled replication forks (Davies et al., 2007; Ouyang et al., 2013; Wu, 2007) and BLM is degraded by adenovirus (Orazio et al., 2011). Future work should also examine the possibility that Mps1 is an essential factor for the enhanced cell death, using siRNA-mediated knockdown and overexpression assays, and delineate the mechanisms involved. At last, it will be interesting to determine whether Claspin and/or the Aurora-A/Plk1 pathway are targets of adenovirus in the absence of drugs.

In light of the findings presented in this thesis, the replication-selective oncolytic adenovirus AdΔΔ could be further engineered in order to potentiate the ability of the E1B19K deletion to enhance chemodrug-induced cell death. Knockdown or

overexpression of identified targets of the combination treatment through insertion of target sequences into the AdΔΔ backbone could be employed. The deletion of E1B19K in the AdΔ19K and AdΔΔ viruses is quite small (approximately 220bp), therefore a further deletion of a viral gene should be introduced in order to accommodate target sequences. One possibility is to delete the E3gp19K gene, which would allow the insertion of an approximately 2000 bp sequence under the control of the E1A-dependent E3 promoter. Deletion of E3gp19K was previously shown to result in increased viral replication and antitumor efficacy, due to activation of cytotoxic T-cells (Wang et al., 2003), and it therefore seems to be beneficiary. Since downregulation of Mre11 and Claspin was demonstrated in this study to enhance cell death induced by E1B19K-deleted adenoviruses and DNA damaging drugs, incorporation of shRNA sequences against Mre11 and Claspin could further increase the cytotoxicity of the combination treatment. In addition, since pharmacological inhibition of Eg5 and Plk1 also potentiated cell death induced by AdΔ19K and gemcitabine, shRNAs targeting Eg5 and Plk1 could also be considered for incorporation into the AdΔΔ virus. Alternatively, insertion of genes whose expression can promote mitotic entry or induce activation of the Aurora-A/Plk1 pathway resulting in Claspin degradation, could enhance mitotic catastrophe induced by the combination treatment. Examples of such genes are the Aurora-A activating cofactors Bora and TPX2.

CHAPTER 5: APPENDIX & REFERENCES

5.1. Appendices

APPENDIX 1: Cell-cycle specific apoptosis - Representative experiments

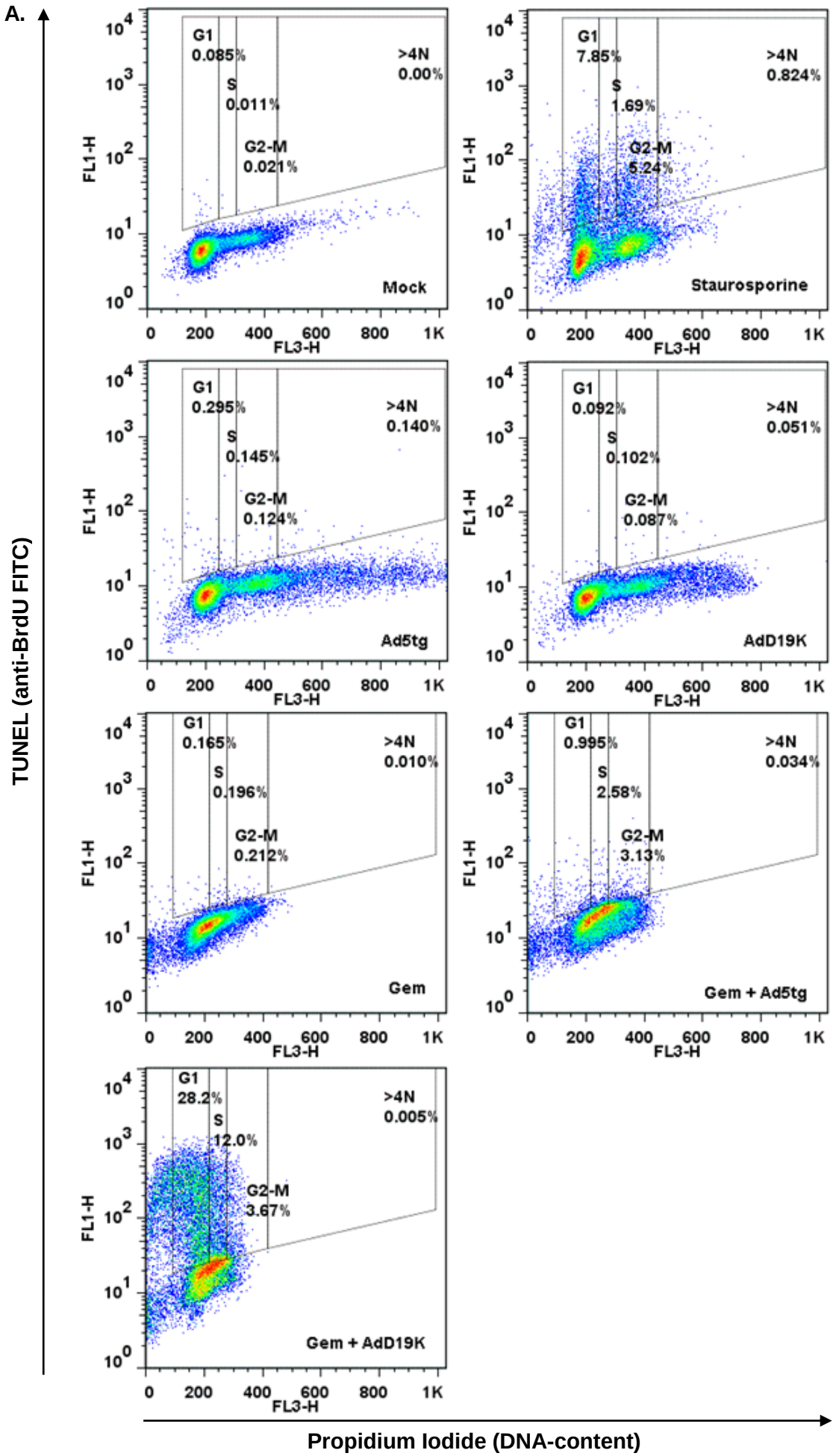
A.
TUNEL (anti-BrdU FITC)
Propidium Iodide (DNA-content)
FL1-H
FL3-H
G1
0.085%
S
0.011%
G2-M
0.021%
>4N
0.00%
Mock
G1
7.85%
S
1.69%
G2-M
5.24%
>4N
0.824%
Staurosporine
G1
0.295%
S
0.145%
G2-M
0.124%
>4N
0.140%
Ad5tg
G1
0.092%
S
0.102%
G2-M
0.087%
>4N
0.051%
AdD19K
G1
0.165%
S
0.196%
G2-M
0.212%
>4N
0.010%
Gem
G1
0.995%
S
2.58%
G2-M
3.13%
>4N
0.034%
Gem + Ad5tg
G1
28.2%
S
12.0%
G2-M
3.67%
>4N
0.005%
Gem + AdD19K

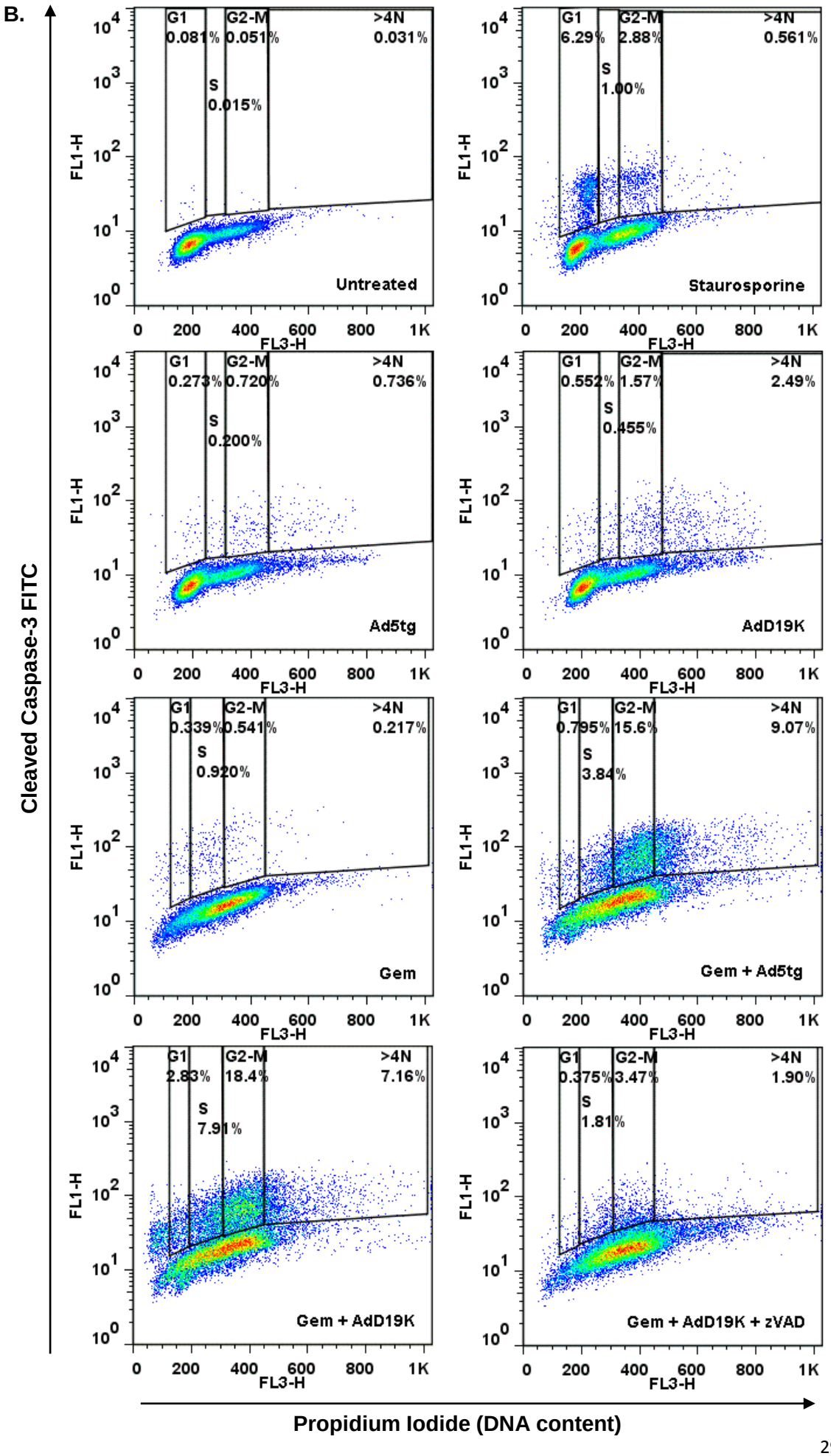
B.
Cleaved Caspase-3 FITC
Propidium Iodide (DNA content)
FL1-H
FL3-H
Untreated
G1 0.081%
G2-M 0.051%
S 0.015%
>4N 0.031%
Staurosporine
G1 6.29%
G2-M 2.88%
S 1.00%
>4N 0.561%
Ad5tg
G1 0.273%
G2-M 0.720%
S 0.200%
>4N 0.736%
AdD19K
G1 0.552%
G2-M 1.57%
S 0.455%
>4N 2.49%
Gem
G1 0.339%
G2-M 0.541%
S 0.920%
>4N 0.217%
Gem + Ad5tg
G1 0.795%
G2-M 15.6%
S 3.84%
>4N 9.07%
Gem + AdD19K
G1 2.83%
G2-M 18.4%
S 7.91%
>4N 7.16%
Gem + AdD19K + zVAD
G1 0.375%
G2-M 3.47%
S 1.81%
>4N 1.90%

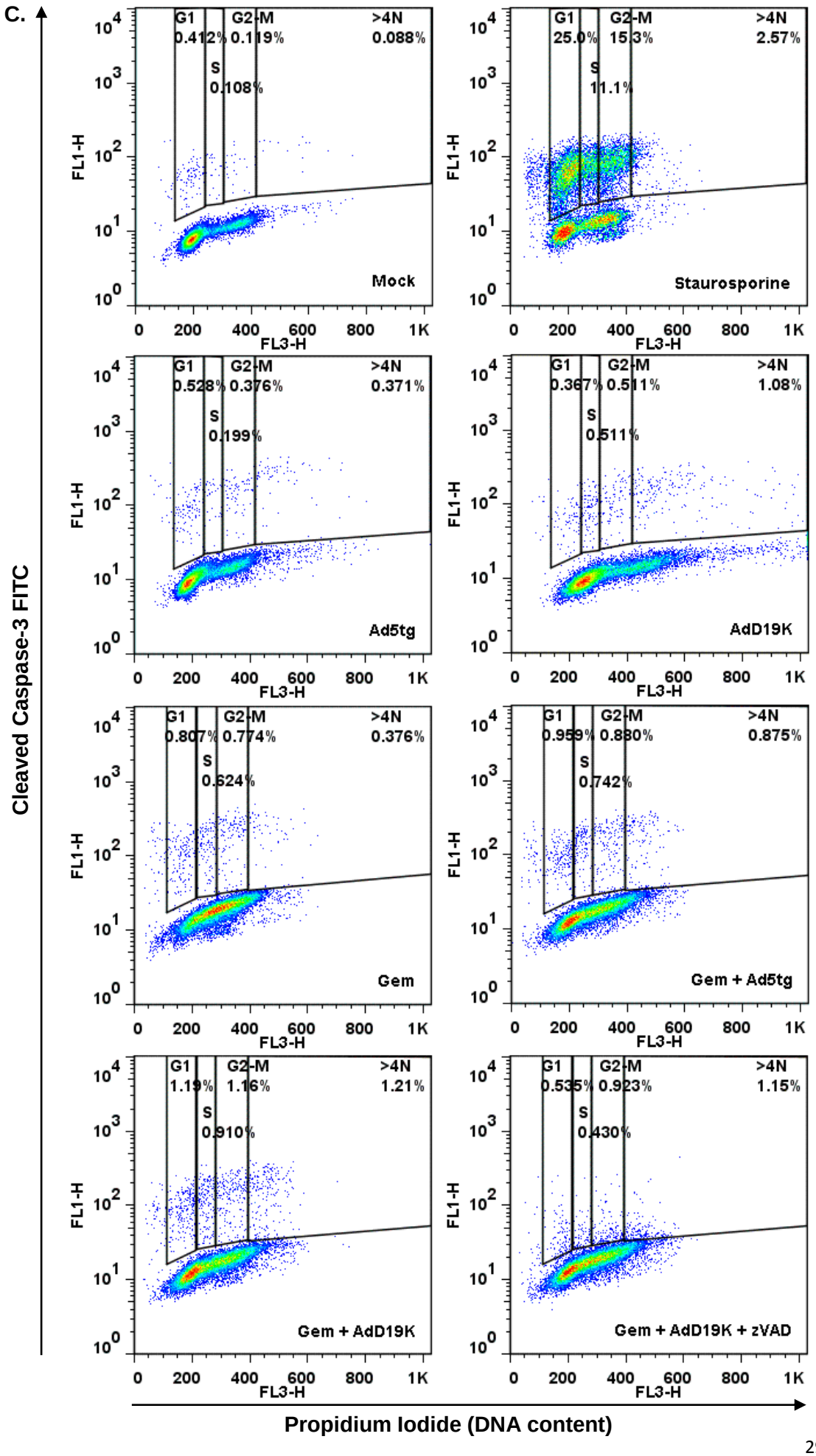
C.
Cleaved Caspase-3 FITC
Propidium Iodide (DNA content)
FL1-H
FL3-H
G1
G2-M
S
>4N
0.412%
0.119%
0.088%
0.108%
Mock
25.0%
15.3%
2.57%
11.1%
Staurosporine
0.528%
0.376%
0.371%
0.199%
Ad5tg
0.367%
0.511%
1.08%
0.511%
AdD19K
0.807%
0.774%
0.376%
0.624%
Gem
0.959%
0.880%
0.875%
0.742%
Gem + Ad5tg
1.19%
1.16%
1.21%
0.910%
Gem + AdD19K
0.535%
0.923%
1.15%
0.430%
Gem + AdD19K + zVAD

Figure 65: Cell-cycle specific apoptosis representative experiments (A) TUNEL/PI assay in PT45 cells **(B)** Cleaved Caspase-3/PI assay in PT45 cells **(C)** Cleaved Caspase-3/PI assay in MIAPaCa-2 cells (72h)

APPENDIX 2: Cell-cycle profiles - Representative experiments

A.

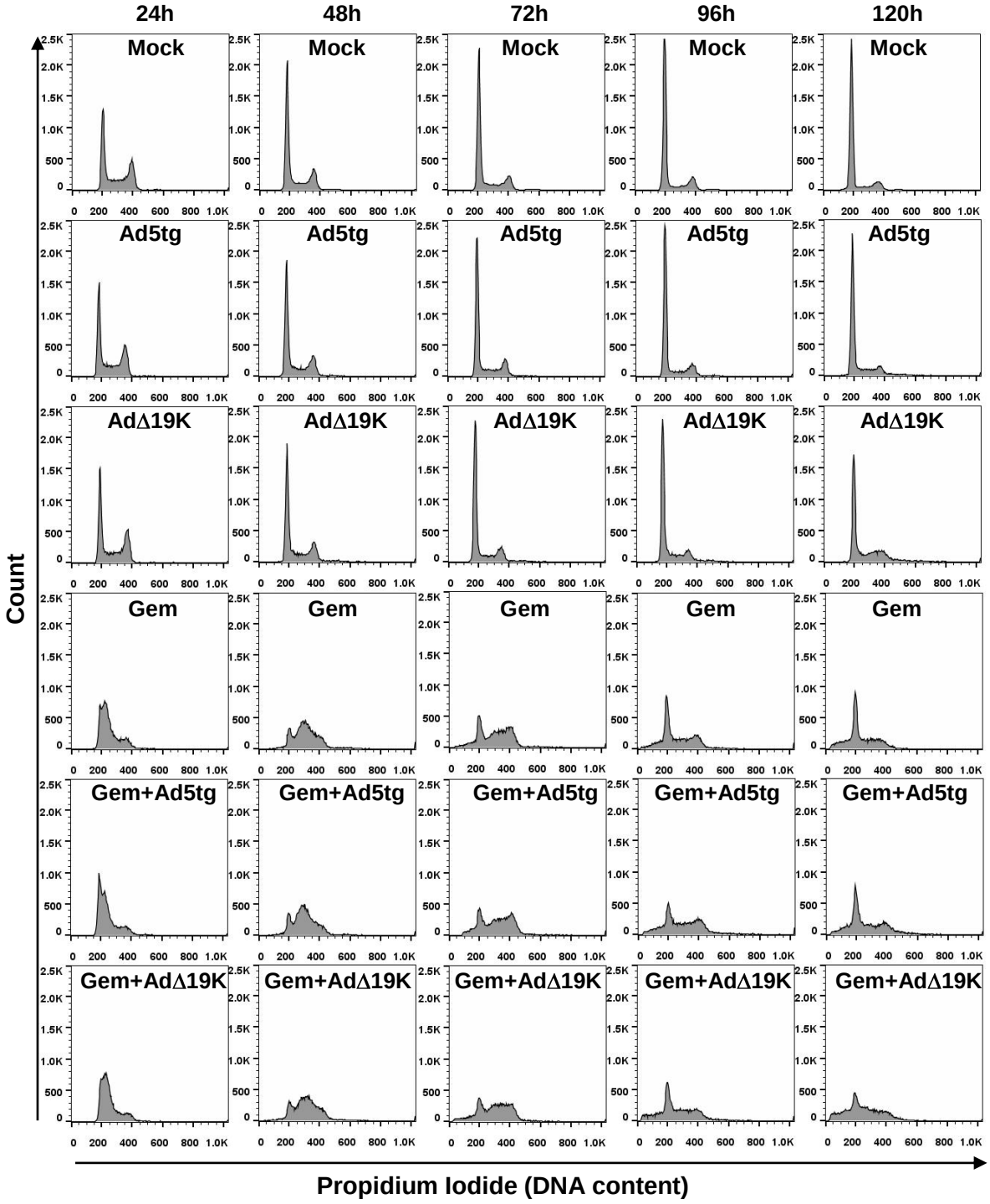

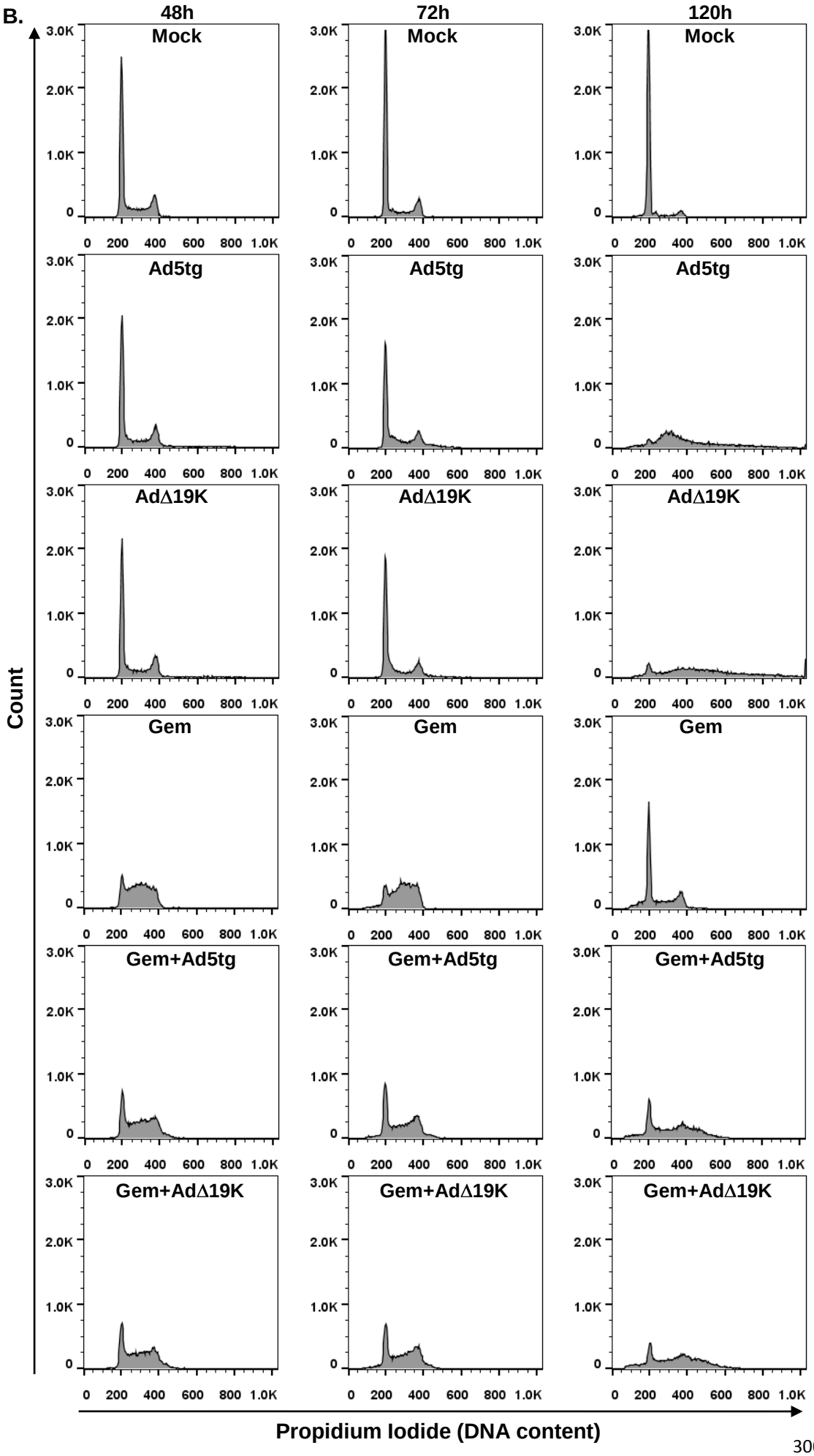
B.
48h
72h
120h
Mock
Ad5tg
AdΔ19K
Gem
Gem+Ad5tg
Gem+AdΔ19K
Count
Propidium Iodide (DNA content)
3.0K
2.0K
1.0K
0
0 200 400 600 800 1.0K

Figure 66: Representative experiments of cell-cycle profiles (A) PT45 **(B)** MIAPaCa-2 cells

APPENDIX 3: Cell-cycle analysis in synchronised cells - Representative dot-plots

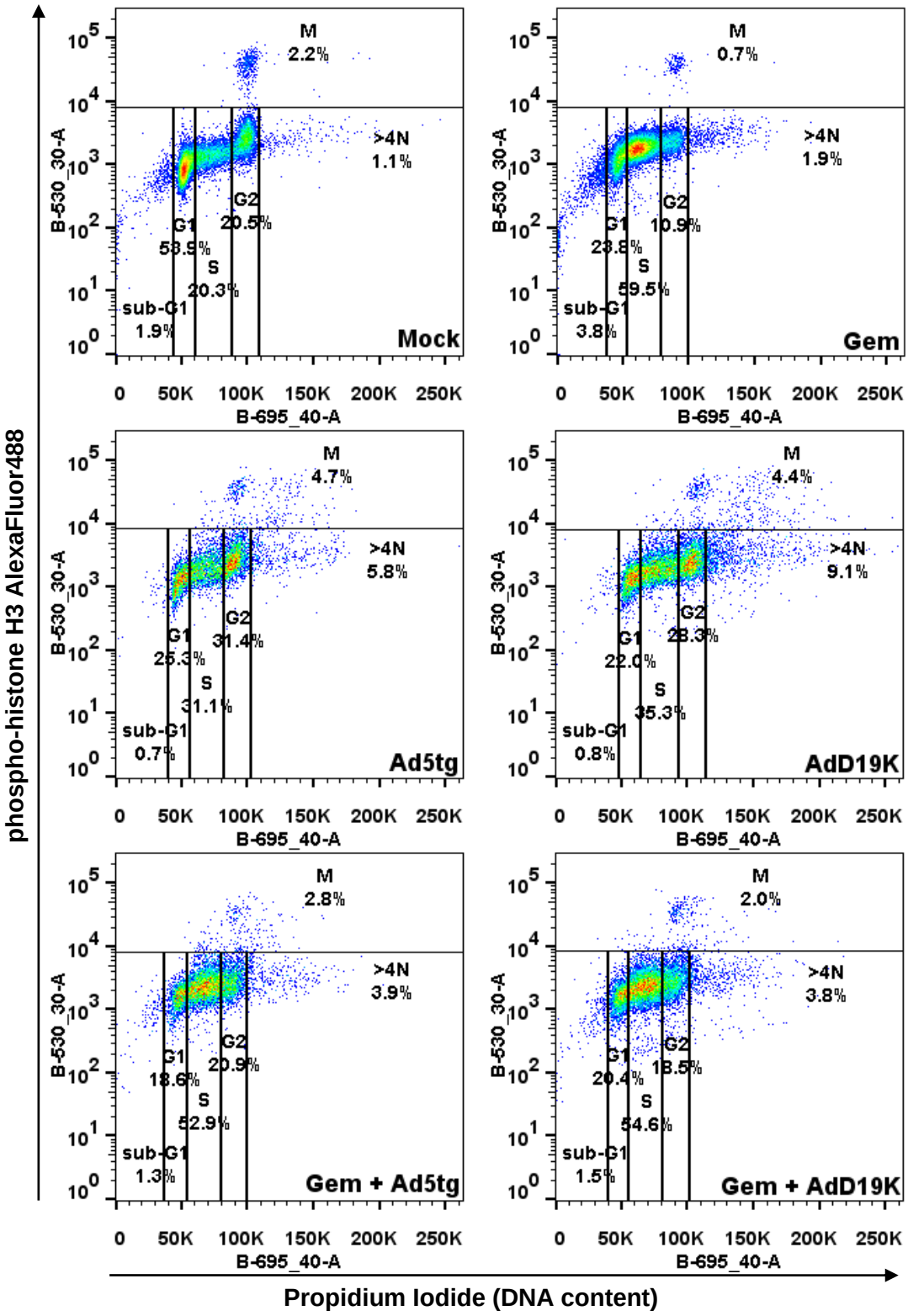

Figure 67: Representative dot-plots from cell-cycle and mitotic index analysis in synchronised cells. Example time-point is 36h

5.2. References

Abou El Hassan, M.A., I. van der Meulen-Muileman, S. Abbas, and F.A. Kruyt. 2004. Conditionally replicating adenoviruses kill tumor cells via a basic apoptotic machinery-independent mechanism that resembles necrosis-like programmed cell death. *J Virol*. 78:12243-51.

Achanta, G., H. Pelicano, L. Feng, W. Plunkett, and P. Huang. 2001. Interaction of p53 and DNA-PK in response to nucleoside analogues: potential role as a sensor complex for DNA damage. *Cancer Res*. 61:8723-9.

Aghi, M., and R.L. Martuza. 2005. Oncolytic viral therapies - the clinical experience. *Oncogene*. 24:7802-16.

Agricola, E., R.A. Randall, T. Gaarenstroom, S. Dupont, and C.S. Hill. 2011. Recruitment of TIF1gamma to chromatin via its PHD finger-bromodomain activates its ubiquitin ligase and transcriptional repressor activities. *Mol Cell*. 43:85-96.

Al-Hajeili, M., A.S. Azmi, and M. Choi. 2014. Nab-paclitaxel: potential for the treatment of advanced pancreatic cancer. *Onco Targets Ther*. 7:187-92.

Al-Hawary, M.M., R.K. Kaza, A.P. Wasnik, and I.R. Francis. 2013. Staging of pancreatic cancer: role of imaging. *Semin Roentgenol*. 48:245-52.

Alemany, R. 2007. Cancer selective adenoviruses. *Mol Aspects Med*. 28:42-58.

Alonso, M.M., C. Gomez-Manzano, B.N. Bekele, W.K. Yung, and J. Fueyo. 2007. Adenovirus-based strategies overcome temozolomide resistance by silencing the O6-methylguanine-DNA methyltransferase promoter. *Cancer Res*. 67:11499-504.

Alvarez-Fernandez, M., V.A. Halim, L. Krenning, M. Aprelia, S. Mohammed, A.J. Heck, and R.H. Medema. 2010. Recovery from a DNA-damage-induced G2 arrest requires Cdk-dependent activation of FoxM1. *EMBO Rep*. 11:452-8.

An, J., Y.C. Huang, Q.Z. Xu, L.J. Zhou, Z.F. Shang, B. Huang, Y. Wang, X.D. Liu, D.C. Wu, and P.K. Zhou. 2010. DNA-PKcs plays a dominant role in the regulation of H2AX phosphorylation in response to DNA damage and cell cycle progression. *BMC Mol Biol*. 11:18.

Andersson, R., U. Aho, B.I. Nilsson, G.J. Peters, M. Pastor-Anglada, W. Rasch, and M.L. Sandvold. 2009. Gemcitabine chemoresistance in pancreatic cancer: molecular mechanisms and potential solutions. *Scand J Gastroenterol*. 44:782-6.

Andreassen, P.R., F.B. Lacroix, O.D. Lohez, and R.L. Margolis. 2001. Neither p21WAF1 nor 14-3-3sigma prevents G2 progression to mitotic catastrophe in human colon carcinoma cells after DNA damage, but p21WAF1 induces stable G1 arrest in resulting tetraploid cells. *Cancer Res*. 61:7660-8.

Apte, M.V., R.C. Pirola, and J.S. Wilson. 2012. Pancreatic stellate cells: a starring role in normal and diseased pancreas. *Front Physiol*. 3:344.

Apte, M.V., and J.S. Wilson. 2012. Dangerous liaisons: pancreatic stellate cells and pancreatic cancer cells. *J Gastroenterol Hepatol*. 27 Suppl 2:69-74.

Apte, M.V., J.S. Wilson, A. Lugea, and S.J. Pandol. 2013. A starring role for stellate cells in the pancreatic cancer microenvironment. *Gastroenterology*. 144:1210-9.

Aranda, S., A. Laguna, and S. de la Luna. 2011. DYRK family of protein kinases: evolutionary relationships, biochemical properties, and functional roles. *FASEB J*. 25:449-62.

Araujo, F.D., T.H. Stracker, C.T. Carson, D.V. Lee, and M.D. Weitzman. 2005. Adenovirus type 5 E4orf3 protein targets the Mre11 complex to cytoplasmic aggresomes. *J Virol*. 79:11382-91.

Archambault, V., and D.M. Glover. 2009. Polo-like kinases: conservation and divergence in their functions and regulation. *Nat Rev Mol Cell Biol*. 10:265-75.

Aressy, B., and B. Ducommun. 2008. Cell cycle control by the CDC25 phosphatases. *Anticancer Agents Med Chem*. 8:818-24.

Attia, S. 2012. Modulation of irinotecan-induced genomic DNA damage by theanine. *Food Chem Toxicol*. 50:1749-54.

Avila, J.L., and J.L. Kissil. 2013. Notch signaling in pancreatic cancer: oncogene or tumor suppressor? *Trends Mol Med*. 19:320-7.

Azorsa, D.O., I.M. Gonzales, G.D. Basu, A. Choudhary, S. Arora, K.M. Bisanz, J.A. Kiefer, M.C. Henderson, J.M. Trent, D.D. Von Hoff, and S. Mousses. 2009. Synthetic lethal RNAi screening identifies sensitizing targets for gemcitabine therapy in pancreatic cancer. *J Transl Med*. 7:43.

Azzariti, A., G. Bocci, L. Porcelli, A. Fioravanti, P. Sini, G.M. Simone, A.E. Quatrale, P. Chiarappa, A. Mangia, S. Sebastian, D. Del Bufalo, M. Del Tacca, and A. Paradiso. 2011. Aurora B kinase inhibitor AZD1152: determinants of action and ability to enhance chemotherapeutics effectiveness in pancreatic and colon cancer. *Br J Cancer*. 104:769-80.

Babiss, L.E., and H.S. Ginsberg. 1984. Adenovirus type 5 early region 1b gene product is required for efficient shutoff of host protein synthesis. *J Virol*. 50:202-12.

Babiss, L.E., H.S. Ginsberg, and J.E. Darnell, Jr. 1985. Adenovirus E1B proteins are required for accumulation of late viral mRNA and for effects on cellular mRNA translation and transport. *Mol Cell Biol*. 5:2552-8.

Bailey, J.M., K.E. DelGiorno, and H.C. Crawford. 2014. The secret origins and surprising fates of pancreas tumors. *Carcinogenesis*. 35:1436-1440.

Bailey, J.M., B.J. Swanson, T. Hamada, J.P. Eggers, P.K. Singh, T. Caffery, M.M. Ouellette, and M.A. Hollingsworth. 2008. Sonic hedgehog promotes desmoplasia in pancreatic cancer. *Clin Cancer Res*. 14:5995-6004.

Baird, S.K., J.L. Aerts, A. Eddaoudi, M. Lockley, N.R. Lemoine, and I.A. McNeish. 2008. Oncolytic adenoviral mutants induce a novel mode of programmed cell death in ovarian cancer. *Oncogene*. 27:3081-90.

Baker, A., K.J. Rohleder, L.A. Hanakahi, and G. Ketner. 2007. Adenovirus E4 34k and E1b 55k oncoproteins target host DNA ligase IV for proteasomal degradation. *J Virol*. 81:7034-40.

Bakhoum, S.F., L. Kabeche, J.P. Murnane, B.I. Zaki, and D.A. Compton. 2014. DNA damage response during mitosis induces whole chromosome mis-segregation. *Cancer Discov*.

Balczon, R., L. Bao, W.E. Zimmer, K. Brown, R.P. Zinkowski, and B.R. Brinkley. 1995. Dissociation of centrosome replication events from cycles of DNA synthesis and mitotic division in hydroxyurea-arrested Chinese hamster ovary cells. *J Cell Biol*. 130:105-15.

Baluchamy, S., N. Sankar, A. Navaraj, E. Moran, and B. Thimmapaya. 2007. Relationship between E1A binding to cellular proteins, c-myc activation and S-phase induction. *Oncogene*. 26:781-7.

Barreto, G., A. Schafer, J. Marhold, D. Stach, S.K. Swaminathan, V. Handa, G. Doderlein, N. Maltry, W. Wu, F. Lyko, and C. Niehrs. 2007. Gadd45a promotes epigenetic gene activation by repair-mediated DNA demethylation. *Nature*. 445:671-5.

Bartek, J., J. Falck, and J. Lukas. 2001. CHK2 kinase--a busy messenger. *Nat Rev Mol Cell Biol*. 2:877-86.

Bartek, J., C. Lukas, and J. Lukas. 2004. Checking on DNA damage in S phase. *Nat Rev Mol Cell Biol*. 5:792-804.

Bartek, J., and J. Lukas. 2007. DNA damage checkpoints: from initiation to recovery or adaptation. *Curr Opin Cell Biol*. 19:238-45.

Barton, K.N., D. Paielli, Y. Zhang, S. Koul, S.L. Brown, M. Lu, J. Seely, J.H. Kim, and S.O. Freytag. 2006. Second-generation replication-competent oncolytic adenovirus armed with improved suicide genes and ADP gene demonstrates greater efficacy without increased toxicity. *Mol Ther*. 13:347-56.

Bassermann, F., D. Frescas, D. Guardavaccaro, L. Busino, A. Peschiaroli, and M. Pagano. 2008. The Cdc14B-Cdh1-Plk1 axis controls the G2 DNA-damage-response checkpoint. *Cell*. 134:256-67.

Batchelor, E., C.S. Mock, I. Bhan, A. Loewer, and G. Lahav. 2008. Recurrent initiation: a mechanism for triggering p53 pulses in response to DNA damage. *Mol Cell*. 30:277-89.

Bayne, L.J., G.L. Beatty, N. Jhala, C.E. Clark, A.D. Rhim, B.Z. Stanger, and R.H. Vonderheide. 2012. Tumor-derived granulocyte-macrophage colony-stimulating factor regulates myeloid inflammation and T cell immunity in pancreatic cancer. *Cancer Cell*. 21:822-35.

Belotserkovskaya, R., and S.P. Jackson. 2014. Keeping 53BP1 out of focus in mitosis. *Cell Res*. 24:781-2.

Beltz, G.A., and S.J. Flint. 1979. Inhibition of HeLa cell protein synthesis during adenovirus infection. Restriction of cellular messenger RNA sequences to the nucleus. *J Mol Biol*. 131:353-73.

Bennett, L.N., and P.R. Clarke. 2006. Regulation of Claspin degradation by the ubiquitin-proteosome pathway during the cell cycle and in response to ATR-dependent checkpoint activation. *FEBS Lett*. 580:4176-81.

Bergman, A.M., G. Giaccone, C.J. van Moorsel, R. Mauritz, P. Noordhuis, H.M. Pinedo, and G.J. Peters. 2000. Cross-resistance in the 2',2'-difluorodeoxycytidine (gemcitabine)-resistant human ovarian cancer cell line AG6000 to standard and investigational drugs. *Eur J Cancer*. 36:1974-83.

Bergman, A.M., H.M. Pinedo, and G.J. Peters. 2002. Determinants of resistance to 2',2'-difluorodeoxycytidine (gemcitabine). *Drug Resist Updat*. 5:19-33.

Berk, A.J. 2005. Recent lessons in gene expression, cell cycle control, and cell biology from adenovirus. *Oncogene*. 24:7673-85.

Bernt, K.M., D.S. Steinwaerder, S. Ni, Z.Y. Li, S.R. Roffler, and A. Lieber. 2002. Enzyme-activated Prodrug Therapy Enhances Tumor-specific Replication of Adenovirus Vectors. *Cancer Res*. 62:6089-98.

Berrozpe, G., J. Schaeffer, M.A. Peinado, F.X. Real, and M. Perucho. 1994. Comparative analysis of mutations in the p53 and K-ras genes in pancreatic cancer. *Int J Cancer*. 58:185-91.

Bertoli, C., J.M. Skotheim, and R.A. de Bruin. 2013. Control of cell cycle transcription during G1 and S phases. *Nat Rev Mol Cell Biol*. 14:518-28.

Besson, A., S.F. Dowdy, and J.M. Roberts. 2008. CDK inhibitors: cell cycle regulators and beyond. *Dev Cell*. 14:159-69.

Bhanot, U., R. Heydrich, P. Moller, and C. Hasel. 2006. Survivin expression in pancreatic intraepithelial neoplasia (PanIN): steady increase along the developmental stages of pancreatic ductal adenocarcinoma. *Am J Surg Pathol*. 30:754-9.

Bhattacharyya, M., J. Francis, A. Eddouadi, N.R. Lemoine, and G. Hallden. 2011. An oncolytic adenovirus defective in pRb-binding (dl922-947) can efficiently eliminate pancreatic cancer cells and tumors in vivo in combination with 5-FU or gemcitabine. *Cancer Gene Ther*. 18:734-43.

Bhonde, M.R., M.L. Hanski, J. Budczies, M. Cao, B. Gillissen, D. Moorthy, F. Simonetta, H. Scherubl, M. Truss, C. Hagemeier, H.W. Mewes, P.T. Daniel, M. Zeitz, and C. Hanski. 2006. DNA damage-induced expression of p53 suppresses mitotic checkpoint kinase hMps1: the lack of this suppression in p53MUT cells contributes to apoptosis. *J Biol Chem*. 281:8675-85.

Bhonde, M.R., M.L. Hanski, J. Stehr, B. Jebautzke, R. Peiro-Jordan, H. Fechner, K.K. Yokoyama, W.C. Lin, M. Zeitz, and C. Hanski. 2010. Mismatch repair system decreases cell survival by stabilizing the tetraploid G1 arrest in response to SN-38. *Int J Cancer*. 126:2813-25.

Biankin, A.V., N. Waddell, K.S. Kassahn, M.C. Gingras, L.B. Muthuswamy, A.L. Johns, D.K. Miller, P.J. Wilson, A.M. Patch, J. Wu, D.K. Chang, M.J. Cowley, B.B. Gardiner, S. Song, I. Harliwong, S. Idrisoglu, C. Nourse, E. Nourbakhsh, S. Manning, S. Wani, M. Gongora, M. Pajic, C.J. Scarlett, A.J. Gill, A.V. Pinho, I. Rooman, M. Anderson, O. Holmes, C. Leonard, D. Taylor, S. Wood, Q. Xu, K. Nones, J.L. Fink, A. Christ, T. Bruxner, N. Cloonan, G. Kolle, F. Newell, M. Pinese, R.S. Mead, J.L. Humphris, W. Kaplan, M.D. Jones, E.K. Colvin, A.M. Nagrial, E.S. Humphrey, A. Chou, V.T. Chin, L.A. Chantrill, A. Mawson, J.S. Samra, J.G. Kench, J.A. Lovell, R.J. Daly, N.D. Merrett, C. Toon, K. Epari, N.Q. Nguyen, A. Barbour, N. Zeps, N. Kakkar, F. Zhao, Y.Q. Wu, M. Wang, D.M. Muzny, W.E. Fisher, F.C. Brunicardi, S.E. Hodges, J.G. Reid, J. Drummond, K. Chang, Y. Han, L.R. Lewis, H. Dinh, C.J. Buhay, T. Beck, L. Timms, M. Sam, K. Begley, A. Brown, D. Pai, A. Panchal, N. Buchner, R. De Borja, R.E. Denroche, C.K. Yung, S. Serra, N. Onetto, D. Mukhopadhyay, M.S. Tsao, P.A. Shaw, G.M. Petersen, S. Gallinger, R.H. Hruban, A. Maitra, C.A. Iacobuzio-Donahue, R.D. Schulick, C.L. Wolfgang, R.A. Morgan, et al. 2012. Pancreatic cancer genomes reveal aberrations in axon guidance pathway genes. *Nature*. 491:399-405.

Bischoff, J.R., D.H. Kirn, A. Williams, C. Heise, S. Horn, M. Muna, L. Ng, J.A. Nye, A. Sampson-Johannes, A. Fattaey, and F. McCormick. 1996. An adenovirus mutant that replicates selectively in p53-deficient human tumor cells. *Science*. 274:373-6.

Blackford, A., O.K. Serrano, C.L. Wolfgang, G. Parmigiani, S. Jones, X. Zhang, D.W. Parsons, J.C. Lin, R.J. Leary, J.R. Eshleman, M. Goggins, E.M. Jaffee, C.A. Iacobuzio-Donahue, A. Maitra, J.L. Cameron, K. Olino, R. Schulick, J. Winter, J.M. Herman, D. Laheru, A.P. Klein, B. Vogelstein, K.W. Kinzler, V.E. Velculescu, and R.H. Hruban. 2009. SMAD4 gene mutations are associated with poor prognosis in pancreatic cancer. *Clin Cancer Res*. 15:4674-9.

Blackford, A.N., R.K. Bruton, O. Dirlik, G.S. Stewart, A.M. Taylor, T. Dobner, R.J. Grand, and A.S. Turnell. 2008. A role for E1B-AP5 in ATR signaling pathways during adenovirus infection. *J Virol*. 82:7640-52.

Botta, G., C. Passaro, S. Libertini, A. Abagnale, S. Barbato, A.S. Maione, G. Hallden, F. Beguinot, P. Formisano, and G. Portella. 2012. Inhibition of autophagy enhances the effects of E1A-defective oncolytic adenovirus dl922-947 against glioma cells in vitro and in vivo. *Hum Gene Ther*. 23:623-34.

Boutros, R., C. Dozier, and B. Ducommun. 2006. The when and wheres of CDC25 phosphatases. *Curr Opin Cell Biol*. 18:185-91.

Boyer, J., and G. Ketner. 1999. Adenovirus Late Gene Expression *In* Adenoviruses: Basic Biology to Gene Therapy P. Seth, editor. R. G. Landes Bioscience, Austin, TX.

Boyer, J., K. Rohleder, and G. Ketner. 1999. Adenovirus E4 34k and E4 11k inhibit double strand break repair and are physically associated with the cellular DNA-dependent protein kinase. *Virology*. 263:307-12.

Braithwaite, A.W., B.F. Cheetham, P. Li, C.R. Parish, L.K. Waldron-Stevens, and A.J. Bellett. 1983. Adenovirus-induced alterations of the cell growth cycle: a requirement for expression of E1A but not of E1B. *J Virol*. 45:192-9.

Braithwaite, A.W., and I.A. Russell. 2001. Induction of cell death by adenoviruses. *Apoptosis*. 6:359-70.

Bramante, S., A. Koski, A. Kipar, I. Diaconu, I. Liikanen, O. Hemminki, L. Vassilev, S. Parviainen, V. Cerullo, S.K. Pesonen, M. Oksanen, R. Heiskanen, N. Rouvinen-Lagerstrom, M. Merisalo-Soikkeli, T. Hakonen, T. Joensuu, A. Kanerva, S. Pesonen, and A. Hemminki. 2014. Serotype chimeric oncolytic adenovirus coding for GM-CSF for treatment of sarcoma in rodents and humans. *Int J Cancer*. 135:720-30.

Branton, P.E. 1999. Early gene expression *In* Adenoviruses: basic biology to gene therapy. P. Seth, editor. TX: Landes, Austin. 39-58.

Branzei, D., and M. Foiani. 2008. Regulation of DNA repair throughout the cell cycle. *Nat Rev Mol Cell Biol*. 9:297-308.

Bressy, C., and K. Benihoud. 2014. Association of oncolytic adenoviruses with chemotherapies: an overview and future directions. *Biochem Pharmacol*. 90:97-106.

Brinkley, B.R. 2001. Managing the centrosome numbers game: from chaos to stability in cancer cell division. *Trends Cell Biol*. 11:18-21.

Briscoe, J., and P.P. Therond. 2013. The mechanisms of Hedgehog signalling and its roles in development and disease. *Nat Rev Mol Cell Biol*. 14:416-29.

Brown, K., M. Dixey, A. Weymouth-Wilson, and B. Linclau. 2014. The synthesis of gemcitabine. *Carbohydr Res*. 387:59-73.

Bruton, R.K., M. Rasti, K.L. Mapp, N. Young, R.Z. Carter, I.A. Abramowicz, G.G. Sedgwick, D.F. Onion, M. Shuen, J.S. Mymryk, A.S. Turnell, and R.J. Grand. 2007. C-terminal-binding protein interacting protein binds directly to adenovirus early region 1A through its N-terminal region and conserved region 3. *Oncogene*. 26:7467-79.

Bryant, K.L., J.D. Mancias, A.C. Kimmelman, and C.J. Der. 2014. KRAS: feeding pancreatic cancer proliferation. *Trends Biochem Sci*. 39:91-100.

Bu, H.Q., J. Luo, H. Chen, J.H. Zhang, H.H. Li, H.C. Guo, Z.H. Wang, and S.Z. Lin. 2012. Oridonin enhances antitumor activity of gemcitabine in

pancreatic cancer through MAPK-p38 signaling pathway. *Int J Oncol*. 41:949-58.

Budhu, A.S., and X.W. Wang. 2005. Loading and unloading: orchestrating centrosome duplication and spindle assembly by Ran/Crm1. *Cell Cycle*. 4:1510-4.

Bunting, S.F., E. Callen, N. Wong, H.T. Chen, F. Polato, A. Gunn, A. Bothmer, N. Feldhahn, O. Fernandez-Capetillo, L. Cao, X. Xu, C.X. Deng, T. Finkel, M. Nussenzweig, J.M. Stark, and A. Nussenzweig. 2010. 53BP1 inhibits homologous recombination in Brca1-deficient cells by blocking resection of DNA breaks. *Cell*. 141:243-54.

Burgess, A., S. Vigneron, E. Brioudes, J.C. Labbe, T. Lorca, and A. Castro. 2010. Loss of human Greatwall results in G2 arrest and multiple mitotic defects due to deregulation of the cyclin B-Cdc2/PP2A balance. *Proc Natl Acad Sci U S A*. 107:12564-9.

Burke, J.M., D.L. Lamm, M.V. Meng, J.J. Nemunaitis, J.J. Stephenson, J.C. Arseneau, J. Aimi, S. Lerner, A.W. Yeung, T. Kazarian, D.J. Maslyar, and J.M. McKiernan. 2012. A first in human phase 1 study of CG0070, a GM-CSF expressing oncolytic adenovirus, for the treatment of nonmuscle invasive bladder cancer. *J Urol*. 188:2391-7.

Burrell, R.A., S.E. McClelland, D. Endesfelder, P. Groth, M.C. Weller, N. Shaikh, E. Domingo, N. Kanu, S.M. Dewhurst, E. Gronroos, S.K. Chew, A.J. Rowan, A. Schenk, M. Sheffer, M. Howell, M. Kschischo, A. Behrens, T. Helleday, J. Bartek, I.P. Tomlinson, and C. Swanton. 2013. Replication stress links structural and numerical cancer chromosomal instability. *Nature*. 494:492-6.

Cabon, L., N. Sriskandarajah, M.Z. Mui, J.G. Teodoro, P. Blanchette, and P.E. Branton. 2013. Adenovirus E4orf4 protein-induced death of p53-/- H1299 human cancer cells follows a G1 arrest of both tetraploid and diploid cells due to a failure to initiate DNA synthesis. *J Virol*. 87:13168-78.

Caldas, C., S.A. Hahn, L.T. da Costa, M.S. Redston, M. Schutte, A.B. Seymour, C.L. Weinstein, R.H. Hruban, C.J. Yeo, and S.E. Kern. 1994. Frequent somatic mutations and homozygous deletions of the p16 (MTS1) gene in pancreatic adenocarcinoma. *Nat Genet*. 8:27-32.

Cancer Research UK. Pancreatic cancer incidence statistics. *Retrieved 04/09/2014, from http://www.cancerresearchuk.org/cancer-info/cancerstats/types/pancreas/incidence/*.

Candelaria, M., E. de la Cruz-Hernandez, E. Perez-Cardenas, C. Trejo-Becerril, O. Gutierrez-Hernandez, and A. Duenas-Gonzalez. 2010. Pharmacogenetics and pharmacoepigenetics of gemcitabine. *Med Oncol*. 27:1133-43.

Canepa, E.T., M.E. Scassa, J.M. Ceruti, M.C. Marazita, A.L. Carcagno, P.F. Sirkin, and M.F. Ogara. 2007. INK4 proteins, a family of mammalian CDK inhibitors with novel biological functions. *IUBMB Life*. 59:419-26.

Cao, Y., Z.X. Jin, X.P. Tong, S. Yue, T. Sakai, T. Kawanami, T. Sawaki, M. Miki, H. Iwao, A. Nakajima, Y. Masaki, Y. Fukushima, Y. Fujita, H. Nakajima, T. Okazaki, and H. Umehara. 2010. Synergistic effects of topoisomerase I inhibitor, SN38, on Fas-mediated apoptosis. *Anticancer Res*. 30:3911-7.

Caporossi, D., and S. Bacchetti. 1990. Definition of adenovirus type 5 functions involved in the induction of chromosomal aberrations in human cells. *J Gen Virol*. 71 (Pt 4):801-8.

Carson, C.T., N.I. Orazio, D.V. Lee, J. Suh, S. Bekker-Jensen, F.D. Araujo, S.S. Lakdawala, C.E. Lilley, J. Bartek, J. Lukas, and M.D. Weitzman. 2009.

Mislocalization of the MRN complex prevents ATR signaling during adenovirus infection. *EMBO J*. 28:652-62.
Carson, C.T., R.A. Schwartz, T.H. Stracker, C.E. Lilley, D.V. Lee, and M.D. Weitzman. 2003. The Mre11 complex is required for ATM activation and the G2/M checkpoint. *EMBO J*. 22:6610-20.
Castedo, M., J.L. Perfettini, T. Roumier, K. Andreau, R. Medema, and G. Kroemer. 2004. Cell death by mitotic catastrophe: a molecular definition. *Oncogene*. 23:2825-37.
Cazales, M., E. Schmitt, E. Montembault, C. Dozier, C. Prigent, and B. Ducommun. 2005. CDC25B phosphorylation by Aurora-A occurs at the G2/M transition and is inhibited by DNA damage. *Cell Cycle*. 4:1233-8.
Cerqueira, N.M., P.A. Fernandes, and M.J. Ramos. 2007. Understanding ribonucleotide reductase inactivation by gemcitabine. *Chemistry*. 13:8507-15.
Cerullo, V., S. Pesonen, I. Diaconu, S. Escutenaire, P.T. Arstila, M. Ugolini, P. Nokisalmi, M. Raki, L. Laasonen, M. Sarkioja, M. Rajecki, L. Kangasniemi, K. Guse, A. Helminen, L. Ahtiainen, A. Ristimaki, A. Raisanen-Sokolowski, E. Haavisto, M. Oksanen, E. Karli, A. Karioja-Kallio, S.L. Holm, M. Kouri, T. Joensuu, A. Kanerva, and A. Hemminki. 2010. Oncolytic adenovirus coding for granulocyte macrophage colony-stimulating factor induces antitumoral immunity in cancer patients. *Cancer Res*. 70:4297-309.
Chakraborty, A.A., and W.P. Tansey. 2009. Adenoviral E1A function through Myc. *Cancer Res*. 69:6-9.
Chan, H.M., M. Narita, S.W. Lowe, and D.M. Livingston. 2005. The p400 E1A-associated protein is a novel component of the p53 --> p21 senescence pathway. *Genes Dev*. 19:196-201.
Chan, J.Y. 2011. A clinical overview of centrosome amplification in human cancers. *Int J Biol Sci*. 7:1122-44.
Chan, K.L., T. Palmai-Pallag, S. Ying, and I.D. Hickson. 2009. Replication stress induces sister-chromatid bridging at fragile site loci in mitosis. *Nat Cell Biol*. 11:753-60.
Chan, K.S., C.G. Koh, and H.Y. Li. 2012. Mitosis-targeted anti-cancer therapies: where they stand. *Cell Death Dis*. 3:e411.
Chandler, N.M., J.J. Canete, and M.P. Callery. 2004. Increased expression of NF-kappa B subunits in human pancreatic cancer cells. *J Surg Res*. 118:9-14.
Chapman, J.R., A.J. Sossick, S.J. Boulton, and S.P. Jackson. 2012. BRCA1-associated exclusion of 53BP1 from DNA damage sites underlies temporal control of DNA repair. *J Cell Sci*. 125:3529-34.
Chartier, C., E. Degryse, M. Gantzer, A. Dieterle, A. Pavirani, and M. Mehtali. 1996. Efficient generation of recombinant adenovirus vectors by homologous recombination in Escherichia coli. *J Virol*. 70:4805-10.
Chattopadhyay, D., M.K. Ghosh, A. Mal, and M.L. Harter. 2001. Inactivation of p21 by E1A leads to the induction of apoptosis in DNA-damaged cells. *J Virol*. 75:9844-56.
Chen, J., and G. Fang. 2001. MAD2B is an inhibitor of the anaphase-promoting complex. *Genes Dev*. 15:1765-70.
Chen, L., D. Chen, M. Gong, M. Na, L. Li, H. Wu, L. Jiang, Y. Qian, G. Fang, and X. Xue. 2009. Concomitant use of Ad5/35 chimeric oncolytic adenovirus with TRAIL gene and taxol produces synergistic cytotoxicity in gastric cancer cells. *Cancer Lett*. 284:141-8.

Chen, P.L., F. Liu, S. Cai, X. Lin, A. Li, Y. Chen, B. Gu, E.Y. Lee, and W.H. Lee. 2005. Inactivation of CtIP leads to early embryonic lethality mediated by G1 restraint and to tumorigenesis by haploid insufficiency. *Mol Cell Biol*. 25:3535-42.

Chen, Y., and R.Y. Poon. 2008. The multiple checkpoint functions of CHK1 and CHK2 in maintenance of genome stability. *Front Biosci*. 13:5016-29.

Cheong, S.C., Y. Wang, J.H. Meng, R. Hill, K. Sweeney, D. Kirn, N.R. Lemoine, and G. Hallden. 2008. E1A-expressing adenoviral E3B mutants act synergistically with chemotherapeutics in immunocompetent tumor models. *Cancer Gene Ther*. 15:40-50.

Cherubini, G., C. Kallin, A. Mozetic, K. Hammaren-Busch, H. Muller, N.R. Lemoine, and G. Hallden. 2011. The oncolytic adenovirus AdΔΔ enhances selective cancer cell killing in combination with DNA-damaging drugs in pancreatic cancer models. *Gene Ther*. 18:1157-65.

Cherubini, G., T. Petouchoff, M. Grossi, S. Piersanti, E. Cundari, and I. Saggio. 2006. E1B55K-deleted adenovirus (ONYX-015) overrides G1/S and G2/M checkpoints and causes mitotic catastrophe and endoreduplication in p53-proficient normal cells. *Cell Cycle*. 5:2244-52.

Cheung-Ong, K., G. Giaever, and C. Nislow. 2013. DNA-damaging agents in cancer chemotherapy: serendipity and chemical biology. *Chem Biol*. 20:648-59.

Chini, C.C., and J. Chen. 2003. Human claspin is required for replication checkpoint control. *J Biol Chem*. 278:30057-62.

Chini, C.C., and J. Chen. 2004. Claspin, a regulator of Chk1 in DNA replication stress pathway. *DNA Repair (Amst)*. 3:1033-7.

Chini, C.C., and J. Chen. 2006. Repeated phosphopeptide motifs in human Claspin are phosphorylated by Chk1 and mediate Claspin function. *J Biol Chem*. 281:33276-82.

Chini, C.C., J. Wood, and J. Chen. 2006. Chk1 is required to maintain claspin stability. *Oncogene*. 25:4165-71.

Chinnadurai, G. 1983. Adenovirus 2 Ip+ locus codes for a 19 kd tumor antigen that plays an essential role in cell transformation. *Cell*. 33:759-66.

Chinnadurai, G. 2002. CtBP, an unconventional transcriptional corepressor in development and oncogenesis. *Mol Cell*. 9:213-24.

Chinnadurai, G. 2009. The transcriptional corepressor CtBP: a foe of multiple tumor suppressors. *Cancer Res*. 69:731-4.

Chiocca, E.A., and S.D. Rabkin. 2014. Oncolytic viruses and their application to cancer immunotherapy. *Cancer Immunol Res*. 2:295-300.

Chiou, S.K., and E. White. 1997. p300 binding by E1A cosegregates with p53 induction but is dispensable for apoptosis. *J Virol*. 71:3515-25.

Chipuk, J.E., T. Moldoveanu, F. Llambi, M.J. Parsons, and D.R. Green. 2010. The BCL-2 family reunion. *Mol Cell*. 37:299-310.

Choi, I.K., J.S. Lee, S.N. Zhang, J. Park, C.H. Sonn, K.M. Lee, and C.O. Yun. 2011. Oncolytic adenovirus co-expressing IL-12 and IL-18 improves tumor-specific immunity via differentiation of T cells expressing IL-12Rbeta2 or IL-18Ralpha. *Gene Ther*. 18:898-909.

Choi, I.K., Y.S. Lee, J.Y. Yoo, A.R. Yoon, H. Kim, D.S. Kim, D.G. Seidler, J.H. Kim, and C.O. Yun. 2010. Effect of decorin on overcoming the extracellular matrix barrier for oncolytic virotherapy. *Gene Ther*. 17:190-201.

Choi, J.W., J.S. Lee, S.W. Kim, and C.O. Yun. 2012. Evolution of oncolytic adenovirus for cancer treatment. *Adv Drug Deliv Rev*. 64:720-9.

Cimprich, K.A., and D. Cortez. 2008. ATR: an essential regulator of genome integrity. *Nat Rev Mol Cell Biol*. 9:616-27.
Clark, C.E., S.R. Hingorani, R. Mick, C. Combs, D.A. Tuveson, and R.H. Vonderheide. 2007. Dynamics of the immune reaction to pancreatic cancer from inception to invasion. *Cancer Res*. 67:9518-27.
Clarke, C.A., and P.R. Clarke. 2005. DNA-dependent phosphorylation of Chk1 and Claspin in a human cell-free system. *Biochem J*. 388:705-12.
Clarke, P.R., and C. Zhang. 2008. Spatial and temporal coordination of mitosis by Ran GTPase. *Nat Rev Mol Cell Biol*. 9:464-77.
Clemenson, C., and M.C. Marsolier-Kergoat. 2009. DNA damage checkpoint inactivation: adaptation and recovery. *DNA Repair (Amst)*. 8:1101-9.
Cleveland, D.W., Y. Mao, and K.F. Sullivan. 2003. Centromeres and kinetochores: from epigenetics to mitotic checkpoint signaling. *Cell*. 112:407-21.
Cleveland, M.H., J.M. Sawyer, S. Afelik, J. Jensen, and S.D. Leach. 2012. Exocrine ontogenies: on the development of pancreatic acinar, ductal and centroacinar cells. *Semin Cell Dev Biol*. 23:711-9.
Collins, E.S., J.E. Hornick, T.M. Durcan, N.S. Collins, W. Archer, K.B. Karanjeet, K.T. Vaughan, and E.H. Hinchcliffe. 2010. Centrosome biogenesis continues in the absence of microtubules during prolonged S-phase arrest. *J Cell Physiol*. 225:454-65.
Connell, C.M., A. Shibata, L.A. Tookman, K.M. Archibald, M.B. Flak, K.J. Pirlo, M. Lockley, S.P. Wheatley, and I.A. McNeish. 2011. Genomic DNA damage and ATR-Chk1 signaling determine oncolytic adenoviral efficacy in human ovarian cancer cells. *J Clin Invest*. 121:1283-97.
Connell, C.M., S.P. Wheatley, and I.A. McNeish. 2008. Nuclear survivin abrogates multiple cell cycle checkpoints and enhances viral oncolysis. *Cancer Res*. 68:7923-31.
Conrad, C., C.R. Miller, Y. Ji, C. Gomez-Manzano, S. Bharara, J.S. McMurray, F.F. Lang, F. Wong, R. Sawaya, W.K. Yung, and J. Fueyo. 2005. Delta24-hyCD adenovirus suppresses glioma growth in vivo by combining oncolysis and chemosensitization. *Cancer Gene Ther*. 12:284-94.
Conroy, T., F. Desseigne, M. Ychou, O. Bouche, R. Guimbaud, Y. Becouarn, A. Adenis, J.L. Raoul, S. Gourgou-Bourgade, C. de la Fouchardiere, J. Bennouna, J.B. Bachet, F. Khemissa-Akouz, D. Pere-Verge, C. Delbaldo, E. Assenat, B. Chauffert, P. Michel, C. Montoto-Grillot, and M. Ducreux. 2011. FOLFIRINOX versus gemcitabine for metastatic pancreatic cancer. *N Engl J Med*. 364:1817-25.
Cook, J.L., T.A. Walker, G.S. Worthen, and J.R. Radke. 2002. Role of the E1A Rb-binding domain in repression of the NF-kappa B-dependent defense against tumor necrosis factor-alpha. *Proc Natl Acad Sci U S A*. 99:9966-71.
Cooper, S. 2003. Reappraisal of serum starvation, the restriction point, G0, and G1 phase arrest points. *Faseb Journal*. 17:333-340.
Costanzo, V. 2011. Brca2, Rad51 and Mre11: performing balancing acts on replication forks. *DNA Repair (Amst)*. 10:1060-5.
Costes, A., and S.A. Lambert. 2012. Homologous recombination as a replication fork escort: fork-protection and recovery. *Biomolecules*. 3:39-71.
Crosio, C., G.M. Fimia, R. Loury, M. Kimura, Y. Okano, H. Zhou, S. Sen, C.D. Allis, and P. Sassone-Corsi. 2002. Mitotic phosphorylation of histone H3:

spatio-temporal regulation by mammalian Aurora kinases. *Mol Cell Biol*. 22:874-85.

Crul, M., R.C. van Waardenburg, S. Bocxe, M.A. van Eijndhoven, D. Pluim, J.H. Beijnen, and J.H. Schellens. 2003. DNA repair mechanisms involved in gemcitabine cytotoxicity and in the interaction between gemcitabine and cisplatin. *Biochem Pharmacol*. 65:275-82.

Cuconati, A., C. Mukherjee, D. Perez, and E. White. 2003. DNA damage response and MCL-1 destruction initiate apoptosis in adenovirus-infected cells. *Genes Dev*. 17:2922-32.

D'Angiolella, V., V. Donato, F.M. Forrester, Y.T. Jeong, C. Pellacani, Y. Kudo, A. Saraf, L. Florens, M.P. Washburn, and M. Pagano. 2012. Cyclin F-mediated degradation of ribonucleotide reductase M2 controls genome integrity and DNA repair. *Cell*. 149:1023-34.

D'Halluin, J.C. 1995. Virus assembly. *Curr Top Microbiol Immunol*. 199 (Pt 1):47-66.

Dalton, W.B., M.O. Nandan, R.T. Moore, and V.W. Yang. 2007. Human cancer cells commonly acquire DNA damage during mitotic arrest. *Cancer Res*. 67:11487-92.

Darzynkiewicz, Z., S. Bruno, G. Del Bino, W. Gorczyca, M.A. Hotz, P. Lassota, and F. Traganos. 1992. Features of apoptotic cells measured by flow cytometry. *Cytometry*. 13:795-808.

Darzynkiewicz, Z., D. Galkowski, and H. Zhao. 2008. Analysis of apoptosis by cytometry using TUNEL assay. *Methods*. 44:250-4.

Davidson, D., Y. Coulombe, V.L. Martinez-Marignac, L. Amrein, J. Grenier, K. Hodkinson, J.Y. Masson, R. Aloyz, and L. Panasci. 2012. Irinotecan and DNA-PKcs inhibitors synergize in killing of colon cancer cells. *Invest New Drugs*. 30:1248-56.

Davies, S.L., P.S. North, and I.D. Hickson. 2007. Role for BLM in replication-fork restart and suppression of origin firing after replicative stress. *Nat Struct Mol Biol*. 14:677-9.

Davison, A.J., M. Benko, and B. Harrach. 2003. Genetic content and evolution of adenoviruses. *J Gen Virol*. 84:2895-908.

Davoli, M.A., J. Fourtounis, J. Tam, S. Xanthoudakis, D. Nicholson, G.S. Robertson, G.Y. Ng, and D. Xu. 2002. Immunohistochemical and biochemical assessment of caspase-3 activation and DNA fragmentation following transient focal ischemia in the rat. *Neuroscience*. 115:125-36.

de Jong, F.A., M.J. de Jonge, J. Verweij, and R.H. Mathijssen. 2006. Role of pharmacogenetics in irinotecan therapy. *Cancer Lett*. 234:90-106.

de Lange, T. 2009. How telomeres solve the end-protection problem. *Science*. 326:948-52.

De Luca, A., R. Mangiacasale, A. Severino, L. Malquori, A. Baldi, A. Palena, A.M. Mileo, P. Lavia, and M.G. Paggi. 2003. E1A deregulates the centrosome cycle in a Ran GTPase-dependent manner. *Cancer Res*. 63:1430-7.

de Sousa Cavalcante, L., and G. Monteiro. 2014. Gemcitabine: metabolism and molecular mechanisms of action, sensitivity and chemoresistance in pancreatic cancer. *Eur J Pharmacol*.

de Stanchina, E., M.E. McCurrach, F. Zindy, S.Y. Shieh, G. Ferbeyre, A.V. Samuelson, C. Prives, M.F. Roussel, C.J. Sherr, and S.W. Lowe. 1998. E1A signaling to p53 involves the p19(ARF) tumor suppressor. *Genes Dev*. 12:2434-42.

Debbas, M., and E. White. 1993. Wild-type p53 mediates apoptosis by E1A, which is inhibited by E1B. *Genes Dev*. 7:546-54.
Dechecchi, M.C., P. Melotti, A. Bonizzato, M. Santacatterina, M. Chilosi, and G. Cabrini. 2001. Heparan sulfate glycosaminoglycans are receptors sufficient to mediate the initial binding of adenovirus types 2 and 5. *J Virol*. 75:8772-80.
Decordier, I., E. Cundari, and M. Kirsch-Volders. 2008. Survival of aneuploid, micronucleated and/or polyploid cells: crosstalk between ploidy control and apoptosis. *Mutat Res*. 651:30-9.
Dianov, G.L., and U. Hubscher. 2013. Mammalian base excision repair: the forgotten archangel. *Nucleic Acids Res*. 41:3483-90.
Diaz-Moralli, S., M. Tarrado-Castellarnau, A. Miranda, and M. Cascante. 2013. Targeting cell cycle regulation in cancer therapy. *Pharmacol Ther*. 138:255-71.
Dilley, J., S. Reddy, D. Ko, N. Nguyen, G. Rojas, P. Working, and D.C. Yu. 2005. Oncolytic adenovirus CG7870 in combination with radiation demonstrates synergistic enhancements of antitumor efficacy without loss of specificity. *Cancer Gene Ther*. 12:715-22.
Dodds, H.M., M.C. Haaz, J.F. Riou, J. Robert, and L.P. Rivory. 1998. Identification of a new metabolite of CPT-11 (irinotecan): pharmacological properties and activation to SN-38. *J Pharmacol Exp Ther*. 286:578-83.
Donzelli, M., and G.F. Draetta. 2003. Regulating mammalian checkpoints through Cdc25 inactivation. *EMBO Rep*. 4:671-7.
Dubrez, L., J. Berthelet, and V. Glorian. 2013. IAP proteins as targets for drug development in oncology. *Onco Targets Ther*. 9:1285-304.
Dunigan, D.D., S.B. Waters, and T.C. Owen. 1995. Aqueous soluble tetrazolium/formazan MTS as an indicator of NADH- and NADPH-dependent dehydrogenase activity. *Biotechniques*. 19:640-9.
Duong, H.Q., Y.B. Hong, J.S. Kim, H.S. Lee, Y.W. Yi, Y.J. Kim, A. Wang, W. Zhao, C.H. Cho, Y.S. Seong, and I. Bae. 2013. Inhibition of checkpoint kinase 2 (CHK2) enhances sensitivity of pancreatic adenocarcinoma cells to gemcitabine. *J Cell Mol Med*. 17:1261-70.
Dyer, M.R., and P.L. Herrling. 2000. Progress and potential for gene-based medicines. *Mol Ther*. 1:213-24.
Elmore, S. 2007. Apoptosis: a review of programmed cell death. *Toxicol Pathol*. 35:495-516.
Elnaggar, M., E. Giovannetti, and G.J. Peters. 2012. Molecular targets of gemcitabine action: rationale for development of novel drugs and drug combinations. *Curr Pharm Des*. 18:2811-29.
Ene-Obong, A., A.J. Clear, J. Watt, J. Wang, R. Fatah, J.C. Riches, J.F. Marshall, J. Chin-Aleong, C. Chelala, J.G. Gribben, A.G. Ramsay, and H.M. Kocher. 2013. Activated pancreatic stellate cells sequester CD8+ T cells to reduce their infiltration of the juxtatumoral compartment of pancreatic ductal adenocarcinoma. *Gastroenterology*. 145:1121-32.
Erkan, M., C.W. Michalski, S. Rieder, C. Reiser-Erkan, I. Abiatari, A. Kolb, N.A. Giese, I. Esposito, H. Friess, and J. Kleeff. 2008. The activated stroma index is a novel and independent prognostic marker in pancreatic ductal adenocarcinoma. *Clin Gastroenterol Hepatol*. 6:1155-61.
Eser, S., A. Schnieke, G. Schneider, and D. Saur. 2014. Oncogenic KRAS signalling in pancreatic cancer. *Br J Cancer*.

Esposito, I., J. Kleeff, I. Abiatari, X. Shi, N. Giese, F. Bergmann, W. Roth, H. Friess, and P. Schirmacher. 2007. Overexpression of cellular inhibitor of apoptosis protein 2 is an early event in the progression of pancreatic cancer. *J Clin Pathol*. 60:885-95.

Esselen, M., S.W. Barth, S. Winkler, S. Baechler, K. Briviba, B. Watzl, S. Skrbek, and D. Marko. 2013. Anthocyanins suppress the cleavable complex formation by irinotecan and diminish its DNA-strand-breaking activity in the colon of Wistar rats. *Carcinogenesis*. 34:835-40.

Ewald, B., D. Sampath, and W. Plunkett. 2007. H2AX phosphorylation marks gemcitabine-induced stalled replication forks and their collapse upon S-phase checkpoint abrogation. *Mol Cancer Ther*. 6:1239-48.

Ewald, B., D. Sampath, and W. Plunkett. 2008. ATM and the Mre11-Rad50-Nbs1 complex respond to nucleoside analogue-induced stalled replication forks and contribute to drug resistance. *Cancer Res*. 68:7947-55.

Falck, J., N. Mailand, R.G. Syljuasen, J. Bartek, and J. Lukas. 2001. The ATM-Chk2-Cdc25A checkpoint pathway guards against radioresistant DNA synthesis. *Nature*. 410:842-7.

Farrell, J.J., H. Elsaleh, M. Garcia, R. Lai, A. Ammar, W.F. Regine, R. Abrams, A.B. Benson, J. Macdonald, C.E. Cass, A.P. Dicker, and J.R. Mackey. 2009. Human equilibrative nucleoside transporter 1 levels predict response to gemcitabine in patients with pancreatic cancer. *Gastroenterology*. 136:187-95.

Fattet, L., A.S. Ay, B. Bonneau, L. Jallades, I. Mikaelian, I. Treilleux, G. Gillet, C. Hesling, and R. Rimokh. 2013. TIF1gamma requires sumoylation to exert its repressive activity on TGFbeta signaling. *J Cell Sci*. 126:3713-23.

Fededa, J.P., and D.W. Gerlich. 2012. Molecular control of animal cell cytokinesis. *Nat Cell Biol*. 14:440-7.

Feldman, L.A., and F. Rapp. 1966. Inhibition of adenovirus replication by 1-beta-D-arabinofuranosylcytosine. *Proc Soc Exp Biol Med*. 122:243-7.

Felsani, A., A.M. Mileo, and M.G. Paggi. 2006. Retinoblastoma family proteins as key targets of the small DNA virus oncoproteins. *Oncogene*. 25:5277-85.

Fenech, M., M. Kirsch-Volders, A.T. Natarajan, J. Surralles, J.W. Crott, J. Parry, H. Norppa, D.A. Eastmond, J.D. Tucker, and P. Thomas. 2011. Molecular mechanisms of micronucleus, nucleoplasmic bridge and nuclear bud formation in mammalian and human cells. *Mutagenesis*. 26:125-32.

Ferguson, M.S., N.R. Lemoine, and Y. Wang. 2012. Systemic delivery of oncolytic viruses: hopes and hurdles. *Adv Virol*. 2012:805629.

Ferreira, C.G., S.W. Span, G.J. Peters, F.A. Kruyt, and G. Giaccone. 2000. Chemotherapy triggers apoptosis in a caspase-8-dependent and mitochondria-controlled manner in the non-small cell lung cancer cell line NCI-H460. *Cancer Res*. 60:7133-41.

Ferreira, T., and W. Rasband. 2012. ImageJ/Fiji 1.46 User Guide
136-138.

Fiandalo, M.V., and N. Kyprianou. 2012. Caspase control: protagonists of cancer cell apoptosis. *Exp Oncol*. 34:165-75.

Fimia, G.M., and M. Piacentini. 2010. Regulation of autophagy in mammals and its interplay with apoptosis. *Cell Mol Life Sci*. 67:1581-8.

Fisher, K.D., and L.W. Seymour. 2010. HPMA copolymers for masking and retargeting of therapeutic viruses. *Adv Drug Deliv Rev*. 62:240-5.
Fisher, R.P. 2012. The CDK Network: Linking Cycles of Cell Division and Gene Expression. *Genes Cancer*. 3:731-8.
Flak, M.B., C.M. Connell, C. Chelala, K. Archibald, M.A. Salako, K.J. Pirlo, M. Lockley, S.P. Wheatley, F.R. Balkwill, and I.A. McNeish. 2010. p21 Promotes oncolytic adenoviral activity in ovarian cancer and is a potential biomarker. *Mol Cancer*. 9:175.
Forrester, N.A., R.N. Patel, T. Speiseder, P. Groitl, G.G. Sedgwick, N.J. Shimwell, R.I. Seed, P.O. Catnaigh, C.J. McCabe, G.S. Stewart, T. Dobner, R.J. Grand, A. Martin, and A.S. Turnell. 2012. Adenovirus E4orf3 targets transcriptional intermediary factor 1gamma for proteasome-dependent degradation during infection. *J Virol*. 86:3167-79.
Fracasso, P.M., K.J. Williams, R.C. Chen, J. Picus, C.X. Ma, M.J. Ellis, B.R. Tan, T.J. Pluard, D.R. Adkins, M.J. Naughton, J.S. Rader, M.A. Arquette, J.W. Fleshman, A.N. Creekmore, S.A. Goodner, L.P. Wright, Z. Guo, C.E. Ryan, Y. Tao, E.M. Soares, S.R. Cai, L. Lin, J. Dancey, M.A. Rudek, H.L. McLeod, and H. Piwnica-Worms. 2011. A Phase 1 study of UCN-01 in combination with irinotecan in patients with resistant solid tumor malignancies. *Cancer Chemother Pharmacol*. 67:1225-37.
Freddie, C.T., Z. Ji, A. Marais, and A.D. Sharrocks. 2007. Functional interactions between the Forkhead transcription factor FOXK1 and the MADS-box protein SRF. *Nucleic Acids Res*. 35:5203-12.
Fredebohm, J., J. Wolf, J.D. Hoheisel, and M. Boettcher. 2013. Depletion of RAD17 sensitizes pancreatic cancer cells to gemcitabine. *J Cell Sci*. 126:3380-9.
Freire, R., M.A. van Vugt, I. Mamely, and R.H. Medema. 2006. Claspin: timing the cell cycle arrest when the genome is damaged. *Cell Cycle*. 5:2831-4.
Freytag, S.O., M. Khil, H. Stricker, J. Peabody, M. Menon, M. DePeralta-Venturina, D. Nafziger, J. Pegg, D. Paielli, S. Brown, K. Barton, M. Lu, E. Aguilar-Cordova, and J.H. Kim. 2002. Phase I study of replication-competent adenovirus-mediated double suicide gene therapy for the treatment of locally recurrent prostate cancer. *Cancer Res*. 62:4968-76.
Freytag, S.O., B. Movsas, I. Aref, H. Stricker, J. Peabody, J. Pegg, Y. Zhang, K.N. Barton, S.L. Brown, M. Lu, A. Savera, and J.H. Kim. 2007a. Phase I trial of replication-competent adenovirus-mediated suicide gene therapy combined with IMRT for prostate cancer. *Mol Ther*. 15:1016-23.
Freytag, S.O., K.R. Rogulski, D.L. Paielli, J.D. Gilbert, and J.H. Kim. 1998. A novel three-pronged approach to kill cancer cells selectively: concomitant viral, double suicide gene, and radiotherapy. *Hum Gene Ther*. 9:1323-33.
Freytag, S.O., H. Stricker, J. Peabody, J. Pegg, D. Paielli, B. Movsas, K.N. Barton, S.L. Brown, M. Lu, and J.H. Kim. 2007b. Five-year follow-up of trial of replication-competent adenovirus-mediated suicide gene therapy for treatment of prostate cancer. *Mol Ther*. 15:636-42.
Freytag, S.O., H. Stricker, J. Pegg, D. Paielli, D.G. Pradhan, J. Peabody, M. DePeralta-Venturina, X. Xia, S. Brown, M. Lu, and J.H. Kim. 2003. Phase I study of replication-competent adenovirus-mediated double-suicide gene therapy in combination with conventional-dose three-dimensional conformal radiation therapy for the treatment of newly diagnosed, intermediate- to high-risk prostate cancer. *Cancer Res*. 63:7497-506.
Frisch, S.M., and J.S. Mymryk. 2002. Adenovirus-5 E1A: paradox and paradigm. *Nat Rev Mol Cell Biol*. 3:441-52.

Fuchs, M., J. Gerber, R. Drapkin, S. Sif, T. Ikura, V. Ogryzko, W.S. Lane, Y. Nakatani, and D.M. Livingston. 2001. The p400 complex is an essential E1A transformation target. *Cell*. 106:297-307.

Fueyo, J., R. Alemany, C. Gomez-Manzano, G.N. Fuller, A. Khan, C.A. Conrad, T.J. Liu, H. Jiang, M.G. Lemoine, K. Suzuki, R. Sawaya, D.T. Curiel, W.K. Yung, and F.F. Lang. 2003. Preclinical characterization of the antiglioma activity of a tropism-enhanced adenovirus targeted to the retinoblastoma pathway. *J Natl Cancer Inst*. 95:652-60.

Fueyo, J., C. Gomez-Manzano, R. Alemany, P.S. Lee, T.J. McDonnell, P. Mitlianga, Y.X. Shi, V.A. Levin, W.K. Yung, and A.P. Kyritsis. 2000. A mutant oncolytic adenovirus targeting the Rb pathway produces anti-glioma effect in vivo. *Oncogene*. 19:2-12.

Fujiwara, T., M. Bandi, M. Nitta, E.V. Ivanova, R.T. Bronson, and D. Pellman. 2005. Cytokinesis failure generating tetraploids promotes tumorigenesis in p53-null cells. *Nature*. 437:1043-7.

Fukasawa, K. 2005. Centrosome amplification, chromosome instability and cancer development. *Cancer Lett*. 230:6-19.

Fukasawa, K. 2007. Oncogenes and tumour suppressors take on centrosomes. *Nat Rev Cancer*. 7:911-24.

Fulda, S. 2009. Apoptosis pathways and their therapeutic exploitation in pancreatic cancer. *J Cell Mol Med*. 13:1221-7.

Gagne, J.F., V. Montminy, P. Belanger, K. Journault, G. Gaucher, and C. Guillemette. 2002. Common human UGT1A polymorphisms and the altered metabolism of irinotecan active metabolite 7-ethyl-10-hydroxycamptothecin (SN-38). *Mol Pharmacol*. 62:608-17.

Gallimore, P.H., and A.S. Turnell. 2001. Adenovirus E1A: remodelling the host cell, a life or death experience. *Oncogene*. 20:7824-35.

Gallorini, M., A. Cataldi, and V. di Giacomo. 2012. Cyclin-dependent kinase modulators and cancer therapy. *BioDrugs*. 26:377-91.

Gandhi, V., J. Legha, F. Chen, L.W. Hertel, and W. Plunkett. 1996. Excision of 2',2'-difluorodeoxycytidine (gemcitabine) monophosphate residues from DNA. *Cancer Res*. 56:4453-9.

Ganem, N.J., H. Cornils, S.Y. Chiu, K.P. O'Rourke, J. Arnaud, D. Yimlamai, M. Thery, F.D. Camargo, and D. Pellman. 2014. Cytokinesis failure triggers hippo tumor suppressor pathway activation. *Cell*. 158:833-48.

Ganem, N.J., and D. Pellman. 2007. Limiting the proliferation of polyploid cells. *Cell*. 131:437-40.

Ganem, N.J., and D. Pellman. 2012. Linking abnormal mitosis to the acquisition of DNA damage. *J Cell Biol*. 199:871-81.

Ganem, N.J., Z. Storchova, and D. Pellman. 2007. Tetraploidy, aneuploidy and cancer. *Curr Opin Genet Dev*. 17:157-62.

Gao, K., W.W. Lockwood, J. Li, W. Lam, and G. Li. 2008. Genomic analyses identify gene candidates for acquired irinotecan resistance in melanoma cells. *Int J Oncol*. 32:1343-9.

Garber, K. 2006. China approves world's first oncolytic virus therapy for cancer treatment. *J Natl Cancer Inst*. 98:298-300.

Garrett, M.D., and I. Collins. 2011. Anticancer therapy with checkpoint inhibitors: what, where and when? *Trends Pharmacol Sci*. 32:308-16.

Gergely, F., and R. Basto. 2008. Multiple centrosomes: together they stand, divided they fall. *Genes Dev*. 22:2291-6.

Gewurz, B.E., and J.W. Harper. 2006. DNA-damage control: Claspin destruction turns off the checkpoint. *Curr Biol*. 16:R932-4.

Ghosn, M., H.R. Kourie, F. El Karak, C. Hanna, J. Antoun, and D. Nasr. 2014. Optimum chemotherapy in the management of metastatic pancreatic cancer. *World J Gastroenterol*. 20:2352-7.

Giannattasio, M., C. Follonier, H. Tourriere, F. Puddu, F. Lazzaro, P. Pasero, M. Lopes, P. Plevani, and M. Muzi-Falconi. 2010. Exo1 competes with repair synthesis, converts NER intermediates to long ssDNA gaps, and promotes checkpoint activation. *Mol Cell*. 40:50-62.

Giberson, A.N., A.R. Davidson, and R.J. Parks. 2012. Chromatin structure of adenovirus DNA throughout infection. *Nucleic Acids Res*. 40:2369-76.

Giovannetti, E., M. Del Tacca, V. Mey, N. Funel, S. Nannizzi, S. Ricci, C. Orlandini, U. Boggi, D. Campani, M. Del Chiaro, M. Iannopollo, G. Bevilacqua, F. Mosca, and R. Danesi. 2006. Transcription analysis of human equilibrative nucleoside transporter-1 predicts survival in pancreas cancer patients treated with gemcitabine. *Cancer Res*. 66:3928-35.

Giunta, S., R. Belotserkovskaya, and S.P. Jackson. 2010. DNA damage signaling in response to double-strand breaks during mitosis. *J Cell Biol*. 190:197-207.

Giunta, S., and S.P. Jackson. 2011. Give me a break, but not in mitosis: the mitotic DNA damage response marks DNA double-strand breaks with early signaling events. *Cell Cycle*. 10:1215-21.

Glover, D.M. 2012. The overlooked greatwall: a new perspective on mitotic control. *Open Biol*. 2:120023.

Gomez-Godinez, V., T. Wu, A.J. Sherman, C.S. Lee, L.H. Liaw, Y. Zhongsheng, K. Yokomori, and M.W. Berns. 2010. Analysis of DNA double-strand break response and chromatin structure in mitosis using laser microirradiation. *Nucleic Acids Res*. 38:e202.

Gomez-Manzano, C., M.M. Alonso, W.K. Yung, F. McCormick, D.T. Curiel, F.F. Lang, H. Jiang, B.N. Bekele, X. Zhou, R. Alemany, and J. Fueyo. 2006. Delta-24 increases the expression and activity of topoisomerase I and enhances the antiglioma effect of irinotecan. *Clin Cancer Res*. 12:556-62.

Goncalves, M.A., and A.A. de Vries. 2006. Adenovirus: from foe to friend. *Rev Med Virol*. 16:167-86.

Gongora, C., L. Candeil, N. Vezzio, V. Copois, V. Denis, C. Breil, F. Molina, C. Fraslon, E. Conseiller, B. Pau, P. Martineau, and M. Del Rio. 2008. Altered expression of cell proliferation-related and interferon-stimulated genes in colon cancer cells resistant to SN38. *Cancer Biol Ther*. 7:822-32.

Good, A.D., W. Duan, J. Anné, and Q.M. Wei. 2011. Cancer Gene Therapy - Developments and Future Perspectives. *In* GENE THERAPY - DEVELOPMENTS AND FUTURE PERSPECTIVES. C. Kang, editor. InTech, Rijeka, Croatia. 299-315.

Gooding, L.R., L. Aquino, P.J. Duerksen-Hughes, D. Day, T.M. Horton, S.P. Yei, and W.S. Wold. 1991. The E1B 19,000-molecular-weight protein of group C adenoviruses prevents tumor necrosis factor cytolysis of human cells but not of mouse cells. *J Virol*. 65:3083-94.

Goodrum, F.D., and D.A. Ornelles. 1998. p53 status does not determine outcome of E1B 55-kilodalton mutant adenovirus lytic infection. *J Virol*. 72:9479-90.

Gottesfeld, J.M., and D.J. Forbes. 1997. Mitotic repression of the transcriptional machinery. *Trends Biochem Sci*. 22:197-202.

Graat, H.C., M.A. Witlox, F.H. Schagen, G.J. Kaspers, M.N. Helder, J. Bras, G.R. Schaap, W.R. Gerritsen, P.I. Wuisman, and V.W. van Beusechem. 2006. Different susceptibility of osteosarcoma cell lines and primary cells to treatment with oncolytic adenovirus and doxorubicin or cisplatin. *Br J Cancer*. 94:1837-44.

Grant, G.D., J. Gamsby, V. Martyanov, L. Brooks, 3rd, L.K. George, J.M. Mahoney, J.J. Loros, J.C. Dunlap, and M.L. Whitfield. 2012. Live-cell monitoring of periodic gene expression in synchronous human cells identifies Forkhead genes involved in cell cycle control. *Mol Biol Cell*. 23:3079-93.

Gray, S.G., A.M. Baird, F. O'Kelly, G. Nikolaidis, M. Almgren, A. Meunier, E. Dockry, D. Hollywood, T.J. Ekstrom, A.S. Perry, and K.J. O'Byrne. 2012. Gemcitabine reactivates epigenetically silenced genes and functions as a DNA methyltransferase inhibitor. *Int J Mol Med*. 30:1505-11.

Gros, A., and S. Guedan. 2010. Adenovirus Release from the Infected Cell as a Key Factor for Adenovirus Oncolysis. *The Open Gene Therapy Journal*. 3:24-30.

Grossman, S.R. 2001. p300/CBP/p53 interaction and regulation of the p53 response. *Eur J Biochem*. 268:2773-8.

Grossman, S.R., M. Perez, A.L. Kung, M. Joseph, C. Mansur, Z.X. Xiao, S. Kumar, P.M. Howley, and D.M. Livingston. 1998. p300/MDM2 complexes participate in MDM2-mediated p53 degradation. *Mol Cell*. 2:405-15.

Guo, Z.S., and D.L. Bartlett. 2014. Oncolytic viruses as platform for multimodal cancer therapeutics: a promising land. *Cancer Gene Ther*. 21:261-3.

Guo, Z.S., Z. Liu, and D.L. Bartlett. 2014. Oncolytic Immunotherapy: Dying the Right Way is a Key to Eliciting Potent Antitumor Immunity. *Front Oncol*. 4:74.

Gupta, A., S. Jha, D.A. Engel, D.A. Ornelles, and A. Dutta. 2013. Tip60 degradation by adenovirus relieves transcriptional repression of viral transcriptional activator EIA. *Oncogene*. 32:5017-25.

Guse, K., T. Ranki, M. Ala-Opas, P. Bono, M. Sarkioja, M. Rajecki, A. Kanerva, T. Hakkarainen, and A. Hemminki. 2007. Treatment of metastatic renal cancer with capsid-modified oncolytic adenoviruses. *Mol Cancer Ther*. 6:2728-36.

Habara, A., K. Kano, H. Nagano, Y. Mano, S. Ikegami, and T. Yamashita. 1980. Inhibition of DNA synthesis in the adenovirus DNA replication complex by aphidicolin and 2',3'-dideoxythymidine triphosphate. *Biochem Biophys Res Commun*. 92:8-12.

Habiro, A., S. Tanno, K. Koizumi, T. Izawa, Y. Nakano, M. Osanai, Y. Mizukami, T. Okumura, and Y. Kohgo. 2004. Involvement of p38 mitogen-activated protein kinase in gemcitabine-induced apoptosis in human pancreatic cancer cells. *Biochem Biophys Res Commun*. 316:71-7.

Hall, A.R., B.R. Dix, S.J. O'Carroll, and A.W. Braithwaite. 1998. p53-dependent cell death/apoptosis is required for a productive adenovirus infection. *Nat Med*. 4:1068-72.

Hallden, G., and G. Portella. 2012. Oncolytic virotherapy with modified adenoviruses and novel therapeutic targets. *Expert Opin Ther Targets*. 16:945-58.

Hamacher, R., R.M. Schmid, D. Saur, and G. Schneider. 2008. Apoptotic pathways in pancreatic ductal adenocarcinoma. *Mol Cancer*. 7:64.

Hamada, S., A. Masamune, and T. Shimosegawa. 2014. Inflammation and pancreatic cancer: disease promoter and new therapeutic target. *J Gastroenterol*. 49:605-17.

Hamdan, S., C.S. Verbeke, N. Fox, J. Booth, G. Bottley, H.S. Pandha, and G.E. Blair. 2011. The roles of cell surface attachment molecules and coagulation Factor X in adenovirus 5-mediated gene transfer in pancreatic cancer cells. *Cancer Gene Ther*. 18:478-88.

Hapke, G., M.B. Yin, J. Wu, C. Frank, and Y.M. Rustum. 2002. Phosphorylation of chk1 at serine-345 affected by topoisomerase I poison SN-38. *Int J Oncol*. 21:1059-66.

Harada, J.N., A. Shevchenko, D.C. Pallas, and A.J. Berk. 2002. Analysis of the adenovirus E1B-55K-anchored proteome reveals its link to ubiquitination machinery. *J Virol*. 76:9194-206.

Hariharan, D., A. Saied, and H.M. Kocher. 2008. Analysis of mortality rates for pancreatic cancer across the world. *HPB (Oxford)*. 10:58-62.

Harley, M.E., L.A. Allan, H.S. Sanderson, and P.R. Clarke. 2010. Phosphorylation of Mcl-1 by CDK1-cyclin B1 initiates its Cdc20-dependent destruction during mitotic arrest. *EMBO J*. 29:2407-20.

Harrison, D., H. Sauthoff, S. Heitner, J. Jagirdar, W.N. Rom, and J.G. Hay. 2001. Wild-type adenovirus decreases tumor xenograft growth, but despite viral persistence complete tumor responses are rarely achieved--deletion of the viral E1b-19-kD gene increases the viral oncolytic effect. *Hum Gene Ther*. 12:1323-32.

Hart, L.S., S.M. Yannone, C. Naczki, J.S. Orlando, S.B. Waters, S.A. Akman, D.J. Chen, D. Ornelles, and C. Koumenis. 2005. The adenovirus E4orf6 protein inhibits DNA double strand break repair and radiosensitizes human tumor cells in an E1B-55K-independent manner. *J Biol Chem*. 280:1474-81.

Hashimoto, S., A. Ishii, and S. Yonehara. 1991. The E1b oncogene of adenovirus confers cellular resistance to cytotoxicity of tumor necrosis factor and monoclonal anti-Fas antibody. *Int Immunol*. 3:343-51.

Hawke, T.J., N. Jiang, and D.J. Garry. 2003. Absence of p21CIP rescues myogenic progenitor cell proliferative and regenerative capacity in Foxk1 null mice. *J Biol Chem*. 278:4015-20.

Hayashi, M.T., A.J. Cesare, J.A. Fitzpatrick, E. Lazzerini-Denchi, and J. Karlseder. 2012. A telomere-dependent DNA damage checkpoint induced by prolonged mitotic arrest. *Nat Struct Mol Biol*. 19:387-94.

Hayashi, M.T., and J. Karlseder. 2013. DNA damage associated with mitosis and cytokinesis failure. *Oncogene*. 32:4593-601.

He, B., X. Huang, X. Liu, and B. Xu. 2013. Cancer targeting gene-viro-therapy for pancreatic cancer using oncolytic adenovirus ZD55-IL-24 in immune-competent mice. *Mol Biol Rep*. 40:5397-405.

He, J., A.J. Page, M. Weiss, C.L. Wolfgang, J.M. Herman, and T.M. Pawlik. 2014. Management of borderline and locally advanced pancreatic cancer: where do we stand? *World J Gastroenterol*. 20:2255-66.

Hecht, J.R., R. Bedford, J.L. Abbruzzese, S. Lahoti, T.R. Reid, R.M. Soetikno, D.H. Kirn, and S.M. Freeman. 2003. A phase I/II trial of intratumoral endoscopic ultrasound injection of ONYX-015 with intravenous gemcitabine in unresectable pancreatic carcinoma. *Clin Cancer Res*. 9:555-61.

Hegarat, N., C. Vesely, P.K. Vinod, C. Ocasio, N. Peter, J. Gannon, A.W. Oliver, B. Novak, and H. Hochegger. 2014. PP2A/B55 and Fcp1 regulate

Greatwall and Ensa dephosphorylation during mitotic exit. *PLoS Genet*. 10:e1004004.
Heijink, A.M., M. Krajewska, and M.A. van Vugt. 2013. The DNA damage response during mitosis. *Mutat Res*. 750:45-55.
Heinemann, V., M. Haas, and S. Boeck. 2012. Systemic treatment of advanced pancreatic cancer. *Cancer Treat Rev*. 38:843-53.
Heinemann, V., R. Labianca, A. Hinke, and C. Louvet. 2007. Increased survival using platinum analog combined with gemcitabine as compared to single-agent gemcitabine in advanced pancreatic cancer: pooled analysis of two randomized trials, the GERCOR/GISCAD intergroup study and a German multicenter study. *Ann Oncol*. 18:1652-9.
Heinemann, V., Y.Z. Xu, S. Chubb, A. Sen, L.W. Hertel, G.B. Grindey, and W. Plunkett. 1990. Inhibition of ribonucleotide reduction in CCRF-CEM cells by 2',2'-difluorodeoxycytidine. *Mol Pharmacol*. 38:567-72.
Heinemann, V., Y.Z. Xu, S. Chubb, A. Sen, L.W. Hertel, G.B. Grindey, and W. Plunkett. 1992. Cellular elimination of 2',2'-difluorodeoxycytidine 5'-triphosphate: a mechanism of self-potentiation. *Cancer Res*. 52:533-9.
Heise, C., T. Hermiston, L. Johnson, G. Brooks, A. Sampson-Johannes, A. Williams, L. Hawkins, and D. Kirn. 2000. An adenovirus E1A mutant that demonstrates potent and selective systemic anti-tumoral efficacy. *Nat Med*. 6:1134-9.
Heise, C., and D.H. Kirn. 2000. Replication-selective adenoviruses as oncolytic agents. *J Clin Invest*. 105:847-51.
Hemminki, A. 2014. Oncolytic immunotherapy: where are we clinically? *Scientifica (Cairo)*. 2014:862925.
Heng, Y.W., and C.G. Koh. 2010. Actin cytoskeleton dynamics and the cell division cycle. *Int J Biochem Cell Biol*. 42:1622-33.
Hernando, E., Z. Nahle, G. Juan, E. Diaz-Rodriguez, M. Alaminos, M. Hemann, L. Michel, V. Mittal, W. Gerald, R. Benezra, S.W. Lowe, and C. Cordon-Cardo. 2004. Rb inactivation promotes genomic instability by uncoupling cell cycle progression from mitotic control. *Nature*. 430:797-802.
Hertel, L.W., J.S. Kroin, J.W. Misner, and J.M. Tustin. 1988. Synthesis of 2-deoxy-2,2-difluoro-D-ribose and 2-deoxy-2,2'-difluoro-D-ribofuranosyl nucleosides. *The Journal of Organic Chemistry*. 53:2406-2409.
Hetzer, M.W. 2010. The nuclear envelope. *Cold Spring Harb Perspect Biol*. 2:a000539.
Hezel, A.F., A.C. Kimmelman, B.Z. Stanger, N. Bardeesy, and R.A. Depinho. 2006. Genetics and biology of pancreatic ductal adenocarcinoma. *Genes Dev*. 20:1218-49.
Hong, Z., J. Jiang, J. Ma, S. Dai, T. Xu, H. Li, and A. Yasui. 2013. The role of hnRPUL1 involved in DNA damage response is related to PARP1. *PLoS One*. 8:e60208.
Horowitz, B., R. Sharf, M. Avital-Shacham, A. Pechkovsky, and T. Kleinberger. 2013. Structure- and modeling-based identification of the adenovirus E4orf4 binding site in the protein phosphatase 2A B55alpha subunit. *J Biol Chem*. 288:13718-27.
Horwitz, M.S. 2004. Function of adenovirus E3 proteins and their interactions with immunoregulatory cell proteins. *J Gene Med*. 6 Suppl 1:S172-83.
Hosoya, N., and K. Miyagawa. 2014. Targeting DNA damage response in cancer therapy. *Cancer Sci*. 105:370-88.
Hruban, R.H., M. Goggins, J. Parsons, and S.E. Kern. 2000. Progression model for pancreatic cancer. *Clin Cancer Res*. 6:2969-72.

Hsiang, Y.H., R. Hertzberg, S. Hecht, and L.F. Liu. 1985. Camptothecin induces protein-linked DNA breaks via mammalian DNA topoisomerase I. *J Biol Chem*. 260:14873-8.

Hsiang, Y.H., and L.F. Liu. 1988. Identification of mammalian DNA topoisomerase I as an intracellular target of the anticancer drug camptothecin. *Cancer Res*. 48:1722-6.

Hsiang, Y.H., L.F. Liu, M.E. Wall, M.C. Wani, A.W. Nicholas, G. Manikumar, S. Kirschenbaum, R. Silber, and M. Potmesil. 1989. DNA topoisomerase I-mediated DNA cleavage and cytotoxicity of camptothecin analogues. *Cancer Res*. 49:4385-9.

Huang, P., S. Chubb, L.W. Hertel, G.B. Grindey, and W. Plunkett. 1991. Action of 2',2'-difluorodeoxycytidine on DNA synthesis. *Cancer Res*. 51:6110-7.

Huang, P., and W. Plunkett. 1995. Induction of apoptosis by gemcitabine. *Semin Oncol*. 22:19-25.

Huang, X., T. Tran, L. Zhang, R. Hatcher, and P. Zhang. 2005. DNA damage-induced mitotic catastrophe is mediated by the Chk1-dependent mitotic exit DNA damage checkpoint. *Proc Natl Acad Sci U S A*. 102:1065-70.

Huen, M.S., and J. Chen. 2010. Assembly of checkpoint and repair machineries at DNA damage sites. *Trends Biochem Sci*. 35:101-8.

Humphrey, T., and G. Brooks. 2004. The Mammalian Cell Cycle. *In* Cell Cycle Control: Mechanisms and Protocols. Vol. 296. T. Humphrey and G. Brooks, editors. Humana Press. 113-115.

Hut, H.M., W. Lemstra, E.H. Blaauw, G.W. Van Cappellen, H.H. Kampinga, and O.C. Sibon. 2003. Centrosomes split in the presence of impaired DNA integrity during mitosis. *Mol Biol Cell*. 14:1993-2004.

Hyun, S.Y., H.I. Hwan, and Y.J. Jang. 2014. Polo-like kinase-1 in DNA damage response. *BMB Rep*. 47:249-55.

Hyun, S.Y., E.M. Rosen, and Y.J. Jang. 2012. Novel DNA damage checkpoint in mitosis: Mitotic DNA damage induces re-replication without cell division in various cancer cells. *Biochem Biophys Res Commun*. 423:593-9.

Ianzini, F., and M.A. Mackey. 1997. Spontaneous premature chromosome condensation and mitotic catastrophe following irradiation of HeLa S3 cells. *Int J Radiat Biol*. 72:409-21.

Ichijima, Y., K. Yoshioka, Y. Yoshioka, K. Shinohe, H. Fujimori, J. Unno, M. Takagi, H. Goto, M. Inagaki, S. Mizutani, and H. Teraoka. 2010. DNA lesions induced by replication stress trigger mitotic aberration and tetraploidy development. *PLoS One*. 5:e8821.

Ikeda, K., and S. Inoue. 2012. TRIM proteins as RING finger E3 ubiquitin ligases. *Adv Exp Med Biol*. 770:27-37.

Ingemarsdotter, C.K., S.K. Baird, C.M. Connell, D. Oberg, G. Hallden, and I.A. McNeish. 2010. Low-dose paclitaxel synergizes with oncolytic adenoviruses via mitotic slippage and apoptosis in ovarian cancer. *Oncogene*. 29:6051-63.

Inoue, H., and K. Tani. 2014. Multimodal immunogenic cancer cell death as a consequence of anticancer cytotoxic treatments. *Cell Death Differ*. 21:39-49.

Inuzuka, H., S. Shaik, I. Onoyama, D. Gao, A. Tseng, R.S. Maser, B. Zhai, L. Wan, A. Gutierrez, A.W. Lau, Y. Xiao, A.L. Christie, J. Aster, J. Settleman, S.P. Gygi, A.L. Kung, T. Look, K.I. Nakayama, R.A. DePinho, and W. Wei. 2011. SCF(FBW7) regulates cellular apoptosis by targeting MCL1 for ubiquitylation and destruction. *Nature*. 471:104-9.

Ito, H., H. Aoki, F. Kuhnel, Y. Kondo, S. Kubicka, T. Wirth, E. Iwado, A. Iwamaru, K. Fujiwara, K.R. Hess, F.F. Lang, R. Sawaya, and S. Kondo. 2006. Autophagic cell death of malignant glioma cells induced by a conditionally replicating adenovirus. *J Natl Cancer Inst*. 98:625-36.

Iwanaga, R., H. Komori, S. Ishida, N. Okamura, K. Nakayama, K.I. Nakayama, and K. Ohtani. 2006. Identification of novel E2F1 target genes regulated in cell cycle-dependent and independent manners. *Oncogene*. 25:1786-98.

Iyer, L., C.D. King, P.F. Whitington, M.D. Green, S.K. Roy, T.R. Tephly, B.L. Coffman, and M.J. Ratain. 1998. Genetic predisposition to the metabolism of irinotecan (CPT-11). Role of uridine diphosphate glucuronosyltransferase isoform 1A1 in the glucuronidation of its active metabolite (SN-38) in human liver microsomes. *J Clin Invest*. 101:847-54.

Jain, A.K., K. Allton, A.D. Duncan, and M.C. Barton. 2014. TRIM24 is a p53-Induced E3-Ubiquitin Ligase that undergoes ATM-Mediated Phosphorylation and Autodegradation during DNA Damage. *Mol Cell Biol*.

Jakob, B., J. Splinter, M. Durante, and G. Taucher-Scholz. 2009. Live cell microscopy analysis of radiation-induced DNA double-strand break motion. *Proc Natl Acad Sci U S A*. 106:3172-7.

Jang, Y.J., J.H. Ji, Y.C. Choi, C.J. Ryu, and S.Y. Ko. 2007. Regulation of Polo-like kinase 1 by DNA damage in mitosis. Inhibition of mitotic PLK-1 by protein phosphatase 2A. *J Biol Chem*. 282:2473-82.

Janssen, A., and R.H. Medema. 2011. Mitosis as an anti-cancer target. *Oncogene*. 30:2799-809.

Janssen, A., M. van der Burg, K. Szuhai, G.J. Kops, and R.H. Medema. 2011. Chromosome segregation errors as a cause of DNA damage and structural chromosome aberrations. *Science*. 333:1895-8.

Jasin, M., and R. Rothstein. 2013. Repair of strand breaks by homologous recombination. *Cold Spring Harb Perspect Biol*. 5:a012740.

Jayaram, S., T. Gilson, E.S. Ehrlich, X.F. Yu, G. Ketner, and L. Hanakahi. 2008. E1B 55k-independent dissociation of the DNA ligase IV/XRCC4 complex by E4 34k during adenovirus infection. *Virology*. 382:163-70.

Jefferies, C., C. Wynne, and R. Higgs. 2011. Antiviral TRIMs: friend or foe in autoimmune and autoinflammatory disease? *Nat Rev Immunol*. 11:617-25.

Jemaa, M., L. Galluzzi, O. Kepp, L. Senovilla, M. Brands, U. Boemer, M. Koppitz, P. Lienau, S. Prechtl, V. Schulze, G. Siemeister, A.M. Wengner, D. Mumberg, K. Ziegelbauer, A. Abrieu, M. Castedo, I. Vitale, and G. Kroemer. 2013. Characterization of novel MPS1 inhibitors with preclinical anticancer activity. *Cell Death Differ*. 20:1532-45.

Jeong, A.L., and Y. Yang. 2013. PP2A function toward mitotic kinases and substrates during the cell cycle. *BMB Rep*. 46:289-94.

Ji, Z., I.J. Donaldson, J. Liu, A. Hayes, L.A. Zeef, and A.D. Sharrocks. 2012. The forkhead transcription factor FOXK2 promotes AP-1-mediated transcriptional regulation. *Mol Cell Biol*. 32:385-98.

Jiang, G., Y. Xin, J.N. Zheng, and Y.Q. Liu. 2011a. Combining conditionally replicating adenovirus-mediated gene therapy with chemotherapy: a novel antitumor approach. *Int J Cancer*. 129:263-74.

Jiang, H., C. Gomez-Manzano, H. Aoki, M.M. Alonso, S. Kondo, F. McCormick, J. Xu, Y. Kondo, B.N. Bekele, H. Colman, F.F. Lang, and J. Fueyo. 2007.

Examination of the therapeutic potential of Delta-24-RGD in brain tumor stem cells: role of autophagic cell death. *J Natl Cancer Inst*. 99:1410-4.
Jiang, H., E.J. White, C. Gomez-Manzano, and J. Fueyo. 2008. Adenovirus's last trick: you say lysis, we say autophagy. *Autophagy*. 4:118-20.
Jiang, H., E.J. White, C.I. Rios-Vicil, J. Xu, C. Gomez-Manzano, and J. Fueyo. 2011b. Human adenovirus type 5 induces cell lysis through autophagy and autophagy-triggered caspase activity. *J Virol*. 85:4720-9.
Jin, J., X.L. Ang, X. Ye, M. Livingstone, and J.W. Harper. 2008. Differential roles for checkpoint kinases in DNA damage-dependent degradation of the Cdc25A protein phosphatase. *J Biol Chem*. 283:19322-8.
Jones, N. 1995. Transcriptional modulation by the adenovirus E1A gene. *Curr Top Microbiol Immunol*. 199 (Pt 3):59-80.
Jones, N., and T. Shenk. 1979. An adenovirus type 5 early gene function regulates expression of other early viral genes. *Proc Natl Acad Sci U S A*. 76:3665-9.
Jones, R.M., P. Kotsantis, G.S. Stewart, P. Groth, and E. Petermann. 2014. BRCA2 and RAD51 promote double-strand break formation and cell death in response to Gemcitabine. *Mol Cancer Ther*.
Jones, S., X. Zhang, D.W. Parsons, J.C. Lin, R.J. Leary, P. Angenendt, P. Mankoo, H. Carter, H. Kamiyama, A. Jimeno, S.M. Hong, B. Fu, M.T. Lin, E.S. Calhoun, M. Kamiyama, K. Walter, T. Nikolskaya, Y. Nikolsky, J. Hartigan, D.R. Smith, M. Hidalgo, S.D. Leach, A.P. Klein, E.M. Jaffee, M. Goggins, A. Maitra, C. Iacobuzio-Donahue, J.R. Eshleman, S.E. Kern, R.H. Hruban, R. Karchin, N. Papadopoulos, G. Parmigiani, B. Vogelstein, V.E. Velculescu, and K.W. Kinzler. 2008. Core signaling pathways in human pancreatic cancers revealed by global genomic analyses. *Science*. 321:1801-6.
Jossen, R., and R. Bermejo. 2013. The DNA damage checkpoint response to replication stress: A Game of Forks. *Front Genet*. 4:26.
Kadeppagari, R.K., N. Sankar, and B. Thimmapaya. 2009. Adenovirus transforming protein E1A induces c-Myc in quiescent cells by a novel mechanism. *J Virol*. 83:4810-22.
Kamileri, I., I. Karakasilioti, and G.A. Garinis. 2012. Nucleotide excision repair: new tricks with old bricks. *Trends Genet*. 28:566-73.
Kanda, M., H. Matthaei, J. Wu, S.M. Hong, J. Yu, M. Borges, R.H. Hruban, A. Maitra, K. Kinzler, B. Vogelstein, and M. Goggins. 2012. Presence of somatic mutations in most early-stage pancreatic intraepithelial neoplasia. *Gastroenterology*. 142:730-733 e9.
Kangasniemi, L., T. Kiviluoto, A. Kanerva, M. Raki, T. Ranki, M. Sarkioja, H. Wu, F. Marini, K. Hockerstedt, H. Isoniemi, H. Alfthan, U.H. Stenman, D.T. Curiel, and A. Hemminki. 2006. Infectivity-enhanced adenoviruses deliver efficacy in clinical samples and orthotopic models of disseminated gastric cancer. *Clin Cancer Res*. 12:3137-44.
Kao, C.Y., A. Tanimoto, N. Arima, Y. Sasaguri, and R. Padmanabhan. 1999. Transactivation of the human cdc2 promoter by adenovirus E1A. E1A induces the expression and assembly of a heteromeric complex consisting of the CCAAT box binding factor, CBF/NF-Y, and a 110-kDa DNA-binding protein. *J Biol Chem*. 274:23043-51.
Kao, Y.T., W.C. Hsu, H.T. Hu, S.H. Hsu, C.S. Lin, C.C. Chiu, C.Y. Lu, T.C. Hour, Y.S. Pu, and A.M. Huang. 2014. Involvement of p38 mitogen-activated protein kinase in acquired gemcitabine-resistant human urothelial carcinoma sublines. *Kaohsiung J Med Sci*. 30:323-30.

Kapoor, T.M., T.U. Mayer, M.L. Coughlin, and T.J. Mitchison. 2000. Probing spindle assembly mechanisms with monastrol, a small molecule inhibitor of the mitotic kinesin, Eg5. *J Cell Biol*. 150:975-88.

Karen, K.A., and P. Hearing. 2011. Adenovirus core protein VII protects the viral genome from a DNA damage response at early times after infection. *J Virol*. 85:4135-42.

Karnitz, L.M., K.S. Flatten, J.M. Wagner, D. Loegering, J.S. Hackbarth, S.J. Arlander, B.T. Vroman, M.B. Thomas, Y.U. Baek, K.M. Hopkins, H.B. Lieberman, J. Chen, W.A. Cliby, and S.H. Kaufmann. 2005. Gemcitabine-induced activation of checkpoint signaling pathways that affect tumor cell survival. *Mol Pharmacol*. 68:1636-44.

Keen, N., E. Brown, C. Crafter, R. Wilkinson, S. Wedge, K.M. Foote, A.A. Mortlock, F.H. Jung, N.M. Heron, and S. Green. 2005. Biological characterisation of AZD1152, a highly potent and selective inhibitor of Aurora kinase activity. *Clinical Cancer Research*. 11:9086S-9086S.

Kelleher, F.C. 2011. Hedgehog signaling and therapeutics in pancreatic cancer. *Carcinogenesis*. 32:445-51.

Kenneth, N.S., S. Mudie, and S. Rocha. 2010. IKK and NF-kappaB-mediated regulation of Claspin impacts on ATR checkpoint function. *EMBO J*. 29:2966-78.

Khuri, F.R., J. Nemunaitis, I. Ganly, J. Arseneau, I.F. Tannock, L. Romel, M. Gore, J. Ironside, R.H. MacDougall, C. Heise, B. Randlev, A.M. Gillenwater, P. Bruso, S.B. Kaye, W.K. Hong, and D.H. Kirn. 2000. a controlled trial of intratumoral ONYX-015, a selectively-replicating adenovirus, in combination with cisplatin and 5-fluorouracil in patients with recurrent head and neck cancer. *Nat Med*. 6:879-85.

Kim, J., J.Y. Cho, J.H. Kim, K.C. Jung, and C.O. Yun. 2002. Evaluation of E1B gene-attenuated replicating adenoviruses for cancer gene therapy. *Cancer Gene Ther*. 9:725-36.

Kim, J.H., Y.S. Lee, H. Kim, J.H. Huang, A.R. Yoon, and C.O. Yun. 2006. Relaxin expression from tumor-targeting adenoviruses and its intratumoral spread, apoptosis induction, and efficacy. *J Natl Cancer Inst*. 98:1482-93.

Kim, J.M., N. Kakusho, M. Yamada, Y. Kanoh, N. Takemoto, and H. Masai. 2008. Cdc7 kinase mediates Claspin phosphorylation in DNA replication checkpoint. *Oncogene*. 27:3475-82.

Kim, K.H., I. Dmitriev, J.P. O'Malley, M. Wang, S. Saddekni, Z. You, M.A. Preuss, R.D. Harris, R. Aurigemma, G.P. Siegal, K.R. Zinn, D.T. Curiel, and R.D. Alvarez. 2012. A phase I clinical trial of Ad5.SSTR/TK.RGD, a novel infectivity-enhanced bicistronic adenovirus, in patients with recurrent gynecologic cancer. *Clin Cancer Res*. 18:3440-51.

Kim, Y.J., and D.M. Wilson, 3rd. 2012. Overview of base excision repair biochemistry. *Curr Mol Pharmacol*. 5:3-13.

Kimball, K.J., M.A. Preuss, M.N. Barnes, M. Wang, G.P. Siegal, W. Wan, H. Kuo, S. Saddekni, C.R. Stockard, W.E. Grizzle, R.D. Harris, R. Aurigemma, D.T. Curiel, and R.D. Alvarez. 2010. A phase I study of a tropism-modified conditionally replicative adenovirus for recurrent malignant gynecologic diseases. *Clin Cancer Res*. 16:5277-87.

Kinkley, S., H. Staege, G. Mohrmann, G. Rohaly, T. Schaub, E. Kremmer, A. Winterpacht, and H. Will. 2009. SPOC1: a novel PHD-containing protein modulating chromatin structure and mitotic chromosome condensation. *J Cell Sci*. 122:2946-56.

Kirn, D. 2000. Replication-selective oncolytic adenoviruses: virotherapy aimed at genetic targets in cancer. *Oncogene*. 19:6660-6669.

Kirn, D., C. Heise, M. Williams, M. Propst, and T. Hermiston. 1998. Adenovirus E1A CR2 mutants as selectively-replicating agents for cancer. *Presented at Cancer Gene Therapy, meeting (R. Sobol and K. Scanlon, organizers). San Diego, Ca.*

Kleger, A., L. Perkhofer, and T. Seufferlein. 2014. Smarter drugs emerging in pancreatic cancer therapy. *Ann Oncol*. 25:1260-1270.

Ko, A.H., M.A. Tempero, Y.S. Shan, W.C. Su, Y.L. Lin, E. Dito, A. Ong, Y.W. Wang, C.G. Yeh, and L.T. Chen. 2013. A multinational phase 2 study of nanoliposomal irinotecan sucrosofate (PEP02, MM-398) for patients with gemcitabine-refractory metastatic pancreatic cancer. *Br J Cancer*. 109:920-5.

Kobayashi, K., B. Bouscarel, Y. Matsuzaki, S. Ceryak, S. Kudoh, and H. Fromm. 1999. pH-dependent uptake of irinotecan and its active metabolite, SN-38, by intestinal cells. *Int J Cancer*. 83:491-6.

Koizumi, K., S. Tanno, Y. Nakano, A. Habiro, T. Izawa, Y. Mizukami, T. Okumura, and Y. Kohgo. 2005. Activation of p38 mitogen-activated protein kinase is necessary for gemcitabine-induced cytotoxicity in human pancreatic cancer cells. *Anticancer Res*. 25:3347-53.

Kolli, S., A.M. Buchmann, J. Williams, S. Weitzman, and B. Thimmapaya. 2001. Antisense-mediated depletion of p300 in human cells leads to premature G1 exit and up-regulation of c-MYC. *Proc Natl Acad Sci U S A*. 98:4646-51.

Komorek, J., M. Kuppuswamy, T. Subramanian, S. Vijayalingam, E. Lomonosova, L.J. Zhao, J.S. Mymryk, K. Schmitt, and G. Chinnadurai. 2010. Adenovirus type 5 E1A and E6 proteins of low-risk cutaneous beta-human papillomaviruses suppress cell transformation through interaction with FOXK1/K2 transcription factors. *J Virol*. 84:2719-31.

Koorstra, J.B., S.R. Hustinx, G.J. Offerhaus, and A. Maitra. 2008. Pancreatic carcinogenesis. *Pancreatology*. 8:110-25.

Kornitzer, D., R. Sharf, and T. Kleinberger. 2001. Adenovirus E4orf4 protein induces PP2A-dependent growth arrest in Saccharomyces cerevisiae and interacts with the anaphase-promoting complex/cyclosome. *J Cell Biol*. 154:331-44.

Koski, A., L. Kangasniemi, S. Escutenaire, S. Pesonen, V. Cerullo, I. Diaconu, P. Nokisalmi, M. Raki, M. Rajecki, K. Guse, T. Ranki, M. Oksanen, S.L. Holm, E. Haavisto, A. Karioja-Kallio, L. Laasonen, K. Partanen, M. Ugolini, A. Helminen, E. Karli, P. Hannuksela, T. Joensuu, A. Kanerva, and A. Hemminki. 2010. Treatment of cancer patients with a serotype 5/3 chimeric oncolytic adenovirus expressing GMCSF. *Mol Ther*. 18:1874-84.

Krajewska, M., and M.A. van Vugt. 2010. Building a great wall around mitosis: evolutionary conserved roles for the Greatwall/MASTL kinases in securing chromosome stability. *Cell Cycle*. 9:3842.

Kramer, A., N. Mailand, C. Lukas, R.G. Syljuasen, C.J. Wilkinson, E.A. Nigg, J. Bartek, and J. Lukas. 2004. Centrosome-associated Chk1 prevents premature activation of cyclin-B-Cdk1 kinase. *Nat Cell Biol*. 6:884-91.

Krystyniak, A., C. Garcia-Echeverria, C. Prigent, and S. Ferrari. 2006. Inhibition of Aurora A in response to DNA damage. *Oncogene*. 25:338-48.

Kulkarni, A., J. Oza, M. Yao, H. Sohail, V. Ginjala, A. Tomas-Loba, Z. Horejsi, A.R. Tan, S.J. Boulton, and S. Ganesan. 2013. Tripartite Motif-containing

33 (TRIM33) protein functions in the poly(ADP-ribose) polymerase (PARP)-dependent DNA damage response through interaction with Amplified in Liver Cancer 1 (ALC1) protein. *J Biol Chem*. 288:32357-69.

Kumagai, A., and W.G. Dunphy. 2000. Claspin, a novel protein required for the activation of Chk1 during a DNA replication checkpoint response in Xenopus egg extracts. *Mol Cell*. 6:839-49.

Kumagai, A., and W.G. Dunphy. 2003. Repeated phosphopeptide motifs in Claspin mediate the regulated binding of Chk1. *Nat Cell Biol*. 5:161-5.

Kunda, P., and B. Baum. 2009. The actin cytoskeleton in spindle assembly and positioning. *Trends Cell Biol*. 19:174-9.

Kurimchak, A., and X. Grana. 2012. PP2A holoenzymes negatively and positively regulate cell cycle progression by dephosphorylating pocket proteins and multiple CDK substrates. *Gene*. 499:1-7.

Kuriyama, R., Y. Terada, K.S. Lee, and C.L. Wang. 2007. Centrosome replication in hydroxyurea-arrested CHO cells expressing GFP-tagged centrin2. *J Cell Sci*. 120:2444-53.

Kuroda, S., T. Fujiwara, Y. Shirakawa, Y. Yamasaki, S. Yano, F. Uno, H. Tazawa, Y. Hashimoto, Y. Watanabe, K. Noma, Y. Urata, and S. Kagawa. 2010. Telomerase-dependent oncolytic adenovirus sensitizes human cancer cells to ionizing radiation via inhibition of DNA repair machinery. *Cancer Res*. 70:9339-48.

Kwiatkowski, N., N. Jelluma, P. Filippakopoulos, M. Soundararajan, M.S. Manak, M. Kwon, H.G. Choi, T. Sim, Q.L. Deveraux, S. Rottmann, D. Pellman, J.V. Shah, G.J. Kops, S. Knapp, and N.S. Gray. 2010. Small-molecule kinase inhibitors provide insight into Mps1 cell cycle function. *Nat Chem Biol*. 6:359-68.

Kwon, M., S.A. Godinho, N.S. Chandhok, N.J. Ganem, A. Azioune, M. Thery, and D. Pellman. 2008. Mechanisms to suppress multipolar divisions in cancer cells with extra centrosomes. *Genes Dev*. 22:2189-203.

Labianca, R., B. Merelli, and S. Mosconi. 2012. Treatment of advanced pancreatic cancer. *Ann Oncol*. 23 Suppl 10:x139-40.

Labib, K., and G. De Piccoli. 2011. Surviving chromosome replication: the many roles of the S-phase checkpoint pathway. *Philos Trans R Soc Lond B Biol Sci*. 366:3554-61.

Lahav, G. 2008. Oscillations by the p53-Mdm2 feedback loop. *Adv Exp Med Biol*. 641:28-38.

Lamfers, M.L., J. Grill, C.M. Dirven, V.W. Van Beusechem, B. Geoerger, J. Van Den Berg, R. Alemany, J. Fueyo, D.T. Curiel, G. Vassal, H.M. Pinedo, W.P. Vandertop, and W.R. Gerritsen. 2002. Potential of the conditionally replicative adenovirus Ad5-Delta24RGD in the treatment of malignant gliomas and its enhanced effect with radiotherapy. *Cancer Res*. 62:5736-42.

Lan, W., and D.W. Cleveland. 2010. A chemical tool box defines mitotic and interphase roles for Mps1 kinase. *J Cell Biol*. 190:21-4.

Lancaster, O.M., and B. Baum. 2014. Shaping up to divide: Coordinating actin and microtubule cytoskeletal remodelling during mitosis. *Semin Cell Dev Biol*.

Lara-Gonzalez, P., F.G. Westhorpe, and S.S. Taylor. 2012. The spindle assembly checkpoint. *Curr Biol*. 22:R966-80.

Lavia, P., A.M. Mileo, A. Giordano, and M.G. Paggi. 2003. Emerging roles of DNA tumor viruses in cell proliferation: new insights into genomic instability. *Oncogene*. 22:6508-16.

Lavoie, J.N., M. Nguyen, R.C. Marcellus, P.E. Branton, and G.C. Shore. 1998. E4orf4, a novel adenovirus death factor that induces p53-independent apoptosis by a pathway that is not inhibited by zVAD-fmk. *J Cell Biol*. 140:637-45.

Lazzaro, F., M. Giannattasio, F. Puddu, M. Granata, A. Pellicioli, P. Plevani, and M. Muzi-Falconi. 2009. Checkpoint mechanisms at the intersection between DNA damage and repair. *DNA Repair (Amst)*. 8:1055-67.

Le Sage, V., and A.J. Mouland. 2013. Viral subversion of the nuclear pore complex. *Viruses*. 5:2019-42.

Lee, W.P., D.I. Tai, S.L. Tsai, C.T. Yeh, Y. Chao, S.D. Lee, and M.C. Hung. 2003. Adenovirus type 5 E1A sensitizes hepatocellular carcinoma cells to gemcitabine. *Cancer Res*. 63:6229-36.

Leitner, S., K. Sweeney, D. Oberg, D. Davies, E. Miranda, N.R. Lemoine, and G. Hallden. 2009. Oncolytic adenoviral mutants with E1B19K gene deletions enhance gemcitabine-induced apoptosis in pancreatic carcinoma cells and anti-tumor efficacy in vivo. *Clin Cancer Res*. 15:1730-40.

Leman, A.R., and E. Noguchi. 2012. Local and global functions of Timeless and Tipin in replication fork protection. *Cell Cycle*. 11:3945-55.

Lenart, P., M. Petronczki, M. Steegmaier, B. Di Fiore, J.J. Lipp, M. Hoffmann, W.J. Rettig, N. Kraut, and J.M. Peters. 2007. The small-molecule inhibitor BI 2536 reveals novel insights into mitotic roles of polo-like kinase 1. *Curr Biol*. 17:304-15.

Leopold, P.L., and R.G. Crystal. 2007. Intracellular trafficking of adenovirus: many means to many ends. *Adv Drug Deliv Rev*. 59:810-21.

Leopold, P.L., and K.K. Pfister. 2006. Viral strategies for intracellular trafficking: motors and microtubules. *Traffic*. 7:516-23.

Leppard, J.B., and J.J. Champoux. 2005. Human DNA topoisomerase I: relaxation, roles, and damage control. *Chromosoma*. 114:75-85.

Leung-Pineda, V., C.E. Ryan, and H. Piwnica-Worms. 2006. Phosphorylation of Chk1 by ATR is antagonized by a Chk1-regulated protein phosphatase 2A circuit. *Mol Cell Biol*. 26:7529-38.

Li, E., D. Stupack, G.M. Bokoch, and G.R. Nemerow. 1998a. Adenovirus endocytosis requires actin cytoskeleton reorganization mediated by Rho family GTPases. *J Virol*. 72:8806-12.

Li, H., H. Zhu, C.J. Xu, and J. Yuan. 1998b. Cleavage of BID by caspase 8 mediates the mitochondrial damage in the Fas pathway of apoptosis. *Cell*. 94:491-501.

Li, J., and D.F. Stern. 2005. Regulation of CHK2 by DNA-dependent protein kinase. *J Biol Chem*. 280:12041-50.

Li, L.H., T.J. Fraser, E.J. Olin, and B.K. Bhuyan. 1972. Action of camptothecin on mammalian cells in culture. *Cancer Res*. 32:2643-50.

Li, S., C. Brignole, R. Marcellus, S. Thirlwell, O. Binda, M.J. McQuoid, D. Ashby, H. Chan, Z. Zhang, M.J. Miron, D.C. Pallas, and P.E. Branton. 2009a. The adenovirus E4orf4 protein induces G2/M arrest and cell death by blocking protein phosphatase 2A activity regulated by the B55 subunit. *J Virol*. 83:8340-52.

Li, S., A. Szymborski, M.J. Miron, R. Marcellus, O. Binda, J.N. Lavoie, and P.E. Branton. 2009b. The adenovirus E4orf4 protein induces growth arrest and mitotic catastrophe in H1299 human lung carcinoma cells. *Oncogene*. 28:390-400.

Li, X., and Z. Darzynkiewicz. 1995. Labelling DNA strand breaks with BrdUTP. Detection of apoptosis and cell proliferation. *Cell Prolif*. 28:571-9.

Liao, W.C., K.L. Chien, Y.L. Lin, M.S. Wu, J.T. Lin, H.P. Wang, and Y.K. Tu. 2013. Adjuvant treatments for resected pancreatic adenocarcinoma: a systematic review and network meta-analysis. *Lancet Oncol*. 14:1095-103.

Libertini, S., A. Abagnale, C. Passaro, G. Botta, S. Barbato, P. Chieffi, and G. Portella. 2011. AZD1152 negatively affects the growth of anaplastic thyroid carcinoma cells and enhances the effects of oncolytic virus dl922-947. *Endocr Relat Cancer*. 18:129-41.

Lichtenstein, D.L., K. Doronin, K. Toth, M. Kuppuswamy, W.S. Wold, and A.E. Tollefson. 2004a. Adenovirus E3-6.7K protein is required in conjunction with the E3-RID protein complex for the internalization and degradation of TRAIL receptor 2. *J Virol*. 78:12297-307.

Lichtenstein, D.L., K. Toth, K. Doronin, A.E. Tollefson, and W.S. Wold. 2004b. Functions and mechanisms of action of the adenovirus E3 proteins. *Int Rev Immunol*. 23:75-111.

Lin, S.Y., K. Li, G.S. Stewart, and S.J. Elledge. 2004. Human Claspin works with BRCA1 to both positively and negatively regulate cell proliferation. *Proc Natl Acad Sci U S A*. 101:6484-9.

Lindqvist, A., M. de Bruijn, L. Macurek, A. Bras, A. Mensinga, W. Bruinsma, O. Voets, O. Kranenburg, and R.H. Medema. 2009. Wip1 confers G2 checkpoint recovery competence by counteracting p53-dependent transcriptional repression. *EMBO J*. 28:3196-206.

Lindsey-Boltz, L.A., and A. Sancar. 2011. Tethering DNA damage checkpoint mediator proteins topoisomerase IIbeta-binding protein 1 (TopBP1) and Claspin to DNA activates ataxia-telangiectasia mutated and RAD3-related (ATR) phosphorylation of checkpoint kinase 1 (Chk1). *J Biol Chem*. 286:19229-36.

Lindsey-Boltz, L.A., O. Sercin, J.H. Choi, and A. Sancar. 2009. Reconstitution of human claspin-mediated phosphorylation of Chk1 by the ATR (ataxia telangiectasia-mutated and rad3-related) checkpoint kinase. *J Biol Chem*. 284:33107-14.

Listovsky, T., and J.E. Sale. 2013. Sequestration of CDH1 by MAD2L2 prevents premature APC/C activation prior to anaphase onset. *J Cell Biol*. 203:87-100.

Liu, B., R. Cong, B. Peng, B. Zhu, G. Dou, H. Ai, X. Zhang, Z. Wang, and X. Xu. 2014. CtIP is required for DNA damage-dependent induction of P21. *Cell Cycle*. 13:90-5.

Liu, D., T. Kojima, M. Ouchi, S. Kuroda, Y. Watanabe, Y. Hashimoto, H. Onimatsu, Y. Urata, and T. Fujiwara. 2009. Preclinical evaluation of synergistic effect of telomerase-specific oncolytic virotherapy and gemcitabine for human lung cancer. *Mol Cancer Ther*. 8:980-7.

Liu, S., S. Bekker-Jensen, N. Mailand, C. Lukas, J. Bartek, and J. Lukas. 2006. Claspin operates downstream of TopBP1 to direct ATR signaling towards Chk1 activation. *Mol Cell Biol*. 26:6056-64.

Liu, S., N. Song, and L. Zou. 2012. The conserved C terminus of Claspin interacts with Rad9 and promotes rapid activation of Chk1. *Cell Cycle*. 11:2711-6.

Liu, S.H., N. Smyth-Templeton, A.R. Davis, E.A. Davis, N. Ballian, M. Li, H. Liu, W. Fisher, and F.C. Brunicardi. 2011. Multiple treatment cycles of liposome-encapsulated adenoviral RIP-TK gene therapy effectively

ablate human pancreatic cancer cells in SCID mice. *Surgery*. 149:484-95.
Liu, T.C., E. Galanis, and D. Kirn. 2007. Clinical trial results with oncolytic virotherapy: a century of promise, a decade of progress. *Nat Clin Pract Oncol*. 4:101-17.
Liu, T.C., G. Hallden, Y. Wang, G. Brooks, J. Francis, N. Lemoine, and D. Kirn. 2004. An E1B-19 kDa gene deletion mutant adenovirus demonstrates tumor necrosis factor-enhanced cancer selectivity and enhanced oncolytic potency. *Mol Ther*. 9:786-803.
Liu, T.C., Y. Wang, G. Hallden, G. Brooks, J. Francis, N.R. Lemoine, and D. Kirn. 2005. Functional interactions of antiapoptotic proteins and tumor necrosis factor in the context of a replication-competent adenovirus. *Gene Ther*. 12:1333-46.
Liu, X., and M. Winey. 2012. The MPS1 family of protein kinases. *Annu Rev Biochem*. 81:561-85.
Livne, A., R. Shtrichman, and T. Kleinberger. 2001. Caspase activation by adenovirus e4orf4 protein is cell line specific and Is mediated by the death receptor pathway. *J Virol*. 75:789-98.
Lockley, M., M. Fernandez, Y. Wang, N.F. Li, S. Conroy, N. Lemoine, and I. McNeish. 2006. Activity of the adenoviral E1A deletion mutant dl922-947 in ovarian cancer: comparison with E1A wild-type viruses, bioluminescence monitoring, and intraperitoneal delivery in icodextrin. *Cancer Res*. 66:989-98.
Loffler, H., B. Rebacz, A.D. Ho, J. Lukas, J. Bartek, and A. Kramer. 2006. Chk1-dependent regulation of Cdc25B functions to coordinate mitotic events. *Cell Cycle*. 5:2543-7.
Lomonosova, E., T. Subramanian, and G. Chinnadurai. 2005. Mitochondrial localization of p53 during adenovirus infection and regulation of its activity by E1B-19K. *Oncogene*. 24:6796-808.
Loncarek, J., P. Hergert, and A. Khodjakov. 2010. Centriole reduplication during prolonged interphase requires procentriole maturation governed by Plk1. *Curr Biol*. 20:1277-82.
Loos, M., J. Kleeff, H. Friess, and M.W. Buchler. 2008. Surgical treatment of pancreatic cancer. *Ann N Y Acad Sci*. 1138:169-80.
Lopez-Contreras, A.J., and O. Fernandez-Capetillo. 2010. The ATR barrier to replication-born DNA damage. *DNA Repair (Amst)*. 9:1249-55.
Lowe, J., H. Cha, M.O. Lee, S.J. Mazur, E. Appella, and A.J. Fornace, Jr. 2012. Regulation of the Wip1 phosphatase and its effects on the stress response. *Front Biosci (Landmark Ed)*. 17:1480-98.
Lu, X., D. Bocangel, B. Nannenga, H. Yamaguchi, E. Appella, and L.A. Donehower. 2004a. The p53-induced oncogenic phosphatase PPM1D interacts with uracil DNA glycosylase and suppresses base excision repair. *Mol Cell*. 15:621-34.
Lu, X., B. Nannenga, and L.A. Donehower. 2005. PPM1D dephosphorylates Chk1 and p53 and abrogates cell cycle checkpoints. *Genes Dev*. 19:1162-74.
Lu, X., T.A. Nguyen, E. Appella, and L.A. Donehower. 2004b. Homeostatic regulation of base excision repair by a p53-induced phosphatase: linking stress response pathways with DNA repair proteins. *Cell Cycle*. 3:1363-6.
Lu, X., T.A. Nguyen, S.H. Moon, Y. Darlington, M. Sommer, and L.A. Donehower. 2008. The type 2C phosphatase Wip1: an oncogenic

regulator of tumor suppressor and DNA damage response pathways. *Cancer Metastasis Rev*. 27:123-35.

Lukas, C., V. Savic, S. Bekker-Jensen, C. Doil, B. Neumann, R.S. Pedersen, M. Grofte, K.L. Chan, I.D. Hickson, J. Bartek, and J. Lukas. 2011. 53BP1 nuclear bodies form around DNA lesions generated by mitotic transmission of chromosomes under replication stress. *Nat Cell Biol*. 13:243-53.

Luo, X., I. Budihardjo, H. Zou, C. Slaughter, and X. Wang. 1998. Bid, a Bcl2 interacting protein, mediates cytochrome c release from mitochondria in response to activation of cell surface death receptors. *Cell*. 94:481-90.

Luttges, J., S. Neumann, R. Jesenofsky, V. Borries, M. Lohr, and G. Kloppel. 2003. Lack of apoptosis in PanIN-1 and PanIN-2 lesions associated with pancreatic ductal adenocarcinoma is not dependent on K-ras status. *Pancreas*. 27:e57-62.

Ma, C.X., S. Cai, S. Li, C.E. Ryan, Z. Guo, W.T. Schaiff, L. Lin, J. Hoog, R.J. Goiffon, A. Prat, R.L. Aft, M.J. Ellis, and H. Piwnica-Worms. 2012. Targeting Chk1 in p53-deficient triple-negative breast cancer is therapeutically beneficial in human-in-mouse tumor models. *J Clin Invest*. 122:1541-52.

Ma, G., K. Kawamura, Q. Li, S. Okamoto, N. Suzuki, H. Kobayashi, M. Liang, Y. Tada, K. Tatsumi, K. Hiroshima, H. Shimada, and M. Tagawa. 2010. Combinatory cytotoxic effects produced by E1B-55kDa-deleted adenoviruses and chemotherapeutic agents are dependent on the agents in esophageal carcinoma. *Cancer Gene Ther*. 17:803-13.

Macurek, L., A. Lindqvist, D. Lim, M.A. Lampson, R. Klompmaker, R. Freire, C. Clouin, S.S. Taylor, M.B. Yaffe, and R.H. Medema. 2008. Polo-like kinase-1 is activated by aurora A to promote checkpoint recovery. *Nature*. 455:119-23.

Maiato, H. 2010. Mitosis: wisdom, knowledge, and information. *Cellular and Molecular Life Sciences*. 67:2141-2143.

Maiato, H., and E. Logarinho. 2014. Mitotic spindle multipolarity without centrosome amplification. *Nat Cell Biol*. 16:386-94.

Mailand, N., S. Bekker-Jensen, J. Bartek, and J. Lukas. 2006. Destruction of Claspin by SCFbetaTrCP restrains Chk1 activation and facilitates recovery from genotoxic stress. *Mol Cell*. 23:307-18.

Maitra, A., N.V. Adsay, P. Argani, C. Iacobuzio-Donahue, A. De Marzo, J.L. Cameron, C.J. Yeo, and R.H. Hruban. 2003. Multicomponent Analysis of the Pancreatic Adenocarcinoma Progression Model Using a Pancreatic Intraepithelial Neoplasia Tissue Microarray. *Mod Pathol*. 16:902-912.

Maity, A., A. Hwang, A. Janss, P. Phillips, W.G. McKenna, and R.J. Muschel. 1996. Delayed cyclin B1 expression during the G2 arrest following DNA damage. *Oncogene*. 13:1647-57.

Mal, A., R.Y. Poon, P.H. Howe, H. Toyoshima, T. Hunter, and M.L. Harter. 1996. Inactivation of p27Kip1 by the viral E1A oncoprotein in TGFbeta-treated cells. *Nature*. 380:262-5.

Mamely, I., M.A. van Vugt, V.A. Smits, J.I. Semple, B. Lemmens, A. Perrakis, R.H. Medema, and R. Freire. 2006. Polo-like kinase-1 controls proteasome-dependent degradation of Claspin during checkpoint recovery. *Curr Biol*. 16:1950-5.

Manchado, E., M. Eguren, and M. Malumbres. 2010. The anaphase-promoting complex/cyclosome (APC/C): cell-cycle-dependent and -independent functions. *Biochem Soc Trans*. 38:65-71.

Mankouri, H.W., D. Huttner, and I.D. Hickson. 2013. How unfinished business from S-phase affects mitosis and beyond. *EMBO J*. 32:2661-71.

Mansilla, S., M. Bataller, and J. Portugal. 2006. Mitotic catastrophe as a consequence of chemotherapy. *Anticancer Agents Med Chem*. 6:589-602.

Manthei, K.A., and J.L. Keck. 2013. The BLM dissolvasome in DNA replication and repair. *Cell Mol Life Sci*. 70:4067-84.

Mao, L., C. Yang, L. Li, L. Nai, L. Fan, J. Wang, W. Li, R. Wen, J. Chen, and J. Zheng. 2014. Replication-competent adenovirus expressing TRAIL synergistically potentiates the antitumor effect of gemcitabine in bladder cancer cells. *Tumour Biol*. 35:5937-44.

Marais, A., Z. Ji, E.S. Child, E. Krause, D.J. Mann, and A.D. Sharrocks. 2010. Cell cycle-dependent regulation of the forkhead transcription factor FOXK2 by CDK.cyclin complexes. *J Biol Chem*. 285:35728-39.

Marcellus, R.C., J.N. Lavoie, D. Boivin, G.C. Shore, G. Ketner, and P.E. Branton. 1998. The early region 4 orf4 protein of human adenovirus type 5 induces p53-independent cell death by apoptosis. *J Virol*. 72:7144-53.

Marteijn, J.A., H. Lans, W. Vermeulen, and J.H. Hoeijmakers. 2014. Understanding nucleotide excision repair and its roles in cancer and ageing. *Nat Rev Mol Cell Biol*. 15:465-81.

Marthiens, V., M. Piel, and R. Basto. 2012. Never tear us apart--the importance of centrosome clustering. *J Cell Sci*. 125:3281-92.

Marti, T.M., E. Hefner, L. Feeney, V. Natale, and J.E. Cleaver. 2006. H2AX phosphorylation within the G1 phase after UV irradiation depends on nucleotide excision repair and not DNA double-strand breaks. *Proc Natl Acad Sci U S A*. 103:9891-6.

Mathew, S.S., and E. Bridge. 2007. The cellular Mre11 protein interferes with adenovirus E4 mutant DNA replication. *Virology*. 365:346-55.

Mathijssen, R.H., W.J. Loos, J. Verweij, and A. Sparreboom. 2002. Pharmacology of topoisomerase I inhibitors irinotecan (CPT-11) and topotecan. *Curr Cancer Drug Targets*. 2:103-23.

Matsuoka, S., G. Rotman, A. Ogawa, Y. Shiloh, K. Tamai, and S.J. Elledge. 2000. Ataxia telangiectasia-mutated phosphorylates Chk2 in vivo and in vitro. *Proc Natl Acad Sci U S A*. 97:10389-94.

Mayer, T.U., T.M. Kapoor, S.J. Haggarty, R.W. King, S.L. Schreiber, and T.J. Mitchison. 1999. Small molecule inhibitor of mitotic spindle bipolarity identified in a phenotype-based screen. *Science*. 286:971-4.

Mazia, D. 1961. How cells divide. *Sci Am*. 205:100-20.

McCleary-Wheeler, A.L., R. McWilliams, and M.E. Fernandez-Zapico. 2012. Aberrant signaling pathways in pancreatic cancer: a two compartment view. *Mol Carcinog*. 51:25-39.

McCormick, F. 2003. Cancer-specific viruses and the development of ONYX-015. *Cancer Biol Ther*. 2:S157-60.

McKenzie, L., S. King, L. Marcar, S. Nicol, S.S. Dias, K. Schumm, P. Robertson, J.C. Bourdon, N. Perkins, F. Fuller-Pace, and D.W. Meek. 2010. p53-dependent repression of polo-like kinase-1 (PLK1). *Cell Cycle*. 9:4200-12.

McNamara, A.V., M. Barclay, A.J. Watson, and J.R. Jenkins. 2012. Hsp90 inhibitors sensitise human colon cancer cells to topoisomerase I poisons by depletion of key anti-apoptotic and cell cycle checkpoint proteins. *Biochem Pharmacol*. 83:355-67.

McNeely, S., C. Conti, T. Sheikh, H. Patel, S. Zabludoff, Y. Pommier, G. Schwartz, and A. Tse. 2010. Chk1 inhibition after replicative stress activates a double strand break response mediated by ATM and DNA-dependent protein kinase. *Cell Cycle*. 9:995-1004.

McSharry, B.P., H.G. Burgert, D.P. Owen, R.J. Stanton, V. Prod'homme, M. Sester, K. Koebernick, V. Groh, T. Spies, S. Cox, A.M. Little, E.C. Wang, P. Tomasec, and G.W. Wilkinson. 2008. Adenovirus E3/19K promotes evasion of NK cell recognition by intracellular sequestration of the NKG2D ligands major histocompatibility complex class I chain-related proteins A and B. *J Virol*. 82:4585-94.

Medema, R.H. 2010. Greatwall in control of recovery. *Cell Cycle*. 9:4264-5.

Medema, R.H., and L. Macurek. 2011. Checkpoint recovery in cells: how a molecular understanding can help in the fight against cancer. *F1000 Biol Rep*. 3:10.

Medendorp, K., J.J. van Groningen, L. Vreede, L. Hetterschijt, W.H. van den Hurk, D.R. de Bruijn, L. Brugmans, and A.G. van Kessel. 2009. The mitotic arrest deficient protein MAD2B interacts with the small GTPase RAN throughout the cell cycle. *PLoS One*. 4:e7020.

Medendorp, K., L. Vreede, J.J. van Groningen, L. Hetterschijt, L. Brugmans, P.A. Jansen, W.H. van den Hurk, D.R. de Bruijn, and A.G. van Kessel. 2010. The mitotic arrest deficient protein MAD2B interacts with the clathrin light chain A during mitosis. *PLoS One*. 5:e15128.

Medina-Kauwe, L.K. 2003. Endocytosis of adenovirus and adenovirus capsid proteins. *Adv Drug Deliv Rev*. 55:1485-96.

Meek, D.W. 2004. The p53 response to DNA damage. *DNA Repair (Amst)*. 3:1049-56.

Melixetian, M., D.K. Klein, C.S. Sorensen, and K. Helin. 2009. NEK11 regulates CDC25A degradation and the IR-induced G2/M checkpoint. *Nat Cell Biol*. 11:1247-53.

Meng, Z., L. Capalbo, D.M. Glover, and W.G. Dunphy. 2011. Role for casein kinase 1 in the phosphorylation of Claspin on critical residues necessary for the activation of Chk1. *Mol Biol Cell*. 22:2834-47.

Michaelis, M., K. Langer, J.U. Vogel, J. Kreuter, H. Rabenau, H.W. Doerr, and J. Cinatl. 2002. In vitro antiviral activity of aphidicolin and its derivates. Synergistic effects of aphidicolin with other antiviral drugs. *Arzneimittelforschung*. 52:393-9.

Michl, P., and T.M. Gress. 2013. Current concepts and novel targets in advanced pancreatic cancer. *Gut*. 62:317-26.

Mikhailov, A., R.W. Cole, and C.L. Rieder. 2002. DNA damage during mitosis in human cells delays the metaphase/anaphase transition via the spindle-assembly checkpoint. *Curr Biol*. 12:1797-806.

Miller, D.L., C.L. Myers, B. Rickards, H.A. Coller, and S.J. Flint. 2007. Adenovirus type 5 exerts genome-wide control over cellular programs governing proliferation, quiescence, and survival. *Genome Biol*. 8:R58.

Millman, S.E., and M. Pagano. 2011. MCL1 meets its end during mitotic arrest. *EMBO Rep*. 12:384-5.

Mini, E., S. Nobili, B. Caciagli, I. Landini, and T. Mazzei. 2006. Cellular pharmacology of gemcitabine. *Ann Oncol*. 17 Suppl 5:v7-12.

Miranda, E., H. Maya Pineda, D. Oberg, G. Cherubini, Z. Garate, N.R. Lemoine, and G. Hallden. 2012. Adenovirus-mediated sensitization to the cytotoxic drugs docetaxel and mitoxantrone is dependent on regulatory domains in the E1ACR1 gene-region. *PLoS One*. 7:e46617.

Miyamoto, S. 2011. Nuclear initiated NF-kappaB signaling: NEMO and ATM take center stage. *Cell Res*. 21:116-30.

Mohammed, S., G. Van Buren Ii, and W.E. Fisher. 2014. Pancreatic cancer: Advances in treatment. *World J Gastroenterol*. 20:9354-9360.

Monaco, L., U. Kolthur-Seetharam, R. Loury, J.M. Murcia, G. de Murcia, and P. Sassone-Corsi. 2005. Inhibition of Aurora-B kinase activity by poly(ADP-ribosyl)ation in response to DNA damage. *Proc Natl Acad Sci U S A*. 102:14244-8.

Moore, M.J., D. Goldstein, J. Hamm, A. Figer, J.R. Hecht, S. Gallinger, H.J. Au, P. Murawa, D. Walde, R.A. Wolff, D. Campos, R. Lim, K. Ding, G. Clark, T. Voskoglou-Nomikos, M. Ptasynski, and W. Parulekar. 2007. Erlotinib plus gemcitabine compared with gemcitabine alone in patients with advanced pancreatic cancer: a phase III trial of the National Cancer Institute of Canada Clinical Trials Group. *J Clin Oncol*. 25:1960-6.

Moore, P.S., B. Sipos, S. Orlandini, C. Sorio, F.X. Real, N.R. Lemoine, T. Gress, C. Bassi, G. Kloppel, H. Kalthoff, H. Ungefroren, M. Lohr, and A. Scarpa. 2001. Genetic profile of 22 pancreatic carcinoma cell lines. Analysis of K-ras, p53, p16 and DPC4/Smad4. *Virchows Arch*. 439:798-802.

Morgan, D.O. 2007. The Cell Cycle. *In* The cell cycle: principles of control. E. Lawrence, editor. New Science Press Ltd. 2-5.

Morgan, M.A., L.A. Parsels, J.D. Parsels, A.K. Mesiwala, J. Maybaum, and T.S. Lawrence. 2005. Role of checkpoint kinase 1 in preventing premature mitosis in response to gemcitabine. *Cancer Res*. 65:6835-42.

Morgan, M.A., L.A. Parsels, L. Zhao, J.D. Parsels, M.A. Davis, M.C. Hassan, S. Arumugarajah, L. Hylander-Gans, D. Morosini, D.M. Simeone, C.E. Canman, D.P. Normolle, S.D. Zabludoff, J. Maybaum, and T.S. Lawrence. 2010. Mechanism of radiosensitization by the Chk1/2 inhibitor AZD7762 involves abrogation of the G2 checkpoint and inhibition of homologous recombinational DNA repair. *Cancer Res*. 70:4972-81.

Mortlock, A.A., K.M. Foote, N.M. Heron, F.H. Jung, G. Pasquet, J.J. Lohmann, N. Warin, F. Renaud, C. De Savi, N.J. Roberts, T. Johnson, C.B. Dousson, G.B. Hill, D. Perkins, G. Hatter, R.W. Wilkinson, S.R. Wedge, S.P. Heaton, R. Odedra, N.J. Keen, C. Crafter, E. Brown, K. Thompson, S. Brightwell, L. Khatri, M.C. Brady, S. Kearney, D. McKillop, S. Rhead, T. Parry, and S. Green. 2007. Discovery, synthesis, and in vivo activity of a new class of pyrazoloquinazolines as selective inhibitors of aurora B kinase. *J Med Chem*. 50:2213-24.

Moss, R.A., and C. Lee. 2010. Current and emerging therapies for the treatment of pancreatic cancer. *Onco Targets Ther*. 3:111-27.

Moufarij, M.A., D.R. Phillips, and C. Cullinane. 2003. Gemcitabine potentiates cisplatin cytotoxicity and inhibits repair of cisplatin-DNA damage in ovarian cancer cell lines. *Mol Pharmacol*. 63:862-9.

Mui, M.Z., M. Kucharski, M.J. Miron, W.S. Hur, A.M. Berghuis, P. Blanchette, and P.E. Branton. 2013. Identification of the adenovirus E4orf4 protein binding site on the B55alpha and Cdc55 regulatory subunits of PP2A: Implications for PP2A function, tumor cell killing and viral replication. *PLoS Pathog*. 9:e1003742.

Mui, M.Z., D.E. Roopchand, M.S. Gentry, R.L. Hallberg, J. Vogel, and P.E. Branton. 2010. Adenovirus protein E4orf4 induces premature APCCdc20 activation in Saccharomyces cerevisiae by a protein phosphatase 2A-dependent mechanism. *J Virol*. 84:4798-809.

Mulvihill, S., R. Warren, A. Venook, A. Adler, B. Randlev, C. Heise, and D. Kirn. 2001. Safety and feasibility of injection with an E1B-55 kDa gene-deleted, replication-selective adenovirus (ONYX-015) into primary carcinomas of the pancreas: a phase I trial. *Gene Ther*. 8:308-15.

Mund, A., T. Schubert, H. Staege, S. Kinkley, K. Reumann, M. Kriegs, L. Fritsch, V. Battisti, S. Ait-Si-Ali, A.S. Hoffbeck, E. Soutoglou, and H. Will. 2012. SPOC1 modulates DNA repair by regulating key determinants of chromatin compaction and DNA damage response. *Nucleic Acids Res*. 40:11363-79.

Muniraj, T., P.A. Jamidar, and H.R. Aslanian. 2013. Pancreatic cancer: a comprehensive review and update. *Dis Mon*. 59:368-402.

Murga, M., S. Bunting, M.F. Montana, R. Soria, F. Mulero, M. Canamero, Y. Lee, P.J. McKinnon, A. Nussenzweig, and O. Fernandez-Capetillo. 2009. A mouse model of ATR-Seckel shows embryonic replicative stress and accelerated aging. *Nat Genet*. 41:891-8.

Murray, J.D., A.J. Bellett, A. Braithwaite, L.K. Waldron, and I.W. Taylor. 1982. Altered cell cycle progression and aberrant mitosis in adenovirus-infected rodent cells. *J Cell Physiol*. 111:89-96.

Musk, P., A. Stowers, and P.G. Parsons. 1990. Effects of antimetabolites on adenovirus replication in sensitive and resistant human melanoma cell lines. *Biochem Pharmacol*. 39:631-7.

Mymryk, J.S., and M.M. Smith. 1997. Influence of the adenovirus 5 E1A oncogene on chromatin remodelling. *Biochem Cell Biol*. 75:95-102.

Nakahira, S., S. Nakamori, M. Tsujie, Y. Takahashi, J. Okami, S. Yoshioka, M. Yamasaki, S. Marubashi, I. Takemasa, A. Miyamoto, Y. Takeda, H. Nagano, K. Dono, K. Umeshita, M. Sakon, and M. Monden. 2007. Involvement of ribonucleotide reductase M1 subunit overexpression in gemcitabine resistance of human pancreatic cancer. *Int J Cancer*. 120:1355-63.

Nakano, Y., S. Tanno, K. Koizumi, T. Nishikawa, K. Nakamura, M. Minoguchi, T. Izawa, Y. Mizukami, T. Okumura, and Y. Kohgo. 2007. Gemcitabine chemoresistance and molecular markers associated with gemcitabine transport and metabolism in human pancreatic cancer cells. *Br J Cancer*. 96:457-63.

Napolitano, L.M., and G. Meroni. 2012. TRIM family: Pleiotropy and diversification through homomultimer and heteromultimer formation. *IUBMB Life*. 64:64-71.

Naud, S., I.M. Westwood, A. Faisal, P. Sheldrake, V. Bavetsias, B. Atrash, K.M. Cheung, M. Liu, A. Hayes, J. Schmitt, A. Wood, V. Choi, K. Boxall, G. Mak, M. Gurden, M. Valenti, A. de Haven Brandon, A. Henley, R. Baker, C. McAndrew, B. Matijssen, R. Burke, S. Hoelder, S.A. Eccles, F.I. Raynaud, S. Linardopoulos, R.L. van Montfort, and J. Blagg. 2013. Structure-based design of orally bioavailable 1H-pyrrolo[3,2-c]pyridine inhibitors of mitotic kinase monopolar spindle 1 (MPS1). *J Med Chem*. 56:10045-65.

Nayak, S., and R.W. Herzog. 2010. Progress and prospects: immune responses to viral vectors. *Gene Ther*. 17:295-304.

Neesse, A., S. Krug, T.M. Gress, D.A. Tuveson, and P. Michl. 2013. Emerging concepts in pancreatic cancer medicine: targeting the tumor stroma. *Onco Targets Ther*. 7:33-43.

Nelson, G., M. Buhmann, and T. von Zglinicki. 2009. DNA damage foci in mitosis are devoid of 53BP1. *Cell Cycle*. 8:3379-83.

Nemerow, G.R., L. Pache, V. Reddy, and P.L. Stewart. 2009. Insights into adenovirus host cell interactions from structural studies. *Virology*. 384:380-8.

Nemunaitis, J., T. Meyers, N. Senzer, C. Cunningham, H. West, E. Vallieres, S. Anthony, S. Vukelja, B. Berman, H. Tully, B. Pappen, S. Sarmiento, R. Arzaga, S. Duniho, S. Engardt, M. Meagher, and M.A. Cheever. 2006. Phase I Trial of sequential administration of recombinant DNA and adenovirus expressing L523S protein in early stage non-small-cell lung cancer. *Mol Ther*. 13:1185-91.

Neuzillet, C., O. Hentic, B. Rousseau, V. Rebours, L. Bengrine-Lefevre, F. Bonnetain, P. Levy, E. Raymond, P. Ruszniewski, C. Louvet, and P. Hammel. 2012. FOLFIRI regimen in metastatic pancreatic adenocarcinoma resistant to gemcitabine and platinum-salts. *World J Gastroenterol*. 18:4533-41.

Nguyen, T.A., S.D. Slattery, S.H. Moon, Y.F. Darlington, X. Lu, and L.A. Donehower. 2010. The oncogenic phosphatase WIP1 negatively regulates nucleotide excision repair. *DNA Repair (Amst)*. 9:813-23.

Nichols, G.J., J. Schaack, and D.A. Ornelles. 2009. Widespread phosphorylation of histone H2AX by species C adenovirus infection requires viral DNA replication. *J Virol*. 83:5987-98.

Nigg, E.A. 2002. Centrosome aberrations: cause or consequence of cancer progression? *Nat Rev Cancer*. 2:815-25.

Nimonkar, A.V., J. Genschel, E. Kinoshita, P. Polaczek, J.L. Campbell, C. Wyman, P. Modrich, and S.C. Kowalczykowski. 2011. BLM-DNA2-RPA-MRN and EXO1-BLM-RPA-MRN constitute two DNA end resection machineries for human DNA break repair. *Genes Dev*. 25:350-62.

Nirula, A., D.J. Moore, and R.B. Gaynor. 1997. Constitutive binding of the transcription factor interleukin-2 (IL-2) enhancer binding factor to the IL-2 promoter. *J Biol Chem*. 272:7736-45.

Nitta, M., O. Kobayashi, S. Honda, T. Hirota, S. Kuninaka, T. Marumoto, Y. Ushio, and H. Saya. 2004. Spindle checkpoint function is required for mitotic catastrophe induced by DNA-damaging agents. *Oncogene*. 23:6548-58.

Nokisalmi, P., S. Pesonen, S. Escutenaire, M. Sarkioja, M. Raki, V. Cerullo, L. Laasonen, R. Alemany, J. Rojas, M. Cascallo, K. Guse, M. Rajecki, L. Kangasniemi, E. Haavisto, A. Karioja-Kallio, P. Hannuksela, M. Oksanen, A. Kanerva, T. Joensuu, L. Ahtiainen, and A. Hemminki. 2010. Oncolytic adenovirus ICOVIR-7 in patients with advanced and refractory solid tumors. *Clin Cancer Res*. 16:3035-43.

Normand, G., and R.W. King. 2010. Understanding cytokinesis failure. *Adv Exp Med Biol*. 676:27-55.

Nowsheen, S., and E.S. Yang. 2012. The intersection between DNA damage response and cell death pathways. *Exp Oncol*. 34:243-54.

Nozawa, T., H. Minami, S. Sugiura, A. Tsuji, and I. Tamai. 2005. Role of organic anion transporter OATP1B1 (OATP-C) in hepatic uptake of irinotecan and its active metabolite, 7-ethyl-10-hydroxycamptothecin: in vitro evidence and effect of single nucleotide polymorphisms. *Drug Metab Dispos*. 33:434-9.

O'Shea, C.C., L. Johnson, B. Bagus, S. Choi, C. Nicholas, A. Shen, L. Boyle, K. Pandey, C. Soria, J. Kunich, Y. Shen, G. Habets, D. Ginzinger, and F. McCormick. 2004. Late viral RNA export, rather than p53 inactivation, determines ONYX-015 tumor selectivity. *Cancer Cell*. 6:611-23.

Obata, T., G.E. Brown, and M.B. Yaffe. 2000. MAP kinase pathways activated by stress: the p38 MAPK pathway. *Crit Care Med*. 28:N67-77.

Oberg, D., E. Yanover, V. Adam, K. Sweeney, C. Costas, N.R. Lemoine, and G. Hallden. 2010. Improved potency and selectivity of an oncolytic E1ACR2 and E1B19K deleted adenoviral mutant in prostate and pancreatic cancers. *Clin Cancer Res*. 16:541-53.

Oda, K., H. Arakawa, T. Tanaka, K. Matsuda, C. Tanikawa, T. Mori, H. Nishimori, K. Tamai, T. Tokino, Y. Nakamura, and Y. Taya. 2000. p53AIP1, a potential mediator of p53-dependent apoptosis, and its regulation by Ser-46-phosphorylated p53. *Cell*. 102:849-62.

Office for National Statistics. 2013. Cancer survival rates, Cancer Survival in England. *Retrived 04/09/2014, from: http://www.ons.gov.uk/ons/rel/cancer-unit/cancer-survival/cancer-survival-in-england--patients-diagnosed-2007-2011-and-followed-up-to-2012/index.html*.

Ohhashi, S., K. Ohuchida, K. Mizumoto, H. Fujita, T. Egami, J. Yu, H. Toma, S. Sadatomi, E. Nagai, and M. Tanaka. 2008. Down-regulation of deoxycytidine kinase enhances acquired resistance to gemcitabine in pancreatic cancer. *Anticancer Res*. 28:2205-12.

Onimaru, M., K. Ohuchida, T. Egami, K. Mizumoto, E. Nagai, L. Cui, H. Toma, K. Matsumoto, M. Hashizume, and M. Tanaka. 2010a. Gemcitabine synergistically enhances the effect of adenovirus gene therapy through activation of the CMV promoter in pancreatic cancer cells. *Cancer Gene Ther*. 17:541-9.

Onimaru, M., K. Ohuchida, E. Nagai, K. Mizumoto, T. Egami, L. Cui, N. Sato, J. Uchino, K. Takayama, M. Hashizume, and M. Tanaka. 2010b. Combination with low-dose gemcitabine and hTERT-promoter-dependent conditionally replicative adenovirus enhances cytotoxicity through their crosstalk mechanisms in pancreatic cancer. *Cancer Lett*. 294:178-86.

Orazio, N.I., C.M. Naeger, J. Karlseder, and M.D. Weitzman. 2011. The adenovirus E1b55K/E4orf6 complex induces degradation of the Bloom helicase during infection. *J Virol*. 85:1887-92.

Orth, J.D., A. Loewer, G. Lahav, and T.J. Mitchison. 2012. Prolonged mitotic arrest triggers partial activation of apoptosis, resulting in DNA damage and p53 induction. *Mol Biol Cell*. 23:567-76.

Orthwein, A., A. Fradet-Turcotte, S.M. Noordermeer, M.D. Canny, C.M. Brun, J. Strecker, C. Escribano-Diaz, and D. Durocher. 2014. Mitosis inhibits DNA double-strand break repair to guard against telomere fusions. *Science*. 344:189-93.

Ottenhof, N.A., R.F. de Wilde, A. Maitra, R.H. Hruban, and G.J. Offerhaus. 2011. Molecular characteristics of pancreatic ductal adenocarcinoma. *Patholog Res Int*. 2011:620601.

Ouyang, K.J., M.K. Yagle, M.J. Matunis, and N.A. Ellis. 2013. BLM SUMOylation regulates ssDNA accumulation at stalled replication forks. *Front Genet*. 4:167.

Pabla, N., S. Huang, Q.S. Mi, R. Daniel, and Z. Dong. 2008. ATR-Chk2 signaling in p53 activation and DNA damage response during cisplatin-induced apoptosis. *J Biol Chem*. 283:6572-83.

Pace, E., M. Melis, L. Siena, F. Bucchieri, A.M. Vignola, M. Profita, M. Gjomarkaj, and G. Bonsignore. 2000. Effects of gemcitabine on cell proliferation and apoptosis in non-small-cell lung cancer (NSCLC) cell lines. *Cancer Chemother Pharmacol*. 46:467-76.

Paillas, S., F. Boissiere, F. Bibeau, A. Denouel, C. Mollevi, A. Causse, V. Denis, N. Vezzio-Vie, L. Marzi, C. Cortijo, I. Ait-Arsa, N. Askari, P. Pourquier, P. Martineau, M. Del Rio, and C. Gongora. 2011. Targeting the p38 MAPK pathway inhibits irinotecan resistance in colon adenocarcinoma. *Cancer Res*. 71:1041-9.

Paillas, S., A. Causse, L. Marzi, P. de Medina, M. Poirot, V. Denis, N. Vezzio-Vie, L. Espert, H. Arzouk, A. Coquelle, P. Martineau, M. Del Rio, S. Pattingre, and C. Gongora. 2012. MAPK14/p38alpha confers irinotecan resistance to TP53-defective cells by inducing survival autophagy. *Autophagy*. 8:1098-112.

Panier, S., and S.J. Boulton. 2014. Double-strand break repair: 53BP1 comes into focus. *Nat Rev Mol Cell Biol*. 15:7-18.

Parato, K.A., D. Senger, P.A. Forsyth, and J.C. Bell. 2005. Recent progress in the battle between oncolytic viruses and tumours. *Nat Rev Cancer*. 5:965-76.

Park, C.H., and K.T. Kim. 2012. Apoptotic phosphorylation of histone H3 on Ser-10 by protein kinase Cdelta. *PLoS One*. 7:e44307.

Parsels, L.A., M.A. Morgan, D.M. Tanska, J.D. Parsels, B.D. Palmer, R.J. Booth, W.A. Denny, C.E. Canman, A.J. Kraker, T.S. Lawrence, and J. Maybaum. 2009. Gemcitabine sensitization by checkpoint kinase 1 inhibition correlates with inhibition of a Rad51 DNA damage response in pancreatic cancer cells. *Mol Cancer Ther*. 8:45-54.

Parsons, J.L., and G.L. Dianov. 2013. Co-ordination of base excision repair and genome stability. *DNA Repair (Amst)*. 12:326-33.

Patil, M., N. Pabla, and Z. Dong. 2013. Checkpoint kinase 1 in DNA damage response and cell cycle regulation. *Cell Mol Life Sci*. 70:4009-21.

Pelka, P., J.N. Ablack, G.J. Fonseca, A.F. Yousef, and J.S. Mymryk. 2008. Intrinsic structural disorder in adenovirus E1A: a viral molecular hub linking multiple diverse processes. *J Virol*. 82:7252-63.

Pelka, P., J.N. Ablack, J. Torchia, A.S. Turnell, R.J. Grand, and J.S. Mymryk. 2009. Transcriptional control by adenovirus E1A conserved region 3 via p300/CBP. *Nucleic Acids Res*. 37:1095-106.

Peng, A. 2013. Working hard for recovery: mitotic kinases in the DNA damage checkpoint. *Cell Biosci*. 3:20.

Peng, A., L. Wang, and L.A. Fisher. 2011. Greatwall and Polo-like kinase 1 coordinate to promote checkpoint recovery. *J Biol Chem*. 286:28996-9004.

Peng, A., T.M. Yamamoto, M.L. Goldberg, and J.L. Maller. 2010. A novel role for greatwall kinase in recovery from DNA damage. *Cell Cycle*. 9:4364-9.

Peschiaroli, A., N.V. Dorrello, D. Guardavaccaro, M. Venere, T. Halazonetis, N.E. Sherman, and M. Pagano. 2006. SCFbetaTrCP-mediated degradation of Claspin regulates recovery from the DNA replication checkpoint response. *Mol Cell*. 23:319-29.

Pesonen, S., I. Diaconu, L. Kangasniemi, T. Ranki, A. Kanerva, S.K. Pesonen, U. Gerdemann, A.M. Leen, K. Kairemo, M. Oksanen, E. Haavisto, S.L. Holm, A. Karioja-Kallio, S. Kauppinen, K.P. Partanen, L. Laasonen, T. Joensuu, T. Alanko, V. Cerullo, and A. Hemminki. 2012. Oncolytic immunotherapy of advanced solid tumors with a CD40L-expressing replicating adenovirus: assessment of safety and immunologic responses in patients. *Cancer Res*. 72:1621-31.

Pesonen, S., L. Kangasniemi, and A. Hemminki. 2011. Oncolytic adenoviruses for the treatment of human cancer: focus on translational and clinical data. *Mol Pharm*. 8:12-28.

Petermann, E., T. Helleday, and K.W. Caldecott. 2008. Claspin promotes normal replication fork rates in human cells. *Mol Biol Cell*. 19:2373-8.

Peters, J.M. 2006. The anaphase promoting complex/cyclosome: a machine designed to destroy. *Nat Rev Mol Cell Biol*. 7:644-56.

Peterson, S.E., Y. Li, B.T. Chait, M.E. Gottesman, R. Baer, and J. Gautier. 2011. Cdk1 uncouples CtIP-dependent resection and Rad51 filament formation during M-phase double-strand break repair. *J Cell Biol*. 194:705-20.

Petitprez, A., V. Poindessous, D. Ouaret, M. Regairaz, G. Bastian, E. Guerin, A.E. Escargueil, and A.K. Larsen. 2013. Acquired irinotecan resistance is accompanied by stable modifications of cell cycle dynamics independent of MSI status. *Int J Oncol*. 42:1644-53.

Petronczki, M., P. Lenart, and J.M. Peters. 2008. Polo on the Rise-from Mitotic Entry to Cytokinesis with Plk1. *Dev Cell*. 14:646-59.

Pfleger, C.M., A. Salic, E. Lee, and M.W. Kirschner. 2001. Inhibition of Cdh1-APC by the MAD2-related protein MAD2L2: a novel mechanism for regulating Cdh1. *Genes Dev*. 15:1759-64.

Pilder, S., J. Logan, and T. Shenk. 1984. Deletion of the gene encoding the adenovirus 5 early region 1b 21,000-molecular-weight polypeptide leads to degradation of viral and host cell DNA. *J Virol*. 52:664-71.

Piya, S., E.J. White, S.R. Klein, H. Jiang, T.J. McDonnell, C. Gomez-Manzano, and J. Fueyo. 2011. The E1B19K oncoprotein complexes with Beclin 1 to regulate autophagy in adenovirus-infected cells. *PLoS One*. 6:e29467.

Polistina, F., G. Di Natale, G. Bonciarelli, G. Ambrosino, and M. Frego. 2014. Neoadjuvant strategies for pancreatic cancer. *World J Gastroenterol*. 20:9374-9383.

Polo, S.E., A.N. Blackford, J.R. Chapman, L. Baskcomb, S. Gravel, A. Rusch, A. Thomas, R. Blundred, P. Smith, J. Kzhyshkowska, T. Dobner, A.M. Taylor, A.S. Turnell, G.S. Stewart, R.J. Grand, and S.P. Jackson. 2012. Regulation of DNA-end resection by hnRNPU-like proteins promotes DNA double-strand break signaling and repair. *Mol Cell*. 45:505-16.

Portugal, J., S. Mansilla, and M. Bataller. 2010. Mechanisms of drug-induced mitotic catastrophe in cancer cells. *Curr Pharm Des*. 16:69-78.

Pourquier, P., C. Gioffre, G. Kohlhagen, Y. Urasaki, F. Goldwasser, L.W. Hertel, S. Yu, R.T. Pon, W.H. Gmeiner, and Y. Pommier. 2002. Gemcitabine (2',2'-difluoro-2'-deoxycytidine), an antimetabolite that poisons topoisomerase I. *Clin Cancer Res*. 8:2499-504.

Pourquier, P., and Y. Pommier. 2001. Topoisomerase I-mediated DNA damage. *Adv Cancer Res*. 80:189-216.

Prescott, D.M., and M.A. Bender. 1962. Synthesis of RNA and protein during mitosis in mammalian tissue culture cells. *Exp Cell Res*. 26:260-8.

Prestwich, R.J., F. Errington, R.M. Diaz, H.S. Pandha, K.J. Harrington, A.A. Melcher, and R.G. Vile. 2009. The case of oncolytic viruses versus the immune system: waiting on the judgment of Solomon. *Hum Gene Ther*. 20:1119-32.

Prigent, C., and S. Dimitrov. 2003. Phosphorylation of serine 10 in histone H3, what for? *J Cell Sci*. 116:3677-85.

Prosser, S.L., K.R. Straatman, and A.M. Fry. 2009. Molecular dissection of the centrosome overduplication pathway in S-phase-arrested cells. *Mol Cell Biol*. 29:1760-73.

Pyronnet, S., J. Dostie, and N. Sonenberg. 2001. Suppression of cap-dependent translation in mitosis. *Genes Dev*. 15:2083-93.

Querido, E., P. Blanchette, Q. Yan, T. Kamura, M. Morrison, D. Boivin, W.G. Kaelin, R.C. Conaway, J.W. Conaway, and P.E. Branton. 2001. Degradation of p53 by adenovirus E4orf6 and E1B55K proteins occurs via a novel mechanism involving a Cullin-containing complex. *Genes Dev*. 15:3104-17.

Radhakrishnan, S., E. Miranda, M. Ekblad, A. Holford, M.T. Pizarro, N.R. Lemoine, and G. Hallden. 2010. Efficacy of oncolytic mutants targeting pRb and p53 pathways is synergistically enhanced when combined with cytotoxic drugs in prostate cancer cells and tumor xenografts. *Hum Gene Ther*. 21:1311-25.

Rainey, M.D., B. Harhen, G.N. Wang, P.V. Murphy, and C. Santocanale. 2013. Cdc7-dependent and -independent phosphorylation of Claspin in the induction of the DNA replication checkpoint. *Cell Cycle*. 12:1560-8.

Rajecki, M., T. af Hallstrom, T. Hakkarainen, P. Nokisalmi, S. Hautaniemi, A.I. Nieminen, M. Tenhunen, V. Rantanen, R.A. Desmond, D.T. Chen, K. Guse, U.H. Stenman, R. Gargini, M. Kapanen, J. Klefstrom, A. Kanerva, S. Pesonen, L. Ahtiainen, and A. Hemminki. 2009. Mre11 inhibition by oncolytic adenovirus associates with autophagy and underlies synergy with ionizing radiation. *Int J Cancer*. 125:2441-9.

Rajeshkumar, N.V., E. De Oliveira, N. Ottenhof, J. Watters, D. Brooks, T. Demuth, S.D. Shumway, S. Mizuarai, H. Hirai, A. Maitra, and M. Hidalgo. 2011. MK-1775, a potent Wee1 inhibitor, synergizes with gemcitabine to achieve tumor regressions, selectively in p53-deficient pancreatic cancer xenografts. *Clin Cancer Res*. 17:2799-806.

Raki, M., A. Kanerva, A. Ristimaki, R.A. Desmond, D.T. Chen, T. Ranki, M. Sarkioja, L. Kangasniemi, and A. Hemminki. 2005. Combination of gemcitabine and Ad5/3-Delta24, a tropism modified conditionally replicating adenovirus, for the treatment of ovarian cancer. *Gene Ther*. 12:1198-205.

Ramachandran, K., H. Miller, E. Gordian, C. Rocha-Lima, and R. Singal. 2010. Methylation-mediated silencing of TMS1 in pancreatic cancer and its potential contribution to chemosensitivity. *Anticancer Res*. 30:3919-25.

Raman, M., S. Earnest, K. Zhang, Y. Zhao, and M.H. Cobb. 2007. TAO kinases mediate activation of p38 in response to DNA damage. *EMBO J*. 26:2005-14.

Ramesh, M., P. Ahlawat, and N.R. Srinivas. 2010. Irinotecan and its active metabolite, SN-38: review of bioanalytical methods and recent update from clinical pharmacology perspectives. *Biomed Chromatogr*. 24:104-23.

Ramesh, N., Y. Ge, D.L. Ennist, M. Zhu, M. Mina, S. Ganesh, P.S. Reddy, and D.C. Yu. 2006. CG0070, a conditionally replicating granulocyte macrophage colony-stimulating factor--armed oncolytic adenovirus for the treatment of bladder cancer. *Clin Cancer Res*. 12:305-13.

Randall, R.E., and S. Goodbourn. 2008. Interferons and viruses: an interplay between induction, signalling, antiviral responses and virus countermeasures. *J Gen Virol*. 89:1-47.

Rao, L., M. Debbas, P. Sabbatini, D. Hockenbery, S. Korsmeyer, and E. White. 1992. The adenovirus E1A proteins induce apoptosis, which is inhibited by the E1B 19-kDa and Bcl-2 proteins. *Proc Natl Acad Sci U S A*. 89:7742-6.

Reid, T., E. Galanis, J. Abbruzzese, D. Sze, J. Andrews, L. Romel, M. Hatfield, J. Rubin, and D. Kirn. 2001. Intra-arterial administration of a replication-selective adenovirus (dl1520) in patients with colorectal carcinoma metastatic to the liver: a phase I trial. *Gene Ther*. 8:1618-26.

Reinhardt, H.C., A.S. Aslanian, J.A. Lees, and M.B. Yaffe. 2007. p53-deficient cells rely on ATM- and ATR-mediated checkpoint signaling through the p38MAPK/MK2 pathway for survival after DNA damage. *Cancer Cell*. 11:175-89.

Reinhardt, H.C., and M.B. Yaffe. 2009. Kinases that control the cell cycle in response to DNA damage: Chk1, Chk2, and MK2. *Curr Opin Cell Biol*. 21:245-55.

Reznik, R., A.E. Hendifar, and R. Tuli. 2014. Genetic determinants and potential therapeutic targets for pancreatic adenocarcinoma. *Front Physiol*. 5:87.

Rieder, C.L. 2011. Mitosis in vertebrates: the G2/M and M/A transitions and their associated checkpoints. *Chromosome Res*. 19:291-306.

Rieder, C.L., and R.W. Cole. 1998. Entry into mitosis in vertebrate somatic cells is guarded by a chromosome damage checkpoint that reverses the cell cycle when triggered during early but not late prophase. *J Cell Biol*. 142:1013-22.

Rieder, C.L., and H. Maiato. 2004. Stuck in division or passing through: what happens when cells cannot satisfy the spindle assembly checkpoint. *Dev Cell*. 7:637-51.

Rivory, L.P., J.F. Riou, M.C. Haaz, S. Sable, M. Vuilhorgne, A. Commercon, S.M. Pond, and J. Robert. 1996. Identification and properties of a major plasma metabolite of irinotecan (CPT-11) isolated from the plasma of patients. *Cancer Res*. 56:3689-94.

Robbins, E., and N.K. Gonatas. 1964. The Ultrastructure of a Mammalian Cell during the Mitotic Cycle. *J Cell Biol*. 21:429-63.

Robert, A., M.J. Miron, C. Champagne, M.C. Gingras, P.E. Branton, and J.N. Lavoie. 2002. Distinct cell death pathways triggered by the adenovirus early region 4 ORF 4 protein. *J Cell Biol*. 158:519-28.

Robert, A., N. Smadja-Lamere, M.C. Landry, C. Champagne, R. Petrie, N. Lamarche-Vane, H. Hosoya, and J.N. Lavoie. 2006. Adenovirus E4orf4 hijacks rho GTPase-dependent actin dynamics to kill cells: a role for endosome-associated actin assembly. *Mol Biol Cell*. 17:3329-44.

Rodriguez-Rocha, H., J.G. Gomez-Gutierrez, A. Garcia-Garcia, X.M. Rao, L. Chen, K.M. McMasters, and H.S. Zhou. 2011. Adenoviruses induce autophagy to promote virus replication and oncolysis. *Virology*. 416:9-15.

Rojas, J.J., M. Cascallo, S. Guedan, A. Gros, J. Martinez-Quintanilla, A. Hemminki, and R. Alemany. 2009. A modified E2F-1 promoter improves the efficacy to toxicity ratio of oncolytic adenoviruses. *Gene Ther*. 16:1441-51.

Roninson, I.B., E.V. Broude, and B.D. Chang. 2001. If not apoptosis, then what? Treatment-induced senescence and mitotic catastrophe in tumor cells. *Drug Resist Updat*. 4:303-13.

Roos, W.P., and B. Kaina. 2006. DNA damage-induced cell death by apoptosis. *Trends Mol Med*. 12:440-50.

Rosewell, A., F. Vetrini, and P. Ng. 2011. Helper-Dependent Adenoviral Vectors. *J Genet Syndr Gene Ther*. Suppl 5.

Rothmann, T., A. Hengstermann, N.J. Whitaker, M. Scheffner, and H. zur Hausen. 1998. Replication of ONYX-015, a potential anticancer adenovirus, is independent of p53 status in tumor cells. *J Virol*. 72:9470-8.

Rozenblum, E., M. Schutte, M. Goggins, S.A. Hahn, S. Panzer, M. Zahurak, S.N. Goodman, T.A. Sohn, R.H. Hruban, C.J. Yeo, and S.E. Kern. 1997. Tumor-suppressive pathways in pancreatic carcinoma. *Cancer Res*. 57:1731-4.

Rucki, A.A., and L. Zheng. 2014. Pancreatic cancer stroma: understanding biology leads to new therapeutic strategies. *World J Gastroenterol*. 20:2237-46.

Rudolf, E., S. John, and M. Cervinka. 2012. Irinotecan induces senescence and apoptosis in colonic cells in vitro. *Toxicol Lett*. 214:1-8.

Rudolf, E., V. Kralova, K. Rudolf, and S. John. 2013. The role of p38 in irinotecan-induced DNA damage and apoptosis of colon cancer cells. *Mutat Res*. 741-742:27-34.

Ruiz van Haperen, V.W., G. Veerman, J.B. Vermorken, and G.J. Peters. 1993. 2',2'-Difluoro-deoxycytidine (gemcitabine) incorporation into RNA and DNA of tumour cell lines. *Biochem Pharmacol*. 46:762-6.

Russell, W.C. 2000. Update on adenovirus and its vectors. *J Gen Virol*. 81:2573-604.

Russell, W.C. 2009. Adenoviruses: update on structure and function. *J Gen Virol*. 90:1-20.

Saladino, C., E. Bourke, P.C. Conroy, and C.G. Morrison. 2009. Centriole separation in DNA damage-induced centrosome amplification. *Environ Mol Mutagen*. 50:725-32.

Salmela, A.-L., and M.J. Kallio. 2013. Mitosis as an anti-cancer drug target. *Chromosoma*. 122:431-449.

Salomoni, P. 2013. The PML-Interacting Protein DAXX: Histone Loading Gets into the Picture. *Front Oncol*. 3:152.

Salomoni, P., and A.F. Khelifi. 2006. Daxx: death or survival protein? *Trends Cell Biol*. 16:97-104.

Samuelson, A.V., M. Narita, H.M. Chan, J. Jin, E. de Stanchina, M.E. McCurrach, M. Fuchs, D.M. Livingston, and S.W. Lowe. 2005. p400 is required for E1A to promote apoptosis. *J Biol Chem*. 280:21915-23.

Sanchez-Perez, T., G. Ortiz-Ferron, and A. Lopez-Rivas. 2010. Mitotic arrest and JNK-induced proteasomal degradation of FLIP and Mcl-1 are key events in the sensitization of breast tumor cells to TRAIL by antimicrotubule agents. *Cell Death Differ*. 17:883-94.

Sankar, N., S. Baluchamy, R.K. Kadeppagari, G. Singhal, S. Weitzman, and B. Thimmapaya. 2008. p300 provides a corepressor function by cooperating with YY1 and HDAC3 to repress c-Myc. *Oncogene*. 27:5717-28.

Sarup, J.C., M.A. Johnson, V. Verhoef, and A. Fridland. 1989. Regulation of purine deoxynucleoside phosphorylation by deoxycytidine kinase from human leukemic blast cells. *Biochem Pharmacol*. 38:2601-7.

Sasaki, C., H. Kitagawa, W.R. Zhang, H. Warita, K. Sakai, and K. Abe. 2000. Temporal profile of cytochrome c and caspase-3 immunoreactivities and TUNEL staining after permanent middle cerebral artery occlusion in rats. *Neurol Res*. 22:223-8.

Sauthoff, H., S. Heitner, W.N. Rom, and J.G. Hay. 2000. Deletion of the adenoviral E1b-19kD gene enhances tumor cell killing of a replicating adenoviral vector. *Hum Gene Ther*. 11:379-88.

Schaeper, U., T. Subramanian, L. Lim, J.M. Boyd, and G. Chinnadurai. 1998. Interaction between a cellular protein that binds to the C-terminal region of adenovirus E1A (CtBP) and a novel cellular protein is disrupted by E1A through a conserved PLDLS motif. *J Biol Chem*. 273:8549-52.

Schafer, A., L. Schomacher, G. Barreto, G. Doderlein, and C. Niehrs. 2010. Gemcitabine functions epigenetically by inhibiting repair mediated DNA demethylation. *PLoS One*. 5:e14060.

Scharer, O.D. 2013. Nucleotide excision repair in eukaryotes. *Cold Spring Harb Perspect Biol*. 5:a012609.

Schneider, G., and R.M. Schmid. 2003. Genetic alterations in pancreatic carcinoma. *Mol Cancer*. 2:15.

Schreiner, S., C. Burck, M. Glass, P. Groitl, P. Wimmer, S. Kinkley, A. Mund, R.D. Everett, and T. Dobner. 2013a. Control of human adenovirus type 5 gene expression by cellular Daxx/ATRX chromatin-associated complexes. *Nucleic Acids Res*. 41:3532-50.

Schreiner, S., S. Kinkley, C. Burck, A. Mund, P. Wimmer, T. Schubert, P. Groitl, H. Will, and T. Dobner. 2013b. SPOC1-mediated antiviral host cell response is antagonized early in human adenovirus type 5 infection. *PLoS Pathog*. 9:e1003775.

Schreiner, S., R. Martinez, P. Groitl, F. Rayne, R. Vaillant, P. Wimmer, G. Bossis, T. Sternsdorf, L. Marcinowski, Z. Ruzsics, T. Dobner, and H. Wodrich. 2012. Transcriptional activation of the adenoviral genome is mediated by capsid protein VI. *PLoS Pathog*. 8:e1002549.

Schreiner, S., P. Wimmer, H. Sirma, R.D. Everett, P. Blanchette, P. Groitl, and T. Dobner. 2010. Proteasome-dependent degradation of Daxx by the viral E1B-55K protein in human adenovirus-infected cells. *J Virol*. 84:7029-38.

Schutte, M., R.H. Hruban, J. Geradts, R. Maynard, W. Hilgers, S.K. Rabindran, C.A. Moskaluk, S.A. Hahn, I. Schwarte-Waldhoff, W. Schmiegel, S.B. Baylin, S.E. Kern, and J.G. Herman. 1997. Abrogation of the Rb/p16 tumor-suppressive pathway in virtually all pancreatic carcinomas. *Cancer Res*. 57:3126-30.

Sedgwick, G.G., K. Townsend, A. Martin, N.J. Shimwell, R.J. Grand, G.S. Stewart, J. Nilsson, and A.S. Turnell. 2013. Transcriptional intermediary factor 1gamma binds to the anaphase-promoting complex/cyclosome and promotes mitosis. *Oncogene*. 32:4622-33.

Seki, A., J.A. Coppinger, C.Y. Jang, J.R. Yates, and G. Fang. 2008. Bora and the kinase Aurora a cooperatively activate the kinase Plk1 and control mitotic entry. *Science*. 320:1655-8.

Sertic, S., S. Pizzi, R. Cloney, A.R. Lehmann, F. Marini, P. Plevani, and M. Muzi-Falconi. 2011. Human exonuclease 1 connects nucleotide excision repair (NER) processing with checkpoint activation in response to UV irradiation. *Proc Natl Acad Sci U S A*. 108:13647-52.

Shah, G.M., M. Robu, N.K. Purohit, J. Rajawat, L. Tentori, and G. Graziani. 2013. PARP Inhibitors in Cancer Therapy: Magic Bullets but Moving Targets. *Front Oncol*. 3:279.

Shao, R., M.C. Hu, B.P. Zhou, S.Y. Lin, P.J. Chiao, R.H. von Lindern, B. Spohn, and M.C. Hung. 1999. E1A sensitizes cells to tumor necrosis factor-

induced apoptosis through inhibition of IkappaB kinases and nuclear factor kappaB activities. *J Biol Chem*. 274:21495-8.

Shao, R., D. Karunagaran, B.P. Zhou, K. Li, S.S. Lo, J. Deng, P. Chiao, and M.C. Hung. 1997. Inhibition of nuclear factor-kappaB activity is involved in E1A-mediated sensitization of radiation-induced apoptosis. *J Biol Chem*. 272:32739-42.

Shashkova, E.V., K. Doronin, J.S. Senac, and M.A. Barry. 2008. Macrophage depletion combined with anticoagulant therapy increases therapeutic window of systemic treatment with oncolytic adenovirus. *Cancer Res*. 68:5896-904.

Shay, J.W., and W.E. Wright. 2011. Role of telomeres and telomerase in cancer. *Semin Cancer Biol*. 21:349-53.

Shen, W., J.K. Tu, X.H. Wang, and Z.X. Fu. 2010. Oncolytic adenovirus mediated Survivin RNA interference and 5-fluorouracil synergistically suppress the lymphatic metastasis of colorectal cancer. *Oncol Rep*. 24:1285-90.

Shen, W., C.Y. Wang, X.H. Wang, and Z.X. Fu. 2009. Oncolytic adenovirus mediated Survivin knockdown by RNA interference suppresses human colorectal carcinoma growth in vitro and in vivo. *J Exp Clin Cancer Res*. 28:81.

Shenk, T.E. 2001. Adenoviridae: The Viruses and their replication. *In* Fields Virology. Fields B. N., D.M. Knipe, and P.M. Howley, editors. PA: Lippincot Williams and Wilkins, Philadelphia.

Sherr, C.J. 1996. Cancer cell cycles. *Science*. 274:1672-7.

Sherr, C.J. 1998. Tumor surveillance via the ARF-p53 pathway. *Genes Dev*. 12:2984-91.

Shi, S., W. Yao, J. Xu, J. Long, C. Liu, and X. Yu. 2012. Combinational therapy: new hope for pancreatic cancer? *Cancer Lett*. 317:127-35.

Shi, X., K.M. Bowlin, and D.J. Garry. 2010. Fhl2 interacts with Foxk1 and corepresses Foxo4 activity in myogenic progenitors. *Stem Cells*. 28:462-9.

Shi, Z., A. Azuma, D. Sampath, Y.X. Li, P. Huang, and W. Plunkett. 2001. S-Phase arrest by nucleoside analogues and abrogation of survival without cell cycle progression by 7-hydroxystaurosporine. *Cancer Res*. 61:1065-72.

Shimada, M., H. Niida, D.H. Zineldeen, H. Tagami, M. Tanaka, H. Saito, and M. Nakanishi. 2008. Chk1 is a histone H3 threonine 11 kinase that regulates DNA damage-induced transcriptional repression. *Cell*. 132:221-32.

Shiotani, B., and L. Zou. 2009. ATR signaling at a glance. *J Cell Sci*. 122:301-4.

Shtrichman, R., and T. Kleinberger. 1998. Adenovirus type 5 E4 open reading frame 4 protein induces apoptosis in transformed cells. *J Virol*. 72:2975-82.

Shtrichman, R., R. Sharf, H. Barr, T. Dobner, and T. Kleinberger. 1999. Induction of apoptosis by adenovirus E4orf4 protein is specific to transformed cells and requires an interaction with protein phosphatase 2A. *Proc Natl Acad Sci U S A*. 96:10080-5.

Shtrichman, R., R. Sharf, and T. Kleinberger. 2000. Adenovirus E4orf4 protein interacts with both Balpha and B' subunits of protein phosphatase 2A, but E4orf4-induced apoptosis is mediated only by the interaction with Balpha. *Oncogene*. 19:3757-65.

Siegel, R., J. Ma, Z. Zou, and A. Jemal. 2014. Cancer statistics, 2014. *CA Cancer J Clin*. 64:9-29.

Siegel, R., D. Naishadham, and A. Jemal. 2012. Cancer statistics, 2012. *CA Cancer J Clin*. 62:10-29.

Singhal, G., E. Leo, S.K. Setty, Y. Pommier, and B. Thimmapaya. 2013. Adenovirus E1A oncogene induces rereplication of cellular DNA and alters DNA replication dynamics. *J Virol*. 87:8767-78.

Sirbu, B.M., and D. Cortez. 2013. DNA damage response: three levels of DNA repair regulation. *Cold Spring Harb Perspect Biol*. 5:a012724.

Small, E.J., M.A. Carducci, J.M. Burke, R. Rodriguez, L. Fong, L. van Ummersen, D.C. Yu, J. Aimi, D. Ando, P. Working, D. Kirn, and G. Wilding. 2006. A phase I trial of intravenous CG7870, a replication-selective, prostate-specific antigen-targeted oncolytic adenovirus, for the treatment of hormone-refractory, metastatic prostate cancer. *Mol Ther*. 14:107-17.

Smith, N.F., W.D. Figg, and A. Sparreboom. 2006. Pharmacogenetics of irinotecan metabolism and transport: an update. *Toxicol In Vitro*. 20:163-75.

Smits, V.A., R. Klompmaker, L. Arnaud, G. Rijksen, E.A. Nigg, and R.H. Medema. 2000. Polo-like kinase-1 is a target of the DNA damage checkpoint. *Nat Cell Biol*. 2:672-6.

Sokolov, M.V., L.B. Smilenov, E.J. Hall, I.G. Panyutin, W.M. Bonner, and O.A. Sedelnikova. 2005. Ionizing radiation induces DNA double-strand breaks in bystander primary human fibroblasts. *Oncogene*. 24:7257-65.

Solier, S., and Y. Pommier. 2014. The nuclear gamma-H2AX apoptotic ring: implications for cancers and autoimmune diseases. *Cell Mol Life Sci*. 71:2289-97.

Sorensen, C.S., L.T. Hansen, J. Dziegielewski, R.G. Syljuasen, C. Lundin, J. Bartek, and T. Helleday. 2005. The cell-cycle checkpoint kinase Chk1 is required for mammalian homologous recombination repair. *Nat Cell Biol*. 7:195-201.

Soria, C., F.E. Estermann, K.C. Espantman, and C.C. O'Shea. 2010. Heterochromatin silencing of p53 target genes by a small viral protein. *Nature*. 466:1076-81.

Spardy, N., K. Covella, E. Cha, E.E. Hoskins, S.I. Wells, A. Duensing, and S. Duensing. 2009. Human papillomavirus 16 E7 oncoprotein attenuates DNA damage checkpoint control by increasing the proteolytic turnover of claspin. *Cancer Res*. 69:7022-9.

Stanford, M.M., C.J. Breitbach, J.C. Bell, and G. McFadden. 2008. Innate immunity, tumor microenvironment and oncolytic virus therapy: friends or foes? *Curr Opin Mol Ther*. 10:32-7.

Stark, G.R., and W.R. Taylor. 2006. Control of the G2/M transition. *Mol Biotechnol*. 32:227-48.

Steegmaier, M., M. Hoffmann, A. Baum, P. Lenart, M. Petronczki, M. Krssak, U. Gurtler, P. Garin-Chesa, S. Lieb, J. Quant, M. Grauert, G.R. Adolf, N. Kraut, J.M. Peters, and W.J. Rettig. 2007. BI 2536, a potent and selective inhibitor of polo-like kinase 1, inhibits tumor growth in vivo. *Curr Biol*. 17:316-22.

Steinwaerder, D.S., C.A. Carlson, and A. Lieber. 2000. DNA replication of first-generation adenovirus vectors in tumor cells. *Hum Gene Ther*. 11:1933-48.

Stephens, C., and E. Harlow. 1987. Differential splicing yields novel adenovirus 5 E1A mRNAs that encode 30 kd and 35 kd proteins. *EMBO J*. 6:2027-35.

Stewart, S.A., and A.A. Bertuch. 2010. The role of telomeres and telomerase in cancer research. *Cancer Res*. 70:7365-71.

Stolarek, R., C. Gomez-Manzano, H. Jiang, G. Suttle, M.G. Lemoine, and J. Fueyo. 2004. Robust infectivity and replication of Delta-24 adenovirus induce cell death in human medulloblastoma. *Cancer Gene Ther*. 11:713-20.

Stracker, T.H., C.T. Carson, and M.D. Weitzman. 2002. Adenovirus oncoproteins inactivate the Mre11-Rad50-NBS1 DNA repair complex. *Nature*. 418:348-52.

Stracker, T.H., T. Usui, and J.H. Petrini. 2009. Taking the time to make important decisions: the checkpoint effector kinases Chk1 and Chk2 and the DNA damage response. *DNA Repair (Amst)*. 8:1047-54.

Strober, W. 2001. Trypan blue exclusion test of cell viability. *Curr Protoc Immunol*. Appendix 3:Appendix 3B.

Strunze, S., M.F. Engelke, I.H. Wang, D. Puntener, K. Boucke, S. Schleich, M. Way, P. Schoenenberger, C.J. Burckhardt, and U.F. Greber. 2011. Kinesin-1-mediated capsid disassembly and disruption of the nuclear pore complex promote virus infection. *Cell Host Microbe*. 10:210-23.

Strunze, S., L.C. Trotman, K. Boucke, and U.F. Greber. 2005. Nuclear targeting of adenovirus type 2 requires CRM1-mediated nuclear export. *Mol Biol Cell*. 16:2999-3009.

Subramanian, T., M. Kuppuswamy, S. Mak, and G. Chinnadurai. 1984. Adenovirus cyt+ locus, which controls cell transformation and tumorigenicity, is an allele of lp+ locus, which codes for a 19-kilodalton tumor antigen. *J Virol*. 52:336-43.

Subramanian, T., S. Vijayalingam, and G. Chinnadurai. 2006. Genetic identification of adenovirus type 5 genes that influence viral spread. *J Virol*. 80:2000-12.

Sultana, A., C.T. Smith, D. Cunningham, N. Starling, J.P. Neoptolemos, and P. Ghaneh. 2007. Meta-analyses of chemotherapy for locally advanced and metastatic pancreatic cancer. *J Clin Oncol*. 25:2607-15.

Sun, C., T. Yamato, T. Furukawa, Y. Ohnishi, H. Kijima, and A. Horii. 2001. Characterization of the mutations of the K-ras, p53, p16, and SMAD4 genes in 15 human pancreatic cancer cell lines. *Oncol Rep*. 8:89-92.

Sun, Y., X. Jiang, S. Chen, N. Fernandes, and B.D. Price. 2005. A role for the Tip60 histone acetyltransferase in the acetylation and activation of ATM. *Proc Natl Acad Sci U S A*. 102:13182-7.

Sun, Y., X. Jiang, and B.D. Price. 2010. Tip60: connecting chromatin to DNA damage signaling. *Cell Cycle*. 9:930-6.

Sun, Y., Y. Xu, K. Roy, and B.D. Price. 2007. DNA damage-induced acetylation of lysine 3016 of ATM activates ATM kinase activity. *Mol Cell Biol*. 27:8502-9.

Suzuki, K., R. Alemany, M. Yamamoto, and D.T. Curiel. 2002. The presence of the adenovirus E3 region improves the oncolytic potency of conditionally replicative adenoviruses. *Clin Cancer Res*. 8:3348-59.

Svejstrup, J.Q., K. Christiansen, Gromova, II, A.H. Andersen, and O. Westergaard. 1991. New technique for uncoupling the cleavage and religation reactions of eukaryotic topoisomerase I. The mode of action of camptothecin at a specific recognition site. *J Mol Biol*. 222:669-78.

Syljuasen, R.G. 2007. Checkpoint adaptation in human cells. *Oncogene*. 26:5833-9.

Syljuasen, R.G., S. Jensen, J. Bartek, and J. Lukas. 2006. Adaptation to the ionizing radiation-induced G2 checkpoint occurs in human cells and depends on checkpoint kinase 1 and Polo-like kinase 1 kinases. *Cancer Res*. 66:10253-7.

Symington, L.S., and J. Gautier. 2011. Double-strand break end resection and repair pathway choice. *Annu Rev Genet*. 45:247-71.

Takatori, E., T. Shoji, S. Kumagai, T. Sawai, A. Kurose, and T. Sugiyama. 2012. Are platinum agents, paclitaxel and irinotecan effective for clear cell carcinoma of the ovary? DNA damage detected with gammaH2AX induced by anticancer agents. *J Ovarian Res*. 5:16.

Takeba, Y., T. Kumai, N. Matsumoto, S. Nakaya, Y. Tsuzuki, Y. Yanagida, and S. Kobayashi. 2007. Irinotecan activates p53 with its active metabolite, resulting in human hepatocellular carcinoma apoptosis. *J Pharmacol Sci*. 104:232-42.

Takekawa, M., M. Adachi, A. Nakahata, I. Nakayama, F. Itoh, H. Tsukuda, Y. Taya, and K. Imai. 2000. p53-inducible wip1 phosphatase mediates a negative feedback regulation of p38 MAPK-p53 signaling in response to UV radiation. *EMBO J*. 19:6517-26.

Takemori, N., C. Cladaras, B. Bhat, A.J. Conley, and W.S. Wold. 1984. cyt gene of adenoviruses 2 and 5 is an oncogene for transforming function in early region E1B and encodes the E1B 19,000-molecular-weight polypeptide. *J Virol*. 52:793-805.

Tanaka, K. 2010. Multiple functions of the S-phase checkpoint mediator. *Biosci Biotechnol Biochem*. 74:2367-73.

Tang, J., T. Agrawal, Q. Cheng, L. Qu, M.D. Brewer, J. Chen, and X. Yang. 2013. Phosphorylation of Daxx by ATM contributes to DNA damage-induced p53 activation. *PLoS One*. 8:e55813.

Tardif, K.D., A. Rogers, J. Cassiano, B.L. Roth, D.M. Cimbora, R. McKinnon, A. Peterson, T.B. Douce, R. Robinson, I. Dorweiler, T. Davis, M.A. Hess, K. Ostanin, D.I. Papac, V. Baichwal, I. McAlexander, J.A. Willardsen, M. Saunders, H. Christophe, D.V. Kumar, D.A. Wettstein, R.O. Carlson, and B.L. Williams. 2011. Characterization of the cellular and antitumor effects of MPI-0479605, a small-molecule inhibitor of the mitotic kinase Mps1. *Mol Cancer Ther*. 10:2267-75.

Tauber, B., and T. Dobner. 2001. Molecular regulation and biological function of adenovirus early genes: the E4 ORFs. *Gene*. 278:1-23.

Taylor, W.R., and G.R. Stark. 2001. Regulation of the G2/M transition by p53. *Oncogene*. 20:1803-15.

Tell, G., F. Quadrifoglio, C. Tiribelli, and M.R. Kelley. 2009. The many functions of APE1/Ref-1: not only a DNA repair enzyme. *Antioxid Redox Signal*. 11:601-20.

Thaci, B., I.V. Ulasov, D.A. Wainwright, and M.S. Lesniak. 2011. The challenge for gene therapy: innate immune response to adenoviruses. *Oncotarget*. 2:113-21.

Thomas, A., and E. White. 1998. Suppression of the p300-dependent mdm2 negative-feedback loop induces the p53 apoptotic function. *Genes Dev*. 12:1975-85.

Thorne, S.H. 2013. The role of GM-CSF in enhancing immunotherapy of cancer. *Immunotherapy*. 5:817-9.

Thornton, T.M., and M. Rincon. 2009. Non-classical p38 map kinase functions: cell cycle checkpoints and survival. *Int J Biol Sci*. 5:44-51.

Tollefson, A.E., K. Toth, K. Doronin, M. Kuppuswamy, O.A. Doronina, D.L. Lichtenstein, T.W. Hermiston, C.A. Smith, and W.S. Wold. 2001. Inhibition of TRAIL-induced apoptosis and forced internalization of TRAIL receptor 1 by adenovirus proteins. *J Virol*. 75:8875-87.

Tong, A.W., N. Senzer, V. Cerullo, N.S. Templeton, A. Hemminki, and J. Nemunaitis. 2012. Oncolytic viruses for induction of anti-tumor immunity. *Curr Pharm Biotechnol*. 13:1750-60.

Toth, K., and W.S. Wold. 2010. Increasing the efficacy of oncolytic adenovirus vectors. *Viruses*. 2:1844-66.

Tsai, M.S., Y.H. Kuo, Y.F. Chiu, Y.C. Su, and Y.W. Lin. 2010. Down-regulation of Rad51 expression overcomes drug resistance to gemcitabine in human non-small-cell lung cancer cells. *J Pharmacol Exp Ther*. 335:830-40.

Tse, A.N., D.S. Klimstra, M. Gonen, M. Shah, T. Sheikh, R. Sikorski, R. Carvajal, J. Mui, C. Tipian, E. O'Reilly, K. Chung, R. Maki, R. Lefkowitz, K. Brown, K. Manova-Todorova, N. Wu, M.J. Egorin, D. Kelsen, and G.K. Schwartz. 2008. A phase 1 dose-escalation study of irinotecan in combination with 17-allylamino-17-demethoxygeldanamycin in patients with solid tumors. *Clin Cancer Res*. 14:6704-11.

Tse, A.N., K.G. Rendahl, T. Sheikh, H. Cheema, K. Aardalen, M. Embry, S. Ma, E.J. Moler, Z.J. Ni, D.E. Lopes de Menezes, B. Hibner, T.G. Gesner, and G.K. Schwartz. 2007. CHIR-124, a novel potent inhibitor of Chk1, potentiates the cytotoxicity of topoisomerase I poisons in vitro and in vivo. *Clin Cancer Res*. 13:591-602.

Tse, A.N., T.N. Sheikh, H. Alan, T.C. Chou, and G.K. Schwartz. 2009. 90-kDa heat shock protein inhibition abrogates the topoisomerase I poison-induced G2/M checkpoint in p53-null tumor cells by depleting Chk1 and Wee1. *Mol Pharmacol*. 75:124-33.

Tsvetkov, L. 2004. Polo-like kinases and Chk2 at the interface of DNA damage checkpoint pathways and mitotic regulation. *IUBMB Life*. 56:449-56.

Turnell, A.S., and R.J. Grand. 2012. DNA viruses and the cellular DNA-damage response. *J Gen Virol*. 93:2076-97.

Turnell, A.S., R.J. Grand, and P.H. Gallimore. 1999. The replicative capacities of large E1B-null group A and group C adenoviruses are independent of host cell p53 status. *J Virol*. 73:2074-83.

Turnell, A.S., R.J. Grand, C. Gorbea, X. Zhang, W. Wang, J.S. Mymryk, and P.H. Gallimore. 2000. Regulation of the 26S proteasome by adenovirus E1A. *EMBO J*. 19:4759-73.

Turnell, A.S., and J.S. Mymryk. 2006. Roles for the coactivators CBP and p300 and the APC/C E3 ubiquitin ligase in E1A-dependent cell transformation. *Br J Cancer*. 95:555-60.

Turnell, A.S., G.S. Stewart, R.J. Grand, S.M. Rookes, A. Martin, H. Yamano, S.J. Elledge, and P.H. Gallimore. 2005. The APC/C and CBP/p300 cooperate to regulate transcription and cell-cycle progression. *Nature*. 438:690-5.

Turner, R.L., J.C. Wilkinson, and D.A. Ornelles. 2014. E1B and E4 oncoproteins of adenovirus antagonize the effect of apoptosis inducing factor. *Virology*. 456-457:205-19.

Tworkowski, K.A., A.A. Chakraborty, A.V. Samuelson, Y.R. Seger, M. Narita, G.J. Hannon, S.W. Lowe, and W.P. Tansey. 2008. Adenovirus E1A targets p400 to induce the cellular oncoprotein Myc. *Proc Natl Acad Sci U S A*. 105:6103-8.

Ueno, N.T., C. Bartholomeusz, J.L. Herrmann, Z. Estrov, R. Shao, M. Andreeff, J. Price, R.W. Paul, P. Anklesaria, D. Yu, and M.C. Hung. 2000. E1A-mediated paclitaxel sensitization in HER-2/neu-overexpressing ovarian cancer SKOV3.ip1 through apoptosis involving the caspase-3 pathway. *Clin Cancer Res*. 6:250-9.

Uetake, Y., and G. Sluder. 2010. Prolonged prometaphase blocks daughter cell proliferation despite normal completion of mitosis. *Curr Biol*. 20:1666-71.

Ulasov, I.V., A.M. Sonabend, S. Nandi, A. Khramtsov, Y. Han, and M.S. Lesniak. 2009. Combination of adenoviral virotherapy and temozolomide chemotherapy eradicates malignant glioma through autophagic and apoptotic cell death in vivo. *Br J Cancer*. 100:1154-64.

Ulasov, I.V., Z.B. Zhu, M.A. Tyler, Y. Han, A.A. Rivera, A. Khramtsov, D.T. Curiel, and M.S. Lesniak. 2007. Survivin-driven and fiber-modified oncolytic adenovirus exhibits potent antitumor activity in established intracranial glioma. *Hum Gene Ther*. 18:589-602.

Ulfendahl, P.J., S. Linder, J.P. Kreivi, K. Nordqvist, C. Sevensson, H. Hultberg, and G. Akusjarvi. 1987. A novel adenovirus-2 E1A mRNA encoding a protein with transcription activation properties. *EMBO J*. 6:2037-44.

Uno, S., and H. Masai. 2011. Efficient expression and purification of human replication fork-stabilizing factor, Claspin, from mammalian cells: DNA-binding activity and novel protein interactions. *Genes Cells*. 16:842-56.

Vakifahmetoglu, H., M. Olsson, and B. Zhivotovsky. 2008. Death through a tragedy: mitotic catastrophe. *Cell Death Differ*. 15:1153-62.

van der Wilt, C.L., J.R. Kroep, A.M. Bergman, W.J. Loves, E. Alvarez, I. Talianidis, S. Eriksson, C.J. van Groeningen, H.M. Pinedo, and G.J. Peters. 2000. The role of deoxycytidine kinase in gemcitabine cytotoxicity. *Adv Exp Med Biol*. 486:287-90.

van Vugt, M.A., A. Bras, and R.H. Medema. 2004. Polo-like kinase-1 controls recovery from a G2 DNA damage-induced arrest in mammalian cells. *Mol Cell*. 15:799-811.

van Vugt, M.A., A.K. Gardino, R. Linding, G.J. Ostheimer, H.C. Reinhardt, S.E. Ong, C.S. Tan, H. Miao, S.M. Keezer, J. Li, T. Pawson, T.A. Lewis, S.A. Carr, S.J. Smerdon, T.R. Brummelkamp, and M.B. Yaffe. 2010. A mitotic phosphorylation feedback network connects Cdk1, Plk1, 53BP1, and Chk2 to inactivate the G(2)/M DNA damage checkpoint. *PLoS Biol*. 8:e1000287.

van Vugt, M.A., and M.B. Yaffe. 2010. Cell cycle re-entry mechanisms after DNA damage checkpoints: giving it some gas to shut off the breaks! *Cell Cycle*. 9:2097-101.

Veltkamp, S.A., D. Pluim, M.A. van Eijndhoven, M.J. Bolijn, F.H. Ong, R. Govindarajan, J.D. Unadkat, J.H. Beijnen, and J.H. Schellens. 2008. New insights into the pharmacology and cytotoxicity of gemcitabine and 2',2'-difluorodeoxyuridine. *Mol Cancer Ther*. 7:2415-25.

Voets, E., and R.M. Wolthuis. 2010. MASTL is the human orthologue of Greatwall kinase that facilitates mitotic entry, anaphase and cytokinesis. *Cell Cycle*. 9:3591-601.

Von Hoff, D.D., T. Ervin, F.P. Arena, E.G. Chiorean, J. Infante, M. Moore, T. Seay, S.A. Tjulandin, W.W. Ma, M.N. Saleh, M. Harris, M. Reni, S. Dowden, D. Laheru, N. Bahary, R.K. Ramanathan, J. Tabernero, M. Hidalgo, D. Goldstein, E. Van Cutsem, X. Wei, J. Iglesias, and M.F. Renschler. 2013. Increased survival in pancreatic cancer with nab-paclitaxel plus gemcitabine. *N Engl J Med*. 369:1691-703.

Vorburger, S.A., and K.K. Hunt. 2002. Adenoviral gene therapy. *Oncologist*. 7:46-59.

Vousden, K.H., and X. Lu. 2002. Live or let die: the cell's response to p53. *Nat Rev Cancer*. 2:594-604.

Wan, Y., J. Han, G. Fan, Z. Zhang, T. Gong, and X. Sun. 2013. Enzyme-responsive liposomes modified adenoviral vectors for enhanced tumor cell transduction and reduced immunogenicity. *Biomaterials*. 34:3020-30.

Wang, D., J. Wang, L. Li, J. Chen, and C. Su. 2012. [Construction of adenovirus carrying dual-target shRNA for Oct-4 and Survivin and its inhibitory effect on human hepatocellular carcinoma cells]. *Sheng Wu Gong Cheng Xue Bao*. 28:623-31.

Wang, H., Z. Liu, Z.P. Wang, F.Y. Li, Y. Zhao, G.P. Chen, and D.C. Li. 2013. [Double-mutated oncolytic adenovirus combined with gemcitabine for treating an orthotopic nude mouse model of bladder cancer]. *Zhonghua Zhong Liu Za Zhi*. 35:412-7.

Wang, H., M. Satoh, G.P. Chen, D.C. Li, H. Hamada, and Y. Arai. 2011. E1A, E1B double-restricted adenovirus enhances the cytotoxicity and antitumor activity of gemcitabine to renal cell carcinoma. *Chin Med J (Engl)*. 124:1082-7.

Wang, W., J.L. Abbruzzese, D.B. Evans, L. Larry, K.R. Cleary, and P.J. Chiao. 1999. The nuclear factor-kappa B RelA transcription factor is constitutively activated in human pancreatic adenocarcinoma cells. *Clin Cancer Res*. 5:119-27.

Wang, X.Q., J.L. Redpath, S.T. Fan, and E.J. Stanbridge. 2006. ATR dependent activation of Chk2. *J Cell Physiol*. 208:613-9.

Wang, Y., G. Hallden, R. Hill, A. Anand, T.C. Liu, J. Francis, G. Brooks, N. Lemoine, and D. Kirn. 2003. E3 gene manipulations affect oncolytic adenovirus activity in immunocompetent tumor models. *Nat Biotechnol*. 21:1328-35.

Warmerdam, D.O., and R. Kanaar. 2010. Dealing with DNA damage: relationships between checkpoint and repair pathways. *Mutat Res*. 704:2-11.

Warren, J.C., A. Rutkowski, and L. Cassimeris. 2006. Infection with replication-deficient adenovirus induces changes in the dynamic instability of host cell microtubules. *Mol Biol Cell*. 17:3557-68.

Watanabe, N., H. Arai, J. Iwasaki, M. Shiina, K. Ogata, T. Hunter, and H. Osada. 2005. Cyclin-dependent kinase (CDK) phosphorylation destabilizes somatic Wee1 via multiple pathways. *Proc Natl Acad Sci U S A*. 102:11663-8.

Watanabe, N., H. Arai, Y. Nishihara, M. Taniguchi, T. Hunter, and H. Osada. 2004. M-phase kinases induce phospho-dependent ubiquitination of somatic Wee1 by SCFbeta-TrCP. *Proc Natl Acad Sci U S A*. 101:4419-24.

Wei, J.H., Y.F. Chou, Y.H. Ou, Y.H. Yeh, S.W. Tyan, T.P. Sun, C.Y. Shen, and S.Y. Shieh. 2005. TTK/hMps1 participates in the regulation of DNA damage checkpoint response by phosphorylating CHK2 on threonine 68. *J Biol Chem*. 280:7748-57.

Weiden, M.D., and H.S. Ginsberg. 1994. Deletion of the E4 region of the genome produces adenovirus DNA concatemers. *Proc Natl Acad Sci U S A*. 91:153-7.

Weis, S.M., and D.A. Cheresh. 2011. alphav Integrins in Angiogenesis and Cancer. *Cold Spring Harb Perspect Med*. 1:a006478.

Weitzman, M.D., and D.A. Ornelles. 2005. Inactivating intracellular antiviral responses during adenovirus infection. *Oncogene*. 24:7686-96.
White, E. 2001. Regulation of the cell cycle and apoptosis by the oncogenes of adenovirus. *Oncogene*. 20:7836-46.
White, E. 2006. Mechanisms of apoptosis regulation by viral oncogenes in infection and tumorigenesis. *Cell Death Differ*. 13:1371-7.
White, E., R. Cipriani, P. Sabbatini, and A. Denton. 1991. Adenovirus E1B 19-kilodalton protein overcomes the cytotoxicity of E1A proteins. *J Virol*. 65:2968-78.
White, E., A. Denton, and B. Stillman. 1988. Role of the adenovirus E1B 19,000-dalton tumor antigen in regulating early gene expression. *J Virol*. 62:3445-54.
White, E., B. Faha, and B. Stillman. 1986. Regulation of adenovirus gene expression in human WI38 cells by an E1B-encoded tumor antigen. *Mol Cell Biol*. 6:3763-73.
White, E., T. Grodzicker, and B.W. Stillman. 1984. Mutations in the gene encoding the adenovirus early region 1B 19,000-molecular-weight tumor antigen cause the degradation of chromosomal DNA. *J Virol*. 52:410-9.
White, E., P. Sabbatini, M. Debbas, W.S. Wold, D.I. Kusher, and L.R. Gooding. 1992. The 19-kilodalton adenovirus E1B transforming protein inhibits programmed cell death and prevents cytolysis by tumor necrosis factor alpha. *Mol Cell Biol*. 12:2570-80.
White, E., and B. Stillman. 1987. Expression of adenovirus E1B mutant phenotypes is dependent on the host cell and on synthesis of E1A proteins. *J Virol*. 61:426-35.
Williams, G.H., and K. Stoeber. 2012. The cell cycle and cancer. *J Pathol*. 226:352-64.
Wilson-Rawls, J., S.L. Deutscher, and W.S. Wold. 1994. The signal-anchor domain of adenovirus E3-6.7K, a type III integral membrane protein, can direct adenovirus E3-gp19K, a type I integral membrane protein, into the membrane of the endoplasmic reticulum. *Virology*. 201:66-76.
Wilson, J.S., R.C. Pirola, and M.V. Apte. 2014. Stars and stripes in pancreatic cancer: role of stellate cells and stroma in cancer progression. *Front Physiol*. 5:52.
Windheim, M., A. Hilgendorf, and H.G. Burgert. 2004. Immune evasion by adenovirus E3 proteins: exploitation of intracellular trafficking pathways. *Curr Top Microbiol Immunol*. 273:29-85.
Wu, L. 2007. Role of the BLM helicase in replication fork management. *DNA Repair (Amst)*. 6:936-44.
Wu, L., Y. Liu, and D. Kong. 2014. Mechanism of chromosomal DNA replication initiation and replication fork stabilization in eukaryotes. *Sci China Life Sci*. 57:482-7.
Wu, Z.H., and S. Miyamoto. 2008. Induction of a pro-apoptotic ATM-NF-kappaB pathway and its repression by ATR in response to replication stress. *EMBO J*. 27:1963-73.
Wurzenberger, C., and D.W. Gerlich. 2011. Phosphatases: providing safe passage through mitotic exit. *Nat Rev Mol Cell Biol*. 12:469-82.
Xia, Z.J., J.H. Chang, L. Zhang, W.Q. Jiang, Z.Z. Guan, J.W. Liu, Y. Zhang, X.H. Hu, G.H. Wu, H.Q. Wang, Z.C. Chen, J.C. Chen, Q.H. Zhou, J.W. Lu, Q.X. Fan, J.J. Huang, and X. Zheng. 2004. Phase III randomized clinical trial of intratumoral injection of E1B gene-deleted adenovirus (H101) combined with cisplatin-based chemotherapy in treating

squamous cell cancer of head and neck or esophagus. *Ai Zheng*. 23:1666-70.

Xu, Y., Y. Sun, X. Jiang, M.K. Ayrapetov, P. Moskwa, S. Yang, D.M. Weinstock, and B.D. Price. 2010a. The p400 ATPase regulates nucleosome stability and chromatin ubiquitination during DNA repair. *J Cell Biol*. 191:31-43.

Xu, Y.Z., and W. Plunkett. 1992. Modulation of deoxycytidylate deaminase in intact human leukemia cells. Action of 2',2'-difluorodeoxycytidine. *Biochem Pharmacol*. 44:1819-27.

Xu, Z., A. Vonlaufen, P.A. Phillips, E. Fiala-Beer, X. Zhang, L. Yang, A.V. Biankin, D. Goldstein, R.C. Pirola, J.S. Wilson, and M.V. Apte. 2010b. Role of pancreatic stellate cells in pancreatic cancer metastasis. *Am J Pathol*. 177:2585-96.

Yadav, D., and A.B. Lowenfels. 2013. The epidemiology of pancreatitis and pancreatic cancer. *Gastroenterology*. 144:1252-61.

Yamamoto, M., and D.T. Curiel. 2010. Current issues and future directions of oncolytic adenoviruses. *Mol Ther*. 18:243-50.

Yamamoto, W., J. Verweij, P. de Bruijn, M.J. de Jonge, H. Takano, M. Nishiyama, M. Kurihara, and A. Sparreboom. 2001. Active transepithelial transport of irinotecan (CPT-11) and its metabolites by human intestinal Caco-2 cells. *Anticancer Drugs*. 12:419-32.

Yang, L., L. Wang, X.Q. Su, X.C. Chen, D. Li, S.T. Luo, H.S. Shi, L.J. Chen, and Y.S. Wang. 2010. Suppression of ovarian cancer growth via systemic administration with liposome-encapsulated adenovirus-encoding endostatin. *Cancer Gene Ther*. 17:49-57.

Yang, L.Y., L. Li, H. Jiang, Y. Shen, and W. Plunkett. 2000. Expression of ERCC1 antisense RNA abrogates gemicitabine-mediated cytotoxic synergism with cisplatin in human colon tumor cells defective in mismatch repair but proficient in nucleotide excision repair. *Clin Cancer Res*. 6:773-81.

Yang, Z., and D.J. Klionsky. 2010. Eaten alive: a history of macroautophagy. *Nat Cell Biol*. 12:814-22.

Yasui, T., K. Ohuchida, M. Zhao, L. Cui, M. Onimaru, T. Egami, H. Fujita, T. Ohtsuka, K. Mizumoto, K. Matsumoto, and M. Tanaka. 2011. Adenoviral therapy is more effective in gemcitabine-resistant pancreatic cancer than in gemcitabine-sensitive cells. *Anticancer Res*. 31:1279-87.

Yasutis, K.M., and K.G. Kozminski. 2013. Cell cycle checkpoint regulators reach a zillion. *Cell Cycle*. 12:1501-9.

Yde, C.W., B.B. Olsen, D. Meek, N. Watanabe, and B. Guerra. 2008. The regulatory beta-subunit of protein kinase CK2 regulates cell-cycle progression at the onset of mitosis. *Oncogene*. 27:4986-97.

Yeeles, J.T., J. Poli, K.J. Marians, and P. Pasero. 2013. Rescuing stalled or damaged replication forks. *Cold Spring Harb Perspect Biol*. 5:a012815.

Yeh, Y.H., Y.F. Huang, T.Y. Lin, and S.Y. Shieh. 2009. The cell cycle checkpoint kinase CHK2 mediates DNA damage-induced stabilization of TTK/hMps1. *Oncogene*. 28:1366-78.

Yin, K., Q. Liu, S. Zhu, and G. Yan. 2008. Adenovirus-mediated siRNA inhibited survivin gene expression induces tumor cell apoptosis in nude mice. *Biosci Trends*. 2:231-4.

Ying, B., and W.S. Wold. 2003. Adenovirus ADP protein (E3-11.6K), which is required for efficient cell lysis and virus release, interacts with human MAD2B. *Virology*. 313:224-34.

Yokoyama, T., E. Iwado, Y. Kondo, H. Aoki, Y. Hayashi, M.M. Georgescu, R. Sawaya, K.R. Hess, G.B. Mills, H. Kawamura, Y. Hashimoto, Y. Urata, T. Fujiwara, and S. Kondo. 2008. Autophagy-inducing agents augment the antitumor effect of telerase-selve oncolytic adenovirus OBP-405 on glioblastoma cells. *Gene Ther*. 15:1233-9.

Yondola, M.A., and P. Hearing. 2007. The adenovirus E4 ORF3 protein binds and reorganizes the TRIM family member transcriptional intermediary factor 1 alpha. *J Virol*. 81:4264-71.

Yoon, A.R., J.H. Kim, Y.S. Lee, H. Kim, J.Y. Yoo, J.H. Sohn, B.W. Park, and C.O. Yun. 2006. Markedly enhanced cytolysis by E1B-19kD-deleted oncolytic adenovirus in combination with cisplatin. *Hum Gene Ther*. 17:379-90.

You, L., Y. Wang, Y. Jin, and W. Qian. 2012. Downregulation of Mcl-1 synergizes the apoptotic response to combined treatment with cisplatin and a novel fiber chimeric oncolytic adenovirus. *Oncol Rep*. 27:971-8.

Yousef, A.F., G.J. Fonseca, M.J. Cohen, and J.S. Mymryk. 2012. The C-terminal region of E1A: a molecular tool for cellular cartography. *Biochem Cell Biol*. 90:153-63.

Yu, D.C., Y. Chen, J. Dilley, Y. Li, M. Embry, H. Zhang, N. Nguyen, P. Amin, J. Oh, and D.R. Henderson. 2001. Antitumor synergy of CV787, a prostate cancer-specific adenovirus, and paclitaxel and docetaxel. *Cancer Res*. 61:517-25.

Yu, D.C., Y. Chen, M. Seng, J. Dilley, and D.R. Henderson. 1999. The addition of adenovirus type 5 region E3 enables calydon virus 787 to eliminate distant prostate tumor xenografts. *Cancer Res*. 59:4200-3.

Yu, F.X., and K.L. Guan. 2013. The Hippo pathway: regulators and regulations. *Genes Dev*. 27:355-71.

Zegerman, P., and J.F. Diffley. 2009. DNA replication as a target of the DNA damage checkpoint. *DNA Repair (Amst)*. 8:1077-88.

Zhang, K.J., J. Zhang, Y.M. Wu, J. Qian, X.J. Liu, L.C. Yan, X.M. Zhou, R.J. Xiao, Y.G. Wang, X. Cao, N. Wei, X.R. Liu, B. Tang, X.Y. Jiao, K. Chen, and X.Y. Liu. 2012. Complete eradication of hepatomas using an oncolytic adenovirus containing AFP promoter controlling E1A and an E1B deletion to drive IL-24 expression. *Cancer Gene Ther*. 19:619-29.

Zhang, X., A.S. Turnell, C. Gorbea, J.S. Mymryk, P.H. Gallimore, and R.J. Grand. 2004. The targeting of the proteasomal regulatory subunit S2 by adenovirus E1A causes inhibition of proteasomal activity and increased p53 expression. *J Biol Chem*. 279:25122-33.

Zhang, X.P., F. Liu, and W. Wang. 2011. Two-phase dynamics of p53 in the DNA damage response. *Proc Natl Acad Sci U S A*. 108:8990-5.

Zhao, D.X., Z.J. Li, Y. Zhang, X.N. Zhang, K.C. Zhao, Y.G. Li, M.M. Zhang, X.W. Yu, M.Y. Liu, and Y. Li. 2014. Enhanced antitumor immunity is elicited by adenovirus-mediated gene transfer of CCL21 and IL-15 in murine colon carcinomas. *Cell Immunol*. 289:155-61.

Zhu, W., L. Wei, H. Zhang, J. Chen, and X. Qin. 2012. Oncolytic adenovirus armed with IL-24 inhibits the growth of breast cancer in vitro and in vivo. *J Exp Clin Cancer Res*. 31:51.

Zhu, W., H. Zhang, Y. Shi, M. Song, B. Zhu, and L. Wei. 2013. Oncolytic adenovirus encoding tumor necrosis factor-related apoptosis inducing ligand (TRAIL) inhibits the growth and metastasis of triple-negative breast cancer. *Cancer Biol Ther*. 14:1016-23.

Zhuo, B., R. Wang, Y. Yin, H. Zhang, T. Ma, F. Liu, H. Cao, and Y. Shi. 2013. Adenovirus arming human IL-24 inhibits neuroblastoma cell proliferation in vitro and xenograft tumor growth in vivo. *Tumour Biol*. 34:2419-26.

Zirkle, R.E., and W. Bloom. 1953. Irradiation of parts of individual cells. *Science*. 117:487-93.

Zlotorynski, E. 2014. DNA damage response: Mitosis: don't 'repair' the telomere! *Nat Rev Mol Cell Biol*. 15:300.